Wei Gao
Daniel L. Schmoldt
James R. Slusser
Editors

UV Radiation in Global Climate Change

Measurements, Modeling and Effects on Ecosystems

TSINGHUA UNIVERSITY PRESS
Springer

Wei Gao
Daniel L. Schmoldt
James R. Slusser

UV Radiation in Global Climate Change

Measurements, Modeling and Effects on Ecosystems

Wei Gao
Daniel L. Schmoldt
James R. Slusser

UV Radiation in Global Climate Change

Measurements, Modeling and Effects on Ecosystems

With 176 figures

TSINGHUA UNIVERSITY PRESS

Springer

Editors
Wei Gao
Natural Resource Ecology Laboratory
Colorado State University, USA
E-mail: wgao@uvb.nrel.colostate.edu

Daniel L. Schmoldt
Cooperative State Research
Education & Extension Service
Waterfront Centre, Ste.3422
800 9th Street SW
Washington DC 20024, USA
E-mail: dschmoldt@csrees.usda.gov

James R.Slusser
Natural Resource Ecology Laboratory
Colorado State University, USA
E-mail: sluss@uvb.nrel.colostate.edu

ISBN 978-7-302-20360-5
Tsinghua University Press, Beijing

ISBN 978-3-642-03312-4 e-ISBN 978-3-642-03313-1
Springer Heidelberg Dordrecht London New York

Library of Congress Control Number: 2009931054

Cover design: Frido Steinen-Broo, EStudio Calamar, Spain

Printed on acid-free paper

Springer is a part of Springer Science+Business Media (www.springer.com)

Wei Gao
Daniel L. Schmoldt
James R. Slusser

全球气候变化中的紫外线辐射：观测、模拟及其对生态系统的影响

UV Radiation in Global Climate Change

Measurements, Modeling and Effects on Ecosystems

With 176 figures

TSINGHUA UNIVERSITY PRESS

Springer

内 容 简 介

大量研究指出紫外线（UV）辐射对生物有机体有害，并且危害人类健康。对地表UV-B辐射强度增加的研究极大地促进了地基和空基相关观测项目的发展；人们还需要进一步对UV辐射的观测、建模和影响进行深入研究。本书各章描述了过去30年来世界范围内与UV辐射相关的研究工作，涉及的领域有：① UV辐射的当前与预测水平及其对生态系统、人类健康、经济与社会的影响；② UV辐射观测仪器的最新发展，地基和空基观测仪器定标进展情况以及观测方法，建模与有关应用；③ 全球气候变化对紫外线辐射的影响。

对于涉及全球气候变化、气象学、气候学、环境科学、生物学和农林科学的大专院校高年级本科生、研究生和教师，本书是一本很有价值的参考书。相关领域的科学家、决策者和普通公众亦能受益于此书。

图书在版编目(CIP)数据

全球气候变化中的紫外线辐射：观测、模拟及其对生态系统的影响= UV Radiation in Global Climate Change: Measurements, Modeling and Effects on Ecosystems: 英文 / 高炜, (美) 施默尔特 (Schmoldt, D. L), (美) 斯拉瑟 (Slusser, J. R.) 主编. —北京：清华大学出版社, 2009.11

ISBN 978-7-302-20360-5

Ⅰ.全…　Ⅱ.①高…　②施…　③斯…　Ⅲ.紫外线–辐射–影响–生态系统–研究–英文

Ⅳ.X122　X171

中国版本图书馆CIP数据核字 (2009) 第 153863 号

责任编辑：赵彤伟
责任校对：
责任印制：

出版发行：清华大学出版社　　**地　　址**：北京清华大学学研大厦 A 座
http://www.tup.com.cn　　**邮　　编**：100084
社 总 机：010-62770175　　**邮　　购**：010-62786544
投稿与读者服务：010-62776969, c-service@tup.tsinghua.edu.cn
质量反馈：010-62772015, zhiliang@tup.tsinghua.edu.cn

印 装 者：
经　　销：全国新华书店
开　　本：153×235　**印张**：35.25　**字数**：797 千字
版　　次：2009 年 11 月第 1 版　**印次**：2009 年 11 月第 1 次印刷
印　　数：1～0000
定　　价：00.00 元

Preface

Over the past three decades, the scientific community has realized the urgency of obtaining a better understanding of the interaction between the earth's atmosphere/biosphere and the sun's radiant energy. Most of the research has focused on the radiant energy balances in the solar and infrared regions of the spectrum, and the way these energy flows affect the climate. During this same time frame, in a related arena, a smaller group of dedicated individuals has concentrated on the role of ultraviolet (UV) radiation as it affects the overall welfare of the planet. Although comprising only a small fraction of the radiation balance that may play a role in global climate change over the next centuries, UV radiation has the capacity to cause direct and more immediate harm to virtually all living organisms and especially to human health. Cumulative high doses of UV radiation are considered a major causal factor in the development of skin cancer and cataracts. Ultraviolet radiation can weaken the human immune system, and can also affect crop production and ocean bio-productivity.

Concerns about the increased levels of UV-B radiation reaching the earth's surface have led to the development of ground- and space-based measurement programs to provide long-term records of its levels. Accurate long-term measurements are difficult to obtain, especially when limited to the bandwidth regions that contain the most harmful solar photons. A core of concerned scientists from across the globe realizes that much work is needed in quantifying the harmful radiation levels and defining their adverse effects. In assessing the effects of UV-B radiation, it is important to realize the complexity of the interactions of living organisms that cause adverse responses with radiant energy directly, as well as in combination with other climate stressors, such as drought, increased temperatures, and CO_2.

This book addresses work that has been conducted throughout the world over the past three decades, such as: (1) current efforts for establishing a climatology of UV radiation; (2) modeling the UV component and its impact on ecosystems, human health, and related economic and social implications; (3) new developments in

UV instrumentation, advances in calibration (ground-based and satellite-based) measurement methods; and (4) the effects of global climate change on UV radiation. All chapters, including the review chapters, have been solicited from renowned scientists in their research fields of UV radiation, meteorology, the environment, and ecosystems. They have presented their work based on research at the global scale, taking into consideration possible future developments. Many new techniques and methods developed from space-ground measurements, mathematical modeling, and remote sensing have recently become available, yet have not previously been presented. This book will be a useful source of reference for undergraduate and graduate students who are involved in the study of global change, environmental science, meteorology, climatology, biology, and agricultural and forest sciences. It will also benefit scientists in related research fields, as well as professors, policy makers, and the general public.

As editors of this book, we wish to express our great appreciation for the contributions of many individuals. We are indebted to the over 50 authors and co-authors within the scientific community who have shared their expertise and contributed much time and effort in the preparation of the book chapters. We also wish to give credit to the numerous funding sources promoting the scientific research performed, and thus the valuable findings shared by the authors. We express our appreciation to the many reviewers and expert scientists who took the time to offer valuable comments and suggestions for the improvement of the book chapters. We acknowledge the management and editorial assistance of Laurie Richards and the technical support of Jonathan Straube of the Natural Resource Ecology Laboratory, Colorado State University and Tsinghua University Press and Springer-Verlag. We especially want to express our appreciation for the support of the Cooperative State Research, Education and Extension Service (CSREES) of the U.S. Department of Agriculture, and the USDA UV-B Monitoring and Research Program at Colorado State University. The efforts of many individuals including Drs. John Moore, John Davis, Steve Liu, Ni-Bin Chang, Mr. George Janson, and Ms. Rita Deike are appreciated.

Dr. Wei Gao
Colorado State University
Fort Collins, CO
Dr. Daniel Schmoldt
U.S. Department of Agriculture
Washington, D.C.

May 2009

Contents

List of Contributors

Julia Lee-Taylor[1], Sasha Madronich[1], Christopher Fischer[1], and Bernhard Mayer[2]
[1]National Center for Atmospheric Research, Boulder, Colorado, USA
[2]Deutsches Zentrum für Luft- und Raumfahrt, Oberpfaffenhofen, Germany

Richard L. McKenzie and J Ben Liley
National Institute of Water and Atmospheric Research (NIWA),
Lauder, Central Otago, New Zealand 9352
NIWA Lauder, Private Bag 50061 Omakau, Central Otago 9352, New Zealand
E-mail: r.mckenzie@niwa.co.nz
E-mail: b.liley@niwa.co.nz

Germar Bernhard, Charles R. Booth, and James C. Ehramjian
5340 Riley Street
Biospherical Instruments Inc., San Diego, CA, USA
E-mail: bernhard@biospherical.com
E-mail: booth@biospherical.com
E-mail: jime@biospherical.com

Claudio Rafanelli, Alessandro Damiani, Elena Benedetti, Sara. De Simone,
Andrea Anav, Luigi Ciattaglia, and Ivo Di Menno
ICES - International Center for Earth Sciences
c/o CNR - Istituto di Acustica “O.M. Corbino”
Area della Ricerca “Roma - Tor Vergata”
via del Fosso del Cavaliere, 100
00133 - Roma, Italy
E-mail: c.rafanelli@e-ices.eu (rafanelli@libero.it)

Jay Herman
Goddard Space Flight Center
Code 613.3
Greenbelt, MD 20771 USA
E-mail: jay.r.herman@nasa.gov

James B. Kerr
Scientist Emeritus of Environment Canada
4396 Kingscote Road, V0R 1N2
Cowichan Bay, British Columbia
E-mail: jbkerr@shaw.ca

Alfio V. Parisi, David J. Turnbull, Peter Schouten, Nathan Downs and Joanna Turner
Centre for Rural and Remote Area Health, University of Southern Queensland, Toowoomba
Queensland, Australia 4350
E-mail: parisi@usq.edu.au

Wei Gao[1], John M. Davis[1], Roger Tree[1], James R. Slusser[1],
and Daniel Schmoldt[2]
[1]United States Department of Agriculture
UV-B Monitoring and Research Program
Natural Resource Ecology Laboratory
Colorado State University, Fort Collins, CO, USA
E-mail: wgao@uvb.nrel.colostate.edu
[2]United States Department of Agriculture
Cooperative State Research, Education, and Extension Service
Washington, DC, USA
E-mail: dschmoldt@csrees.usda.gov

Knut Stamnes,[1] Børge Hamre,[2] and Jakob J. Stamnes[2]
[1]Light and Life Laboratory, Department of Physics and Engineering Physics,
Stevens Institute of Technology, Hoboken, NJ 07030, USA
E-mail: Knut.Stamnes@stevens.edu
[2]Department of Physics and Technology, University of Bergen, Postboks 7800, 5020 Bergen, Norway
Børge.Hamre@ift.uib.no
E-mail: Jakob.Stamnes@ift.uib.no

Wei Gao[1], Zhiqiang Gao[1,2], and Ni-Bin Chang[3]
[1]USDA UV-B Monitoring and Research Program,
Natural Resource Ecology Laboratory,
Colorado State University, Fort Collins, CO, USA
E-mail: wgao@uvb.nrel.colostate.edu
E-mail: zgao@uvb.nrel.colostate.edu
[2]Institute of Geographical Sciences and Natural Resources Research,
Chinese Academy of Sciences, Beijing, China
[3]Department of Civil and Environmental Engineering,

University of Central Florida, Orlando, FL 32816, USA
E-mail: nchang@mail.ucf.edu

William F. Barnard[1] and Brian N. Wenny[2]
[1]North Carolina State University
Department of Marine, Earth, and Atmospheric Sciences
Campus Box 8208
Raleigh, North Carolina 27695-8208, USA
E-mail: SBarn46193@aol.com
[2]MODIS Characterization Support Team (MCST) Sigma Space Corp.
10210 Greenbelt Road, Suite 500
Lanham, MD 20706
E-mail: brian.wenny@gmail.com

Gordon M. Heisler
USDA Forest Service Northeastern Research Station,
c/o SUNY ESF, 5 Moon Library, Syracuse, NY 13210, USA
E-mail: gheisler@fs.fed.us

Ronald J. Ryel[1], Stephan D. Flint[1], and Paul W. Barnes[2]
[1]Department of Wildland Resources and the Ecology Center, Utah State University
Logan, UT 84322-5230, USA
E-mail: ron.ryel@usu.edu
[2]Department of Biological Sciences, Loyola University New Orleans, LA 70118, USA
E-mail: pwbarnes@loyno.edu

K. Raja Reddy[1], P.V. Vara Prasad[2], and Shardendu K. Singh[1]
[1]Deaprtment of Plant and Soil Sciences, Box 9555, 117 Dorman Hall
Mississippi State University, Mississippi State, MS 39762, USA
E-mail: krreddy@pss.msstate.edu
[2]Department of Agronomy, Kansas State University, Manhattan, KS 66506, USA
E-mail: vara@ksu.edu

Joseph H. Sullivan[1], Linda C. Pope, Betsy M. Sutherland[2], Paula V. Bennett[2], James E. Blum[3], Ann E. Stapleton[4], and Dennis C. Gitz III[5]
[1]Department of Plant Science and Landscape Architecture, 2122 Plant Sciences Building University of Maryland, College Park, MD 20742, USA
E-mail: jsull@umd.edu
[2]Brookhaven National Laboratory, P.O. Box 5000
Upton, NY 11973-5000, USA

E-mail: bms@bnl.gov
[3]Department of Mathematics and Statistics
University of North Carolina at Wilmington, Wilmington, NC 28403, USA
E-mail: blumj@uncw.edu
[4]Department of Biology and Marine Biology
University of North Carolina at Wilmington, Wilmington, NC 28403, USA
E-mail: stapletona@uncw.edu
[5]USDA-ARS, 3810 4th Street, Lubbock, Texas 79415, USA

Richard H. Grant[1], Kent G. Apostol[2], and Hans F. Schmitz[1]
[1]Department of Agronomy, Purdue University, West Lafayette, IN 47907-2054, USA
E-mail: rgrant@purdue.edu
E-mail: hschmitz@purdue.edu
[2]Department of Biological Sciences, Bethel University, St. Paul, MN 55112, USA
E-mail: k-apostol@bethel.edu

Katherine M. Warpeha and Lon S. Kaufman
Department of Biological Sciences m/c 567
University of Illinois at Chicago
900 S. Ashland Ave
Chicago, IL 60607, USA
E-mail: kwarpeha@uic.edu
E-mail: lkaufman@uic.edu

Yadong Qi[1], Gordon M. Heisler[2], Wei Gao[3], Thomas C. Vogelmann[4], and Shuju Bai[5]
[1]Urban Forestry Program, P.O. Box 11288, Southern University
Baton Rouge, LA 70813, USA
E-mail: yadong_qi@subr.edu
[2]USDA Forest Service Northeastern Research Station, c/o SUNY ESF,
5 Moon Library, Syracuse, NY 13210, USA
E-mail: gheisler@fs.fed.us
[3]USDA UV-B Radiation Monitoring Program, and Senior Research Scientist, Natural Resource Ecology Laboratory, Colorado State University
Fort Collins, CO 80523-1499, USA
E-mail: wgao@uvb.nrel.colostate.edu
[4]Botany Department, University of Vermont, Burlington, VT 05405, USA
E-mail: Thomas.Vogelmann@uvm.edu
[5]Department of Computer Science, Southern University
Baton Rouge, LA 70813, USA
E-mail: bais@cmps.subr.edu

1 A Climatology of UV Radiation, 1979 – 2000, 65S – 65N

Julia Lee-Taylor[1], Sasha Madronich[1], Christopher Fischer[1], and Bernhard Mayer[2]

[1] National Center for Atmospheric Research, Boulder, Colorado, USA
[2] Deutsches Zentrum für Luft- und Raumfahrt, Oberpfaffenhofen, Germany

Abstract Solar ultraviolet (UV) radiation reaching earth's surface is of interest because of its role in the induction of various biological and chemical processes, including skin cancer. We present climatological distributions of monthly mean surface-level UV radiation, calculated using the Tropospheric Ultraviolet-Visible (TUV) radiative transfer model with inputs of ozone column amounts and cloud reflectivities (at 380 nm) measured by satellite instruments (Total Ozone Mapping Spectrometers (TOMS), aboard Nimbus-7, Meteor-3, and Earth Probe). The climatology is averaged over the years 1979 – 2000 for UV-A (315 nm – 400 nm), UV-B (280 nm – 315 nm), and radiation weighted by the action spectra for the induction of erythema (skin-reddening), pre-vitamin D_3 synthesis, and non-melanoma carcinogenesis. Coverage is global, excluding the poles.

Comparisons with concurrent ground-based UV radiation measurements archived at the World Ozone and Ultraviolet Data Center show agreement at the 10% – 20% level, except at high latitudes where the large surface albedo of snow and ice invalidates the use of satellite-observed reflectivity in estimating cloud cover. The climatology may be useful in epidemiological studies that assess the role of long-term environmental exposure to UV radiation.

Keywords UV climatology, erythema, vitamin D synthesis, TUV model

1.1 Introduction

Solar ultraviolet radiation transmitted through the atmosphere to earth's surface is known to induce various biological and chemical processes, many of which are harmful to living tissues and some materials (see UNEP, 2006, for a review). Examples of processes relevant to human health include skin-reddening (erythema), synthesis of vitamin D within skin, and induction of various skin cancers. The

long-term geographical distribution of surface UV radiation is of considerable interest towards understanding these effects. However, environmental UV levels are highly variable due to daily and seasonal cycles at different latitudes, and to variations in atmospheric transmission (mainly attributable to variations in ozone, clouds, and aerosols) and surface reflections. Ultraviolet radiation measurements by ground-based instruments are too few, and their record relatively short, to construct a unified picture of its average global distribution.

An alternative method of estimating surface UV levels with long-term global coverage relies on satellite-based observations of earth's atmosphere and surface, combined with a computer model of the propagation of UV radiation through the atmosphere. This methodology is already in use on a NASA website (http://jwocky.gsfc.nasa.gov/ery_uv/ery_uv1.html, which uses data from the TOMS ozone-monitoring satellite instruments to generate maps of erythemal UV for specific days. Other applications of the technique have illuminated interesting aspects of the problem, i.e., estimation of zonal mean irradiances at different UV wavelengths, of trends due to ozone changes, of cloud effects, and of geographical distributions based on monthly averaged ozone and clouds (e.g., Frederick and Lubin, 1988; Madronich, 1992; Eck et al., 1995; Frederick and Erlick, 1995; Herman et al., 1996a; Lubin et al., 1998; Herman et al., 1999; Sabziparvar et al., 1999; Herman et al., 2000; McKenzie et al., 2001). Here we use satellite-based observations of atmospheric ozone and clouds to derive a climatology of erythemal UV radiation with nearly global coverage (excluding the polar regions), averaged over the years 1979 – 2000. We developed a fast method for the explicit calculation of UV daily doses for each day of the whole time period. Averaging daily UV doses, rather than calculating monthly doses on the bases of monthly-averaged cloudiness and ozone, reduces possible uncertainties connected with the non-linear relationship between atmospheric parameters (e.g., total ozone and clouds) and surface UV radiation. Comparisons with long-term measurements at 22 UV monitoring stations allow some assessment of the reliability of this technique. Climatologies such as those presented here can be useful in epidemiological studies that assess the role of long-term environmental exposure to ultraviolet radiation, such as those discussed in Chapter 2 (McKenzie and Liley).

1.2 Method

UV broadband irradiances (W m^{-2}) are computed as integrals over wavelength λ (nm) of spectral irradiances $E(\lambda)$ (W m^{-2} nm^{-1}) weighted by appropriate spectral functions $S(\lambda)$ (typically unit-less):

$$\text{Irradiance} = \int S(\lambda)\, E(\lambda)\, \mathrm{d}\lambda$$

$E(\lambda)$ is a function of solar zenith angle (SZA) and surface elevation, as well as

optical depth profiles of atmospheric absorbers and scatterers (e.g., ozone and clouds). The values of $S(\lambda)$ are unity for UV-A and UV-B in the respective wavelength ranges of 315 nm – 400 nm and 280 nm – 315 nm, and zero outside these ranges. Figure 1.1 shows the wavelength dependence for three action spectra with relevance to human health: (1) erythema (McKinlay and Diffey, 1987), (2) pre-vitamin D_3 production in human skin (Holick et al., 2006, after MacLaughlin et al., 1982), and (3) photocarcinogenesis of non-melanoma skin cancers (CIE, 2006). The erythema action spectrum has been accepted for the calculation of the instantaneous UV index (defined as the UV_{ery} irradiance multiplied by 40 (ICNIRP, 1995; WMO, 1997)), and the time-integrated standard erythemal dose (SED = 100 J m^{-2} (CIE, 1998)). In practice, use of this CIE spectrum emphasizes the ozone-sensitive region of 295 nm – 320 nm, peaking near 305 nm with minor contributions from longer wavelengths (Madronich et al., 1998; Micheletti et al., 2003). The other two functions are somewhat similar, in that they maximize at around 305 nm wavelength, and decrease by several orders of magnitude by 330 nm.

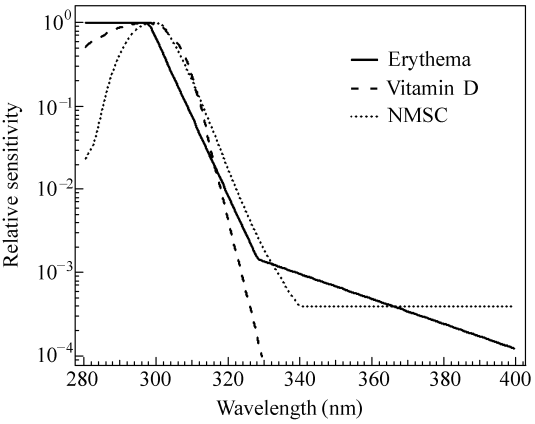

Figure 1.1 Spectral functions for erythema: solid line (McKinlay and Diffey, 1987); synthesis of pre-vitamin D3: dashed line (MacLaughlin et al., 1982; Holick et al., 2006); and non-melanoma carcinogenesis: dotted line (CIE, 2006)

Compilation of a global UV climatology is computationally intensive, requiring the calculation of $E(\lambda)$ at all relevant wavelengths, at each geographical location, and over diurnal cycles for each day of each year. To reduce computational time, we used the TUV model (Madronich and Flocke, 1997) to pre-tabulate values of weighted UV irradiances as a function of SZA (0° to 96° in 1° steps), ozone column (43 DU – 643 DU in steps of 10 DU), and surface elevation (0, 3, and 8 km above sea level), for cloud-free and aerosol-free conditions. The omission of UV absorption by aerosols can lead to overestimates of irradiance for polluted locations; this limitation will be discussed in more detail later. $E(\lambda)$ at earth's surface was computed at 1 nm steps from 280 nm – 400 nm. The spectral irradiance

incident at the top of the atmosphere was taken from the Atlas3/SUSIM measurements (D. Prinz, pers. comm., 1998). Vertical profiles (appropriate for mid-latitude, annual average conditions) for air density, temperature, and ozone were taken from the U.S. Standard Atmosphere (USSA, 1976) with, however, the ozone profile re-scaled to the actual ozone column (see below). The propagation of solar radiation through the atmosphere was computed with a 4-stream discrete ordinates method (Stamnes et al., 1988), with pseudo-spherical correction for improved accuracy at low sun conditions (Petropavlovskikh, 1995). A Lambertian surface albedo of 5% was assumed at all wavelengths.

The atmospheric ozone column and cloud reflectivity at 380 nm (R) were taken from the TOMS data from three satellites: (1) Nimbus-7, Level 3/Version 8 (McPeters et al., 1996), Nov. 1, 1978 to Dec. 31, 1992; (2) Meteor-3, Level 3/Version 8 (Herman et al., 1996b), Aug. 22, 1991 to Dec. 11, 1994; and (3) Earth Probe, Level 3/Version 8 (McPeters et al., 1998), July 7, 1996 to June 30, 2000. The geographical resolution of the measurements was 1.25° longitude by 1.00° latitude. For each grid point, only one satellite overpass per day occurred (*ca*. local noon). We therefore assumed constant ozone and reflectivity values for the entire day. Local values of the ozone column, SZA and surface elevation were used to compute the clear-sky irradiances at 30-minute intervals over half days by interpolation of the pre-tabulated values. Assuming symmetry about local noon, these data were integrated over 24 hours to obtain the daily UV-A, UV-B, and erythemal doses. A correction for variations in the earth-sun distance was applied as a function of date. A reduction factor F for cloud cover, identical to that used by Eck et al. (1995), was then applied:

$$1/F = \begin{cases} 1-(R-0.05)/0.9, & R \leqslant 50\% \\ 1-R, & R > 50\% \end{cases}$$

For cloud-free and aerosol-free conditions, total reflectivity at 380 nm is dominated by Rayleigh scattering and surface reflections, the latter being rather small at UV wavelengths unless snow or ice is present. The TOMS algorithm attributes excess reflectivity to clouds or scattering aerosols, without distinguishing between the two. When high surface albedo is encountered (e.g., snow or ice), this method erroneously interprets the high surface reflectivity as cloud cover, thus artificially reducing surface UV irradiance. Polar regions are therefore excluded from our analysis. For non-polar regions, including mountainous regions, we did not attempt to correct for snow cover. The calculated UV doses for such areas should therefore be considered as lower limits.

The calculation of UV doses should in principle be carried out for each location and each day over the satellite record (ca. 1979 – 2000). However, gaps in the satellite record exist, so that for some days and/or locations, no doses could be computed. These missing days require some consideration to avoid biases in any

long term averages and trends. For each location, monthly averaged doses were calculated for each of the 247 months in the combined dataset, but were considered valid only if at least half of the days in that month had data. No attempt was made to discriminate between the months in which data gaps typically occurred during the early part of the month and when they typically occurred during the latter part of the month. In some cases, measurements for the same location and days were available from two different satellites; in such cases, monthly means for each satellite were computed, then averaged together to obtain a single mean for that month.

Climatological monthly values were computed for each location by averaging all valid values for that month over multiple years (e.g., climatological January is the mean of all valid January values over 1979 – 2000, etc.). For most of this chapter, we consider averages over the full 22 years (1979 – 2000), but for some of the discussion below, we also considered the time periods 1979 – 1989 and 1990 – 2000 separately. Climatological annual values were computed as the mean of all valid climatological monthly values, specifically (mean of all Jans. + mean of all Febs. + ⋯ + mean of all Decs.)/12.

The second period (1990 – 2000) is missing some data (all of 1995, Jan – Jun 1996, Jul – Dec 2000). We tested the effects of these missing data on the calculated changes by temporarily removing the analogous months from the 1979 – 1989 record and comparing the resulting climatology to that of the complete 1979 – 1989 period. Differences of $< \pm 0.2\%$ were obtained. This is on the order of ~1/10 of the clear sky changes between the two periods 1979 – 1989 and 1990 – 2000, and on the order of <1/10 of the changes in the "all sky" values between these two periods.

For a comparison with the satellite-derived estimates, we used measurements of UV irradiances by ground-based spectroradiometers, obtained from the World Ozone and UV Data Center archive (WOUDC; data downloaded June 2002). Measured UV_{ery} doses are reported as daily integrals of spectral observations integrated over wavelength with the McKinlay and Diffey (1987) erythemal action spectrum weighting. The archives include 22 non-polar stations; 10 in Canada (Meteorological Service of Canada, MSC); 4 in Japan (Japan Meteorological Agency, JMA); 2 in the Taiwan region ("Central Weather Bureau of Taiwan, CWBT"), and 1 each in Obninsk, Russia (Institute of Experimental Meteorology-Scientific Production Association (IEM-SPA)), Poprad-Ganovce, Slovakia (Slovak HydroMeteorological Institute (SHMI)); Mauna Loa, HI (MSC); San Diego, CA; Ushuaia, Argentina; and Palmer Station, Antarctica (all US National Science Foundation (NSF) sites). The NSF sites operated double monochromators (Biospherical Instruments, Inc), while all other sites operated Brewer single monochromators. Our satellite-based irradiance values for station locations were derived for the locations and altitudes of the ground-based stations.

1.3 Results

1.3.1 Satellite-Derived UV Climatologies

The geographical distributions of daily UV radiation doses at earth's surface, averaged over the entire time period of (Nov. 1, 1978 – June 30, 2000) are shown in Figs. 1.2 – 1.6. The upper panel in each figure shows values calculated by considering the effects of both ozone and clouds, as estimated from TOMS data, and are thus assessed to be nearest to the actual values experienced over this time period. The lower panels show climatological distributions estimated for hypothetical cloud-free skies (i.e., estimated from the ozone distributions without correcting for the presence of clouds).

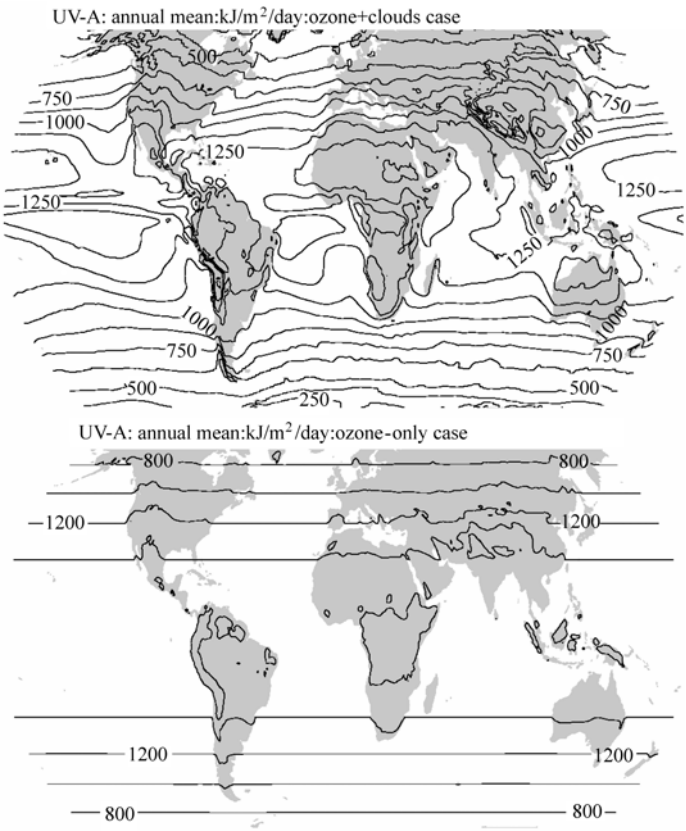

Figure 1.2 Climatological daily doses of UV-A at earth's surface, derived from satellite (TOMS) observations of the atmospheric ozone column and cloud reflectivity at 380 nm and averaged annually over Nov 1, 1978 – June 30, 2000, with (upper) and without (lower) correcting for the presence of clouds

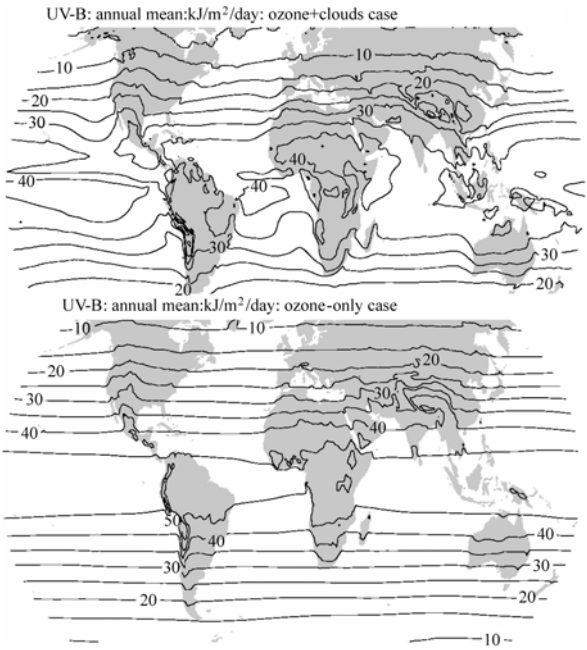

Figure 1.3 Climatological daily doses of UV-B at earth's surface, as Fig. 1.2

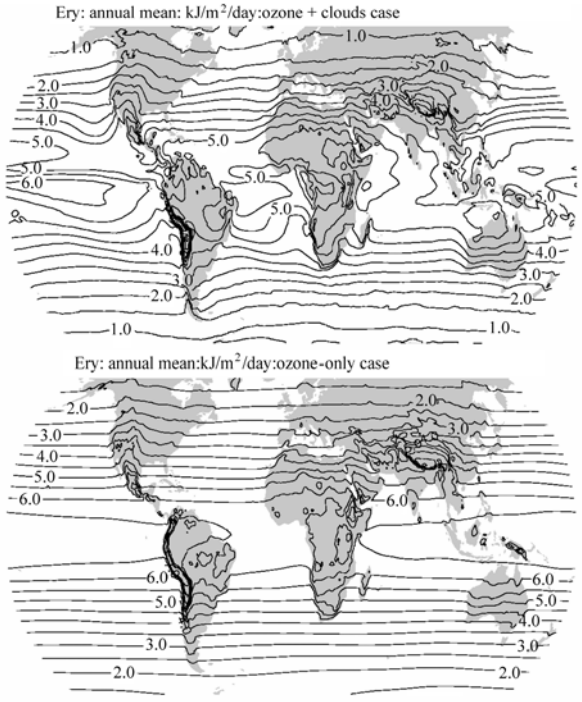

Figure 1.4 Climatological daily doses of erythemal UV at earth's surface, as Fig. 1.2

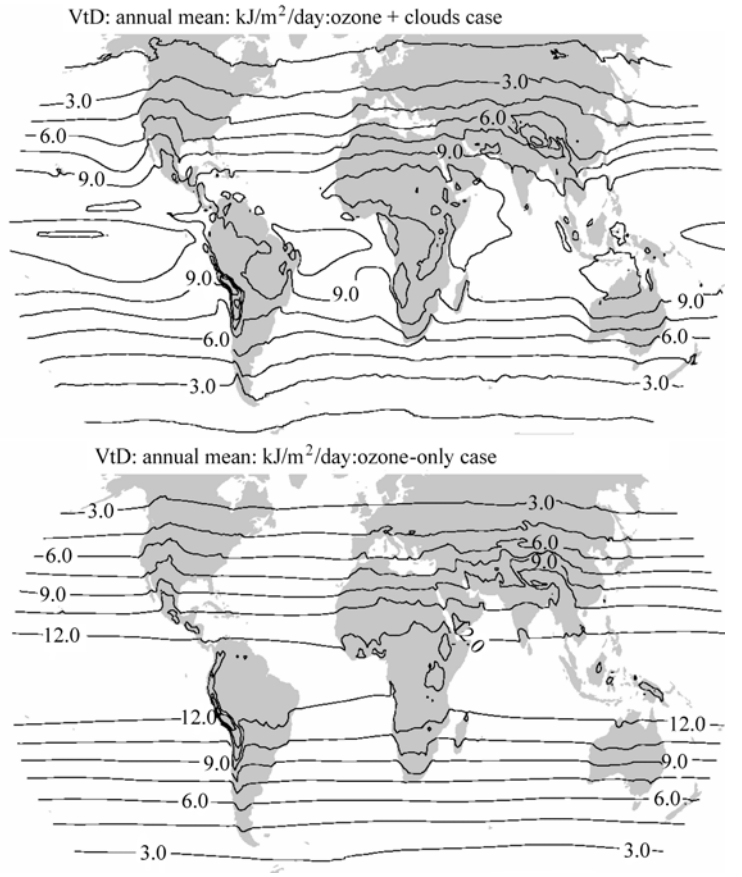

Figure 1.5 Climatological daily doses of UV weighted for pre-vitamin D_3 synthesis at earth's surface, as Fig. 1.2

The zonally homogeneous distribution of UV-A calculated for cloud-free conditions shows almost exclusive dependence on solar position, with only small variations due to surface topography. Ozone column variations induce additional zonal variations in the distributions of cloud-free UV-B and UV weighted for either erythema or other biological response functions. However, the strongest longitudinal variations in the surface UV dose rate distributions are caused by climatological cloud distributions.

As expected, the highest doses are generally seen in the tropics, up to ca. 6 kJ m^{-2} day^{-1} (60 SED day^{-1}) for erythemal UV in the eastern Pacific and eastern Africa, but with substantial cloud-related reductions over western South America, parts of West Africa, and just north of the equator in the eastern and central Pacific. Middle latitudes of both hemispheres show a general pole-ward decrease from about 5 to 1 kJ m^{-2} day^{-1}, with some regional highs associated with higher elevations, smaller ozone columns, and infrequent cloudiness (e.g., the Andes

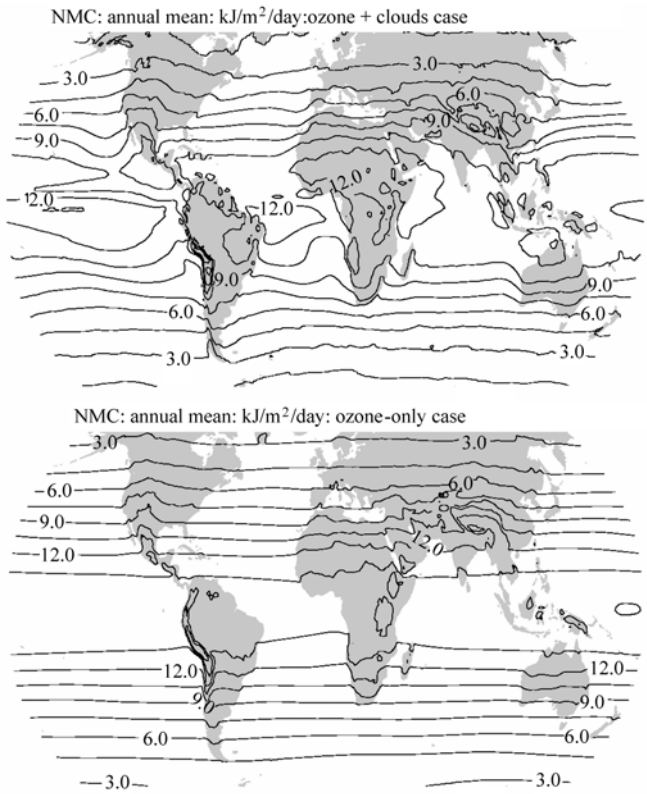

Figure 1.6 Climatological daily doses of UV weighted for non-melanoma carcinogenesis at earth's surface, as Fig. 1.2

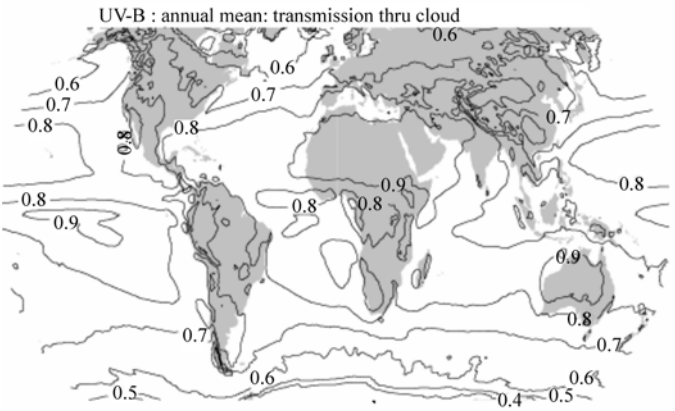

Figure 1.7 Climatological annual mean cloud-related UV reduction factors for daily doses of UV-A derived from satellite (TOMS) observations of the atmospheric ozone column and cloud reflectivity at 380 nm for Nov 1, 1978 – June 30, 2000. Cloud-related UV reduction factors for the other UV functions discussed in this chapter are similar

Mountains, the Tibetan Plateau, central Mexico, and the southwestern U.S.). Lower values for those latitudes are noted for East Asia and the coastal eastern Pacific, associated with more frequent cloud cover. Figure 1.7 shows the cloud-related UV reduction factor, calculated as the ratio of the cloud-corrected climatological daily UV dose (upper panels of Figs. 1.2 – 1.6) to the climatological daily dose before cloud-correction (lower panels of Figs. 1.2 – 1.6).

The seasonal variations of the 22-year UV dose climatologies are shown in Figs. 1.8 – 1.11. (The seasonal variability of UV weighted for non-melanoma carcinogenesis is similar in magnitude and distribution to that of UV weighted for pre-vitamin D3 synthesis, so it is not shown.) The latitudinal distributions are generally consistent with the annual variation of the subsolar point in the tropics, giving strong seasonal variations at temperate latitudes (out of phase by six months between the two hemispheres).

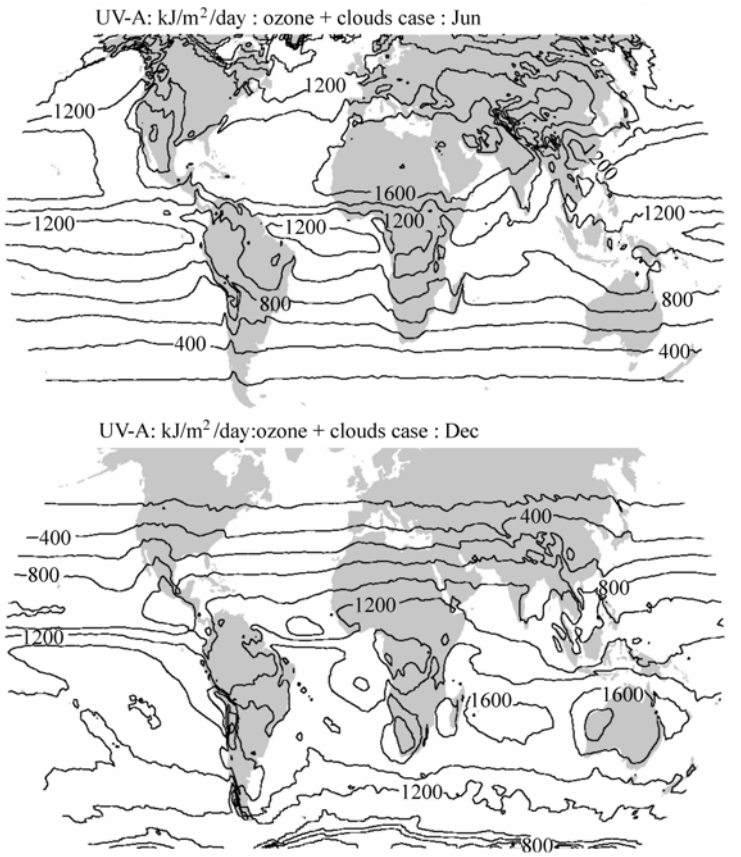

Figure 1.8 Seasonal variability of daily doses of UV-A. The figure shows the daily doses averaged over the period Dec. 1, 1978 – June 30, 2000 for the months of June (upper) and December (lower)

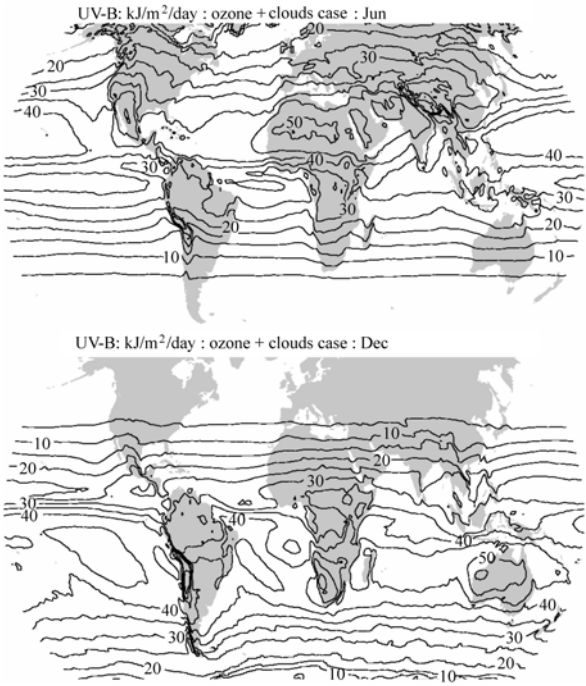

Figure 1.9 Seasonal variability of daily doses of UV-B, as Fig. 1.8

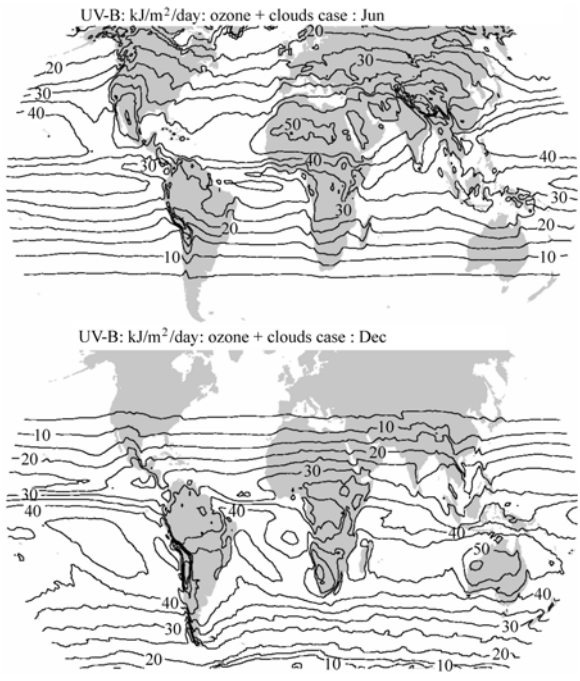

Figure 1.10 Seasonal variability of daily doses of erythemal UV, as Fig. 1.8

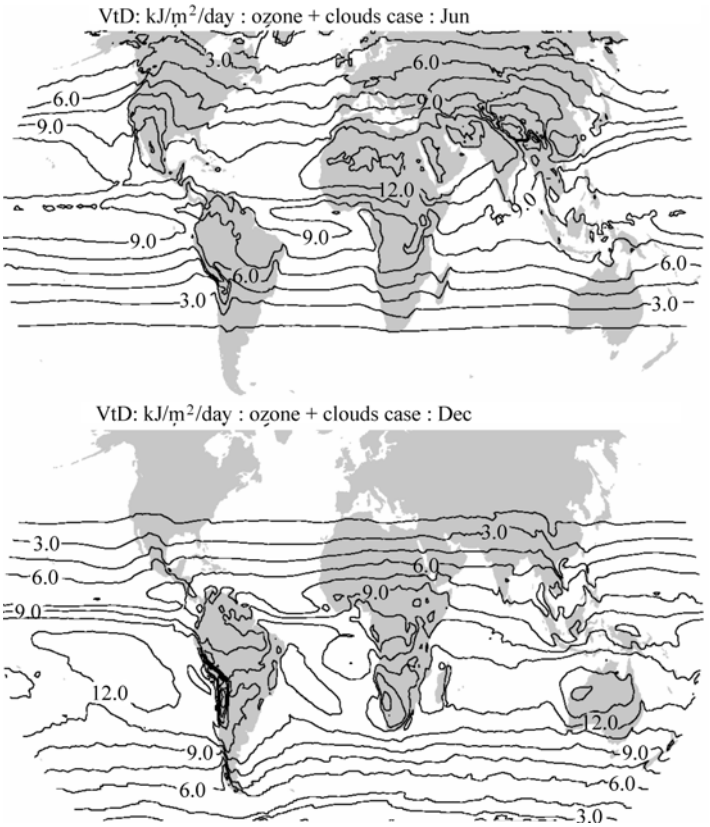

Figure 1.11 Seasonal variability of daily doses of UV weighted for pre-vitamin D_3 synthesis, as Fig. 1.8

Detailed analysis of temporal trends is beyond the scope of this work, but some indications may be obtained by comparing the climatological values averaged over 1990 – 2000 with those averaged over 1979 – 1989. Figure 1.12 shows the changes in erythemal doses between these two 11-year periods. The total dose rate changes combine the effects of changes in the ozone column (Fig. 1.12, top panel) and changes in cloudiness (Fig. 1.12, center panel). The upper panel clearly shows the increase in surface UV resulting from stratospheric ozone reductions, not only in the Antarctic region, but also at mid-latitudes. The center panel shows a reduction in cloudiness, maximizing over north-central Europe, possibly as a result of the introduction of cleaner fuel-burning technologies in the west, combined with a contraction of heavy industry in the east. Increases in cloudiness are seen over the Bay of Bengal and over the Humboldt Current off the west coast of South America, possibly owing to the enhanced El Niño conditions prevalent during the 1990s. The apparent reductions in cloudiness around the coasts of

southern Alaska and Hudson Bay may partly be artifacts related to decadal-scale changes in snow and ice cover. The lower panel shows the net change in the annual mean global distribution of erythemal UV dose rates. Significant changes are seen to have occurred, with annual mean dose rate increases of 8% or more in some regions, including north-central Europe, the eastern seaboard of the US, Siberia, and the Antarctic Ocean. Other regions experienced annual mean dose rate reductions of up to 6%.

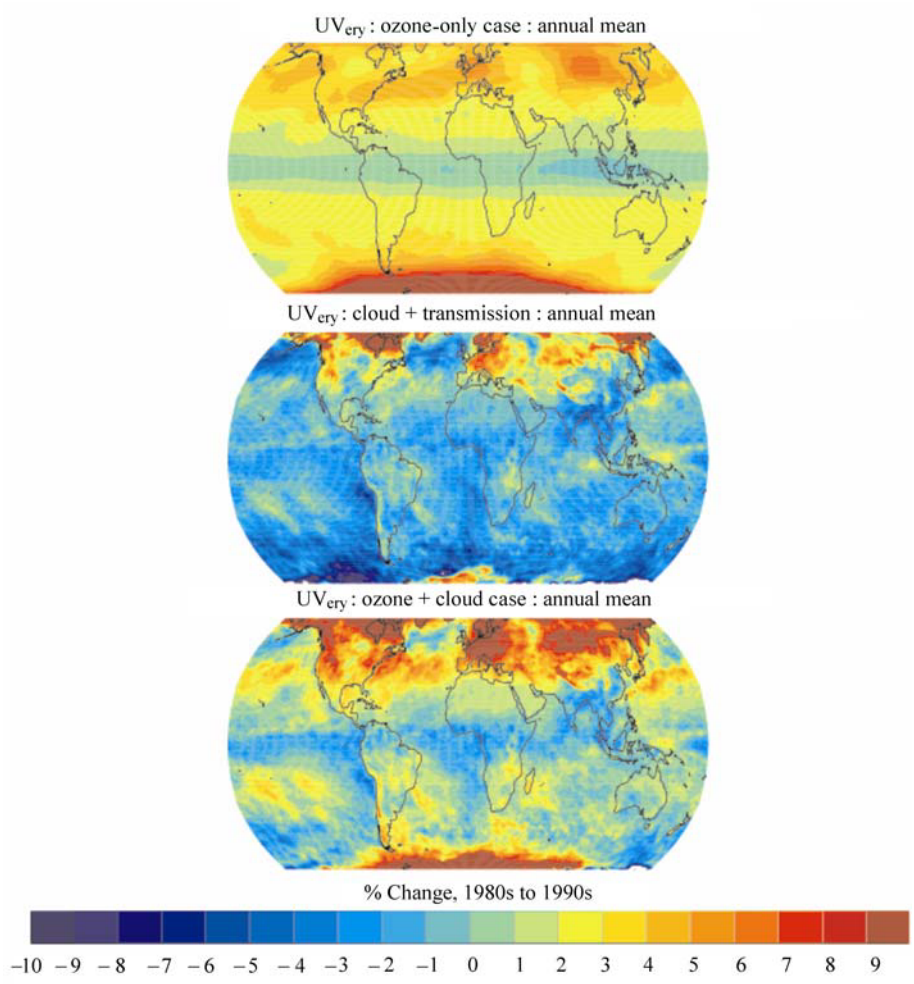

Figure 1.12 Changes in average daily doses of erythemal UV between the periods of 1979 – 1989 and 1990 – 2000. Change in values calculated from the TOMS ozone data only (upper); change in cloud reduction factor (center); change in annual mean net daily erythemal UV dose (lower)

1.3.2 Comparison with Ground-Based Measurements

Comparisons with ground-based measurements are shown in Fig. 1.13 for annual averages of the daily UV_{ery} dose. Temporal overlap between the satellite observations and the ground-based observations is only available at some stations (see Table 1.1), and then only for a few years. The satellite-derived estimates show a long-term trend due to stratospheric ozone depletion, as has been reported previously (Herman et al., 1996a), whether or not cloud cover is considered. Note that the satellite-derived values apply to an extended region of typically 10^4 km^2, while the ground-based observations pertain to a single, often urban, location. Figure 1.13 shows that the satellite-derived annual averages tend to overestimate measurements by averages of 5% for remote northern locations, 11% for Canadian cities, and 30% for polluted mid-latitude urban regions (San Diego and cities in Japan and cities in the Taiwan region). Herman et al. (1999) found similar differences for the measurements at Toronto, showing also that these were not seasonally dependent, except for snow-covered periods. These discrepancies remain under investigation and may stem from both measurements and satellite-derived values. Because of the imperfect cosine response of the entrance optics, Brewer instruments may underestimate true irradiances by 2% – 7% according to Bais et al. (1998), or by 6% ± 2% according to Herman et al. (1999). Network for the

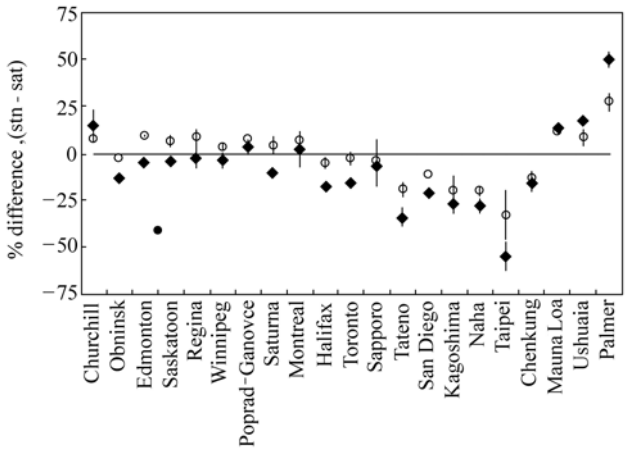

Figure 1.13 Differences between ground-based and satellite-derived annual mean daily erythemal UV doses. Points show the mean of differences for all years where both ground-based and satellite-derived values are available. Lines show the standard deviations at each station. Filled diamonds = satellite-derived UV values including adjustment for the presence of clouds, and mean ground-based values; open circles = satellite-derived UV values without cloud adjustment and maximum ground-based values. Stations are listed in order of decreasing latitude. See Table 1.1 for station details

Table 1.1 Details of ground-based Brewer spectrophotometer stations referenced in Fig. 1.13

Station	Agency*	Station I.D.	Latitude (°)	Longitude (°)	Altitude (m)
Churchill	MSC	77	58.8	−94.1	35
Obninsk	IEM-SPA	307	55.1	36.6	0
Edmonton	MSC	21	53.6	−114.1	766
Saskatoon	MSC	241	52.1	−106.7	550
Regina	MSC	338	50.2	−104.7	592
Winnipeg	MSC	320	49.9	−97.2	239
Poprad-Ganovce	SHMI	331	49.0	20.3	706
Saturna	MSC	290	48.8	−123.1	178
Montreal	MSC	319	45.5	−73.8	24
Halifax	MSC	321	44.7	−63.6	31
Toronto	MSC	65	43.8	−79.5	198
Sapporo	JMA	12	43.1	141.3	19
Tateno	JMA	14	36.1	140.1	31
San Diego	NSF	239	32.8	−117.1	0
Kagoshima	JMA	7	31.6	130.6	283
Naha	JMA	190	26.2	127.7	29
Taipei	"CWBT"	95	25.0	121.5	30
Chenkung	"CWBT"	306	23.1	121.4	10
Mauna Loa	MSC	31	19.5	−155.6	3397
Ushuaia	NSF	339	−54.5	−68.2	7
Palmer	NSF	292	−64.5	−64.0	0

* Agency abbreviations: Meteorological Service, Canada (MSC); Institute of Experimental Meteorology-Scientific Production Association (IEM-SPA), Russia; Swedish Meteorological and Hydrological Institute (SHMI); Japan Meteorological Agency (JMA); National Science Foundation (NSF), USA; "Central Weather Bureau of Taiwan (CWBT)." The World Ultraviolet Radiation Data Centre (WOUDC), where the data is archived, has a stated goal of annually intercalibrating the instruments.

Detection of Atmospheric Composition Change (NDACC) quality ground based instruments, which have superior cosine responses and include corrections for these errors, also show much lower UV irradiances than satellite derived values in polluted locations, but good agreement in pristine locations (McKenzie et al., 2001). The TOMS-based method does not account for UV-absorbing aerosols, which according to Herman et al. (1999) lead to a systematic overestimate of ca. 8% ± 2% at Toronto. Aerosols are likely to be significant at other locations during pollution episodes (e.g., Wenny et al., 1998), or if an area suffers routinely from pollution (e.g., the Southeast Asian sites). Smaller errors (e.g., 5% or less) are associated with several other factors (e.g., instrument calibrations, extraterrestrial irradiances used in the model), but at present there is no basis for estimating the sign of any resulting bias. The strong disagreement at Palmer Station, where we underestimate the irradiance by 50%, illustrates the consequence of using

TOMS-observed reflectivity to infer cloudiness at high-latitude locations. The high reflectivity recorded by the satellite may be due to snow and ice rather than to clouds, thus leading to a significant underestimate of the UV_{ery} reaching the surface.

Using a similar TOMS-based technique, Frederick and Erlick (1995) computed noon-time erythemal irradiances, as well as their trends and interannual variability, for regions of 6° latitude by 10° longitude centered over New Zealand, Malaysia, Sweden and the eastern U.S. Lubin et al. (1998) used monthly mean ozone from TOMS and monthly mean cloud cover data derived from the Earth Radiation Budget Experiment (ERBE) to compute global UV_{ery} distributions for several months during 1988 and 1989. Sabziparvar et al. (1999) presented a global climatology of daily doses for January, April, July, and October, computed from monthly-averaged climatological ozone (TOMS, 1985 – 1989) and cloud data (International Satellite Cloud Climatology Project (ISCCP), 1983 – 1991). Global distributions of UV_{ery} for 1988 (January, March, July, and September) are presented by Herman et al. (1999), who also carried out detailed comparisons to observations obtained with the Toronto Brewer instrument. Our results are generally consistent with these studies, for example, predicting the strong latitudinal gradients as well as most of the regional anomalies. However, detailed values are not directly comparable because of our use of daily rather than monthly ozone and cloud data, and our integration over an extended time period (1978 – 2000).

1.3.3 Discussion of Uncertanties

We recognize a number of limitations in our study that can hopefully be addressed by future work. The parameterization of cloud effects via the 380 nm reflectivity is obviously crude compared to the complexity of real cloudiness, and its failure in the presence of high albedo surfaces has been discussed. Other sources of cloud information exist and show promise in extending the climatology to higher latitudes (e.g., Mayer and Madronich, 1998). Additionally, pollutants present in the lower atmosphere can attenuate surface UV irradiances. Regional-scale absorbing aerosols, probably associated with plumes of biomass burning, have been detected by the TOMS instrument (Krotkov et al., 1998), although quantification remains a challenging area of research. On smaller scales, such as highly polluted urban areas, substantial absorption of UV radiation is possible from smog-generated ozone, SO_2, NO_2, and absorbing aerosols (e.g., soot) in the lower atmosphere. These absorbers are not easily detected from satellite platforms, so that a climatology based on direct ground-based UV radiation measurements, if available, is preferable for such locations.

The presence of snow, whether seasonal or year-round, creates another challenge. The misinterpretation of snow cover as cloud in the satellite data leads to

underestimates of ambient UV. This underestimate stems not only from the inappropriate application of the cloud-related UV reduction factor, but also from the use of a surface albedo of 5%, whereas the reflectivity of snow is usually much higher and causes stronger surface-atmosphere radiative coupling. Hence, even our "cloud-free" climatology may be an underestimate for UV dose in snowy regions. If snow cover is interspersed with lower albedo surfaces such as forest, the bias will be reduced, but not eliminated. Another factor is the increase in effective UV dose received just above a snow surface by reflection from that surface. At higher latitudes and low altitudes, persistent widespread snow is likely to be present only during winter when UV irradiance is already low due to large SZAs. In mountainous regions, snow cover may also persist at lower latitudes, and for longer seasons. In each case, the climatologies presented here underestimate the actual ambient UV dose.

The results shown here do not give the short-term variations in erythemal UV, although some of the inter-annual variability may be inferred from Fig. 1.12. Daily data (1979 – 1994 and 1996 – 2000) are available and were used to compute the long-term averages; however, space limitations preclude their presentation here.

1.4 Conclusions

By using satellite ozone and reflectivity measurements as input to a column radiative transfer model, we have derived near-global climatologies of UV radiation at earth's surface, weighted for UV-A, UV-B, human erythema induction, pre-vitamin D_3 synthesis, and non-melanoma carcinogenesis. These climatologies are potentially of direct utility to epidemiological studies of the effects of UV exposure, especially if geographical gradients are of interest. For example, the induction of non-melanoma skin cancers is thought to be associated with long-term cumulative exposure to UV radiation, while melanoma mutational subtypes are associated with UV radiation exposure at different life stages (e.g., Thomas et al., 2007). The weighted UV distributions described in this chapter are available for free download from the NCAR Community Data Portal (http://cdp.ucar.edu). To find the datasets, navigate the "browse" menu through the directory structure: ACD > ACD Models > TUV > Erythemal UV. A technical note (Lee-Taylor and Madronich, 2007) that includes color versions of the figures in this chapter is also available.

Acknowledgements

This work was supported by the Department of Energy through grants 03-00ER62587.001 and DE-A105-94ER61879 to the National Center for Atmospheric

Research. The National Center for Atmospheric Research is sponsored by the National Science Foundation. Ground-based UV data was obtained from the archive of the World Ozone and Ultraviolet Radiation Data Center (http://www.woudc.org).

References

Bais A, Kazadzis S, Balis D, Zerefos C, and Blumthaler M (1998) Correcting global solar ultraviolet spectra recorded by a Brewer spectroradiometer for its angular response error, Appl. Optics, 37, 6339 – 6344

CIE (Commission Internationale de l'Eclairage) (1998) Erythema Reference Action Spectrum and Standard Erythema Dose, CIE S 007/E-1998, Vienna

CIE (2006) Photocarciongenesis Action Spectrum (Non-Melanoma Skin Cancers), CIE S 019/E:2006, Vienna

Eck TF, Bhartia PK, and Kerr JB (1995) Satellite estimation of spectral UVB irradiance using TOMS derived total ozone and UV reflectivity, Geophys. Res. Lett., 22, 611 – 614

Frederick JE and Lubin D (1988) The budget of biologically active ultraviolet radiation in the Earth-atmosphere system, J. Geophys. Res., 93, 3825 – 3832

Frederick JE and Erlick C (1995) Trends and interannual variations in erythemal sunlight, 1978 – 1993, Photochem. Photobiol., 62, 476 – 484

Herman JR, Bhartia PK, Kiemke J, Ahmad Z, and Larko D (1996a) UV-B increases (1979 – 1992) from decreases in total ozone, Geophys. Res. Lett., 23, 2117 – 2120

Herman JR, Bhartia PK, Krueger AJ, McPeters RD, Wellemeyer CG, Seftor CJ, Jaross G, Schlesinger BM, Torres O, Labow G, Byerly W, Taylor SL, Swissler T, Cebula RP, and Gu XY (1996b) Meteor-3 Total Ozone Mapping Spectrometer (TOMS) Data Products User's Guide, NASA Ref. Pub. 1393, Goddard Space Flight Center, Greenbelt, MD

Herman JR, Krotkov N, Calarier E, Larko D, and Labow G (1999) Distribution of UV radiation at the earth's surface from TOMS-measured UV-backscattered radiances, J. Geophys., Res., 104, 12059 – 12076

Herman JR, Piacentini RD, Ziemke J, Celarier E, and Larko D (2000) Interannual variability of ozone and UV-B exposure, J. Geophys. Res., 105, 29189 – 29193

Holick M (Chair), Bouillon R, Eisman J, Garabedian M, Kleinschmidt J, Suda T, Terenetskaya I, and Webb A (2006) Action Spectrum for the Production of Pre-vitamin D_3 in Human Skin, CIE Technical Report TC 6-54, Vienna

ICNIRP (International Commission on Non-Ionizing Radiation Protection), Global Solar UV-Index, 1995-1

Krotkov NA, Bhartia PK, Herman JR, Fioletov V, and Kerr J (1998) Satellite estimation of spectral surface UV in the presence of tropospheric aerosols. 1 Cloud-free case, J. Geophys. Res., 103, 8779 – 8793

Lee-Taylor J, and Madronich S (2007) Climatology of UV-A, UV-B, and Erythemal Radiation at the Earth's Surface, 1979 – 2000, NCAR Technical Note TN-474+STR, Boulder, CO

Lubin D, Jensen EH, and Gies HP (1998) Global surface ultraviolet radiation climatology from TOMS and ERBE data, J. Geophys. Res., 103, 26061 – 26091

MacLaughlin JA, Anderson RR, and Holick MF (1982) Spectral character of sunlight modulates photosynthesis of pre-vitamin D_3 and its photoisomers in human skin. Science 216 (4549): 1001 – 1003

Madronich S (1992) Implications of recent total atmospheric ozone measurements for biologically active ultraviolet radiation reaching the earth's surface, Geophys. Res. Lett., 19, 37 – 40

Madronich S, and Flocke S (1997) Theoretical estimation of biologically effective UV radiation at the earth's surface, in Solar Ultraviolet Radiation-Modeling, Measurements and Effects (Zerefos, C., ed.). NATO ASI Series Vol. I52, Springer-Verlag, Berlin

Madronich S, McKenzie RE, Björn LO, and Caldwell MM (1998) Changes in biologically active ultraviolet radiation reaching the earth's surface, J. Photochem. Photobiol. B:Biology, 46, 5 – 19

Mayer B and Madronich S (1998) Calculation of ultraviolet radiation quantities using TOMS ozone and ISCCP cloud data, Eos Trans., 79, F170

McKenzie RL, Seckmeyer G, Bais A, and Madronich S (2001) Satellite retrievals of erythemal UV dose compared with ground-based measurements at Northern and Southern Latitudes, J. Geophys. Res., 206, 24051 – 24062

McKinlay AF and Diffey BL (1987) A reference action spectrum for ultraviolet induced erythema in human skin. In: Passchier W.R. and Bosnjakovic, B.F.M. (eds.) Human Exposure to Ultraviolet Radiation: Risks and Regulations. Elsevier, Amsterdam

McPeters RD, et al. (1996) Nimbus-7 Total Ozone Mapping Spectrometer (TOMS) Data Products User's Guide, NASA Reference Publication 1384, National Aeronautics and Space Administration, Washington, D.C.

McPeters RD, et al. (1998) Earth Probe Total Ozone Mapping Spectrometer (TOMS) Data Products User's Guide, NASA Tech. Pub. 1998-206895, Goddard Space Flight Center, Greenbelt, MD

Micheletti MI, Piacentini RD, and Madronich S (2003) Sensitivity of biologically active UV radiation to stratospheric ozone changes: effects of action spectrum shape, Photochem. Photobio., 78, 456 – 461

Petropavlovskikh I (1995) Evaluation of photodissociation coefficient calculations for use in atmospheric chemical models, Ph. D. Thesis, U. of Brussels and NCAR/CT-159, Boulder

Sabziparvar AA, Shine KP, and Forster PM de F (1999) A model-derived global climatology of ultraviolet radiation at the earth's surface, Photochem. Photobiol., 69, 193 – 202

Stamnes K, Tsay S, Wiscombe S, and Jayaweera K (1988) A numerically stable algorithm for discrete-ordinate-method radiative transfer in multiple scattering and emitting layered media, Appl. Opt., 27, 2502 – 2509

Thomas NE, Edmiston SN, Alexander A, Millikan RC, Groben P, Hao H, Tolbert D, Berwick M, Busam K, Begg CB, Mattingly D, Ollila DW, Tse CK, Hummer A, Lee-Taylor J, and Conway K (2007) Number of Nevi and Early Life Ambient UV Exposure Are Associated with BRAF-Mutant Melanoma, Cancer Epidemiology Biomarkers and Prevention, 16(5), 991 – 997

UNEP (United Nations Environment Programme), Environmental Effects of Ozone Depletion and Its Interactions with Climate Change: 2006 Assessment (Leun van der, Bornman JC, J, and X. Tang, eds.) United Nations Environment Programme, Nairobi, 2006

USSA (US Standard Atmosphere) (1976) National Oceanic and Atmospheric Administration (NOAA), National Aeronautics and Space Administration (NASA), United States Air Force, Washington DC

Wenny BN, Schafer JS, DeLuisi JJ, Saxena VK, Barnard WF, Petropavlovskikh IV, and Vergamini AJ (1998) A study of regional aerosol radiative properties and effects on ultraviolet-B radiation, J. Geophys. Res., 103, 17083 – 17097

WMO (World Meteorological Organization) (1997) Report of the WMO-WHO Meeting of Experts on Standardization of UV Indices and their Dissemination to the Public, WMO/GAW Report No. 127, Geneva

WOUDC (World Ozone and UV Data Center) (2002) http://www.woudc.org/

2 Balancing the Risks and Benefits of Ultraviolet Radiation

Richard L. McKenzie and J Ben Liley

National Institute of Water & Atmospheric Research (NIWA),
Lauder, Central Otago, New Zealand 9352
NIWA Lauder, Private Bag 50061 Omakau, Central Otago 9352, New Zealand
E-mail: r.mckenzie@niwa.co.nz
E-mail: b.liley@niwa.co.nz

Abstract The relatively small long-term change in ultraviolet (UV) radiation is compared with its substantial geographical variability. Action spectra published by the International Commission on Illumination (CIE) are then used to examine diurnal, seasonal, and latitudinal variations in erythemally-weighted (sunburning) UV—a health risk, and vitamin D-weighted UV—a health benefit. Vitamin D weighted UV is more strongly dependent on ozone and solar zenith angle (SZA). Consequently, its diurnal, seasonal, and geographic variability is more pronounced than for erythemally weighted UV. An algorithm is developed and used to relate vitamin D production to the widely-used UV Index. The exposure times needed to produce erythema, or sufficient vitamin D, are calculated as a function of UV Index[1] (UVI), using published physiological criteria. In the summer at noon, there should be sufficient UV at mid-latitudes to photosynthesize optimal vitamin D in ~1 minute for full body exposure, whereas skin damage occurs after ~15 minutes. Further, while it should be possible to photosynthesize vitamin D in the winter at mid latitudes, the amount of skin that must be exposed is larger than on the hands and face alone. This raises the question of whether the action spectrum for vitamin D production is correct, since it has been reported that production of vitamin D is not possible in the winter at mid-latitudes. Because the benefits of UV depend on the area of skin exposed, it is preferable to expose large skin areas to sunlight for shorter times than to expose small areas for correspondingly larger times.

Keywords solar UV irradiance, ozone, erythema, vitamin D

1 UVI = 40 × UV_{Ery}, where the latter is in units of W m^{-2}.

2.1 Introduction

There has been increased interest in understanding the variability and trends in ultraviolet (UV) radiation since it was realized that the world's protective ozone layer was at risk from a build-up of anthropogenic trace gases in the atmosphere. Good progress has been made through improvements in instrumentation, calibration procedures, and data quality assurance. The widespread adoption of a standardized metric for reporting UV radiation risk—namely erythemally weighted UV (UV_{Ery}[1], in W m^{-2}), or the UV Index (WHO, 2002) ($UVI = 40 \times UV_{Ery}$), has also facilitated meaningful comparisons.

Assessments of our understanding of UV radiation and its effects on the environment are updated regularly. The most recent of these assessments predicts that although the ozone layer will gradually recover over the next few decades, the outlook for future UV is less certain (UNEP, 2006; 2007; WMO, 2007). Despite the progress in instrumentation, any changes in UV_{Ery} attributable to ozone depletion have been difficult to detect, because of: (1) uncertainties in UV measurement, (2) a relatively low sensitivity of UV_{Ery} to changes in ozone, and (3) the effects of other changes in atmospheric composition (e.g., changes in aerosols and clouds).

2.2 Long Term Changes in UV_{Ery}

While the effects of ozone depletion on UV_{Ery} have been large in the Antarctic region (Kerr et al., 2003), the effects have been relatively small in populated areas at lower latitudes. At mid-southern latitudes, summertime ozone, and therefore UV_{Ery}, is influenced by the export of ozone-poor air from the Antarctic ozone hole (Roy et al., 1990). Long term measurements at Lauder, New Zealand (45°S, 170°E, altitude 370 m) provide some of the strongest evidence outside the Antarctic region for increases in UV_{Ery} attributable to ozone depletion. Results are shown in Fig. 2.1. The increases in peak UV_{Ery} due to ozone depletion were relatively modest, ~10% – 15%, with a peak in late 1990s, and a decrease since that time. Other measurement sites, which are generally more polluted, show larger variabilities from sources other than ozone (WMO, 2007). These findings demonstrate that, outside the region affected by the Antarctic ozone hole, changes in UVI due to changes in ozone are rather small and are within the range of variability from other causes. Outside polar regions, ozone levels are expected to return to pre-1980 levels around the middle of the 21st century. Inside polar regions, the recovery is expected to be delayed by a further 10 to 20 years due to an interaction with global warming whereby the expected cooler stratospheric

1 Erythemally weighted UV irradiance. UV radiation weighted by the erythema action spectrum.

temperatures will tend to favor the more widespread development of polar stratospheric clouds. Reactions on the surface of these clouds can greatly accelerate ozone depletions, as currently happens each spring in Antarctica (WMO, 2007). The relatively small magnitude of changes in ozone and UV, and the optimistic outlook for the future, are attributable to the success of the Montreal Protocol and its subsequent amendments and adjustments.

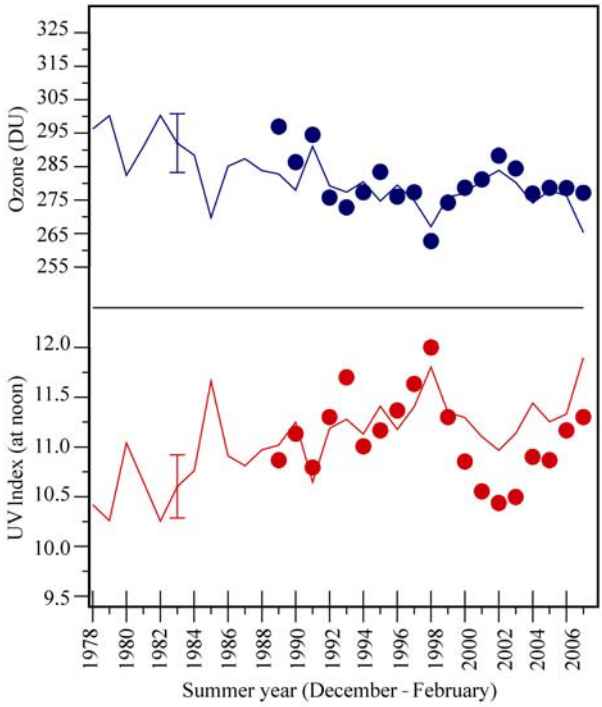

Figure 2.1 Upper panel: Mean ozone (Dobson Units, 1 DU = 2.69×10^{16} molecule cm^{-2}) at Lauder, New Zealand for the summers of 1978 – 1979 through 2007 – 2008. Lower panel: Corresponding estimates of UV Index. Summer is defined as the period from December through February. The solid lines show the changes in summertime ozone that have occurred since the 1970s and the deduced changes in clear-sky UV expected from these changes in ozone. The symbols (from 1989 – 1990 on) show measured values of ozone and the summertime peak UV Index, both derived from the UV spectroradiometer (McKenzie et al., 2000)

2.3 Geographical Variability in UV_{Ery}

In contrast to these ozone-induced changes in UV_{Ery}, the geographical and seasonal changes (as well as diurnal changes) are large. These geographical variabilities are usually derived from satellite-borne sensors that monitor solar UV radiation

that is backscattered from the earth. It should be noted that estimates of UV_{Ery} from a satellite are sometimes too large in polluted locations because extinctions within the atmospheric boundary layer are not well probed by these sensors (McKenzie et al., 2001; 2003). Thus, extinctions by tropospheric clouds and aerosols, as well as variations in the profiles of ozone and temperature, can lead to errors in the retrieved surface UV irradiances.

Compared with noon intensities, the corresponding daily total doses of available UV radiation show much larger seasonal variabilities because of the longer hours of daylight in summer. Daily doses for the solstice months, as derived from the Ozone Monitoring Instrument (OMI) on the UARS satellite, are shown in Fig. 2.2. Generally, the daily doses of UV are a maximum at locations where the noon solar zenith angle (SZA) approaches zero, and tend to decrease rapidly in moving to locations where the noon SZA is larger. Thus, the highest daily doses of UV tend to occur in the tropics, and the lowest doses occur in polar regions where they fall to zero in mid winter for all latitudes within the Arctic or Antarctic circles (latitudes > 68°). There are two notable departures from this overall pattern, caused by the springtime Antarctic ozone hole and the effects of high altitudes, as discussed later.

At mid-latitudes (~40° – 50° in both hemispheres), the daily UV_{Ery} dose in summer is comparable with that in the tropics. However, in the winter, it is less than 10% of the summer dose. As the latitude increases, the seasonal swing becomes more and more marked.

2.4 Peak UV

For some biological processes, peak UV intensity may be more important than the mean value, and while we cannot be sure about evolutionary pressures, it is possible that UV intensities were much greater during the earlier history of the planet than at present (Björn and McKenzie, 2007). However, from our current perspective, changes in UV over the past, and future, few decades are more relevant. It is likely that peak UV over these time scales has already occurred, since it is expected that ozone will continue to recover throughout the 21st century (WMO, 2007).

2.4.1 Peak UV Index

Here we examine the geographical distribution of peak UV. There is considerable geographic variability, as illustrated in Fig. 2.3 (Liley and McKenzie, 2006), which shows calculated peak values of the UVI based on over 20 years of measurements from the NASA Total Ozone Monitoring Spectrometer (TOMS)

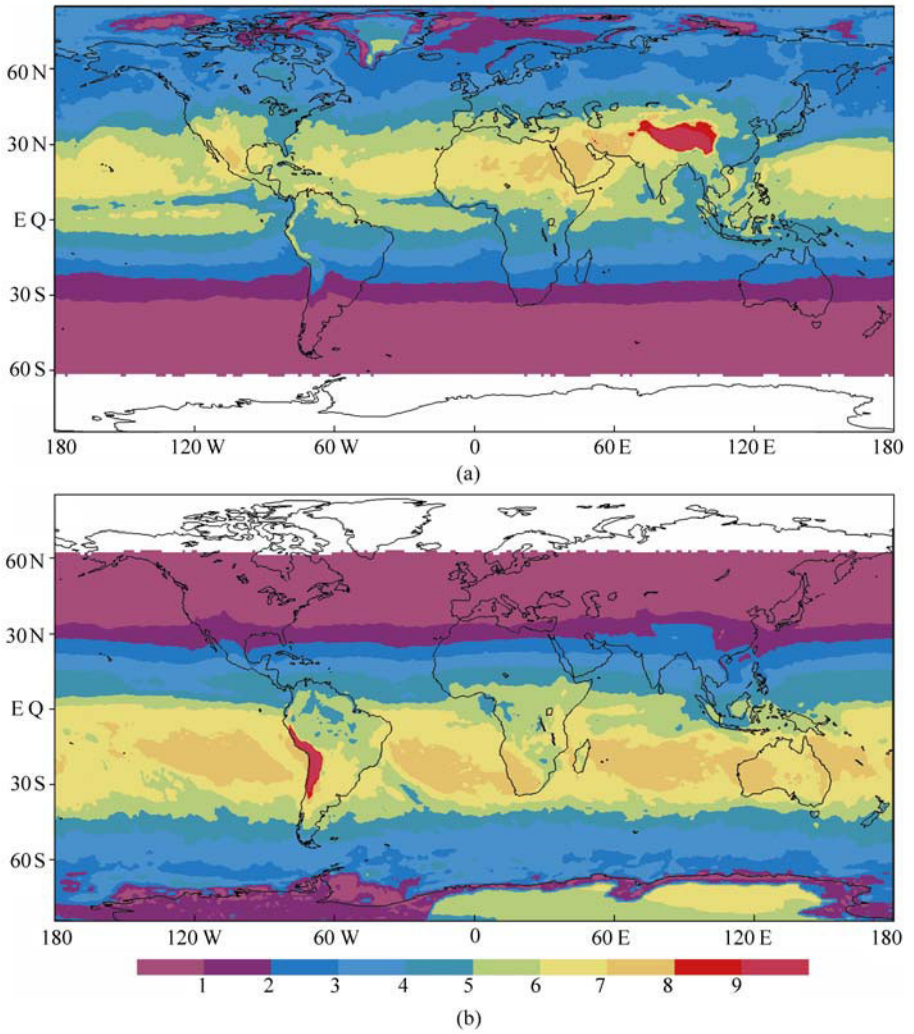

Figure 2.2 Global distribution of the average cloud corrected erythemal daily dose (in kJ m^{-2} per day) for June 2005 (upper panel) and December 2005 (lower panel) derived from OMI measurements. These surface UV irradiance images were supplied by Aapo Tanskanen of the Meteorological Institute. OMI is a joint effort of KNMI, NASA, and FMI, and is managed by NIVR/Netherlands. The unshaded (white) areas are those with no UV data coverage

satellite-borne instruments. Generally, the peak UVI values decrease from equator to pole. However, at mid-latitudes, and even at high latitudes, peak values can approach those in the tropics. UV doses can also be exceptionally high in the high-altitude Altiplano region of South America, where the UVI can reach values of 25 during the month of February when the noon sun is approximately

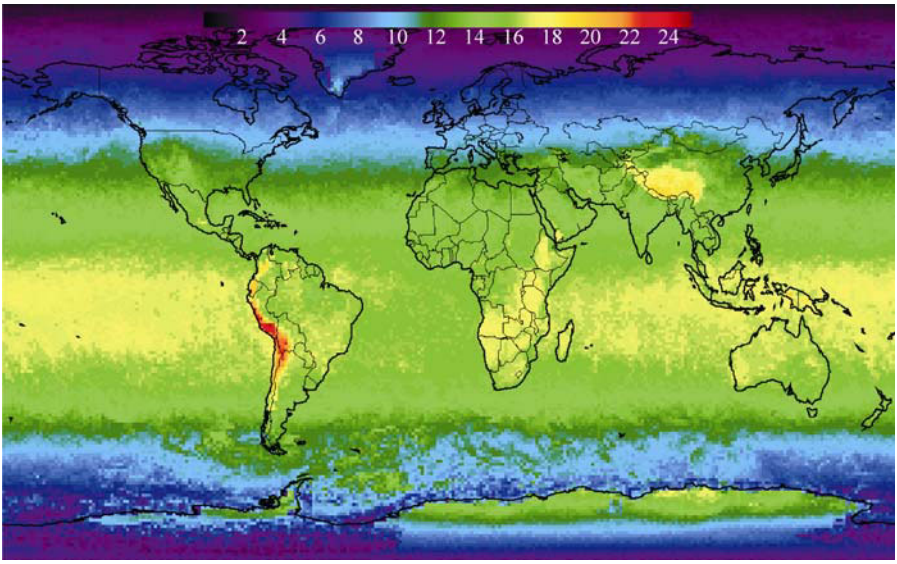

Figure 2.3 Global values of the peak UVI derived from 20 years of TOMS satellite data

overhead (Liley and McKenzie, 2006). Fittingly, the location of this peak is near Cuzco, Peru (13.5°S, 72°W, alt: ~3300 m a.s.l), which was the capital of the ancient sun-worshipping Inca civilization. In locations including the city of La Paz (population ~1 million), so called "extreme" UVI values (UVI > 10) are reached on two out of three days every year (F. Zaratti, Personal communication, 2006).

These global peak UVI values are nearly a factor of two greater than at unpolluted mid-latitude, lower-altitude sites, such as Lauder, New Zealand (45°S). Although the intensities there are not extreme in a global sense, they are approximately 40% higher than at corresponding latitudes in the Northern Hemisphere, and are more reminiscent of those at latitude 5° closer to the equator and 2000 m higher in altitude (Fig. 2.4). These differences are caused by: (1) the phasing of the Earth's orbit about the sun (closest in January and furthest in July), (2) lower ozone amounts in the Southern Hemisphere summer, and (3) the generally lower pollution in the Southern Hemisphere.

Overall differences are much smaller in the winter, so in the Southern Hemisphere the summer-winter contrast in UV_{Ery} is also more marked. These huge seasonal changes in UV radiation have important implications for human health. High UV irradiance in summer contributes to skin cancer, while low irradiance in winter results in ailments associated with vitamin D deficiency. In New Zealand, for example, the skin cancer rates are among the highest in the world, yet a significant fraction of the population has insufficient vitamin D in the winter (Livesey et al., 2007). Tanning of the skin, induced by the high summertime UV

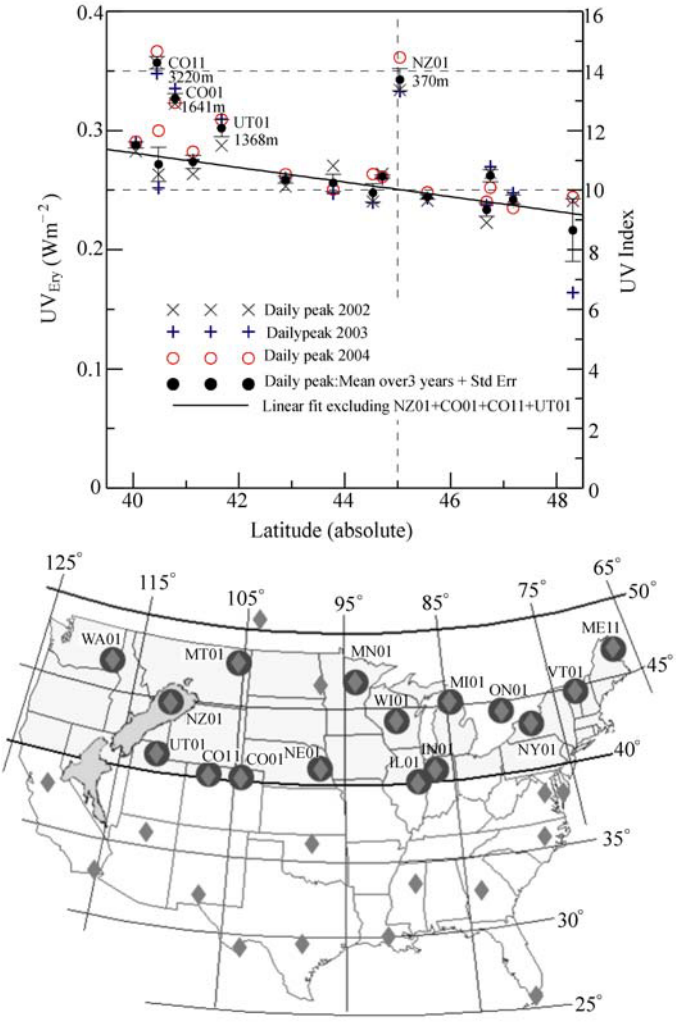

Figure 2.4 Upper panel: Peak UV at 45˚S (Lauder, NZ—labeled NZ01) compared with sites in North America of comparable latitude. The high-altitude sites in North America, which tend to be at lower latitudes, are labeled (CO11, CO01, UT01). Lower panel: The sites selected, which are a subset of the USDA UV network sites maintained by the University of Colorado. The Lauder site is shown on the inverted map of New Zealand, which is superimposed over its corresponding range of latitudes in North America

irradiance, may further exacerbate the winter problem since the increased pigmentation in response to sun exposure blocks UV penetration into the skin and so inhibits the production of vitamin D. Other factors, such as skin type, and lifestyle choices, which in turn are influenced by parameters, such as ambient temperature, also contribute to the high rates of skin cancer in New Zealand.

2.4.2 Peak UV Daily Dose

Unlike the peak UVI values, the peak daily UV doses derived from satellite data also depend on the length-of-day and on cloud patterns. The precise geographic location for these peak UV doses depends on the temporal averaging period and the spectral weighting function in question. Table 2.1 shows peak values of monthly mean daily UV doses and their locations for several different weighting functions. In all cases, the peak values occur in the Altiplano region, although for these monthly means, the peak occurs at a slightly higher latitude—where the summer day-length is longer than for the peak instantaneous UVI shown in Fig. 2.3. Whereas the peak UVI occurred in the February/March period (close to the period when the sun moves directly overhead), the peak monthly means occur closer to the summer solstice. The daily dose of erythemally weighted UV can exceed 12 kJ m^{-2} (or 120 SED (standard erythemal dose)) on cloudless days (Lee-Taylor and Madronich, 2007), which corresponds to ~50 MED (minimum erythemal dose) for fair skinned individuals. For all of the weightings listed, the peak occurs in January, generally at latitude 22.5°S. In the case of UVA radiation, which is independent of ozone, the peak value occurs at higher latitude. The peak values for the month of December are only slightly less than those for January and all occur near latitude 5°S.

Table 2.1 Global peak in UV doses, calculated from monthly values, including the effects of clouds, which in each case reduce the clear-sky values by 10% ± 1%. All peak sites are in the Atacama Desert of the Andes (up to ~5,000 m) near the border of Chile, Bolivia, and Argentina. All are south of Cuzco, where the peak UVI occurred in February. For snow-covered surfaces, doses are about 35% greater. With the alternative definition of UVB (280 nm – 320 nm), the peak doses are approximately a factor of 2 greater (137 kJm^{-2} per day). Data extracted from a 20-year climatology (Lee-Taylor and Madronich, 2007)

Weighting	Month	Max Value (kJm^{-2}day^{-1})	Latitude (°S)	Longitude (°W)
Erythema	01	11.8	22.5	66.9
	12	*10.5*	*25.5*	*68.1*
Vitamin D	01	21.3	22.5	66.9
	12	*19.0*	*25.5*	*68.1*
Non Melanoma Skin Cancer (NMSC)	01	23.4	22.5	66.9
	12	*21.0*	*25.5*	*68.1*
UVA (315 nm – 400 nm)	01	2220	26.5	68.1
	12	*2060*	*25.5*	*69.4*
UVB (280 nm – 315 nm)	01	74.0	22.5	66.9
	12	*67.2*	*25.5*	*68.1*

During the latter period of the springtime Antarctic ozone hole, when solar elevations are higher and day length is longer, daily UV doses at high southern latitudes can reach values comparable with mid to low latitudes, such as San Diego (Kerr et al., 2003; Bernhard et al., 2008).

2.5 Comparing Weighting Functions for Erythema and Vitamin D

The weighting functions for erythema (McKinlay and Diffey, 1987) and for vitamin D production (Bouillon et al., 2006), as published by the International Commission on Illumination (CIE), are compared in Fig. 2.5 (upper panel). Each of these is arbitrarily normalized to unity at its maximum value. The figure also includes typical global solar irradiance spectra measured at a mid-latitude site at local noon on cloudless days close to the summer and winter solstices. The resolution of the spectra is approximately 0.9 nm at full-width half-maximum (fwhm), and the detailed structure is mainly due to absorption in the sun's atmosphere. The sharp decrease at wavelengths shorter than 315 nm is due to absorption by atmospheric ozone. All of these curves are plotted on a logarithmic vertical scale. Although the erythemal weighting function extends to longer wavelengths, the vitamin D weighted irradiance for the summer spectrum is about twice as large as for erythema because of its increased contribution between 300 nm and 315 nm. The weighted integrals for erythema (UV_{Ery}) and vitamin D (UV_{VitD}[1]) are compared in the middle panel of Fig. 2.5, with a linear vertical scale. In all cases, the contribution from UVA is small, especially in the case of vitamin D-weighted UV. For the summer spectrum shown, the weighted irradiances, which are given by the integrated areas under these curves, are: $UV_{Ery} = 0.28$ W m^{-2} and $UV_{VitD} = 0.54$ W m^{-2} (UV_{VitD} is reduced by ~5% if the weighting function is cut at 315 nm, see discussion below). For the winter spectrum, the weighted irradiances are: $UV_{Ery} = 0.026$ W m^{-2} and $UV_{VitD} = 0.027$ W m^{-2} (UV_{VitD} is reduced by ~10% if the weighting function is cut at 315 nm). The lower panel of Fig. 2.5 shows the same weighted irradiances, but focuses on the wavelength region from 290 nm to 330 nm only. There are substantial differences in the spectral shape of these weighted irradiances between summer and winter. In the winter, the contribution from longer wavelength components has a greater relative importance.

1 UV radiation weighted by the action spectrum for production of pre-vitamin D.

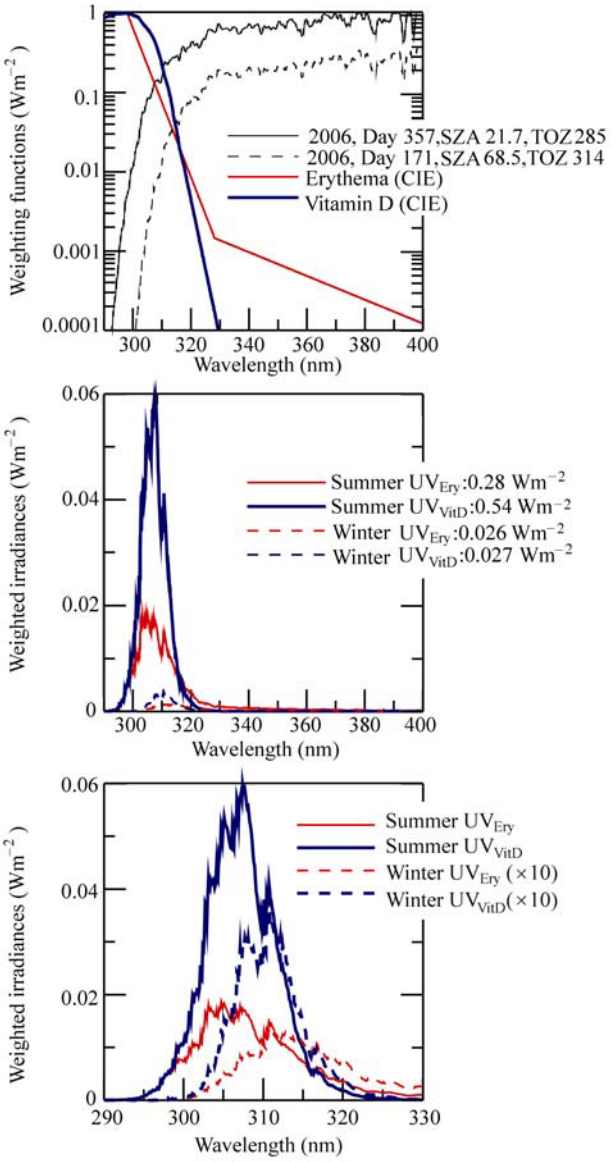

Figure 2.5 Upper panel: Weighting functions for erythema and vitamin D production, along with sample spectra measured at Lauder New Zealand at noon in the summer and winter. Middle panel: Weighted irradiances for the spectra shown in the upper panel. Lower panel: Detail of the weighted irradiances between 290 nm and 330 nm, with winter values (dashed curves) scaled up by a factor of 10

2.6 Seasonal and Diurnal Variation of UV_{Ery} and UV_{VitD}

Spectral measurements of solar UV irradiances, which have been undertaken over several years by NIWA (National Institute of Water and Atmospheric Research) at Lauder, New Zealand, have been used to demonstrate the seasonal and diurnal variability of vitamin D weighted UV and erythemally weighted UV irradiances at this mid-latitude site. Results for these weighted irradiances for a wide range of observing conditions at Lauder are shown in Figs. 2.6 and 2.7. The changes over one year of observations (Fig. 2.6) are due to the combined effects of changes in SZA, clouds, ozone, and earth-sun separation. While the mean of daily values, including cloud effects, is about 70% of the clear sky mean, on some days clouds attenuate the irradiances to less than 30% of the clear sky values. The upper envelopes approximately correspond to clear sky conditions (though there are occasional higher values attributable to cloud enhancements), and represent the

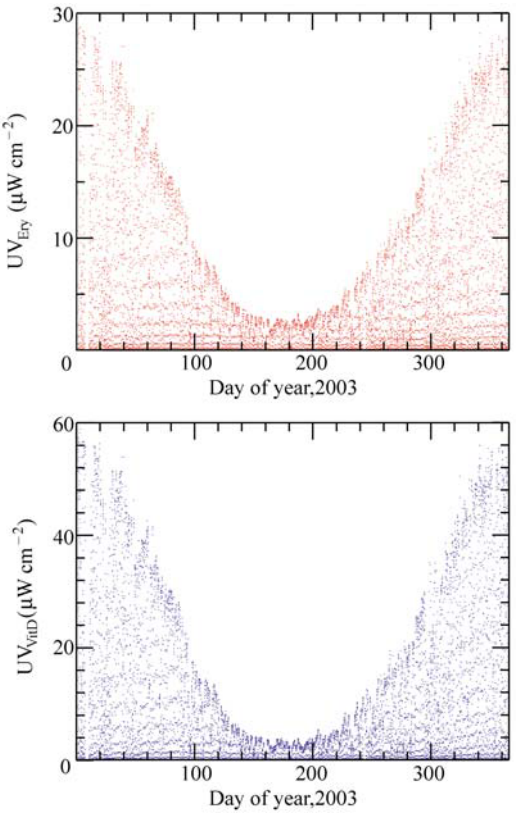

Figure 2.6 Seasonal variation in weighted irradiances at Lauder, New Zealand—45°S. Upper panel: UV_{Ery}. Lower panel: UV_{VitD}

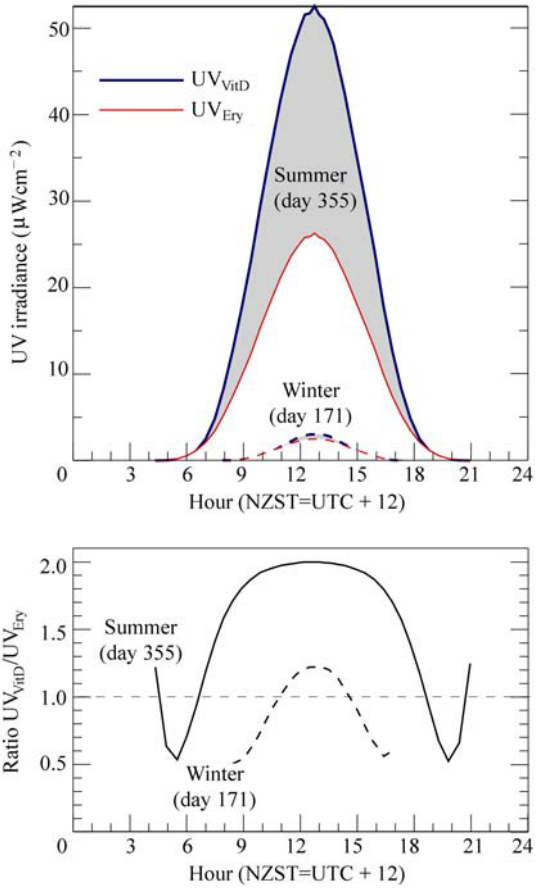

Figure 2.7 Upper panel: Diurnal variations in vitamin D-weighted and erythemally-weighted UV irradiances on clear days near the summer and winter solstice periods at Lauder, New Zealand, 45°S, in 2003. Lower panel: Corresponding ratios of UV_{VitD}/UV_{Ery}. On the summer day, the total ozone was 300 DU and the minimum SZA was 21.6°. On the winter day, the total ozone was 310 DU and the minimum SZA was 68.5°

seasonal variability in noon-time UV irradiances. The seasonal variation in vitamin D weighted UV (Fig. 2.6) is very large at this site, with noon values at mid winter being only 5% of those in summer. This seasonal swing is significantly larger than for UV_{Ery}, where the winter values are about 10% of those in summer. The large swings are in contrast to the situation found for noon-time UV_{vitD} at several sites in the USA over several months (Kimlin et al., 2007), where UV_{VitD} remained relatively constant over the summer months. However, those were based on measurements at lower latitudes where seasonal changes are smaller. Furthermore, in the northern hemisphere, the seasonal changes in sun-earth separation tend to cancel some of the effects due to seasonal changes in SZA.

Figure 2.7 shows the diurnal variability of UV_{Ery} and UV_{VitD} and their ratios on a summer day and a winter day at Lauder. The total column amount of ozone was stable through both of these days, and was quite similar: 300 DU for the summer day, and 310 DU for the winter day. Most of the disparity is therefore attributable to differences in SZA and earth-sun separation. The peak UV_{Ery} is a factor of 10 less than for the summer day, and the peak UV_{VitD} is nearly a factor of 20 less than the summer peak. At larger SZAs, the UV_{VitD}/UV_{Ery} ratio is greatly reduced compared with that for high sun, resulting in lower ratios in the winter compared with the summer, and lower ratios at twilight compared with midday. The decrease in this ratio with increasing SZA arises because UV_{Ery} includes a contribution from the UVA region, which is less attenuated. At the largest SZA (SZA > 85°), there is a reversal in this trend which arises because at these SZAs, the direct beam contribution is negligible, and most of the radiation is from Rayleigh scattering from the zenith sky for which the scattering efficiency reduces with wavelength.

2.7 Global Climatologies of UV_{Ery} and UV_{VitD}

Global UV climatologies (Lee-Taylor and Madronich, 2007), which were calculated with the TUV[1] radiative transfer model (Madronich and Flocke, 1995), were used to directly compare vitamin D weighted UV and erythemally weighted UV. In both cases, the weighting functions are as adopted by the CIE, extending to 400 nm in the case of $UV_{Ery,}$ (McKinlay and Diffey, 1987), and to 330 nm in the case of UV_{VitD} (Bouillon et al., 2006). If the truncated version of the vitamin D action spectrum had been used, the peak value would be reduced by approximately 5%, with larger percentage reductions for smaller doses (see discussion of Fig. 2.5). The climatologies are based on over 20 years (1979 – 2000) of satellite-derived data from the NASA TOMS instruments. Since temporal changes in ozone have been relatively small over most of the globe, these climatologies still apply for present-day ozone fields, and for those expected in the future. In the Antarctic region, ozone amounts have been lower in spring, but the summer and winter conditions illustrated have been less affected by the springtime ozone hole. Furthermore, as ozone is expected to recover in the future, the mean UV intensities, over the period the satellite data is used, are likely to be similar to the means over the next few years.

Zonal means of these UV climatologies are shown for solstice months in Fig. 2.8. The UV doses are largest at the sub-solar latitudes, and decrease rapidly as the latitude diverges from the sub-solar point. At the summer solstice, the clear-sky doses in the southern hemisphere summer are significantly larger than in the northern hemisphere. The winter values in the southern hemisphere are much

1 Tropospheric UV radiative transfer model developed at NCAR, USA.

more comparable with those in the northern hemisphere. The UV_{VitD} doses show a stronger latitudinal gradient than the UV_{Ery} doses. When cloud effects are included, these tend to reduce the doses of both UV_{VitD} and UV_{Ery} in the southern hemisphere more than in the northern hemisphere, especially at latitudes pole-ward of about 60˚S.

The upper panel of Fig. 2.9 shows the cloud effect expressed as a ratio of the clear sky values to cloudy sky values. For cloudless skies, this ratio is unity, and decreases as clouds increase. These cloud transmissions tend to reduce towards higher latitudes. In the southern hemisphere summer, there is a rapid reduction in cloud transmission between latitudes 60˚S and 70˚S, indicating that cloud cover in this region is quite persistent in the summer, as has been previously noted (Herman et al., 2001). The lower panel of Fig. 2.9 shows the ratio UV_{VitD}/UV_{Ery} for these daily doses. Near the latitudes with peak UV, the daily doses of vitamin D-weighted UV are approximately twice those of erythemally weighted UV. This shows that the daily doses are dominated by the contributions from near noon when the SZA is smallest. The decrease is more rapid in the case of vitamin D-weighted UV, and the ratios reduce to below unity at latitudes where the UV is low (e.g., approaching the poles).

The equinox months are compared in Fig. 2.10. Note that the peak values, which occur near the equator at these times, are less than the peak values in the southern hemisphere summer near 20˚S. The effects of the springtime Antarctic

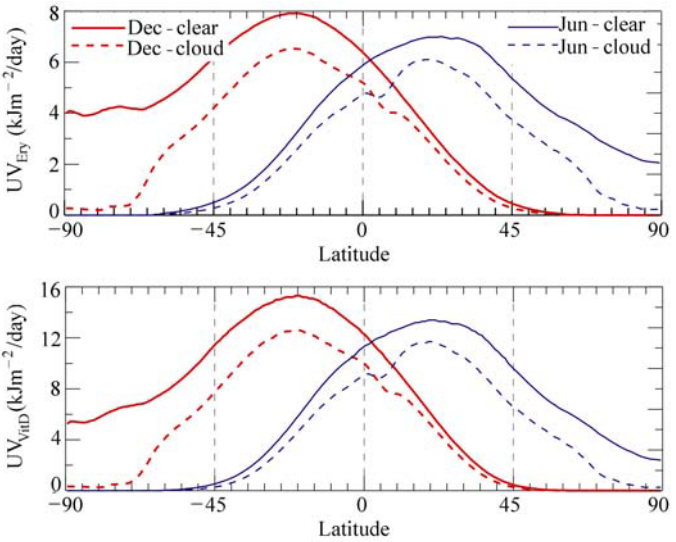

Figure 2.8 Latitudinal distribution of the UV_{Ery} and UV_{VitD} daily dose, calculated for the two solstice months. Solid curves are for clear skies, and broken curves include cloud effects. In this figure and Figs. 2.9 – 2.11, north latitudes are positive and south altitudes are negative

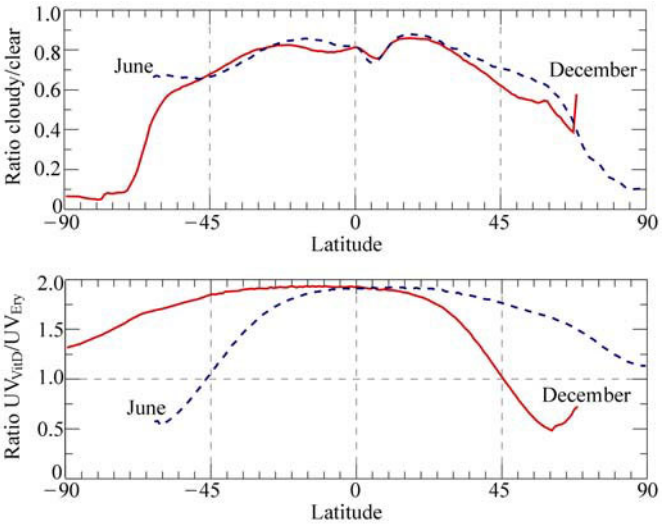

Figure 2.9 Upper panel: Latitudinal distribution of the cloud transmission ratios. Lower panel: Ratio UV_{VitD}/UV_{Ery} calculated from the daily doses in the two solstice months

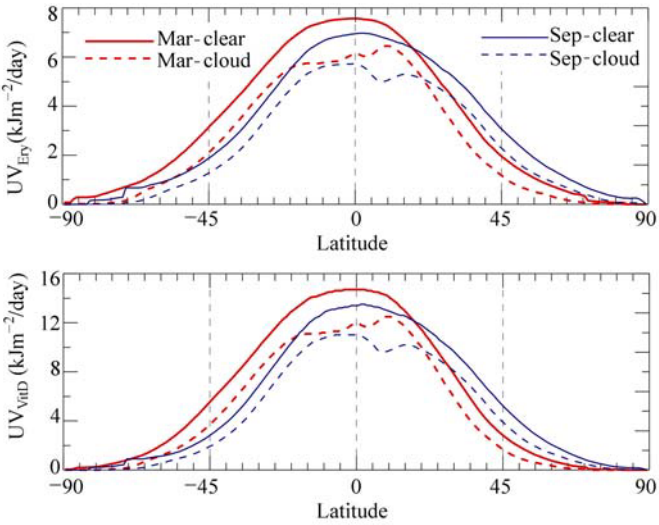

Figure 2.10 Latitudinal distribution of the UV_{Ery} and UV_{VitD} daily dose, calculated for the two equinox months. Solid curves are for clear skies and broken curves include cloud effects

ozone hole are just detectable poleward of about 60°S. Note that contrary to public concern in New Zealand and Australia about high levels of UV radiation during this period, the doses, even as far south as 45°S, are in fact smaller than at 45°N. This is because, despite the presence of the ozone hole over Antarctica, the

ozone amounts at mid-latitudes in both hemispheres are much larger in spring than in autumn. However, at the higher latitudes of the southern tip of South America (50°S – 55°S), the ozone hole does lead to significant UV increases in populated regions during spring and early summer (Bernhard et al., 2008).

The annual doses are compared in Fig. 2.11. In this case, the maxima occur in the tropics and tend to be slightly larger in the southern hemisphere, with the exception of the Antarctic region, where they are lower than at corresponding Arctic latitudes. This shows that in an annually averaged sense, the effect of increased cloud cover in that region dominates over any effects due to the ozone hole.

In the following section, we use the spectral measurements at Lauder to develop relationships between UV_{VitD} and UV_{Ery}. These are tested against calculations with a radiative transfer model and then applied to calculating the optimal times for exposure to sunlight to maintain adequate levels of vitamin D without incurring sunburn.

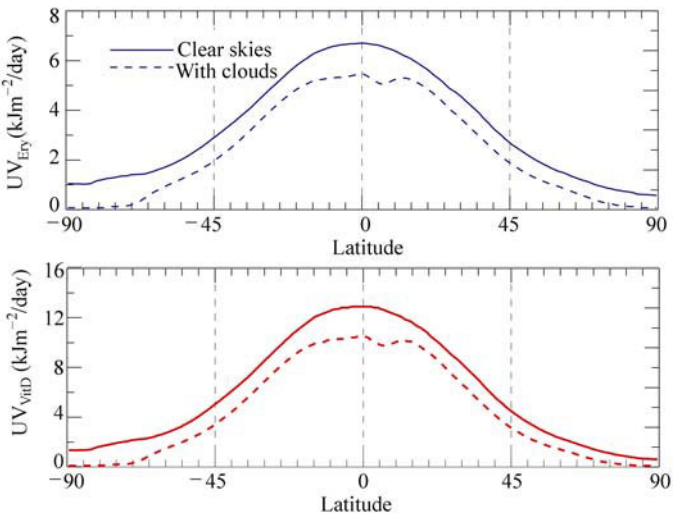

Figure 2.11 Latitudinal distribution of the UV_{Ery} and UV_{VitD} mean daily dose averaged over all months. Solid curves are for clear skies and broken curves include cloud effects

2.8 Relationship Between UV_{VitD} and UV_{Ery}

The relationship between UV_{VitD} and UV_{Ery}, as deduced from several years of spectral UV data from Lauder, New Zealand, is shown in Fig. 2.12. At first impression, the plot in the upper panel seems to indicate a close proportionality between the two quantities, with UV_{VitD} being approximately $2 \times UV_{Ery}$ (for

standard normalization). However, at lower values, which are characteristic of the situation throughout winter months, this proportionality breaks down. For the truncated version of the action spectrum, the plot is very similar (not shown), but the slope is reduced by approximately 3%.

The relationship is examined in more detail in the lower panel of Fig. 2.12, where the ratio UV_{VitD}/UV_{Ery} is plotted as a function of SZA. The ratio is ~2 when the SZA is small, and reduces to a value close to unity at SZA ~70°. The ratio reaches a minimum for SZA ~85° and increases thereafter. As expected, the departures from proportionality with UV_{Ery} are more marked, and the ratios are slightly lower, with a truncated version of the action spectrum (not shown). There are groupings of the data at 5-degree steps in SZA, which occur because these are the preferred sampling intervals in the spectral measurements. Several spectra are also taken at 15-minute intervals over a 2-hour period around the solar noon. The largest vertical separation in points occurs at intermediate SZAs, where there is a distinct bimodal distribution of data at each SZA. This is a consequence of the seasonal variations in ozone. In the spring, when ozone amounts are larger, the ratio is smaller than in autumn when ozone amounts are smaller.

Although UV_{VitD} is not directly proportional to UV_{Ery}, it is possible to estimate UV_{VitD} from UV_{Ery} using a radiative transfer model if ozone and SZA are known (McKenzie et al., 2008). The measured ratios in Fig. 2.12 are consistent with those calculated with the TUV radiative transfer model.

In summary,

$$UV_{VitD} = R(\text{ozone, SZA})\, UV_{Ery} \tag{2.1}$$

where the values of their ratio (R) are given as a function of ozone and SZA (see Fig. 2.12, and the appendix in (McKenzie et al., 2008)).

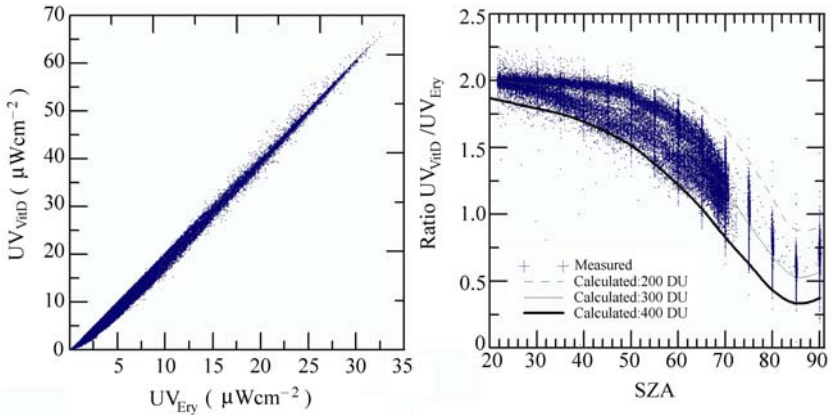

Figure 2.12 Left panel: Relationship between UV_{VitD} and UV_{Ery} based on 100,000 spectra measured at Lauder, New Zealand over the period 1998 to 2007. Right panel: Ratio UV_{VitD}/UV_{Ery} as a function of SZA

2.9 Production of Vitamin D from Sunlight

While there is considerable uncertainty regarding the wavelength dependence for vitamin D production, it has been suggested that there is insufficient vitamin D produced in the winter poleward of about 40° (Webb et al., 1988).[1] Based on that work, we may take an upper limit threshold for insufficient vitamin D production as the daily available dose at the latitude of Boston, 42°N. This threshold is about 0.7 kJ m^{-2} per day (see Fig. 2.8). Under the same conditions, erythemally weighted UV dose is approximately 0.55 kJ m^{-2} per day, with a corresponding peak UVI = 1.3 at noon. Yet at the same location in summer, the erythemally weighted UV dose can exceed 5 kJ m^{-2}, with corresponding peak UVI ~9. It is apparent that the only places where the minimum required vitamin D-weighted UV radiation is exceeded throughout the winter months are at latitudes between 40°S and 40°N. On the other hand, the peak UVI at all of these latitudes can often exceed 10 (i.e., "extreme" UV) during the summer months, so at some times of the year, there is a risk of skin damage in as short a time as 15 – 20 minutes. Surprisingly, therefore, it appears that there is no region on the planet which is "just right;" where there is no risk of sunburn in summer, yet ample UV for vitamin D production in the winter. Public advice regarding personal behavior in response to UV variability needs further development, and should recognize both the benefits and the risks of UV exposure.

2.10 Calculation of Optimal Times for Exposure to Sunlight

The optimal time for exposure to sunlight that is needed to receive adequate UV for vitamin D production, but without inducing erythema, depends strongly on latitude and season. Here we develop algorithms for calculating the time in terms of the widely used UVI.

We can calculate the time taken (t_E in minutes) to induce skin damage (one minimum erythemal dose) using

$$t_E = \frac{4000}{60} \cdot \frac{\mathrm{MEDF} \cdot \mathrm{SPF}}{\mathrm{UVI}} \tag{2.2}$$

where the factor 4000/60 accounts for the conversions from UV_{Ery} to UVI and seconds to minutes; UVI is the UV Index ($= 40 \times UV_{Ery}$, where UV_{Ery} has units of W m^{-2}); and MEDF is a factor to take into account the differences in skin color. It is expressed as the number of SED (1 SED = 100 J m^{-2} of erythemally-

1 However, higher vitamin D levels have been associated with winter UV exposures among Tasmanian school children (Jones et al., 1999) suggesting that vitamin D synthesis can occur in winter at latitudes higher than 40°S.

weighted UV) required to induce erythema (Diffey et al., 1997) according to the Fitzpatrick skin classification (Fitzpatrick, 1988), (see Table 2.2), and SPF is the sun protection factor of any sun block applied.

Table 2.2 Skin type classifications according the Fitzpatrick scale (Fitzpatrick, 1988)

Skin Type	Description	SED to Burn (MEDF)
Ⅰ	Celtic (always burns)	2 – 3
Ⅱ	Pale (burns easily)	2.5 – 3
Ⅲ	Caucasian (may burn)	3 – 5
Ⅳ	Mediterranean (burns rarely)	4.5 – 6
Ⅴ	S. American (rarely burns)	6 – 20
Ⅵ	Negroid (rarely burns)	6 – 20

For example, for unprotected type Ⅱ skin (SPF = 1), assuming 1 MED = 2.5 SED, the time taken to receive an erythemal dose at UVI = 12 would be 13.9 minutes. Under the same conditions, with a correctly-applied sun block of SPF = 20, it would take approximately 278 minutes (> 4.5 hours) for damage to occur. Two caveats should be mentioned here. Firstly, over such a large period, there will be changes in the UVI, so the mean UVI value should be applied. Second, it is implicitly assumed that reciprocity between time and UVI applies; meaning that a constant UVI dose of 10 for one hour, say, would give the same erythemal effect as a constant UVI value of 1 for 10 hours. This reciprocity has not been demonstrated for sunlight, although it does seem to apply for a range of UVI values greater than ~5 using artificial lamps that emit much higher proportions of UV-B (UV radiation in the range 280 nm – 315 nm) and UV-C (UV radiation in the range 100 nm – 280 nm) radiation (Meanwell and Diffey, 1989). According to the current WHO guidelines, some protection to avoid sunburn is advised whenever the UVI exceeds 3. At this UV level, for a fair skinned person, that corresponds to a period of approximately one hour before skin damage is detectable as mild erythema (skin reddening). On the other hand, our dietary intake of vitamin D is generally far below the level required to maintain optimal levels of blood serum vitamin 25(OH)D, so some UV exposure is desirable to maintain healthy vitamin D levels. Unlike the risk of erythema, the beneficial effects of UV radiation depend on the area of skin exposed. If twice the area is exposed, then twice the benefit is received (assuming all skin areas have a similar capacity for producing vitamin D). We use relationships derived from published physiological considerations to estimate the range of optimal exposures for various skin types as a function of UVI. We could also develop a similar relationship as a function of SZA, but that would ignore the effect of ozone, which can be appreciable.

Following the procedure described in more detail elsewhere (McKenzie et al., 2008), the time (t_D) required to photosynthesize sufficient vitamin D for a given value of UVI_j can be expressed in terms of the corresponding time (t_{D0}) at some reference condition (UVI_0), as follows:

$$t_D = t_{D0} \cdot \frac{UVI_0}{UVI} \cdot \frac{R_0}{R} \cdot \frac{A_0}{A} \cdot \frac{MEDF}{MEDF_0} \cdot \frac{SPF}{SPF_0} \tag{2.3}$$

where R (SZA, TOZ[1]) is the ratio of UV_{Ery}/UV_{VitD} for that value of UVI, as discussed above; A is the area of skin surface exposed; and the remaining terms are as defined above.

We assume that optimal vitamin D levels are easily maintained by a daily intake of 1,000 IU of vitamin D3. If an intake of 400 IU is sufficient, as some have suggested, then the times to achieve the desired UV dose would be decreased by a factor of 2.5 over those that we calculate. From the figures provided earlier (Holick, 2002; 2007), a full body exposure of type Ⅱ skin under high sun conditions (UVI = 10) produces 1,000 IU in less than one minute.

In that case, the reference conditions are as follows:

$UVI_0 = 10$ (peak UV for mid latitudes in the NH)
$R_0 = 2$
$T_{D0} = 1$
$A_0 = 1$ (full body exposure)
$MED_0 = 2.5$ (skin type Ⅱ)
$SPF_0 = 1$ (no sunscreen applied).

With these substitutions, Eq. (2.3) simplifies to:

$$t_D = 8 \cdot \frac{MEDF \cdot SPF}{UVI \cdot R \cdot A} \tag{2.4}$$

which should be compared with Eq. (2.2) for erythema.

The resulting times are shown graphically in Fig. 2.13 (McKenzie et al., 2008). The shaded area at top right gives times when erythema occurs on exposed skin for each UVI value. The shaded area at bottom left gives the times when there is insufficient UV to maintain optimal levels of vitamin D, even for full body exposures. The other three curves give the approximate exposure times needed to maintain vitamin D for different areas of the exposed body. For full body exposures, there is a wide window between the time for sufficient UV and the time for too much UV. As the fraction of body that is exposed decreases, the window of optimum UV exposure times also decreases. If only hands and face are exposed, there is generally only a small window between receiving insufficient UV for vitamin D production and too much UV for skin damage (erythema).

1 Total ozone column (in Dobson Units, where 1 DU = 2.69×10^{16} molecule cm^{-2} in a vertical column).

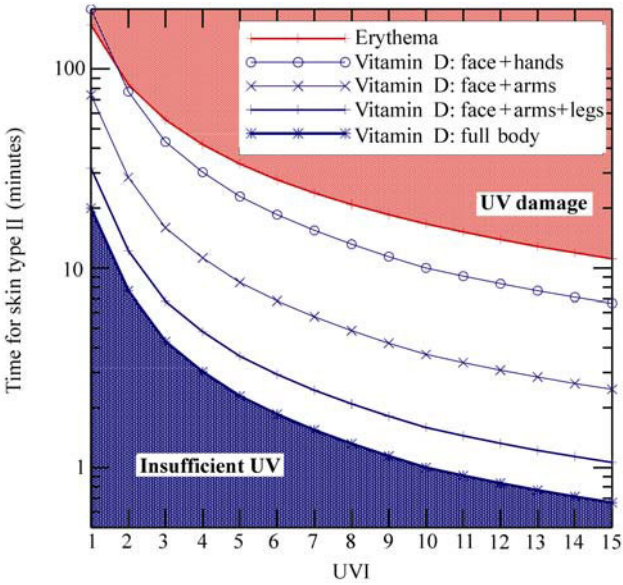

Figure 2.13 Range of exposure times required for optimal UV (white region), plotted as a function of UVI. The area labeled "UV damage" represents times when too much UV is received, leading to erythema (skin-reddening). The region marked "Insufficient UV" represents the time when insufficient amounts of UV are received to maintain an intake of 1,000 IU for full body exposure. For skin type Ⅳ, these exposure times should be multiplied by 2, and for skin type Ⅵ they should be multiplied by approximately 5

For SZA = 63°, which corresponds to noon on a mid-winter day at latitude ~41°, the UVI is typically between 2 and 3 (i.e., UVI "low"), and the ratio of UV_{VitD}/UV_{Ery} is about 1.6. The time to produce a minimum erythemal dose for skin type Ⅱ is between one and two hours. The time to achieve 1,000 IU of vitamin D is about six minutes for full body exposure ($A = 1.0$), and about one hour if only the hands and face are exposed ($A = 0.1$).

These optimal exposure times calculated above should be considered as very approximate. In particular, there is some uncertainty regarding the applicability of the action spectrum for vitamin D, and the possible role of temperature in converting pre-vitamin D to vitamin D3 (Matsuoka et al., 1989). If the action spectrum were confined to shorter wavelengths, then the R values would be reduced commensurately. For example, if the upper limit were reduced from 330 nm to 315 nm, the R values would typically be 5% – 10% lower, so the required exposure time would be increased by a similar factor. There is also the question of how well the radiation received by the skin relates to that incident on a horizontal surface. We also note that the relationships derived here are from high quality spectral measurements and they are specific to a single location with its own particular conditions. Although we consider the results should be generally

applicable elsewhere, the minimum R values do depend on the range of ozone variability. At locations where ozone amounts are higher (such as at high northern latitudes), the minimum R values would be smaller, and at locations with lower ozone amounts (such as within the tropics), the minimum R values would be larger.

As the UVI becomes smaller, it becomes more difficult to produce sufficient vitamin D without inducing erythema. For low sun conditions typical of midday in the mid-latitude winter (SZA ~65°), where $R_j \sim 1$, the skin area exposed must be more than 12%. This means that for these low sun conditions, it is difficult to receive sufficient vitamin D from exposing the hands and face alone since that area is less than 12% of the full body—though the radiation received may significantly exceed that on a horizontal surface assumed here (Moan et al., 2008). For still larger SZA, larger fractions of the body would have to be exposed to produce sufficient vitamin D without erythema. However, that is of academic interest only, because at those low UVI values, there is insufficient time in a day to produce either of those outcomes.

During the winter, when cold temperatures may preclude exposures of large areas of skin, it may not be possible to receive adequate UV for optimal vitamin D synthesis. When exposures are limited to the hands and face, there is a relatively small margin of error between getting sufficient UV for vitamin D production and not getting too much for sunburn. The calculations show that the best advice would be to expose as much area as possible for the minimum time necessary. For high sun conditions, the time for skin damage is about twice the time for sufficient vitamin D production if only the hands and face are exposed. And when the UVI is 1 or less, it is not possible to get sufficient UV for vitamin D without acquiring a mild erythemal dose. Under such conditions, of course, there will generally be substantial changes in UVI over the long periods of exposure needed.

Finally, we note that this margin between UV sufficiency (for vitamin D) and UV excess (for sunburn) depends critically on the assumption that sufficient vitamin D is made in one minute. In Fig. 2.13, we assumed that one minute of exposure to UVI = 10 provided sufficient UV to maintain vitamin D levels. In that case, whenever the UVI is less than 2, one cannot manufacture sufficient vitamin D from exposure to hands and face alone without inducing erythema. If, for example, the time was 1.5 minutes, then the vitamin D curves in Fig. 2.13 all move up, and the curve for exposure to hands and face intersects the curve for erythema when UVI = 6. Conversely, if lower doses of vitamin D are sufficient, then those curves move downward.

2.11 An Inconsistency

The above discussion points to an inconsistency between the CIE spectrum for vitamin D (Bouillon et al., 2006) and the statements made in the literature about

our ability to photosynthesize vitamin D in summer and winter, namely:

- that a few minutes daily exposure to sunlight in summer is sufficient at mid-latitudes (Holick, 2002; 2007), and
- that no vitamin D is produced in Boston in winter (Webb et al., 1988).

The first statement above is based on the supposition that 1 MED full body exposure corresponds to an oral dose of 10,000 IU to 25,000 IU of vitamin D. For a fair skinned person, 1 MED (i.e., 2.5 SED) is accumulated in approximately 14 minutes when UVI = 12 ($UV_{Ery} = 0.3$ W m^{-2}). The vitamin D produced from this is more than 10 times the recommended daily dose of up to ~1,000 IU (Chel et al., 1998; Bischoff-Ferrari et al., 2006; Holick, 2007; Vieth et al., 2007), so that a full body exposure for less than one minute should suffice to meet daily requirements in the summer (see Fig. 2.13). This exposure time is consistent with that recommended in Holick's popular book, "The UV Advantage" (2003), where it is stated (p164) that to maintain adequate vitamin D, one should "expose 25% of your body surface to 25% of 1 MED two to three times per week." Since 1 MED is received in about 15 minutes at noon in summer, that corresponds to less that one minute of full body exposure per day at noon in summer. In the winter, the vitamin D weighted UV incident on a horizontal surface is approximately 1/20th of the summer value at mid-latitudes, but since the sun is lower in the sky in winter, a larger fraction would be incident on vertically oriented cylindrical surfaces that better approximate the exposed surface of our body (Moan et al., 2008). Therefore, sufficient vitamin D should easily be produced in less than 20 minutes of full body exposure. For darker skinned individuals, the exposure time required would be longer, but the amount of vitamin D produced should not be zero. This inconsistency remains, regardless of whether the long wavelength limit of the action spectrum for vitamin D extends to 315 nm or 330 nm.

There is, of course, the question of whether individuals would be prepared to expose a large enough area of their bodies at the temperatures in winter. They probably would not. However, even for more limited exposures, the vitamin D produced would be non-zero. The experiments to determine the action spectrum of pre-vitamin D did not use live subjects. Instead they used samples of skin tissue exposed in a petri dish (Webb et al., 1988). It is surprising that these did not yield any vitamin D since these exposure periods were for three hours over the midday period. This raises the question of whether the action spectrum has been specified sufficiently. For example, it is known that the conversion from pre vitamin D to vitamin D is temperature dependent (Holick, 2007), so it is reasonable to assume some temperature dependence in the overall conversion from sunlight to blood serum vitamin 25(OH)D. Although the temperature-dependent reaction takes place in the skin, the temperature can vary significantly from normal body temperature of 37°C. Some have suggested that there is a threshold below which vitamin D is not produced (Hollis, 2005), but the evidence for this is not strong. More likely, any perceived threshold is actually caused by an inability to detect the smaller amounts produced.

Notwithstanding the above arguments, there is ample evidence that individuals do not receive sufficient UV to maintain optimal vitamin D during the winter (Livesey et al., 2007). This may be in part because of our modern lifestyles, where outdoor exposure is not the norm, even in the summer months. A recent study in New Zealand found that schoolchildren typically received less than 5% of the local ambient daily UV dose, even in the summer (Wright et al., 2007). Another study in Germany found that even outdoor workers receive only 5% – 10% of the ambient daily dose, which is a factor of five more than indoor workers (Knuschke et al., 2007).

2.12 Conclusions

Past increases in the UV that humans are exposed to have been small. In contrast, there are huge geographical and seasonal differences in UV, which have more important implications for health than the small trends. Highest UV intensities occur in the tropics, but latitude for latitude, the peak UV intensities are relatively much higher in the Southern Hemisphere.

There are even larger geographical and seasonal variabilities for beneficial UV. In the summer, the UV_{VitD} is approximately twice UV_{Ery}, but the two are approximately equal for mid-latitude winter conditions. At high latitudes in the winter hemisphere, UV_{Ery} becomes larger than UV_{VitD}. The results are similar for both clear-sky calculations and for all sky conditions.

Despite these departures from proportionality at larger SZA, vitamin D weighted UV can still be estimated from knowledge of erythemally weighted UV (or UVI). An algorithm to estimate vitamin D production from UVI shows that the production of vitamin D from sunlight is dominated by the midday period when UV intensities are at a maximum. When the sun is high in the sky, such as near noon at mid to low latitudes in the summer, sufficient vitamin D can be produced from a few minutes of sun exposure to the face and hands. But the exposure time should be limited to less than approximately 15 minutes to avoid erythema. A better strategy would be to expose a larger fraction of the body for a shorter time period, preferably when the sun is lower in the sky. When the UVI is 3, skin damage occurs after approximately one hour, but sufficient vitamin D can still be produced in a few minutes.

There should be sufficient UV radiation available in the mid latitude winter to produce vitamin D. However, under those conditions it is necessary to expose larger areas than hands and face alone. Because of the low temperatures, this proviso sets a practical limit on our ability to maintain adequate levels of vitamin D in the winter; a situation which is exacerbated by our modern lifestyle in which periods spent outdoors are greatly diminished. The situation could be improved by promoting physical outdoor activities, such as jogging, during the midday

period in winter when the peak UVI is low. During the winter at mid latitudes, most people will probably require supplementation of vitamin D from other sources. These could be dietary (e.g., increased consumption of oily fish, fortification of foods, or from vitamin D supplements), or from exposure to higher UV intensities from holidays abroad, or from artificial sources. The latter options carry risk of overexposure.

Further work is needed to resolve the inconsistency in the literature between the action spectrum of vitamin D and statements that have been made about the production of vitamin D in summer and winter. In particular, if the rate of production stated for the summer is correct, then it should be possible to produce vitamin D at mid latitudes in the winter, contrary to the current advice.

Acknowledgements

This review is based on recent UNEP Effects Panel reports (UNEP, 2008), and a paper in press (McKenzie et al., 2008). We acknowledge the contributions from our co-author, Lars Olof Björn. We are grateful to NIWA Lauder staff including Michael Kotkamp for maintaining the spectral UV observations, Dan Smale for carrying out the radiative transfer calculations, and Paul Johnston for many useful insights. We also thank Dr. Sasha Madronich of the National Center of Atmospheric Research (NCAR), Boulder, CO, USA, for providing the UV climatologies.

References

Bernhard G, Booth CR, and Ehramjian JC (2008) Climatology of Ultraviolet Radiation at High Latitudes. In: Gao W, Schmoldt D, Slusser J (eds) UV Radiation in Global Change: Measurements, Modeling and Effects on Ecosystems. Springer-Verlag, Tsinghua University Press, Beijing, China

Bischoff-Ferrari HA, Giovannucci E, Willett WC, Dietrich T, and Dawson-Hughes B (2006) Estimation of optimal serum concentrations of 25-hydroxyvitamin D for multiple health outcomes. American Journal of Clinical Nutrition 84: 18 – 28

Björn LO and McKenzie RL (2007) Attempts to probe the ozone layer and the UV-B levels of the past. Ambio 36(5): 366 – 371

Bouillon R, Eisman J, Garabedian M, Holick M, Kleinschmidt J, Suda T, Terenetskaya I, and Webb A (2006) Action spectrum for the production of previtamin D3 in human skin. CIE, Vienna, p.12

Chel VGM, Ooms ME, Popp-Snijders C, Pavel S, Schothorst AA, Meulemans CCE, and Lips P (1998) Ultraviolet irradiation corrects vitamin D deficiency and suppresses secondary hyperparathyroidism in the elderly. Journal of Bone and Mineral Research 13(8): 1238 – 1242

Diffey BL, Jansén CT, Urbach F, and Wulf HC (1997) The Standard Erythema Dose: a new photobiological concept. Photodermatology, Photoimmunology and Photomedicine 13: 64 – 66

Fitzpatrick TB (1988) The validity and practicality of sun-reactive skin types Ⅰ through Ⅵ. Archives of Dermatology 124: 869 – 871

Herman JR, Larko D, Celarier E, and Ziemke J (2001) Changes in the earth's UV reflectivity from the surface, clouds and aerosols. J. Geophys. Res. 106(D6): 5353 – 5368

Holick MF (2002) Vitamin D: the underappreciated D-lightful hormone that is important for skeletal and cellular health. Current Opinion in Endocrinology, Diabetes 8: 87 – 98

Holick MF (2007) Vitamin D deficiency. New England Journal of Medicine 357: 266 – 281

Holick MF and Jenkins M (2003) The UV Advantage. IBooks Inc., New York, p.224

Hollis BW (2005) Circulating 25-hydroxyvitamin D levels indicative of vitamin D sufficiency: Implications for establishing a new effective dietary intake recommendation for vitamin D1. Journal of Nutrition 135: 317 – 322

Jones G, Blizzard C, Riley M, Parameswaran V, Greenaway T, and Dwyer T (1999) Vitamin D levels in prepubertal children in Southern Tasmania: prevalence and determinants. European Journal of Clinical Nutrition 52: 824 – 829

Kerr JB, Seckmeyer G, Bais AF, Bernhard G, Blumthaler M, Diaz SB, Krotkov NA, Lubin D, McKenzie RL, Sabziparvar AA, and Verdebout J (2003) Surface ultraviolet radiation: Past and future. In: Ajavon A-L, Albritton DL, Megie G, Watson RT (eds) WMO Scientific Assessment of Ozone Depletion: 2002. World Meteorological Organization, Global Ozone Research and Monitoring Project, Report No. 47, p.498

Kimlin MG, Olds WJ, and Moore MR (2007) Location and vitamin D synthesis: Is the hypothesis validated by geophysical data? Journal of Photochemistry and Photobiology B: Biology 86: 234 – 239

Knuschke P, Unverricht I, Ott G, and Jansen M (2007) Personenbezogene messung der UV-Exposition von Arbeitnehmern im freien, Bundesanstalt fur Arbeitsschutz und Arbeitsmedian (BAUA), Dortmund/Berlin/Dresden, p.195

Lee-Taylor J and Madronich S (2007) Climatology of UV-A, UV-B, and erythemal radiation at the earth's surface, 1979 – 2000. In: NCAR Technical Note, NCAR, Boulder, p.52

Liley JB and McKenzie RL (2006) Where on Earth has the highest UV? In: UV Radiation and its Effects: an update, pp. 26 – 37, http://www.niwascience.co.nz/rc/atmos/uvconference

Livesey J, Elder P, Ellis J, McKenzie R, Liley B, and Florkowski C (2007) Seasonal variation in vitamin D levels in the Canterbury population in relation to available UV radiation. New Zealand Medical J 120:1262; URL: http://www.nzma.org.nz/journal/ 120-1262/2733/

Madronich S and Flocke S (1995) Theoretical estimation of biologically effective UV radiation at the earth's surface. In: Zerefos CS, Bais AF (eds) Solar Ultraviolet Radiation. NATO, Series Ⅰ: Advanced Study Institute. Springer, Berlin, pp.23 – 48

Matsuoka LY, Wortsman J, Haddad JG, and Hollis BW (1989) In Vivo threshold for cutaneous synthesis of vitamin-D3. Journal of Laboratory and Clinical Medicine 114(3): 301 – 305

McKenzie RL, Bodeker GE, Connor BJ, Johnston PV, Kotkamp M, and Matthews WA (2000) Increases in summertime UV radiation in New Zealand: an update. In: Bojkov RD, Shibasaki K (eds) Quadrennial Ozone Symposium, EORC/NASDA, Tokyo, pp.237 – 238

McKenzie RL, Seckmeyer G, Bais AF, Kerr JB, and Madronich S (2001) Satellite retrievals of erythemal UV dose compared with ground-based measurements at northern and southern midlatitudes. Journal of Geophysical Research 106(D20): 24051 – 24062

McKenzie R, Smale D, Bodeker G, and Claude H (2003) Ozone profile differences between Europe and New Zealand: Effects on surface UV irradiance and its estimation from satellite sensors. Journal of Geophysical Research 108(D6):4179 doi:10.1029/ 2002JD002770

McKenzie RL, Liley JB, and Björn LO (2008) UV Radiation: Balancing Risks and Benefits. Photochemistry and Photobiology, DOI: 10.1111/j.1751-1097.2008.00400.x

McKinlay AF and Diffey BL (1987) A reference action spectrum for ultra-violet induced erythema in human skin. In: Passchier WF, Bosnajakovic BFM (eds) Human Exposure to Ultraviolet Radiation: Risks and Regulations. Elsevier, Amsterdam, pp.83 – 87

Meanwell EF and Diffey B (1989) Reciprocity of ultraviolet erythema in human skin. Photodermatology 6: 146 – 148

Moan J, Porojnicu AC, Dahlback A, and Setlow RB (2008) Addressing the health benefits and risks, involving vitamin D or skin cancer, of increased sun exposure. Proceedings of the National Academy of Sciences 105(2): 668 – 673

Roy CR, Gies HP, and Elliot G (1990) Ozone depletion. Nature 347: 235 – 236

UNEP (United Nations Environment Programme) (2006) Environmental effects of ozone depletion and its interactions with climate change: Progress report, 2005. Photochemical and Photobiological Sciences 5: 13 – 24 DOI: 10.1039/b515670j

UNEP (2007) Environmental effects of ozone depletion and its interactions with climate change: 2006 assessment Photochemical and Photobiological Sciences, UNEP Special Issue 6(3): 201 – 332

UNEP (2008) Environmental effects of ozone depletion and its interactions with climate change: Progress report, 2007. Photochemical and Photobiological Sciences 7: 15 – 27, DOI: 10.1039/b717166h, 2008

Vieth R, Bischoff-Ferrari H, Boucher BJ, Dawson-Hughes B, Garland CF, Heaney RP, Holick MF, Hollis BW, Lamberg-Allardt C, McGrath JJ, Norman AW, Scragg R, Whiting SJ, Willett WC, and Zittermann A (2007) The urgent need to recommend an intake of vitamin D that is effective. American Journal of Clinical Nutrition 85: 649 – 650

Webb AR, Kline L, and Holick MF (1988) Influence of season and latitude on the cutaneous synthesis of vitamin D3: Exposure to winter sunlight in Boston and Edmonton will not promote vitamin D3 synthesis in human skin. Journal of Clinical Endocrinology and Metabolism 67(2): 373 – 378

WHO (2002) Global Solar UV Index: A practical guide, World Health Organization (WHO), World Meteorological Organization (WMO), United Nations Environment Program (UNEP), and International Commission on Non-Ionising Radiation Protection (ICNRP), Geneva, Switzerland, p.28

WMO (World Meteorological Organization) (2007) Scientific Assessment of Ozone Depletion: 2006. Geneva, Switzerland

Wright CY, Reeder AI, Bodeker GE, Gray A, and Cox B (2007) Solar UVR exposure, concurrent activities and sun-protective practices among primary schoolchildren. Photochemistry and Photobiology 83: 749 – 758

3 Climatology of Ultraviolet Radiation at High Latitudes Derived from Measurements of the National Science Foundation's Ultraviolet Spectral Irradiance Monitoring Network

Germar Bernhard, Charles R. Booth, and James C. Ehramjian

5340 Riley Street
Biospherical Instruments Inc., San Diego, CA, USA
E-mail: bernhard@biospherical.com
E-mail:booth@biospherical.com
E-mail:jime@biospherical.com

Abstract Solar ultraviolet (UV) radiation has been measured at seven sites of the National Science Foundation's UV Spectral Irradiance Monitoring Network (UVSIMN) for up to 20 years. Data are used to establish a UV climatology for each site and to quantify differences between sites. Most locations are at high latitudes and include the South Pole; two research stations at the Antarctic coast (McMurdo and Palmer); the city of Ushuaia at the tip of South America; the Arctic village of Barrow; and Summit, a research camp established at the top of Greenland's ice sheet. UV levels at San Diego, California were also analyzed as an example of a lower-latitude location. The climatologies focus on the UV Index, which was derived from measured solar spectra of global irradiance. For each site and day of year, the average, median, and maximum UV Index at solar noon, as well as 10^{th} and 90^{th} percentile values, were calculated. Measurements were also compared with pre-ozone-hole UV levels estimated from historical measurements of total ozone. The analysis indicates a large effect of the ozone hole on the UV Index at the three Antarctic sites, and to a lesser extent at Ushuaia. UV Indices measured at South Pole during the ozone hole period (October and November) are 20% – 80% larger than measurements at comparable solar elevations during summer months. During October and November, the average UV Index between 1991 and 2006 was 55% – 85% larger than the estimate for the years 1963 – 1980. The UV Index at McMurdo shows a similar asymmetry about the solstice. In October and November, the average UV Index is about 30% – 60% higher now than it was historically. The largest UV Index ever measured at Palmer was 14.8. This value exceeds the maximum UV Index of 12.0 observed at San Diego. While the average

UV Index at Ushuaia is fairly symmetrical about the solstice, maximum UV Indices as high as 11.5 have occurred in October at times when the ozone hole passed over the city. The annual cycle of UV radiation at Barrow is governed by large seasonal changes of total ozone, albedo, and cloud cover. The UV Index does not exceed 5 due to less severe ozone depletion over the Arctic: changes in UV over the last 30 years are on average less than ±8%. A comparison of UV levels at network locations reveals that differences between sites greatly depend upon the selection of the quantity used for the comparison. Average noontime UV Indices at San Diego during summer are considerably larger than noontime UV levels under the ozone hole at all Antarctic sites. The difference diminishes, however, when daily doses are compared because of the effect of 24 hours of sunlight during Antarctic summers. Data analysis further revealed that broken clouds at the South Pole can enhance spectral UV irradiance at 400 nm by up to 30% above the clear-sky value due to multiple reflections between the snow-covered surface and the cloud ceiling.

Keywords solar ultraviolet radiation, Antarctica, Arctic

3.1 Introduction

When the ozone hole was discovered in 1984 (Chubachi, 1984; Farman et al., 1985), there was concern about increased levels of ultraviolet radiation in Antarctica. UV radiation was not measured in Antarctica at that time, prompting the U.S. National Science Foundation (NSF) to establish a UV monitoring program, which is now known as the "NSF Ultraviolet Spectral Irradiance Monitoring Network (UVSIMN)" (Booth et al., 1994). Similar monitoring activities also commenced in the 1980s and 1990s in Canada (Fioletov et al., 2001), Europe (e.g., Gröbner et al., 2006), New Zealand (McKenzie et al., 1999), the United States (Kaye et al., 1999), and other regions. The UVSIMN network currently consists of six sites at high latitudes and a system at San Diego, California. It has been operated by Biospherical Instruments Inc. (BSI) since 1988. An overview of network sites is provided in Table 3.1 and Fig. 3.1. The program employs SUV-100 and SUV-150B spectroradiometers, which measure global spectral irradiance between 280 nm and 600 nm with a bandpass of about 1.0 nm (SUV-100) or 0.63 nm (SUV-150B) full width at half maximum (FWHM). Results have been used in about 100 peer-reviewed publications as well as for scientific assessments of ozone depletion published by the World Meteorological Organization (e.g., WMO, 2007). A complete list of references and additional information about the network can be found in Operations Reports (e.g., Bernhard et al., 2006a) and at the project's website http://www.biospherical.com/NSF.

Table 3.1 Network sites

Site	Latitude	Longitude	Elevation	Established	Used in Study
South Pole, Antarctica	90°00'S	—	2841 m	Feb 1988	Jan 1991 – Jan 2007
McMurdo, Antarctica	77°50'S	166°40'E	183 m	Mar 1988	Dec 1989 – Jan 2007
Palmer, Antarctica	64°46'S	64°03'W	21 m	May 1988	Mar 1990 – Apr 2006
Ushuaia, Argentina	54°49'S	68°19'W	25 m	Nov 1988	Nov 1988 – Jun 2005
San Diego, California	32°46'N	117°12'W	22 m	Oct 1992	Oct 1992 – Aug 2006
Barrow, Alaska	71°19'N	156°41'W	8 m	Dec 1990	Jan 1991 – Apr 2007
Summit, Greenland	72°35'N	38°27'W	3200 m	Aug 2004	Aug 2004 – Nov 2006

Figure 3.1 Map of UVSIMN sites (created by Eric Gaba based on a Fuller map). Vertical lines indicate latitudes of 0°, ±20°, ±40°, and ±60°. (The Fuller Projection Map design is a trademark of the Buckminster Fuller Institute © 1938, 1967 and 1992. All rights reserved, http://www.bfi.org)

In this chapter, a climatology of UV radiation at UVSIMN sites is presented. UV radiation at high latitude sites is distinct from conditions at lower latitudes due to small solar elevations; up to 24 hours of sunlight during spring and summer; extended periods of darkness during winter; the annually occurring ozone hole over Antarctica and recent episodes of severe ozone depletion over the Arctic; high surface albedo from seasonal or year-round snow and ice cover; small influence of clouds in the interior of Antarctica and Greenland due to low atmospheric water content; and small aerosol optical depth. Large changes in UV radiation due to the ozone hole can be expected, although other factors are also important. However, a confirmation of trends in UV based on measurements of the UVSIMN remains elusive. By analyzing measurements from South Pole, Palmer, and McMurdo, Bernhard et al. (2004; 2005; 2006b) concluded that linear trend estimates are by and large not significant at the 95.5% confidence level. Significant linear trends were observed only for the months of February and March at McMurdo (owing to changes in cloudiness and/or albedo), and for February at Palmer. Several factors contribute to this finding: (1) the network's operation started only in the late 1980s after the ozone hole had already been observed; (2) time-series of about 15 – 18 years are still considered short for reliable trend detection (Weatherhead et al., 1998); (3) there is a large year-to-year variability in total ozone, cloudiness, and albedo at most network sites, which obstructs the

detection of possible long-term changes; (4) measurement uncertainties affect the detection of trends; and (5) the stratospheric chlorine loading (and the potential for ozone depletion) was highest at the turn of the century (WMO, 2007), approximately in the middle of UVSIMN time-series. The last factor suggests that changes in UV radiation over the period of UVSIMN operations should be described with a second-order rather than a linear function. In addition to the availability of ozone-depleting chemicals, the depth and extent of the ozone hole is also largely controlled by meteorology, planetary wave activity, and stratospheric temperatures (Rex et al., 2004; WMO, 2007). These factors show large changes from year to year. Despite these variabilities, the largest UV intensities at austral UVSIMN sites were observed in 1997 and 1998 when stratospheric chlorine concentrations were at their maximum (Bernhard et al., 2004, 2005, 2006b). While we do not attempt trend estimates in this study, we do estimate past UV levels at five network sites from historical measurements of total ozone, and contrast these estimates with the climatology established from recent measurements of the UVSIMN. This analysis documents large changes in the Antarctic UV climate that have occurred during the last 40 years.

3.2 Data Analysis

3.2.1 Data

Measurements from all sites with the exception of San Diego are based on "Version 2 NSF Network Data" (Bernhard et al., 2004), available at http://www.biospherical.com/NSF/Version2. Version 2 data have been corrected for the cosine error of the instruments, have a wavelength uncertainty of less than $\pm$.04 nm ($\pm 1\sigma$), and were normalized to a uniform bandwidth of 1 nm FWHM. The expanded standard uncertainty of erythemal irradiance (CIE action spectrum by McKinlay and Diffey, 1987) and spectral irradiance at 400 nm varies between 4.2% and 6.8% (coverage factor 2, equivalent to a confidence level of 95.5%, or 2σ-level). Measurements are complemented with calculations of the radiative transfer model UVSPEC/libRadtran (Mayer and Kylling, 2005). Measurements during clear skies agree with model calculations to within $\pm$5% on average. More details on Version 2 data and model spectra from South Pole, McMurdo, Palmer, Barrow, and Summit can be found in publications by Bernhard et al. (2004, 2005, 2006b, 2007, 2008).

Version 2 data for San Diego, including model spectra, are not available as of this writing. Measurements from San Diego are based on the original "Version 0" data release (Booth et al., 1994; Bernhard et al., 2006a). Data were scaled up by 5%, which is the typical difference between Version 0 and 2 for erythemal irradiance observed at the other sites. Version 2 corrections are of less importance for San

Diego because of the smaller solar zenith angles (SZAs) occurring at this site. Nevertheless, San Diego data have an additional uncertainty of about 3%.

3.2.2 Establishment of Climatologies

Climatologies discussed in this study are based on measurements near local solar noon and daily doses. The latter were derived by integrating measurements over 24-hour periods. Spectra were measured hourly until 1997 and quarter-hourly thereafter. The following times (provided in Universal Time) were associated with noon: McMurdo: 01:00; Palmer: 16:00; South Pole: 00:00; Ushuaia: 17:00; San Diego: 20:00; Barrow: 22:00; and Summit: 15:00. To set up a climatology for noontime irradiance, we calculated for every site and every day of year the average, median, and maximum, as well as the 10^{th} and 90^{th} percentiles, using data from the periods indicated in the last column of Table 3.1. As the maximum may not always occur at noon due to changing clouds and total ozone, we also calculated the maximum within ± 2 hours (± 12 hours for South Pole) of the times indicated above. This value is denoted "daily maximum."

Figure 3.2(a) shows the resulting climatology for the UV Index (i.e., erythemal irradiance multiplied with 0.4 $cm^2/\mu W$ (WHO, 2002)) at the South Pole. The time-axis of the plot starts at winter solstice (22 December). Individual measurements are indicated by small dots. Average and median are plotted as red and green lines, respectively. Ten percent of the measurements are below (above) the lower (upper) blue line. The daily maximum is indicated by a thin grey line. All lines exhibit a large day-to-day variability. To facilitate interpretation, an 11-day running-average filter was applied to the average, median, and 10^{th} and 90^{th} percentiles. The resulting graph is plotted in Fig. 3.2(b) and will be discussed further below.

3.2.3 Estimates of Historical UV Indices

Based on historical ozone data and model calculation, the climatology of the UV Index for years preceding the development of the ozone hole was estimated for all sites with the exception of San Diego and Summit. The procedure is explained using South Pole as an example. Historical total ozone data at South Pole are available from observations of Dobson spectrophotometers performed by the Global Monitoring Division (GMD) of NOAA's Earth System Research Laboratory (ESRL) (Climate Monitoring and Diagnostics Laboratory, 2004). Measurements started in 1963. Data from 1963 – 1980 were used for estimating past UV levels.

Year-to-year variability of UV at South Pole is mainly influenced by total ozone. Variations of surface albedo in the UV and visible wavelength range are smaller than $\pm 1\%$ (Grenfell et al., 1994). Except at times following volcanic eruptions, the aerosol optical depth at 500 nm is typically only 0.012 (Shaw,

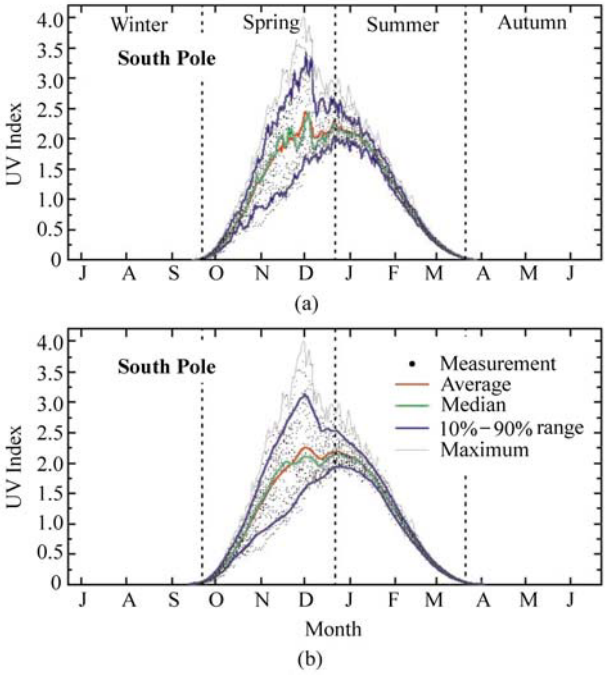

Figure 3.2 Climatology of UV Index at South Pole. Measurements at 00:00 UT of the years 1991 – 2007 are indicated by black dots. Average and median are plotted as red and green lines. 10% of the measurements are below (above) the lower (upper) blue line. The daily maximum is indicated by a thin grey line. The plot starts at the winter solstice. Summer solstice, and vernal and autumnal equinoxes are indicated by broken lines. Panel (a): Unsmoothed data. Panel (b): Same data as in (a), but with an 11-day running-average applied to the average, median, 10% and 90% lines

1982). Attenuation by clouds is small due to the low atmospheric water vapor content and the moderation of cloud effects by the high (>0.96) albedo (Nichol et al., 2003). By comparing measurements with the clear-sky model, it was determined that the average attenuation of spectral irradiance at 345 nm is only 6%. Cloud transmission at South Pole has also been determined from measurements of total irradiance (0.3 μm – 3.0 μm) using pyranometers (Dutton et al., 2004). Although this study did not indicate a significant linear trend of cloud transmission between 1976 and 2001, an oscillation on a decadal timescale was observed with a small downward trend in the late 1970s, followed by an upward trend between 1982 and 1995, and a downward trend thereafter. The small relative changes in cloud transmission of about ±2% reported by Dutton et al., (2004) have a very small effect ($<\pm1\%$) on the UV Index due to the diminished cloud influence at shorter wavelengths (Bernhard et al., 2004). Based on these considerations we assumed that all parameters affecting the radiative transfer did not change during the last 40 years, with the exception of atmospheric ozone concentrations. The historical clear-sky UV Index for the years 1963 – 1980 was

consequently modeled based on the average parameters used for processing South Pole Version 2 data of the years 1991 – 2007, with the exception of total ozone which was taken from the GMD Dobson data set.

The range of historical UV levels for a given day is mostly controlled by year-to-year changes in total ozone and cloudiness. To account for the variability introduced by clouds, we integrated measured and modeled spectra from the years 1991 – 2007 over the wavelength interval 337.5 nm – 342.5 nm, calculated the ratio of measurement to model, and used the results for estimating cloud-induced variability in UV intensities. This result was also applied to historical measurements. This approach assumes that year-to-year cloud-variability did not change during the last four decades, which is justified considering the small effect of clouds on UV discussed earlier. We also note that the wavelength interval of 337.5 nm – 342.5 nm is virtually unaffected by atmospheric ozone concentrations, and attenuation by clouds has only a weak wavelength dependence between 300 nm and 340 nm (Seckmeyer et al., 1996). The ratio of measurement to model for the 337.5 nm – 342.5 nm interval is therefore also appropriate for quantifying the effect of clouds on the UV Index. We estimate that the overall uncertainty in calculated historical UV Indices due to cloud effects is ±2%.

Results of these calculations are shown in Fig. 3.3. The red line is the historical average UV Index estimated from the average total ozone column of the years 1963 – 1980 measured with the Dobson, and the average attenuation by clouds of about 6% derived from Version 2 data. Figure 3.3 also includes the estimated 10th and 90th percentiles from the historical variability of total ozone (thin black lines in Fig. 3.3) and year-to-year differences in cloud transmission estimated from recent measurements (broken black lines). The two ranges were combined in quadrature to estimate the 10th and 90th percentiles for both effects (blue lines). During summer, variations induced by ozone and clouds are of similar magnitude. Variations during spring are dominated by ozone.

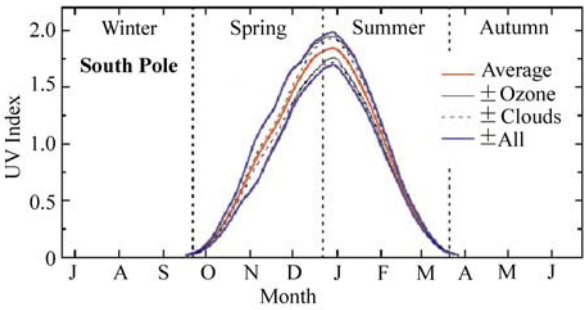

Figure 3.3 Estimate of the historical UV Index at South Pole. The red line is the average. The ranges defined by the 10th and 90th percentiles caused by variability of total ozone and cloud transmission are indicated by thin black and broken black lines respectively. The two ranges were combined in quadrature resulting in the span indicated by blue lines

A comparison of UV Indices measured during the years 1991 – 2007 and UV Indices modeled for the years 1963 – 1980 is shown in Fig. 3.4(a). An 11-day moving average was applied to all lines, except the line of the daily maximum. To better emphasize differences between the two periods, the average, and 10th and 90th percentiles from the current measurements were ratioed against the respective data from the historical period. The results are shown in Fig. 3.4(b). The difference of measurements performed before and after the solstice (22 December) is further highlighted in Fig. 3.5. Data from 21 December were ratioed against data from 23 December, data from 20 December were ratioed against data from 24 December, and so forth. If atmospheric conditions had been the same before and after the solstice, the ratio would be close to unity and only slightly ($< \pm 1\%$) affected by the different earth-sun distance before and after the mid-summer mark. Figure 3.5 shows that the actual situation is very different. Results shown in Figs. 3.4 and 3.5 are further discussed below.

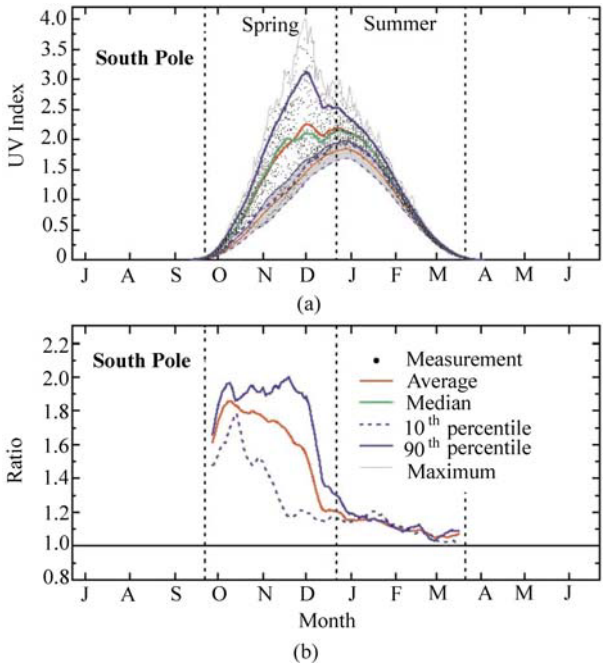

Figure 3.4 Comparison of UV Index measured during the last 17 years with historical estimate for South Pole. Panel (a): Individual measurements, average, median, range of 10th – 90th percentiles, and daily maximum. Recent measurements are indicated by thick lines; historical data are indicated by thin lines and grey-shading. Panel (b): Ratio of recent-to-historical data for average, and 10th and 90th percentiles

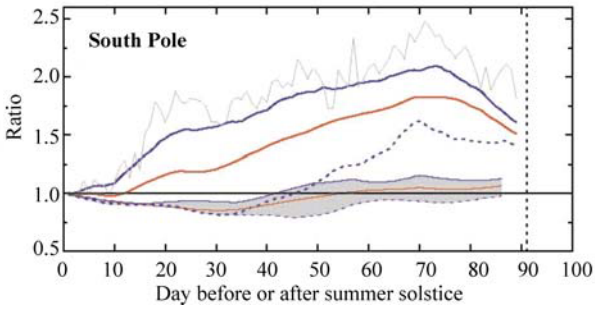

Figure 3.5 Comparison of the UV Index at the South Pole for periods before and after the summer solstice (22 December). Data from 21 December were ratioed against data from 23 December, data from 20 December were ratioed against data from 24 December, and so forth. Ratios of recent measurements are indicated by thick lines; historical data are indicated by thin lines and grey-shading. Red lines refer to the average noontime UV Index, broken and solid blue lines to the 10^{th} and 90^{th} percentiles, respectively. The thin grey line is the ratio for the daily maximum of recent data. The broken vertical line indicates the equinox

3.3 UV Index Climatology

A similar analysis as described previously for the South Pole was also performed for McMurdo, Palmer, Ushuaia, San Diego, and Barrow. The data record for Summit is still too brief for meaningful interpretation. A description of results for each site is provided below.

3.3.1 South Pole

The effect of the ozone hole is quite pronounced in measurements from the South Pole (Figs. 3.4 and 3.5). There is a strong asymmetry between spring and summer. The daily maximum and 90^{th} percentile peak at the end of November, shortly before the time when the annual ozone hole typically starts to disintegrate (Fig 3.4(a)). The maximum UV Index ever observed was 4.0 and was measured on 30 November 1998.

There is a striking difference between recent measurements and the estimate for historical data. During October and November, recent measurements from the years 1991 – 2007 are on average 55% – 85% larger than in the past (red line in Fig. 3.4(b)). The difference for the 90^{th} percentile is about 95%. Recent data peak at the end of November, but the peak is absent in the historical estimate. Past UV Indices for January and February are 10% – 20% lower than contemporary data. By comparing GMD Dobson total ozone data of the years 1963 – 1980 with data of the years 1991 – 2005, we found that the increase in UV radiation for these two

months can also be attributed to changes in total ozone. Compared to the earlier period, monthly average total ozone for the years 1991 – 2005 are lower by the following percentages: January: 12%; February: 7%; October: 48%; November: 35%; and December: 19%. Differences for all months are statistically significant.

Figure 3.5 indicates that contemporary measurements taken before the solstice are larger than UV Indices measured after the mid-summer mark (i.e., ratios are larger than one). Not surprisingly, the difference increases with the time from the solstice. On 13 October (70-day mark), the average and 90th percentile are larger by 82% and 102% respectively, than on the conjugate day of 2 March. Maximum UV Indices measured on the two days differ by 140% (grey line in Fig. 3.5). This pattern is very different from the situation prevalent before the development of the ozone hole. Prior to the 1980s, the reconstructed UV Index was smaller before the solstice: the thin red line in Fig. 3.5 is smaller than one up to day 50 from the solstice, and close to one thereafter.

Figures 3.4(a) and 3.5 also indicate that the 10th percentile is lower in spring than summer, both for recent and historical data. This characteristic is a consequence of the natural annual cycle of ozone concentrations caused by the Brewer-Dobson circulation (Holton et al., 1995). This phenomenon leads to a poleward transport of ozone from the tropics during the winter and early spring, resulting in an ozone maximum in spring and a minimum in autumn. During times in the spring when either the South Pole is outside the perimeter of the ozone hole or the ozone hole has already closed for the year, total ozone tends to be larger than in summer. Such situations lead to lower UV Indices in spring relative to summer. In contrast, when the ozone hole is over the South Pole, ozone concentrations are smaller than during the summer, explaining the annual cycle of the 90th percentile.

3.3.2 McMurdo Station

McMurdo is affected by the ozone hole from September until early December (Fig. 3.6(a)). The maximum UV Index was 7.6 and occurred in November; UV Indices measured after the solstice were below 5.5. The 90th percentile also exhibits a distinct maximum in late November. The average UV Index is fairly symmetric within ± 40 days about the solstice, but the 10th percentile is lower in the spring than in the summer. This feature is again a consequence of the Brewer- Dobson circulation. Historical UV Indices for McMurdo were estimated from total ozone measured by TOMS on NASA's Nimbus-7 satellite (McPeters and Labow, 1996). Measurements began in 1978, when the ozone hole had already started to develop. Model calculations were based on the average ozone column measured between 1978 and 1981. The UV irradiance derived from this calculation is therefore likely already larger than UV intensities prevailing in the 1960s. Due to the short reference period, it was not possible to calculate a range of historical UV Indices

caused by variations in ozone during the pre-ozone-hole period. The grey range in Fig. 3.6(a) reflects variation by cloudiness only. Cloud effects are considerably larger compared to the South Pole due to optically thicker clouds at the Antarctic coast and lower surface albedo, ranging from 0.84 during winter and early spring to about 0.74 in summer (Bernhard et al., 2006b). Contemporary measurements are significantly above the historical estimate for all months. Figure 3.7(a) shows that the average UV Index for October and November is 30% – 60% larger now than it was historically. The 90th percentile is higher by 70% – 110%. The increase in the ratio of contemporary to historical data during September reflects the gradual photochemical loss in stratospheric ozone concentrations as the ozone

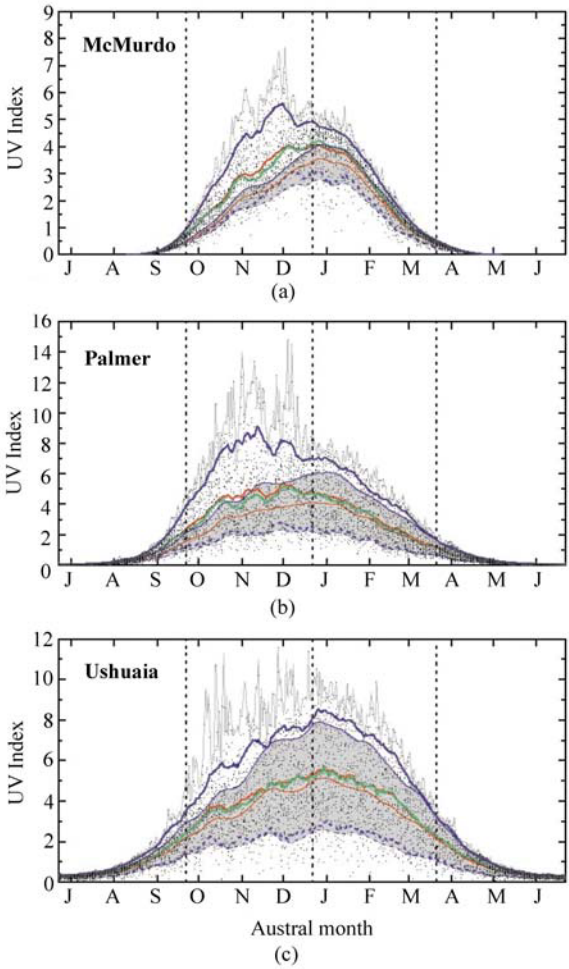

Figure 3.6 Same as Fig. 3.4(a), but for McMurdo (Panel (a)), Palmer (Panel (b)), and Ushuaia (Panel (c))

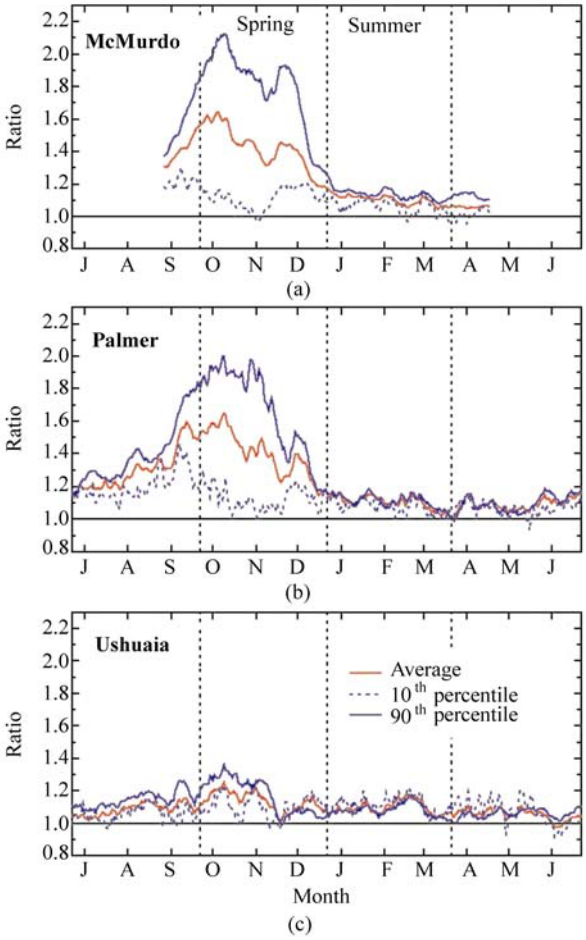

Figure 3.7 Same as Fig. 3.4(b), but for McMurdo (Panel (a)), Palmer (Panel (b)), and Ushuaia (Panel (c))

hole forms at the end of winter. For January through March, differences are on the order of 8% – 15%. Increased UV levels for these months are a consequence of lower total ozone values during the 1980s and 1990s, also observed for months not directly affected by the ozone hole (WMO, 2007). Approximately the same increase in the UV Index of 5% – 15% was observed at all austral network sites during summer months (compare Figs. 3.4(b) and 3.7(a), (b), (c)).

3.3.3 Palmer Station

The patterns of measured and historical UV Indices at Palmer are similar to those at McMurdo, but the magnitudes are different. The highest UV Index occurs in

spring, reaching a maximum of 14.8. The 90th percentile is considerably enhanced during spring. Particularly large UV-B levels were observed in November and early December during years when the polar vortex became unstable and air masses with low ozone concentration moved toward the Antarctic Peninsula. In combination with the relatively high solar elevations in those months, it led to UV intensities exceeding San Diego's summer levels. UV Indices at Palmer during summer were always lower than 8. Historical measurements were estimated based on the average ozone column calculated from TOMS/Nimbus-7 measurements of the years 1978 – 1980. The grey range in Fig. 3.6(b) indicates variability by clouds only. This variability is much larger than the effect of ozone variations on historical UV Indices at South Pole (Fig. 3.3). The range indicated in Fig. 3.6(b) should be a good estimate for the actual variability at Palmer if past year-to-year changes in total ozone were similar at South Pole and Palmer. We believe that this assumption is justified. Recent measurements for mid-September to mid-November are on average 30% – 60% larger than the historical average (Fig. 3.7(b)). The differences for the 90th percentile are between 60% – 100%.

3.3.4 Ushuaia

Ushuaia is less affected by the ozone hole than the three Antarctic sites due to its lower latitude (Fig. 3.6(c)). The average and 10th and 90th percentiles tend to be lower in spring than summer, as is expected from the natural annual cycle of ozone. Large UV levels may occur between September and December when the edge of the ozone hole moves over Ushuaia. During those events, the daily maximum UV Index measured in October was as high as 11.5. Historical measurements are based on the average TOMS/Nimbus-7 ozone column of the years 1978 – 1981. The grey range in Fig. 3.6(c) indicates variability by clouds only. The discrepancy between recent and historical data is much smaller than for Antarctic sites. The difference for October is about 18% for the average and 25% – 30% for the 90th percentile (Fig. 3.7(c)). Some increases in the UV Index are also evident for January and February, but little change has been observed for the months March – July.

3.3.5 San Diego

San Diego is located at 32°N where the depletion of stratospheric ozone has been small: total ozone averaged over the latitude band 35°N – 60°N was about 3% lower during the period 2002 – 2005 than during 1964 – 1980 (WMO, 2007). The maximum summer-time UV Index is 12.0 (Fig. 3.8(a)). The average and 90th percentile for July are about 9.5 and 11, respectively. UV levels are generally lower during the months preceding the summer solstice due to a combination of

larger ozone columns in spring compared to summer (the average ozone column for May is 320 DU; that for July is 295 DU), and frequent coastal fog during the months of May and June, also known as "June gloom". This is particularly evident in the dip of the 10th percentile around 1 June. Model calculations and historical data are not available for San Diego.

3.3.6 Barrow

Barrow is located at the Arctic coast. Land and ocean adjacent to the instrument are typically covered by snow between October and June. The UV albedo is 0.83 ± 0.08 ($\pm 1\sigma$) between November and May and smaller than 0.1 during the summer months (Bernhard et al., 2007). Clouds are more frequent in summer than in spring. The small differences between the 10th and 90th percentiles in March and April (Fig. 3.8(b)) are attributable to high albedo and low cloudiness during these months. Barrow is affected by ozone depletion between February and April, but the magnitude is much smaller than at Antarctic sites. Depletion events are typically short and lead to spikes in the UV Index of up to one UV Index unit only. The largest daily maximum UV Indices of $4.5 - 5$ are observed in May and June when low ozone episodes coincide with high albedo conditions.

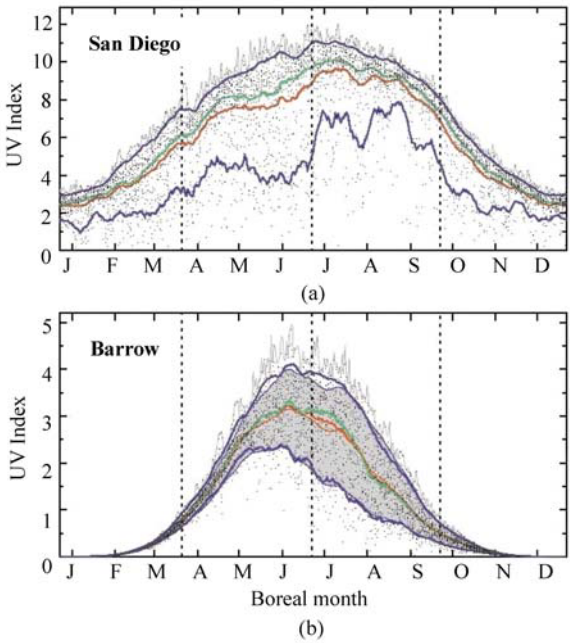

Figure 3.8 Same as Fig. 3.4(a), but for San Diego (Panel (a)) and Barrow (Panel (b)). Historical data were not calculated for San Diego

Total ozone at Barrow has been measured by GMD/ESRL with Dobson photometers since 1973. Historical UV intensities for Barrow were calculated in a similar way as UV levels were at South Pole using Dobson measurements from the years 1973 – 1980. Dutton et al. (2004) have reported a statistically significant decrease of effective cloud transmission from 0.64 in 1976 to 0.61 in 2001 based on their analysis of pyranometer data. When estimating past UV Indices, we did not consider this change. First, it is unknown whether the downward trend was already present during the 1960s, and second, changes in cloud transmission were likely smaller in the UV, particularly in spring when attenuation by clouds is reduced by high albedo.

To estimate the range of historical UV, we also considered year-to-year changes in surface albedo. The grey area in Fig. 3.8(b) includes changes in total ozone estimated from the years 1973 – 1980, as well as variations due to clouds and albedo estimated from the years 1991 – 2006. UV Indices measured since 1991 are very similar to the historical estimate. For the months February through April, the average increase is 4% – 7% only, and the increase for the 90th percentile is 7% – 13%. Differences for summer months are smaller and may even be negative: recent measurements for August are about 5% below the historical estimate. Differences of this magnitude are within the uncertainty of the data. This shows that there was little change in UV levels during the last 30 years at Barrow, with the exception of several spikes observed during recent low-ozone episodes.

3.4 Climatology of UV-A Irradiance

Figure 3.9 shows the climatology of UV-A irradiance (spectral irradiance integrated between 315 nm and 400 nm) for all UVSIMN sites but Summit. All plots show individual measurements, as well as the average, median, and 10th and 90th percentiles, and overall daily maximum. Since long-term changes in cloud cover and albedo are not considered in this study, historical estimates are virtually identical with recent measurements and are therefore not included in Fig. 3.9. Changes in total ozone have practically no influence on UV-A irradiance. Patterns in Fig. 3.9 show mostly seasonal variations in cloudiness, surface albedo, and to a lesser extent, atmospheric aerosol loading.

UV-A irradiance at the South Pole is very symmetric about the solstice due to constant high albedo year-round, and little influence by clouds. Daily maximum UV-levels are considerably above the 90th percentile, indicating that enhancement of UV radiation by scattered clouds—which is a well-known effect at mid-latitude sites (Mims and Frederick, 1994)—can also occur at the South Pole. The maximum enhancement is about 30%. Enhancement of the spectral integral 400 nm – 600 nm can be as high as 70%. An extreme example is shown in Fig. 3.10, which displays three spectra measured at 19:00 UT, 19:15 UT, and 19:30 UT on 17 December 2000 at South Pole. During the first spectrum starting at 19:00 UT, the sun was

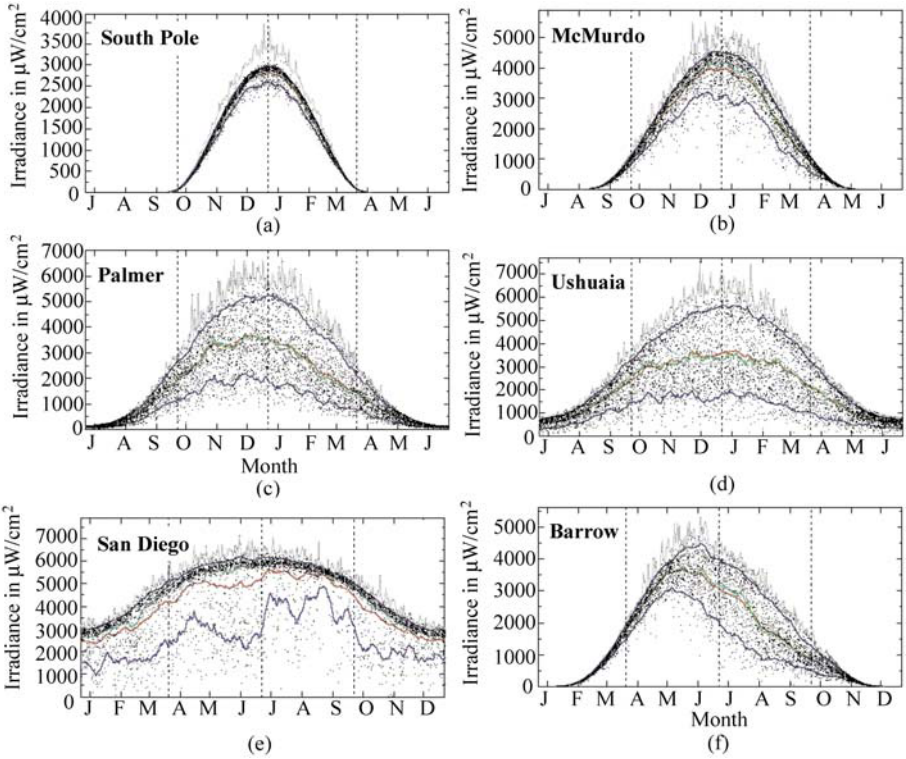

Figure 3.9 UV-A irradiance measured at South Pole (Panel (a)), McMurdo (Panel (b)), Palmer (Panel (c)), Ushuaia (Panel (d)), San Diego (Panel (e)), and Barrow (Panel (f)). Individual measurements, average, median, and 10th and 90th percentiles, as well as daily maximum, are shown as in Fig. 3.2(b)

hidden by a stable cloud, leading to a reduction of UV and visible irradiance of about 10% – 20% compared to the clear-sky model (Fig. 3.10(b), red line). Measurements were also compared against a second model spectrum where a wavelength-independent cloud optical depth of 1.83 was used as an additional model input parameter. The ratio of the measured spectrum with this model spectrum (Fig. 3.10(b), orange line) is close to one and virtually independent of wavelength, confirming that the radiation field during the period of the scan (approximately 13 minutes) was very stable. Measurements of total irradiance with a pyranometer also indicate constant conditions (Fig. 3.10(c)). During the second spectrum, starting at 19:15 UT (Fig. 3.10, green lines), total irradiance increased sharply during the first part of the scan; spectral irradiance increased up to 60% relative to the clear-sky model. Total irradiance increased by up to 72%. As reflections from nearby obstacles can be excluded, this pattern can only be explained by enhancement due to scattered clouds surrounding the (unoccluded) disk of the sun. Photons passing through a hole in the cloud are scattered multiple times between the snow-covered surface and the cloud-ceiling. This effect leads to

a large enhancement of downwelling radiation and cannot be observed at locations with small surface albedo. The third spectrum starting at 19:30 UT (Fig. 3.10, blue lines) agrees well with the clear-sky model. Pyranometer measurements were close to the value expected for clear-sky.

UV-A irradiance at McMurdo (Fig. 3.9(b)) is generally symmetric about the solstice. Radiation levels are somewhat smaller in January than December, probably

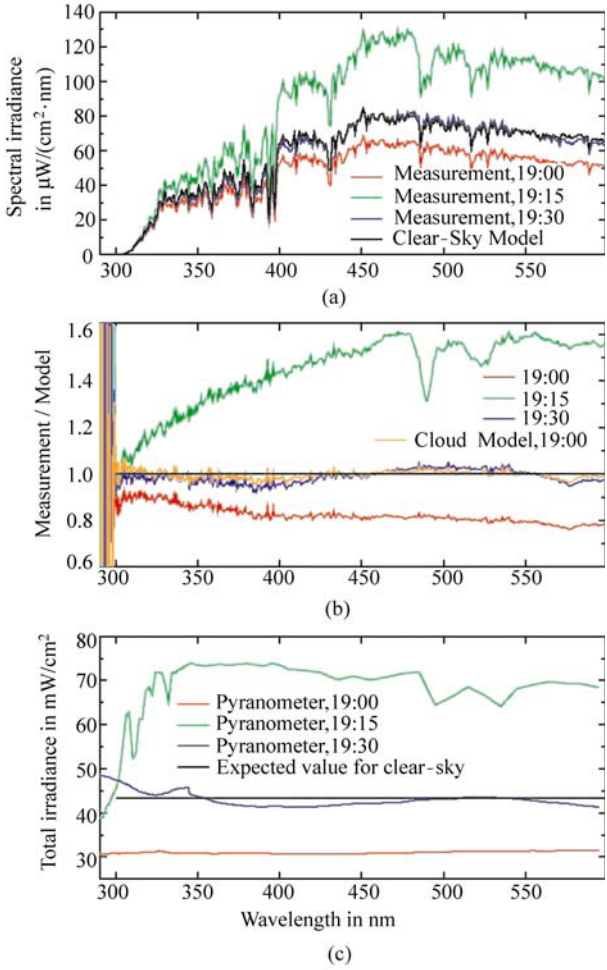

Figure 3.10 Enhancement of global irradiance by a broken cloud at South Pole. Panel (a): Three spectra of global irradiance measured on 17 December 2000 at 19:00 UT, 19:15 UT, and 19:30 UT. The clear-sky model spectrum for 19:00 is also shown. Panel (b): Ratios of measured and modeled spectra. Panel (c): Total irradiance measured by a pyranometer during the recording of the three spectra and plotted against the wavelength being sampled by the spectroradiometer as a surrogate of time

due to smaller albedo in summer when compared with spring. UV-A irradiance at Palmer (Fig. 3.9(c)) shows a much larger variability than observed at South Pole and McMurdo due to frequent cloud cover with optical depths typically ranging between 20 and 50 (Ricchiazzi et al., 1995). The ocean surrounding Palmer freezes over during the winter. Terrain and glaciers at Palmer are typically covered by snow up to mid-December. Surface albedo is therefore larger in winter and spring than in summer. This leads to the small asymmetry in the annual cycle UV-A irradiance discernable in Fig. 3.9(c). Ushuaia, like Palmer, is affected by persistent cloudiness, leading to a large difference of the 10^{th} and 90^{th} percentiles (Fig. 3.9(d)). The Beagle Channel adjacent to Ushuaia does not freeze, but snow typically enhances the effective surface albedo to approximately 0.2 to 0.3 between June and October, leading to some enhancement of UV-A during the winter. UV-A irradiance during spring and summer is almost symmetric about the solstice. The clear-sky limit of UV-A irradiance at San Diego (Fig. 3.9(e)) is symmetric about the solstice, but the average and 10^{th} percentile are affected by seasonal patterns in cloudiness. Cloud attenuation is largest during May and June, whereas most days in August are cloud-free at solar noon. Enhancement of UV-A irradiance by scattered clouds beyond the clear-sky limit is remarkably small, and less pronounced than at the South Pole. This is attributable to low surface albedo (<0.05) and the near absence of broken cumulus clouds, which can enhance UV radiation at other mid-latitude locations by up to 25% (WMO, 2007). UV-A irradiance at Barrow displays a strong annual cycle due to seasonal differences in cloudiness (more prevalent in summer) and surface albedo (0.83 ± 0.08 between November and May; smaller than 0.1 during summer). The effect of the two factors has been quantitatively described by Bernhard et al. (2007).

3.5 Comparison of Radiation Levels at Network Sites

There are substantial differences in the UV climatology between the various UVSIMN sites. A large portion of the differences can be traced to their geographical locations as lower latitudes experience higher sun elevations and more UV, all other factors being equal. However, the contention that low levels of UV will occur in Polar Regions because of the high latitude is shown here to not be true. Measurements from the seven network sites are presented below. The comparison is based on the average and maximum UV Index, as well as average and maximum erythemal daily dose. The results reveal that differences between the sites depend very much on the selection of the physical quantity used for the comparison.

High levels of UV radiation absorbed during short time-periods, ranging from minutes to hours, can be most detrimental for some organisms. This includes humans who may receive a "sunburn" after an exposure time of less than 20 minutes for UV Indices above 7 (Vanicek et al., 2000). The average noontime and daily

maximum UV Index are therefore useful for quantifying the risk of getting sunburned. UV-B radiation is a risk factor for developing basal and squamous cell carcinoma (Moan and Dahlback, 1992), and the UV Index also provides guidance in avoiding overexposure with regard to cancer prevention. The "daily dose" is an appropriate quantity for investigating cumulative UV exposures over an extended time-period. This is relevant for plants and animals that cannot avoid the sun. This quantity, however, does not capture the impact of transient high levels of UV-B that may occur during episodic combinations of clear skies (or partly cloudy skies and high albedo) and severe ozone depletion. Such incidents may have biological significance in systems that do not obey reciprocity in terms of exposure intensity versus duration. This is particularly relevant for microorganisms, which have only a short life cycle, such as plankton (Moline et al., 1997). The maximum daily dose may be the best measure for quantifying the effect on these organisms.

Figure 3.11 shows a comparison of the noontime UV Index from the seven sites. The data are identical to those indicated by red lines in Figs. 3.4(a), 3.6, and 3.8. Measurements at San Diego exceed those at the other sites due to its lower latitude, and range between 2.5 during winter and 9.5 during summer.

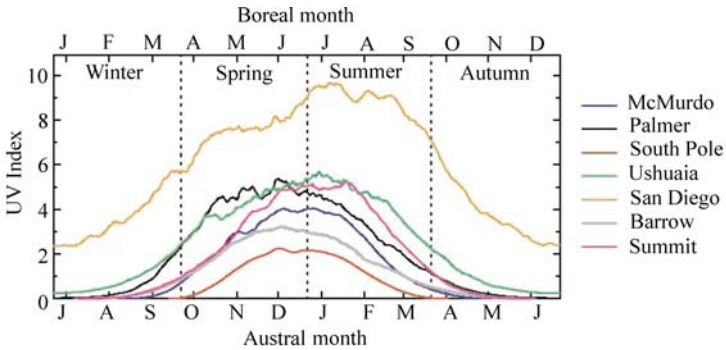

Figure 3.11 Comparison of average noontime UV Index from all sites

The average noontime UV Index at Palmer, Ushuaia, and Summit, observed close to the summer solstice, is about 5, or about 55% of the typical summer UV Index at San Diego. Average UV Indices for South Pole, Barrow and McMurdo extend up to 2, 3, and 4, respectively. The divergence relative to San Diego is even larger during autumn and winter when some sites experience extended periods of darkness.

The differences between sites show completely different patterns when maxima, rather than average values, are compared. Figure 3.12 shows the maximum daily UV Index, which was indicated by thin grey lines in Figs. 3.6 and 3.8. At Palmer Station, the maximum observed UV Index was 14.8. This value is 23% larger than the highest UV Index of 12.0 measured at San Diego. The maximum UV Index at

Ushuaia was 11.5, which is comparable to summer-time values at San Diego. Maximum UV Indices at McMurdo, South Pole and Barrow are considerably smaller than at San Diego; however, the differences are considerably smaller when compared to average noontime values.

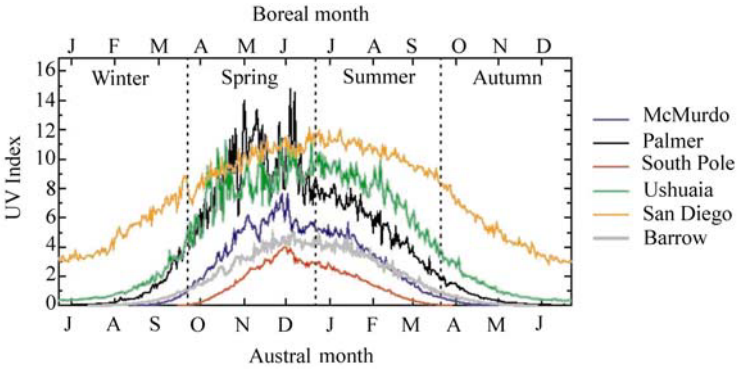

Figure 3.12 Comparison of daily maximum UV Index from all sites, but Summit

The picture changes again when comparing average daily erythemal doses (Fig. 3.13). The effect of 24 hours of sunlight during Arctic and Antarctic summers reduces the consequence of latitude differences. Although average summer doses at San Diego are still highest, average December UV doses at McMurdo, Palmer Station, South Pole, and Ushuaia, as well as June doses at Summit, amount to 65% − 95% of typical mid-summer San Diego conditions. Note that average daily doses at McMurdo and South Pole are very similar between mid-January and March but differ significantly in mid-November when doses at South Pole exceed those at McMurdo by up to 35%. The reasons are threefold: first, the influence of the ozone hole on UV levels is more pronounced at South Pole than at the Antarctic coast; second, the solar elevation at South Pole is constant for 24 hours;

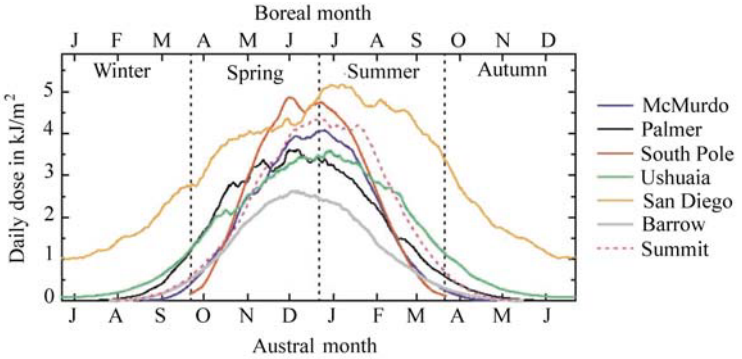

Figure 3.13 Comparison of average daily erythemal dose from all sites

and third, albedo at McMurdo is at its annual minimum during January and February. Average daily erythemal dose at Barrow is the lowest of all network sites mostly because ozone depletion in the northern hemisphere is much less severe than over Antarctica.

The importance of UV radiation for high latitudes becomes most obvious when comparing maximum daily doses. Figure 3.14 shows that the largest daily erythemal doses ever measured at South Pole and Palmer are 18% and 32%, respectively, higher than the San Diego record. Maximum doses at McMurdo and Ushuaia are comparable to San Diego levels. Note that the difference between McMurdo and South Pole is much smaller when maximum daily doses rather than maximum noontime UV Indices (Fig. 3.11) are compared. We attribute this to the difference in the diurnal cycle of the sun at these sites: at McMurdo, radiation levels peak at local solar noon whereas at the South Pole, there is virtually no change in solar elevation during a given 24-hour period.

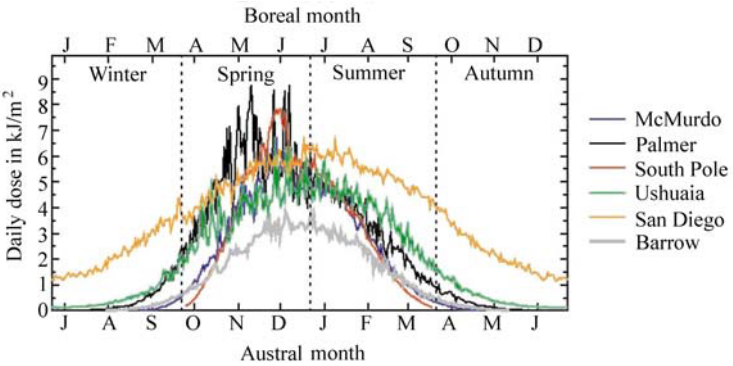

Figure 3.14 Comparison of maximum daily erythemal dose from all sites, but Summit

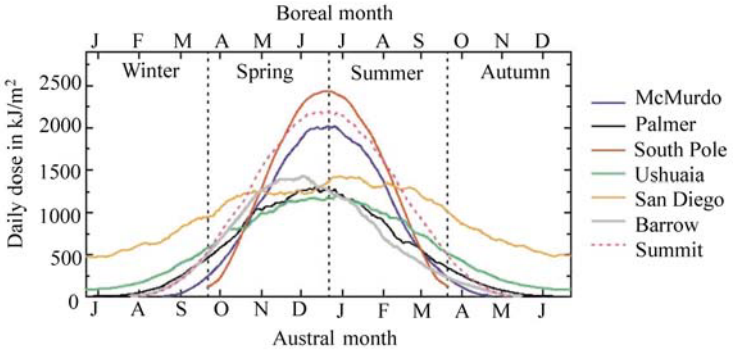

Figure 3.15 Comparison of average daily UV-A dose from all sites

The effect of 24 hours of sunlight is best shown when comparing the average daily UV-A dose (Fig. 3.15). Since UV-A spectral irradiance is practically independent

of atmospheric ozone concentrations, there are no ozone-related features in this figure. UV-A doses at the summer solstice at McMurdo, Summit, and South Pole exceed San Diego doses by 71% − 88%. In addition to 24 hours of sunlight, this difference can be explained by high surface albedo, and in the cases of South Pole and Summit, high altitude.

3.6 Conclusions and Outlook

Measurements of solar UV irradiance performed during the last 18 years at six high-latitude locations and San Diego have revealed large differences of the sites' UV climates. The ozone hole has a large effect on the UV Index at the three Antarctic sites, and to a lesser extent at Ushuaia. UV Indices measured at South Pole during the ozone hole period are on average 20% − 80% larger than measurements at comparable solar elevations during summer months. When the ozone hole passed over Palmer Station late in the year, the UV Index was as high as 14.8 and exceeded the maximum UV Index of 12.0 observed at San Diego. The maximum UV Index at Ushuaia was 11.5, which is comparable with summer-time measurements at San Diego. UV Indices at the two Arctic sites Barrow and Summit are lower than at southern-hemisphere sites as ozone columns are generally larger in the northern hemisphere, and ozone depletion is less severe.

A comparison of UV levels at the network sites revealed that differences between sites depend greatly on the data product used. Average noontime UV Indices at San Diego during summer are considerably larger than at Antarctic sites under ozone-hole conditions, but the difference disappears when daily doses are compared. This contradicts the common notion that UV levels at high latitudes are small because of small solar elevations.

Reconstructions of historical UV Indices based on long-term ozone records and climatological cloud and aerosol patterns indicate that contemporary UV Indices measured during the ozone hole period at Antarctic sites are on average 30% − 85% larger than estimates for the past. These reconstructions were based on the assumption that cloud, albedo, and aerosol conditions have not changed over the last 40 years. Analysis of pyranometer data from South Pole and Barrow indicated that this assumption is justified. Similar long-term observations are not available from other UVSIMN locations, and estimates of historical UV irradiance at those sites are therefore more uncertain. Clearly, the reconstruction of UV levels from proxy data has a larger uncertainty than actual measurements. Operation of the UVSIMN is expected to continue, providing the opportunity to assess future developments of high-latitude UV climate more accurately than in the past. These measurements will help document changes in UV levels due to the expected recovery of the ozone layer (WMO, 2007) and the impact of climate change, which will likely modify stratospheric temperatures; ozone (column and profile); surface

albedo (e.g., due to changes in the timing of snow melt (Stone et al., 2002)); clouds (frequency and optical properties), aerosols (e.g., changes in Arctic haze (Bodhaine and Dutton, 1993)), and atmospheric circulation patterns (Knudsen and Anderson, 2001).

Acknowledgements

Operation of the UVSIMN and this study were supported by the National Science Foundation's Office of Polar Programs via a subcontract to Biospherical Instruments Inc. from Raytheon Polar Services Company (RPSC). Extended thanks go to Vi Quang of BSI for assisting in data processing. Dobson measurements for South Pole and Barrow were retrieved from http://www.esrl.noaa.gov/gmd/ozwv/dobson/. TOMS Nimbus-7 total ozone data were accessed via the website http://toms.gsfc.nasa.gov/n7toms/n7_ovplist_a.html. We thank Ellsworth Dutton from NOAA for discussions regarding cloud effects at the South Pole.

References

Bernhard G, Booth CR, and Ehramjian JC (2004) Version 2 Data of the National Science Foundation's Ultraviolet Radiation Monitoring Network: South Pole. J. Geophys. Res. 109:D21207, doi:10.1029/2004JD004937

Bernhard G, Booth CR, and Ehramjian JC (2005) UV Climatology at Palmer Station, Antarctica. In: Bernhard G, Slusser JR, Herman JR, Gao W (eds) Ultraviolet Ground- and Space-based Measurements, Models, and Effects V. Proceedings of SPIE International Society of Optical Engineering 5886, pp.588607-1 − 588607-12

Bernhard G, Booth CR, Ehramjian JC, and Quang VV (2006a) NSF Polar Programs UV Spectroradiometer Network 2004 − 2005 Operations Report, Volume 14.0, p.257, Biospherical Instruments Inc., San Diego, CA, http://www.biospherical.com/NSF

Bernhard G, Booth CR, Ehramjian JC, and Nichol SE (2006b) UV climatology at McMurdo Station, Antarctica, Version 2 Data of the National Science Foundation's Ultraviolet Radiation Monitoring Network. J. Geophys. Res. 111:D11201, doi:10.1029/2005JD005857

Bernhard G, Booth CR, Ehramjian JC, Stone R, and Dutton EG (2007) Ultraviolet and visible radiation at Barrow, Alaska: Climatology and influencing factors on the basis of Version 2 National Science Foundation network data. J. Geophys. Res. 112:D09101, doi:10.1029/2006JD007865

Bernhard G, Booth CR, and Ehramjian JC (2008) Comparison of UV irradiance measurements at Summit, Greenland; Barrow, Alaska; and South Pole. Antarctica. Atmos. Chem. Phys. 8: 4799 − 4810, http://www.atmos-chem-phys.net/8/4799/

Bodhaine BA and Dutton EG (1993) A long-term decrease in Artic haze at Barrow, Alaska. Geophys. Res. Lett. 20: 947 − 950

Booth CR, Lucas TB, Morrow JH, Weiler CS, and Penhale PA (1994) The United States National Science Foundation's polar network for monitoring ultraviolet radiation. Weiler CS, Penhale PA (eds). Antarc. Res. Ser. 62: 17 − 37

Chubachi S (1984) Preliminary results of ozone observations at Syowa Station from February 1982 to January 1983. Mem. Natl. Inst. Polar Res. Jap., Spec. Issue 34: 13 − 19

Climate Monitoring and Diagnostics Laboratory (CMDL) (2004) Summary Report 27, 2002 − 2003. Schnell RC, Buggle A-M, Rosson RM (eds) U.S. Dept. of Commerce, Boulder, CO

Dutton EG, Farhadi A, Stone RS, Long CN, and Nelson DW (2004) Long-term variations in the occurrence and effective solar transmission of clouds as determined from surface-based total irradiance observations. J. Geophys. Res. 109:D03204, doi:10.1029/2003JD003568

Farman JC, Gardiner BG, and Shanklin JD (1985) Large losses of total ozone in Antarctica reveal seasonal ClO_x/NO_x interaction. Nature 315: 207 − 210

Fioletov VE, McArthur LJB, Kerr JB, and Wardle DI (2001) Long-term variations of UV-B irradiance over Canada estimated from Brewer observations and derived from ozone and pyranometer measurements. J. Geophys. Res. 106(D19): 23009 − 23028, 10.1029/2001JD000367

Grenfell TC, Warren SG, and Mullen PC (1994) Reflection of solar radiation by the Antarctic snow surface at ultraviolet, visible, and near infrared wavelengths. J. Geophys. Res. 99(D9): 18669 − 18684

Gröbner J, Blumthaler M, Kazadzis S, Bais A, Webb A, Schreder J, Seckmeyer G, and Rembges D (2006) Quality assurance of spectral solar UV measurements: results from 25 UV monitoring sites in Europe, 2002 to 2004. Metrologia 43: S66 − S71, DOI:10.1088/0026-1394/43/2/S14

Holton JR, Haynes PH, McIntyre ME, Douglass AR, Rood RB, and Pfister L (1995) Stratosphere-troposphere exchange. Rev. Geophys. 33(4): 403 − 440

Kaye JA, Hicks BB, Weatherhead EC, Long CS, and Slusser JR (1999) U.S. Interagency UV Monitoring Program established and operating. EOS 80(10): 113 − 116

Knudsen BM and Andersen SB (2001) Longitudinal variation in springtime ozone trends Nature 413: 699 − 700

Mayer B and Kylling A (2005) Technical note: the libRadtran software package for radiative transfer calculations — description and examples of use. Atmos. Chem. Phys. 5: 1855 − 1877, http://www.atmos-chem-phys.org/acp/5/1855/

McKenzie R, Connor B, and Bodeker G (1999) Increased summertime UV radiation in New Zealand in response to ozone loss. Science 285(5434): 1709 − 1711, DOI:10.1126/science. 285.5434.1709

McKinlay AF and Diffey BL (eds) (1987) A reference action spectrum for ultraviolet induced erythema in human skin. In: Commission International de l'Éclairage (CIE). Research Note 6(1): 17 − 22

McPeters RD and Labow GJ (1996) An assessment of the accuracy of 14.5 years of Nimbus 7 TOMS Version 7 ozone data by comparison with the Dobson network. Geophys. Res. Lett. 23(25): 3695 − 3698

Mims FM and Frederick JE (1994) Cumulus clouds and UVB. Nature 371: 291

Moan J and Dahlback A (1992) The relationship between skin cancers, solar radiation, and ozone depletion. British Journal of Cancer 65: 916 − 921

Moline MA, Prézelin BB, Schofield O, and Smith RC (1997) Temporal dynamics of coastal Antarctic phytoplankton: environmental driving forces and impact of a 1991/1992 summer diatom bloom on the nutrient regimes. In: Battaglia B, Valencia J, Walton DWH (eds) Antarctic Communities. Cambridge Press, London, 67 − 72

Nichol SE, Pfister G, Bodeker GE, McKenzie RL, Wood SW, and Bernhard G (2003) Moderation of cloud reduction of UV in the Antarctic due to high surface albedo. J. Appl. Meteorol. 42(8): 1174 − 1183

Rex M, Salawitch RJ, von der Gathen P, Harris NRP, Chipperfield MP, and Naujokat B (2004) Arctic ozone loss and climate change. Geophys. Res. Lett. 31:L04116, doi:10.1029/2003GL018844

Ricchiazzi P, Gautier C, and Lubin D (1995) Cloud scattering optical depth and local surface albedo in the Antarctic: simultaneous retrieval using ground-based radiometry. J. Geophys. Res. 100(D10): 21091 − 21104

Shaw GE (1982) Atmospheric turbidity in the Polar regions. J. Appl. Meteorol. 21: 1080 − 1088

Seckmeyer G, Erb R, and Albold A (1996) Transmittance of a cloud is wavelength-dependent in the UV-range. Geophys. Res. Lett. 23(20): 2753 − 2756

Stone RS, Dutton EG, Harris JM, and Longenecker D (2002) Earlier spring snowmelt in northern Alaska as an indicator of climate change. J. Geophys. Res. 107(D10): 4089, doi:10.1029/2000JD000286

Vanicek K, Frei T, Litynska Z, and Schmalwieser A (2000) UV-Index for the public, COST-713 Action. Office for Official Publications of the European Communities, Luxembourg. ISBN 92-828-8142-3, 27

Weatherhead EC, Reinsel CG, Tiao GC, Meng X-L, Choi D, Cheang W-K, Keller T, DeLuisi JJ, Wuebbles DJ, Kerr JB, Miller AJ, Oltmans SJ, and Frederick JE (1998) Factors affecting the detection of trends: statistical considerations and applications to environmental data. J. Geophys. Res. 103(D14): 17149 − 17161

World Health Organization (WHO) (2002) Global solar UV Index: a practical guide. ISBN 9241590076, Geneva, Switzerland. http://www.unep.org/PDF/Solar_Index_Guide.pdf. p.28

World Meteorology Organization (WMO) (2007) Scientific assessment of ozone depletion: 2006, Global ozone research and monitoring project, Geneva, Switzerland, Report No. 50, p.572

4 UV Solar Radiation in Polar Regions: Consequences for the Environment and Human Health

Claudio Rafanelli, Alessandro Damiani, Elena Benedetti, Sara. De Simone, Andrea Anav, Luigi Ciattaglia, and Ivo Di Menno

ICES-International Center for Earth Sciences
c/o CNR-Istituto
di Acustica "O.M. Corbino"
Area della Ricerca "Roma-Tor Vergata"
via del Fosso del Cavaliere, 100
00113-Roma, Italy
E-mail: c.rafanelli@e-ices.eu (rafanelli@libero.it)

Abstract Over the past few years, some preventive measures have been adopted for restricting the growth of human impact on the terrestrial environment and to limit gaseous emissions into the atmosphere, (e.g., the Vienna Convention for the Protection of the Ozone Layer, 1985, and the Montreal Protocol, 1987). The monitoring of minor atmospheric gases presently assumes a double significance: (1) to better understand the photochemistry process involved and the environmental problems they produce; and (2) to test the effectiveness of adopted mitigation techniques. Studies on stratospheric ozone are particularly relevant because it is a filter for ultraviolet (UV) and has a high sensitivity to chlorofluorocarbon (CFC) presence. During the past 20 years, the trend of ozone depletion has been strongly negative. Some signals have recently been observed that seem to indicate there has been a slight recovery, even if the evidence for this tendency is disguised by the difficulty in separating the anthropogenic impact from the natural variability. Human impact is much more discernible in polar regions making them privileged areas for carrying out this type of research.

In light of these considerations, studies on solar radiation flux have become important for investigating the properties of the atmosphere and its minor components, and also for evaluating the available radiant energy for technical applications. Moreover, the ever-increasing interest in regard to the consequences of human activity on the biosphere has further contributed to the development of these studies, especially in the UV spectral region. As a result, there has been an increase in the number of instrument sites and radiometric networks. Many decisions affecting civil society are made using data from these networks and consequently, it is essential that the effects of

environmental factors are well understood.

Few fields of research involve such a mixture of measurement techniques, instrumental characteristics, and physical atmospheric properties. The major environmental factors include radiative transfer of solar UV through the atmosphere, atmospheric physics, and aerosol composition and content. The management of international networks and the development of instruments are the main limiting factors for good data acquisition.

This work gives a concise review and provides guidance regarding the consequences and risks of solar UV radiation on environmental and human health.

Keywords ozone, ozone hole, personal dosimeter, polar regions, radiometer, skin cancer, UV radiation

4.1 Introduction

The North and South Poles are the best areas on earth for the evaluation of global effects and the study of climatic change. The majority of developed countries have established their scientific bases in one of these areas to perform their research because the local atmospheric circulation highlights modifications to planetary background values. Moreover, the Poles are privileged zones for studying solar electromagnetic flux that reaches the ground, e.g. within the ultraviolet region, because due to the ozone hole event, it is possible to investigate the large variability of the UV radiation, particularly during the spring season.

Ultraviolet radiation is defined as the portion of the electromagnetic spectrum between X-rays and visible light, which is between wavelengths of 40 nm and 400 nm (energy comprised between 30 eV and 3 eV). The UV spectrum can be divided into broad bands: vacuum UV (40 nm − 190 nm), far UV (190 nm − 220 nm), UV-C (220 nm − 290 nm), UV-B (290 nm − 320 nm), and UV-A (320 nm − 400 nm) (Zeman, 2008). Solar UV-C, UV-B, and UV-A enter the earth's atmosphere, but only UV-B and UV-A reach the ground because UV-C is blocked in the stratosphere by the ozone layer (Chapman, 1930). Thus, the discovery of stratospheric ozone (O_3) depletion due to disposal of CFCs in the atmosphere (Molina and Rowland, 1973; Farman et al., 1985; Bojkov et al., 1995) is very evident in the polar regions, and the consequent rise of UV levels in the troposphere has underlined two of the most important effects of human activity on the environment (Solomon, 1999) and on global change (IPCC, 2007). Additionally, increased UV due to a decline in O_3 has affected the biosphere with implications for human health, as well as for fauna and flora (Caldwell et al., 1986; Worrest et al., 1989; Bigelow et al., 1998; Chaney and Sliney, 2005; UNEP, 2002). Additionally, UV radiation interacts with the DNA chain, which can produce cellular changes. This hazard can be responsible for the development of skin cancers and eye disease in humans (Slaper et al., 1996; WHO, 1999; 2006).

Ozone depletion was so evident that, shortly after its discovery, an international agreement, the "Vienna Convention for the Protection of the Ozone Layer", was signed in 1985 in an attempt to preserve the ozone layer. Two years later, the well-known "Montreal Protocol on Substances that Deplete the Ozone Layer," with its subsequent adjustments and amendments, was also designed. Thus, "Ozone Hole Protection" became a flag for environmental protection.

A strong widening of the ozone hole in the austral hemisphere, and a less intense ozone hole developing in the northern hemisphere, were recently observed (Bojkov et al., 1998; Uchino et al., 1999). In the Arctic, the consequences of depletion phenomena can be more serious due to the high density of human presence subjected to increased UV radiation. In September 2003, the surface of the austral polar vortex reached a new maximum (an extension of more than 12% compared with the previous maximum in 2000). Inside the ozone hole, the region with a very low O_3 concentration also grew. Furthermore, on Sept. 27, 2002, the vortex split into two parts (Fig. 4.1, Orsolini et al., 2005). These could be signs of an evolution in the dynamics of the polar vortex and consequently, of the ozone hole (Alvarez-Madrigal and Pérez-Peraza, 2005).

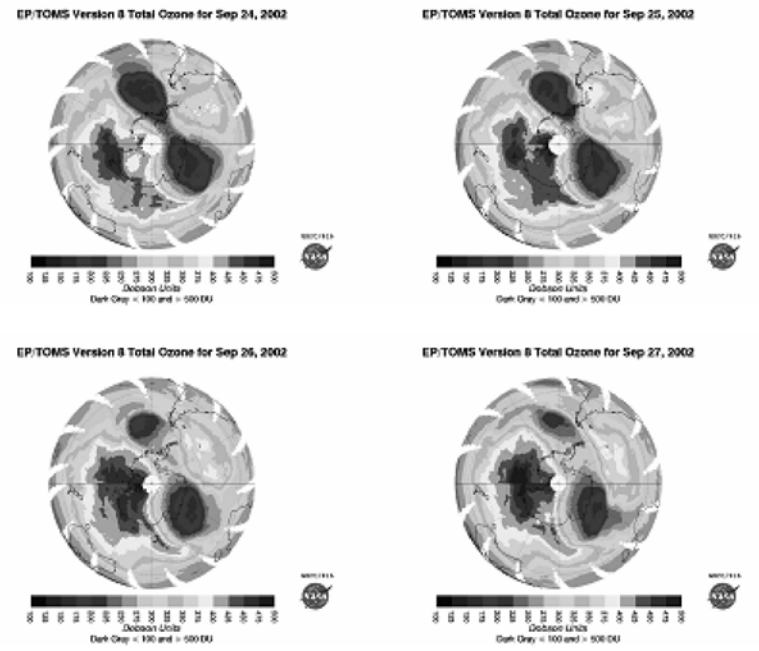

Figure 4.1 Ozone hole during splitting event in September 2002

The development of numerous measurement sites and long-term monitoring programs is necessary to understand these processes, to model the trends, and to study the ground effects. To this end, the international community is forming

collaborations for monitoring minor atmospheric gases, particularly the ozone levels at ground level (Roscoe et al., 2005a), using data taken by airborne instruments (Giovanelli et al., 2005) and from satellites (Banks et al., 1978; Russell Ⅲ et al., 1993; Krueger, 2001; Schoeberl et al., 2006; Waters et al., 2006). After more than 25 years of application, these studies allow for an evaluation of the effects of environmental protection treaties.

Polar vortices develop a confining action for chemical substances that exist at those latitudes, and the low temperatures promote Polar Stratospheric Cloud (PSC) development. During the polar night, photolysis processes do not occur. During the following spring, UV solar radiation activates the catalytic cycles of Cl and Br on the PSC surface, and the destruction of ozone begins. Therefore, studies on the precursors of depletion in the high atmosphere during the polar nights (Orsolini and Jackson, 2008) are necessary to understand the chemistry that generates ozone reduction (Strawa et al., 2002; Voigt et al., 2003; Tilmes et al., 2004).

4.2 Networks and Databanks

An increased distribution of Arctic stations has been encouraged since the Arctic Conference met in Stockholm, Sweden in 1956, in preparation for the International Geophysical Year (IGY) of 1957. Moreover "… the sensitivity of instruments should be increased so that measurements could be made using moonlight, a standard method of measuring the ozone content of surface air should be developed…, …the establishment of an aerological and actinometric station on the Greenland ice cap was strongly recommended ..." (WMO, 2006a).

An increased interest regarding the impact of human activity on the global ecosystems has contributed to the development of measurements of solar UV radiation, particularly in the UV spectral region. As a result, there has been a growing number of instrument sites, radiometric networks, and apparatus improvements; many of which are managed by either national or international organizations. One of the most noted is the World Meteorological Organization (WMO) the United Nations official authoritative voice on weather, climate, and water where its involvement influenced policy for ozone, UV, and climate change. The WMO *Global Atmospheric Watch* (WMO-GAW) (Volker and Barrie, 2006) forecasts the ozone hole trend, and issues the *Antarctic Ozone Bulletin* and the *Arctic Ozone Bulletin*.

The World Ozone and Ultraviolet Radiation Data Centre (WOUDC, http://www.msc-smc.ec.gc.ca/woudc/), part of the Global Atmosphere Watch (GAW) Program, consists of two component parts: the World Ultraviolet Radiation Data Centre (WUDC) and the World Ozone Data Centre (WODC). It produced its first data publication, *Ozone Data for the World*, in 1964.

There are presently six ozone data categories (types) and three UV data types

registered at the WOUDC. The ozone data archive contains the following data categories: Lidar vertical profiles, Ozonesonde vertical profiles, total column ozone (daily and monthly values), and Umkehr N-value and C-Umkehr vertical profiles. The UV data archive contains the following data categories: Broadband, Multi-band and Spectral.

The authors of this chapter, members of the Italian National Antarctic Program (PNRA), participate in the measuring of greenhouse gases (GHG), ozone, and UV radiation at stations in the Arctic and Antarctic regions, in cooperation with Direccion Nacional del Antartico/Istituto Antartico Argentino (DNA/IAA, Buenos Aires), the Norwegian Institute for Air Research (NILU, Kieler), and the Norwegian Polar Institute (NP, Tromsø). They manage a sampling site in Jubany Base (King George Island, Antarctic Peninsula) to monitor background levels of carbon dioxide (CO_2). They also contribute to ozone and UV monitoring by using Brewer spectrophotometers at the Belgrano Ⅱ Base (Antarctica), in Ushuaia (Tierra del Fuego, Argentina), and in the Arctic region, at the Italian base of CNR Dirigibile Italia in Ny Ålesund (Svalbard Island, Norway).

The Network for the Detection of Atmospheric Composition Change (NDACC), composed of more than 70 high-quality, remote-sensing research stations, is currently involved in the observation of the physical and chemical state of the stratosphere and upper troposphere to better assess the impact of stratospheric changes on the underlying troposphere and also on global climate. The various sites in the network are shown in Fig. 4.2. The Network for the Detection of Stratospheric Change (NDSC) is a part of this network.

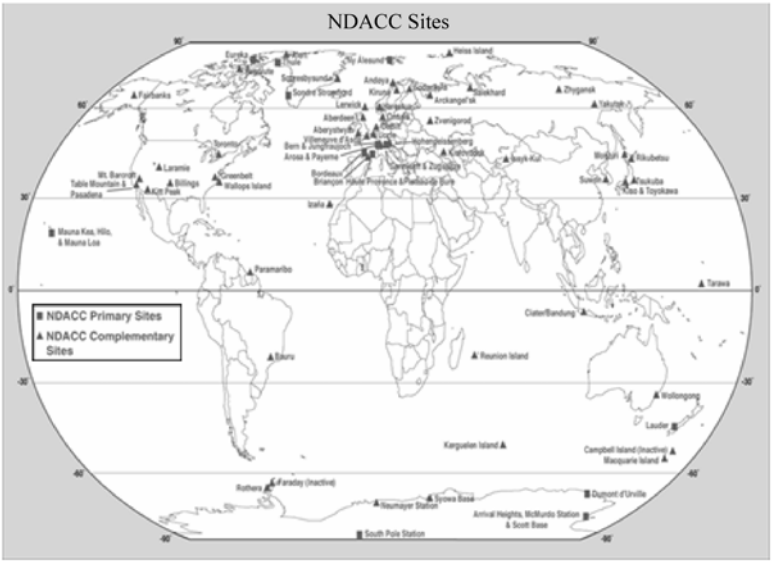

Figure 4.2 The NDACC network

The NSF Polar UV Monitoring Network, based on the SUV-100 spectroradiometer (Biospherical Instrument Inc., Bernhard et al., 2007) is a good reference source for UV measurements at ground level. The map of the network is displayed in Fig. 4.3.

Figure 4.3 Map of the NSF Polar UV monitoring network

The Global Climate Observing System (GCOS) is intended to be a long-term, user-driven operational system for monitoring the climate system, detecting and evaluating climate change, assessing the impact of climate variability and change, and is viewed as an application for national economic development. It is capable of providing the comprehensive observations required for research to improve the understanding, modeling, and prediction of the climate system. GCOS addresses the total climate system including physical, chemical, and biological properties, and atmospheric, oceanic, terrestrial, hydrologic, and cryospheric components. The map of the GCOS network is shown in Fig. 4.4.

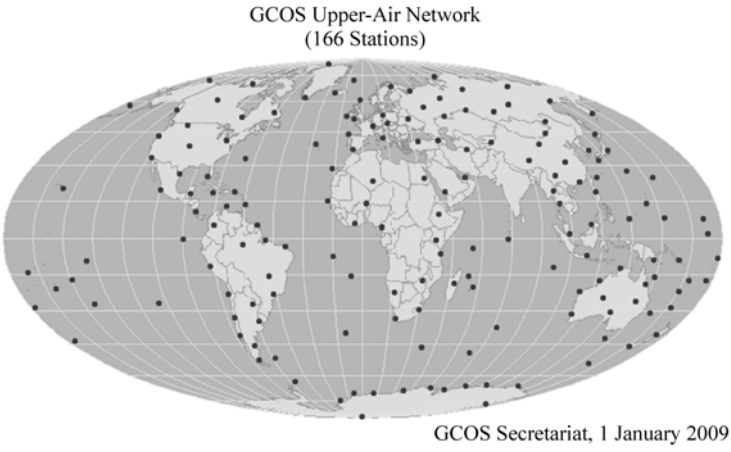

Figure 4.4 The GCOS network

Several projects promoted by the Scientific Committee on Antarctic Research (SCAR) manage sampling campaigns, networks, and data-banks to study the effects on the environment and biosphere in polar regions. The *Evolution and Biodiversity in the Antarctic: the Response of Life to Change* (EBA) (see SCAR-EBA, 2008) describes the past, explains the present, and predicts the future, with an international, multidisciplinary program. This program combines the research communities and aims of the past SCAR programs of RiSCC, EVOLANTA, and EASIZ (see http://www.scar.org/researchgroups/lifescience/). In particular, EBA studies the evolution and diversity of life in the Antarctic, and their influence on the properties and dynamics that currently exist in the Antarctic ecosystems and the Southern Ocean system. It attempts to make predictions on how organisms and communities respond to environmental change, both currently and in the future. By integrating research in marine, terrestrial, and freshwater ecosystems in a new manner, EBA hopes to advance evolutionary and ecological science globally, using model systems and organisms from the Antarctic.

Through a single web-portal, the SCAR Action Group on Marine Biodiversity Information (SCAR-MarBIN), mainly funded by the Belgian Science Policy, aims to offer free and open access to Antarctic Marine Biodiversity Data (see http://www.scarmarbin.be) which also includes a variety of scientific and technical services. SCAR-MarBIN is a core of the International Polar Year (IPY, 2007–2008) initiative, and acts as the information component of the Census of Antarctic Marine Life (CAML). For the atmosphere, databank web sites exist for each National Program, e.g., in Europe, Pangea of AWI, Germany, http://www.pangaea.de; NILU, Norway, http://polarportal.nilu.no/; British Antarctic Survey (BAS) (2008), UK, http://www.antarctica.ac.uk/bas_research/data/index.php; etc.

The management of this vast number of networks and databanks from across the globe, incorporating varying research strategies and types of instrumentation, requires a sizeable organization to efficiently install, maintain, and calibrate these instruments, ensuring quality assurance and quality control (QA/QC), for data collected from international databanks (see WMO, 2006b; WMO, 2007 and its references; Tüg et al., 2003; Diaz et al., 2005; Lakkala et al., 2005; Bernhard, 2008). This is, however, beyond the limits of the present work.

4.3 Impact of Solar UV on the Environment

The most important effect of solar UV on the environment is its photochemical interaction with oxygen, producing ozone, a GHG (greenhouse gas). The photochemistry of ozone behaves in different ways on the biosphere, depending on its height from the ground. The behavior of ozone at ground level demonstrates itself by its damaging effects on both human health (through inhaled air), and on vegetation. Because it is a major source of atmospheric oxidants, it regulates atmospheric composition and maintains a habitable atmosphere (IPCC, 2007). At

ground level, ozone is formed when nitrogen oxides (NO_x) and volatile organic compounds (VOC) react with sunlight. Nitrogen oxide is a by-product of high-temperature combustion created by fire, automobile emissions, and power plants. Volatile organic compounds include organic chemicals that vaporize easily, such as gasoline. Therefore, ozone is found in higher concentrations in urban areas resulting in dangerous effects on health.

The second behavior we discuss here is in the stratosphere (Chapman, 1930). About 90% of the ozone in the earth's atmosphere resides in the stratosphere, forming the "ozone layer" which shields life on earth from harmful UV radiation. In the mid-1970s, it was recognized that anthropogenic chlorofluorocarbons (CFCs) could deplete the ozone layer. Observation of the ozone layer indicated that depletion was occurring due to the buildup of CFCs and Halons in the stratosphere.

The discovery in the mid 1980s of dramatic stratospheric ozone depletion in Antarctica, which is commonly referred to as the ozone hole, and the consequent rising of UV levels in the troposphere, resulted in increased studies into the possibility of damaging effects on human health and biosphere.

The O_3 concentration, as Total Ozone Content (TOC) in Dobson Units (DU; 1 DU = $2.7 \cdot 10^{16}$ O_3 molecules $\cdot$ cm^{-2}) has fallen from about 350 DU in 1978, to less than 100 during the ozone hole season (approximately from the end of August to the end of November). The historical pictures elaborated by NASA for the ozone depletion in polar regions, October 1980 through 2004 and March 1979 through 1998, respectively, are shown in Figs. 4.5 and 4.6. The more recent conditions of Antarctic are shown in Fig. 4.6(b).

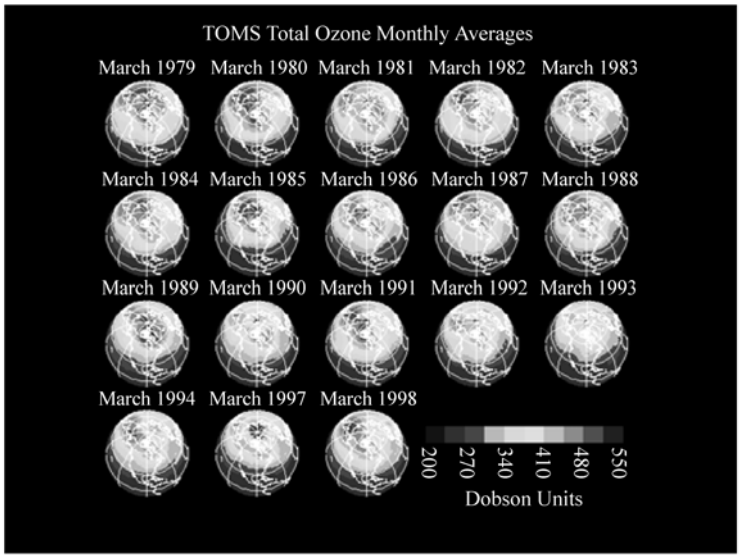

Figure 4.5 Historical picture of NASA with Arctic ozone depletion trend in March (monthly averages)

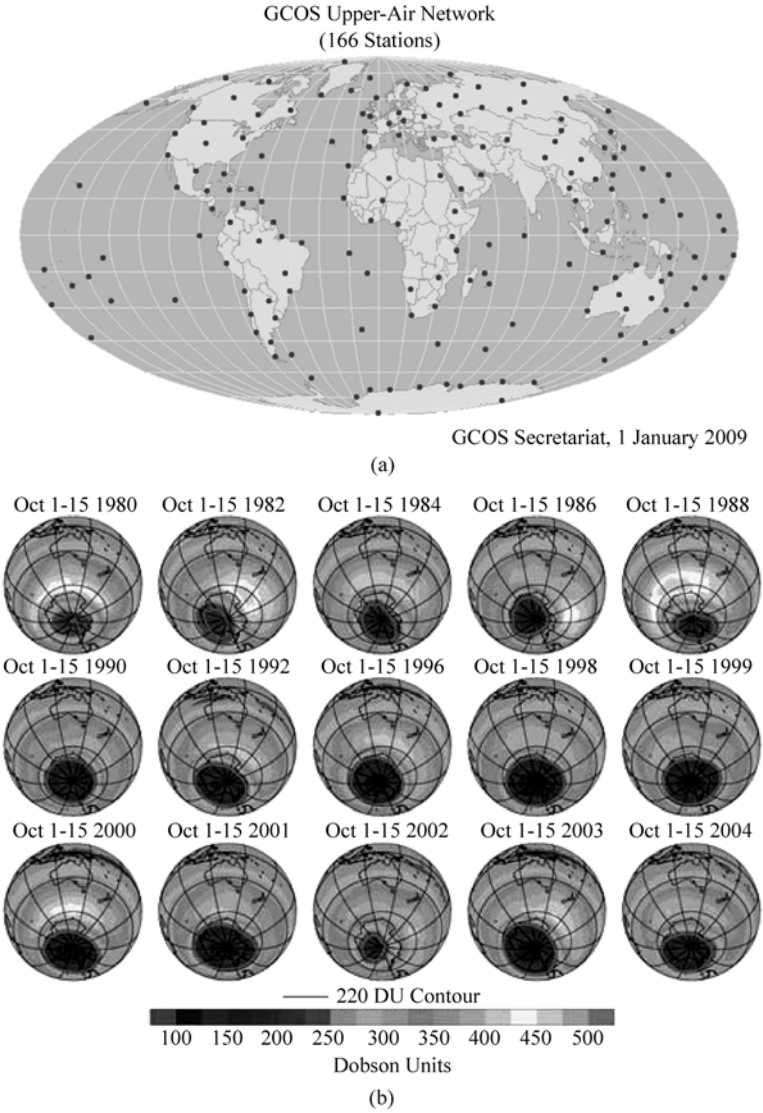

Figure 4.6 (a) Historical picture of NASA with Antarctic ozone depletion trend in October (monthly averages); (b) Antarctic ozone depletion trend, since 1980 to 2004 (October averages)

The O_3 trends registered between 1975 and 2005 are shown in Fig. 4.7(a), for Belgrano, and Fig. 4.7(b) for Ushuaia. In Fig. 4.7(a), Belgrano, the O_3 is displayed as October mean values measured at ground level by the Brewer spectrophotometer and the Total Ozone Mapping Spectrometer (TOMS), the sensors installed on several satellites during their flying period (1979−2005). Comparisons are made with the absolute minimum values registered inside the ozone hole. A negative

trend is clearly evident since the 1970s, with a sharp depletion since 1980. However, a stable tendency seems to have begun since the end of the 1990s (Knudsen et al., 2004; Velders, 2008). The day of the year during 1980 to 2005 when the ozone hole opens and closes (internationally defined as ozone concentration less or greater than 220 DU) is shown in Fig. 4.8(a). The opening period increases from approximately 270 DU to 210 DU. The period of closure moves from 300 DU to 350 DU. During the final part of the period, stabilization appears in the trend. Therefore, as shown in Fig. 4.8(b), the length of the ozone hole period increases from 20 days to 120 days, showing a constant trend after 1997. Is this an effect of the Montreal Protocol enforcement or a consequence of a constraining of the vortex? The answer to this question will be a future goal of research (Egorova et al., 2001; Tabazadeh and Cordero, 2004).

The Arctic polar vortex is not as stable as the Antarctic vortex, and abrupt ingress of warm air phenomena can occur (Salby and Garcia, 1990). These sudden warmings are due to streams of air from the southern latitudes aided by very active planetary waves (Stowasser et al., 2002; Latysheva et al., 2007; Manney et al., 2008). Antarctica had higher O_3 values during 1998 and 2002 when the vortex

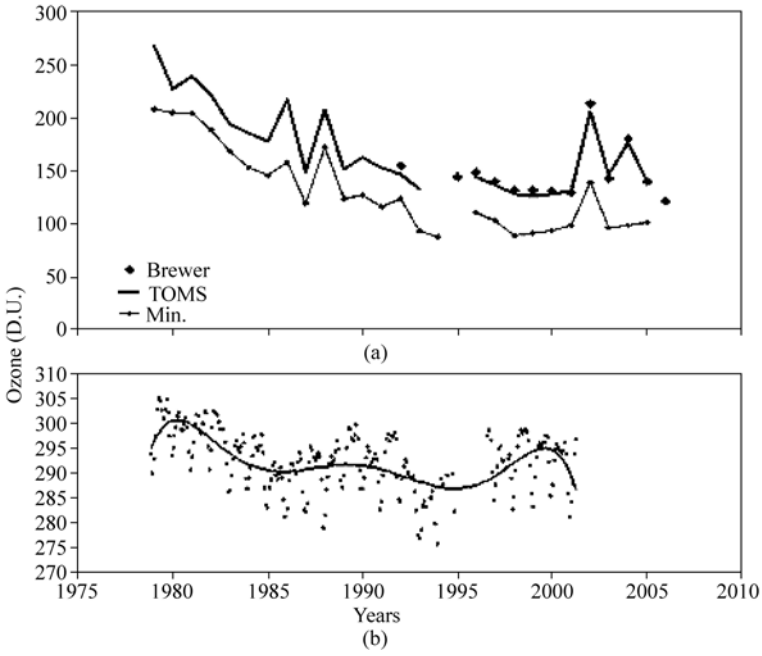

Figure 4.7 The O_3 trends registered between the years of 1975 − 2005: (a) in Belgrano-mean values during October by Brewer (dots) and TOMS (solid line) compared with the absolute minima (dotted line) registered inside the ozone hole; and (b) over Ushuaia-monthly mean values by Total Ozone Mapping Spectrometer (TOMS); the line is a generic fit to highlight the trend

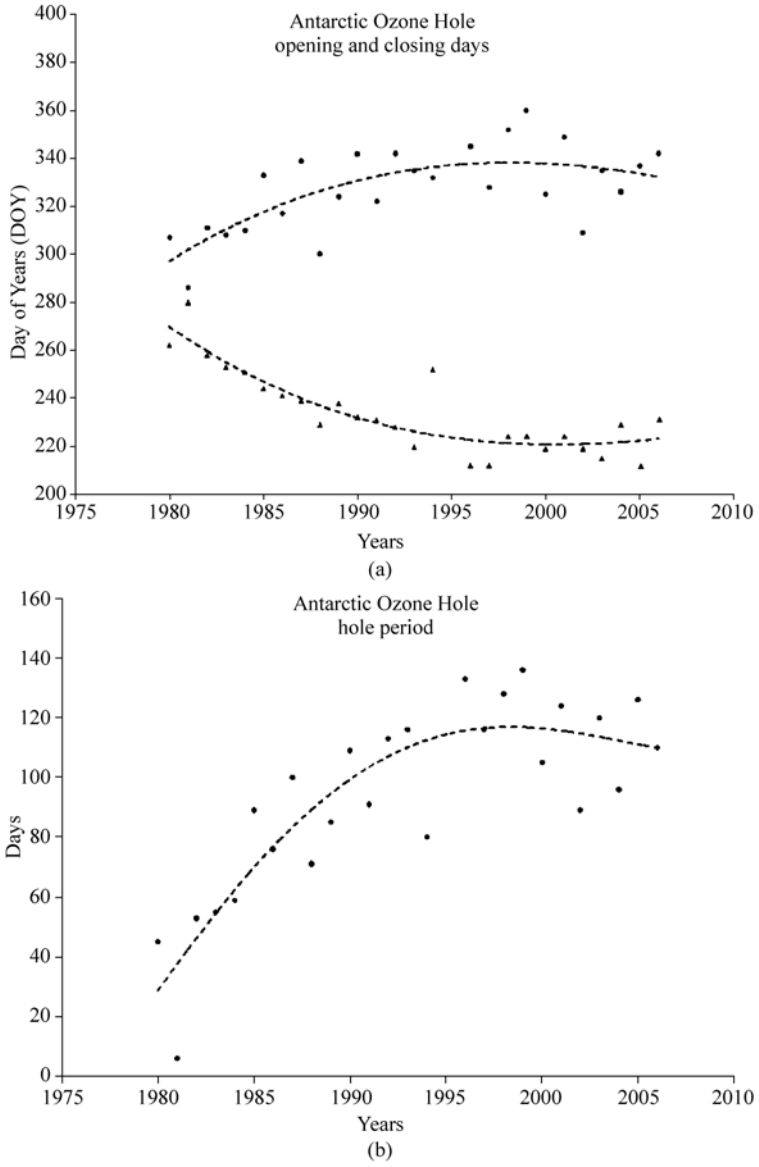

Figure 4.8 (a) Ozone hole in Antarctica, days of the year of opening and closing. Satellite data from TOMS; and (b) ozone hole in Antarctica, length ozone hole season. Satellite data from TOMS

area was not as wide and the temperatures were warmer. In particular, a major warming in September 2002 produced an early closing of the hole as a consequence of the splitting event (Grooß et al., 2005).

These studies are necessary to understand the dynamic inside the vortex and to distinguish natural trends from anthropogenic ones (Roscoe et al., 2005b). In fact,

ozone concentration is not only influenced by man-made CFCs, but also by natural phenomena connected to volcanic eruptions (Tie and Brasseur, 1995; Grainger and Highwood, 2003), Quasi Biennial Oscillation (QBO) (Garcia and Solomon, 1987; Baldwin and Dunkerton, 1998; Han et al., 2000; Sitnov, 2004), and solar activity (Labitzke and van Loon, 1997; Shindell et al., 1999; Todorovich and Vujovic, 2008). This is well depicted in Fig. 4.7(b), where the ozone trend over Ushuaia is shown. Even when dealing with a short record, the 11-year solar cycle trend appears in the data superimposed on the depletion due to CFC presence in the atmosphere. This is due to major increases of extreme UV radiation, responsible for ozone creation, compared with the larger UV wavelengths during the maximum amount of solar activity.

Moreover, the sun also influences the terrestrial atmosphere by sporadic activity (e.g., flares). After large explosions on the sun's surface, Solar Energetic Particles (SEPs) are able to enter the terrestrial magnetosphere and produce additional ionization at polar latitudes (Storini et al., 2005). During and after these events, the chemistry in the mesosphere and stratosphere changes, and the ozone concentration undergoes a large degree of variability (Damiani et al., 2006; Damiani et al., 2008) since the HO_x and NO_x that is produced trigger catalytic cycles of O_3 destruction. Depending on the seasonal conditions, these effects can be long lasting and could alter the background values. The absence of solar radiation during the winter does not allow NO production from the chemical reactions between N_2O and atomic oxygen. Moreover, the transport from the low latitudes of air masses that have a high concentration of NO is blocked by the vortex. In these conditions, caused by the descending air masses from the mesosphere to the stratosphere (Engel et al., 2005; Müller et al., 2007), the NO_x produced at elevated altitudes by SEPs assumes high relevance (Randall et al., 2006; Seppälä et al., 2007). However, a low percentage of TOC variability can be attributed to these phenomena since the effects are concentrated on the middle atmosphere.

These phenomena obviously happen throughout the year, but due to the dark winters in the polar regions, the absence of solar radiation limits continuous sampling by ground-based measurements or by satellite instruments. For this reason, the stratospheric ozone is occasionally sampled at ground level by spectrophotometers using the solar UV reflected by the moon disk. Of course this possibility is only viable during limited periods of the polar night, depending on both the phase of the moon disk and the air mass factor (the optical path length in the atmosphere). In other periods, the UV fluxes are too dim for the sensitivity of the instruments. The winter surface air temperatures are not as cold as in the Arctic. The minimum air temperature at ground level is higher than −26℃; therefore, it is possible to leave instruments outdoors and to carry out ozone and sulfur dioxide measurements (Rafanelli et al., 2008). Unfortunately, the very low winter surface temperatures and the frequent presence of katabatic winds in the Antarctic make open-air measurement in the polar night a sporadic event, which can only be accomplished with ozone-sondes on balloons.

4.3.1 Effect of the Environment on Solar UV

As described above, environmental effects resulting from UV radiation exposure do exist; however, several effects are also produced by the environmental components on the solar UV flux during its passage through the atmosphere. The presence of numerous substances, components (e.g., NO_2, SO_2), and aerosol particles due to fire, air pollution, dust, etc. (Fig. 4.9), modifies UV diffusion and scattering, creating measurement, sampling, and modeling problems.

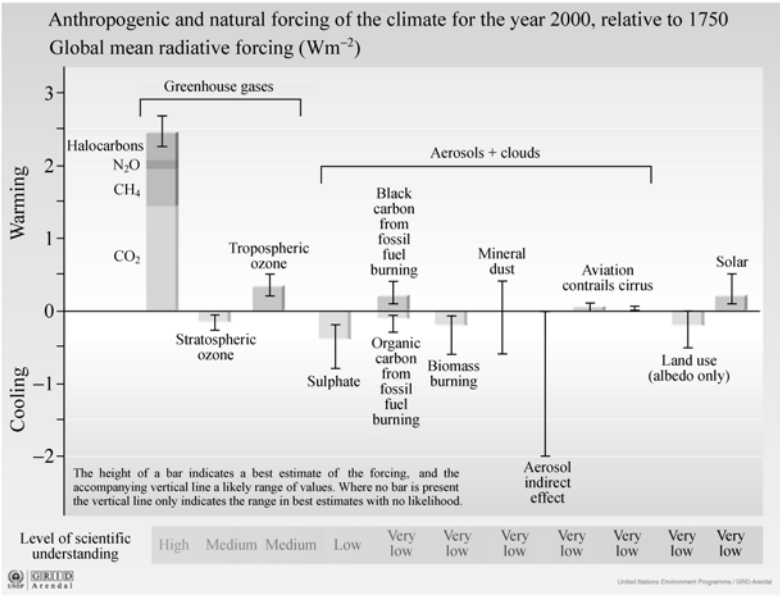

Figure 4.9 Atmospheric component affecting the radiative forcing in the atmosphere

The presence of clouds in the sky is one of the very important factors (Rafanelli et al., 2002) that affect radiation measurements at ground level (Rafanelli, 2001). Clear sky conditions are essential for the calibration of broadband or multi-filter radiometers (those with moderately wide, pass-band filters). The calibration is performed with clear sky conditions to obtain isotropic diffusion of radiation in the atmosphere. The same conditions are repeatable at every calibration. With the presence of clouds, the isotropic condition fails because the transmission through the layers is no longer isotropic, and selective wavelength absorption is produced. Therefore, different positions of clouds produce different effects on the global dose measured. The shape of the spectral window of the pass-band filters used in the instruments does not have a box contour as is theoretically required. As a result, the clouds modify the response of the instrument, make radiometer calibration unreliable, and thus, their data is not completely reliable. Alternatively, with the use of spectral instruments, the clouds are not influential due to the narrow window in each wavelength.

Furthermore, many models and algorithms are developed for clear sky conditions and are not valid in cloudy conditions. The vertical profiles from the evaluations of the Brewer measurements (Umkehr model) are shown in Fig. 4.10 (a), (b), (c); panel (a) shows the profile of the clear sky under normal conditions, and panel (b) shows the profile where the edge of the ozone hole is positioned over Ushuaia. In panel (c), the cloudy conditions produce negative model results. Indeed, the cloudy

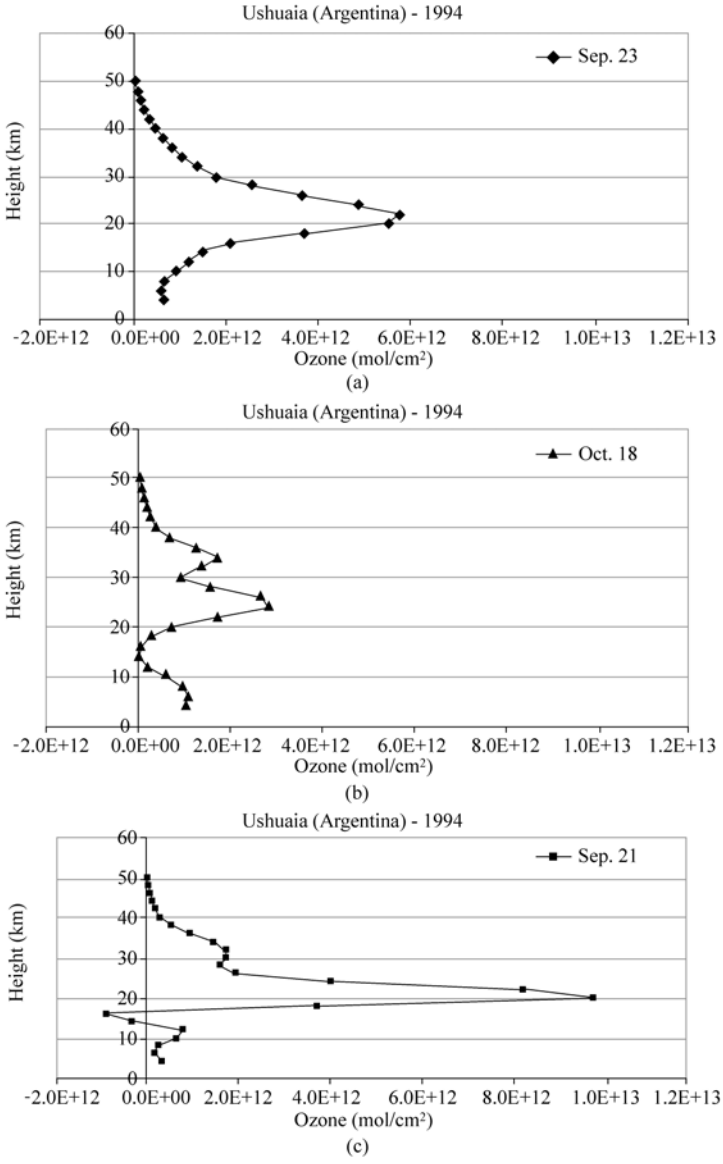

Figure 4.10 Ozone vertical profiles by Umkehr model: (a) normal situation; (b) under ozone hole; (c) in cloudy conditions. Source: Rafanelli et al., 1998

weather conditions, often present at high latitudes, does not allow for frequent use of this technique. This is unfortunate since it would be very beneficial to have such a simple and inexpensive method in place for measuring vertical profiles in remote regions (Rafanelli et al., 1998).

Currently, cloud cover is only studied for meteorological reasons, yet its linkage with solar radiation is also important (Moriconi et al., 1998; Simic et al., 2007).

A prototype of a Total Sky Camera (TSC) is shown in Fig. 4.11 (Rafanelli et al., 2001). The pictures of the sky and the digitized output are depicted in Fig. 4.12 (Rafanelli et al., 2005). This system, in conjunction with hardware and software, can evaluate the coverage and localization of clouds related to the sun's position.

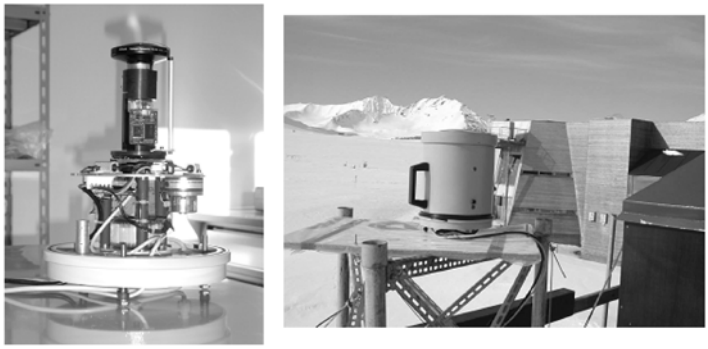

Figure 4.11 Total Sky Camera (TSC); inside view and outdoor location

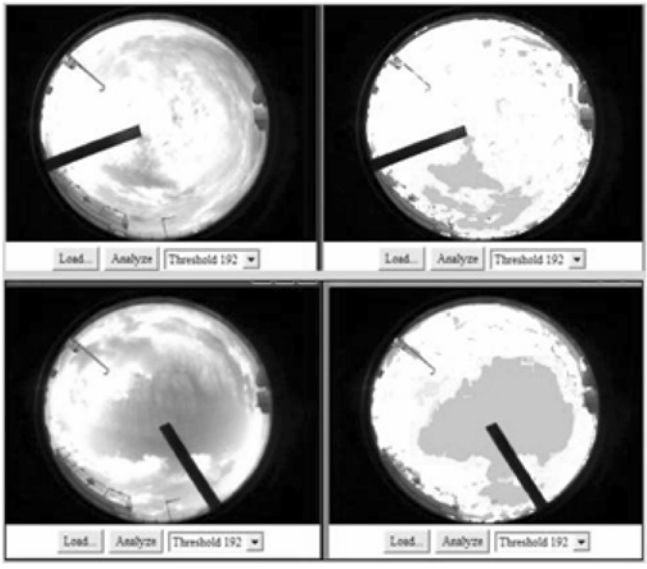

Figure 4.12 Pictures of the sky by TSC (left) and software output (right). Source: Rafanelli et al., 2005. The black band is to shadow the sun

Studies of cloud effects on UV are possible by synchronizing the shooting with the solar UV spectra. For example, the ratio 305/380 nm vs. PAR (Photosynthetically Active Radiation), sampled with a multi-channel radiometer, is shown in Fig. 4.13. In clear sky conditions, the trend follows the solar zenith angle (SZA), while in cloudy conditions, there is no pattern (Rafanelli et al., 2006). It is possible to model the cloud effect, producing a long time series of spectra and corresponding images.

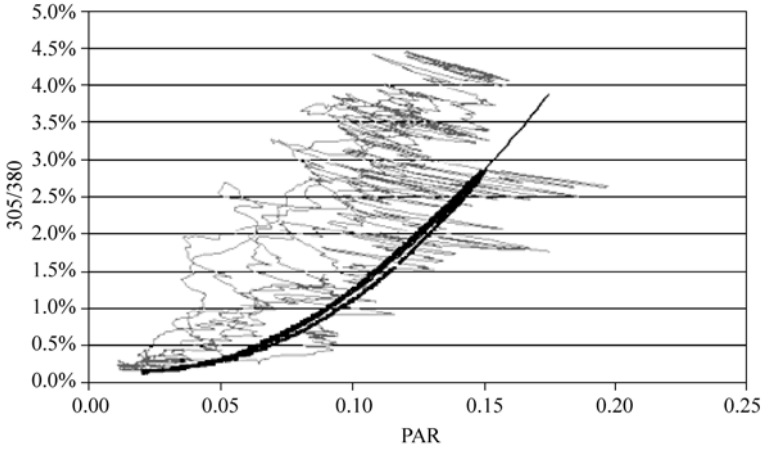

Figure 4.13 Scatter plot of ratio 305/380 nm vs. PAR. Data gathered by multichannel radiometer. Black line in clear sky conditions, grey dots for cloudy sky. Source: Rafanelli et al., 2006

4.4 Impact of Solar UV on Human Health

The potential consequences of global climatic change (GCC) with regard to human health have recently been the subject of numerous reviews (e.g., Leaf, 1989; Longstreth, 1991; Epstein, 1998; Longstreth, 1999). For the most part, the possibility of increased negative effects could only occur when the incidence of disease is linked to the tropics or other warm weather regions. However, it is also clear that in most locations, GCC will only affect the risk of disease if the disease already exists at that location or in a location that is geographically contiguous. There is great concern that the risk of malaria may increase with GCC in developed as well as developing nations, and it has also been contended that most developed nations that conquered the disease in the past may experience a serious resurgence.

Solar UV radiation changes are considered as contributing factors to GCC. Solar UV radiation can affect human health both positively and negatively. Small amounts of exposure can be beneficial to humans and is essential for the production of vitamin D. Ultraviolet radiation is also useful for the treatment of several diseases, including rickets, psoriasis, eczema, and jaundice, under medical

supervision. The benefits of treatment versus the risks of exposure are a matter of clinical judgment.

Prolonged human exposure to solar UV radiation may result in acute and chronic health effects on the skin, in the eyes, and on the immune system. Sunburn (erythema) is the best-known acute effect of excessive UV radiation exposure (Lindfors and Vuilleumier, 2005). Over the longer term, UV radiation induces degenerative changes in skin cells, fibrous tissue, and blood vessels leading to premature skin aging, photodermatoses, and actinic keratoses. Another long-term effect is an inflammatory reaction of the eye. In the most serious cases, skin cancer and cataracts can occur (De Gruijl et al., 2003). The relationship between the exposure to UV radiation and the level of disease is shown in Figs. 4.14 and 4.15.

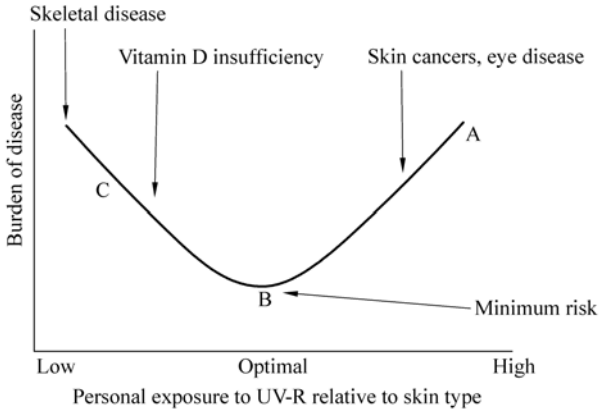

Figure 4.14 Relationship of exposure to UV-R and burden of disease. Source: WHO, Ultraviolet radiation and the INTERSUN Programme

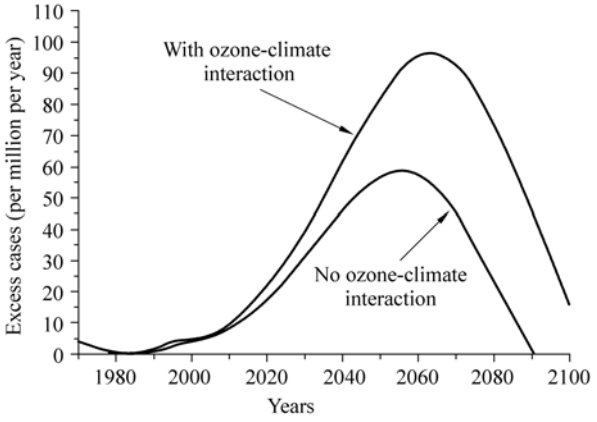

Figure 4.15 Increase in skin cancer incidence in northwestern Europe with and without ozone-climate interaction

These effects are evident in laboratory experiments. DNA damage induced by UV radiation is wavelength dependent, whereas UV-A only causes indirect damage to DNA, proteins, and lipids through reactive oxygen intermediates. On the other hand, UV-B causes both indirect and direct damage because of the strong absorption by the DNA molecule at wavelengths below 320 nm. The most abundant products formed by irradiation with UV-B are cyclobutane pyrimidine dimmers (CPD). Experiments on bacteria have highlighted several repair mechanisms in response to UV-induced damage. These mechanisms are usually classified into dark repair (DR) and photoreactivation (Zenoff et al., 2006).

On the other hand, quantifying risks for humans is difficult because the risk depends on styles of human life which evolve in the time. Nevertheless, epidemiological and experimental studies have confirmed that UV radiation is a definite risk factor for certain types of cataracts, with peak efficacy in the UV-B waveband. The causal link between squamous cell carcinoma and cumulative solar UV exposure has been well-established. New findings regarding the genetic basis of skin cancer, including studies on genetically modified mice, have confirmed the epidemiological evidence that UV radiation contributes to the formation of basal cell carcinomas and cutaneous melanomas. The animal models, for the latter, have demonstrated that UV exposure at a very young age is more detrimental than exposure in adulthood. Although suppression of certain immune responses following UV exposure has been recognized, the impact of this suppression on the control of infectious and autoimmune diseases is largely unknown. However, studies on several microbial infections have indicated significant consequences in terms of symptoms or reactivation of disease. The possibility that the immune response to vaccination could be depressed by UV-B exposure is of considerable concern (De Gruijl et al., 2003).

Studies conducted world-wide have shown that excessive solar UV exposure was the cause for the loss of approximately 1.5 million days of work (0.1% of the total global burden of disease) and 60,000 premature deaths in the year 2000. The greatest damage resulting from excessive exposure to UV radiation is cortical cataracts, cutaneous malignant melanoma, and sunburn (although the latter estimates are highly uncertain due to paucity of data). Notably, a zero UV exposure would not result in a minimum disease burden, but rather a high disease burden due to diseases caused by vitamin D deficiency (McMichael et al., 2006).

A very low percentage of the Antarctica population has been exposed to UV, attributed in part to the fact that the majority of its residents consist of scientific and logistic personnel, well-educated in health risks. In the recent past, however, approximately more than 30,000 tourists per year have ventured into these latitudes (Fig. 4.16; BAS, 2008; IAATO, 2008). Additionally, the number of tourists in the Arctic region continues to increase (e.g., 1.2 million in Alaska in 1999; Fay, 2000). Low Arctic temperatures force residents to wear warmer clothing suitable for the climate, even during the full summer season. A real health risk that exists during the summer is possible damage to the eyes due to a relatively high SZA

due to direct sun. The high albedo, for ice and snow presence, is an additional issue. Unfortunately, both residents and tourists are ill-informed in regard to the UV risks present in the polar regions.

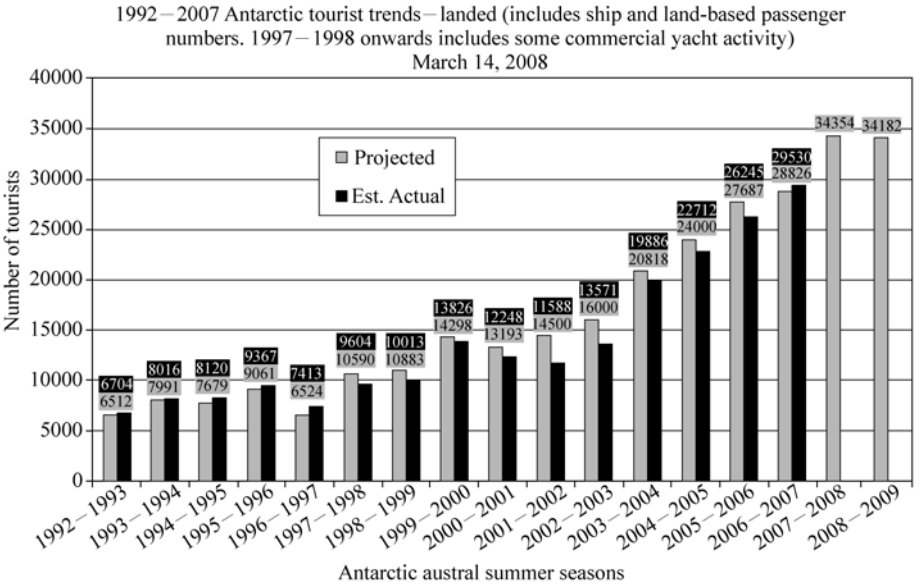

Figure 4.16 Tourist presence in Antarctica. Source: International Association of Antarctica Tour Operators (IAATO)

Thus, the study of solar UV in Antarctic latitudes is beneficial because the reduced thickness of the atmosphere, the clear air, and the absence of local sources of ozone at those latitudes allow one to measure the background levels with high accuracy (Pazmiño et al., 2005). Moreover, the deep and rapid variations in TOC, into the vortex, promote the study of the model's response and the ability to carry out experimental campaigns on fauna and flora with varying environmental conditions useful to translate the results in countries at lower latitudes.

Cataracts are a major cause of blindness. This condition can be adequately treated by surgery, but when not treated, it often leads to permanent blindness with grave social/economic consequences. For example, in 1998 an estimated 135 million people worldwide were visually impaired and 45 million people developed blindness with cataracts as the leading cause (Mariutti et al., 2003; WHO, 2008a).

Epidemiological studies show that the etiology of cataracts is complicated and involves many risk factors. Taking into consideration all the risk factors, the only effective preventive interventions are to stop smoking and to reduce ocular UV-B exposure (Taylor, 1999).

The dependence of cataract formation on the wavelength of the UV radiation is important in establishing whether increases in ambient UV-B exposure due to ozone depletion will have an impact. Cataracts in humans develop slowly with

age, and the process is difficult to investigate experimentally, especially in human subjects, but can be done with the use of isolated lenses and in animals. The problem with these experiments is that the cataracts are induced in a matter of hours, days, or weeks. Careful comparisons show that the commonly UV-induced anterior subcapsular opacification in animals is not adequate for modeling the age-related cataracts observed in humans. The wavelength dependence of cataract formation can be inferred from the basic mechanism; however, the knowledge currently available on this subject is still inadequate. It is essential, therefore, that the study of dosimetry is utilized, particularly personal dosimetry, thus facilitating an increased knowledge of the damaging effects of UV.

4.4.1 Information and Protection Programs

The most important, effective, and rapid action for the reduction of the health risks caused by UV exposure is to provide people, across the globe, with accurate information. Possession of adequate knowledge of the cause and effect of sunburn, tanning methodology, and the best known practices for sun exposure, is the only way to reduce UV radiation induced health risks. Thus, over the last 20 years, many international, national, governmental, and private institutions have published numerous articles, and produced web-portals and web-sites to explain, inform, and display the most effective preventative practices and solutions. The knowledge of ozone depletion over Antarctica, the ozone hole, and the risks of sun exposure, is not only confined to specialists, but is now diffused worldwide among the general population, even if to varying degrees.

The World Health Organization (WHO), United Nations Environment Programme (UNEP), World Meteorological Organization (WMO), and International Commission on Non-ionizing Radiation Protection (ICNIRP) are the most influential international institutions in this field of research. A visit to their web-portal is an educational experience. Other national portals are also available as additional sources of valuable information. Another very informative source is the WHO INTERSUN Programme (WHO, 2008b), created as a result of Agenda 21 actions (UN Conference on Environment and Development, Rio de Janeiro, Brazil, June 3 − 14, 1992). Agenda 21 is a comprehensive plan of action to be taken globally, nationally, and locally by various organizations within the United Nations system, governments, and major groups involved in every area of human impacts on the environment. In addition, there are numerous publications available as relevant sources of information (e.g., Global Solar UV Index: A Practical Guide of WHO, 2002).

All of these instruments of information are based on the Global Solar UV Index (GSUVI), the official tool used to evaluate the risks of sun exposure. The purpose of the GSUVI is to provide uniform information to the public about daily UV exposure levels and protective measures that should be taken, with various index values.

Ultraviolet index values can range from zero upward. Summertime UV-I values can range up to 20 in many countries located close to the equator. Summer maxima in Europe are generally not more than 8, but can be higher, especially at beach resorts. While not yet standardized worldwide, the GSUVI values can generally be described as low (1 and 2), moderate (3 and 4), high (5 and 6), very high (7 and 8), and extreme (greater than 9).

Other UV indices also exist; therefore, it is necessary to be aware of the correct usage of the information obtained from them. In particular, the WHO warns that there is a real danger for public confusion over the use of multiple UV indices, together with a universal GUVI recommended by international organizations since 1995 (WHO, 1998).

Some of these multiple indices are promoted by sunscreen or cosmetic manufacturers for commercial purposes and used by local authorities who are unaware of the standardized and internationally accepted GSUVI. The GSUVI estimates the maximum skin damaging UV measured over a period of 10 to 30 minutes at solar noon on a given day. The higher the UV-I, the greater the exposure to skin and eye damaging UV, and the less time it takes for this damage to occur (WHO, 1998). The WHO emphasizes that a real danger currently exists that the use of standardized GSUVI in conjunction with many other UV indices currently in existence could lead to public confusion regarding critical messages on health.

4.4.2 Dosimetry, UV Modeling, and Instruments

Every wavelength causes differing biological effects. Four Action Spectra for different biological targets are shown in Fig. 4.17. It is evident that UV-B is the main culprit for harmful UV consequences, in particular erythema. Convolving a solar UV irradiance spectrum with the specific action spectrum and then integrating

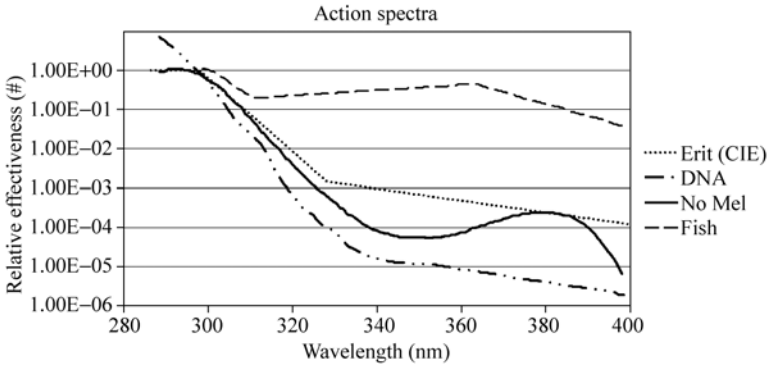

Figure 4.17 Action spectra for several biological targets. Source: Di Menno et al., 2007

it (effective spectrum) over time, the effective dose (ED) is obtained; this is the link to evaluating solar UV risk. The ED integrated over time provides the available environmental dose (AED), i.e., the dose available outdoors during the time considered. Measurements are often expressed in terms of exposure ratios (ER) or fraction of environmental dose falling on a horizontal surface (maximum available dose).

To evaluate the individual dose (ID), (i.e., the dose absorbed by a target exposed outside without considering the time spent indoors), it is necessary know the effective time of exposure. Measurements carried out by ground-based radiometric instruments give the AED, but no information on ID. Moreover, for a human body, not all the parts are exposed to the sun in the same manner, depending on the solar angle view for the surface exposed (i.e., skin or eyes). Therefore a personal dosimeter is an essential requirement for evaluating the ID (Fig. 4.18(a), (b), (c)).

(a) (b) (c) (d)

Figure 4.18 (a) Commercial electronic dosimeters; Examples of personal dosimeters; (b) Rafanelli et al. 2002; (c) Kimlin and Parisi, 1999; (d) Electronic dosimeter and dosimeter badge by polysulphone film

To describe in detail the real individual habits of sun exposure, long-term studies using personal dosimetry are needed. Furthermore, the dosimeter can be placed on different parts of the body to measure the solar angle view. The dosimetric

science for the AED utilizes broadband radiometers in a single site or in network architecture. These instruments are known as biometers and have a spectral response approximating the action spectrum of the phenomena under examination, mostly erythema. They are cheap, but have small differences in construction (e.g., in spectral response). Large differences can occur in the results, thus not permitting a reliable comparison between equipment from different manufacturers (Rafanelli, 2001). On the other hand, the use of more complex instruments (e.g., spectroradiometers), could present serious management and budgetary problems. For these reasons, multichannel broadband radiometers are becoming more widely established for measuring UV irradiance, although not at high resolution, but only in several spectral bands. Multi-channel radiometers are calibrated in physical units, so models reconstructing the continuous UV spectrum are necessary to compute the AED (i.e., Dahlback, 1996; Rafanelli et al., 2000).

Valid examples of multi-channel radiometers are the GUV 511 (Biospherical Inc., USA; Di Menno et al., 2002), with four filters at 305, 320, 340, 380 nm; and the NILU UV Irradiance Meter, NILU Prod. AS, Norway (Dahlback et al., 2007) with five filters at 305, 312, 320, 340, and 380 nm. Both can also perform the PAR measurement. A result of the modeling application for some biological effects is shown in Fig. 4.19. In each plot, the difference between the effective dose computed by spectral and modeled data is less than 8% (Anav et al., 2004).

An alternative approach involves biodosimeters that use simple biological systems (bacteria, spores, and biological cells or molecules) and measure AED directly for the biological effect studied. Biodosimeters are cheap, small devices that require no external power and thus, are widely accepted for both natural and artificial UV dose control. However, biodosimeters have a number of disadvantages. They indicate a damaging effect of UV because UV absorption of a DNA molecule is the basis of a biological response. They require laboratory analysis to evaluate the dose and an in-situ control is not possible. The comparison between different biodosimeters is very hard because they act as "black boxes," the AED is measured in specific biological units and not as comparable physical units, J/m^2.

A practical personal dosimeter is based on polysulphone badges with plastic film that changes its transmission after UV exposure (Diffey, 1984; McKinlay and Diffey, 1987; Diffey, 1989; Mariutti et al., 2003). This dosimeter (Figs. 4.18(c) and 4.20) also agrees with daily GSUVI data and comparisons of AED measurements do not need to be corrected (Wester, 2006).

As previously stated, to measure the AED, the knowledge of the pass band filter shape is important in order to make comparisons between different instruments, such as multi-channel or broadband radiometers. In the spectral UV region, a very small difference in the shape can produce a large discrepancy in the results of a comparison (Anav et al., 1996; Di Menno et al., 2002). However, the major problem in accurately evaluating irradiance is the presence of clouds in the sky (Mariutti et al., 2002). Thus, the use of spectroradiometers is the best option, but they do involve a longer sampling time.

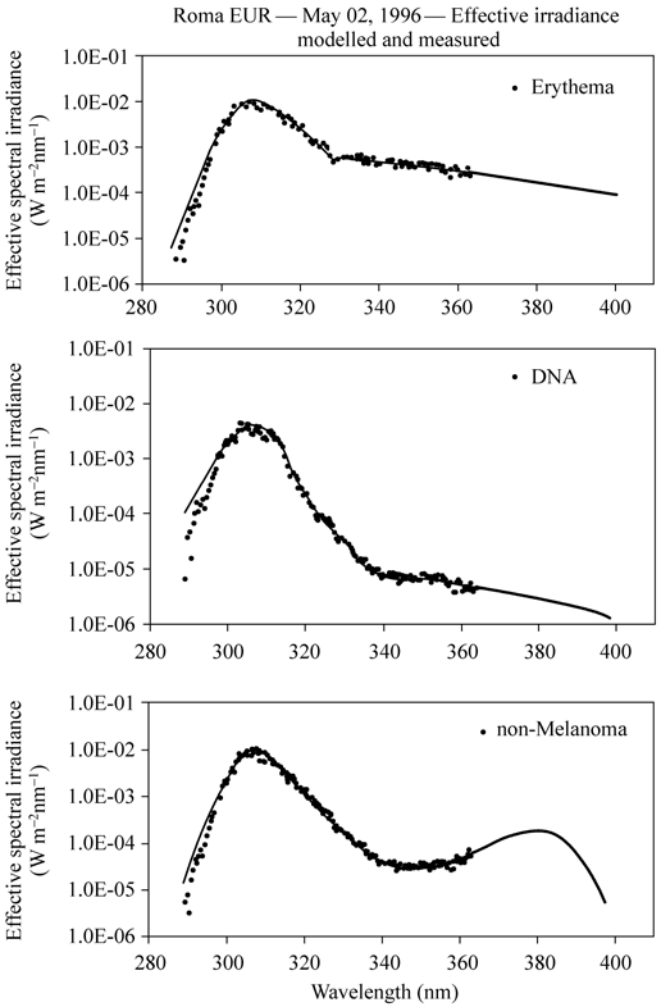

Figure 4.19 Effective spectral irradiance comparisons between the WL4UV model (lines) and Brewer data (dots) for (from top to bottom): Erythema, DNA, and no melanoma. Data carried out in Rome Italy, May 2, 1996 at SZA = 27.30°. Source: Anav et al., 2004

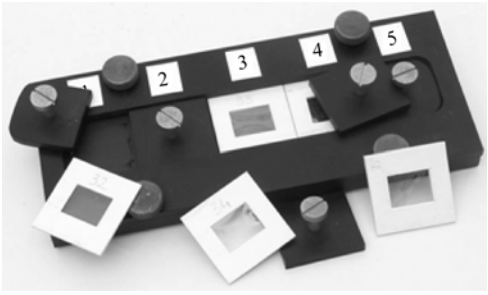

Figure 4.20 Personal dosimeter, badges in polysulphone. Source: courtesy of G.F. Mariutti

Modern technology can solve or attenuate the problems. In Di Menno et al. (2007), a new CCD and optical fiber spectrograph (fast spectroradiometer) is shown. The specifications of the instrument are: (1) pass-band range: 250 nm − 400 nm; (2) spectral resolution: 0.25 nm FWHM (improvement of the CCD efficiency making it possible to have a 0.10 nm as FWHM); (3) high signal/noise ratio, very fast acquisition; and (4) automatic management, small size and lightweight with low power consumption. In addition, the use of high quality commercial components and an expert knowledge of the technical specifications of each part, crown it all.

The key to obtaining such a high performance has been the adoption of a new shape for the optical fiber junction to the monochromator box. Commonly, the bush has a circular shape, but in this case, a large part of the beam falls outside the slit at the entrance of the monochromator. By rearranging the bush into a square profile, almost all the beam enters into the monochromator. This solution is shown in Fig. 4.21. With this key feature, the energy inlet increases from 1% to 40%. This allows the measurement of solar UV wavelengths less than 280 nm, which is useful for indoor measurements that are applied to artificial UV sources. The preliminary results of a comparison with a Brewer spectrophotometer, used as a reference, are shown in Fig. 4.22. This allows the application of the UV differential spectral analysis technique to evaluate the concentrations of many compounds present in the atmosphere. Finally, the small dimensions of the instrument allow its use in a configuration suitable for polar night campaigns.

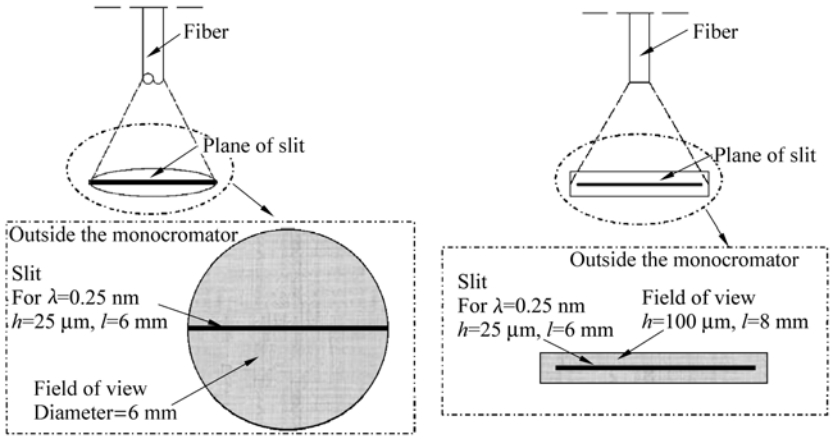

Figure 4.21 Circular and square shapes for optical fiber junction with monocromator box. Source: Di Menno et al., 2007

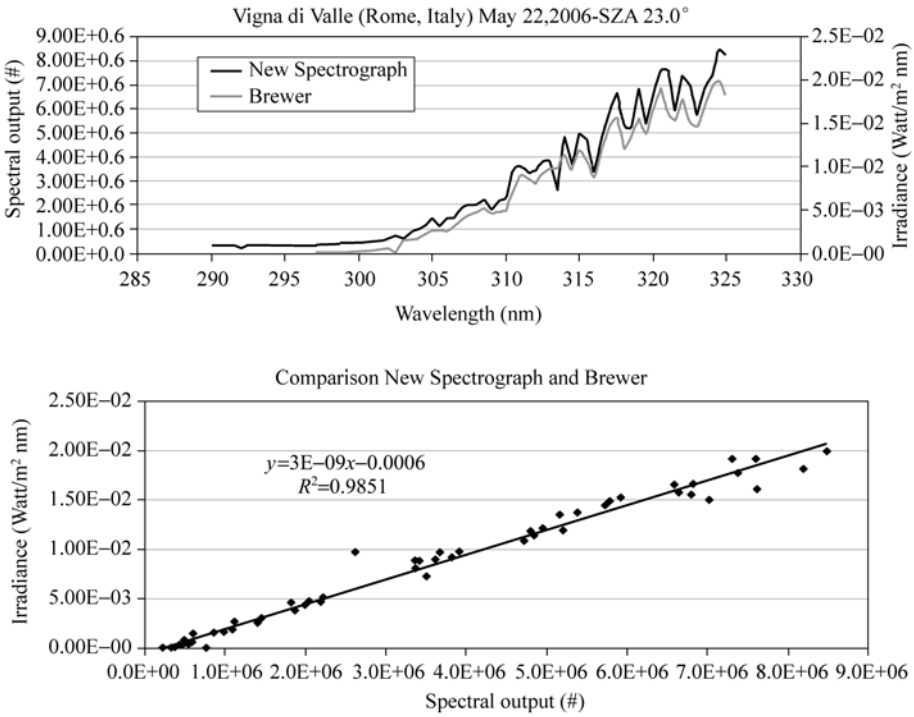

Figure 4.22 Preliminary results of a comparison between Spectrograph vs. Brewer. Source: Di Menno et al., 2007

4.5 Concluding Remarks

A better understanding of the dual effects of solar UV radiation is essential for the environment and for life on earth. It positively affects the planetary energy balance and it auto-produces the UV filter by photochemistry of ozone in the stratosphere. The polar regions are privileged areas for conducting research to advance our knowledge of the physics and consequences of these topics. The negative environmental effects are dependent on humanly induced polluting activities, such as releasing CFCs into the atmosphere. New habits recently adopted by a large percentage of the world's population have had a great effect on the consequences of UV exposure for human health. Frequent exposure to large areas of the skin, especially during the middle of the day, increases the risk of damage.

Exposure to artificial sources of UV rays, such as tanning beds or other types of UV lamps, has purposely not been discussed here as it is beyond the scope of the paper. However, this is an important issue because doses absorbed from artificial mercury lamps, in many cases used without any supervision by qualified personnel,

adds to the UV exposure already received from natural UV doses, which results in an increased risk of skin damage.

For a "correct usage of UV", the words from the Global Solar UV Index—A Practical Guide of WHO (WHO, 2002) are to be noted: "*A marked increase in the incidence of skin cancers has been observed in fair-skinned populations worldwide since the early 1970s. This is strongly associated with personal habits in relation to sun exposure and its ultraviolet (UV) component, and the societal view that a tan is desirable and healthy. Educational programmes are urgently needed to raise awareness of the damaging effects of UV radiation, and to encourage changes in lifestyle that will arrest the trend towards more and more skin cancers.*"

Another topic to be investigated is the absorption of UV rays from artificial sources by employees and professionals working with arc welders or germicide UV lamps. This research requires very fast spectrographs, where the bottom of the spectral range is less than 280 nm, and additional studies on indoor spaces mapping the UV reflecting surfaces that increase the dose by diffuse radiation in the work place.

References

Alvarez-Madrigal M and Pérez-Peraza J (2005) Analysis of the evolution of the Antarctic ozone hole size. J. Geophys. Res. 110, D02107, DOI:10.1029/2004JD004944

Anav A, Moriconi ML, Giannoccolo S, and Di Menno M (1996) Field measurements of global UV-B radiation: a comparison between a broad-band radiometer and a Brewer spectrophotometer. Il Nuovo Cimento C(4), Vol. 14, July − August, pp. 505 − 516

Anav A, Rafanelli C, Di Menno I, and Di Menno M (2004) An algorithm for irradiance and effective dose rates using solar spectral UV irradiance at few selected wavelengths. Rad. Prot. Dosim. V. 111 (3), 239 − 250

Baldwin MP and Dunkerton TJ (1998) Quasi-biennial modulation of the southern hemisphere stratospheric polar ozone. Geophys. Res. Lett. 25: 3343 − 3346

Banks PM, Huntress WT, Hudson RD, Reber CA, Barth CA, Farmer CB, Geller MA, Gille JC, London J, Megill LR, Russell JM III, Roble RG, Stolarski RS, and Waters JW (1978) Upper Atmosphere Research Satellite Program. JPL Publication 78 − 54

British Antarctic Survey (BAS) (2008) http://www.antarctica.ac.uk/about_antarctica/tourism/index.php

Bernhard G, Booth CR, Ehramjian JC, Stone R, and Dutton EG (2007) Ultraviolet and visible radiation at Barrow, Alaska: Climatology and influencing factors on the basis of version 2 National Science Foundation network data. J. Geophys. Res. 112: D09101, DOI:10.1029/2006JD007865

Bernhard G (2008) Instrumental and Methodological Developments in UV Research. Proceedings of Quadrennial Ozone Symposium 2008. Tromsø Jun 29th − Jul. 5th

Bigelow DS, Slusser JR, Beaubien AF, and Gibson JH (1998) The USDA Ultraviolet Radiation Monitoring Program. Bulletin of the American Meteorological Society 79: 601 − 615

Bojkov RD, Bishop L, and Fioletov VE (1995) Total ozone trends from quality controlled ground based data (1964 − 1994). J. Geoph. Res. 100: 25867 − 25876

Bojkov RD, Balis DS, and Zerefos CS (1998) Characteristics of the ozone decline in the northern Polar and middle latitudes during the winter/spring. Meteorolog. Atmos. Phys. 69: 119 − 135

Caldwell MM, Camp LB, Warner CW, and Flint SD (1986) Action Spectra and their key role in assessing biological consequences of solar UV-B radiation change. In: Worrest RC, Caldwell MM (eds) Stratospheric Ozone Reduction, Solar Ultraviolet Radiation and Plant Life. Springer − Verlag, pp. 87 − 111

Chaney EK and Sliney DH (2005) Re-evaluation on the ultraviolet hazard action spectrum. The impact of spectral bandwidth. Health Physics Society 89: 322 − 332

Chapman S (1930) A theory of upper-atmospheric ozone. Memoirs of the Royal Meteorological Society 3: 103 − 125

Dahlback A (1996) Measurements of biologically effective UV doses, total ozone abundances, and cloud effects with multi-channel, moderate bandwidth filter. Applied Optics 35: 6514 − 6521

Dahlback A, Gelsor N, Stamnes J, and Gjessing Y (2007) UV measurements in the 3000 − 5000 m altitude region in Tibet. J. Geophys. Res. 112: D9, D09308, 10.1029/2006JD007700

Damiani A, Storini M, Laurenza M, Rafanelli C, Piervitali E, and Cordaro EG (2006) Southern ozone variations induced by solar particle events during 15 January–5 February 2005. J. Atmospheric and Solar-Terrestrial Physics 68(17): 2042 − 2052

Damiani A, Storini M, Laurenza M, Diego P, and Rafanelli C (2008) Ozone variability related to several SEP events occurring during solar cycle no. 23. J. Adv. Space Res. DOI:10.1016/ j.asr.2008.06.006

De Gruijl FR, Longstreth J, Norval M, Cullen AP, Slaper H, Kripke ML, Takizawag Y, and van der Leun JC (2003) Health effects from stratospheric ozone depletion and interactions with climate change. Photochem. Photobiol. Sci. 2: 16 − 28

Diaz S, Booth CR, Armstrong R, Brunat C, Cabrera S, Camilion C, Casiccia C, Deferrari G, Fuenzalida H, Lovengreen C, Paladini A, Pedroni J, Rosales A, Zagarese H, and Vernet M (2005) Multichannel radiometer calibration: a new approach. Applied Optics 44: 26

Diffey BL (1984) Personal ultraviolet radiation dosimetry with polysulphone film badges. Photodermatology 1: 151 − 157

Diffey BL (1989) Ultraviolet radiation dosimetry with polysulphone film. In: Diffey BL (ed) Radiation Measurement in Photobiology, Academic Press, New York, 136 − 159

Di Menno I, Moriconi ML, Di Menno M, Casale GR, and Siani AM (2002) Spectral ultraviolet measurements by a multichannel monitor and a Brewer spectroradiometer: a field study. Rad. Prot. Dosimetry. 102(3): 259 − 263

Di Menno I, Rafanelli C, De Simone S, and Di Menno M (2007) High performance spectrograph for solar UV 250 − 400 band. Proceedings of Optics and Photonics, San Diego, CA, Aug. 26 − 30

Egorova TA, Rozanov EV, Schlesinger ME, Andronova NG, Malyshev SL, Karol IL, and Zubov VA (2001) Assessment of the effect of the Montreal Protocol on atmospheric ozone. Geophys. Res. Lett. 8: 2389 − 2392

Engel A, Möbius T, Haase HP, Bönisch H, Wetter T, Schmidt U, Levin I, Reddmann T, Oelhaf H, Wetzel G, Grunow K, Huret N, and Pirre M (2005) On the observation of mesospheric air inside the arctic stratospheric polar vortex in early 2003. Atmos. Chem. Phys. Discuss. 5: 7457 − 7496

Epstein PR (1998) Global warming and vector-borne disease. Lancet 351: 1737 − 1738

Farman JC, Gardiner BG, and Shanklin JD (1985) Large losses of total ozone in Antarctica reveal seasonal CLO_x/NO_x interaction. Nature 315: 207 − 210

Fay G (2000) Marketing and Guiding Alaska Tourism-Defining our Roles. Proceedings of the 7th Annual Ecotourism in Alaska Conference, Feb. 3rd, Anchorage, AK

Garcia RR and Solomon S (1987) A possible relationship between interannual variability in Antarctic ozone and the quasi-biennial oscillation. Geophys. Res. Lett. 14: 848 − 851

Giovanelli G, Bortoli D, Petritoli A, Castelli E, Kostadinov E, Ravegnani F, Redaelli G, Volk CM, Cortesi U, Bianchini G, and Carli B (2005) Stratospheric minor gas distribution over the Antarctic Peninsula during the APE-GAIA campaign. International Journal of Remote Sensing 26(16): 3343 − 3360

Grainger RG and Highwood EJ (2003) Changes in stratospheric composition, chemistry, radiation and climate caused by volcanic eruptions. Geological Society, London, Special Publications 213: 329 − 347

Grooß J, Konopka P, and Müller R (2005) Ozone chemistry during the 2002 Antarctic vortex split. J. Atmos. Sci. 62(3): 860 − 870

Han Z, Chongping J, and Libo Z (2000) QBO Signal in total ozone over Tibet. Advances Atmos. Sci. 17(4): 562 − 568

International Association of Antarctica Tour Operators (IAATO) (2008) http://www.iaato.org/index.html

International Panel on Climate Change (IPCC) (2007) The Physical Science Basis. UNEP-WMO

Kimlin MG and Parisi (1999) Ultraviolet protective capabilities of hats under two different atmospheric conditions. http://www.photobiology.com/photobiology99

Knudsen BM, Harris NRP, Andersen SB, Christiansen B, Larsen N, Rex M, and Naujokat B (2004) Extrapolating future Arctic ozone losses. Atmos. Chem. Phys. 4: 1849 − 1856

Krueger AJ (2001) Mapping of total ozone from space. Geoscience and Remote Sensing Symposium, 2001. IGARSS 01; IEEE 2001 International 3: 1032 − 1034, DOI:10.1109/IGARSS.2001.976737

Labitzke K and van Loon H (1997) Total ozone and the 11-yr sunspot cycle. Journal of Atmospheric and Solar Terrestrial Physics 59(1): 9 − 19

Lakkala K, Redondas A, Meinander O, Torres C, Koskela T, Cuevas E, Taalas P, Dahlback A, Deferrari G, Edvardsen K, and Ochoa H (2005) Quality assurance of the solar UV network in the Antarctic. Journal of Geophysical Research 110(15): D15101.1 − D15101.12

Latysheva IV, Belousova EP, Ivanova AS, and Potemkin VL (2007) Circulation conditions of the abnormally cold winter of 2005/2006 over Siberia. Journal of Russian Meteorology and Hydrology 32(9): DOI 10.3103/S106837390709004X

Leaf A (1989) Potential health effects of global climatic and environmental changes. N. Engl. J. Med. 321: 1577 − 1583

Lindfors A and Vuilleumier L (2005) Erythemal UV at Davos (Switzerland), 1926 − 2003, Estimated usage of total ozone, sunshine duration, and snow depth. Journal Geophysical Research 110:D02104, doi:10.1029/2004jd005231

Longstreth J (1991) Anticipated public health consequences of global climate change. Environ. Health Perspect. 96: 139 − 144

Longstreth J (1999) Public health consequences of global climate change in the United States. Environ. Health Perspect. 107(1): 169 − 179

Manney GL, Krüger K, Pawson S, Minschwaner K, Schwartz MJ, Daffer WH, Livesey NJ, Mlynczak MG, Remsberg EE, Russell III JM, and Waters JW (2008) The evolution of the stratopause during the 2006 major warming: Satellite data and assimilated meteorological analyses. J. Geophys. Res. 113:D11115, DOI:10.1029/2007JD009097

Mariutti GF, Rafanelli C, Bortolin E, Anav A, and Polichetti A (2002) A test in the Arctic area for personal UV dosimetry. Proceedings of the LXXXVIII National Congress of Italian Physics Society, Alghero, Sept. 26 − Oct. 1, 2002

Mariutti GF, Bortolin E, Polichetti A, Rafanelli C, Anav A, Di Menno I, Casale G, and Di Menno M (2003) UV dosimetry in Antarctica (Baia Terranova): Analysis of data from polysulphone films and GUV 511 radiometer. Proceedings of Optical Science and Technology, SPIE 48th Annual Meeting, San Diego, CA, Aug. 3 − 8

McKinlay AF and Diffey BL (1987) A reference action spectrum for UV induced erythema in human skin. In: Passchier WF, Bosnjakovich BFM (eds) Human Exposure to Ultraviolet Radiation: Risks and Regulations, International Congress Series, pp. 83 − 87

McMichael T, Smith W, Armstrong B, and Lucas R (2006) Solar ultraviolet radiation: Global burden of disease from solar ultraviolet radiation. Environmental Burden of Disease Series, No. 13, WHO Editor, Geneva, Switzerland

Molina MJ and Rowland FS (1973) Stratospheric sink for clorofluoromethanes: Chlorine catalyzed destruction or ozone. Nature 249: 810 − 814

Moriconi ML, Rafanelli C, Anav A, Di Menno I, and Di Menno M (1998) Solar radiation and clouds: Polar experimental data and modeling. Proceedings of 4th NySMAC Scientific Seminar, The Arctic and Global Change: Multidisciplinary Approach and International Efforts at Ny Ålesund, Ravello, Italy, March 5 − 6

Müller R, Tilmes S, Grooß JU, Engel A, Oelhaf H, Wetzel G, Huret N, Pirre M, Catoire V, Toon G, and Nakajima H (2007) Impact of mesospheric intrusions on ozone-tracer relations in the stratospheric polar vortex. J. Geophys. Res. 112:D23307, DOI:10.1029/2006JD008315

Orsolini YJ and Jackson DR (2008) An estimation of Arctic ozone loss in recent winters based on assimilation of EOS/MLS and SBUV observations. Geophysical Research Abstracts 10:EGU2008-A-06645

Orsolini YJ, Randall CE, Manney GL, and Allen DR (2005) An observational study of the final breakdown of the southern hemisphere stratospheric vortex in 2002. Journal of the Atmospheric Sciences 62(3): 735

Pazmiño AF, Godin-Beekmann S, Ginzburg M, Bekki S, Hauchecorne A, Piacentini RD, and Quel EJ (2005) Impact of Antarctic polar vortex occurrences on total ozone and UVB radiation at southern Argentinean and Antarctic stations during the 1997 − 2003 period. J. Geophys. Res. 110:D03103, DOI:10.1029/2004JD005304

Rafanelli C (2001) Environmental factors on solar UV measurements. Rad. Prot. Dosim. 97: 423 − 428

Rafanelli C, Ciattaglia L, Anav A, Valenti C, and Di Menno M (1998) Polar Umkehr profiling during the ozone hole period. Proceedings of 4th NySMAC Scientific Seminar, The Arctic and Global Change: Multidisciplinary Approach and International Efforts at Ny Ålesund, Ravello, Italy, Mar. 5 − 6, 1998

Rafanelli C, Anav A, Di Menno I, Di Menno M, Ciattaglia L, Diaz SB, and Iturraspe R (2000) UV Green Model, SUV 100 & Brewer spectra: an intercomparison in Ushuaia. Proceedings of 2nd SPARC General Assembly, SPARC 2000, Mar del Plata, Argentina, Nov. 6 − 10, 2000

Rafanelli C, Leonardi RM, and Di Menno M (2001) Evaluation of cloud effects on solar UV-B spectral irradiance by a new automatic ground-based Total-Sky Camera. Proceedings of IX Workshop on Italian Research in Antarctic Atmosphere, Roma, Italy, Oct. 22 − 24, 2001

Rafanelli C, Anav A, and Di Menno I (2002) Cloud effect on solar UV-B irradiance at ground: a campaign in the Arctic region. Proceedings of LXXXVIII National Congress of Italian Physics Society, Alghero, Italy, Sept. 26 − Oct. 1, 2002

Rafanelli C, Casagrande G, Piervitali E, Casu G, Malaspina F, Foti F, and Vuerich E (2005) Automatic cloud coverage evaluation by a ground based Total-Sky Camera. Proceedings of WMO Technical Conference on Meteorological and Environmental Instruments and Methods of Observation, Bucharest, Romania, May 4 − 7, 2005

Rafanelli C, Anav A, Di Menno I, and Di Menno M (2006) The solar UV as an environmental factor: measurements and model. In: Blume Y, Durzan DJ, Smertenko P (eds) Cell Biology and Instrumentation: UV Radiation, Nitric Oxide and Cell Death in Plants. IOS Press, NATO Sciences Series, vol. 371

Rafanelli C, De Simone S, Damiani A, Lund C, Erdvardsen K, Svenoe T, and Benedetti E (2008) A first attempt to evaluate the total ozone column by Brewer Spectrophotometer during the arctic winter. Proceedings of Quadrennial Ozone Symposium 2008, Tromsø Jun 29 − July 5, 2008

Randall CE, Harvey VL, Singleton CS, Bernath PF, Boone CD, and Kozyra JU (2006) Enhanced NO_x in 2006 linked to strong upper stratospheric Arctic vortex. Geophys. Res. Lett. 33:L18811, DOI:10.1029/2006GL027160

Roscoe HK, Colwell SR, Shanklin JD, Karhu JA, Taalas, P, Gil M, Yela M, Rodriguez S, Rafanelli C, Cazeneuve H, Villanueva C A, Ginsburg M, Diaz SB, de Zafra R L, Muscari G, Redaelli G, and Dragani R, (2005a) Measurements from ground and balloons during APE-GAIA. A polar ozone library. Advances in Space Research 36: 835 − 845

Roscoe HK, Shanklin JD, and Colwell SR (2005b) Has the Antarctic vortex split before 2002? Journal of the Atmospheric Sciences 62(3): 581 − 588

Russell III JM, Gordley LL, Park JH, Drayson SR, Hesketh WD, Cicerone RJ, Tuck AF, Frederick JE, Harries JE, and Crutzen PJ (1993) The halogen occultation experiment. J. Geophys. Res. 98, D6: 10777 − 10797

Salby ML and Garcia RR (1990) Dynamical perturbations to the ozone layer. Physics Today 43: 38 − 46

SCAR-EBA (2008) Describe the past, understand the present, predict the future. http://www.eba.aq/

Schoeberl MR, Douglass AR, Hilsenrath E, Bhartia PK, Beer R, Waters JW, Gunson MR, Froidevaux L, Gille JC, Barnett JJ, Levelt PF, and DeCola P (2006) Overview of the EOS aura mission. IEEE TGARS 44(5): 1066 − 1074

Seppälä A, Verronen PT, Clilverd MA, Randall CE, Tamminen J, Sofieva V, Backman L, and Kyrölä E (2007) Arctic and Antarctic polar winter, NO_x and energetic particle precipitation in 2002/2006. Geophys. Res. Lett. 34:L12810, DOI:10.1029/2007GL029733

Shindell D, Rind D, Balachandran N, Lean J, and Lonergan P (1999) Solar Cycle Variability, Ozone, and Climate. Science 284: 305 − 308

Simic S, Weihs P, Vacek A, Kromp-Kolb H, and Fitzka M (2007) Ozone and spectral UV measurements in Austria during 1994 − 2006: Climatology and investigations of long- and short-term changes. Proceedings of One Century of UV Radiation Research, Davos, Switzerland, Sept. 18 − 20, 2007

Sitnov SA (2004) QBO effects manifesting in ozone, temperature, and wind profiles. Annales Geophysicae 22: 1495 − 1512

Slaper H, Velders GJM, Daniel JS, de Gruijl FR, and van der Leun JC (1996) Estimates of ozone depletion and skin cancer incidence to examine the Vienna Convention achievements. Nature 384: 256 − 258; DOI:10.1038/384256a0

Solomon S (1999) Stratospheric ozone depletion: a review of concepts and history. Reviews of Geophysics 37(3): 275 − 316

Storini M, A Damiani, and C Rafanelli (2005) Search of solar induced effects on the ozone layer: 1996-2004. Proceeding of 10th Scientific Assembly of the IAGA, Toulouse, France, July 18 − 29, 2005

Stowasser M, Oelhaf H, Ruhnke R, Wetzel G, Friedl-Vallon F, Kleinert A, Kouker W, Lengel A, Maucher G, Nordmeyer H, Reddmann Th, Trieschmann O, von Clarmann T, Fischer H, and Chipperfield MP (2002) A characterization of the warm 1999 Arctic winter by observations and modeling: NO_y partitioning and dynamics, J. Geophys. Res. 107(D19), 4376, DOI:10.1029/2001JD001217

Strawa A, Drdla K, Fromm M, Pueschel RF, Hoppel KW, Browell EV, Hamill P, and Dempsey DP (2002) Discriminating types Ia and Ib stratospheric clouds in POAM satellite data. J. Geophys Res. 107, DOI:10.1029/2001JD000458

Tabazadeh A and Cordero EC (2004) New Directions: Stratospheric ozone recovery in a changing atmosphere. Atmospheric Environment 38: 647 − 649

Taylor HR (1999) Epidemiology of age-related cataract. Eye 13: 445 − 448

Tie X and Brasseur G (1995) The response of stratospheric ozone to volcanic eruptions: Sensitivity to atmospheric chlorine loading. Geophysical Research Letters 22: 3035 − 3038

Tilmes S, Müller R, Grooß J-U, and Russell JM III (2004) Ozone loss and chlorine activation in the Arctic winters 1991 − 2003 derived with the tracer-tracer correlations. Atmos. Chem. Phys. 4: 2181 − 2213

Todorovich N and Vujovic D (2008) Solar activity, cyclone circulation, and negative anomalies of total ozone content. Geophysical Research Abstracts 10, EGU2008-A-11192

Tüg H, Hanken T, and Schrems O (2003) Spectral UV-measurements at NDSC sites in the Arctic (Ny-Ålesund, Spitsbergen) and Antarctica (Neumayer Station). Geophysical Research Abstracts 5: 13022

Uchino O, Bojkov RD, Balis DS, Akagi K, Hayashi M, and Kajihara R (1999) Essential characteristics of the Antarctic spring ozone decline, update to 1998. Geophysical Research Letters 26: 1377 − 1380

UNEP (United Nations Environment Programme) (2002) Environmental Effects of Ozone Depletion and its Interactions with Climate Change: 2002 Assessment, Geneva, Switzerland

Velders G (2008) Importance of the Montreal Protocol for ozone layer and climate. WMO/UNEP Ozone Research Managers,Geneva, Switzerland, May 19, 2002

Voigt C, Larsen N, Deshler T, Kröger C, Schreiner J, Mauersberger K, Luo B, Adriani A, Cairo F, Di Donfrancesco G, Ovarlez J, Ovarlez H, Dörnbrack A, Knudsen B, and Rosen J (2003) In situ mountain-wave polar stratospheric cloud measurements: Implications for nitric acid trihydrate formation. J. Geophys. Res. 108(D5): DOI:10.1029/2001JD001185

Volker AM and Barrie L (2006) The WMO GAW Programme. Proceeding of Inter-commission Task Team on Quality Management Framework (ICTC-QMF), Geneva, Switzerland, April 25 − 27, 2006

Waters JW, Froidevaux L, Harwood RS, et al. (48 authors) (2006) The Earth Observing System Microwave Limb Sounder (EOS MLS) on the Aura satellite. IEEE TGARS 44: 1075 − 1092

Wester U (2006) Polysulphone and spore-film UV-dosimeters compared to two radiation transfer models and an instrument that measures the UV index: an evaluation for a UV-dosimetry study of preschool children in Stockholm. JR Slusser, K Schäfer, A Comerón (eds) Proceedings of Remote Sensing of Clouds and the Atmosphere XI. Vol. 6362

WHO (World Health Organization) (1998) Press Release WHO/5, Geneva, Switzerland, July 17, 1998

WHO (1999) Ultraviolet radiation: solar radiation and human health. WHO fact sheet 227. http://www.who.int/mediacentre, Geneva, Switzerland

WHO (2002) Global Solar UV Index. In: WHO (ed) A Practical Guide. Geneva, Switzerland

WHO (2006) Static Fields Environmental Health. Criteria Monograph 232, http://www.who.int/mediacentre, Geneva, Switzerland

WHO (2008a) http://www.who.int/blindness/en/index.html, Geneva, Switzerland

WHO (2008b) Ultraviolet radiation and the INTERSUN Programme. http://www.who.int/uv/health/en/, Geneva, Switzerland

WMO (World Meteorological Organization) (2006a) WMO Bulletin 55(4). October, Geneva, Switzerland

WMO (2006b) Guide to meteorological instruments and methods of observation. WMO 8, 7th edition, Geneva, Switzerland

WMO (2007) http://www.empa.ch/gaw, Geneva, Switzerland

Worrest RC, Smythe KD, and Tait AM (1989) Linkages between climate change and stratospheric ozone depletion. In: White JC (ed) Global Climate Change Linkages: Acid Rain, Air Quality, and Stratospheric Ozone. Elsevier Science, New York, ISBN 0-444-01515-9, pp. 67 − 78

Zeman G (2008) Ultraviolet Radiation. Health Physics Society, http://hps.org/hpspublications/articles/uv.html

Zenoff VF, Siñeriz F, and Farías ME (2006) Diverse responses to UV-B radiation and repair mechanisms of bacteria isolated from high-altitude aquatic environments. Appl. Environ. Microbiol. 72(12): 7857 − 7863

5 Changes in Ultraviolet and Visible Solar Irradiance 1979 to 2008

Jay Herman

Goddard Space Flight Center
Code 613.3
Greenbelt, MD 20771 USA
E-mail: jay.r.herman@nasa.gov

Abstract A description is presented of instruments and requirements for measuring ultraviolet (UV) and visible irradiance and estimating long-term changes in irradiance from the ground-based and satellite data The 30-year changes in zonal average UV irradiances are estimated from changes that have occurred in ozone amount and cloud cover as a function of latitude and season. Ozone changes have been obtained from a multiple satellite time series starting with Nimbus-7/Total Ozone Mapping Spectrometer (TOMS) in 1979 and continuing to the end of 2008 with the Solar Backscatter Ultraviolet (SBUV-2) series, Earth-Probe TOMS, and Ozone Monitoring Instrument (OMI). The changes in cloud cover have been obtained using the 340 nm reflectivity data from the same series of satellite instruments, except for Earth-Probe TOMS. The results show large increases in UV-B (280 nm − 315 nm) irradiance in both hemispheres, mostly caused by changes in ozone amounts. The largest increases have occurred in the Southern Hemisphere for clear-sky conditions when compared to the same latitudes in the Northern Hemisphere. Since 1979, an increase of 5% − 8% has occurred in clear-sky DNA damage action spectra weighted irradiance P_{DNA} during most of the spring and summer, with increases ranging from 12% to 15% between 30°S and 40°S and 18% to 22% between 40°S and 50°S. Increases in erythemal irradiance are about half that of P_{DNA}. There were only small changes in the equatorial zone (±23°), where sea level UV irradiances are largest because of naturally low ozone amounts and the nearly overhead sun.

Keywords ultraviolet, trends, RAF, erythemal, spectrometer, pyranometer

5.1 Introduction

Determining the amount of ultraviolet (290 nm − 400 nm) and visible (VIS,

400 nm − 700 nm) radiation that reaches the earth's surface is a fundamental problem that has occupied scientists and governments from the earliest times. In highly organized major civilizations, the primary reason for the intense interest was to determine the factors (sunlight, drought, and temperature) that affected agriculture, and through agriculture, the wealth and population of nations. The quantitative interest in changing amounts of solar radiation is a more modern endeavor that still has an agricultural underpinning, but has expanded into direct human health effects, effects on land and ocean biology, materials damage, and global warming. In addition to these long-term effects (years-to-decades) from changing solar radiation, there are short-term phenomena (minutes-to-yearly), such as the effects of solar radiation on boundary layer and tropospheric photochemistry, clouds and aerosols, and local and global weather. Short-term changes in ozone and cloud cover change the amount of solar radiation reaching the earth's surface and affect each year's agriculture, the extent of human and other biological exposure, and damage to materials. The extent of human exposure and the corresponding health effects are difficult to quantify because of the mobility of people, the great variety of resistance to UV damage caused by skin type (Hemminki, 2002) and other genetic factors, in addition to the effects of culture and diet on mitigating UV exposure. An example is seen in the relative incidence of skin cancer between Japanese and Caucasians living in the U.S. For the Japanese, the non-melanoma skin cancer rate is about 1 per 100,000, while for Caucasians the rate is about 15 per 100,000 (Qiu and Marugame, 2008). Even the low cancer rate reported for the Japanese-American ethnic group is about double the rate reported in Japan.

Instrumental methods for measuring or estimating solar radiation amounts have gradually evolved from simple ground-based instrumentation that essentially measured the heating effect of all solar radiation (e.g., pyranometers and standardized water evaporation containers, Fig. 5.1) to spectrometers capable of good spectral resolution (0.5 nm) in the UV and VIS range. Before 1979, the only sources of UV and VIS data were obtained from sparsely scattered ground stations of varying accuracy and precision. The longest reconstructed time series of solar UV irradiance from measurements of ozone amounts goes back to 1928 at Arosa, Switzerland (Staehelin and Weiss, 2001; Staehelin et al., 1998), and another near Moscow, Russia goes back to 1968 (Chubarova, 2008) based on direct UV measurements. There have been calibrated measurements of total column ozone since the late 1950s at several stations from which clear-sky UVB (280 nm − 315 nm) can be derived. Attempts have been made to reconstruct the ozone time series back to the late 1600s by estimating the UV-B (280 nm − 315 nm) stress on biological systems, particularly on pine and spruce trees (Zuev and Bonderenko, 2001), and by other biological proxies (Rozema et al., 2002). Networks of standardized evaporation pans (Roderick and Farquhar, 2002), and pyranometers (Stanhill and Cohen, 2001) appear to have detected a long-term reduction in solar irradiance at the earth's surface that seems to be associated with increased cloud and aerosol amounts; a concept popularly known as "global dimming."

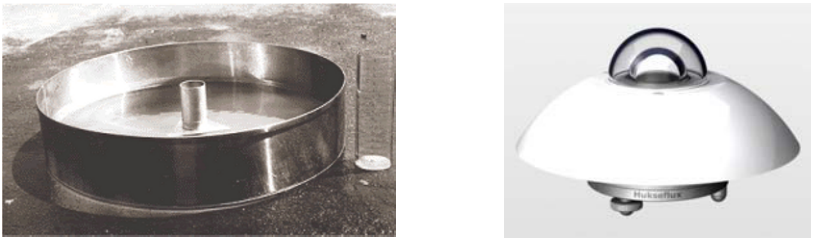

(a) (b)

Figure 5.1 (a) Standardized evaporation pan for measurement of water evaporation installed on a wooden platform in a grassy location. The pan is filled with water and exposed to sunlight; (b) An example of a pyranometer used for measuring total solar irradiance

Then and now, the preponderance of UV measuring stations are located in the Northern Hemisphere, mostly in Europe and North America, with gradually increasing numbers in Asia. There are a few stations in South America (Argentina, Chile, and Brazil), New Zealand, Australia, and Africa. A well-calibrated polar network of seven stations has been maintained by the U.S. National Science Foundation in Antarctica (Palmer, McMurdo, and South Pole Stations); Ushuaia, Argentina; Barrow, Alaska; Summit, Greenland; and San Diego, California. These have been augmented in recent years by the worldwide distribution of well-calibrated sun and sky photometers as part of AErosol RObotic NETwork (AERONET) (Holben et al., 1998). Reliable satellite measurements of ozone derived from back-scattered UV radiation started in late 1978, with an earlier attempt from the BUV instrument (1970 − 1977) on the Nimbus-4 satellite. Since November 1978, satellite UV data consists of daily measurements of ozone amount and cloud reflectivity from Nimbus-7/Total Ozone Mapping Spectrometer (TOMS) and the Solar Backscatter Ultra-Violet (SBUV) instrument, continued with the NOAA SBUV-2 series, Ozone Monitoring Instrument (OMI), and Global Ozone Monitoring Experiment (GOME). These data provide global coverage using an independent calibration for each instrument that can be validated with respect to existing ground stations. Global coverage has been especially important for understanding processes over the oceans, in Africa, parts of Asia, and most of the Southern Hemisphere, where ground-based data are sparse or non-existent. The availability of satellite data has intensified the efforts to develop reliable ground-based instrumentation and to perfect their calibration, for direct measurements of both UV irradiance and atmospheric composition (ozone, sulfur dioxide, aerosols, and more recently, nitrogen dioxide and formaldehyde).

Satellite measurements of ozone amount, reflectivity, and some aerosol properties have enabled good estimates of radiation reaching the ground using laboratory measured absorption and scattering coefficients in radiative transfer calculations that include polarization effects. The principal sources of error in satellite-based estimates of UV and VIS radiation are from the properties and amounts of absorbing aerosols, which are not easily measured from satellites. When satellite measurements of ozone and reflectivity are combined with ground-based

measurements of aerosols (or in very clean atmospheres), estimates of UV and VIS radiation reaching the ground compare well with ground-based data (Kalliskota et al., 2000). The best estimates of VIS wavelength aerosol properties in the atmosphere come from a large network of AERONET CIMEL sunphotometers that are strategically located in many parts of the world. The AERONET data consist of estimates of aerosol extinction at six wavelengths (340, 380, 440, 670, 870 and 1,020 nm), absorption optical depths at four wavelengths (440, 670, 870 and 1,020 nm) and particle size distribution. These aerosol parameters are essential for VIS and UV radiative transfer calculations. However, extrapolation of aerosol absorption from the VIS to the UV has proved to be incorrect (Krotkov et al., 2005; Cede et al., 2006) leading to errors in calculated UV fluxes at the surface and photolysis rates in the troposphere.

Currently, comparisons of satellite-based estimates of UV irradiance with ground-based measurements show overestimates that can range up to 40% when unmeasured aerosol loadings are large. For unpolluted sites, the agreement is within 2% or 3%, consistent with known instrument calibration errors for both satellite and ground-based instruments. For UV radiation, this is implies that the relation between ozone and absorption of UV-B is well understood, as is the relationship between UV-A (315 nm − 400 nm) and VIS irradiances and aerosols (scattering and absorbing). For a comparison of ground-based measurements with satellite estimates of solar radiation, the major outstanding problems are outlined as follows:

(1) Accounting for the aerosol absorption optical depth from 300 nm to 1,000 nm.
(2) Satellite estimation of UV and VIS radiation over snow and ice.
(3) Measurements of ozone, reflectivity, and UV+VIS radiation at high latitudes and solar zenith angles (SZAs) (latitudes of 65° and SZA >70°) both from the ground and from satellites.
(4) Establishment of international transfer standards and transfer methods that are better than the current limit of about 3%.
(5) Creating common stable calibrations between all types of ground-based instruments at different locations.
(6) Accounting for the differences between ground-based and satellite measurements caused by their different fields of view (FOV).
(7) Improved understanding of radiance and irradiance transmission by clouds, which becomes increasingly important as the FOV becomes smaller.

The amount of solar ultraviolet UV and VIS radiation reaching the earth's surface, and the fraction reflected back to space, is primarily governed by the amount of cloud cover, and to a lesser extent, by Rayleigh scattering, aerosols, and various absorbing gases (e.g., O_3, NO_2, H_2O). Unlike the weakly surface reflected UV and blue radiation, most of the VIS solar radiation is moderately reflected by the ground and vegetation. For UV-B irradiance, ozone, aerosols, and cloud cover are the most important atmospheric components limiting the amount radiation able to reach the ground. Ultraviolet-A irradiances reaching the

ground are limited by aerosols and cloud cover.

Figure 5.2 shows an example of solar flux measured above the atmosphere by the Solar-Stellar Irradiance Comparison Experiment (SOLSTICE) (McClintock et al., 2000) and the space shuttle borne Atlas-3/Solar Ultraviolet Spectral Irradiance Monitor (SUSIM) (Brueckner et al., 1994) spectrometers, and the calculated solar irradiance reaching the ground for overhead sun and 300 Dobson Units (DU) of ozone. Atlas-3/SUSIM was a high spectral resolution instrument (0.15 nm), which clearly shows the solar Fraunhofer line structure, especially the calcium K and H lines at 393.3 nm and at 396.9 nm (see inset in Fig. 5.2). SOLSTICE was an independent lower resolution instrument that agrees quite well with Atlas-3/SUSIM. These data are a good starting point for UV radiative transfer calculations in the atmosphere to provide estimates of UV irradiance reaching the ground.

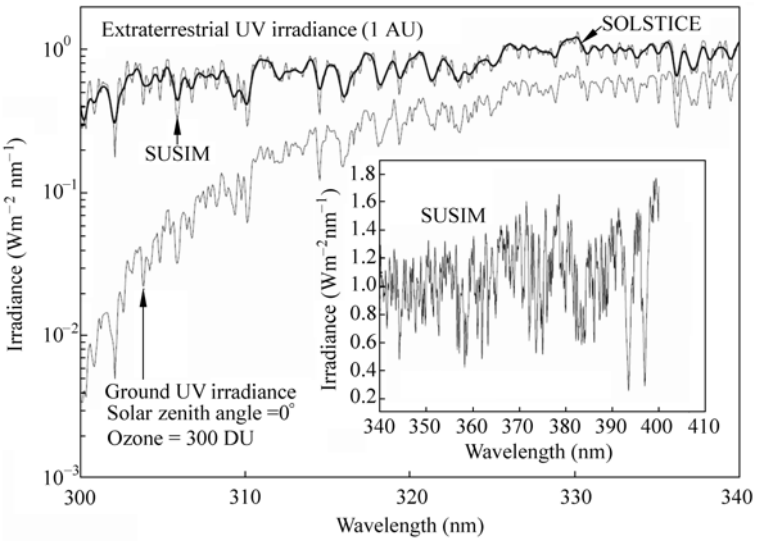

Figure 5.2 The extraterrestrial solar UV irradiance measured by SOLSTICE and Atlas-3/SUSIM instruments above the atmosphere normalized to a sun-earth distance of 1 astronomical unit, and the calculated irradiance at the ground for 300 DU of ozone and overhead sun. Only the inset, 340 nm − 410 nm is shown at full resolution of 0.15 nm. 1 DU = 2.67×10^{16} molecules/cm^2

Ozone absorbs a wavelength-dependent fraction of the solar UV radiation in the 200 nm to 340 nm range, with peak absorption at 255.4 nm. Almost no solar photons with wavelengths shorter than 280 nm reach the earth's surface because of ozone (Hartley and Huggins bands) and molecular oxygen absorption (Schumann-Runge band and continuum absorption). There is still strong absorption at 310 nm, where a 1% change in ozone leads to an approximate 1% change in irradiance for SZA = 45°. At wavelengths less than 305 nm, the increasingly large ozone absorption coefficient leads to a proportionally large increase in irradiance for a

small decrease in ozone (e.g., at SZA = 45°, a 1% decrease in ozone can produce a 2.2% increase in 305 nm irradiance).

Clouds and scattering aerosols reduce solar radiation at all wavelengths λ by reflecting a fraction of the energy back to space, which depends on the aerosol's refractive index and particle size. Except in cases of dense smoke or dust, scattering aerosols (e.g., sulfates) usually reduce radiation reaching the surface by less than 10%. Under special conditions, clouds can locally increase UV from 1% to 10% by cloud edge reflections. Extremely heavy cloud cover (black thunderstorm) can decrease UV and VIS by almost 100%, while even moderate cloud thickness can change the UV-B spectral distribution because of the additional ozone absorption caused by multiple scattering.

In addition to the above effects, VIS wavelengths are modulated by H_2O, and those in the Near-IR (NIR) (700 nm − 3,000 nm) are modulated by changes in CO_2, CH_4, and H_2O, within their respective absorption bands. There is an additional small amount of absorption for UV-A and blue wavelengths from NO_2 and HCHO, and for UV-B from SO_2, in addition to a stronger absorption for UV and VIS from smog in urban or industrial areas.

Ultraviolet and VIS radiation at the surface are generally highest near the equator following the seasonally changing sub-solar point (latitude between ±23.3°), where ozone amounts are low and the SZA is the smallest. For any specific latitude, larger amounts of solar radiation are seen at high altitude sites because of reduced Rayleigh scattering, especially those with predominantly dry and clear weather and large surface reflectivity (e.g., from snow or ice cover).

Understanding, modeling, and measuring the factors that affect the amount of UV and VIS radiation reaching the earth's surface are important, since changes in these radiation amounts impact agricultural and ocean productivity, global energy balance, and human health. Changes in UV radiation can affect human health adversely through skin cancer (Diffey, 1991), eye cataracts (Taylor, 1990), and suppression of the immune system (Vermeer et al., 1991), yet positively through increased vitamin D production (Grant, 2002; Holick, 2004). Changes in UV radiation can also significantly affect ecosystem biology (Smith et al., 1992; Ghetti et al., 2006).

The focus of this chapter is the estimation or detection of UV irradiance changes that can be measured directly from the ground, or estimated using satellite-based or ground-based measurements that characterize the optical properties of the atmosphere. Section 5.2 describes a subset of the instrumentation widely deployed today, as well as two new instruments recently deployed and validated for measurements of atmospheric optical properties. Section 5.3 is devoted to a discussion of estimating long-term trends in UV irradiance based on satellite derived ozone and reflectivity amounts. The concept of radiation amplification factor (RAF) is reviewed for the purpose of estimating monochromatic irradiance changes from Beer's Law. A second, apparently empirical, power law form is introduced for deriving irradiance trends when changes are estimated for action

spectra weighted wavelength integrated irradiances. In a later section, it is shown that the empirical power law form can be numerically derived from the Beer's Law form. Section 5.4 presents a brief discussion of UV irradiance in the Polar Regions. Section 5.5 briefly discusses the effects of UV irradiance on human health. Section 5.6 discusses the UV Index and commonly used units for irradiance and exposure (time integral of irradiance). Section 5.7 introduces the concept of action spectra and discusses their application, gives accurate fitting functions for four of these spectra, derives the power law RAF for each of these spectra, and shows a comparison of theory with data obtained for the erythemal action spectrum. Estimated annual zonal average irradiance changes are presented for monochromatic irradiances (305 nm − 325 nm), erythemal irradiances, and monthly zonal average irradiance (305 nm), as well as the DNA damage action spectrum.

5.2 Instrumentation

Instrumentation for measuring solar radiation reaching the ground falls into a few main classes, which have been described at length in specialized literature and reports. The earliest reliable device for quantitative measurements of solar radiation was a pyranometer (Kerr et al., 1967), which converted the sun's photon energy into heat and then into a voltage or current proportional to the energy-weighted integrated solar photon flux (Fig. 5.1(a)). Pyranometers are still deployed at many sites, some of which have the longest broadband data records for well-calibrated highly stable instruments. The basic pyranometer measurement is the solar irradiance in watts/m^2 over a hemispherical field of view, which includes both direct and diffuse (scattered) photons, and a wavelength range from 280 nm to 3,000 nm. The detector is a black-coated thermopile with a nearly perfect cosine response for photons incident at different angles. The pyranometer's stability makes it ideal for detecting small long-term changes in solar irradiance caused by changes in the atmosphere (clouds and aerosols), changes in surface reflectivity, and of course, changes in solar output. The stability suggests an application for determining the amount of UV irradiance by combining pyranometer data for cloud transmission estimates with an instrument capable of determining the column amount of ozone Ω, and radiative transfer calculations. Ω is usually determined from the ratio of two or more measured narrow-band narrow FOV direct-sun viewing solar irradiances, and more recently by matching the entire absorption spectrum for a moderate wavelength range. This reduces two calibration problems: (1) the need for absolute radiometric calibration, and (2) the need for determining UV measuring instrument's cosine response to direct and diffuse radiances from different angles. While the combination is not a direct measurement of UV irradiance, it offers a solution to difficult calibration and stability problems inherent in direct measurements.

All other instruments that attempt to directly measure the direct plus diffuse photons (known as global flux) have a common calibration problem; namely, determining cosine response to the angle of the incident photons on a diffuser material (flat plate or some specially shaped diffuser). Most instruments rely on a laboratory-derived correction to their approximation of the ideal cosine response (e.g., Brewer spectrometers) instead of achieving a nearly perfect cosine response from hardware. An example of the latter is given by a commercially available UV spectrometer (290 nm − 400 nm with 1 nm resolution) developed at the National Institute of Water and Atmospheric Research in New Zealand. Unprotected diffuser materials (e.g., Teflon) are usually porous and susceptable to transmission changes from atmospheric pollution and from natural aging, which affects both the radiometric calibration and the cosine response. Such instruments require periodic recalibration to correct for changes in diffuser properties, detector sensitivity, and changes in the internal optics. One popular commercial instrument, the Multi-Filter Rotating Shadowband Radiometer (UV-MFRSR), uses an exposed diffuser element (no quartz window or dome in front of the Teflon diffuser) with the result that the optical transmission decreases from pollution effects and partly recovers after every rainfall. Hand-cleaning the diffuser with alcohol is only partialy effective.

Currently deployed instruments include broadband instruments, which measure the solar radiation from all directions using a diffuser over a specific wavelength range, which is usually less than viewed by a pyranometer. Most are tailored to have a response to different wavelengths that approximates some biological or application absorption spectrum (action spectrum $A(\lambda)$). The most frequently approximated action spectrum is the erythemal action spectrum, which provides a measurement of the skin reddening effect for exposure to UV-A and UV-B (McKinlay and Diffey, 1987). Next are multi-spectral filter instruments that measure solar radiation from all directions, or in a narrow field of view, using several narrow wavelength bands (usually less than 10 bands from 1 nm to 10 nm wide) at the same time or sequentially (e.g., the Yankee Environmental System Ultraviolet-Multifilter Rotating Shadowband Radiometer (UV-MFRSR), and the CIMEL Sunphotometer, Fig. 5.3). These instruments require calibration for the detector response, filter transmission function, and diffuser element (if any). All of these instruments, except for the pyranometer, suffer from out of band wavelength responses, scattered and stray light in the optics and detectors, and noise in either analog amplifiers or analog to digital converters. These problems can affect data quality and instrument stability if the instruments are not frequently monitored and calibrated.

The CIMEL sunphotometer, Fig. 5.3(a), is used by AERONET for worldwide aerosol characterization (440, 500, 675, 870, and 1,020 nm) for measuring atmospheric aerosol optical thickness, absorption, particle size, and a filter at 939 nm for measuring atmospheric water vapor. There are two additional channels (340 nm and 380 nm) that are only used for aerosol extinction optical depth. The

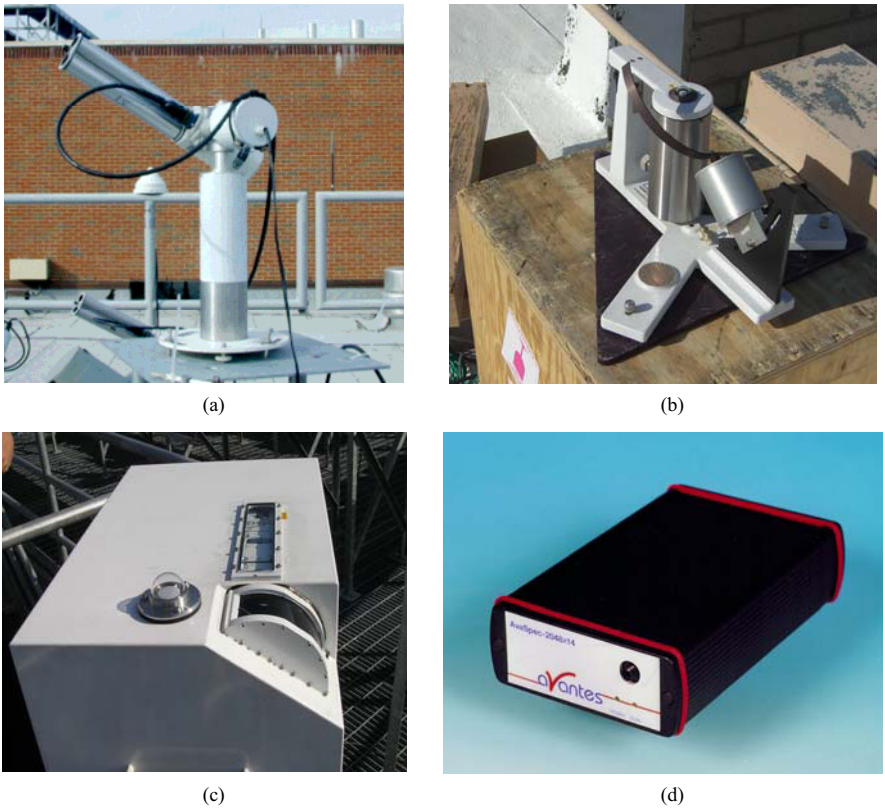

Figure 5.3 (a) Commercial AERONET CIMEL Sunphotometer for direct-sun and sky irradiances using two independent apertures, mounted on a sun-tracker; (b) Commercial modified UV-MFRSR (Shadowband) mounted on a fixed baseplate located at GSFC. The 300 nm channel has been replaced by 440 nm and a quartz dome is over the diffuser; (c) Commercial Brewer double monochromator measuring from 270 nm – 365 nm with a 0.5 nm resolution. This Brewer has been modified at GSFC with a curved quartz window and depolarizer to permit accurate measurements of sky radiances; (d) Miniature commercial spectrometer measuring from 270 nm – 525 nm with 0.5 nm resolution. The spectrometer is connected to an optical head by a fiber optic cable. This, or other commercial spectrometers, form the basis of the Pandora spectrometer system

instrument automatically determines and tracks the sun's position, and collects data in automated sequences of measurements, which include almucantar and principal plane with a 1.2° FOV. The CIMEL sunphotometers are calibrated at a central facility at Goddard Space Flight Center (GSFC) in the laboratory and against standard CIMELS, which are calibrated at Mauna Loa, Hawaii using the Langley method (Slusser et al., 2000). While the AERONET CIMELs have been extremely successful in determining aerosol properties (optical depth, absorption, and particle size distribution) in the VIS wavelengths, they cannot determine

aerosol absorption at UV wavelengths.

The UV-MFRSR (Fig. 5.3(b)) measures global radiation in seven wavelength bands (300, 305, 311, 317, 325, 332, 368 nm with 2 nm bandpass) using a cosine approximating diffuser assembly over seven separate detectors. The instrument measures whole sky (2π steradians) with and without the sun blocked by a curved metal band, which permits estimating the direct sun irradiance from the difference. The U.S. Department of Agriculture UV-B Monitoring and Research Program (UVMRP) has developed and maintains the largest network of UV-MFRSR's (over 36), which are field calibrated using the Langley method (Slusser et al., 2000) to measure global and direct sun irradiance and derive aerosol optical depths and ozone amounts from the short wavelength channels (Goering et al., 2005). While the primary purpose was for the furtherance of agricultural productivity in the US, the network has also provided a long-term database useful for irradiance related human health studies and satellite validation of ozone and UV irradiance estimates along with other traditional Brewer and Dobson spectrometers (Gao et al., 2001).

The combination of global and direct-sun irradiance can be used to deduce UV aerosol attenuation and absorption optical depths when the UV-MFRSR calibration is matched to the CIMEL sunphotometer. At GSFC and Colorado State University, the UV-MFRSR has been modified to improve its performance for aerosol detection by replacing the 300 nm channel with one for 440 nm to match one of the CIMEL sunphotometer's almucantar wavelength channels. With this modification, the UV-MFRSR can extend the CIMEL aerosol characterization into the UV wavelengths while matching the CIMEL results at 440 nm. The combined use of the CIMEL and the modified UV-MFRSR resulted in finding that the absorption of many urban aerosols have spectral dependencies in the UV that are different than those extrapolated from the visible CIMEL channels (Krotkov et al., 2005; Cede et al., 2006). The differences can be used to identify whether the aerosols are black carbon or the more strongly absorbing organic hydrocarbons. The results can also be used to calculate the reduction of UV irradiance by absorbing aerosols and to improve the estimation of tropospheric photolysis rates.

While useful work is still being done with filter spectroradiometers and broadband instruments, much more information can be derived from high spectral resolution spectrometers (e.g., the global network of Brewer spectrometers represented in the U.S. by the NOAA-EPA network of single-grating Brewers, the NSF/Biospherical network, at NASA by a modified (polarization insensitive) double-grating Brewer (Fig. 5.3(c)) (Cede et al., 2006), and by recently developed instruments using high quality commercial Charge Coupled Device (CCD) and Complementary Metal Oxide Semiconductor (CMOS) spectrometers (Fig. 5.3(d)).

The most versatile UV-VIS instruments are full spectrometers (prism, single- and double-grating dispersion elements) that are able to measure continuously in wavelength over a specified range in both narrow (less than 2°) and whole-sky FOV. The best known of these are the widely deployed Brewer spectrometers (single- and double-scanning grating versions with a single detector), which are

capable of both narrow FOV and whole-sky viewing through separate ports (Fig. 5.3(c)). The Brewer double grating instrument (283 nm – 364 nm) with resolution of about 0.5 nm full width half maximum (FWHM) is especially capable for measurements of ozone in the 300 nm – 315 nm range because of its extremely low amount of scattered or stray light (photons of one wavelength affecting the count rates of another wavelength). These instruments measure one wavelength at a time and can suffer random errors from the effects of a changing atmosphere during the duration of a measurement. This effect is minimized, but not eliminated, by a slit mask used to measure six closely spaced wavelengths in a short period of time. At GSFC, each Brewer wavelength is integrated multiple times for 0.1147 seconds, or about 0.7 seconds for all six wavelengths anywhere in the Brewer spectrometer's range. A modified version of the Brewer spectrometer has been built at GSFC, which removes the polarization sensitivity of the narrow FOV port by adding a depolarizer in front of the grating and a curved fused silica window, to replace the standard flat-plate window so that the viewing direction is always perpendicular to the window surface (Fig. 5.3(c)). This eliminates the Fresnel effect for diffuse polarized skylight. The modification permits the measurement of accurate sky radiances in the presence of an unknown amount or type of aerosol. The GSFC Brewer has successfully used measured sky-radiances to determine ozone profiles in the troposphere and stratosphere every 20 minutes throughout the day (Tzortziou et al., 2008). Another commercially available moderate size double monochromator spectrometer system has been developed in New Zealand by the National Institute of Water and Atmospheric Research (NIWA) that is technically competitive with the Brewer spectrometer. It has a wider spectral range (280 nm – 450 nm), but a coarser spectral resolution (1 nm FWHM).

There is a new class of portable narrow or wide FOV instruments that simultaneously measure all wavelengths in a specified range using a single grating as the dispersion device and a multi-pixel CCD or CMOS detector. When carefully characterized and calibrated, the narrow FOV CCD/CMOS spectrometer-based systems can measure UV and VIS radiances and derive trace gas amounts (O_3, SO_2, HCHO, BrO, NO_2, H_2O), aerosol properties (optical depth, absorption, and particle size) (Herman et al., 2009a), and ozone altitude profiles.

A small portable spectrometer based system (Pandora, Figs. 5.3(d) and 5.4(a)) that is accurate, but inexpensive, has been developed at GSFC. The CCD version consists of a temperature controlled 1/8 m symmetric Czerny-Turner commercial spectrometer (Fig. 5.3(d)) using a backthinned 2048×14 pixel CCD detector (270 nm to 525 nm with a resolution of 0.5 nm FWHM) coupled to a small custom-built optical head (Fig. 5.4(a), 1.6° circular FOV collimator, lens and filter wheel system, and electronics) by a 10 m UV-VIS transmitting fiber optic cable. The head is mounted on a computer controlled small sun-tracker device, which also permits pointing to anywhere in the sky (the fiber optic cable depolarizes the input). The plans, machine drawings, specifications, and software are freely available upon request.

For an accurate detection of trace gas amounts, the slit function, wavelength, and radiometric calibration must be accurately determined and maintained during operation by an active temperature control (20°C± 1°C) of the entire spectrometer. High signal to noise (SNR) and precision are achieved by averaging successive measurements (a few milliseconds exposure) over several seconds. The small automated sun tracker permits the instrument to operate in direct-sun viewing, almucantar, and principal plane modes for determination of aerosol properties in the same manner as the CIMEL, but as a continuous function of wavelength in both the VIS and UV ranges. The narrow FOV precludes measuring irradiance directly; but indirectly, the irradiance can be deduced by combining solar irradiance and sky radiance measurements with radiative transfer calculations.

A much larger portable spectrometer system (MFDOAS, Fig. 5.4(b); Herman et al., 2009a) with even higher precision for a given exposure time, but with the same accuracy, has been developed at Washington State University. It measures both sun and sky radiances (see Tables 5.1 and 5.2). The MFDOAS instrument consists of separate telescopes for direct sun or scattered sky, a filter wheel containing various filters and polarizers, a spectrometer/CCD-detector system, a pointing device, a computer, and a water-based cooler to maintain constant temperature.

MF-DOAS incorporates a modified commercial, single-pass Czerny-Turner spectrograph with a focal length of 300 mm (f/4). A 400-groove/mm diffraction grating, with a blaze wavelength of 400 nm, is used to disperse light. The spectrometer has a fixed 100 μm entrance slit, resulting in a 0.83 nm (7.8 pixels

(a)

(b)

Figure 5.4 (a) Pandora optical head and sun-tracker mounted on a tripod and attached to a small spectrometer (Fig. 5.3(d)) with a 10 m fiber optic cable; (b) MFDOAS spectrometer mounted on its base and sun-tracker. The water-cooled spectrometer is controlled by with a computer in its base

Table 5.1 Pandora characteristics

Wavelength interval	270 nm – 520 nm
Spectral resolution (FWHM)	0.42 nm – 0.52 nm
Oversampling	8 pixels
Spectrometer slit width	50 μm
Grating line density	1200 mm^{-1}
Grating blaze wavelength	250 nm
CCD array size (pixels)	14×2048
CCD pixel size (μm)	25
80% full well S/N (1 sigma)	300:1
CCD dynamic range	16 bit
Minimum integration time	4 ms
FOV (sun and sky)	1.6°

Table 5.2 MFDOAS characteristics

Wavelength interval	282 nm – 498 nm
Spectral resolution (FWHM)	0.83 nm
Oversampling	7.8 pixels
Spectrometer slit width	100 μm
Grating line density	400 mm^{-1}
Grating blaze wavelength	400 nm
CCD array size (pixels)	512×2048
CCD pixel size (μm)	13.5×13.5
80% full well S/N (400 rows)	5640:1
CCD dynamic range	16 bit
Integration time	20 ms – 60 s
FOV (sun)	1.5°

FWHM) average spectral resolution. The wavelength coverage is from 282 nm to 498 nm. The CCD is thermoelectrically cooled to −70°C. Direct sunlight enters the instrument through a 25 cm black anodized, baffled snout with a quartz window for weather control. A biconvex lens focuses the sunlight onto an 8 cm spectralon integrating sphere that moves into the spectrometer's FOV during the direct-sun measurements. A series of baffles inside the telescope limit the direct-sun field of view to about 1.5°. The sky FOV is a narrow rectangle that is 1° wide. Use of an integrating sphere assures equal illumination of the optics and minimizes the effect of pointing errors, eliminating a critical source of spectral residual error. Light from the scattered sky or the direct sun passes through two filter wheels containing optional depolarizers, a spectral flattening filter, and UV-transmitting and UV-cutoff filters.

The two independently developed instruments have been compared during two

campaigns at GSFC and JPL's Table Mountain Facility in California (TMF) and found to agree very closely (Herman et al., 2009a). During these campaigns, both instruments measured $C(NO_2)$, the column amount of NO_2, in the atmosphere using direct-sun observations of atmospheric absorption. The precision achieved was 0.01 DU (1 DU $= 2.67 \times 10^{16}$ molecules/cm^2) with an accuracy of ± 0.05 DU compared to the minimum $C(NO_2)$ in the atmosphere of 0.1 DU. This level of precision and accuracy is sufficient to measure UV and VIS radiances, as well as trace gas amounts (O_3, SO_2, NO_2, H_2O and aerosols). The measured trace gas and aerosol amounts can be used to calculate UV irradiances and radiances over the entire 300 nm to 400 nm range.

The large dynamic intensity range as a function of wavelength can cause a well-known spectrometer system problem of stray light from longer wavelengths affecting the radiometric response of the shorter wavelengths. This problem is minimized by using bandpass filters (e.g., UV-340 filter) that block the visible and pass the UV so that ozone amounts can be measured (305 nm – 320 nm) by the same instrument that measures NO_2 (400 nm – 450 nm). The best performance is obtained by use of a double filter wheel with one wheel containing neutral density ND filters, open hole, and blocked hole, and the other containing function filters (e.g., UV-340, polarization filters, open hole etc.). The blocked hole is essential for the measurement of spectrometer dark current correction in between each measurement of radiance for the same exposure time as the radiance measurement. The use of fiber optic cables to connect the optical head to the spectrometer (Pandora) has advantages (modularity, light weight, depolarization, and remote operation) and disadvantages (radiometric stability, calibration, controlling the FOV, and some fragility) compared to direct coupling of the optical head to the spectrometer (MFDOAS). While these problems are not trivial, they have been mostly overcome.

For all of these instruments, the key factors are the absolute accuracy of the calibration and the long-term stability (precision) of the instrument. Absolute accuracy is achieved by measuring the output of a standard lamp that has been verified by an appropriate standards organization (e.g., the National Institute Standards and Technology (NIST), in the U.S., or one of the European standards laboratories). The quality of the transfer of calibration is dependent on a meticulous laboratory setup between the standard lamp and the instrument in question. Currently, the best transfer of calibration produces an accuracy of between 2% and 3% under the assumption that the instrument has been fully characterized in the laboratory before the use of a standard lamp (slit functions, filter transmission functions, wavelength calibration, temperature sensitivity, stray and scattered light, etc.). The achievable accuracy will be a combination of the instrument characterization errors and the lamp transfer radiometric calibration. Note: To determine the wavelength dependent slit functions over the entire wavelength range or the filter functions, the detector must have many light sensitive elements within the projection of the grating's spectral resolution onto the detector at its

full width at half the maximum height (FWHM) or the width of the filter bandpass at FWHM. For wavelength scanning spectrometers, the scanning step size must be much less than the spectral resolution FWHM to accurately determine the slit function.

Good long-term stability of the instrumentation is needed to detect possible changes in the amount of radiation reaching the ground. The stability can be determined by repeated checks against standard lamps in the laboratory or by techniques applied to the data obtained in the field. The most common of these is a procedure that attempts to derive the solar irradiance above the atmosphere by measuring solar irradiance at the ground as a function of SZA (Langley method). This gives a series of measured instrument counts as a function of the amount of atmosphere between the instrument and the sun. If the atmosphere is approximately stable over the period of the measurements, the series of measurements can be extrapolated back to zero atmospheres. The details of a modified Langley method are described in Herman et al. (2009a). Repeating this procedure frequently for the life of the instrument can give a measure of the instrument's stability or precision. The best Langley procedures are performed at extremely clean sites such as Mauna Loa, Hawaii, where the interference from changing aerosol and boundary layer ozone amounts is at a minimum. The combination of frequent standard lamp calibration and in the field Langley procedure provides a precision between 2% and 3%. Some instruments, such as a well-maintained double Brewer spectrometer, are known to be very stable against standard lamps and can produce a radiance precision near 1% if the instrument is modified to be polarization insensitive (Fig. 5.3(c)).

In addition to ground-based instruments, there have been several spectrometers located on satellites since 1979, which are able to provide accurate estimates of ozone and cloud transmission T (through measured cloud and aerosol Lambert Equivalent Reflectivity R (Herman et al., 2001a; 2009b; see Section 5.3.4), where T is approximately $1-R$). The estimate for T has been improved by detailed radiative transfer solutions for plane parallel clouds of different optical thickness. The resulting cloud transmission factor C_T (Krotkov et al., 1998) gives results that are close to the simple expression $C_T=(1-R)/(1-R_G)$, where R_G is the measured surface reflectivity and $R_G<R<1$ (Herman et al., 2001b). This expression for C_T has been given by Krotkov et al. (1998), and can be derived from a Stokes calculation (see Section 5.3.5) for a transmitting and reflecting surface over a reflecting ground (Herman et al., 2009b). Ultraviolet and VIS irradiance, at ground-level or within the atmosphere, can be accurately estimated using radiative transfer calculations that include the appropriate absorbing gases, aerosol scattering and absorption, surface reflectivity, and cloud transmission. Frequently, the calculated amount of radiation is overestimated by 10% to 20% because of the lack of knowledge regarding aerosol absorption, even when the aerosol optical depth is known, especially in urban areas (Herman et al., 1999).

Instrumental requirements for making long-term UV irradiance measurements

are well understood in terms of calibration and stability for both spectrometers and broadband radiometers (WMO, 1999; 2003; 2007). The degree to which further improvements are made to a given instrument type should be dictated by the scientific goals of an application. For example, different accuracy and precision are needed for estimating transmission through the atmosphere in the presence of trace absorbing gases, changes in UV and VIS radiances and irradiances needed for estimating changes in atmospheric chemistry photolysis rates, climate change studies, or for use in various applications (estimations of solar radiation amounts vs. cancer incidence, material damage, atmospheric photochemistry, and biological productivity).

Biological or material damage applications are usually expressed in terms of "action" spectra, which are an estimate of the relative strength of a given process (e.g., skin reddening) for a given wavelength per unit of incident solar radiation. The biological action spectra are usually poorly known and have a wide variation within a species depending on skin or surface type, genetics, species adaptation to its local environment, and from species to species. In other words, knowing the solar radiation change to within a few percent, or even 10%, is good enough for most biological and materials damage process studies. Of more importance is determining the changes in exposure to solar radiation either in the same location or by moving to lower latitudes where there is usually more solar irradiance.

Higher accuracy and precision are needed for understanding physical processes, such as contributions to atmospheric energy balance related to global warming or for estimations of photolysis rates for atmospheric chemistry studies. The estimated surface heat imbalance between the surface re-radiation and the atmosphere is about $+9$ watts/m^2 (Lin et al., 2008), so that a contribution of 1 watt/m^2 would be a significant portion of the uncertainty. For the UV range from 300 nm to 400 nm, there are approximately 100.7 watts/m^2 at the top of the atmosphere and about half that at the surface, so that detecting a 1-watt/m^2 change in the UV band over a decade would require 2% long-term precision.

5.3 Detection of Long-Term Change

Long-term ground-based UV spectral irradiance measurements must be carefully made and analyzed to preclude variations due to clouds that could be mixed into UV trend estimates, or whose variability can mask the detection of small changes. If ground-based data are filtered for cloud-free observations, then UV-B changes caused by the variability in ozone amounts are easily observed in multi-year data records. Aerosols and other forms of pollution can also produce apparent changes in UV irradiance that masks the effect of ozone changes. These changes can be taken into account if measurements are made simultaneously within the UV-B range (e.g., 305 nm) and outside of the ozone absorbing range (e.g., 324 nm). The lack of ability to separate aerosol and pollution effects from ozone-induced

changes limits the usefulness of broadband instruments (300 nm – 400 nm) for understanding the observed irradiance changes.

Radiometric and wavelength calibration of spectrometers used for irradiance trend estimates must be carefully maintained to detect the relatively small changes caused by ozone and aerosols. Making accurate spectral measurements can be difficult, since the natural UV spectrum at the ground changes by several orders of magnitude from 300 nm to 400 nm. A slight wavelength misalignment can cause significant errors in the measured UV-B irradiance amount. Wavelength misalignment is less important for broadband wavelength integrated quantities, such as erythemal irradiance. Equally difficult are measurements of UV irradiance ratios at both small (near noon) and large SZAs (near sunrise or sunset) because of the large dynamic range required. The use of sensitive CCD spectrometers and multiple neutral density filters can mitigate the intensity problem at the expense of some additional calibration. Experience to date with the backthinned CCD Pandora spectrometers indicates both the spectrometers and the optics are stable with field calibration and suited for both short- and long-term measurements.

5.3.1 Radiation Amplification Factor

An alternate method for the estimation of long-term changes in UV-B irradiance can be devised by combining measured ozone values with radiative transfer calculations. These calculations can be simplified for estimating irradiance change by neglecting scattering effects. For clear-sky, constant cloud, and constant aerosol conditions, changes in monochromatic UV-B irradiance dF show a well-defined inverse relation with changes in the amount of ozone dΩ in the atmosphere based on laboratory measurements of the ozone UV absorption coefficient α (e.g., Zerefos et al., 2001). This has been most clearly demonstrated using a spectroradiometer measuring ozone and erythemally weighted irradiance (300 nm – 400 nm) at Mauna Loa, Hawaii on 132 clear mornings between July 1995 and July 1996 (WMO report, 1999). The relationship of a change in irradiance dF at a single wavelength to a small change in column ozone amount dΩ is approximately given in Eq. (5.1).

$$\mathrm{d}F/F = -\mathrm{d}\Omega/\Omega\,\alpha\Omega\sec(\theta) = -\mathrm{d}\Omega/\Omega\,(\mathrm{RAF}) \tag{5.1}$$

The differential relationship is derived from the standard Beer's Law of irradiance F attenuation in an absorbing atmosphere, $F = F_{\mathrm{o}}\exp(-\alpha\Omega\sec(\theta))$, where Ω = the ozone column amount in DU (1 DU = 1 milli-atm-cm or 2.69×10^{16} molecules/cm^2), α = the ozone absorption coefficient (in cm^{-1}), θ = the SZA, and F_{o} is the irradiance at the top of the atmosphere. The quantity $\alpha\Omega\sec(\theta)$ is the slant path optical depth, which was also named the Radiation Amplification Factor, or RAF(Ω,θ) (Madronich, 1993) when Eq. (5.1) was used for estimating irradiance change. When varying cloud reflectivity dR is included, $F = F_{\mathrm{o}}\exp$

$(-\alpha\Omega\sec(\theta))\,(1-R)/(1-R_G)$ and the fractional change in irradiance is

$$dF/F = -d\Omega/\Omega\,\alpha\Omega\,\sec(\theta) + dC_T/C_T \tag{5.2}$$

where C_T = the cloud + aerosol transmission = $(1-R)/(1-R_G)$,
and R = the reflectivity of the ground R_G + cloud R_C system ($R_G < R < 1$).

Equation (5.2) has proven to be quite accurate for estimating monochromatic irradiance changes for small changes in Ω under a wide variety of conditions, especially for cloud-free conditions. A comparison was run between radiative transfer solutions RTS and Eq. (5.1) for 1% change from three ozone values, 275 DU, 375 DU, and 475 DU for the wavelength range 290 nm to 350 nm, and SZA = 30° (Herman et al., 1999). The largest difference between the RTS and Eq. (5.1) was 0.2% at 290 nm for 275 DU, and less than 0.1% for wavelengths larger than 310 nm.

Figure 5.5 shows a specific example of the cloud-free monochromatic RAF for $\Omega = 0.33$ atmosphere-cm = 330 DU and SZA = 45°, and shows the ozone absorption coefficient (cm^{-1}) for the wavelength range from 240 nm to 340 nm. The RAF method accurately estimates small monochromatic UV irradiance changes compared to clear-sky radiative transfer (Herman et al., 1999). For example, radiative transfer shows that a 1% decrease in O_3 produces a 2.115% increase in 305 nm irradiance, while the RAF method estimates a 2.064% increase ($\Omega = 375$ DU, $\theta = 30°$). There are wavelength dependent deviations from Eqs. (5.1) and (5.2) under optically thick clouds caused by multiple scattering increasing the optical path for ozone absorption. If there is a 1% change in ground reflectivity from a

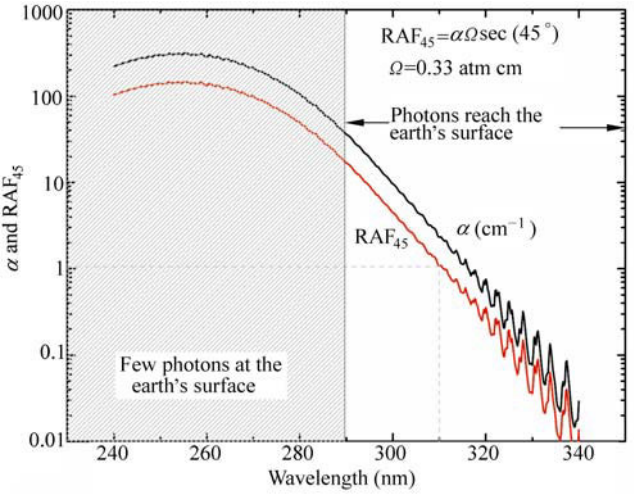

Figure 5.5 Ozone absorption coefficient α (cm^{-1}) and the RAF_{45} for an SZA = 45° and ozone amount of 330 DU ($\Omega = 0.330$ atm cm). Note that at 310 nm, the $RAF_{45} \sim 1$, so that a 1% increase in O_3 would produce a 1% decrease in 310 nm irradiance

nominal reflectivity of $R_G = 5$ RU ($R_G = 0.05$) for clear skies, the change in downward irradiance is less than 0.35% due to backscattering from the atmosphere. If there is optically thick cloud cover, the change increases to about 0.8%.

The RAF method has also been validated using measurements of ozone and UV irradiance at Mauna Loa, Hawaii. Figure 5.6 shows that when clear-sky measurements of monochromatic irradiance are carefully made for a 1% change in ozone amounts, but no change in aerosols, the measured and calculated changes agree quite well. Later, it is shown that an empirical power-law RAF method agrees with monochromatic Eq. (5.1) for small ozone changes, but also applies for action spectrum weighted irradiances with larger ozone changes. The empirical power law can be obtained (numerically) from Beer's Law (see Section 5.7).

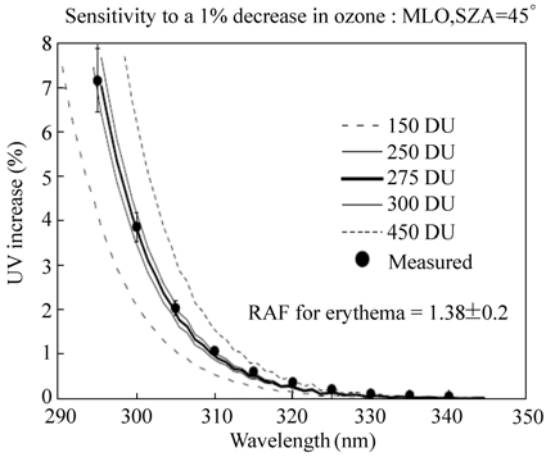

Figure 5.6 Validation of RAF method using the measured (dark circles) changes in ozone and UV irradiance from Mauna Loa, Hawaii (WMO, 1999)

Fioletov et al. (1997) reported an extensive analysis of UV-B irradiance and its dependence on total ozone. The analysis provides an empirical wavelength-by-wavelength measure of the increase of UV-B irradiance for a 1% decrease of total ozone. The values for UV change with ozone change were found to be essentially the same for clear and cloudy conditions (except for very heavy clouds), and are in good agreement with model results for longer wavelengths and moderate SZA. The conclusion is in agreement with the approximation in Eqs. (5.1) and (5.2).

Both theory and observations show that reductions in ozone lead to increases in UV erythemal and UV-B monochromatic radiation at the earth's surface. For mid-latitudes, changes in measured erythemal irradiance can be approximated using Eq. (5.1) with the monochromatic RAF = 1.3 to 1.4 at mid-latitudes when the ozone amount changes by 1%. However, an empirical power law form gives a better approximation to erythemal irradiance change with ozone than Eq. (5.1). A detailed discussion of RAF is given in Section 5.7.

Satellite estimates of ozone and reflectivity are retrieved separately, each with its own error budget. Ozone is retrieved with about 1% accuracy, especially on a zonal average basis. Zonal average reflectivity is retrieved with an accuracy of about 2 RU or 0.02 ($0 < R < 1$). The differences $d\Omega$ and dR have the same accuracy as Ω and R, since they are simply the difference from a fixed reference value. When Eqs. (5.1) and (5.2) are used for estimating UV trends in this study (see Section 5.3.7), the reference values used are the average value of ozone or reflectivity in the first year as a function of latitude.

The implication of this and following sections is that it may be easier to measure changes in ozone amounts and cloud plus aerosol transmission combined with radiative transfer calculations of UV irradiance change than it is to measure the changes in UV irradiance with very stable and well-calibrated instrumentation. This method will miss some features of UV irradiance, such as the momentary increase above clear sky amounts caused by reflections from the sides of clouds and will not be accurate in mountainous regions where the terrain reflectivity affects the irradiance more than in relatively flat regions. Even in mountainous regions, Eq. (5.2) will still represent the change in irradiance caused by satellite-detected changes in stratospheric and tropospheric ozone amounts. However, changes in scene reflectivity from the sides of mountains can affect the amount of UV irradiance in a manner that is usually not detected by ozone-measuring satellites. The method will also miss any absorption effects (usually small) caused by other trace gases (e.g., NO_2 and SO_2) and absorbing aerosols. Currently there are no long-term measurements of these quantities and their changes over wide areas.

5.3.2 Different Definitions of RAF

An alternate power-law form for estimating action spectrum weighted irradiance change is commonly used for large changes in ozone amount, which empirically matches data quite well (Booth and Madronich, 1994; Blumthaler et al., 1995). This form is given in Eq. (5.3).

$$F_1/F_2 = (\Omega_1/\Omega_2)^{-\mathrm{RAF}(\theta)} \tag{5.3}$$

where Ω_1 and Ω_2 are two values of ozone that correspond to two values of irradiance, F_1 and F_2, respectively. The RAF(θ) is an empirically selected set of constants to match Eq. (5.3) to observed data. For small changes in Ω, equation (5.3) is approximately the same as Eq. (5.1) by expanding $F_1/F_2 = [1 + (\Omega_1 - \Omega_2)/\Omega_2)]^{-\mathrm{RAF}} = 1 - \mathrm{RAF}\,[(\Omega_1 - \Omega_2)/\Omega_2)] + \cdots$, so that $(F_1 - F_2)/F_2 = -\mathrm{RAF}\,(\Omega_1 - \Omega_2)/\Omega_2 + \cdots$ for $(\Omega_1 - \Omega_2) << \Omega_2$.

The primary use for the power-law form is for processes that span a wide wavelength range that includes UV-B and UV-A. The best-known example is the erythemal action spectrum weighted irradiance $A_{\mathrm{ERY}}(\lambda)F(\lambda)$, where the weighting is given by the McKinlay and Diffey (1987) action spectrum $A_{\mathrm{ERY}}(\lambda)$ (see

Section 5.7). Since the power law form is empirical, measurements or radiative transfer calculations, as a function of ozone amount, must be made to estimate $RAF_{ERY}(\theta)$. For large SZAs the UV-B portion of the irradiance diminishes rapidly and the product $A_{ERY}(\lambda)F(\lambda)$ is dominated by UV-A, which has almost no sensitivity to ozone change. As a function of latitude, the mid-day $RAF_{ERY}(\theta)$ is approximately constant in low and middle latitudes, and then decreases at high latitudes (high SZA) (Bodhaine et al., 1997). This behavior appears to be quite different from the monochromatic RAF in Eq. (5.1) (see Section 5.7).

The existence of two definitions of RAF (Beer's Law, equation (5.1) and Power Law, Eq. (5.3)) can cause some confusion. The physically based Beer's Law formulation can also be used to derive monochromatic $\Delta F/F$ for large changes in ozone $\Delta\Omega/\Omega$. Let $F_1 = F_0 \exp(-\alpha\Omega_1 \sec(\theta))$ and $F_2 = F_0 \exp(-\alpha\Omega_2 \sec(\theta))$, then define $\Delta F_{12}/F_2 = (F_1 - F_2)/F_2$ and $\Delta\Omega_{12}/\Omega_2 = (\Omega_1 - \Omega_2)/\Omega_2$. The result is given in Eq. (5.4).

$$\Delta F_{12}/F_2 = \exp(-\alpha\Omega_2 \sec(\theta)\, \Delta\Omega_{12}/\Omega_2) - 1 \tag{5.4}$$

In Section 5.7, we show that the use of Eq. (5.4) Beer's Law leads directly to the Power Law after integrating over the wavelength range corresponding to an action spectrum. In the following sections, $\Delta\Omega_{12}/\Omega_2$ is small, so that the change for near-monochromatic dF/F can be estimated from Eq. (5.1) or (5.4).

5.3.3 Estimating UV Trends: Discussion

Satellite observations of UV and VIS irradiance can be used to distinguish regional and global changes in derived atmospheric properties (e.g., ozone, sulfur dioxide, reflectivity, aerosol distribution, nitrogen dioxide, UV-irradiance) in contrast to purely local observations from ground-based instruments. The estimates are based on a single well-calibrated instrument that is used over extended periods (Herman et al., 1991; Herman et al., 1996). For example, the $\pm 52^\circ$ side scanning Nimbus-7/TOMS measured six radiance channels (312, 317, 331, 340, 360, and 380 nm, 1-nm wide) producing a full global map in each channel once per day for the period October 1978 to January 1993. As with most satellite instruments, the accuracy and precision were maintained using in-flight earth radiance and solar irradiance data to detect and correct changes from the pre-launch laboratory calibration. The data series obtained by Nimbus-7/TOMS has been extended through the present (2009) using the NOAA SBUV-2 series of spectrometers and the hyperspectral spectrometer OMI (270 nm – 500 nm with a resolution of about 0.5 nm).

Satellite derived geophysical quantities (column ozone amounts, values of aerosol optical depth, scene reflectivities (cloud, aerosol, plus ground), and a ground reflectivity climatology) are used to estimate the solar UV irradiance at the ground. Since the entire process is based on remote sensing, complicated retrieval

algorithms, and radiative transfer model calculations, the results must be validated against a small set of well-calibrated ground-based measurements distributed in a variety of regions that observe under different atmospheric and geographic conditions. The main purpose of these validation measurements is to provide timely warning that either the satellite or the ground-based instruments are experiencing calibration drift, or that there is some missing physical parameter in the satellite algorithm that can only be supplied from ground-based ancillary data (e.g., aerosol absorption).

UV radiation reaching the earth's surface varies on all time scales, from seconds to seasons to years. In today's atmosphere, the multi-year UV-B variations are principally controlled by changes in stratospheric ozone, changes in the extent of cloud cover, and other longer-term changes such as in the amount of aerosol and pollution. Day-to-day ozone-caused changes from stratospheric and tropospheric dynamics can be significant, but are usually smaller than changes due to cloud cover, because the stratospheric abundance of ozone usually changes as a moderate percentage (~15%) of its seasonally changing mean value. The broad, seasonally repeatable cloud patterns can also cause changes in daily and monthly time scales as the weather changes. On longer time scales (decadal), most regional changes in cloud cover have been small (Herman et al., 2009b), so that global and zonal average changes in UV-B due to long-term ozone depletion are dominant over cloud-change effects. In some regions (e.g., northern Europe), decadal-term cloud changes are also important. Ultraviolet-A changes are controlled by all of the above factors, except ozone.

Ozone data from Nimbus-7/TOMS, obtained during June for the entire 5° longitudinal zone centered at 40°N, shows that the day-to-day ozone amount can vary by 50 DU, the approximate mean value of 350 DU, or $\mathrm{d}\Omega/\Omega = \pm 0.14$. The day-to-day June ozone variation is obtained from figures similar to those shown in Herman et al. (1995). Using an average noon SZA for June of about 23° and an ozone absorption coefficient for 305 nm $\alpha = 4.75\ \mathrm{cm}^{-1}$ yields a typical 305 nm irradiance change $\mathrm{d}F/F = -\mathrm{d}\Omega/\Omega\,\alpha\Omega\sec(\theta) = \pm 0.14 \times 4.75 \times 0.35 \times 1.09 = \pm 0.25$. In other words, for clear-sky conditions, the 305 nm irradiance typically varies by ±25% during June, just from to day-to-day ozone changes. As will be discussed later, the day-to-day variability of clear-sky 40°N UV June irradiance is much larger than the change caused by the long-term June decreases in ozone from 1979 to 2008.

Other factors, such as Rayleigh scattering and land/ocean surface reflectivity, affect the magnitude of measured or theoretically estimated UV irradiance. However, these factors do not significantly affect the short- or long-term changes in irradiance, since their changes are small. Hourly or daily changes in Rayleigh scattering follow the small changes in atmospheric pressure, which usually are less than 2%. There have been no long-term changes in mean atmospheric pressure. The UV surface reflectivity R_G is small (3 RU − 10 RU) and almost constant with time, except in regions seasonally or permanently covered with snow or ice. Based on radiative

transfer studies, clear-sky atmospheric backscattering to the surface contributes less than 0.2 R_G to the measured UV irradiance, which is quite small for most ice/snow-free scenes (Herman et al., 1999).

5.3.4 Reduction of UV Irradiance by Clouds and Aerosols

A measured daily cycle of UV reaching the surface will show large UV irradiance reductions from clear-sky conditions as clouds pass over a site while blocking the view of the sun. These reductions are frequently in excess of those caused by measured ozone changes from climatological values for wavelengths longer than 305 nm. In general, the effect of clouds and aerosols reduces the UV and VIS amounts at all wavelengths reaching the earth's surface. When using satellite data to estimate the amount of UV reaching the surface, the average amount of UV radiation reduction caused by clouds, plus scattering aerosols, can be estimated from the Lambert Equivalent scene Reflectivity (LER), which varies significantly between locations on the coarse resolution scale of the satellite instrument (50 km to 100 km). The cloud reflectivity estimation can only be done for snow and ice-free conditions,

The LER of a scene is calculated by requiring that the measured radiance I_{SM} match the calculated radiance I_S at the observing position of the satellite by adjusting a single free parameter R in the formal solution of the radiative transfer equation in Eq. (5.5).

$$I_S(\Omega,\Theta,R,P_O) = \frac{RI_d(\Omega,\Theta,P_O)f(\Omega,\Theta,P_O)}{1-RS_b(\Omega,P_O)} + I_{dO}(\Omega,\Theta,P_O) = I_{SM} \qquad (5.5)$$

Ω = column ozone amount
Θ = viewing geometry (SZA, satellite look angle, azimuth angle)
R = LER at P_O, $0 < R < 1$
P_O = pressure of the reflecting surface (e.g., ground or cloud)
S_b = fraction scattered back to P_O from the atmosphere
I_d = sum of direct and diffuse irradiance reaching P_O
f = fraction of radiation reflected from P_O reaching the satellite
I_{dO} = radiance scattered back from the atmosphere for $R = R_G = 0$ at $P = P_O$

The quantities S_b, I_d, f, and I_{dO} are calculated from a radiative transfer solution and stored in tables. From Eq. (5.5),

$$R = \frac{I_{SM} - I_{dO}}{I_d f + (I_{SM} - I_{dO})S_b} \qquad (5.6)$$

The quantities in Eq. (5.6) are calculated from the TOMRAD vector radiative transfer program for a pure Rayleigh atmosphere for different values of R and P_O to create a table lookup capability. The details of the implementation are given in

the paper written by Dave (1964) from which TOMRAD was developed. Essentially, the quantities S_b and f are calculated for unit upward irradiance leaving the surface at P_O. In the case of S_b, it is the fraction that scatters back to the surface, and in the case of f, it is the fraction that reaches the satellite. I_{dO} is computed for the case $R_g = 0$.

The earth's reflectivity as represented by the LER is not the same as the angularly dependent reflectivity of a surface containing structures (grass, vegetation, mountains, clouds, etc.). The angular effects caused by structures in the surface and in clouds are minimized by scene averaging from the coarse resolution of the observations. In order to use the LER to estimate change in reflectivity, the observing geometry must be approximately constant over the life of the satellite, or corrections must be made to account for the change in angular dependence of the observations. Most of the satellites used to construct the reflectivity time series were in near-noon sun-synchronous orbits. This means that any location on the earth's surface was observed at approximately the same angle for the same day of each year. Long-term changes in LER represent changes in the scene reflectivity (clouds, aerosols, and surface) for each location. Comparisons of LER between seasons contain an angular effect caused by the seasonal change in the noontime SZA from the changing solar declination angle $\pm 23.3^\circ$.

The Nimbus-7/TOMS instrument obtained daily global coverage for ozone and LER for over 13 years at a spatial resolution that varied between 50×50 km^2 to 100×100 km^2. For any given location on the earth's surface, frequency of occurrence histograms were constructed from satellite derived reflectivity values (Fig. 5.7) (Herman et al., 2001b). These histograms showed that the most commonly occurring values of R were about 3 RU − 5 RU greater than the surface reflectivity, and represent haze or very sparse cloud cover. Central Europe, represented by Germany, is quite different from North American sites in that the most frequent values are around 10 RU (127 days; 3.9%) or around 50 RU (128 days; 3.9%), with almost the same number of days (80 to 128 days; 2.4% to 3.9%) having 10 RU to 70 RU. Greenland is another extreme, where the reflectivity is always high because of the ice cover. Nevada and Virginia are similar, except that Nevada has a lower average reflectivity representing less cloud cover. Another extreme case is represented by Australia, where the average reflectivity (due to cloud cover) is very low, and cumulative UV exposure is high compared to the same latitude in the U.S.

Satellite observations of reflected UV indicate that reflectivities for typical mid-latitude cloud covered scenes have a wide range of values, which can reach 90 RU over high altitude cloud tops, which most frequently occurs in the tropics. Under snow-free conditions, the surface reflectivity R_G is usually between 2 RU and 4 RU, reaching about 10 RU in the Libyan Desert and similar small areas (e.g., Andes Mountain high deserts). Area-averaged clear-sky UV surface irradiance is then approximately reduced as a linear function of the cloud plus aerosol reflectivity, which can be written in terms of effective transmission. The cloud transmission is approximately given by $C_T = (1 - R)/(1 - R_G)$, where $R_G < R < 1$.

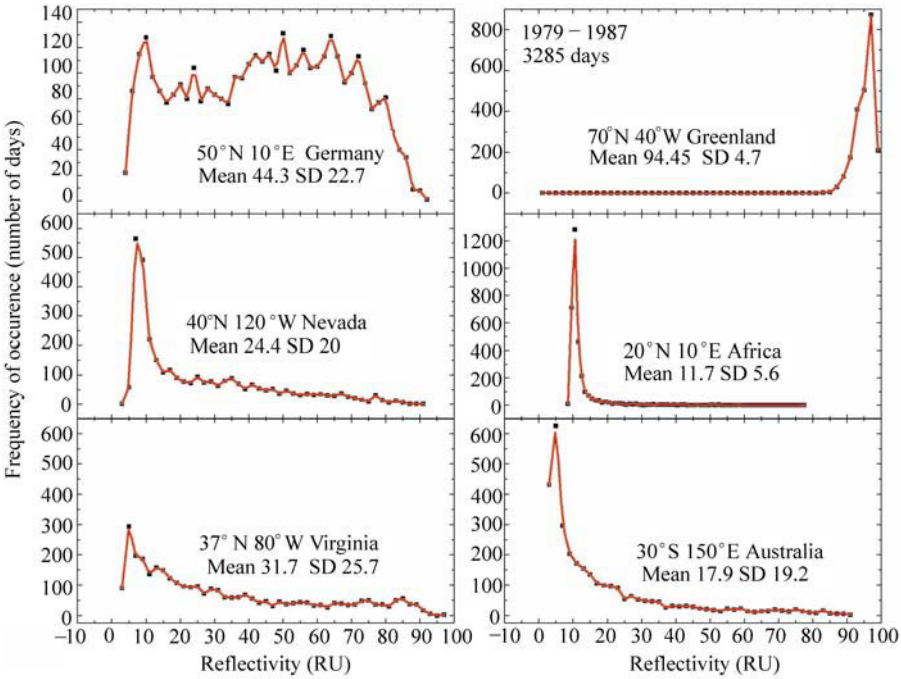

Figure 5.7 Frequency of occurrence of reflectivity values 1979 – 1987 (3285 days) for six different locations. The mean and standard deviation (SD) are in RU (1 RU = 1%). Based on Herman et al. (2001b)

5.3.5 Stokes Derivation of $C_T=(1-R)/(1-R_G)$

A satellite viewing the earth's surface observes a combined reflectivity $R=R_{SYSTEM}$ from the clouds and the ground. Assume that the cloud-ground system can be approximated by a two-layer Stokes problem with atmospheric effects neglected. Assume that the clouds have different transmission and reflections properties for diffuse T_D, R_D and direct-sun T_C, R_C. The arrows in Fig. 5.8 represent the partial contributions to the upward and downward fluxes.

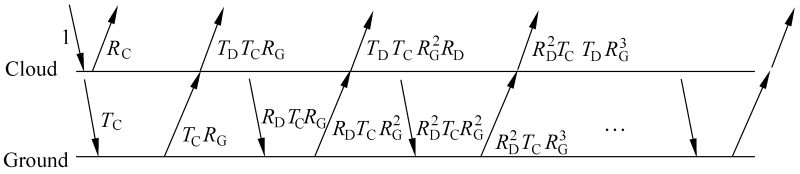

Figure 5.8 Stokes diagram for C_T for unit irradiance incident on a cloud of transmittance T_C over a surface of reflectance R_G. The cloud and surface have diffuse transmittance and reflectivity of T_D and R_D

$$R_{SYSTEM} = R_C + R_G T_C T_D \left[1 + R_G R_D + (R_G R_D)^2 + \cdots\right]$$

$$= R_C + R_G T_D T_C / (1 - R_G R_D) \tag{5.7}$$

$$C_T = T_C \left[1 + R_G R_D + (R_G R_D)^2 + \cdots\right] = T_C / (1 - R_G R_D) \tag{5.8}$$

Using Eq. (5.8), rewrite Eq. (5.7) as

$$1 - R_{SYSTEM} = 1 - R_C - R_G T_D T_C / (1 - R_G R_D) = 1 - R_C - R_G T_D C_T \tag{5.9}$$

Assume $T_C = 1 - R_C$ and $T_D = 1 - R_D$, rewrite (5.8) as $C_T (1 - R_G R_D) = 1 - R_C$.

Now Eq. (5.9) becomes $1 - R_{SYSTEM} = C_T (1 - R_G R_D) - R_G C_T (1 - R_D)$

$$= C_T (1 - R_G) \tag{5.10}$$

Finally, $C_T = (1 - R_{SYSTEM})/(1 - R_G)$ (5.11)

where

R_G = Reflectivity of the ground

R_C = Direct beam cloud reflectivity

R_D = Diffuse flux cloud reflectivity

R_{SYSTEM} = Reflectivity of the combined ground-cloud system

T_C and T_D are the corresponding cloud transmissivities

Assume $R = R_{SYSTEM}$ as an approximation of the reflectivity seen by the satellite

A problem exists for high reflectivity scenes observed by UV/VIS satellite instruments, such as those covered by snow or ice. Snow/ice covered scenes cannot be distinguished from cloud cover by radiance observations in the UV wavelengths. Because of this, the use of C_T to estimate the amount of UV radiation at the surface in the presence of snow is likely to be in error. For example, the very high reflectivity values observed in Greenland (Fig. 5.7) are almost independent of the cloud cover. Radiative transfer solutions for clouds over snow/ice surfaces show that the maximum reflectivity is obtained for clear-sky scenes, which is reduced somewhat in the presence of clouds over snow/ice (Krotkov et al., 1998).

Long-term changes in regional cloud and aerosol reflectivity must be considered when estimating long-term changes in UV irradiance. However, for most populated regions of the earth, long-term (decadal) cloud and aerosol scattering changes have been shown to be small, even where they are statistically significant (Herman et al., 2001a; Herman et al., 2009b). Local values of aerosol amounts and absorption are currently estimated from the widely distributed AERONET network of ground-based sunphotometers (Holben et al., 2001), and for clear-sky scenes, from satellite data (Torres et al., 2002a, b).

5.3.6 UV Absorption

The amount of UV radiation reaching the earth's surface is affected by air pollution, i.e., absorption by aerosols (black carbon, dust, and smoke), tropospheric O_3, NO_2, and other gases. These can cause typical reductions in UV radiation by up to 15% in polluted sites, but with much higher reductions occurring in certain highly polluted cities, e.g., occasionally in Los Angeles and frequently in Beijing. NO_2 causes small reductions, mainly to UV-A, since its absorption cross-section peaks near 410 nm, yet is still significant at 330 nm. Aerosols of most types affect UV and VIS radiation at all wavelengths. Pollution abatement, especially in highly polluted regions, can decrease the atmospheric reflectivity and absorption, which has the effect of increasing the amount of UV and VIS radiation reaching the ground. The reductions in surface UV can be much higher in regions affected by smoke (e.g., biomass burning) or by the major dust storms that frequently occur in Africa and parts of China.

Absorption of UV and VIS irradiance/radiance is used to determine the amount of pollution (O_3, SO_2, HCHO, NO_2, H_2O) in the atmosphere by matching the measured and calculated spectrum reaching ground-based spectrometers or reflected back to a satellite spectrometer (e.g., OMI and GOME) (Cede et al., 2006; Wenig et al., 2006).

5.3.7 Estimating Zonal Average UV Change

Since changes in cloud, plus aerosol, reflectivity have been small over the 1979 to 2008 period, except in some local regions (Herman et al., 2009b), the zonal average change in UVB radiation is dominated by changes in ozone amounts. For this purpose, the changes can be estimated from Eq. (5.1) or (5.3), or including the observed LER change term as in Eq. (5.2). The ozone data set is based on a combination of satellite data from Nimbus-7/TOMS, the SBUV-2 series of satellite data, EP/TOMS, and AURA/OMI organized into monthly average and zonal average time series. The time of the day is taken as local noon, so that the SZA is the latitude $L \pm \delta$ (the solar declination angle δ) depending on the day of the year T. When $t = 12$ (noon), $\mathrm{SZA} = L - \delta$ from Eq. (5.12).

$$\cos(\mathrm{SZA}) = \cos(L)\cos(\delta)\cos[\pi(t-12)/12] + \sin(L)\sin(\delta) \tag{5.12}$$

A useful, but moderate, accuracy estimate for δ (degrees) as a function of the day of the year T (days from 1 to 365) is given in Eq. (5.13). Knowledge of SZA is needed to evaluate Eqs. (5.1) to (5.4) to estimate UV or VIS changes from satellite data discussed in Section 5.3.8.

$$\delta = \frac{180}{\pi}\arcsin\left[c\cos(\theta + d)\right] \tag{5.13}$$

$\theta = 0.5a(2 + b^2)T + 2ab\sin(T) + 0.25ab^2\sin(2T)$
$a = 0.017{,}202{,}166$
$b = 0.016{,}75$
$c = -0.397{,}68$
$d = 0.177{,}84$

5.3.8 Estimating UV Trends: Satellites

Global estimates of surface UV irradiance F_λ as a function of latitude, longitude, and wavelength λ have been calculated from satellite measurements of atmospheric backscattered UV radiances and the small amount reflected from the surface. The long-term precision and stability of a satellite instrument's in-flight calibration, especially the single-channel radiances used to estimate cloud transmission and reflectivity, make it very useful for estimating trends in F_λ. In the absence of a widely distributed, closely-spaced surface network of well-calibrated UV spectrometers, satellite UV irradiance estimates are extremely useful, especially over ocean areas where there are no other measurements.

There are two ways of estimating the UV irradiance reaching the ground from satellite remote sensing of ozone, aerosol, and reflectivity. First, one can enter these quantities into a detailed radiative transfer model to compute cloud transmission C_T using Mie theory to approximate the cloud and aerosol properties, in addition to Rayleigh scattering and ozone absorption (Krotkov et al., 1998; 2001). The second approximate method, is to estimate the irradiance reaching the ground for a Rayleigh scattering and ozone absorbing atmosphere F_{CLEAR}, and then add the cloud and aerosol transmission as a correction factor based on the measured fractional scene $R\,(0 < R < 1)$ and surface reflectivity R_G, $T \approx (1 - R)/(1 - R_G)$, where $0 < T < 1$. The irradiance at the surface is then approximately

$$F_{SURFACE} = T\,F_{CLEAR} \tag{5.14}$$

The two methods quite closely agree (Krotkov et al., 2001), except when there is enough multiple scattering within a cloud to give enhanced ozone absorption at wavelengths less than about 310 nm where C_T is the better estimate. Irradiances from both the C_T and the simplified methods are frequently higher than measured irradiance values on the ground, usually caused by an underestimate in the satellite calculation of aerosol amounts and aerosol absorption (Krotkov et al., 1998; 2001; Herman et al., 1999; Kalliskota, 2000). The differences become much less when the aerosol amount is small or is known from ground-based measurements. Other sources of differences between ground-based measurements and satellite estimates of UV irradiance arise from the large satellite field of view (50×50 km^2 at nadir for TOMS and 13×24 km^2 for OMI) compared to the smaller ground-based field of view, in addition to the terrain height differences within a satellite field of view.

A recent comparison of measured UV erythemal irradiance from ground-based measurements and OMI satellite estimates has been made (Tanskanen et al., 2007). The comparison shows that for flat, snow-free regions with modest loadings of absorbing aerosols or trace gases, the OMI-derived daily erythemal doses have a median overestimation of 0% to 10%, and that 60% to 80% of the satellite estimated erythemal doses are within ±20% compared to ground-based measurements.

Similar errors occur when interpolating between widely separated ground-based stations, where the aerosol, ozone, and cloud amounts vary between the stations. Given the need for global coverage of F_λ, and the sparsely located ground-based stations, calculations of F_λ from satellite-observed column ozone abundances and cloud reflectivities, which are validated by ground-based measurements, are a useful method for estimating regional, zonal averages, and global UV irradiance trends.

The year-to-year shifts in cyclic weather patterns (e.g., clouds, ozone transport, etc.) by even a tenth of a degree in latitude and longitude (~10 km), strongly affect ground-based UV measurements and their estimates of UV irradiance trends, but have a minimal effect on area-averaged satellite ozone and reflectivity measurements (and the UV estimates derived from them). Therefore, the surface UV changes deduced from ozone amounts and reflectivity measured by satellites, F_λ, are expected to be equivalent to those from cloud-filtered, ground-based observations of UV irradiance, and are superior for estimating regional and global changes. Satellite measurements provide both regional and global long-term coverage, which can be used to construct zonal and regional averages and long-term trends, which have much less geophysical variance from clouds than corresponding ground-based measurements. However, most satellite measurements are from low earth polar orbits that pass over a given site only once a day, and so represent the precise cloud conditions for that local time (usually from 10:30 to 13:30 hours), which misses the morning to afternoon variation. For the purposes of UV trends, the estimations are usually calculated for solar noon geometry using ozone amount and cloud reflectivity from sun-synchronous satellite near-noon measurements.

The use of satellite estimates presupposes ground-based measurements for validation and as a bridge between successive satellite instruments, if there are gaps. However, the determination of local UV irradiance is best achieved by ground-based measurements of either the irradiance or the atmospheric properties (ozone, aerosols, and clouds) above the observation site from which the irradiance can be calculated.

Satellite-observed long-term changes in mid-latitude zonal average ozone amounts suggest that there were significant UV increases for both erythemal irradiance and individual UV-B F_λ. The zonal average irradiance increase, relative to 1980, for the latitude band between 30°N and 40°N peaked in 1993 at about 20% (erythemal irradiance) and 40% (305 nm irradiance). Fortunately, these increased percentage changes occurred during the winter months when the SZAs are large, so that the absolute irradiances were comparatively small and the biological effects

were minimal. The calculated annual average irradiance increase during 1993 was about 7% and 14%, for erythemal and 305 nm irradiances, respectively. By 2007, ozone had partially recovered so that the irradiance increase moderated to 4% and 8%, respectively. Model calculations show that the recovery is a direct consequence of the implementation of the Montreal Protocol, and its subsequent amendments, limiting the introduction of ozone destroying substances into the atmosphere.

The long-term (30-year) monthly and zonal average (5° bands) ozone time series can be used to estimate changes in monochromatic irradiance reaching the earth's surface using the RAF from Eqs. (5.1) and (5.2), and the estimate of the SZA as a function of latitude and season from Eqs. (5.12) and (5.13). Sample results are shown in Fig. 5.9 for latitude bands centered on 32.5°S and 32.5°N where the ozone change dO_3/O_3 is approximately −3% over 30 years. Since there has been no significant change in zonal average cloud cover (Herman et al., 2009b) at these latitudes, the increase in 305 nm irradiance dF/F is about 6% over 30 years for the summer months centered on June (Herman, 2009). While this increase is significant, it appears that the decrease in ozone and increase in irradiance has leveled off starting in the late 1990s.

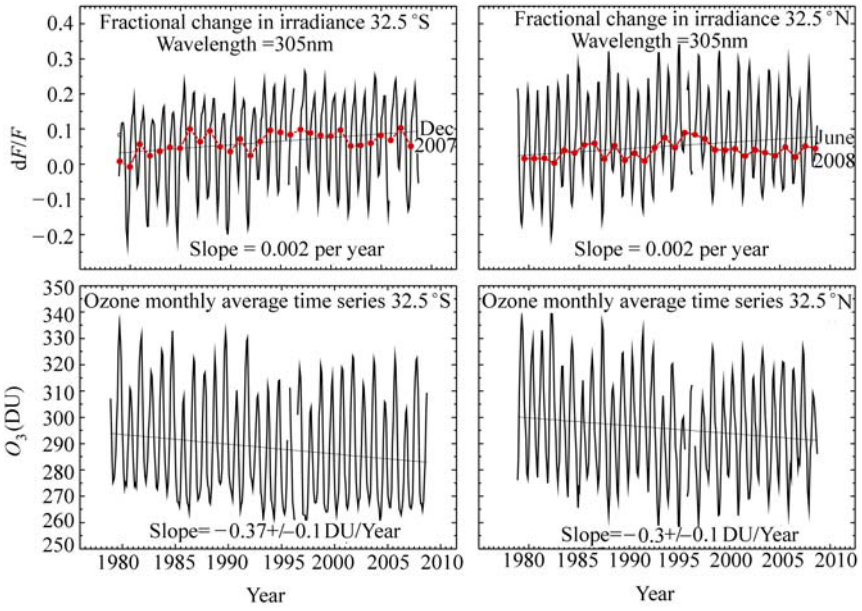

Figure 5.9 Fractional change in 305 nm irradiance dF/F (upper panels) caused by a change in ozone (lower panels) in two latitude bands centered on 32.5°S and 32.5°N of 5° width. The red dots represent the summer solstice months of December (−32.5°S) and June (32.5°N). The monthly average ozone values are available from the GSFC website based on merged data from multiple satellites (http://hyperion.gsfc.nasa.gov/Data_services/merged/index.html)

The two principal causes for change in irradiance at the earth's surface, dO_3/O_3 and dR/R are shown in Figs. 5.10 and 5.11. The change in reflectivity is based on the preliminary analysis of reflectivity (Herman et al., 2009b; Herman, 2009) for the entire 1979 to 2008 period. The current best-calibrated nadir-view zonal averaged LER values are averaged values from the temporally overlapping satellites listed in Table 5.3. The final numbers are expected to be slightly different than those in Fig. 5.11, so that the cloud-transmission correction to the 305 nm irradiance caused by variability in cloud cover will also change in the final analysis.

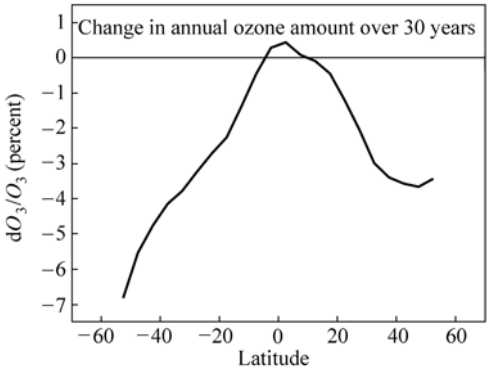

Figure 5.10 The 30-year percent change in zonal average annual ozone amount as a function of latitude

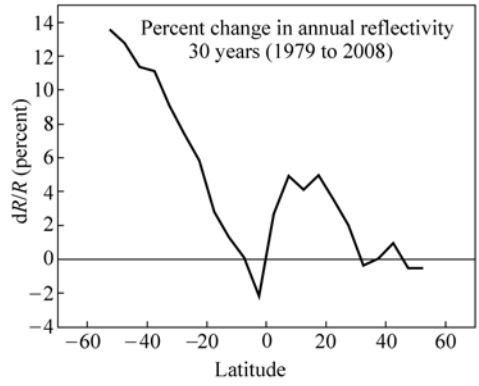

Figure 5.11 The 30-year percent change in zonal average annual reflectivity caused by clouds and aerosols (preliminary estimate)

Based on these numbers, an analysis for the annual mean change of 305 nm irradiance can be carried out for multiple latitudes with the results shown in Fig. 5.12. The changes in 305 nm irradiance are quite large at higher latitudes in both hemispheres, but especially in the Southern Hemisphere where it amounts to an

Table 5.3 Satellite instruments for ozone and reflectivity

1979 – 1992	Nimbus-7/TOMS (N7)	Full global coverage every day. Only a few missing days from1980 to 1992. Ozone plus reflectivity. Near noon orbit
1985 – 2008	SBUV-2 Series (N-9, N-11, N-16, N-17, N-18)	Nadir viewing only. Only a few missing days. Ozone plus reflectivity. N-9 and N-11 have a drifting orbit
2004 – 2008	Ozone Monitoring Instrument (OMI)	Full global coverage every day with few missing days. OMI produces both ozone and reflectivity values. 1:30 p.m. orbit

approximate 13% increase at 50°S latitude near the southern tip of South America. As shown in Fig. 5.12, the percent change in irradiance is dominated by changes in ozone amounts, except near the equator where the change in C_T dominates. The apparent leveling off with latitude of ozone change between 35°N and 50°N does not appear as strongly in the irradiance change because of the sec(θ) term in the expression for dF_{12}/F_2. The increase in cloudiness (decrease in C_T) at high southern latitudes moderates the irradiance increases caused by ozone decreases. While these estimated irradiance changes are significant, they are caused by small changes in ozone amount compared to the mean ozone value, which would permit the use of Eqs. (5.1) and (5.2), or the more accurate direct use of Beer's Law (Eq. (5.4)) as shown in Fig. 5.12.

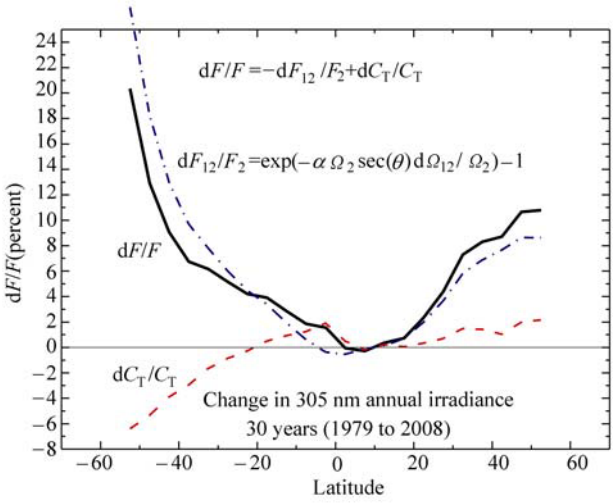

Figure 5.12 The annual average change in annual 305 nm irradiance (solid line) caused by changes (preliminary) in reflectivity and cloud transmission C_T (dashed line) and the change in ozone amount Ω (dot-dash line)

5.3.9 Estimating UV Trends: Ground-Based

An excellent example of UV trend detection is from ground-based measured solar irradiances at 305 nm and 324 nm at Thessaloniki, Greece. The irradiances shown in Fig. 5.13 are for cloud-free skies at a constant SZA of 63° (WMO, 2007, an extension of Bias et al., 1993). These data are obtained from a carefully maintained Brewer spectrometer located in an industrial area that is subjected to moderate amounts of pollution generated locally and also reaching Greece from other countries in Europe. There are also occasional dust episodes originating in northern Africa.

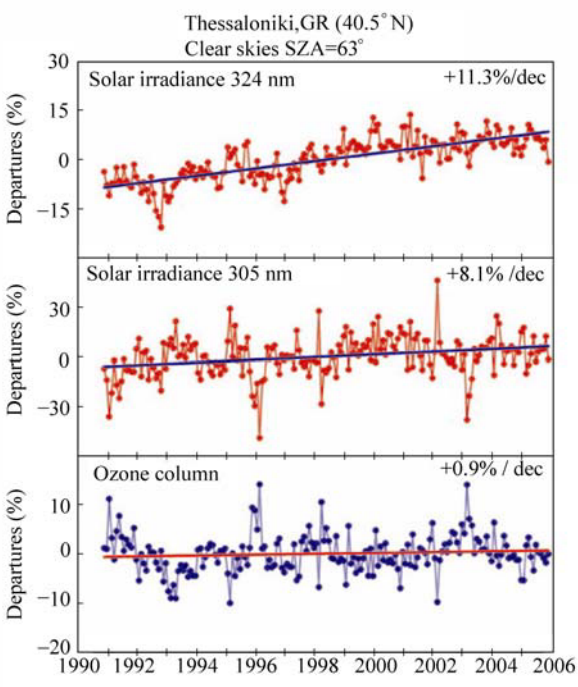

Figure 5.13 Combined effects of ozone, aerosols, and other absorbing components on UV radiation. Long-term variability in monthly mean solar spectral irradiances at 324 nm (upper panel) and at 305 nm (middle panel) measured at Thessaloniki, Greece, under clear skies at 63° SZA, shown as departures from the long-term (1990 – 2006) averages. The lower panel shows the corresponding departures in the ozone column of 375 DU (from WMO, 2007)

The radiation at 324 nm should not be significantly affected by ozone so that the cause of the upward trend at 324 nm (11.3% per decade) is almost certainly due to aerosol and pollution decreases. Decreasing amounts of aerosol and pollution that cause the upward trend at 324 nm will also affect 305 nm by approximately

the same amount. Combining the changes seen for 324 nm with those observed for 305 nm (8.1% per decade) implies that the effect of increasing ozone amounts (0.9% per decade) on 305 nm irradiance is a statistically significant decrease of $\sim(11.3-8.1)\%=3.2\%$ per decade.

An easy way to check this conclusion is through the RAF defined as part of Eq. (5.1); $\mathrm{RAF}=-\alpha\Omega\sec(\theta)=-4$ for $\Omega=375$ DU, and $\theta=63^\circ$, the average measured values for Thessaloniki. Based on the RAF and the observed ozone change of 0.9% per decade, the change in 305 nm UV irradiance $\mathrm{d}F/F=\mathrm{RAF}\,\mathrm{d}\Omega/\Omega$ should be $\sim-4(0.9)\%=-3.6\%$ per decade, consistent with the measurements of −3.2% and −3.4% per decade discussed above. In addition to the smaller ozone effects, Fig. 5.13 shows that a decline in air pollutants can cause increases in surface UV irradiance of 11.3% per decade in a local industrial site, such as Thessaloniki, Greece.

When data from cloudy and clear days are present in the UV time series, the measured trends in UV radiation at individual stations can have sufficient variation (typically 0% − 50%, and occasionally larger due to cloud cover) to make estimated long-term trends lose statistical significance. As shown in a report by WMO (2007), trend estimates for Toronto for the period of 1998 through 2005 were $(1.5\pm5)\%$ per decade (1 standard deviation, 1σ) (WMO, 2007) during a period in which the total ozone amount was relatively constant. Even using unfiltered Toronto UV radiation data going back to 1990, no statistically significant trend is observable in the extended Toronto UV data despite ozone decreases that took place during the 1990s, due to the variability introduced by clouds. To relate the estimated trends to ozone changes requires knowledge of changes in aerosol and cloud amounts, which can be obtained from a wavelength not affected by ozone.

Fioletov et al. (2001) have made ground-based estimates of erythemal irradiance changes from two Brewer spectrometer stations (Montreal and Edmonton), and found that the UV-B trends were similar to those expected from changes in ozone alone, but with much larger uncertainty because of clouds and aerosols.

5.4 UV in the Polar Regions

The expansion of the Antarctic polar vortex during the 1990s, both in spatial and temporal extent into early summer, has increased the frequency of elevated UV-B episodes over sub-Antarctic populated areas (Rousseaux et al., 1999). These episodes are no longer just small pockets of ozone depleted stratospheric air coming from the break-up of the polar vortex, but include occasional excursions of the polar vortex edge over Ushuaia, Argentina and Punta Arenas, Chile. This occurred 44 times in the years 1997, 1998, and 2000 combined, with some episodes lasting three to four days. Surface measurements show average erythemal UV increases of about 70% over Ushuaia (54.47°S) since 1997, and episodic total UV-B increases of up to 80% over Punta Arenas (53.08°S) (WMO, 2007).

Diaz et al. (2003) show that Barrow, Alaska, has experienced UV-B increases related to springtime ozone depletion in March and April, but these increases are a factor of ten smaller than those observed at the southern high latitudes. Summertime low-ozone episodes in the Arctic also affect surface UV-B irradiances. These summertime events result from gas-phase chemistry involving nitrogen and hydrogen cycles, which become very efficient during the 24-hour insolation that occurs in the Arctic summer. During summer 2000, two low- ozone episodes brought about erythemal UV increases in order of 10%−15%, each lasting more than five days (WMO, 2007).

The measured amounts of UV irradiance at Palmer Station, Antarctica (64°S) and San Diego, CA (32°N), show that for all seasons, other than spring in Antarctica, there is a decrease in UV-B irradiance caused by the increased path through the atmosphere resulting in less UV-B than observed in San Diego (Fahey, 2007). The Antarctic ozone depletion that occurs each spring causes the UV-B portion of the erythemally-weighted irradiance to increase dramatically to where it exceeds even the summertime values observed in San Diego. Similar wide-area springtime low ozone amounts do not occur in the Arctic region because of the degree of meteorological wave activity in the north that leads to a weaker polar vortex and higher ozone amounts. Southern Hemisphere ozone depletion events have extended further north over Southern Africa, parts of Australia, and New Zealand.

5.5 Human Exposure to UV

From the viewpoint of human exposure to UV, the maximum clear-sky UV irradiance and exposure occurs in the equatorial zone latitudes, ±23.3°, following the seasonal sub-solar point, and at high mountain altitudes. In general, UV erythemal, UV-A, and UV-B irradiance decreases with increasing latitude outside of the equatorial zone, due to the decreases in maximum daily noon solar elevation angles and for UV-B increases in ozone amount. An exception occurs for UV-B wavelengths at southern mid- to high-latitudes when reduced ozone amounts from the Antarctic ozone hole remain late into the spring and are pushed away from Antarctica toward the lower latitudes. For example, UV measurements indicate that the equatorial UV-B irradiance levels can occur in the southern part of South America for several days.

Global images of daily-integrated UV erythemal exposure (kJ per m^2), averaged during the months of January (Southern Hemisphere summer), July (Northern Hemisphere summer), and the two equinox months of September and March, are shown in Fig. 5.14 (based on WMO, 1999). Because of cloud cover, the high equatorial clear-sky irradiances do not translate into the highest monthly cumulative exposures. The maximum erythemal doses near the equator occur when the sun is directly overhead during March, which has lower cloud cover than during September. The difference is related to the annual cycle of the cloud cover associated with

the Intertropical Convergence Zone (ITCZ), which is usually over the equator in September, but is south of the equator in March. Two examples of very high UV exposures occur in the South American Andes (e.g., the sparsely populated Atacama Desert in Chile at 4,400 m to 5,600 m altitude, and in the city Cuzco, Peru) during January and in the Himalayan Mountains (over 100 peaks exceeding 7,000 meters) during July, as shown in Fig. 5.14. In both Southern Hemisphere cases, the sun is nearly overhead in January when the earth is also closest to the sun. Excluding high altitude locations, the largest monthly UV exposures occur in Australia and South Africa during summer (January) because of the very low amount of day-to-day cloud cover from late spring to early autumn. Other mid-latitude, low altitude relatively cloud-free areas also receive high doses, e.g., summertime (July) in the southwest U.S. and the Mediterranean countries.

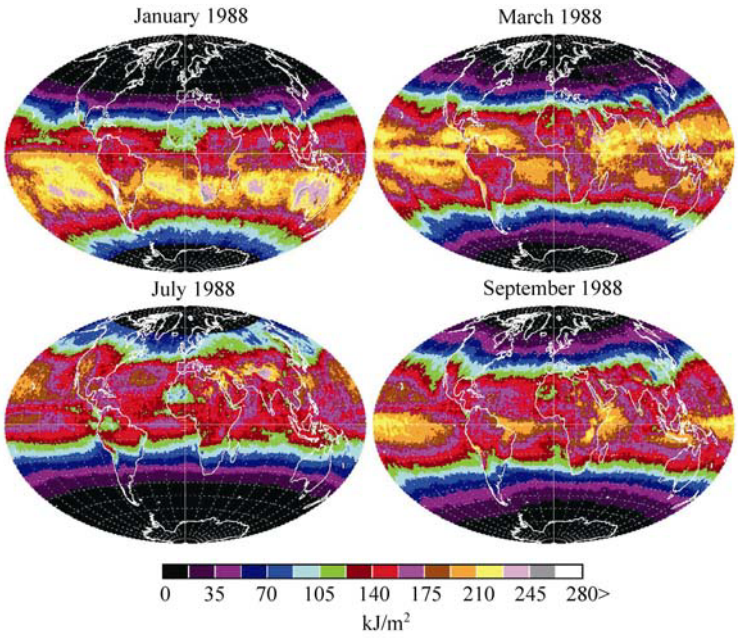

Figure 5.14 Erythemal exposure kJ per m^2 for the months of January, March, July, and September 1988 (from WMO, 1999) based on Nimbus-7/TOMS ozone and reflectivity data. These extreme levels are not seen in the September 1988 panel because the sun is just beginning to rise over Antarctica and the 1988 ozone depletion was not extreme

Other factors contribute to the high Southern Hemisphere UV doses. There is a five million km decrease (3%) in Earth-Sun distance (perihelion near January 3) during the Southern Hemisphere summer, as compared to the Northern Hemisphere summer (aphelion near July 4), causing a 6% increase in summer irradiance in the Southern Hemisphere for a couple of weeks around perihelion. Average

summer ozone in the Southern Hemisphere (270 DU) is lower than the Northern Hemisphere (320 DU) by about 13% which would lead to a 13% increase in 310 nm and a 26% increase in 305 nm irradiance. The exact percentage of increase is a function of latitude. In general, the Southern Hemisphere has fewer pollution aerosols, which can cause a small increase in UV irradiance relative to the Northern Hemisphere.

After latitude, the biggest factor affecting mid- and low-latitude exposure to UV radiation is the amount of cloud cover during the summer months. Satellite measurements of reflectivity indicate that there are some regions where there are long-term reflectivity increases (more cloud cover) over land in a few places, such as over the Indian Ocean, parts of Morocco and Algeria, northern Mexico/ southern U.S., and Canada. However, there are decreases in cloud cover over central U.S., northern Europe (60°N, 20°E), Kazakhstan (80°E 45°N), Argentina-Chile, and also smaller decreases over Australia and New Zealand that produce corresponding increases in time-integrated solar irradiance (exposure) reaching the ground (Herman et al., 2009b). While the decreasing cloud reflectivity increases solar radiation reaching the ground, changes in ozone are important for UV-B since it affects the clear-sky days when the irradiance is at a maximum for that day and latitude.

In Australia and other countries, any increase in UV exposure is especially detrimental to the European portion of the population that has minimal natural UV protection for skin cancer (Diffey, 1991; and a more general reference for health impact, Lucas et al., 2006), eye cataracts (Taylor, 1991), suppression of the immune system (Vermeer et al., 1991), and to ecosystem biology (Ghetti et al., 2006). Based on U.S. National Institute of Health (NIH) data (Devesa et al., 1999), similar skin cancer problems are present in the U.S., with more skin cancer occurring at lower latitudes where the UV exposure is higher. The seriousness of the very high UV exposure problem is observed in Australia where skin cancer rates have increased dramatically (20% for basal cell, to 788 per 100,000, and over 90% for squamous cell, to 321 per 100,000 carcinomas) based on household surveys in 1985, 1990, and 1995 (Staples et al., 1998). This compares to the U.S. National Cancer Institute's estimate (Devesa et al., 1999) of 14.5 per 100,000 for the U.S. Skin cancer incidence by skin type has been estimated by the U.S. National Cancer Institute's Surveillance, Epidemiology, and End Results (SEER) Program, which states that Caucasian people have the highest melanoma incidence, followed by a much lower rate for Hispanics, African Americans, and with the lowest incidence for Asian Pacific islanders.

The effects of custom or culture can be seen in Europe with large populations of light-skinned people living at fairly high latitudes (e.g., Stockholm, Sweden at 59.3°N, London, England at 51.5°N). However, there is a major difference in non-melanoma cancer incidence rates between citizens of Sweden (15 per 100,000) and the citizens of the United Kingdom (5 per 100,000) based on data from 1995 (Qiu and Marugame, 2008).

At higher latitudes in the Northern Hemisphere, where there is much more cloud cover than in Australia (e.g., central Europe 50°N, northern U.S., and Canada), a small decrease in cloud cover and ozone may produce the beneficial effect of increasing natural vitamin D production from increased UV-B exposure during the spring and summer months (Grant, 2002; McKenzie et al., 2003; Holick, 2004) without producing greatly enhanced rates of skin cancer. In the U.S., NIH data shows (Devesa et al., 1999) that increased solar exposure appears to correlate by latitude with decreases in some internal cancers along with increases in skin cancer.

5.6 UV Index and Units

Erythemal irradiance is frequently expressed in terms of the UV index = 25 mW per m^2 = 2.5 μW per cm^2. The index is an arbitrary unit such that very high values reported by weather services have a UV index of 10 (25 μW per cm^2). Erythemal exposure or dose is a time-integrated quantity normally expressed in kJ per m^2. Many high altitude locations with extreme UV amounts can exceed 10 on clear days. The weather service for the populated region near Cuzco, Peru, frequently reports a UV index of 10 to 11 for extended periods and occasionally has a UV index that reaches 25, the latter based on TOMS ozone data analysis (Liley and McKenzie, 2006). Spectral irradiance is expressed in mW per m^2 per nm. The solar irradiance has a peak value of about 2,100 mW m^{-2} nm^{-1} at about 450 nm. Sky radiance is expressed in mW m^{-2} nm^{-1} per steradian. Zenith sky irradiance for 0.5° FOV is of the order of 10^{-5} of the solar irradiance in the vicinity of 400 nm, but the ratio increases with decreasing wavelength because of increasing Rayleigh scattering in the UV wavelengths.

5.7 Action Spectra and Irradiance Trends

An action spectrum $A(\lambda)$ is a weighting function of wavelength λ that estimates the relative strength of a process (e.g., biological process or material degradation) for each wavelength in a range from λ_1 to λ_2. The action spectrum is multiplied by the irradiance $I(\lambda,t)$ to obtain a production function $P_{\mathrm{ACT}}(t)$. A direct comparison of dose amounts for any causal effect is not given by $A(\lambda)$, but just indicates the relative effect of each wavelength. Frequently, what is wanted is the time integrated effect of the process E_{F} over a specified time interval t_1 to t_2. The quantities P_{ACT} and E_{F} can be used to estimate the relative effect of exposure to solar radiation on different days at some specified time, or cumulatively over some portion of a day or longer (Eqs. (5.15) and (5.16)).

$$P_{\mathrm{ACT}}(t) = \int_{\lambda_1}^{\lambda_2} I(\lambda,t)A(\lambda)\mathrm{d}\lambda \tag{5.15}$$

$$E_{\mathrm{F}} = \int_{t_1}^{t_2} P(t)\mathrm{d}t \tag{5.16}$$

Typical action spectra have been estimated for skin reddening for Caucasian males, plant damage, vitamin D production, non-melanoma cancer production, and DNA damage, etc. The vitamin D action spectrum $A_{\text{Vit-D}}$ is based on a digitization of the action spectrum graph presented by McLaughlin et al. 1988. The vitamin D production was obtained in the laboratory from "surgically separated skin." An accurate functional fit (Fig. 5.15(a)) to the published graph is given ($250\ \text{nm} < \lambda < 315\ \text{nm}$) in Table 5.2 along with functional fits to the graphs (Figs. 5.15(b), (c), (d)) for three other more common action spectra, A_{DNA} damage, plant growth A_{PLA}, and erythemal A_{ERY}.

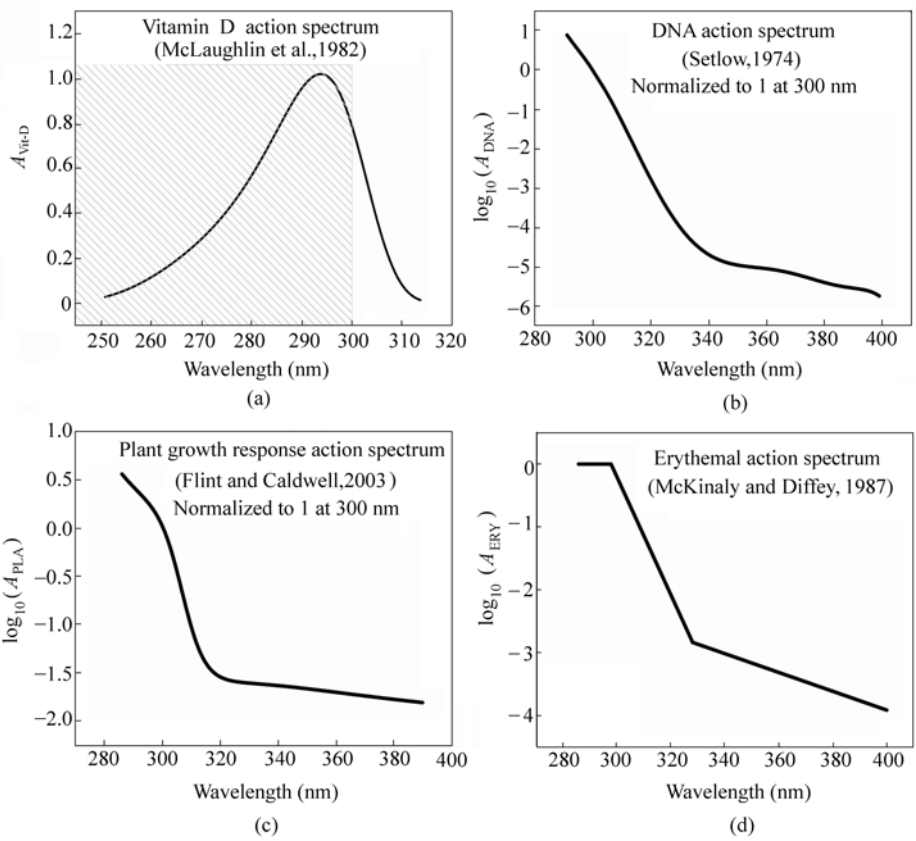

Figure 5.15 (a) Fit to vitamin D action spectrum (McLaughlin et al., 1982), $250\ \text{nm} < \lambda < 314\ \text{nm}$; (b) Fit to DNA damage action spectrum from (Setlow, 1974), $290\ \text{nm} < \lambda < 400\ \text{nm}$; (c) Fit to plant growth response action spectrum (Flint and Caldwell, 2003), $285\ \text{nm} < \lambda < 390\ \text{nm}$; (d) Fit to erythemal action spectrum (McKinlay and Diffey, 1987), $250\ \text{nm} < \lambda < 400\ \text{nm}$

Figures 5.16 and 5.17 show the result of multiplying respective action spectra by the solar flux (Fig. 5.2) at the ground for an atmosphere with 300 DU of ozone and SZA = 0° (typical or the equatorial band with overhead sun). From a practical perspective, wavelengths below 300 nm have little effect at sites near sea level, because there are too few photons that are able to penetrate the atmosphere. Altitude must be taken into account at higher altitude sites, even though most of the short wavelength photons are absorbed by stratospheric ozone, but the numbers that do penetrate the stratosphere are not reduced as much by Rayleigh multiple scattering compared to the boundary layer atmosphere. The effect for DNA damage and vitamin D production decreases rapidly for longer wavelengths, especially for larger SZA typical of mid-latitudes. The erythemal effect persists into the UV-A

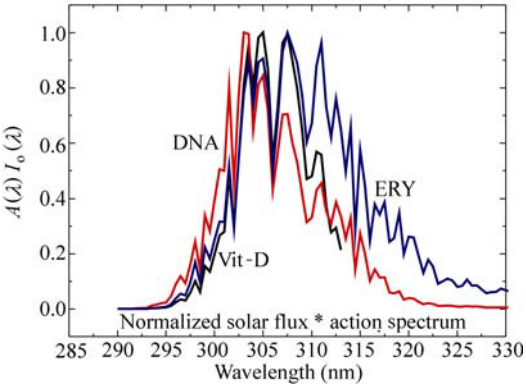

Figure 5.16 Action spectra (DNA, vitamin D, and ERY) multiplied by the solar flux at the ground for 300 DU of ozone and SZA = 0°

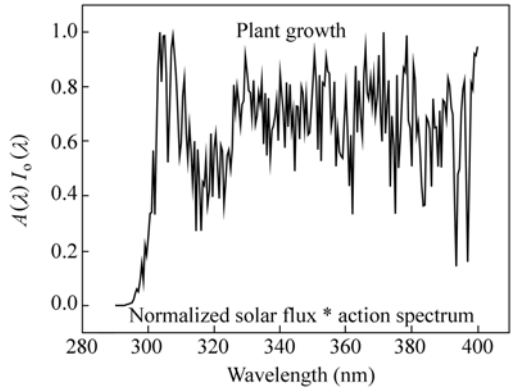

Figure 5.17 Action spectrum (plant growth) multiplied by the solar flux at the ground for 300 DU of ozone and SZA = 0°

range, which is why it is important for sunscreen preparations to protect to as long a wavelength as is possible. Finally, the plant growth spectrum (Fig. 5.15(c)) spans both UV-B and UV-A, and extends into the VIS wavelengths.

The accuracy of action spectra are usually not specified since they are meant to convey the response that occurred during a particular set of experiments that are highly specific to the particular samples that were examined. This is particularly true for the three spectra that pertain to human response to UV light. None of these spectra apply to any specific individual or group of people, but are just indicative of a process. The spectra can be used to give an idea of how a process would change if there were a change in the UV irradiance for a sample that had an approximate average response that was similar to the above spectra. The best-known example of this is the use of the UV index based on the erythemal action spectrum. Here the accuracy of the UV index is limited to no better than 10% (i.e., an integer scale from 0 to 10), but nonetheless, the index is useful for estimating when conditions are likely to cause harm from exposure to UV irradiance. All of the action spectra should be considered in a similar manner.

As discussed in Section 5.3.1, the behavior with respect to ozone change of action spectrum weighted summed irradiances is not the same as for monochromatic irradiances. The fractional change is approximated by a power law in RAF described in Section 5.3.2, which has been demonstrated to hold for a wide range of ozone values Ω with constant RAF for each SZA. Rearranging Eq. (5.3) in terms of fractional differences,

$$(F_1 - F_2)/F_2 = [1 + (\Omega_1 - \Omega_2)/\Omega_2]^{-\mathrm{RAF}(\theta)} - 1 \qquad (5.17)$$

However, the RAF(θ), where θ = SZA, must be empirically derived for each action spectrum and each SZA. This has been done for the erythemal irradiance F_{ERY} using measurements from Mauna Loa, Hawaii (Bodhaine et al., 1997). The resulting variation of RAF(θ) with SZA is shown in Fig. 5.18, along with a theoretical calculation based on Eq. (5.4) applied to each wavelength and summed with erythemal weighting. This shows that the empirical power law behavior $F_1/F_2 = (\Omega_2/\Omega_1)^{\mathrm{RAF}(\theta)}$ can be explained by application of the physically based Beer's Law for absorption in the atmosphere. The behavior with SZA is as expected from a mix of UV-B and UV-A wavelengths, as the importance of UV-B decreases with increasing SZA. In addition to standard action spectra, a recent WMO report (Seckmeyer et al., 2005) has developed an RAF(θ,Ω) analysis for the specific response of particular types of broadband instruments that are intended to approximate the erythemal response function. They also present an analysis of RAF(θ,Ω) for the exact erythemal weighting function A_{ERY} (Table 5.4) for the ozone range from 100 DU to 600 DU. In all of the work discussed here RAF(θ,Ω) = RAF(θ) by limiting the range of Ω to 200 DU < Ω < 600 (see Appendix 5.1).

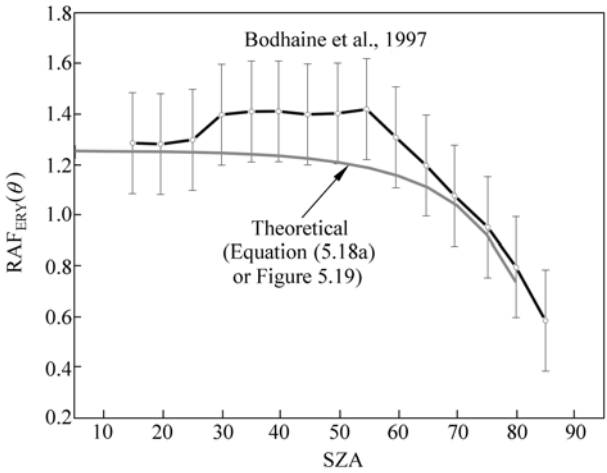

Figure 5.18 $\mathrm{RAF_{ERY}}(\theta)$ variation with $0 < \theta < 85^\circ$ for the erythemal action spectrum from data obtained at Muana Loa, Hawaii (Bodhaine et al., 1997) compared with a theoretical calculation based on summation over wavelengths using A_{ERY} and Eq. (5.4) yielding the form of Eq. (5.17), which is fitted by Eq. (5.18a) for erythemal irradiance (Herman, 2009)

Table 5.4 Function fit to four UV action spectra of Fig. 5.8

Fit to vitamin D spectrum (McLaughlin et al., 1988) $A_{\mathrm{Vit\text{-}D}}$ $250\ \mathrm{nm} < \lambda < 314\ \mathrm{nm}$
$\log_{10}(A_{\mathrm{Vit\text{-}D}}) = (A + C\lambda^{0.5} + E\lambda + G\lambda^{1.5})/(1 + B\lambda^{0.5} + D\lambda + F\lambda^{1.5})$
$A = -0.9601647127133382$ $B = -0.1771944277419561$ $C = 0.1798847906875285$
$D = 0.01044079180885732$ $E = -0.01118449188229313$ $F = -0.00020464360877287360$
$G = 0.0002309087838152358$
Fit to DNA damage spectrum (Setlow, 1974) A_{DNA} $290\ \mathrm{nm} < \lambda < 400\ \mathrm{nm}$
$\log_{10}(A_{\mathrm{DNA}}) = (A + C\lambda^{0.5} + E\lambda)/(1 + B\lambda^{0.5} + D\lambda + F\lambda^{1.5})$
$A = -0.1090717334891702$ $B = -0.1578036701734071$ $C = 0.01546956801974633$
$D = 0.008268275171175154$ $E = -0.000529417616572146$ $F = -0.0001436582640327567$
Fit to plant growth response action spectrum (Flint and Caldwell, 2003) A_{PLA}
$\log_{10}(A_{\mathrm{PLA}}) = (A + C\lambda^{0.5} + E\lambda)/(1 + B\lambda^{0.5} + D\lambda + F\lambda^{1.5})$ $285\ \mathrm{nm} < \lambda < 390\ \mathrm{nm}$
$A = -2.747265993518105$ $B = -0.1791860260727771$ $C = 0.4772684658484249$
$D = 0.01068302156756403$ $E = -0.02764643975624155$ $F = -0.0002119599411078172$
$G = 0.0005339842703179307$
Fit to erythemal action spectrum (McKinlay and Diffey. 1987) A_{ERY}
$\log_{10}(A_{\mathrm{ERY}})$ $250\ \mathrm{nm} < \lambda < 400\ \mathrm{nm}$
$\log_{10}(A_{\mathrm{ERY}}) = 0$ $250\ \mathrm{nm} < \lambda < 298\ \mathrm{nm}$
$\log_{10}(A_{\mathrm{ERY}}) = 0.094(298 - \lambda)$ $298\ \mathrm{nm} < \lambda < 328\ \mathrm{nm}$
$\log_{10}(A_{\mathrm{ERY}}) = 0.015(139 - \lambda)$ $328\ \mathrm{nm} < \lambda < 400\ \mathrm{nm}$

Theoretically calculated $\mathrm{RAF}(\theta)$ values for all four action spectra in Fig. 5.15 are given in Fig. 5.19, and the fitting functions for each RAF in Table 5.5,

Eqs. (15.8a~15.8d), for the ozone range from 200 DU to 600 DU, which gives an RAF(θ) that is independent of the ozone value. If the range is extended to 100 DU, the RAF(θ,Ω) depends on the ozone amount and SZA. The behavior of some action spectra RAFs with SZA (e.g., DNA) is similar to single wavelength RAFs for relatively narrow action spectra mostly contained in the UV-B region; namely, increasing RAF with SZA. More broadly-based spectra have RAF values that are nearly constant for SZA < 40°, and decrease for larger values of SZA. Very wide spectra, such as the Plant Growth spectrum, decrease for all SZA > 0.

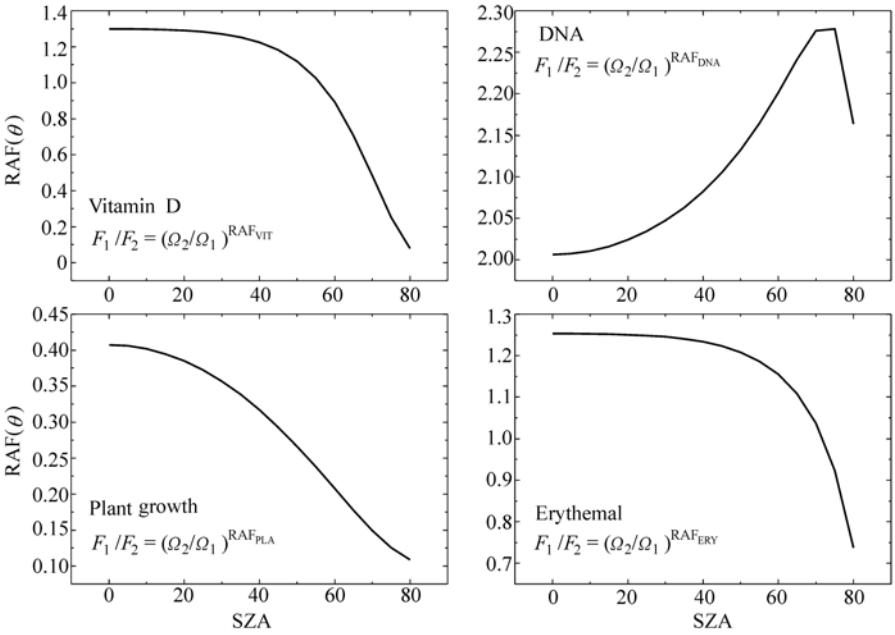

Figure 5.19 The variation of RAF with SZA for the four spectra in Fig. 5.15. Note that RAF_{ERY} and RAF_{VIT} look similar because of different scales (200 DU < Ω < 600 DU)

The reason that scattering can be neglected when calculating change in irradiance is that the scattered radiance is linearly proportional to the direct solar beam when stratospheric ozone is the primary absorber. The calculation may not be accurate for strongly absorbed wavelengths at large SZA when the direct solar beam is very small compared to the scattered irradiance. When this happens, the path through the atmosphere to the ground is the expected slant path through the stratosphere, which changes to a nearly vertical path for scattered irradiance that occurs lower in the atmosphere (Umkehr effect). This shortens the optical path and reduces the sensitivity to ozone change that occurs in the troposphere. If ozone changes in the stratosphere are much larger than in the troposphere, $F_1/F_2 = (\Omega_2/\Omega_1)^{RAF(\theta)}$ is still a good approximation, since scattering can be neglected for estimations of irradiance change.

Table 5.5 Fitting functions for the action spectra RAF of Fig. 5.19

$$\mathrm{RAF}_{\mathrm{ERY}} = (A + C\theta^{0.5} + E\theta)/(1 + B\theta^{0.5} + D\theta + F\theta^{1.5}) \quad (5.18a)$$

$A = 1.253034387380404$ $B = -0.1893942742785442$
$C = -0.2374988749526192$ $D = 0.008753703248421607$
$E = 0.01109085001133105$ $F = 2.163425112458424\mathrm{D}{-05}$

$$\mathrm{RAF}_{\mathrm{DNA}} = (A + C\theta^{2} + E\theta^{4})/(1 + B\theta^{2} + D\theta^{4}) \quad (5.18b)$$

$A = 2.006603342348651$ $B = -0.000222243468041799$
$C = -0.0004040537916876323$ $D = 1.23788082612675\mathrm{D}{-08}$
$E = 1.861486615239331\mathrm{D}{-08}$

$$\mathrm{RAF}_{\mathrm{VIT}} = (A + C\theta^{0.5} + E\theta + G\theta^{1.5})/(1 + B\theta^{0.5} + D\theta + F\theta^{1.5}) \quad (5.18c)$$

$A = 1.300000361376985$ $B = -0.2561979971919163$
$C = -0.3331173671966876$ $D = 0.02040664839011024$
$E = 0.02657302492632673$ $F = -0.0004560385514125725$
$G = -0.0006221828632328866$

$$\mathrm{RAF}_{\mathrm{PLA}} = (A + C\theta^{0.5} + E\theta)/(1 + B\theta^{0.5} + D\theta) \quad (5.18d)$$

$A = 0.4073412230744607$ $B = -0.1992738307220675$
$C = -0.08017040437930313$ $D = 0.01140308620531996$
$E = 0.004045533964044966$

The percent change in zonal average clear-sky erythemal irradiance as a function of latitude can be estimated from the 30-year monthly and zonal averaged ozone time series by using Eqs. (5.17) and (5.18a) (Fig. 5.20). The estimations are restricted to latitudes between 53°S to 53°N because the estimation of the RAF was for SZA < 80°. During the winter solstice, at 53° latitude, the noon SZA is 76°. The estimation of RAFs for large SZA > 80° could be done with a spherical geometry corrected radiative transfer analysis.

The results in Fig. 5.20 show that there have been large changes in potentially damaging UV-B radiation at all wavelengths. The monochromatic changes were estimated from Eq. (5.4) because some of the ozone changes were sufficiently large as to result in a small error using the differential form in Eq. (5.1). The high latitude values may have a very small error caused by neglecting the spherical geometry correction to sec(SZA) for winter conditions at 52.5° latitude when the noon SZA reached 75.8°. The effect would be to slightly reduce the optical path and the estimated change in irradiance. At lower latitudes, the effect is negligible.

Since the DNA damage RAF, which is dominated by the behavior between 300 nm and 310 nm (Fig. 5.16), is similar in shape with respect to SZA to the monochromatic RAF, the percent increase will be much larger for DNA damage than for the erythemal spectrum. Figures 5.21 and 5.22 present the monthly percent change of 100 $\mathrm{d}F_{12}/F_2$ in 305 nm irradiance and the DNA damage weighted irradiance $P_{\mathrm{DNA}}(\mathrm{Month}, \theta)$ from 1979 to 2008. As expected, the change in percent is similar for low latitudes where the ozone change is fairly small. For larger Ω

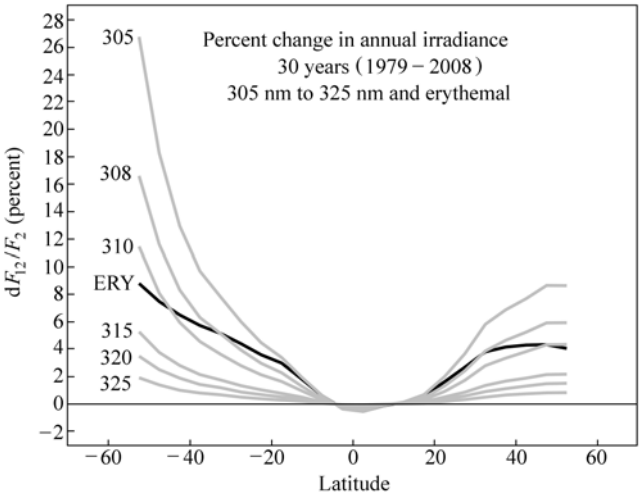

Figure 5.20 The percent change in annual clear-sky erythemal irradiance (ERY solid black) for 30 years during the period 1979 to 2008, based on Eqs. (5.17) and (5.18a), and the monthly and zonal averaged ozone time series. The change in monochromatic 305, 308, 310, 315, 320, and 325 nm irradiance from Eq. (5.4) are also shown (gray)

changes at high southern latitudes, the behavior is somewhat different because of increased contribution to P_{DNA} (Eq. (5.15)) from wavelengths smaller than 305 nm for the summer months. The same summer effect is smaller at high northern latitudes because the ozone change is less (annual ozone change 3.5% compared to 7%, Fig. 5.22).

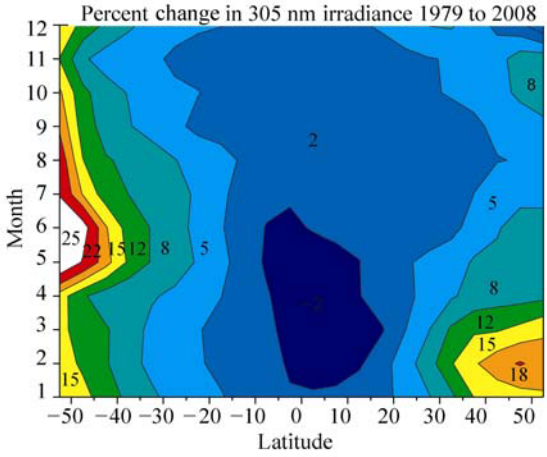

Figure 5.21 Percent change in clear-sky 305 nm irradiance from 1979 to 2008 as a function of month and latitude calculated from Eq. (5.4) and the monthly zonal average ozone data

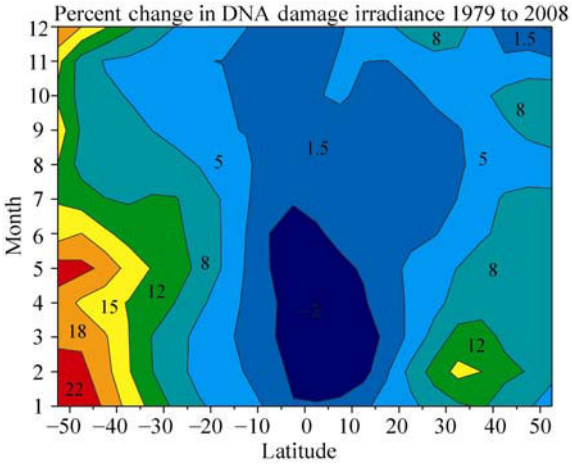

Figure 5.22 Percent change in clear-sky DNA damage spectrum weighted irradiance from 1979 to 2008 as a function of month and latitude calculated from Eq. (5.17), Table 5.2, and the monthly zonal average ozone data

From the viewpoint of population in the higher latitudes of the Northern Hemisphere, the increases in clear-sky P_{DNA} have been 5% − 8% during most of the spring and summer months when the solar UV irradiance exposure is at a maximum (more clear days as well as seasonally declining ozone going into the summer). The changes have been much larger in the higher latitudes of the Southern Hemisphere during the spring and summer months, ranging from 12% to over 20%, and extend to lower latitudes (a 12% to 15% increase between 30°S and 40°S and 18% to 22% between 40°S and 50°S). These are serious increases in damaging UV irradiance that likely would have been much worse in the absence of the chlorine limiting agreement contained in the Montreal Protocols and subsequent agreements.

5.8 UV Summary

Quantitative UV measurements have been made for the past 50 years with gradually growing sophistication in the instruments. Requirements for determining UV irradiance changes at the earth's surface are currently well understood and have been implemented at a number of sites. Measurements from ground-based instruments and estimations from satellite instruments around the globe show a mixture of UV-B increases and decreases that depend on changes in local cloud cover, and ozone and aerosol amounts.

Measurements of ozone and cloud plus aerosol reflectivity from satellites have been used to estimate the changes in UV-B for the past 30 years using data collected since 1979. The estimation of irradiance change can be obtained using radiative

transfer calculations, or from a simplified, yet accurate, approach using the "Radiation Amplification Factor." Based on the satellite ozone record, the summer average, clear-sky UV erythemal irradiance P_{ERY}, averaged over the 32.5°N latitude band, increased by about 8% from 1979 to the mid-1990s. Since the mid-1990s, P_{ERY} has decreased so that the current level is about 7% higher than it was at the start of the record in 1979. Similar, changes have occurred in the 32.5°S latitude band where the increase was about 7% in 2008 (Fig. 5.9). At higher latitudes, the annual average increase has been about 8% near the tip of South America (50°S), and about 4.5% at 50°N (Fig. 5.20).

Because of increased sensitivity to ozone changes at 305 nm (near the peak of the DNA damage weighted irradiance P_{DNA}), the increases have been substantially larger. The change in annual average 305 nm at 32.5°S is about 8%, rising to about 23% at 50°S. In the Northern Hemisphere, the changes have been somewhat smaller, about 6% at 32.5°N and 8.5% at 50°N. These changes are large enough to cause concern for an increase in diseases related to sun exposure. The larger changes for 305 nm irradiance and P_{DNA}, which occurred at higher latitudes, were only partially moderated by a strongly latitude-dependent apparent increase in cloud and aerosol cover (preliminary estimate). When change in cloud cover is included, average annual increase in 305 nm irradiance at 50°S was about 17% over 30 years, while the increase at 50°N was about 11%. Clouds will have approximately the same effect on all UV wavelengths. Since, the change caused by just ozone was larger in the Southern Hemisphere than in the Northern Hemisphere, it implies that danger from human exposure on clear days has increased more in the Southern Hemisphere than in the Northern Hemisphere. The increases for DNA damage irradiance P_{DNA} have been substantially larger than for P_{ERY}, since the weighting is more towards the shorter wavelengths. The effect is much larger in the Southern Hemisphere during spring and summer than in the Northern Hemisphere at higher latitudes, 30° to 50° (Fig. 5.22).

Ground-based measurements of surface UV trends present a challenge that can be overcome with proper filtering of the data for cloud-free conditions along with simultaneous aerosol measurements. Ultraviolet estimates from satellite measurements of ozone, aerosols, and cloud reflectivity are averages over large areas on the order of 25 km to 100 km, which minimizes many problems with local variability of cloud and aerosol amounts. Both ground and satellite UV estimates are critically dependent on establishing and maintaining an accurate calibration over the lifetime of an instrument and between successive instruments. Ground-based measurements are essential to provide validation of satellite calibration and as a bridge between successive satellite instruments.

While the Northern Hemisphere UV irradiance maximum in 1993 was associated with the massive equatorial Mt. Pinatubo eruption in 1991 (Kerr and McElroy, 1993, Bhartia et al., 1993), a portion of the total increase occurred before 1991 and was associated with ozone destruction from chlorine loading in the atmosphere

before being limited by the Montreal Protocol. Though there have been significant zonal average ozone decreases over 30 years at most latitudes (except the equator), even larger chlorine-driven ozone decreases and UV-B increases were prevented by this and subsequent agreements that were effective for limiting releases of chloroflourocarbons (CFCs) and other chlorine bearing compounds, with CFCs being almost completely phased out by 1995.

Because of the large observed changes in UV-B irradiance at mid- and high-latitudes, it is very important that we continue monitoring from both space and the ground. For space, it is essential that we have continuous well-calibrated data sets from successive near-noon, sun-synchronous satellites, with at least a one-year overlap. The calibration of satellite instruments is an extended effort that must be performed over the life of the satellite using in-flight data leading to occasional reprocessing (perhaps once every two years) of the entire dataset. Comparisons with ground-based UV irradiance and radiance data play an essential role in traditional validation and identification of problems with either satellite or ground-based instruments. For this purpose, a few well-characterized and maintained spectrometers are preferable to large networks of lesser instruments. The few instruments should be located in both clean and moderately polluted sites, and in key locations (e.g., mountains) where satellite estimations may be intrinsically in error. More effort should be put into instruments and procedures that characterize the atmosphere in terms of absorption, scattering, and composition rather than just measuring irradiance.

Appendix 5.1 Calculating RAF(θ)

If the RAF is calculated directly from the power law definition $F_1/F_2 = (\Omega_2/\Omega_1)^{\mathrm{RAF}}$ or $\mathrm{RAF} = \ln(F_1/F_2)/\ln(\Omega_2/\Omega_1)$, the result will have a dependence on ozone amount for any range of Ω_1 relative to the reference amount Ω_2 (Fig. 5.A1).

In this study, the RAF is calculated as the best fit to the function $U(\Omega_2/\Omega_1)^{\mathrm{RAF}}$ with the requirement that U is approximately 1 (Fig. 5.A2). This approximation works well for the entire range of SZA (Fig. 5.A3), the ozone range 200 DU to 600 DU, and for all four action spectra discussed in this study. The result is a small error in the estimation of action spectra irradiance change, if the ozone independent RAF is used in the power law formula. If more accuracy is needed for the erythemal spectrum, the parameter $U(\theta)$ is given by $U_{\mathrm{ERY}} = (A + C\theta^{0.5} + E\theta)/(1 + B\theta^{0.5} + D\theta + F\theta^{1.5})$ with the coefficients given in Table 5.A1. $0.95 < U_{\mathrm{ERY}}(\theta) < 0.99$. Similar functions can be derived for other action spectra.

If the range is extended to $100\ \mathrm{DU} < W < 600\ \mathrm{DU}$, then the functional form changes (Fig. 5.A4) for $\mathrm{SZA} < 50^\circ$ and the form $U(\Omega_2/\Omega_1)^{\mathrm{RAF}}$ with an RAF value independent of Ω can no longer be used.

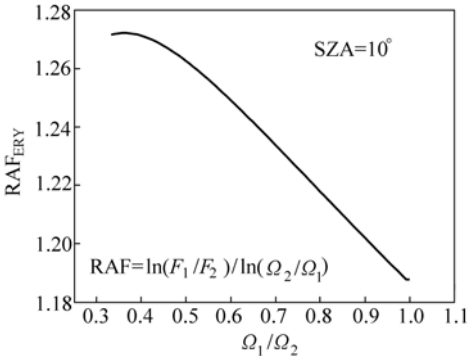

Figure 5.A1 RAF computed from its definition, $\mathrm{RAF} = \ln(F_1/F_2)/\ln(\Omega_2/\Omega_1)$

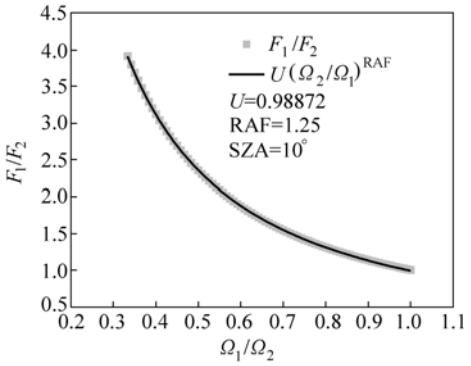

Figure 5.A2 RAF computed as best fit to irradiance ratios F_1/F_2 (gray squares) using $U(\Omega_2/\Omega_1)^{\mathrm{RAF}}$ (black line)

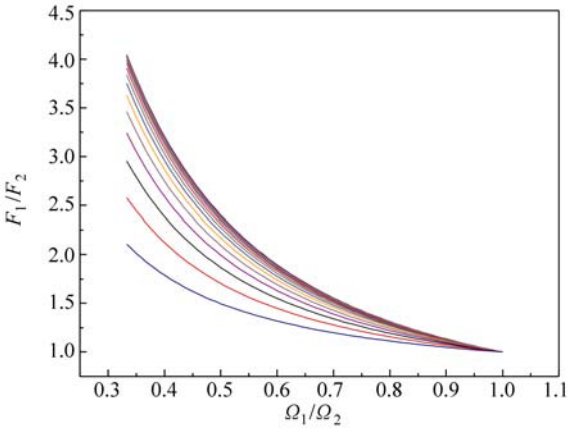

Figure 5.A3 F_1/F_2 for $0° < \mathrm{SZA} < 80°$ for 200 DU $< W <$ 600 DU

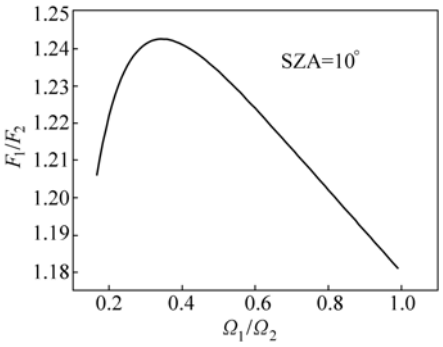

Figure 5.A4 Irradiance ratios when the ozone range is extended $100 < \Omega < 600$

Table 5.A1 $U_{ERY} = (A + C\theta^{0.5} + E\theta)/(1 + B\theta^{0.5} + D\theta + F\theta^{1.5})$

$A = 0.9893339422829114$	$B = -0.2091512249939112$
$C = -0.2065389508416529$	$D = 0.01116628089647472$
$E = 0.01084565669362034$	$F = -0.00001740267964926986$

Acknowledgements

This research was partly supported by the NASA MEASURES project for the reflectivity data. In addition, I would like to acknowledge the OMI, SBUV-2, and TOMS satellite analysis team for making the merged ozone time series available.

References

Bhartia PK, Herman JR, and Torres O (1993) Effect of Mt. Pinatubo aerosols on total ozone measurements from backscatter ultraviolet (BUV) experiments. J. Geophys. Res. 98: 18547 – 18554

Blumthaler M, Salzgeber M, and Ambach W (1995) Ozone and ultraviolet-B irradiances: experimental determination of the radiation amplification factor. Photochem Photobio 61: 159 – 162

Bodhaine BA, Dutton EG, Hofmann DJ, McKenzie RL, and Johnston PV (1997) UV measurements at Mauna Loa: July 1995 to July 1996. J. Geophys. Res. 102(D15): 19265 – 19273

Booth CR, Madronich S (1994) Radiation amplification factors: Improved formulation accounts for large increases in ultraviolet radiation associated with Antarctic ozone depletion. In: Weiler CS, Penhale PS (eds) Ultraviolet radiation in Antarctica: measurement and biological effects. Antarct Res Ser 62: 39 – 52

Brueckner C, Floyd LE, Lund PA, Prinz DK, and Vanhoosier ME (1994) In: Pap JM, Frolich C, Hudson HS, Solanki S (eds) The Sun as a Variable Star: Solar and Stellar Irradiance Variations. Cambridge Univ. Press, Cambridge, UK

Cede A, Herman J, Richter A, Krotkov N, and Burrows J (2006) Measurements of nitrogen dioxide total column amounts at Goddard Space Flight Center using a Brewer Spectrometer in direct sun mode. J. Geophys. Res. 111, D05304, DOI:10.1029/2005JD006585

Chubarova NY (2008) UV variability in Moscow according to long-term UV measurements and reconstruction model. Atmos. Chem. Phys. Discuss. 8: 893 – 906

Dave JV (1964) J. Opt. Soc. America, 54: 307

Devesa SS, Grauman DJ, Blot WJ, Pennello G, Hoover RN, and Fraumeni JF Jr. (1999) Atlas of cancer mortality in the United States, 1950 – 1994. Washington, DC: US Govt Print Off, NIH Publ. No. (NIH) 99 – 4564

Díaz S, Nelson D, Deferrari G, and Camilión C (2003) A model to extend spectral and multiwavelength UV irradiances time series: Model development and validation. J. Geophys. Res., 108(D4): 4150, doi:10.1029/2002JD002134

Diffey BL (1991) Solar ultraviolet radiation effects on biological systems. Review in Physics in Medicine and Biology 36(3): 299 – 328

Fahey DW (Lead Author) (2007) Twenty Questions and Answers About the Ozone Layer: 2006 Update, in Scientific Assessment of Ozone Depletion: 2006. Global Ozone Research and Monitoring Project Report No. 50, World Meteorological Organization, Geneva

Flint SD, and Caldwell MM (2003) A biological spectral weighting function for ozone depletion research with higher plants. Physiologia Plantarum 117: 137 – 144

Gao W, Slusser J, Gibson J, Scott G, and Bigelow D (2001) Direct-Sun column ozone retrieval by the ultraviolet multifilter rotating shadow-band radiometer and comparison with those from Brewer and Dobson spectrophotometers. J. Applied Optics 40: 3149 – 3156

Ghetti F, Bagnoli C, and Checcucci G (2006) Response to UV-B Radiation: Weighting Functions and Action Spectra, Environmental UV Radiation: Impact on Ecosystems and Human Health and Predictive Models Proceedings of the NATO Advanced Study Institute on Environmental UV Radiation: Impact on Ecosystems and Human Health and Predictive Models, Pisa, Italy, June 2001

Goering CD, L'Ecuyer TS, Stephens GL, Slusser JR, Scott G, Davis J, Barnard JC, and Madronich S (2005) Simultaneous retrievals of column ozone and aerosol optical properties from direct and diffuse solar irradiance measurements. J. Geophys. Res. 110, O5, D05204, 10.1029/2004JD005330

Hemminki K, Xu G, Kause L, Koulu LM, Zhao C, and Jansen CT (2002) Demonstration of UV-dimers in human skin DNA in situ 3 weeks after exposure. Carcinogenesis 23: 605 – 609

Herman JR, Hudson R, McPeters R, Stolarski R, Ahmad Z, Gu X-Y, Taylor S, and Wellemeyer C (1991) A new self-calibration method applied to TOMS/SBUV backscattered ultraviolet data to determine long term global ozone change. J. Geophys. Res. 96: 7531 – 7545

Herman JR, Newman PA, McPeters RD, Krueger AJ, Bhartia PK, Seftor CJ, Torres O, Jaross G, Cebula RP, Larko D, and Wellemeyer C (1995) Meteor-3/Total Ozone Mapping Spectrometer observations of the 1993 ozone hole. J. Geophys. Res. 100: 2973 – 2983

Herman JR, Bhartia PK, Ziemke J, Ahmad Z, and Larko D (1996) UV-B radiation increases (1979 – 1992) from decreases in total ozone. Geophys. Res. Lett. 23: 2117 – 2120

Herman JR, Krotkov N, Celarier E, Larko D, and Labow G (1999) Distribution of UV radiation at the Earth's surface from TOMS-measured UV-backscattered radiances. J. Geophys. Res. 104: 12059 – 12076

Herman JR, Larko D, and Ziemke J (2001a) Changes in the Earth's Global UV Reflectivity from Clouds and Aerosols. J. Geophys. Res. 106: 5353 – 5368

Herman JR, Celarier E, and Larko D (2001b) UV 380 nm reflectivity of the Earth's surface, clouds, and *aerosols*. J. Geophys. Res. 106: 5335 – 5351

Herman J, Cede A, Spinei E, Mount G, Tzortziou M, and Abuhassan N (2009a) NO_2 column amounts from ground-based PANDORA and MF-DOAS spectrometers using the Direct-Sun DOAS Technique: Intercomparisons and application to OMI validation. J. Geophys. Res. 114, D13307, doi: 10.1029/2009JD011848

Herman JR, Labow G, Hsu NC, and Larko D (2009b) Changes in cloud cover (1998 – 2006) derived from reflectivity time series using SeaWiFS, N7-TOMS, EP-TOMS, SBUV-2, and OMI radiance data. J. Geophys. Res. 114:D01201, DOI: 10.1029/2007JD009508

Herman JR (2009) Global Increase in UVB During the past 30 years 1979 to 2008. Accepted, J. Geophys. Res. 114: D01201, doi: 10.1029/2007JD009508

Holben BN, Eck TF, Slutsker I, Tanre D, Buis JP, Setzer A, Vermote E, Reagan JA, Kaufman Y, Nakajima T, Lavenu F, Jankowiak I, and Smirnov A (1998) AERONET — A federated instrument network and data archive for aerosol characterization. Rem. Sens. Environ. 66: 1 – 16

Holben BN, Tanre D, Smirnov A, Eck TF, Slutsker I, Abuhassan N, Newcomb WW, Schafer J, Chatenet B, Lavenue F, Kaufman YJ, Vande J Castle, Setzer A, Markham B, Clark C, Frouin R, Halthore R, Karnieli A, O'Neill NT, Pietras C, Pinker RT, Voss K, and Zibordi G (2001) An emerging ground-based aerosol climatology: Aerosol optical depth from AERONET. J. Geophys. Res. 106: 12067 – 12097

Holick MF (2004) Sunlight and vitamin D for bone health and prevention of autoimmune diseases, cancers, and cardiovascular disease. American Journal of Clinical Nutrition 80(6): 1678S – 1688S

Kalliskota S, Kaurola J, Taalas P, Herman JR, Celarier EA, and Krotkov NA (2000) Comparison of daily UV doses estimated from Nimbus-7/TOMS measurements and ground-based spectroradiometric data. J. Geophys. Res. 105: 5059 – 5067

Kerr JB, and McElroy CT (1993) Evidence for large upward trends of ultraviolet-B radiation linked to ozone depletion. Science 262: 1032 – 1034

Kerr JP, Thurtell GW, and Tanner CB (1967) An Integrating Pyranometer for Climatological Observer Stations and Mesoscale Networks. Journal of Applied Meteorology 6: 688 – 694

Krotkov NA, Bhartia PK, Herman JR, Fioletov V, and Kerr J (1998) Satellite estimation of spectral surface UV irradiance in the presence of tropospheric aerosols 1: Cloud free case. J. Geophys. Res. 103: 8779 – 8793

Krotkov NA, Herman JR, Bhartia PK, Ahmad Z, and Fioletov V (2001) Satellite estimation of spectral surface UV irradiance 2: Effect of horizontally homogeneous clouds. J. Geophys. Res. 106: 11743 – 11759

Krotkov N, Bhartia PK, Herman J, Slusser J, Scott G, Labow G, Vasilkov AP, Eck TF, Dubovik O, and Holben BN (2005) Aerosol ultraviolet absorption experiment (2002 to

2004), Part 2: Absorption optical thickness, refractive index, and single scattering albedo. Opt. Eng. 44(4) 041005: 1 – 17

Liley, BJ, and McKenzie RL (2006) Where on Earth has the highest UV? UV Radiation and its Effects: An Update. NIWA Science, Hamilton, NZ

Lin B, Stackhouse Jr PW, Minnis P, Wielicki BA, Hu Y, Sun W, Fan T-F, and Hinkelman LM (2008) Assessment of global annual atmospheric energy balance from satellite observations. J. Geophys. Res. 113, D16114, doi:10.1029/2008JD009869

Lucas R, McMichael T, Smith W, and Armstrong B (2006) Solar ultraviolet radiation: Global burden of disease from solar ultraviolet radiation. Environmental Burden of Disease Series, No. 13, WHO Report

Madronich S (1993) The atmosphere and UV-B radiation at ground level. In: Björn LO, Young AR (eds) Environmental UV Photobiology. Plenum Press, New York, pp. 1 – 39

McClintock W, Rottman GJ, and Woods T (2000) Solar Stellar Irradiance Experiment Ⅱ (SOLSTICE Ⅱ) for the NASA Earth Observing System's Solar Radiation and Climate Experiment mission. SPIE 4135: 225 – 234

McKenzie RL, Bjorn LO, Bais A, and Hyasd M (2003) Changes in biologically active ultraviolet radiation reaching the earth's surface. Photochemical Photobiological Sciences 2: 5 – 15

McKinlay AF, and Diffey BL (1987) A reference action spectrum for ultraviolet induced erythema in human skin. In: Passchier WR, Bosnjakovic BFM (eds.) (1987) Human Exposure to Ultraviolet Radiation:Risks and Regulations. Elsevier, Amsterdam

Qiu D, and Marugame T (2008) Comparison of time trends in skin cancer incidence (1973 – 1997) in East Asia, Europe and USA, from cancer incidence in five continents. Japan J. of Clinical Oncology 38: 234 – 236

Roderick ML, and Farquhar GD (2002) The cause of decreased pan evaporation over the past 50 years. Science 298: 1410 – 1411

Rousseaux MC, Ballaré CL, Giordano CV, Scope AL, Zima AM, Szwarcberg-Bracchitta M, Searles PS, Caldwell MM, and Díaz SB (1999) Ozone depletion and UV-B radiation: Impact on plant DNA damage in southern South America. Proceedings of the National Academy of Sciences USA 96(26): 15310 – 15315

Rozema J, Van Geel B, Björn LO, Lean J, and Madronich S (2002) Toward solving the UV puzzle. Science 296 31: 1621 – 1622

Seckmeyer G, Bias A, Bernhard G, Blumthaler M, Booth CR, Lantz K, Mckenzie RL, Disterhoft P, and Webb A (2005) Instruments to measure Solar Ultraviolet radiation, Part 2: Broadband Instruments Measuring Erythemally Weighted Solar Irradiance. World Meteorological Organization Report 164, WMO TD-No.1289

Setlow RB (1974) The wavelengths in sunlight effective in producing cancer: a theoretical analysis. Proceedings of the National Academy of Sciences USA 71: 3363 – 3366

Slusser J, Gibson J, Bigelow D, Kolinski D, Disterhoft P, Lantz K, and Beaubien A (2000) Langley method of calibrating UV filter radiometers. Journal of Geophysical Research 105: 4841 – 4849

Staehelin J, Renaud A, Bader J, McPeters R, Viatte P, Hoegger B, Bugnion V, Giroud M, and Schill H (1998) Total ozone series at Arosa (Switzerland): Homogenization and data comparison. Journal of Geophysical Research 103(D5): 5827 – 5841

Staehelin J, and Weiss AK (2001) Swiss history of atmospheric ozone research and results of long-term Swiss ozone measurements. Ozone: Science and Engineering 23: 461 – 466

Stanhill G, and Cohen S (2001) Global dimming: A review of the evidence for a widespread and significant reduction in global radiation with discussion of its probable causes and possible agricultural consequences. Agricultural and Forest Meteorology 107(4): 255 – 278

Torres O, Herman JR, Bhartia PK, and Sinyuk A (2002a) Aerosol properties from EP-TOMS near UV observations. Advances in Space Research 29: 1771 – 1780

Torres O, Herman JR, Bhartia PK, and Sinyuk A (2002b) A long term record of aerosol optical thickness from TOMS observations and comparison to AERONET measurement. Journal of Atmospheric Science 59: 398 – 413

Tzortziou M, Krotkov NA, Cede A, Herman JR, and Vasilkov A (2008) A new technique for retrieval of tropospheric and stratospheric ozone profiles using sky radiance measurements at multiple view angles: Application to a Brewer spectrometer. Journal of Geophysical Research 113:D06304, doi:10.1029/2007JD009093

Wenig MO, Bucsela EJ, Celarier EA, Gleason JF, Cede AM, Herman JR, Veefkind P, and Brinksma E (2006) Validation study of two years of OMI NO_2 data. Advanced Environmental Monitoring

WMO (World Meteorological Organization) (1999) Scientific assessment of ozone depletion: 1998. Global Ozone Research and Monitoring Project, Report No. 50, Geneva

WMO (2003) Scientific assessment of ozone depletion: 2002. Global Ozone Research and Monitoring Project, Report No. 47, Geneva

WMO (2007) Scientific assessment of ozone depletion: 2006. Global Ozone Research and Monitoring Project, Report No. 50, Geneva

Zerefos C, Balis D, Tzortziou M, Bais A, Tourpali K, Meleti1 C, Bernhard G, and Herman J (2001) A note on the interannual variations of UV-B erythemal doses and solar irradiance from ground-based and satellite observations. Annales Geophysicae 19: 115 – 120

Zuev VV, Bondarenko SL (2001) Relationship between long-period variability of atmospheric ozone layer with wood density variations caused by UV-B radiation. Atmospheric and Oceanic Optics 12: 1 – 4

6 The Brewer Spectrophotometer

James B. Kerr

Scientist Emeritus of Environment Canada
4396 Kingscote Road, V0R 1N2
Cowichan Bay, British Columbia
E-mail: jbkerr@shaw.ca

Abstract In the late 1960s and early 1970s, concerns were raised regarding the vulnerability of stratospheric ozone to anthropogenic activities and the consequential increase of ultraviolet-B (UVB) radiation at the earth's surface. These concerns prompted the development of new scientific instrumentation for monitoring the state of the ozone layer and levels of surface UV radiation. Included in the list of instrumentation is the ground-based Brewer spectrophotometer. The Brewer spectrophotometer has now been in operation at some sites for more than 25 years and has participated in numerous specialized field campaigns. Site instruments have been stable over long periods of time and function reliably in unattended operation for periods of several days under a wide range of operating conditions. The Brewer spectrophotometer has proven to be a valuable scientific tool that has made significant contributions to our understanding of the ozone layer and the dependence of surface UV radiation on stratospheric ozone and other atmospheric variables. This chapter discusses the history of the development of the Brewer spectrophotometer, describes the design and operation of the instrument, outlines the methods and algorithms used to measure the geophysical variables, and reviews some scientific results of operational and specialized measurements.

Keywords atmospheric ozone, ultraviolet radiation, radiation instrumentation, measurement techniques

6.1 Introduction

The Brewer spectrophotometer is a modified Ebert grating spectrometer that has been designed to measure the intensity of radiation at targeted UV and visible wavelengths. Pointing capabilities of the instrument allow the measurement of

direct irradiance, global irradiance, or sky radiance from a specified direction, including the zenith. The column amount of atmospheric constituents that absorb or scatter solar or lunar radiation can be determined using differential optical absorption spectroscopy (DOAS) techniques. Atmospheric gases that are measured using their absorption properties include ozone, sulfur dioxide (SO_2), and nitrogen dioxide (NO_2). In addition, aerosol optical depth can be determined from measurements of direct solar irradiance.

Today nearly 200 Brewer instruments have been manufactured and are operating in about 40 countries. The early instruments have operated almost continuously for about 25 years at some sites. Instruments operate unattended outdoors under a wide range of weather conditions encountered at tropical, high latitude, and high altitude sites. Ozone measurement records spanning up to 25 years have provided a wealth of valuable information that has contributed toward our understanding of the changing ozone layer. Measurement records of spectral UV radiation are more than 15 years in length at several sites and allow analysis for long-term changes in UV radiation. Brewer instruments account for about 75% of spectral UV data reported to global and regional databases (WMO, 2007).

6.2 History

An early version of a grating spectrometer was developed at Cambridge University, UK and used by David Wardle in the winter of 1963 – 1964 to make measurements of total column ozone during the polar night at Resolute, Canada using stellar radiation as a light source (Wardle, 1965). The instrument was later brought to the University of Toronto where subsequent versions of grating spectrometers were developed with Alan Brewer, Jim Kerr, and Tom McElroy. These instruments were used for short-term research projects that demonstrated the capability of grating spectrophotometers for measuring atmospheric ozone (Brewer and Kerr, 1973; Kerr, 1973) and nitrogen dioxide (Brewer et al., 1973). Brewer (1973) proposed that a grating spectrophotometer could be developed with the goal of supplementing the Dobson ozone spectrophotometer (Dobson, 1957) and the M-83 filter ozonometer (Gustin et al., 1985), which were the only ground-based operational instruments in use at the time. Kerr, McElroy, and Wardle moved to the Atmospheric Environment Service (AES) of Environment Canada in Downsview, Ontario in the early 1970s where the goal of developing an operational grating instrument to measure surface UV irradiance and atmospheric ozone was kept alive.

One major consideration regarding the development of a viable instrument with potential for widespread use as an operational network instrument was commercialization. It was realized that it would be necessary for the instrument to be manufactured commercially by a company capable of making specialized

scientific equipment and supporting it over a long period of time. During the later part of the 1970s, the first pre-production prototype instruments (Mark Ⅰ) were developed and manufactured by SED Systems of Saskatoon, Canada.

The Mark Ⅰ prototype instruments were tested in operational use over a period of several months, and in field intercomparison experiments (Kerr et al., 1981; Parsons et al., 1981). Significant information regarding the calibration, stability, and reliability of the instruments was acquired during this period of operation. Much of what was learned regarding the possible improvements that were needed to address shortcomings was noted and included in the development of the production version (Mark Ⅱ), which has the same optical layout and configuration as the earlier version.

The design and development of the Mark Ⅱ version was carried out jointly by AES and SED Systems and focused mainly on providing fully automatic operation. Full automation of the instrument was considered to be important because the general trend for monitoring geophysical variables was evolving toward automatic measurement in order to reduce manpower and increase data volume. The Dobson spectrophotometer is not automated, and the introduction of a fully automated instrument would offer a distinct advantage.

There were several aspects that needed to be considered to enable unattended operation over different time periods over several days. The first consideration was that of data recording. The first commercial prototype provided a serial port that could output data to a printer. However, manual operations were required to align the instrument, set it up, and then initiate an observation. The requirement for manual operation was addressed by installing several stepping motors to make mechanical adjustments, which would otherwise require manual setup. About this time, personal computers were becoming available, offering a means to fulfill data recording and mechanical positioning requirements at a relatively low cost. The first “control computer” for the automated Brewer instrument was the Commodore PET, which was programmed to schedule and carry out sequences of measurements and tests. The advent of modern day personal computer technology and communication technology has significantly improved and simplified the reliability of data management tasks such as data storage, reporting, and analysis.

In the early 1980s, Brewer instruments were manufactured (by a new company called Sci-Tec Instruments Inc.) and commenced operation at Canadian sites as well as several sites operated by foreign institutes. Three Brewer instruments were established as the calibration “triad” in Downsview (Kerr et al., 1985), and the same three instruments comprise the triad today (Fioletov et al., 2005). Brewer instruments replaced the existing five Dobson instruments in the Canadian ozone-monitoring network after an overlap period of at least three years (Kerr et al., 1988). In addition, the Canadian network expanded to 12 sites beginning in the late 1980s (Kerr, 1994). Around the same time, Brewer instruments were upgraded to measure spectral UV irradiance and appropriate calibration facilities and standards were developed to allow this measurement on an absolute scale.

The Brewer instrument proved to be stable on an absolute scale over long periods of time (Kerr and McElroy, 1993). UV spectral measurement records using Brewer instruments commenced at several sites around the world in the early 1990s (Bais et al., 1994; Ito et al., 1994; Vandersee and Köhler, 1994).

During this time, two new versions of the Brewer instrument were developed: the Mark Ⅲ and the Mark Ⅳ. The Mark Ⅲ is a double monochromator, which was developed to reduce stray light that can be a problem in single monochromators. The Mark Ⅳ has a modified grating, which allows the option to measure radiation at visible wavelengths to determine atmospheric NO_2, as well as the standard UV wavelengths used to determine ozone, SO_2, and spectral UV irradiance. In the late 1990s, a Mark Ⅴ version of the instrument was developed to measure radiation at wavelengths in visible red light (600 nm – 650 nm) where ozone is measured using the Chappuis absorption bands. This instrument can measure ozone at low sun angles ($< 10^\circ$ solar elevation) and is particularly suitable at high latitude locations (WMO, 2006; Tanskanen et al., 2007).

Since 1990, workshops for users of Brewer instruments have been held about every two years. These meetings have been hosted by agencies in Europe, North America, and Asia. In addition, the developers from AES (now the Meteorological Service of Canada, MSC) and manufacturers of the instrument, and the commercial companies that service and calibrate field instruments, also attend these workshops. The purpose of the workshops is to offer interested users a platform to present results and experiences from using Brewer instruments. The meetings also allow users and supporting groups the opportunity to interact with each other. The workshops are organized as a series of seminars under various topics, such as measurement type (e.g., UV, total ozone, etc.), calibration procedures, data analysis, and data archiving. Results presented at the workshops are formally published as WMO reports (e.g., WMO, 1994; WMO, 2006).

In 1996, Sci-Tec Instruments Inc. merged with Kipp and Zonen Inc. and production of the instruments was later transferred to Delft, Holland. Today only the Mark Ⅲ version of the instrument is manufactured, and the Mark Ⅱ and Mark Ⅳ instruments are no longer produced. However, technical service and support is still provided for these existing instruments.

6.3 The Instrument

The optical components of the Brewer spectrophotometer are comprised of three parts: (1) the fore-optics, (2) the spectrometer, and (3) the photomultiplier housing, as illustrated in Fig. 6.1 (from Fig. 2.5 of the Brewer Instruction Manual, courtesy of Kipp and Zonen). Additional information regarding the optical components can be found in Fig. 2.4 of the Brewer Instruction Manuals. The fore-optics direct incoming radiation onto the entrance slit of the spectrometer. The

spectrometer disperses and focuses a spectrum of the incident radiation across a set of exit slits. For the Mark Ⅱ and Mark Ⅳ instruments, the photomultiplier counts photons of radiation that pass through the exit slits. The Mark Ⅲ version of the instrument has a second spectrometer (recombining spectrometer) that mirrors the dispersing spectrometer of the Mark Ⅱ and Mark Ⅳ versions.

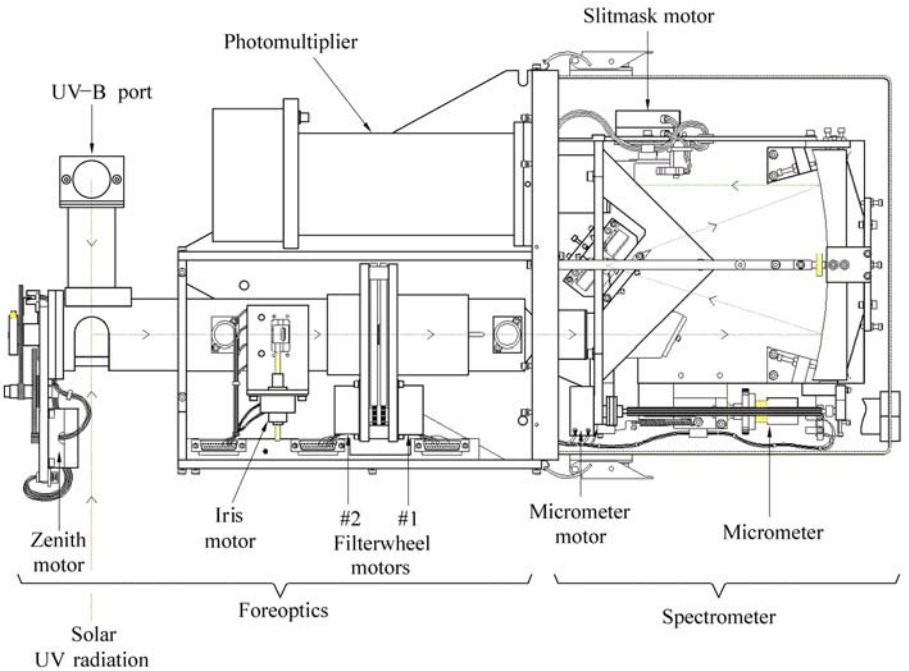

Figure 6.1 Optical layout of the single monochromator (Mark Ⅱ and Mark Ⅳ) versions of the Brewer Spectrophotometer. This diagram shows the foreoptics, the spectrometer, and the photomultiplier components of the instrument. For the Mark III double monochromator, the dispersing spectrometer is the same as that shown here and the recombining spectrometer is the mirror image located behind (beneath) the base plane of the spectrometer illustrated above. The photomultiplier housing for the Mark Ⅲ is located beneath the foreoptics. (Illustration from Brewer Instruction Manual, courtesy of Kipp and Zonen)

A photograph of the Mark Ⅲ version is shown in Fig. 6.2. The optical components and supporting electronics of the Brewer instrument are enclosed in a weatherproof container that is painted white to minimize radiative heating. The cover for the instrument has a sloping quartz window to allow UV radiation onto the fore-optics of the instrument for direct sun, direct moon, and zenith sky measurement. Mounted on the top of the instrument is a Teflon diffuser covered by a quartz dome for measurements of global irradiance. The enclosed instrument sits on top of an azimuth drive box, which rotates the instrument in azimuth with

a precision of about 0.025°. Normally the azimuth drive aligns the instrument so that the quartz window faces the sun.

Figure 6.2 Photograph of the Mark III version of the Brewer Spectrophotometer (Courtesy of Kipp and Zonen)

6.3.1 The Fore-Optics

A 45° fused quartz prism is located at the head of the fore-optics tube and reflects incoming radiation (by total internal reflection) at right angles along the horizontal optical path of the instrument. The zenith prism plays an important role in selecting the appropriate source of radiation for lamp tests, sky measurements, direct sun or moon measurements, or UV spectral measurements. The prism rotates about the optical axis of the fore-optics so that radiation originating from zenith angles between 0° and 90° can be directed along the axis. In this mode, the instrument measures the radiance at the respective zenith angle. Rotation of the zenith prism is done by a computer controlled stepping motor (called the zenith motor), which acts through a set of reducing gears to position the desired direction with a precision of 0.128°.

A lamp housing containing a mercury lamp and a quartz iodine lamp is located below the zenith prism. When the zenith prism is directed so that it points downward (zenith angle of 180°), radiation from the lamps is directed along the optical path. The mercury lamp is used to check the wavelength setting of the instrument and adjust it if necessary. The quartz iodine lamp provides a radiation source to check the relative wavelength response of the instrument.

Radiation incident on a horizontal Teflon diffuser on top of the cover is viewed by rotating the zenith prism to view horizontally towards the UV port shown in Fig. 6.1. The UV port consists of another 45° prism that is mounted on the fore-optics tube and positioned directly below the horizontal diffuser. The UV port prism reflects radiation transmitted through the horizontal diffuser at right angles toward the zenith prism, which in turn, reflects radiation at right angles along the optical path. In this mode, the instrument measures global irradiance.

Radiation passing along the fore-optics axis then passes through a lens that focuses radiation from infinity onto the plane of an iris. The iris is used for only direct sun or moon measurement. When the azimuth and zenith are aligned toward the sun or moon, the focused image of the target passes through the aperture of the iris, which is closed to about five solar diameters (e.g., Cede et al., 2003). This prevents most of the scattered sky radiation around the solar or lunar disk to pass through to the spectrometer. Scattered sky radiation can become important when the sun is low, or at relatively large aerosol or cloud optical depths. For all other measurements, the iris remains open and does not block any radiation passing along the optical axis.

After passing through the plane of the iris, radiation is collimated by a second lens and then passes through two filter wheels which can both hold up to six filters. The first wheel consists of an open position and neutral density filters with increasing optical depth in the five remaining positions. Progressive filter positions decrease radiation by a factor of about 3. A second six-position filter wheel inserts filters that include ground quartz for direct sun measurements and polarization filters. The ground quartz filter is used to diffuse direct sun radiation, which reduces errors that may result from the effects of slight misalignment. After passing by the filter wheels, radiation is then focused onto the entrance slit of the spectrometer.

6.3.2 The Spectrometer

The Brewer instrument uses a modified Ebert grating spectrometer (Fastie, 1952) to disperse incoming radiation into a spectrum. The first optical element of the spectrometer is a tilted quartz lens. The purpose of the lens is to correct for optical aberrations, which are inherent in an Ebert spectrometer. Both of the lens surfaces correct for an aberration. An off-axis spherical concave surface of the lens compensates for coma due to the asymmetry of the Ebert spectrometer. The second surface is cylindrical convex and is used to correct for astigmatism.

The optical path continues to a spherical mirror where radiation is collimated and directed toward the grating. Radiation is dispersed at the grating and directed toward the spherical mirror where the spectrum is focused on the plane of the exit slits.

There are six exit slits that are approximately evenly spaced across the focal plane. The shortest wavelength slit is for wavelength calibration using a grouping of mercury emission lines near 302.1 nm or the single emission line at 296.68 nm.

The other five slits correspond to wavelengths that take advantage of the structure of both the ozone and SO_2 absorption spectra at UV wavelengths. Figure 6.3 shows the wavelength positions of the six slits with the absorption spectra of ozone and SO_2. The absorption spectrum of ozone differs from that of SO_2 and, as a result, it is possible to quantify both absorbers (Kerr et al., 1981).

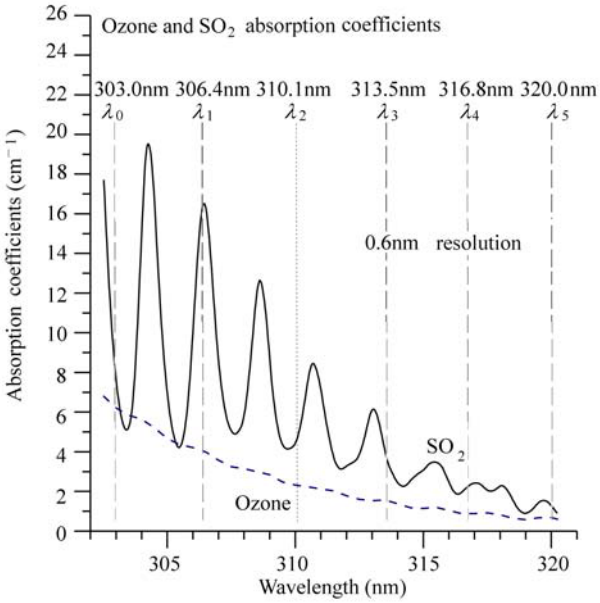

Figure 6.3 Absorption coefficients for ozone and SO_2 smoothed to the resolution of the Brewer instrument. Operational wavelengths of the Brewer Spectrophotometer (λ_1 to λ_5) and the wavelength used for special applications (λ_0) are shown. The absorption features for SO_2 are significantly different than those for ozone, making it possible to measure both constituents simultaneously. It should be noted that under polluted conditions, column SO_2 is usually less than 5 Dobson Units (DU), and stratospheric ozone values typically range between 200 and 500 DU. The amount of UV-B absorbed by SO_2 is therefore generally less than 5% that of ozone. However, absorption by SO_2 can be significant under plumes from major volcanic eruptions (Kerr et al., 1982; Krueger, 1983). Absorption coefficients are those of Bass and Paur (1985) at $-45^{\circ}C$, and the coefficients for SO_2 are those of McGee and Burris (1987) at $-63^{\circ}C$

The slits are covered by a cylindrical mask with openings that are positioned by a stepping motor to open one slit at a time. In operation, the time required to switch from one wavelength to another is about 0.016 sec, and the sampling time at each wavelength position is seven times the switching time (about 0.115 sec). A sampling cycle progresses from a lower wavelength (e.g., wavelength 1) to an upper wavelength (say wavelength 5) and back. The range of the sampling cycle and the number of sampling cycles in a sample are programmable.

The cylindrical mask also contains a position that blocks all slits as well as opening two slits at a time. The purpose of the blocking position is to provide a quick sample of the instrument's dark count (i.e., the signal that the instrument registers without any radiation). Dark count is normally measured as part of the sampling sequence and is subtracted from the counts registered at each wavelength channel. The purpose of the double slit opening is to allow a quick measurement of the instrument's dead time. Dead time is measured by comparing the photon counts when both slits are opened with the sum of photon counts when the two slits are opened individually. This test is done quickly and automatically as part of the daily operational schedule.

An 1,800 line/mm holographic grating is used in the second order for the Mark Ⅱ instrument and a 1,200 line/mm grating is used in the third order for the Mark Ⅳ instrument. The grating is mounted on a set of cross-springs that serves as a frictionless bearing to allow the control of rotation with virtually no hysteresis over the operational wavelength range. Rotation of the grating is controlled by a stepping motor which drives a micrometer acting at the end of a lever arm. The drive between the stepping motor to the micrometer is geared so that one motor step is equivalent to a shift of about 0.007 nm of the spectrum across the exit slit plane. For the existing design of the Brewer instrument, the mechanical limits of the grating rotation allow for a range of wavelengths spanning from about 285 nm (measured on the shortest slit) to 365 nm (measured using the longest slit). Extension of this wavelength range without loss of hysteresis and wavelength precision is difficult. The wavelength setting can be measured to about 0.1 micrometer step (Gröbner et al., 1998; Kerr, 2002), but the wavelength positioning is limited to 1.0 micrometer steps.

The double monochromator (Mark Ⅲ) uses basically the same dispersion spectrometer as that of the Mark Ⅱ and Mark Ⅳ with a 3,600 line/mm holographic grating used in the first order. The main difference is that a 45° mirror is placed ahead of the cylindrical slit mask to reflect radiation 90° downward onto the horizontal focal plane where radiation passes through the exit slits and into the recombining spectrometer, which is the mirror image of the dispersing spectrometer. Both gratings (holographic with 3,600 line/mm) for the Mark Ⅲ are individually controlled to allow automatic measurement and adjustment of the wavelength alignment of the two spectrometers. Further descriptions of the double monochromator regarding wavelength stability (Gröbner et al., 1998) and spectral characteristics (Bais et al., 1996; Wardle et al., 1997) are reported in the literature.

6.3.3 The Photomultiplier Housing

A light proof, hermetically sealed, dehumidified cylindrical housing houses the photomultiplier with electronics for high voltage power and for the high-speed amplifier for photon counting. High voltage DC power to operate the photomultiplier

is usually set at a voltage between 1,200 and 1,400 volts, depending on tube characteristics. A photon arriving at the light sensitive cathode initiates a burst of electrons that cascades and is amplified as is passes through the various stages of the tube. The burst of electrons arriving at the anode is then amplified to yield a pulse that is counted in the counting register. A discriminator level is set at about 30 milli-volts to filter out low voltage pulses, which are more likely electronic noise and not light signal.

An order-blocking filter is placed between the exit slits and the cathode of the photomultiplier to remove radiation from grating orders that are not used. For the Mark Ⅱ instruments, the second order radiation (~280 nm－350 nm) is used and the first order (~560 nm－700 nm) is blocked by a nickel sulfate/UG-11 filter combination. In the Mark IV, the first order (~840 nm－1,050 nm) is not used and a filter wheel inserts an order-blocking filter. Second order visible radiation (~420 nm－525 nm) for measurements of NO_2 is selected with a BG-12 filter, and third order (~280 nm－350 nm) for measurements of ozone, SO_2, and spectral UV radiation is selected by a nickel sulfate/UG-11 filter combination. An order-blocking filter is not used in the Mark Ⅲ instruments that are equipped with gratings operating in the first order.

6.3.4 Support Electronics

An on-board microcomputer coordinates the movement of the six (Mark Ⅱ and Mark Ⅲ) or seven (Mark Ⅳ and Mark Ⅴ) stepping motors located in the instrument as well as the azimuth drive located in the mounting box beneath the instrument. This microcomputer provides the time base for coordinating the movement of the slit mask and the accumulation of photon counts in appropriate memory registers. It also controls the switching of the lamps, and monitors various supply voltages and temperature readings at different locations inside the instrument. Wired communication with a separate control computer, which is usually located indoors, is done through an RS-232 communication port. The microcomputer accepts ASCⅡ commands, executes each command task, and signals the task completion back to the control computer. Multiple commands can be sequenced and executed in order of sequence.

Instruments operating in cold climates are heated to limit the lower range of operation. Should the temperature drop below a specified value (between 5°C and 20°C), a thermostat switches on the heaters inside the instrument box. Some Brewer instruments have been modified to operate in a thermally regulated (both heated and cooled) environment that allows minimal temperature variability.

Other electronics inside the instrument include power supplies for several components of the instrument. These components include the mercury and standard lamps, the high voltage for the photomultiplier, drive supplies for the stepping motors, and the heaters.

6.3.5 The Control Computer

The control computer is a personal desktop or laptop computer that communicates directly with the microcomputer on the Brewer instrument via a RS-232 serial link. The control computer allows operation of the Brewer instrument either manually by entering commands from a menu or automatically by entering a sequence of commands that is scheduled as a function of solar zenith angle (SZA) or time of day. Nearly all of the data collected by Brewer instruments is collected during automatic operation. The manual mode is used mainly for setup, special tests, or debugging operations.

The control computer is programmed using GWBasic allowing users of the instrument to develop customized measurements or tests. Versions of the control program have been developed that use other computer languages, i.e., Matlab; however, these programs are not in general use. Preliminary results of measurements are calculated and summarized in real time allowing quick identification of instrumental problems.

Many operators automatically retrieve a daily file of raw data remotely (usually overnight) from field instruments using communication links such as telephone or the internet. Daily data files are typically 100 KB to 200 KB in size depending on observation schedule, location, and time of year, and are often archived into a central database on a day-to-day basis. Preliminary data results are reported in near real time for use in applications, such as UV Index forecast or public distribution of real time total ozone and UV Index values. In addition, programs can be uploaded remotely to the Brewer control computer allowing schedule changes or special tests to be carried out without on-site intervention.

6.4 Corrections Applied to Data

There are a number of corrections that are applied during the processing of the photon count data. The requirements for corrections arise from the unique characteristics of each instrument. Corrections include those for dark count, dead time, stray light, temperature response, neutral density filter attenuation, cosine response, and polarization effect.

6.4.1 Dark Count

Correction for the dark count is fairly straightforward and involves the subtraction of the dark count from the signal count. Dark counts arise from thermal noise and are generated spontaneously in photomultiplier tubes. The dark count is temperature dependent and varies from tube to tube. The dark count can also change with

time and is dependent on the history of light exposure. As mentioned earlier, the dark count is measured as part of a sample and is stored on all data records.

6.4.2 Dead Time

The correction for dead time is required because the photon counting process is non-linear. A photon pulse generated by the photomultiplier and amplifier has a finite width of about 30 nanoseconds (ns). Thus, two or more photons arriving within 30 ns merge into a single pulse, which is registered as one count. The probability for missed counts increases with the count rate, and as the count rate increases, the registered counts eventually saturate. The maximum operating count rate for the Brewer instrument is limited to about 2 million counts per second (MHz). Under this condition, the average photon spacing is about 15 times the photon pulse width, and correction for dead time can be accurately made. Prior to every measurement, targeted radiation is sampled, and if the count rate is too high, the appropriate neutral density filter is inserted to reduce the count rate below 2 MHz. If the count rate is low (<0.5 MHz), the thickness of the neutral density is reduced, if possible.

The correction assumes the following model:

$$N = N_o \exp(-tN_o) \tag{6.1}$$

where N is the measured photon count rate.

N_o is the corrected photon count rate.

t is the dead time.

With knowledge of t, it is possible to solve iteratively for N_o from N. At maximum measured count rate ($N = 2$ MHz), the correction required is about $+6.5\%$ for an instrument with dead time of 30 ns.

As discussed in Section 6.3.2, the slit mask of the Brewer spectrophotometer is designed to measure dead time quickly and automatically by using a mask position where two slits (slit #2 and slit #4) are opened together. This allows a two-source linearity measurement by counting the photons with two slits opening individually, as well as with both opening together. Three equations are described for N_2, N_4 and N_{2+4}, where N_2 = number of photons counted with slit #2 opened, N_4 = number of photons counted with slit #4 opened, and N_{2+4} = number of photons counted with both slits opened. From these three equations, three unknowns (N_{o2}, N_{o4}, and t) can be solved iteratively since it is known that $N_{o2} + N_{o4} = N_{o2+4}$. Results of this internal two-source test compare very well with conventional, but more cumbersome, tests using two external radiation sources.

In operation, the dead time is measured and recorded on a daily basis using two intensity settings, and the results are used as an indicator of instrument performance. Measured dead times for the two intensity levels should agree and should remain fairly stable with time. These tests are useful to warn operators of

possible problems associated with the setting or stepping of the slit mask, as well as photon counting circuitry.

6.4.3 Stray Light

Stray light is an inherent problem with spectrometers. Stray light is light that arrives at the focal plane at a wavelength position shifted from the primary wavelength position. The amount of stray light generally decreases with the difference between the shifted wavelength and the primary wavelength (Wardle et al., 1997). Use of holographic gratings reduces this problem; however, for single monochromators, stray light from nearby wavelengths is typically 10^{-3} to 10^{-4} times that of the primary wavelength.

Stray light is an important consideration for making UV measurements. The rapid increase of ozone absorption with decreasing wavelength (Fig. 6.3) causes UV radiation at the earth's surface to increase by several orders of magnitude over a relatively short wavelength range, particularly when the sun is low in the sky. This means that stray light from longer wavelengths can make up a significant fraction of the signal measured at shorter wavelengths where there is relatively little radiation.

It is possible to apply a correction for the stray light present in a single monochromator (Kerr, 2002). This is done by measuring the distribution of light from a monochromatic source (laser) that is dispersed in the spectrometer and scattered to nearby wavelengths from the primary wavelength. Once this dependence is known, it is possible to calculate the spectrum of stray light and subtract it from the measured spectrum.

The problem of stray light is significantly reduced with the double Brewer monochromator. In this case, the second pass through the recombining spectrometer effectively reduces stray light to about 10^{-7} to 10^{-8} times that of the primary wavelength (Wardle et al., 1997). Use of the double Brewer instrument increases the accuracy of ozone and UV measurements and extends the range of operation to lower sun angles.

6.4.4 Temperature Response

Brewer instruments are sensitive to temperature. The temperature dependence is mainly due to the transmission properties of the nickel sulfate filter, which is used as part of the order-blocking filter combination for UV operation and is necessary to reduce stray light in the spectrometer. The temperature dependence is linear; however, it increases non-linearly with increasing wavelength (Kerr, 2002). Temperature of the instrument near the nickel sulfate filter is measured, so the response can be determined and corrections can be made. Sensitivity to

temperature is measured both under controlled cold chamber conditions as well as field operational conditions. Typical temperature sensitivities range from about −0.5%/°C to +0.1%/°C and vary from instrument to instrument. Temperature response corrections have been routinely made to ozone measurements prior to submission and analysis of data records. Temperature response has also been measured and applied to spectral UV data (Weatherhead et al., 2001; Siani et al., 2003; Garane et al., 2006). Uncertainty of the temperature corrections is about ±0.05%/°C. The double monochromator Mark III version of the Brewer instrument has significantly less stray light, and the nickel sulfate filter is not required for order blocking. Temperature response of the Mark III is therefore less of a problem.

6.4.5 Neutral Density Filters

A series of five neutral density filters is located in a filter wheel of the fore-optics and can be inserted into the optical path should the intensity of incoming radiation require reduction. The filters increase in density by factors of about 3 up to a density of about 300 (Kerr, 2002). For operational measurements of ozone using the standard DOAS technique (described in Section 6.5), there is no need to account for the presence of a filter. This is because the filters are nearly neutral, so they attenuated all wavelengths nearly equal, and there is essentially zero differential optical absorption from wavelength to wavelength. In reality, the filters are not exactly neutral; however, optical density gradients are linear with wavelength and any effects linear with wavelength are removed by the Brewer DOAS technique for measuring ozone (see Section 6.5).

Knowledge of the attenuation characteristics of the neutral density filters is essential for absolute spectroscopy applications and for measurements of aerosol optical depth. Absolute applications include the measurement of global or direct spectral UV irradiance. Routine measurements are made of global spectral UV irradiance (Kerr and McElroy, 1993) and special measurements have been developed to measure direct irradiance (Bais, 1997; Gröbner and Kerr, 2001). For measurements of aerosol optical depth (e.g., Bais, 1997; Kerr, 2002), accurate knowledge of the optical thickness of the neutral density filters is crucial since it is difficult to distinguish between the nearly neutral optical depth of a filter with that of atmospheric aerosols.

6.4.6 Cosine Response

Traditionally, the measurement of surface radiation has been made to quantify the downward flux incident on a horizontal surface. This is used for studies involving the radiative transfer of flux through the atmosphere and at the earth's surface.

The downward flux is the total radiation integrated over the celestial hemisphere weighted with the cosine of the zenith angle.

Most radiation monitoring instruments, including the Brewer, are designed to replicate the cosine response to incident radiation. The Teflon diffuser of the Brewer approximates the cosine response; however, at large zenith angles, the response falls below the cosine function (Fioletov et al., 2002). Measurements of global irradiance are therefore in error by values that range up to −10% depending on wavelength, SZA (solar zenith angles), and clarity of the sky. The cosine response is instrument dependent (Bais et al., 2005) and, with proper measurement, correction for the departure from the cosine response is applied to the data with the aid of a radiative transfer model or another parameterization technique (Bais et al., 1998; Fioletov et al., 2002). The uncertainty of the corrected values is about 2%. Also, work has been carried out to improve the cosine response of the sensor (Gröbner, 2003), and these new diffusers are available.

6.4.7 Internal Polarization

It has been demonstrated that there is a sensitivity dependence on SZA for measurements of direct radiation due to polarization effects between components of Brewer spectrophotometers (Cede et al., 2004; 2006a). Unpolarized radiation from direct sun becomes increasingly polarized as the incident angle through the quartz window increases from normal transmission (SZA = 35°), and the direction of enhanced polarization is along the axis parallel to the length of the window. This polarization interacts with the grating, which is more sensitive to radiation polarized on the axis perpendicular to the grating grooves. At SZA = 0°, the polarization axis of the grating is aligned parallel to the polarization axis transmitted through the window. With increasing SZA, the angle between the two axes of polarization increases. Thus, for window transmission normalized to SZA = 35°, the apparent transmission is enhanced for SZA < 35° and reduced for SZA > 35°.

Corrections can be applied to direct radiation data provided the degree of polarization of the grating sensitivity is known. It should be noted that the degree of polarization is not necessarily the same for all instruments. Calculations by Cede et al. (2004; 2006a) assume 100% polarization (extreme case) for the grating response. In general, the degree of polarization for the grating is less than 100%, and for single spectrometers (Mark Ⅱ and Mark Ⅳ), the polarization is significantly less than 100% since there is only one grating.

Corrections can also be achieved by the use of hardware modifications. Use of a cylindrical quartz window with the axis centered on the axis of rotation for the zenith prism would ensure that direct radiation always passes through the window at right angles. Also, a depolarizer inserted in the fore-optics removes the polarization effect (Cede et al., 2006a). Use of a Teflon diffuser instead of the ground quartz diffuser for measurements of direct radiation also avoids this effect since the

Teflon has been found to be an effective depolarizer, whereas the ground quartz removes very little polarization.

The internal polarization effects do not impact the operational measurements of ozone and other atmospheric gases that use DOAS techniques. These techniques measure the relative absorption at different wavelengths and the wavelength dependence of the polarization effect was found to be negligible (Cede et al., 2006a). However, corrections for the polarization effects should be applied for absolute measurements of the extraterrestrial spectra, aerosol optical depth, aerosol single scattering albedo, and estimates of actinic flux (Webb et al., 2002). Measurements of global UV irradiance are not affected since the Teflon diffuser on top of the instrument has been found to be an effective depolarizer.

6.5 Measurement of Total Ozone

The second most important atmospheric variable affecting surface UV radiation after cloud cover is total column ozone. Ozone strongly absorbs radiation in the UV and accounts for the sharp cutoff of the solar spectrum at about 290 nm. The most common measurement made by Brewer instruments is that of total column ozone, which is the amount of ozone in a column of the atmosphere compressed to standard temperature (STP = 273 °K and pressure = 1,013.25 mb). Column ozone is measured in Dobson Units (DU = 10^{-3} cm ozone at STP). Total ozone measurements are routinely reported to the World Ozone and UV Data Centre (WOUDC) in Toronto. Direct sun measurements are the preferred measurement type because they are the most accurately defined. Measurements are also made using zenith sky radiance, global irradiance, and direct irradiance from the moon.

6.5.1 Measurement Technique

The standard algorithm used for determining total ozone with the Brewer instrument is a DOAS technique using radiation measured at four of the operational UV wavelengths, (λs shown in Fig. 6.3): 310.1 nm ($\lambda = 2$), 313.5 nm ($\lambda = 3$), 316.8 nm ($\lambda = 4$), and 320.0 nm ($\lambda = 5$). Bandpasses for the slits are approximately triangular in shape (Gröbner et al., 1998) with a full-width-half intensity (FWHI) of about 0.6 nm (Kerr, 2002). The DOAS method for measuring total ozone is based on the following equation (Kerr et al., 1981), which quantifies the intensity of direct solar radiation at the earth's surface:

$$\log(I_\lambda) = \log(I_{o\lambda}) - \beta_\lambda m \times p/p_o - \tau_\lambda \sec(\mathrm{SZA}) - \alpha_\lambda O_3 \mu \tag{6.2}$$

where I_λ is the measured intensity of radiation at wavelength λ.

$I_{o\lambda}$ is the extraterrestrial intensity at wavelength λ.

β_λ is the Rayleigh scattering coefficient at λ.
m is the effective pathlength of direct radiation through air.
p is the pressure at the station.
p_o is standard pressure (1,013.25 millibars).
τ_λ is the aerosol optical depth at λ.
sec (SZA) is the secant of the solar zenith angle (SZA).
α_λ is the ozone absorption coefficient at λ.
O_3 is the column amount of atmospheric ozone.
μ is the ratio of the effective pathlength of direct radiation through ozone to the vertical path.

The intensity of radiation at the four operational wavelengths over the 10 nm range is represented by the 4 I_λ values shown in Eq. (6.2). The measurement of ozone takes advantage of the curvature of ozone absorption as a function of wavelength over the wavelength range (Fig. 6.3). The four equations ($\lambda = 2-5$) are linearly combined and rearranged to yield the following:

$$F + \Delta\beta m = F_o - \Delta\tau \sec(\mathrm{SZA}) - \Delta\alpha O_3 \mu \tag{6.3}$$

where $F = \log(I_2) - 0.5 \log(I_3) - 2.2 \log(I_4) + 1.7 \log(I_5)$
$F_o = \log(I_{o2}) - 0.5 \log(I_{o3}) - 2.2 \log(I_{o4}) + 1.7 \log(I_{o5})$
$\Delta\beta = \beta_2 - 0.5\,\beta_3 - 2.2\,\beta_4 + 1.7\,\beta_5$
$\Delta\tau = \tau\delta_2 - 0.5\,\tau\delta_3 - 2.2\,\tau\delta_4 + 1.7\,\tau\delta_5 \sim 0$
$\Delta\alpha = \alpha_2 - 0.5\,\alpha_3 - 2.2\,\alpha_4 + 1.7\,\alpha_5$

The linear combination is weighted to minimize effects of small shifts in wavelength (i.e., $\Delta F_o/\Delta\lambda$ is near a stationary point) and to eliminate SO_2 absorption. The weighting also makes any function linear with wavelength equal to zero (i.e., $\lambda_2 - 0.5\lambda_3 - 1.7\lambda_4 + 2.2\lambda_5 = 0$). Thus aerosol scattering ($\Delta\tau\delta$), which is approximately linear with wavelength over the relatively small wavelength range, becomes negligible in Eq. (6.3). The effects of Rayleigh scattering ($\Delta\beta m$) in Eq. (6.3) are calculated using the Rayleigh scattering coefficients of Bates (1984). The amount of total ozone is then readily calculated from the equation using $O_3 = (F_o - F - \Delta\beta m)/\Delta\alpha\mu$ provided values for F_o and $\Delta\alpha$ are known. The precision over a long period of time for a direct sun measurement made with a well-calibrated and well-maintained Brewer instrument is demonstrated to be better than $\pm 1\%$ (Fioletov et al., 2005). Values of F_o and $\Delta\alpha$ (calibration constants) are unique for each instrument and depend on the detailed band passes of the slits of each instrument. All instruments in operation require the determination of the calibration constants. Determination of the calibration constants is discussed further in Section 6.5.2.

The Brewer instrument is also used to derive total ozone from measurements of polarized radiation scattered from the zenith sky. The zenith radiation measured at the four wavelengths is weighted to yield the value F_{zs}, in the same manner as F for direct sun shown in Eq. (6.3). Many pairs of direct sun and zenith sky observations taken over a period of more than a year are used to establish a statistical relationship that relates F_{zs} as a function of F_o, total ozone (derived from direct sun data), and

airmass (μ). The measurement pairs are made under a wide range of total ozone and airmass values. Once the relationship is established, total ozone can be determined from a measurement of F_{zs} made when the sun is not available.

The precision of the zenith sky measurement is not as good as that for the direct sun (Dobson, 1957; Brewer and Kerr, 1973) and is observed to be about $\pm 2\%$ under most conditions without heavy clouds provided the zenith sky algorithm has been derived for the specified instrument and location. Radiation polarized parallel to the solar plane is used since it has been shown that this radiation is less sensitive to the presence of thin clouds (Brewer and Kerr, 1973). When heavy convective clouds are present, the apparent total ozone can increase substantially (Fioletov et al., 1997; Mayer et al., 1998; Kerr and Davis, 2007). This is likely caused by enhanced absorption due to multiple scattering through ozone within the clouds.

Total ozone derived from zenith sky measurements also depends on the vertical distribution of ozone, particularly when the SZA is large. For example, the majority of zenith radiation passes vertically through a layer of ozone near the ground since most of the radiation is scattered above the layer. However, for a layer near the top of the atmosphere, the effective pathlength is relatively longer since most of the scattering occurs below the layer and radiation from the sun that is scattered toward the instrument passes through the layer obliquely.

Total ozone is also derived from measurements of global radiation (Fioletov et al., 1997; Kerr and Davis, 2007) and measurements using the focused sun (Josefsson, 1992) or moon (Kerr, 1989a) as a light source. Measurements using global irradiance are useful for situations when the direct sun is not available. Focused sun measurements are used at high latitudes at times of the year when the solar elevation does not reach 15°. Measurements using the moon as a light source are useful for obtaining data when the sun is below the horizon. This is particularly beneficial for obtaining data from high latitudes during winter when the sun is absent most of the time.

6.5.2 Calibration

Calibration of an instrument requires the determination of the calibration constant F_o and the effective ozone absorption coefficient $\Delta\alpha$ as discussed in the previous section. Determination of $\Delta\alpha$ is done for all instruments by applying laboratory measurements of the slit transmission functions to the ozone absorption coefficient spectrum. The absorption spectrum of Bass and Paur (1985) has been used operationally since this is used by other operational ground-based (Dobson) and satellite-based (Total Ozone Mapping Spectrometer (TOMS)) instruments. Other ozone absorption spectra are available (e.g., Molina and Molina, 1986; Brion et al., 1993), and if these spectra are applied to the Brewer instrument, differences of up to a few percent in total ozone result.

The slit transmission functions are determined by measuring the signal of emission lines at accurately known wavelengths as they are scanned individually across each exit slit by moving the micrometer. Emission lines from mercury, cadmium, neon, and other elements are used (Gröbner et al., 1998). The known wavelengths are then used to determine the wavelength setting as a function of micrometer step for each slit, and the shape of the transmission as a function of wavelength is accurately determined for each slit. Operational measurements involving wavelength scans (e.g., global UV scans) use the wavelength dispersion function to select wavelength settings during the scans.

There are two methods to determine the extraterrestrial calibration constant (F_o from Eq. (6.3)): (1) the primary calibration method, and (2) the calibration transfer method. Primary calibrations are done by use of the Langley plot technique, also called the zero airmass extrapolation technique (Kerr et al., 1985). If the aerosol term ($\Delta\delta$ (SZA)) in Eq. (6.3) is ignored then, the measured value (F), plus the calculated Rayleigh term ($\Delta\beta m$) is a linear function of airmass (μ) with the value F_o as the intercept. Therefore, if measurements are made under a range of μ (e.g., $1 < \mu < 3.5$) throughout a day when ozone remains constant, then a plot of (F + $\Delta\beta m$) versus μ would yield a straight line with intercept F_o.

Extraterrestrial calibrations of Brewer instruments are carried out regularly at Mauna Loa Observatory (MLO), Hawaii (19.5°N, 155.6°W, 3400 m above sea level). This site offers stable observing conditions required for the calibrations and a low μ value at noon ($\mu < 1.2$) for most of the year. The high altitude of MLO is above most tropospherical contamination and the tropical location ensures minimal day-to-day variability of stratospheric ozone. In reality, ozone does not remain constant during the day at MLO and typically varies by about ± 2 DU ($1 - \sigma$) throughout any given day (see Kerr, 2002), resulting in an uncertainty of F_o that would cause an error in total ozone of about 1.5%. Calibrations are therefore averaged over a 10-day period to reduce the effects of daytime ozone variability. The calibrations are done in two parts. The results of the first part are applied to past data and those of the second part are used for future data. Any changes or upgrades to the instrument (e.g., realignment, replacing or cleaning optical components, etc.) are carried out between the first and second parts.

The calibration reference for the global Brewer network is a triad of instruments based in Toronto. These instruments have been calibrated independently from the basic physical principles described above. There are three instruments to ensure the integrity and continuity of the reference. For example, if one instrument should develop a problem, the problem instrument is quickly identified as the outlier and measures are taken to correct the problem promptly. Historically since 1982, there has been at least one of the three instruments in operation at all times, fulfilling the objective of providing the continuous availability of a calibration reference. Normally, all three instruments are operating together and analysis of their long-term records shows agreement between the instruments comprising the triad better than 1% over a 20 year period (Fioletov et al., 2005).

The second method for determining F_o for an instrument is by the calibration transfer method, which uses an instrument with a known F_o. Simultaneous direct sun measurements are made with the calibrated instrument and one or more uncalibrated instruments. The total ozone value (O_3) from the calibrated instrument is used to determine the F_o of the uncalibrated instrument using $F_o = F + \Delta\beta m + \Delta\alpha O_3 \mu$ (from Eq. (6.3) with the $\Delta\delta$ sec (SZA) set equal to zero). In practice, F_o is determined from the results of many side-by-side measurements made over the period of one or two days to provide a large range of airmass.

Calibration of operational field instruments is done by use of a traveling standard. This process uses an instrument, which is calibrated using the primary standard triad in Toronto. This traveling instrument is then transported to a site where it is used as the calibration reference for the field instrument. In practice, several regional field instruments are calibrated in one trip. After calibration of the field instrument(s), the traveling standard returns to Toronto for a follow-up calibration check. This operational process has the advantage that both the triad reference, as well as the field instruments, remain in operation continuously and are not subject to any risks involved with transporting an instrument.

Another method by which field instruments are calibrated is through intercomparison field campaigns. This method has been used traditionally for Dobson instruments, and Brewer instruments have often participated in these Dobson intercomparisons to ensure agreement between Brewer and Dobson references (e.g., Komhyr et al., 1989). Also, in some situations, it is more efficient for several field Brewer instruments to be calibrated by a traveling standard during a regional intercomparison campaign. Overall, the intercomparison campaign method is less desirable than the one-on-one site calibration method since the absence of field instruments during the intercomparison leaves gaps in the data records at field sites and instruments are subject to damage during transport to and from the intercomparisons.

6.6 Measurement of Spectral UV Radiation

The Brewer Mark Ⅱ instrument measures global spectral irradiance (mW/m^2/nm) incident on the horizontal Teflon diffuser for wavelengths between 290 nm and 325 nm at a resolution of about 0.58 nm and a sampling interval of 0.5 nm (Kerr and McElroy, 1993). Later versions of the instrument have extended the wavelength range to include irradiance at wavelengths up to 365 nm (Bais, 1997; Gröbner et al., 1998).

For the short scans (290 nm − 325 nm), the shortest operational exit slit (normally set a 306.3 nm for ozone measurements) is used. The grating is rotated via the micrometer stepping motor to locate radiation centered at the specified wavelength on slit 1. Samples progress from 290 nm to 325 nm and then back to 290 nm.

Radiation is sampled for about one second at each wavelength setting, and the grating is repositioned to the next wavelength setting 0.5 nm away. A complete scan takes about three minutes. The extended scan (290 nm – 365 nm) takes longer, but is usually sampled in one direction: from the shortest to longest wavelength. The extended scan also switches to the longest wavelength slit part way through the scan to allow coverage to 365 nm.

Measurement of spectral UV irradiance is an absolute measurement, which is intrinsically more difficult than the DOAS measurement method used for total ozone. Calibration and data processing therefore require additional attention in order to obtain high quality spectra that are accurate on an absolute scale. Data processing should include corrections for dark count, dead time, neutral density filters, stray light, temperature response, and cosine response as discussed in Section 6.4.

Spectral UV data measured by Brewer instruments are regularly reported to the WOUDC (http://www.msc-smc.ec.gc.ca/woudc/) as well as the European Ultraviolet Database (EUVDB; http://uv.fmi.fi/uvdb). Here the data are archived, checked for quality, and flagged should there be any problems. These data are readily available to the scientific community.

Calibration on an absolute scale is carried out using 1,000 W quartz lamps with known irradiance output traceable to a national standards institute, such as the National Institute for Standards and Technology (NIST) in the United States. Calibrated lamps are supplied with known emissivity as a function of wavelength with an estimated accuracy of about ±2% on an absolute scale. Typically, several primary (supplied by a standards institute) and secondary lamps (calibrated by comparison to a primary) are used for periodic calibrations. Analysis of the long-term calibration records for some Brewer instruments has shown that the output stability and degradation with age varies significantly from lamp-to-lamp. Calibration results vary by as little as ±1.5% for some lamps and as much as ±4% for others. Newly calibrated primary lamps usually agree to within ±2%; however, some degrade very rapidly with age and others have remained constant for many hours of operation over the period of several years.

For instrument calibration, the power to a lamp is accurately controlled to ensure that it is operated at the specified current and voltage. The lamp is placed vertically above the horizontal diffuser at an accurately determined distance inside a blackened housing or a dark room to block external radiation and to minimize radiation reflected from the lamp. From the lamp emissivity data and the geometric setup, it is possible to determine the irradiance at the location of the diffuser. Scans of the lamp are made and, using the known irradiance, the responsivity of the Brewer instrument as a function of wavelength is determined. The responsivity is determined for radiation arriving vertically downward from the zenith. Additional measurements must be made to determine the responsivity as a function of zenith angle. Correction for the departure of the responsivity from the cosine function can be applied to data.

Generally the lamp irradiance is significantly less than that seen with the instrument exposed to full sunlight. It is therefore important to ensure that the instrument responds linearly to radiation over the range that encompasses both calibration and measurement. The frequent testing of the linearity (as discussed in Section 6.4.2), and its application during data processing, ensure the linear response of the instrument and the accuracy of the data.

The pointing capabilities of the Brewer instrument also allow for the absolute measurement of direct irradiance provided absolute calibration is carried out for the direct sun port (Bais, 1997; Gröbner and Kerr, 2001). This calibration is not done as part of a routine operation of field instruments. However, special methods have been developed to determine the responsivity of the direct measurement by using lamps viewed through the pointing prism, or by comparison of a direct measurement through the prism with a direct measurement on the diffuser (Kazadzis et al., 2005). Careful consideration must be made for neutral density filter transmission, instrument temperature, internal polarization, and stray light.

Absolute measurements of direct irradiance can be used to determine the absolute intensity of the solar spectrum using the Langley extrapolation method. Extrapolated measurements of the solar spectrum using well-calibrated Brewer instruments have shown agreement to within ±3% compared with spectral measurements made from a satellite (Bais, 1997; Gröbner and Kerr, 2001).

Brewer instruments have participated in many intercomparison campaigns for UV instruments. Instrument intercomparisons are often used as a check to quantify differences between individual instruments and various instrument types (e.g., Thompson et al. 1997; Bais et al., 2002). During intercomparisons, individual instruments are calibrated using their normal operating procedures and then used to measure global irradiance simultaneously with other calibrated instruments. With the participation of several instruments, all measuring the same signal, it is possible to determine measurement uncertainty from differences between instruments and to identify problem instruments. Intercomparisons have been used to standardize calibration and operational procedures and, overall, the quality of UV measurements has improved significantly with time as a result of knowledge gained through the intercomparisons.

6.7 Measurement of Other Atmospheric Variables

In addition to total ozone and spectral UV radiation, the Brewer instrument is capable of measuring other atmospheric variables that affect the wavelength distribution and angular distribution of surface UV radiation through absorption and scattering processes. These variables include the vertical profile of ozone, column sulfur dioxide (SO_2), column nitrogen dioxide (NO_2), aerosol optical depth, and effective temperature of atmospheric ozone.

6.7.1 Vertical Profile of Ozone

The traditional method used to derive the vertical profile of ozone is the Umkehr method (Gotz et al., 1934), which has been adapted for use with the Brewer instrument (Mateer et al., 1985; McElroy and Kerr, 1995). Measurements are made of radiation scattered from the zenith sky at twilight during sunrise or sunset for solar zenith angles between 90° and about 75°. Zenith sky radiation as a function of wavelength depends on total ozone, the solar zenith angle, and the vertical distribution of ozone. It is therefore possible to determine the vertical profile of ozone from measurements made as the SZA passes between 90° and 75°. It takes between one and three hours to cover this SZA range depending on latitude and time of year. One condition for good quality Umkehr measurements of the vertical profile of ozone is that the sky remains clear during the observing period. The fully automated capabilities of the Brewer instrument allow measurements to be attempted every morning and every evening during twilight. Good quality measurements can be selected during the analysis of the data set.

6.7.2 Atmospheric SO_2

Surface UV radiation is affected by the presence of atmospheric SO_2, which has strong absorption bands at UV wavelengths (Fig. 6.3). Sources of atmospheric SO_2 are both manmade and natural. Measurements of SO_2 are important for tracking and assessing impacts of emissions from pollution sources, such as coal burning power plants. Measurements are also important for tracking and quantifying naturally occurring SO_2 emitted by volcanoes. Pollution sources typically result in a few DU of column SO_2 unless observations are made near a source. Column SO_2 in the vicinity of a volcanic eruption can be more significant (Kerr et al., 1982; Krueger et al., 1995). Ground-based measurements of atmospheric SO_2 using the Brewer instrument have played an important role in the development and validation of satellite-based SO_2 measurements (Schaefer et al., 1997) used primarily for detecting and tracking volcanic emissions.

The SO_2 absorption spectrum at UV wavelengths has significantly more structure than that of ozone as shown in Fig. 6.3. The differences in structure allow the measurement of SO_2 in addition to ozone. The presence of SO_2 in the atmosphere can add a false signal to total ozone measured with the Dobson instrument (Kerr et al., 1985). However, the operational total ozone algorithm for the Brewer instrument (Eq. (6.3)) is insensitive to SO_2. The Brewer algorithm for measuring SO_2 uses the peak absorption feature at 306.3 nm (Fig. 6.3) and is described in detail by Kerr et al. (1985). Column SO_2 is usually measured using the direct sun method since it the most accurate method and values are reported to the WOUDC

when available. SO_2 can be seen on zenith sky measurements if values are significantly large, particularly during the passage of debris from a volcanic eruption (e.g., Kerr et al., 1982).

6.7.3 Atmospheric NO_2

Surface UV radiation is also affected by atmospheric NO_2, which absorbs at UV wavelengths. Atmospheric NO_2 typically absorbs a small percentage of global radiation at the earth's surface. Sources of atmospheric NO_2 are both manmade and natural. Pollution from sources such as automobiles and aircraft account for NO_2 near the ground, in addition to regions in the troposphere and lower stratosphere. NO_2 occurs naturally in the stratosphere and plays an important role in the photochemistry of stratospheric ozone. Measurements of NO_2 are therefore important for both pollution studies, as well as in the study of the stratosphere.

NO_2 absorbs radiation in the visible as well as the UV region of the spectrum. Its absorption in the UV has little structure and is nearly linear with wavelength, so it does not interfere with UV ozone measurements. However, at visible wavelengths between 420 nm and 450 nm, NO_2 absorption is highly structured with wavelength allowing its measurement (Brewer et al., 1973). Several researchers now monitor NO_2 routinely using DOAS techniques with the visible absorption features (Hofmann et al., 1995, and references therein). The Brewer Mark Ⅳ instrument uses the set of five wavelengths positioned at wavelengths in the visible and an algorithm weighted to optimize NO_2 absorption as described in detail by Kerr (1989b).

6.7.4 Aerosol Optical Depth

Atmospheric aerosols play an important role in scattering and absorbing radiation as it passes through the atmosphere. The intensity and angular distribution of surface radiation are affected by the aerosols' optical depth (τ in Eq. (6.2)), vertical distribution, and absorption and scattering characteristics. Aerosol optical depth (τ) is comprised of two components: absorbing and scattering (i.e., $\tau = \tau_{abs} + \tau_{scat}$). Aerosols typically reduce surface UV irradiance by a few percent and can reduce surface irradiance by more than 50% in some cases.

There are a number of sources of atmospheric aerosols. Natural sources include volcanoes, dessert dust, and smoke from forest fires. Manmade sources include pollution from industrial activity (smog). The measurement of aerosols is important for several scientific applications ranging from local to global issues. Local issues include the prediction of smog alerts in the vicinity of cities and tracking of smoke from forest fires. Regional issues include transport of pollution across

borders. Global issues include the impact of widespread manmade aerosols on our changing climate and the impact of volcanic aerosols on the ozone layer.

The Brewer instrument is capable of determining τ using measurements of direct solar radiation provided the extraterrestrial response of the instrument is accurately known and appropriate corrections are applied. Measurements must be made at several wavelengths in order to quantify and correct for the absorption of absorbing atmospheric gases such as ozone, SO_2, and NO_2.

Extraterrestrial values (log ($I_{o\lambda}$) terms in Eq. (6.2)) are determined by making measurements of log (I_λ) (in Eq. (6.2)) at a clean site (e.g., MLO) to determine the values of log (I_λ) $+\beta_\lambda m + \alpha_\lambda O_3 \mu$ from many measurements made throughout a day. A plot of these values against sec (SZA) yields a straight line with intercept log ($I_{o\lambda}$). Intercept values made at several wavelengths averaged over a period of several days are used as the extraterrestrial reference for the particular instrument. Once the extraterrestrial values are known, it is possible to determine τ_λ from measurements made at a field site using Eq. (6.2).

Corrections that must be applied to the measurements include dark count, dead time, instrument temperature, neutral density filter, internal polarization, and stray light (if required). These corrections must be applied both to the calibration measurements as well as to the field site measurements. Further details of the methods of instrument calibration and the method for measuring τ are discussed in Kerr (2002) and Arola and Koskela (2004). Results of optical depth measurements using the Brewer instrument have been reported by many researchers (Bais, 1997; Kerr, 1997; Carvalho and Henriques, 2000; Jaroslawski and Krzyscin, 2000; Jaroslawski and Krzyscin, 2005; Meleti and Cappellani, 2000; Gröbner et al., 2001; Kirchhoff et al., 2001; Kerr, 2002; Cheymol and De Backer, 2003; Gröbner and Melita, 2004; Kazadzis et al., 2007).

6.7.5 Effective Temperature of Atmospheric Ozone

The temperature of atmospheric ozone influences the amount of UV radiation reaching the surface. The absorption of radiation by ozone in the UV is temperature dependent and generally increases with temperature. The effective temperature of atmospheric ozone (i.e., average temperature of column ozone weighted by ozone concentration) can vary by up to 20°C depending on latitude and season. Over this temperature range, ozone absorption can change by up to 10% at some wavelengths.

It is possible to measure the effective temperature of ozone since the spectrum of the temperature dependence has features that can be used as a dependent vector in a DOAS analysis. The methods used to measure effective ozone temperatures and the multiyear records of the effective ozone temperatures at Toronto are reported by Kerr (2002) and Kerr and Davis (2007).

6.8 The Brewer Spectrophotometer as a Powerful Research Tool

The original development of the Brewer spectrophotometer and subsequent upgrades have provided users with pre-programmed routines for making a suite of the most common types of operational measurements, set-up, tests, and calibrations. Pre-programmed routine measurements include global UV scans, Umkehr measurements, measurements of total ozone, SO_2, and NO_2 using direct sun, zenith sky, or global radiation. Operational tests include standard lamp and mercury lamp tests to set wavelength, wavelength shutter motor test, and dead time test. Calibrations include the slit function dispersion measurement and responsivity calibration for global measurements.

Software operating on the control computer offers interested users the opportunity to develop customized programs to carry out specialized types of measurements and support tests. Customized measurements take advantage of the fact that all operational mechanical adjustments are controlled with stepping motors. Depending on the objective of a specialized measurement, some hardware modification may be required. However, most hardware modifications are relatively minor and fairly easy to implement. For example, a custom filter may replace or supplement an existing filter in one of the three filter wheels. Some of these specialized measurements have been discussed in pervious sections (Bais, 1997; Wardle et al., 1997; Gröbner et al., 1998; Gröbner and Kerr, 2001; Kerr, 2002; Kerr and Davis, 2007). Other customized measurements include that developed to measure NO_2 using an advanced scanning technique (Cede et al., 2006b) and a new method developed to measure tropospheric and stratospheric ozone profiles using sky radiance measurements at multiple viewing angles (Tzortziou et al., in press).

There is further potential for use of the Brewer instrument to explore other possible scientific applications. Pointing capabilities allow the investigation of the dependence of spectral irradiance as a function of direction. Measurement of radiation in the first order of the Mark Ⅱ instrument (600 nm − 650 nm) could allow the measurement of ozone using the Chappuis band. Measurements could then be made at low solar elevations since ozone absorption is smaller and Rayleigh scattering is significantly less at these wavelengths than those in the UV. A new scan type, called the “group-scan method,” has recently been developed (Kerr, 2002) and could be applied to the measurement of NO_2 at visible wavelengths, resulting in improved accuracy for measurements of NO_2.

Brewer instruments have also participated in numerous scientific field campaigns that are intended to study various aspects regarding atmospheric composition and surface UV radiation. Measurements made by Brewer instruments provide important input to detailed investigations of photochemical and physical processes involved in our understanding of the ozone layer and surface UV radiation. In some cases, special measurements and schedules are developed to ensure critical measurements

are made at appropriate times. Contributions made to campaigns include measurements of atmospheric variables such as total ozone (e.g., Kerr et al., 1994; Margitan et al., 1995), aerosol optical depth (e.g., Gröbner et al., 2001), or surface UV radiation (e.g., Bais et al., 2001).

6.9 Summary

The Brewer spectrophotometer has been in operation at some sites almost continuously for up to 25 years. It has also been proven reliable in numerous specialized field campaigns and intercomparisons. In general, the instruments have proven to be quite stable over long periods of time and function reliably in unattended operation for periods of several days under a wide range of operating conditions.

The Brewer spectrophotometer is a valuable scientific tool that has made significant contributions to our understanding of the ozone layer and the dependence of surface UV radiation on stratospheric ozone and other atmospheric variables. Several dozen papers have been published that focus on the instrument itself, and several hundred papers have been published reporting scientific results that include data from Brewer spectrophotometers.

Acknowledgements

The author would like to thank three anonymous reviewers for providing many constructive comments and suggestions for the chapter.

References

Arola A, and Koskela T (2004) On the sources of bias in aerosol optical depth retrieval in the UV range. J. Geophys. Res. 109:D08209, DOI:10.1029/2003JD004375

Bais AF (1997) Absolute spectral measurements of direct solar ultraviolet irradiance with a Brewer spectrophotometer. Appl. Opt. 36(21): 5199 – 5204

Bais AF, Zerefos CS, Meleti C, and Ziomas IC (1994) Comparison of UV-B measurements performed with a Brewer spectrophotometer and a new UVB-1 broadband detector. In: Hudson RD (ed) Ozone in the Troposphere and Stratosphere. Proceedings of the Quadrennial Ozone Symposium, Charlottesville, VA, 1992. NASA Conference Publication 3266: 786 – 789

Bais AF, Zerefos CS, and McElroy CT (1996) Solar UVB measurements with the double- and single-monochromator Brewer ozone spectrophotometers. Geophys. Res. Lett. 23: 833 – 836

Basi AF, Kazadzis S, Balis D, Zerefos CS, and Blumthaler M (1998) Correcting global solar ultraviolet spectra recorded by a Brewer spectroradiometer for its angular response error. Appl. Opt. 37: 6339 – 6344

Bais AF, Gardiner BG, Slaper H, Blumthaler M, Bernhard G, McKenzie R, Webb AR, Seckmeyer G, Kjeldstad B, Koskela T, Kirsch PJ, Gröbner J, Kerr JB, Kazadzis S, Leszcznski K, Wardle D, Josefsson W, Brogniez C, Gillotay D, Reinen H, Weihs P, Svenøe T, Eriksen P, Kuik F, and Redondas A (2001) SUSPEN intercomparison of ultraviolet spectroradiometers. J. Geophys. Res. (106): 12509 – 12525

Bais AF, Kazadtzis S, Garane K, Kouremeti N, Gröbner J, Blumthaler M, Seckmeyer G, Webb AR, Koskela T, Görtz P, and Schreder J (2005) Portable device for characterizing the angular response of UV spectroradiometers. Appl. Opt. 44: 7136 – 7143

Bass AM, and Paur RJ (1985) The ultraviolet cross-sections of ozone, I, The measurements, in atmospheric ozone. In: Zerefos CS, Ghazi A, Reidel D (eds) Proceedings of the Quadrennial Ozone Symposium, Halkidiki, Greece, 1984. Dordrecht, Holland, pp.606 – 610

Bates DR (1984) Rayleigh scattering by air. Planet. Space Sci. 32: 785 – 790

Brewer AW (1973) A replacement for the Dobson spectrophotometer? PAGEOPH 106 – 108: 919 – 927

Brewer AW, and Kerr JB (1973) Total ozone measurements in cloudy weather. PAGEOPH 106 – 108: 928 – 937

Brewer AW, McElroy CT, and Kerr JB (1973) Nitrogen dioxide concentrations in the atmosphere. Nature 246: 129 – 133

Brion J, Chakir A, Daumont D, Malicet J, and Parisse C (1993) High-resolution laboratory absorption cross section of O_3: Temperature effect. Chem. Phys. Lett. 213: 610 – 612

Carvalho F, anb Henriques D (2000) Use of the Brewer spectrophotometer for aerosol optical depth measurements in the UV region. Adv. Space Res. 25: 997 – 1006

Cede A, Labow G, Kowalewski M, Krotkov N, and Dubovik O (2003) Deriving aerosol parameters from absolute UV sky radiance measurements using a Brewer double spectrometer. In: Slusser JR, Herman JR, Gao W (eds) Ultraviolet Ground- and Space-based measurements, Models, and Effects Ⅲ. San Diego, CA. Proc. SPIE 5156: 323 – 329

Cede A, Labow G, Kowalewski M, and Herman J (2004) The effect of polarization sensitivity of Brewer spectrometers on direct sun measurements. In: Slusser JR, Herman JR, Gao W (eds) Ultraviolet Ground- and Space-Based Measurements, Models, and Effects Ⅳ. Denver, CO. Proc. SPIE 5545: 131 – 137

Cede A, Kowalewski M, Kazadzis S, Bais A, Kouremeti N, Blumthaler M, and Herman J (2006a) Correction of direct irradiance measurements of Brewer spectrophotometers due to the effect of internal polarization. Geophys. Res. Lett. 33:L02806, DOI:10.1029/2005GL024860

Cede A, Herman J, Richter A, Krotkov N, and Burrows J (2006b) Measurements of nitrogen dioxide total column amounts using a Brewer double spectrophotometer in direct sun mode. J. Geophys. Res. 111: D05304, DOI:10.1029/2005JD006585

Cheymol A, and De Backer H (2003) Retrieval of the aerosol optical depth in the UVB at Uccle from Brewer ozone measurements over a long time period-1984 – 2002. J. Geophys. Res. 108:4800, DOI:10.1029/2003JD003758

Dobson GMB (1957) Observers' handbook for the ozone spectrophotometer. Ann. Int. Geophys. Year 5, 1: 46 – 49

Fastie WG (1952) A small plane grating monochromator. J. Opt. Soc. Amer. 42: 641 – 651

Fioletov VE, Kerr JB, and Wardle DI (1997) The relationship between total ozone and spectral UV irradiance and its use for deriving total ozone from UV measurements. Geophys. Res. Lett. 24: 2977 – 3000

Fioletov VE, Kerr JB, Wardle DI, Krotkov N, and Herman JR (2002) Comparison of Brewer ultraviolet irradiance measurements with total ozone mapping satellite retrievals Opt. Eng. 41(12): 3051 – 3161

Fioletov VE, Kerr JB, McElroy CT, Wardle DI, Savastiouk V, and Grajnar TS (2005) The Brewer reference triad. Geophys. Res. Lett. 32:L20805, DOI:10.1029/ 2005GL024244

Garane K, Bais AF, Kazadzis S, Kazantzidis A, and Meleti C (2006) Monitoring of UV spectral irradiance at Thessaloniki (1990 – 2005): Data re-evaluation and quality control. Ann. Geophys. 24: 3215 – 3228

Gotz FWP, Meetham AR, and Dobson GMB (1934) The vertical distribution of ozone in the atmosphere. Proc. R. Soc. London A 145: 416 – 446

Gröbner J (2003) Improved entrance optic for global irradiance measurements with a Brewer spectrophotometer. Appl. Opt. 42: 3516 – 3521

Gröbner J, and Kerr JB (2001) Ground-based determinations of the spectral ultraviolet extraterrestrial solar irradiance: Providing a link between space-based and ground-based solar UV measurements. J. Geophys. Res. 106: 7211 – 7217

Gröbner J, and Meleti C (2004) Aerosol optical depth in the UVB and visible wavelength range from Brewer spectrophotometer direct irradiance measurements: 1991-2002. J. Geophys. Res. 109: D09202, 10.1029/2003JD004409

Gröbner J, Wardle DI, McElroy CT, and Kerr JB (1998) Investigation of the wavelength accuracy of Brewer spectrophotometers. Appl. Opt. 37(36): 8352 – 8360

Gröbner J, Vergaz R, Cachorro VE, Henriques DV, Lamb K, Redondas A, Vilaplana JM, and Rembges D (2001) Intercomparison of aerosol optical depth measurements in the UVB using Brewer spectrophotometers and a Li-Cor spectrophotometer. Geophys. Res. Lett. 28: 1691 – 1694

Gustin GP, Sokolenko SA, Dudko BG, and Lagutina VV (1985) Ozonometer M-124, (in Russian) Tr. Glav. Geofiz. Obs. im. A. I. Voeikova 499: 60 – 67

Hofmann D, Bonasoni P, De Maziere M, Evangelisti F, Giovanelli G, Goldman A, Goutail F, Harder J, Jakoubek R, Johnston P, Kerr J, Matthews WA, McElroy T, Mckenzie R, Mount G, Platt U, Pommereau JP, Sarkissian A, Simon P, Solomon S, Stutz J, Thomas A, Van Roozendael M, and Wu E (1995) Intercomparison of UV/visible spectrometers for measurements of stratospheric NO_2 for the Network for the Detection of Stratospheric Change. J. Geophys. Res. 100: 16765 – 16791

Ito T, Sakoda Y, Matsubara K, Kajihara R, Uekubo T, Kobayashi M, Shitamichi M, Euno T, and Ito M (1994) UV-B radiation amplication factor determined based on the simultaneous observation of total ozone and global spectral irradiance In: Hudson RD (ed) Ozone in the Troposphere and Stratosphere: Proceedings of the Quadrennial Ozone Symposium, Charlottesville, VA, 1992. NASA Conference Publication 3266: 657 – 662

Jaroslawski J, and Krzyscin JW (2000) Aerosol optical depth in the UV range derived from direct sun ozone observations performed by the Brewer spectrophotometer Mark Ⅱ. No 064, Belsk, Poland. Quadrennial Ozone Symposium, Natl. Space Dev. Agency of Japan

Jaroslawski JP, and Krzyscin JW (2005) Importance of aerosol variations for surface UV-B level: Analysis of ground-based data taken at Belsk, Poland, 1992-2004. J. Geophys. Res. 110:D16201, 10.1029/2005JD005951

Josefsson WAP (1992) Focused sun observations using a Brewer ozone spectrophotometer. J. Geophys. Res. 97: 15813 – 15819

Kazadzis S, Bais A, Kouremeti N, Gerasopoulos E, Garane K, Blumthaler M, Schallhart B, and Cede A (2005) Direct spectral measurements with a Brewer spectroradiometer: absolute calibration and aerosol optical depth retrieval. Appl. Opt. 44: 1681 – 1690

Kazadzis S, Bais AF, Amiridis V, Balis D, Meleti C, Kouremeti B, Zerefos CS, Rapsomanikis S, Petrakakis N, Kelesis A, Tzoumaka P, and Kelektsoglou K (2007) Nine years of UV aerosol optical depth measurements at Thessaloniki, Greece. Atmos. Chem. Phys. 7: 2091 – 2101

Kerr JB (1973) Short-time period fluctuations in the total ozone PAGEOPH 106 – 108: 977 – 980

Kerr JB (1989a) Observations of Arctic total ozone with the Brewer spectrophotometer during the polar winter using the moon as a light source. In: Bojkov RD, Fabian P, Deepak A (eds) Ozone in the Atmosphere. Proceedings of the Quadrennial International Ozone Symposium, Hampton, VA, pp. 728 – 731

Kerr JB (1989b) Ground-based measurements of nitrogen dioxide using the Brewer spectrophotometer. In: Bojkov RD, Fabian P, Deepak A (eds) Ozone in the Atmosphere. Proceedings of the Quadrennial International Ozone Symposium, Hampton, VA, pp.340 – 343

Kerr JB (1994) Decreasing ozone causes health concern. Environ. Sci. Technol. 28: 514A – 518A

Kerr JB (1997) Observed dependencies of atmospheric UV radiation and trends. In: Zerefos CS, Bais AF (eds) Solar Ultraviolet Radiation: Modeling, Measurements, and Effects. NATO ASI Ser., Ser. I, 52: 259 – 266

Kerr JB (2002) New methodology for deriving total ozone and other atmospheric variables from Brewer spectrophotometer direct sun spectra. J. Geophys. Res. 107: D23, 4731, DOI:10.1029/2001JD001227

Kerr, JB, and McElroy CT (1993) Evidence for large upward trends of ultraviolet-B radiation linked to ozone depletion. Science 272: 1032 – 1034

Kerr JB, and Davis JM (2007) New methodology applied to deriving total ozone and other atmospheric variables from global irradiance spectra. J. Geophys. Res. 112: D21301, DOI: 10.1029/2007JD008708

Kerr JB, McElroy CT, and Olafson RA (1981) Measurements of ozone with the Brewer spectrophotometer. In: London J (ed) Proceedings of the Quadrennial International Ozone Symposium. Natl. Cent. for Atmos. Res., Boulder, CO, pp.74 – 79

Kerr JB, Evans WFJ, and Mateer CL (1982) Measurements of SO_2 in the Mount St. Helens debris. In: Deepak A (ed) Atmospheric Effects and Potential Climatic Impact of the 1980 Eruptions of Mount St. Helens. NASA Conference Publication 2240, Hampton, VA, pp.219 – 223

Kerr JB, Evans WFJ, and Asbridge IA (1985) Recalibration of Dobson field spectrophotometers with a traveling Brewer spectrophotometer standard. In: Zerefos CS, Ghazi A, Reidel D (eds) Atmospheric Ozone. Proceedings of the Quadrennial Ozone Symposium, Halkidiki, Greece, 1984. Dordrecht, Holland, pp.381 – 386

Kerr JB, Asbridge IA, and Evans WFJ (1988) Intercomparison of total ozone measured by the Brewer and Dobson spectrophotometers at Toronto. J. Geophys. Res. 93: 11129 – 11140

Kerr JB, Fast H, McElroy CT, Oltmans SJ, Lathrop JA, Kyro E, Paukkunen A, Claude H, Köhler U, Sreedharan CR, Takao T, and Tsukagosji Y (1994) The 1991 WMO international ozonesonde intercomparison at Vanscoy, Canada. Atmos. Ocean 32: 685 – 716

Kirchhoff VWJH, Silva AA, Costa CA, Paes Leme N, Pavão HG, and Zaratti F (2001) UV-B optical thickness observations of the atmosphere. J. Geophys. Res. 106: 2963 – 2973

Komhyr WD, Grass RD, Evans RD, and Leonard RK (1989) Results of international Dobson and Brewer spectrometer calibrations, Arosa, Switzerland. In: Bojkov RD, Fabian P, Deepak A (eds) Ozone in the Atmosphere. Proceedings of the Quadrennial International Ozone Symposium. Hampton, VA, pp.776 – 779

Krueger AJ (1983) Sighting of El Chichon sulfur dioxide clouds with the Nimbus 7 Total Ozone Mapping Spectrometer. Science 220: 1377 – 1378

Krueger AJ, Walter LS, Bhartia PK, Schnetzler CC, Krotkov NA, Sprod I, and Bluth GJS (1995) Volcanic sulfur dioxide measurements from the total ozone mapping spectrometer instruments, J. Geophys. Res. 100: 14057 – 14076

Margitan JJ, Barnes RA, Brothers GB, Butler J, Burris J, Connor BJ, Ferrare RA, Kerr JB, Komhyr WD, McCormick MP, McDermid IS, McElroy CT, McGee TJ, Miller AJ, Owens M, Parrish AD, Parsons CL, Torres AL, Tsou JJ, Walsh TD, and Whiteman D (1995) Stratospheric Ozone Intercomparison Campaign (STOIC) 1989: Overview. J. Geophys. Res. 100: 9193 – 9207

Mateer CL, Kerr JB, and Evans WFJ (1984) Ozone profiles derived from Umkehr observations obtained with the Brewer ozone spectrophotometer. In: Zerefos CS, Ghazi A, Reidel D (eds) Atmospheric Ozone. Proceedings of the Quadrennial Ozone Symposium, Halkidiki, Greece, 1984. Dordrecht, Holland, pp.407 – 411

Mayer B, Kylling A, Madronich S, and Seckmeyer G (1998) Enhanced absorption of UV radiation due to multiple scattering in clouds: Experimental evidence and theoretical explanation. J. Geophys. Res. 103: 31241 – 31254

McElroy CT, and Kerr JB (1995) Table Mountain ozone intercomparison: Brewer ozone spectrophotometer Umkehr observations. J. Geophys. Res. 100: 9293 – 9300

McGee TJ, and Burris Jr J (1987) SO_2 absorption cross sections in the near UV. J. Quant. Spectrosc. Radiat. Transfer 37: 165 – 182

Meleti C, and Cappellani F (2000) Measurements of aerosol optical depth at Ispra: Analysis of the correlation with UV-B, UV-A, and total solar irradiance. J. Geophys. Res. 105: 4971 – 4978

Molina LT, and Molina MJ (1986) Absolute absorption cross sections of ozone in the 185 to 350 nm wavelength range. J. Geophys. Res. 91: 14501 – 14508

Parsons CL, Gerlach JC, Williams ME, and Kerr JB (1981) Preliminary results of an intercomparison of total ozone spectrophotometers. In: London J (ed) Proceedings of the Quadrennial International Ozone Symposium. National Center for Atmospheric Research, Boulder, CO, pp. 80 – 87

Schaefer SJ, Kerr JB, Millan MM, Realmuto VJ, Krueger AJ, Krotkov NA, Seftor C, and Sprod IE (1997) Geophysicists unite to validate volcanic SO_2 measurements. EOS Trans. AGU 78(21): 217 – 223

Siani AM, Benevento G, and Casale GR (2003) Temperature dependence of Brewer UV measurements at Rome station. In: Slusser JR, Herman JR, Gao W (eds) Ultraviolet Ground- and Space-Based Measurements, Models, and Effects III, August 2003, San Diego, CA. Proc. SPIE 5156: 355 – 366

Tanskanen A, Lindfors A, Määttä A, Krotkov N, Herman J, Kaurola J, Koskela T, Lakkala K, Fioletov V, Bernhard G, McKenzie R, Kondo Y, O'Neill M, Slaper H, den Outer P, Bais AF, and Tamminen J. (2007) Validation of daily erythemal doses from Ozone Monitoring Instrument with ground-based UV measurement data. J. Geophys. Res. 112: D24S44, DOI:10.1029/2007/ 2007JD008830

Thompson A, Early EA, DeLuisi J, Disterhoft P, Wardle D, Kerr J, Rives J, Sun Y, Lucas T, Mestechkina T, and Neale P (1997) The 1994 North American interagency intercomparison of ultraviolet monitoring spectroradiometers. J. Res. Natl. Inst. Stand. Technol. 102: 279 – 322

Tzortziou M, Krotkov NA, Cede A, Herman JR, Vassilkov A. A new technique for retrieval of tropospheric and stratospheric ozone profiles using sky radiance measurements at multiple view angles — Application to a Brewer spectrometer. J. Geophys. Res. (in press)

Vandersee W, and Köhler U (1994) UV observations with a Brewer spectrophotometer at Hohenpeissenberg. In: Hudson RD (ed) Ozone in the Troposphere and Stratosphere. Proceedings of the Quadrennial Ozone Symposium, Charlottesville, VA, June 1992. NASA Conference Publication 3266: 742 – 745

Wardle DI (1965) The measurement of atmospheric ozone at night. PhD Thesis, Cambridge University, Trinity College, UK

Wardle DI, McElroy CT, Kerr JB, Wu E, and Lamb K (1997) Laboratory tests on the double Brewer spectrophotometer. In: Bojkov RD, Visconti G (eds) Proceedings of the Quadrennial Ozone Symposium, L'Aquila, Italy, 1996, pp. 997 – 1000

Weatherhead E, Theisen D, Stevermer A, Enagonio J, Rabinovitch B, Disterhoft P, Lantz K, Meltzer R, Sabburg J, DeLuisi J, Rives J, and Shreffler J (2001) Temperature dependence of the Brewer ultraviolet data. J. Geophys. Res. 106: 34121 – 34129

Webb AR, Bais AF, Blumthaler M, Gobbi GP, Kylling A, Schmitt R, Thiel S, Barnaba F, Danielsen T, Junkermann W, Kazantzidis A, Kelly P, Kift R, Liberti GL, Misslbeck M, Schallhart B, Schreder J, and Topaloglou C (2002) Measuring spectral actinic flux and irradiance: Experimental results from the Actinic Flux Determination from Measurements of Irradiance (ADMIRA) project. J. Atmos. Ocean Tech. 19: 1049 – 1062

WMO (World Meteorological Organization) (1994) Second WMO consultation on measurements by Brewer spectrophotometer, Charlottesville, VA, June, 1992. Global Ozone Research and Monitoring Project, Geneva, Switzerland, Report No. 30, p.56

WMO (2006) The Ninth Biennial WMO Consultation on Brewer Spectrophotometer Operation, Calibration, and Data Reporting, Delft, The Netherlands, May-June, 2005. Global Atmosphere Watch, Geneva, Switzerland, Report No. 175, p.69

WMO (2007) Scientific assessment of ozone depletion, 2006. Global Ozone Research and Monitoring Project, Geneva, Switzerland, Report No. 50, p.572

7 Techniques for Solar Dosimetry in Different Environments

Alfio V. Parisi, David J. Turnbull, Peter Schouten,
Nathan Downs and Joanna Turner

Centre for Rural and Remote Area Health, University of
Southern Queensland, Toowoomba
Queensland, Australia 4350
E-mail: parisi@usq.edu.au

Abstract Minimization of solar UV exposures is necessary to reduce the risks of detrimental sun-related effects caused by overexposure to sunlight and vitamin D deficiency related diseases. Furthermore, agricultural production can be influenced by changes in solar UV and visible radiation due to atmospheric variability. Consequently, there is a requirement for a full understanding of the solar radiation environment. This chapter describes the development of dosimetric techniques for the measurement of solar UV exposures in different conditions in order to provide an improved characterization of the solar radiation environment for humans and plants. The erythemal exposures during normal daily activities and the effectiveness of UV protective strategies have been measured with polysulphone dosimeters. These dosimeters have also been miniaturized in order to increase the number of environments in which they can be used. Additionally, polysulphone dosimeters have been employed with appropriate calibration to evaluate the pre-vitamin D_3 effective UV exposure on humans, along with the UVB (280 nm − 320 nm) exposures to plant leaves. The dynamic range of polysulphone has been extended by the development of a dosimeter that is based on polyphenylene oxide with a dynamic range that is approximately four times longer than that of polysulphone.

Keywords UV, dosimeter, polysulphone, PPO, erythema, plants

7.1 Introduction

The costs of excessive solar UV exposures are high with over 1 million non-melanoma cases and 59,940 melanoma cases in the USA during 2007 (American

Cancer Society, 2008). In 2007, there were 2,740 deaths from nonmelanoma and 8,110 deaths from melanoma in the USA. Additionally, there is the incalculable cost of the associated human suffering and disfigurement. The risk of the detrimental sun-related effects can be lowered by the reduction of human exposures to solar UV radiation. On the positive side, exposures to UVB wavelengths (280 nm – 320 nm) are required for the production of vitamin D (Holick, 2004a). The solar UVB waveband acts as an initiator of the synthesis of vitamin D_3 by the photolysis of 7-dehydrocholesterol in the human skin, to pre-vitamin D_3. This vitamin plays an important role in calcium metabolism and is essential for good bone development, prevention of rickets in children, and prevention of osteoporosis, osteomalacia, and fractures in the elderly (Holick, 2004b). Vitamin D can also be obtained through vitamin D supplements and a small number of foods; however, the simplest way to obtain vitamin D is from moderate exposure to sunlight (Holick, 2004a). Exposures of 1 MED (minimum erythemal dose) to the entire body produce serum vitamin D that is equivalent to 10,000 IU to 25,000 IU of vitamin D (Holick, 2004b). Furthermore, optimisation of adequate sun exposure to maintain adequate serum vitamin D levels, while avoiding excessive exposures that increase the risk of skin cancer, is also the most cost effective way of maintaining adequate vitamin D levels without the additional burden of vitamin D supplements. Adequate levels of vitamin D can be maintained by exposures of 1/6 to 1/3 MED to 15% of the body (Samanek et al., 2006). It is estimated that 90% – 95% of the vitamin D levels required in the human body are obtained from exposure to sunlight (Holick, 2004a).

Agricultural production and natural vegetation can be influenced by changed levels of solar UV and visible radiation due to atmospheric change. The UVB has been shown to produce biological damage in higher plants (Caldwell, 1971). The wavelengths extending into the UVA (320 nm – 400 nm) waveband have also been found to produce a response in plants with an action spectrum for plant growth inhibition in higher plants that extends to 366 nm being recently developed (Flint and Caldwell, 2003). The action spectrum for a biological reaction provides the effectiveness of each wavelength for producing that reaction (Ambach and Blumthaler, 1993).

In order to optimize the UV exposure of humans and to reduce the influence of UV exposures on both agricultural crops and natural vegetation, a complete understanding of the solar radiation environment is necessary. As recommended by the World Health Organization (WHO, 1994), monitoring of personal UV exposures is important in order to establish the percentage of the ambient solar UV received by the population. Solar UV dosimeters are an important tool in this research. Dosimeters that have been developed for UV research fall into two categories; namely, the thin film type and the spore or biofilm type. The latter types are based on spores or biological specimens that are UV sensitive (e.g., Quintern et al., 1992; Quintern et al., 1997; Munakata et al., 1998). For the thin film type, dosimeters fabricated from a polysulphone thickness of 30 μm – 45 μm possess a

spectral response that approximates the erythemal action spectrum (CIE, 1992). This chapter reports on the use of thin film dosimeters in different environments in order to provide an improved characterization of the solar radiation environment for humans and plants.

7.2 UV Dosimetry and Minimization Strategies

UV radiation incident on the earth's surface is comprised of both a direct component and a diffuse component. The combination of the diffuse and direct UV is termed the global UV. As the direct component is incident directly from the sun, it is easier to minimize by simply blocking its path. However, the diffuse UV component is incident from all directions due to atmospheric and environmental scattering and can constitute a significant proportion of the UV exposure to the human body. The relative amounts of direct and diffuse UV compared to global UV depend on the solar zenith angle (SZA). For example, the ratio of the diffuse UV to global UV increases with increasing SZA (Blumthaler and Ambach, 1991). This is due to the longer path through the atmosphere. Furthermore, the ratio of diffuse UV to global UV is higher at the shorter wavelengths due to the higher degree of scattering at the shorter wavelengths.

Numerous studies have employed UV dosimeters to investigate the efficacy of different strategies utilized to minimize exposures to diffuse UV and direct UV. Tree shade is widely employed and Parisi et al. (2000a, 2000b) utilized manikin forms with dosimeters placed at specific anatomical sites in tree shade to measure the UV exposure ratios under Australian gum trees. The exposure ratios of global UV radiation in a shaded environment to an unshaded environment ranged from 0.16 to 0.49 for the different anatomical sites. It was also found that exposure ratios for the legs ranged from 0 to 0.75 for the different anatomical sites for a sitting posture in summer compared to 0.14 to 0.39 for a standing posture. Furthermore, tree shade provided reductions in personal annual erythemal UV exposures by a factor of 2 to 3 and 4 to 6 in the contribution to the risk of basal cell carcinomas and squamous cell carcinomas, respectively, compared to not employing the protection of tree shade.

Erythemal UV exposures to the faces of school children wearing hats while playing sports were measured with polysulphone dosimeters over the period of an hour. The mean facial exposures of unprotected students (no hat) to protected students (hat) varied from 140 ± 82 Jm^{-2} to 99 ± 33 Jm^{-2}, respectively (Downs and Parisi, 2008). The cosine response of the polysulphone film used in these dosimeters has been found to be within approximately 20% of the cosine function for angles of incidence up to 70° (Krins et al., 2000). Parisi and Wilson (2005) measured erythemal UV exposures beneath different types of clothing with dosimeters and found that the highest exposure under a high ultraviolet protection factor (UPF) knitted garment was only 1.5% of that of full sun exposure. Parisi et al. (1999)

employed dosimeters to measure the solar UPF for different stocking thicknesses and colors and found that the highest UPF of 4.6 was provided by 50 denier stockings with the lowest UPF of 1.4 provided by 15 denier stockings. Dosimetric measurements behind different thicknesses of glass (Parisi et al., 2007) found that the glass filtered solar UV ranged from 59% to 70% compared to the unfiltered UV and was only influenced to a small extent by the thickness of the glass and the solar zenith angle. It was also found that laminated window glass only transmitted 12% of incident UV radiation and that windscreen laminated glass transmitted approximately 2.6%. All new cars use laminated windscreen glass that transmits minimal UV. Turnbull and Parisi (2005) measured exposures to the human form while using shade structures. An example of polysulphone dosimeters employed on a human form manikin to measure the UV protection of a shade device is provided in Fig. 7.1. This research found that during summer and winter, significant decreases in exposure of up to 65% for summer and 57% for winter can be attained when comparing the use and non-use of polycarbonate sheeting for side-on UV protection.

Figure 7.1 A human form manikin with dosimeters placed at various anatomical sites measuring the UV protection provided by a shade umbrella

7.3 Miniaturization of Polysulphone Dosimeters

Miniaturized polysulphone dosimeters were employed to take high density measurements on living and manikin subjects under various environmental conditions to facilitate detailed mapping of the erythemal UV exposure to unprotected skin (Downs and Parisi, 2007; 2008). These dosimeters are cost-effective and provide accurate short-term UV exposure measurements for personal and environmental applications that may require a large number of dosimeters. Such applications may include UV exposure measurements to humans, animals, and plants.

Polysulphone film employed in the manufacturing of miniaturized dosimeters is adhered to flexible cardboard frames measuring approximately 1.5 cm×1 cm having a clear circular aperture of 6 mm. The smaller flexible, lightweight dosimeter can be placed along curved surfaces and attached to complex surface topography not readily accessible to conventionally sized dosimeters, including the eyes, ears, and fingers of life-sized manikin models. The miniaturized dosimeter can also be conveniently attached to human subjects with the use of medical tape. An example of the application of miniaturized dosimeters used to measure UV exposures on the hand is given in Fig. 7.2.

Figure 7.2 UV exposure measured by application of miniaturized polysulphone dosimeters placed on the hand of a life-sized manikin

Miniaturized polysulphone dosimeters undergo the same UV induced photo-degradation as conventional polysulphone film dosimeters and can be calibrated on a horizontal plane in proximity to a calibrated spectroradiometer or radiometer. Typically this involves the measurement of pre- and post-exposure polysulphone film absorbance at 330 nm (ΔA_{330}) taken at four different dosimeter film sites which are averaged to account for a variation in film absorbance and plotted with respect to the cumulative UV exposure measured by a spectroradiometer or radiometer. The change in absorbance is measured at 330 nm as this is approximately the wavelength at which the maximum change occurs (Davis et al., 1976a). Polysulphone film calibrated in this manner is typically weighted to the erythemally effective UV, but alternative action spectra, including the vitamin D action spectrum, can also be used. The dose response calibration of polysulphone dosimeters is related to the total atmospheric ozone amount and the solar zenith angle (Casale et al., 2006). This requires the calibration curve to be determined under the same atmospheric conditions of the field study.

The calibrated UV exposure measured using conventional polysulphone dosimeters is accurate to within 10% for a ΔA_{330} less than 0.3 and 30% for a ΔA_{330} less than 0.4 (Diffey, 1987). Comparative measurements made using miniaturized

polysulphone dosimeters give the uncertainty in calibrated UV exposure at 24% for a ΔA_{330} less than 0.35 (Downs and Parisi, 2008), the approximate equivalent of 1,500 Jm^{-2} of erythemally effective UV. Increases in calibrated uncertainty with greater periods of exposure are due to the dynamic saturation of the polysulphone. Figure 7.3 illustrates the increasing calibrated uncertainty with increasing exposure. In this figure, sets of three miniaturized polysulphone dosimeters were removed at predetermined time intervals extending up to nine hours of exposure during a clear summer day, and measured at a subtropical latitude. Greater variability in the change of absorbance can be observed for dosimeters removed after longer periods of exposure.

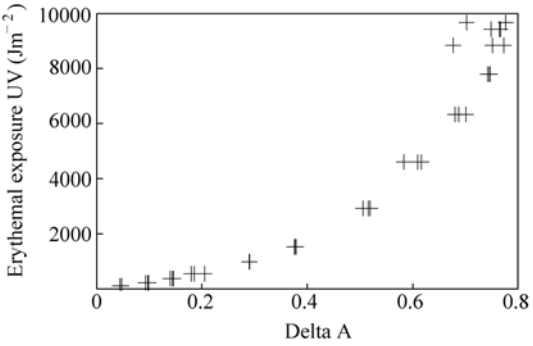

Figure 7.3 Calibration of miniaturized polysulphone dosimeters measured over a nine-hour period in summer

7.4 Measurements on Plants

UVB radiation can be damaging to plant physiology and plant growth (Teramura and Sullivan, 1994), but solar visible radiation is important to the photosynthesis process in plants. This radiation (400 nm − 700 nm) is referred to as photosynthetically active radiation (PAR). Both PAR and UV radiation within the solar spectrum have to be accounted for as the plant response to UVB depends on solar visible radiation exposure (Caldwell et al., 1995). PAR can have a direct influence on plant response to UVB radiation. Plant response to UVB radiation during growth can be a function of PAR levels. There may be an observed reduction in plant growth and mass with reduced PAR and increasing UV radiation, and different plant species may not respond in the same way. Rather than relying on large equipment that is too bulky for measuring solar spectral irradiance or broadband UV within a plant canopy, a combination of dosimeters can be used to evaluate the UVB and PAR incident on a plant canopy. A UVB and PAR dosimeter package allows the measurement of exposure at different locations within the canopy, or locations on the plant itself (Parisi et al., 2003). This is important as

leaf angle, leaf reflectance, and shading will affect the UVB and PAR exposures on plants, as well as the relative proportions of UVB to PAR.

The dosimeter package consists of two sensors: a polysulphone dosimeter to measure the UVB and a second dosimeter material to extend the wavelength range to measure the PAR (Parisi et al., 1998; 2003). The second dosimeter material, made from 35 mm AGFA 25 APX photographic film, responds to visible radiation which is easy to obtain, simple to process, responds to visible wavelengths. Additionally, the optical density (absorbance) can be measured using appropriate equipment, such as a dual beam spectrophotometer (Shimadzu, model UV-160, Kyoto, Japan) with maximum absorbance measured at a wavelength of 800 nm. The PAR dosimeter is constructed by cutting the unexposed film into 30 mm lengths in total darkness and mounting it in a black plastic holder with an opening of 10 mm×20 mm. This opening is covered with cardboard when not exposed and also acts as a shutter. The exposure time of the PAR dosimeter can be adjusted using filters made of exposed and developed AGFA 25 APX film. Once the dosimeter has been exposed, the film is processed using a standardized procedure (Parisi et al., 2003), and the absorbance is measured. Calibration of the PAR dosimeter (Fig. 7.4) is used to determine photosynthetic photon flux by exposing a number of PAR dosimeters for varying periods of time and then comparing them to simultaneously measured visible spectral irradiance using a scanning spectroradiometer recording at 1 nm increments. The PAR dosimeter is dose rate independent, has a very small dark reaction (within 1%−2% of original measured values after periods of one and seven days), is temperature stable from 20℃ to 45℃ and has a cosine response agreement of 13% or better for solar zenith angles smaller than 20° and up to 21% for solar zenith angles up to 60° (Parisi et al., 1998). The overall error of the PAR dosimeter is 20%.

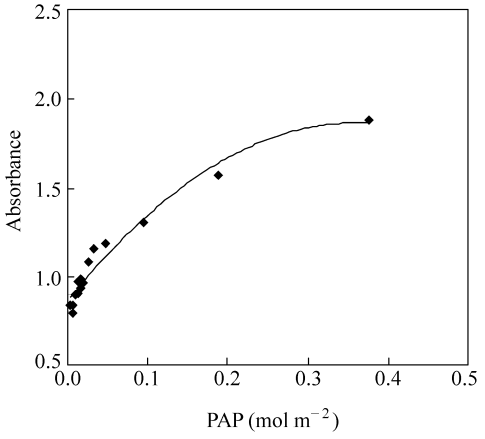

Figure 7.4 Calibration of the photosynthetically active radiation dosimeter for photosynthetically active photons or PAP (Parisi et al., 1998)

7.5 Long-Term UV Dosimeters

One of the main dosimetric materials for UV exposures has been the polymer polysulphone, which was first employed in the 1970s by Davis et al. (1976a). Despite its immense usefulness, the polysulphone dosimeter is restricted as it is only capable of measuring solar exposures approximately less than ten hours during a clear summer day at a subtropical location before reaching the maximum optical saturation point. Furthermore, the uncertainty of polysulphone increases to 30% for a ΔA_{330} between 0.3 and 0.4 (Diffey, 1987). This makes the long-term measurement of UV a difficult task logistically as polysulphone dosimeters would have to be continually replaced on location in order to achieve a continuous stream of measurements. Another dosimeter was formulated in the 1970s, again by Davis et al. (1976b), this time using a polymer called poly 2,6-dimethyl-1,4-phenylene oxide, or just PPO in short. The PPO dosimeter was fabricated using similar methods to polysulphone and was just as easy to use, however instead of having a short responsive lifetime, PPO was capable of receiving a subtropical UV exposure over a period of time no less than five to ten days before complete saturation at the same level of accuracy as its polysulphone counterpart. It can be seen that the potential of the PPO dosimeter was far more substantial than the polysulphone dosimeter; however, in recent years most solar radiation researchers have chosen to use polysulphone.

The PPO dosimeter has recently experienced a revival with a varied amount of research being performed both on it and with it. The optical properties of PPO have been trialled for in-air use and calibrated to the erythemal action spectrum (Lester et al., 2003) and also to short UVA wavelengths (320 nm – 340 nm) by implementation of a Mylar filter (Turnbull and Schouten, 2008), similar to the methodology used by Parisi et al. (2005) when calibrating the prototype phenothiazine dosimeter to the UVA waveband. Figure 7.5 graphically shows how much more erythemal UV solar exposure the PPO dosimeter can handle in comparison to the polysulphone dosimeter. It demonstrates that on a typical summer's day, polysulphone can receive an approximate dosage of 2,500 J/m^2 before reaching its exposure limit at its characteristic sampling wavelength of 330 nm (ΔA_{330}). Comparatively, the PPO dosimeter can accept close to a further 25,000 J/m^2 before optical saturation at its own particular sampling wavelength of 320 nm (ΔA_{320}). This is a ten-fold increase in exposure capability during summertime (low solar zenith angle conditions).

The high exposure capability of the PPO dosimeter means that it is also ideal for underwater measurements that would usually be awkward to achieve by using traditional spectroradiometric and radiometric instrumentation. Schouten et al. (2007) tested the PPO dosimeter in a controlled underwater environment using solar UVB simulation focusing on dose response calibration trends, cosine response, interdosimeter variability, dark reaction, UVA/visible wavelength responsivity, and additionally, exposure additivity. The information gathered from this investigation

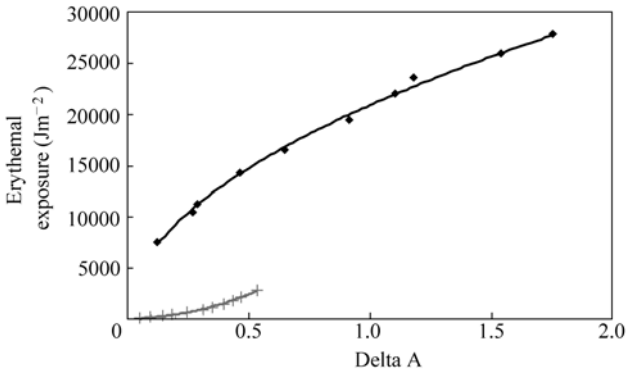

Figure 7.5 PPO dosimeter (♦) and polysulphone dosimeter (+) calibration to the erythemal action spectrum (CIE, 1987). Polysulphone dosimeter calibration data obtained from Turnbull and Parisi (2005)

showed that PPO was viable for underwater measurements with only a slight decrease in accuracy introduced when compared with in-air measurements, which was caused by watermarking on the PPO film surface. This research also made the important finding that calibrations made in-air could not be used as proxies to calculate underwater exposures.

This initial trial research has since been extended (Schouten et al., 2008) by obtaining calibration regimes at different depths to the real solar UVB spectrum for the PPO dosimeter in four different water types (clear water, sea water, dam water, and creek water) over a wide range of solar zenith angles and under fluctuating ozone conditions. This work found that at shallow depths, calibrations could be transferred from one water type to another with only a relatively small reduction in total uncertainty on the condition that each water type was within a certain spectral transmission (or absorption) range. It was also discovered that PPO calibrations are sensitive to atmospheric ozone variations. This means that if researchers wish to measure UVB with the PPO dosimeter, calibrations would have to be made just before, after, or during the measurement campaign to reduce the response error brought on by ozone attenuation causing changes in the solar spectrum of the UVB wavelengths.

7.6 Vitamin D Effective UV Dosimetry

The action spectrum for the synthesis of pre-vitamin D_3 shows that only the short wavelength UV is effective (CIE, 2006) for this process. This action spectrum can be approximated by the spectral response of polysulphone (CIE, 1992). Using polysulphone dosimeters, the transmission of pre-vitamin D_3 effective UV through clothing has been investigated (Hutchinson and Hall, 1984; Parisi and Wilson, 2005). Many factors influence the UV exposure to an individual, and therefore,

the synthesis of pre-vitamin D_3, including clothing, use of sunscreen, pigmentation of the skin, age, and latitude of residence (Matsuoka et al., 1990; 1992; Webb, 2006). The face, arms, and hands contain approximately 15% of the skin area of the human body. UV exposure of 1 MED to these parts would produce serum vitamin D equivalent to 1,500 IU − 3,750 IU (Samanek et al., 2006). Most research conducted on UV transmission through clothes is generally from the perspective of protection from UV; however, some of the incident UV can transmit through clothing and has been measured at various body sites under garments with polysulphone dosimeters for pre-vitamin D_3 effective UV (Parisi and Wilson, 2005).

This work can be extended for the quantification with polysulphone dosimeters of pre-vitamin D_3 effective UV to humans in different environments. Figure 7.6 shows a typical calibration curve for pre-vitamin D_3 effective UV in winter at a sub-tropical site.

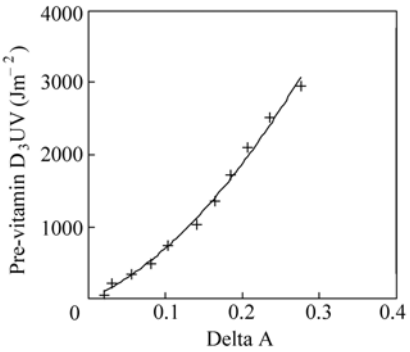

Figure 7.6 Calibration of polysulphone dosimeters for pre-vitamin D_3 effective UV exposures on a winter's day (Parisi and Turnbull, 2006)

7.7 Discussion and Conclusions

The use of UV polysulphone dosimeters to quantify erythemal exposures to humans during normal daily activities in different environments and to determine the effectiveness of UV minimization strategies has been reported. Miniaturization of these dosimeters to a diameter of 6 mm has allowed an increase in the density of the UV exposure measurements, along with an increase in the potential number of environments in which they can be used. Additionally, polysulphone dosimeters employed in conjunction with a dosimeter sensitive to the visible waveband have been employed to measure the UVB exposures and the photosynthetically active radiation to plant leaves. With appropriate calibration, polysulphone dosimeters have measured the pre-vitamin D_3 effective UV to humans in order to quantify the amount of UV producing this vitamin that is essential for the well being of humans. The dynamic range of polysulphone at a

sub-tropical site is approximately one day in summer. For periods of exposure longer than this, the polysulphone dosimeters have to be replaced on a daily basis or alternatively a dosimeter based on polyphenylene oxide with a dynamic range that is approximately ten times longer than that of polysulphone has been employed for erythemal and UVB exposures.

References

Ambach W, and Blumthaler M (1993) Biological effectiveness of solar UV radiation in humans. Experientia 49: 747 – 753

American Cancer Society (2008) URL: http://www.cancer.org/docroot/PRO/content/PRO_1_1x_Skin_Cancer.pdf.asp?sitearea = PRO, accessed on 7 Feb, 2008

Blumthaler M, and Ambach W (1991) Spectral measurements of global and diffuse solar ultraviolet-B radiant exposure and ozone variations. Photochem. Photobiol. 54: 429 – 432

Caldwell MM (1971) Solar ultraviolet radiation and the growth and development of higher plants. In: AC Giese (Editor), Photophysiology, Vol. 6. Academic Press, New York, pp.131 – 177

Caldwell MM, Teramura AH, Tevini M, Bornman JF, Bjorn LO, and Kulandaivelu G (1995) Effects of increased solar ultraviolet radiation on terrestrial plants. Ambio 24: 166 – 173

Casale GR, Borra M, Colosimo A, Colucci M, Militello A, Siani AM, and Sisto R (2006) Variability among polysulphone calibration curves. Phys. Med. Biol. 51: 4413 – 4427

CIE (International Commission on Illumination) (1987) A reference action spectrum for ultraviolet induced erythema in human skin. CIE J. 6: 17 – 22

CIE (1992) Personal dosimetry of UV radiation. Technical Report. Publication No. CIE 98, Wien, Austria

CIE (2006) Action spectrum for the production of previtamin D_3 in human skin. CIE 174: 2006

Davis A, Deane GHW, and Diffey BL (1976a) Possible dosimeter for ultraviolet radiation. Nature 261: 169 – 170

Davis A, Deane GHW, Gordon D, Howell GV, and Ledbury KJ (1976b) A worldwide program for the continuous monitoring of solar UV radiation using poly (phenylene oxide) film, and consideration of the results. J. Appl. Poly. Sci. 20: 1165 – 1174

Diffey BL (1987) A comparison of dosimeters used for solar ultraviolet radiometry. Photochem. Photobiol. 46: 55 – 60

Downs NJ, and Parisi AV (2007) Three dimensional visualisation of human facial exposure to solar ultraviolet. Photochem. Photobiol. Sci. 6: 90 – 98

Downs N, and Parisi AV (2008) Patterns in the received facial ultraviolet exposure of school children measured at a sub-tropical latitude. Photochem. Photobiol. 84(1): 90 – 100

Flint SD, and Caldwell MM (2003) A biological spectral weighting function for ozone depletion research with higher plants. Physiol. Plant. 117: 137 – 144

Holick MF (2004a) Vitamin D: Importance in the prevention of cancers, type 1 diabetes, heart disease and osteoporosis. Am. J. Clin. Nutr. 79: 362 – 371

Holick MF (2004b) Sunlight and vitamin D for bone health and prevention of autoimmune diseases, cancers, and cardiovascular disease. Am. J. Clin. Nutr. 80: S1678 – S1688

Hutchinson G, and Hall A (1984) The transmission of ultraviolet light through fabrics and its potential role in the cutaneous synthesis of vitamin D. Human Nutrition: Applied Nutrition 38A: 298 – 302

Krins A, Bolsee D, Dorschel B, Gillotay D, and Knuschke P (2000) Angular dependence of the efficiency of the UV sensor polysulphone film. Rad. Prot. Dos. 87: 261 – 266

Lester RA, Parisi AV, Kimlin MG, and Sabburg J (2003) Optical properties of poly (2,6-dimethyl-1,4-phenylene oxide) film and its potential for a long term solar ultraviolet dosimeter. Phys. Med. Biol. 48: 3685 – 3698

Matsuoka LY, Wortsman J, Haddad JG, and Hollis BW (1990) Skin types and epidermal photosynthesis of vitamin D_3. J. Am. Acad. Derm. 23: 525 – 526

Matsuoka LY, Wortsman J, Dannenberg MJ, Hollis BW, Lu Z, and Holick MF (1992) Clothing prevents ultraviolet-B radiation-dependent photosynthesis of vitamin D_3. J. Clin. Endocrinol. Metab. 75: 1099 – 1103

Munakata N, Ono M, and Watanabe S (1998) Monitoring of solar-UV exposure among schoolchildren in five Japanese cities using spore dosimeter and UV-coloring labels. Jpn. J. Cancer Res. 89: 235 – 245

Parisi AV, and Wilson CA (2005) Pre-vitamin D_3 effective ultraviolet transmission through clothing during simulated wear. Photodermatol. Photoimmunol. Photomed. 21(6): 303 – 310

Parisi AV, and Turnbull DJ (2006) Solar UV dosimetry. UV radiation and its effects: an update (2002) Conf, 19 – 21 Apr, 2006, Dunedin, NZ

Parisi AV, Wong CF, and Randall C (1998) Simultaneous assessment of photosynthetically active and ultraviolet solar radiation. Agric. For. Meteorol. 92(2): 97 – 103

Parisi AV, Kimlin MG, Meldrum LR, and Relf CM (1999) Field measurements on protection by stockings from solar erythemal ultraviolet radiation. Rad. Prot. Dos. 86(1): 69 – 72

Parisi AV, Kimlin MG, Wong JCF, Lester R, and Turnbull DJ (2000a) Reduction in the personal annual solar erythemal ultraviolet exposure provided by Australian gum trees. Rad. Prot. Dos. 92(4): 307 – 312

Parisi AV, Kimlin MG, Wong JCF, and Wilson M (2000b) Personal exposure distribution of solar erythemal ultraviolet radiation in tree shade over summer. Phys. Med. Biol. 45(2): 349 – 356

Parisi AV, Galea VJ, and Randall C (2003) Dosimetric measurements of the visible and UV exposures on field grown soybean plants. Agric. For. Meteorol. 120: 153 – 160

Parisi AV, Kimlin MG, Turnbull DJ, and Macaranas J (2005) Potential of phenothiazine as a thin film dosimeter for UVA exposures. Photochem. Photobiol. Sci. 4: 907 – 910

Parisi AV, Turnbull DJ, and Kimlin MG (2007) Dosimetric and spectroradiometric investigations of glass filtered solar UV. Photochem. Photobiol. 83: 777 – 781

Quintern LE, Horneck G, Eschweiler U, and Buecker H (1992) A biofilm used as ultraviolet dosimeter. Photochem. Photobiol. 55: 389 – 395

Quintern LE, Furusawa Y, Fukutsu K, and Holtschmidt H (1997) Characterization and application of UV detector spore films: the sensitivity curve of a new detector system provides good similarity to the action spectrum for UV-induced erythema in human skin. J. Photochem. Photobiol. B: Biol. 37: 158 – 166

Samanek AJ, Croager EJ, Gies P, Milne E, Prince R, McMichael AJ, Lucas RM, and Slevin T (2006) Estimates of beneficial and harmful sun exposure times during the year for major Australian population cities. Med. J. Aust. 184: 338 – 341

Schouten PW, Parisi AV, and Turnbull DJ (2007) Evaluation of a high exposure solar UV dosimeter for underwater use. Photochem. Photobiol. 83: 931 – 937

Schouten PW, Parisi AV, and Turnbull DJ (2008) Field calibrations of a long term UV dosimeter for aquatic UVB exposures. J. Photochem. Photobiol. B: Biol. 91: 108 – 116

Teramura AH, and Sullivan JH (1994) Effects of UV-B radiation on photosynthesis and growth of terrestrial plants. Photosynth. Res. 39: 463 – 473

Turnbull DJ, and Parisi AV (2005) Increasing the ultraviolet protection provided by public shade structures. J. Photochem. Photobiol. B: Biol. 78(1): 61 – 67

Turnbull DJ, and Schouten PW (2008) Utilising polyphenylene oxide for high exposure solar UVA dosimetry. Atmos. Chem. Phys. 8: 2129 – 2141

Webb AR (2006) Who, what, where and when — influences on cutaneous vitamin D synthesis. Prog. Biophys. Mol. Biol. 92: 17 – 25

WHO (World Health Organization) (1994) Environmental Health Criteria 160: Ultraviolet Radiation. Geneva, p. 256

8 An Ultraviolet Radiation Monitoring and Research Program for Agriculture

Wei Gao[1], John M. Davis[1], Roger Tree[1], James R. Slusser[1], and Daniel Schmoldt[2]

[1] United States Department of Agriculture UV-B Monitoring and Research Program
Natural Resource Ecology Laboratory
Colorado State University, Fort Collins, CO, USA
E-mail: wgao@uvb.nrel.colostate.edu
[2] United States Department of Agriculture
Cooperative State Research, Education, and Extension Service
Washington, DC, USA
E-mail: dschmoldt@csrees.usda.gov

Abstract The United States Department of Agriculture (USDA) Ultraviolet-B Monitoring and Research Program (UVMRP) was initiated in 1992 through a grant to Colorado State University (Fort Collins, CO, USA), authorized by Congress under the USDA Cooperative State Research Education and Extension Service (CSREES) Special Research Grant authority, to provide the agricultural science research community with the information necessary to determine if changing levels of UV-B radiation would threaten food and fiber production in the United States. The UVMRP consists of three major components: (1) monitoring solar radiation with an emphasis on UV-B radiation; (2) research to determine the effects of UV radiation on specific plants and crops; and (3) crop growth and production assessment modeling to assess the impact of climate change scenarios on crop production. The monitoring network, consisting of UV and visible solar radiation measurement instrumentation installed at 37 climatological sites, is described in this chapter, along with the basic algorithms used to process the data and the calibration methods designed to provide accurate long term data records. Procedures developed to provide aerosol optical depth, columnar ozone, and enhanced products, such as integrated irradiances weighted with biological spectral weighting functions and summed over selected time periods, are also described. An updated, flexible web page interface that allows users to access various data products is documented. The UVMRP's role in UV-B agricultural effects studies is summarized, including contributions by scientists at several collaborating

universities. The UVMRP's component that models agricultural sustainability by coupling a state of the science climate forecasting model to crop growth models in order to obtain the impact of climate change scenarios on crop yield is introduced. Future directions of UVMRP are also presented.

Keywords USDA UVMRP, ultraviolet, solar UV-B radiation, monitoring network, crop damage, UV climatology, agricultural sustainability, column ozone, crop yield

8.1 Introduction

Over the past few decades, the atmospheric science community has found it beneficial to establish routine programs to monitor various surface radiation quantities. During the early 1970s, a focus on the potential national benefit for using solar radiation as an energy source prompted the National Oceanic Atmospheric Association (NOAA) to begin monitoring solar radiation at its Climate Monitoring and Diagnostics Laboratory, currently known as the Earth System Research Laboratory (ESRL); see http://www.esrl.noaa.gov/gmd/publications/annrpt23/chapter3_2.htm. Although this initial interest in solar energy waned somewhat before its recent revival, the launch of the first meteorological satellites excited climate scientists by making estimates of the earth's radiation budget feasible from space. The first part of this effort started in the mid 1980s with the Earth Radiation Budget Experiment (ERBE), during which time surface monitoring of the radiation budget fields received renewed attention (Barkstrom, 1984). In the years that followed, as the need for more accurate estimates of the solar radiation budget for application in higher resolution climate models became desirable, and the concern over global climate change increased, the US Department of Energy funded the development of the Atmospheric Radiation Monitoring Program in 1989 (see http://www.arm.gov/about/). Satellite observations revealed another potential impact of anthropogenic activity during the 1980s, namely the observed depletion of stratospheric ozone in the Antarctic area (Farman et al., 1985; WMO, 1989; Stolarski et al., 1992) and the Arctic. These observations raised serious concerns in the scientific community of concomitant increases in ultraviolet-B (UV-B) radiation reaching the earth's surface (Frederick and Snell, 1988; Scotto et al., 1988; Grant, 1988; Worrest et al., 1989; Blumthaler and Ambach, 1990; Smith et al., 1992; Kerr and McElroy, 1993; Jaque et al., 1994; Herman et al., 1996) and its detrimental effects on plants, animals, ecosystems, and human health. These concerns led to the establishment of a network for monitoring solar radiation that was not concerned with the total solar and infrared spectrum, but rather specifically focused on the challenge of monitoring the UV radiation reaching the earth's surface, for evaluation of potential impact on crop yield and nutrition, and for assessing possible impacts on human and animal health (Caldwell et al., 1986;

Teramura et al., 1990). The purpose of this chapter is to document the activities associated with the monitoring of UV radiation, which has become one focus of the United States Department of Agriculture's UV-B Monitoring and Research Program.

8.2 Introduction to the USDA UVMRP (Purpose and History)

The beginnings of the USDA UVMRP stem from a series of USDA sponsored workshops, held for the purpose of determining the type of response that might be necessary to address the potential threat of UV radiation to US agriculture (Gibson 1991, 1992; Science and Policy Associates, 1992; O'Hara and O'Hara, 1993). Workshop participants, representing various universities, research institutions, and governmental agencies, recommended that the USDA establish a monitoring network to support research for determining the geographical distribution and temporal trends of the effects of UV-B radiation on plants and animals.

The USDA UVMRP was initiated in 1992, through a grant to Colorado State University (Fort Collins, CO, USA) authorized by Congress under the USDA Cooperative State Research Education and Extension Service (CSREES) Special Research Grant authority, to provide the agricultural science research community with the information necessary to determine if changing levels of UV-B radiation would threaten food and fiber production in the U.S. (Bigelow et al., 1998). The primary objective of the program was defined as providing information to the agricultural research community about the geographic and temporal distribution of UV-B irradiance in the U.S. It was recognized later, however, that there was a critical need for experimental and modeling research to examine the effects of enhanced UV-B radiation levels on crops and animals in order to meet the USDA objectives and to cope with the emerging challenges from the scientific community, such as the quantification of the effects, their variations among species and biochemical processes, their interactions with other biotic and abiotic factors, and gene control responses to UV-B radiation. Although some recent measurements indicate the start of a turnaround in stratospheric ozone, its recovery will likely take decades and is influenced by many factors (Staehelin et al., 2001; Newchurch et al., 2003; Reinsel et al., 2005; WMO, 2007). Great uncertainties exist in the future levels of surface UV radiation because it will be additionally affected by changes in clouds and aerosols (Bredahl et al., 2004; Kerr, 2005; McKenzie et al., 2007). The effects of UV radiation on plants, animals, ecosystems, and human health are complex and interact with other stress factors (Rozema et al., 1997; Yuan et al., 1998; Grant, 1999; Tegelberg et al., 2002; Gao et al., 2002, 2003; Caldwell et al., 2003; Clarke and Harris, 2003; Flint et al., 2003; Kulandaivelu and Tevini, 2003; Kakani et al., 2003; Reddy et al., 2003; Warren et al., 2003; Bassman, 2004; Turtola et al., 2005). Observations of visible and UV solar radiation reaching the

ground are necessary in order to quantify changes in atmospheric transmission which in turn drive the terrestrial ecosystems.

The UVMRP consists of three major components: (1) quality solar measurement and research in atmospheric radiation transfer, especially in UV wavelengths; (2) research to determine the effects of enhanced UV radiation on specific plants and agricultural crops to develop methods to lessen these effects and ensure crop productivity; (3) crop growth and production assessment modeling that accurately responds to various precipitation, temperature, and solar radiation scenarios. This chapter describes the UVMRP with an emphasis on the Program's data and derived products, the web-accessible database, and its role in facilitating research on agricultural effects, establishment of crop growth, and a production assessment modeling system.

8.3 Monitoring Network

8.3.1 Sites and Coverage

The design goal of the network was to have a 5° latitude × 10° longitude equal-area representation of the continental U.S. with additional coverage of Alaska and Hawaii (Bigelow et al., 1998). However, the existing distribution of the observation sites is not ideal because of logistical difficulties in securing acceptable sites in each latitudinal zone (Bigelow and Slusser, 2000). As of 2008, 34 climatological sites in the U.S., with 2 additional collaborating climatological sites in Canada and one in New Zealand, are operating in the network (Fig. 8.1). Sites were selected to represent each grid rectangle based upon their long-term viability, proximity to agricultural, biological, ecological, and ongoing UV research sites, unobstructed sky view, and availability of phone, internet, and power supply. The sites in Canada and New Zealand were set up for the purpose of maintaining a scale for comparison of each country's radiation archives. In addition, ad hoc research sites are temporarily set up and maintained for specific research purposes for a period of time. Six high resolution U1000 spectroradiometers were sited at research sites where key collaborative research allowed interdisciplinary uses of the data, although the high maintenance of the U1000s eventually led to discontinuing their deployment. Instruments at a research site may be turned off and on at any time, and additional instruments can be installed and run for a period of time depending on the purpose of the research project, especially during the campaigns of inter-comparisons between instruments from different manufacturers. On the other hand, the climatological sites require less sophisticated instrumentation than at research sites, and the instruments at a climatological site operate continuously without intentional interrupts except for routine maintenance. In this chapter, we focus on the climatological sites only.

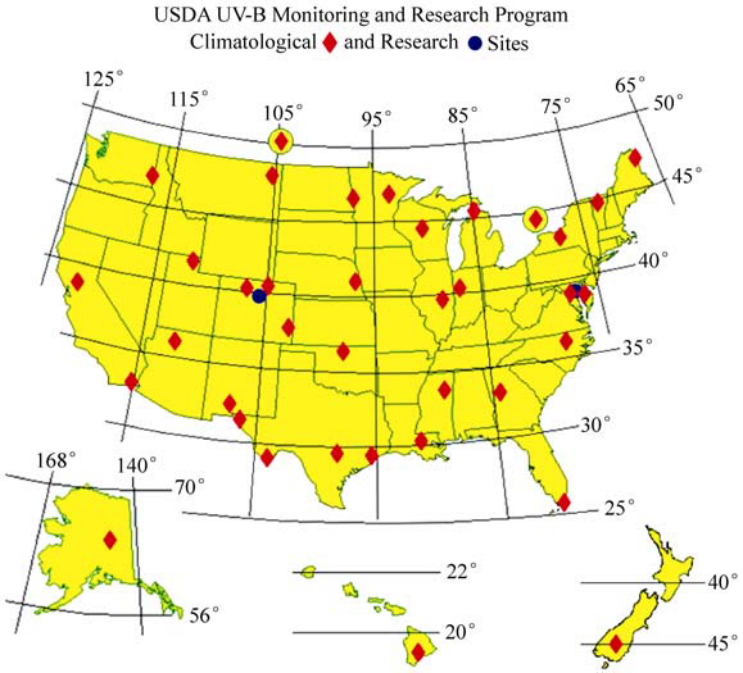

Figure 8.1 The UVMRP monitoring network coverage from 1993 through year-end 2008

8.3.2 Data Products Provided by UVMRP

The USDA UVMRP provides a wide variety of products to the broader scientific community. Although the primary stakeholders of UVMRP are focused on agricultural applications, many users of the data access the products via the web page or by special request for use in human health research, atmospheric science studies, industrial coating testing and analysis, defense contractor work, and for a few proprietary applications.

The data provided by UVMRP may be divided into measurement data and derived products. Many quantities are measured and the values are available on the UVMRP web site within 24 hours (http://uvb.nrel.colostate.edu). This also applies to some of the derived products. Table 8.1 presents a list of quantities categorized as either direct measurements or derived quantities, along with the instrument used to collect the data. Section 8.4 elaborates on the data collection process in general, and the processing applied to arrive at useful quantities. Section 8.5 follows with a discussion of the processing of the derived data products.

Table 8.1 The primary measurements and derived quantities available to users of the USDA UVMRP website. Other related quantities are available upon request

Data Product	Brief Description	Primary or Derived	Instrument Name
UV spectral irradiance	300, 305, 311, 317, 325, 332 and 368 nm wavelengths	Primary	YES* Inc. UV-MFRSR
UV erythemal irradiance	280 nm − 320 nm (erythemally weighted)	Primary	YES Inc. UVB-1 pyranometer
Visible spectral irradiance	415, 500, 615, 673, 870, and 940 nm wavelengths	Primary	YES Inc. VIS-MFRSR
PAR	400 nm − 700 nm Photosynthetically Active Radiation	Primary	LI-COR** Inc. LI-190SA Quantum Sensor
Surface reflected irradiance	Used to indicate presence of snow covered surface	Primary	LI-COR Inc. LI-210SA photometer
UVA broadband irradiance	320 nm − 400 nm broadband irradiance (at only 7 sites)	Primary	Solar Light*** Model 501A -UV-A radiometer
Ambient air temperature and relative humidity	Standard meteorological values	Primary	Vaisala**** HMP 35A or HMP 45D
Ambient barometric pressure	Standard meteorological values (at only 14 sites)	Primary	Vaisala Inc. Model PTB-101 or PTB-110
Aerosol optical depth	332 nm and 368 nm instantaneous or daily averaged	Derived from MFRSR	
Column ozone	Daily value	Derived from UV-MFRSR	
Synthetic spectrum	300 nm − 400 nm irradiance at 1 nm resolution	Derived from UV-MFRSR	
UV climatology	UV-A, UV-B, Erythemal, Flint, Caldwell, Vitamin D as daily, monthly, and annual sums	Derived from synthetic spectrum	

* Yankee Environmental Systems, Turners Falls, MA
** LI-COR Biosciences, Lincoln, NE
*** Solar Light, Glenside, PA
**** Vaisala Inc., Vantaa, Finland

8.4 Data Collection and Processing

Two data loggers are installed at each site to collect and transfer the direct measurements from the instruments referred to in Table 8.1. One data logger is used to collect the data every 15 seconds from the VIS-MFRSR, UVB-1 pyranometer, temperature/humidity sensors, and the downward looking LI-COR 210SA photometer. The other is for the UV-MFRSR, PAR Quantum sensor, and barometer (and UV-A radiometer where applicable) that are sampled every 20 seconds. The difference between the sampling frequencies results from a longer required dwell time of the UV-MFRSR instrument. The data are aggregated into 3-min averages and stored in each data logger. Figure 8.2 shows an example of a UVMRP station.

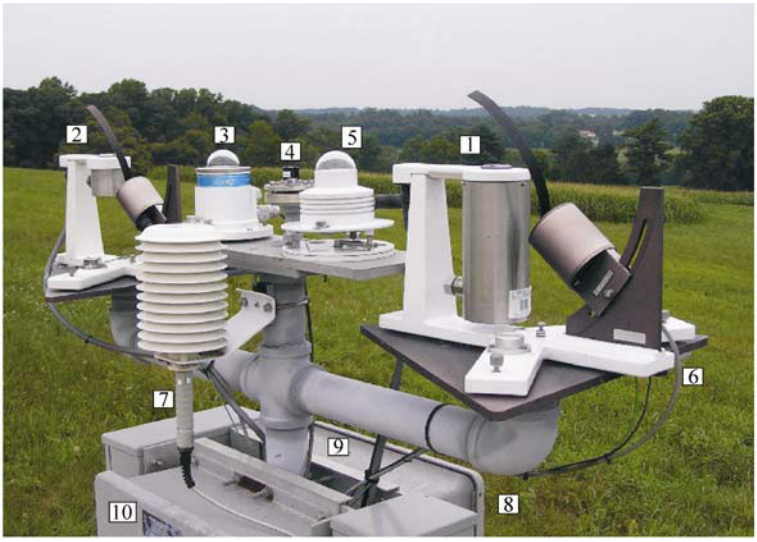

Figure 8.2 The layout of instruments at a typical climatological site in the UVMRP monitoring network. (1) UV-B Multi-Filter Rotating Shadowband Radiometer (UV-MFRSR); (2) Visible Multi-Filter Rotating Shadowband Radiometer (vis-MFRSR); (3) UVB-1 Pyranometer (erythemal); (4) Photosynthetically Active Radiation (PAR or Quantum Sensor); (5) UV-A biometer (only at 7 sites); (6) Downward-looking photometer; (7) Air temperature and relative humidity sensor; (8) Barometric pressure (14 sites, inside datalogger enclosure); (9) UV-MFRSR Datalogger; (10) Vis-MFRSR Datalogger

The instruments are located at sites with unobstructed horizons and are positioned at a level of 1.5 m above the ground. The temperature and relative humidity measurements are intended to be used in applications that require these data to be collocated with the radiation measurements and are not intended as substitutes for the National Weather Service (NWS) data, since these sensors are not installed in conformance to NWS standards. The data loggers are driven by AC power with rechargeable batteries in line to act as a backup in case the AC power fluctuates or outages occur for a short period of time. The "raw voltage" measurements from the station data loggers are transferred to the UVMRP data server every day through dedicated phone lines or the Internet. The raw voltages are processed into their corresponding physical quantities at the UVMRP headquarters located at Colorado State University, Fort Collins, CO, USA. Data quality control measures are applied daily. Discussion in this section will focus on the UV-B data, including UV-MFRSR and UVB-1 measurements.

Before 1997, characterization and calibration of the UV-MFRSR, VIS-MFRSR, and UVB-1 instruments were done annually at YES or at the Atmospheric Science Research Center (ASRC) at the State University of New York (SUNY)-Albany, NY, USA. Since 1997, annual characterization and calibration of the UV-MFRSR and UVB-1 instruments have been performed at the Central UV Calibration Facility

(CUCF), which is housed within NOAA's ESRL. The CUCF was initiated and developed in collaboration with the Optical Technology Division of the National Institute of Standards and Technology (NIST) and works to transfer the NIST standards of spectral irradiance to the U.S. solar UV radiation monitoring community in an accurate, long-term, repeatable, and cost-efficient manner (Disterhoft, 2005). The characterization and calibration of VIS-MFRSR instruments are based on the original YES values. Because many of the VIS-MFRSR instruments have been deployed for many years, the users are warned of this on the UVMRP website and are encouraged to use Langley calibrations, which are updated monthly. Until recently, the UV-MFRSRs were cycled through the calibration process at CUCF on an annual basis. Beginning in 2006, program priorities and fiscal constraints significantly lengthened the period between laboratory calibrations. Until this situation is resolved, the users of these data may wish to consult the most recent deployment date listed for the instrument at the site of interest via the UVMRP web page under "Site Location Deployment History", to check for last lamp calibration date. Then the choice of using lamp or Langley calibrations for spectral UV data may be made. The PAR sensors are sent to LI-COR for recalibration at their recommended two-year interval. The rest of the instruments, LI-COR 210SA photometers, and temperature-humidity probes, are calibrated by the manufacturers before they are deployed.

8.4.1 UV-MFRSR Data Processing

The UV-MFRSR uses independent interference filter-photodiode detectors and an automated rotating shadow band to measure the total horizontal and diffuse horizontal UV solar irradiance at seven wavelengths concurrently (Michalsky et al., 1988; Harrison et al., 1994). Direct normal irradiance is determined within the data logger by subtracting the diffuse from the total signal, followed by a correction for imperfect cosine response. The UV-MFRSR instruments provide synchronized measurements of spectral irradiances within the UV wavelength region. The direct normal measurement provides an input required for retrieval of atmospheric optical properties, including air mass components, such as the aerosol optical depths and columnar ozone content that may not be feasible from the total irradiance signal alone. Essential adjustments to the UV-MFRSR measurements include removal of dark current bias voltages and a correction for deviations of the sensors from an ideal cosine response. The corrected voltages are then converted into irradiances by multiplying by a calibration factor.

8.4.1.1 Dark Current Bias Removal

Certain extraneous voltages may be generated by the electronics of the observation system, including data loggers, amplifiers, circuits, and connecting wires. These

signals are measured at night in the absence of solar radiation using voltages averaged from one hour prior to, and one hour after, the time of minimum solar elevation over the three day period preceding the current data processing day. For a more detailed discussion of the dark current voltage bias removal, please view the USDA UVMRP website (http://uvb.nrel.colostate.edu/UVB/index.jsf), under the "Monitoring Network," then the "Data Processing Procedures" links.

8.4.1.2 Cosine Correction

The direct beam irradiance measured on a horizontal surface is given by the product of the incident normal irradiance and the cosine of the solar zenith angle (SZA). However, the detectors of the UV-MFRSR do not have perfect cosine responses, especially at higher incidence angles. The correction for the deviation of the response from an ideal cosine response is known as cosine correction or angular correction. The non Lambertian response of the UV-MFRSR instruments has been described by Harrison et al. (1994). Characteristics of the cosine responses of the UV-MFRSR instruments used in the network are described by Bigelow et al. (1998). The actual angular responses of an instrument are a function of solar zenith and azimuth angles and were determined annually by YES (in the initial periods of network operation and by CUCF since 1997). The cosine response is determined through laboratory measurements based on an independent radiometric characterization of individual detectors made through the diffuser along two orthogonal planes (Michalsky et al., 1995). With knowledge of angular responses along north-south and east-west azimuths, correction factors for direct normal voltages are interpolated according to solar zenith and azimuth angles at the time of measurement.

An imperfect cosine response affects the measurement of the diffuse horizontal irradiance in addition to the direct normal component (Leszczynski et al., 1998). Experimental results show that the uncertainties in diffuse irradiance due to the assumption of a homogeneous sky radiance distribution are within ±1.5% in the UV-B band for varying atmospheric and geographic conditions (Gröbner et al., 1996). This assumption is employed in processing the diffuse irradiance values of the UV-MFRSR.

8.4.1.3 Out-of-Band Correction

In the original design of the UV-MFRSR the two channels at 300 nm and 305 nm used silicon-carbide (SiC) photodiodes and the remaining five channels used gallium-phosphide (GaP) photodiodes. By the end of 1997, this instrument design had been deployed at the 22 sites, which comprised the climatological network at that time. In December of 1997, the first of many failures of GaP photodiodes occurred ultimately resulting in a solution developed jointly by UVMRP and YES which involved the replacment of the GaP photodiodes with silicon (Si) versions. The GaP photodiodes were replaced with silicon in all UVMRP UV-MFRSRs by

the end of 2002. Thus, the UV-MFRSRs now use Si photodiodes in the 311 nm through 368 nm channels and retain the original SiC photodiodes for the two channels centered at 300 nm and 305 nm (Janson et al., 2004).

Ideally, a radiometer should be designed to reject all radiation outside the designated wavelength region, i.e., in the 2 nm wide wavelength band of each of the seven channels. However, laboratory tests showed that the replacement Si photodiodes allowed out-of-band light from the NIST traceable tungsten-halogen lamps during the calibration procedure to contribute to the calibration signal, resulting in an inaccurate calibration (Lantz et al., 2005). Further studies revealed that the contribution of out-of-band light to the signal depended on several factors, including the channel, the individual instrument, and the lamp used for the laboratory calibration. Further analysis revealed that the out-of-band light contributing to the signal is mainly from wavelengths longer than 570 nm. This contribution of out-of-band light is commonly referred as "red light leakage" or "red leakage" for simplicity. To characterize the contribution of out-of-band light to the signal, each of the UV-MFRSR instruments were measured for out-of-band rejection using short-pass cutoff filters in the field with the sun as the radiation source and in the laboratory using the lamp as the radiation source. Results are given in Tables 8.2 and 8.3. Forty-seven UV-MFRSR instruments were tested in the field for out-of-band light and showed negligible signal within the detection limit of the measurements when the sun is used as the radiation source (Table 8.2). The largest average percent contribution is in the 317 nm channel. The average contribution of out-band-light is 0.4% of the total solar signal, with a maximum of 1.3% for this channel. The implications are that the Langley plot calibrations, which are described below, are not affected by red light leakage to any significant extent. All UV-MFRSR instruments were tested in the laboratory for out-of-band light using a FEL-type quartz-tungsten-halogen lamp as the radiation source and a 400 nm long pass filter. As shown in Table 8.3, there is a significant percentage of out-of-band light contributing to the signal when a lamp is used as the calibration source. The most significant contribution from the out-of-band light is in the 317 nm channel where the average is 22.1%. All of the channels with Si photodiodes have a detectable out-of-band contribution to the total lamp signal. The two channels using SiC photodiodes have no measurable out-of-band signal.

Table 8.2 Percent contributions of out-of-band light to the measured solar signal from 47 filter radiometers (from Lantz et al., 2005)

	300 nm	305 nm	311 nm	317 nm	325 nm	332 nm	368 nm
Average	0.1%	0.0%	0.2%	0.4%	0.1%	0.1%	0.1%
Maximum	0.0%	0.3%	0.5%	1.3%	0.3%	0.4%	0.5%
Minimum	0.0%	0.0%	0.0%	0.0%	0.0%	0.0%	0.0%

Table 8.3 Percent contributions of out-of-band light to the measured lamp signal during calibration with a FEL-type quartz-tungsten-halogen lamp from 40 filter radiometers (from Lantz et al., 2005)

	300 nm	305 nm	311 nm	317 nm	325 nm	332 nm	368 nm
Average	0.0%	0.0%	8.8%	22.1%	12.1%	11.2%	4.0%
Maximum	0.1%	0.1%	28.4%	35.7%	28.5%	23.1%	10.5%
Minimum	0.0%	0.0%	4.2%	6.6%	3.9%	4.9%	1.1%

The calibration factors corrected for out-of-band signals for the Si photodiodes are applied to the corrected voltages (after the dark current voltage bias and cosine correction) to convert them into irradiances, which are the lamp calibrated channel data provided to the public through an internet website. Earlier versions of the UV-MFRSR instruments that used the GaP photodiodes participated in several North American Interagency Inter-comparisons of Ultraviolet Spectroradiometers conducted during 1995 – 1997. The measurements of the UV-MFRSR instruments agreed with the filter-weighted irradiances of the participating spectroradiometers with a ±5% uncertainty at local noon (Early et al., 1998a, 1998b; Lantz et al., 2002). Collocated measurements show that after the out-of-band corrections are applied, the irradiances measured by a representative UV-MFRSR instrument using Si photodiodes agree with the filter-weighted irradiance measurements from a U1000 spectroradiometer within the uncertainty of ±1.5% (Lantz et al, 2005) for the seven channels. All lamp calibrated UV-MFRSR data accessed via the UVMRP website has now been corrected for the out-of-band radiation leakage.

8.4.2 Erythemally Weighted UV Irradiance

One of the data types most frequently requested from UVMRP is a compilation of erythemally weighted irradiance over a specified geographic region and time period. The UVMRP employs YES UVB-1 pyranometers to measure the Commission Internationale de l'Eclairage (CIE) weighted erythemal irradiances (McKinlay and Diffey, 1987) at each climatological site. Initially, the UVB-1 pyranometers were calibrated and characterized annually by the instrument manufacturer. Comparisons between collocated radiometers show an agreement of better than ±2.3% when SZA is less than 80°, while absolute errors might reach 10% when SZA is greater than 80° (Bigelow et al., 1998; McKenzie et al., 2006). Since 1997, the broadband pyranometers have been calibrated and characterized annually by CUCF. Characterizations include the tests of cosine response and spectral response. The scale factor for erythemal calibration is determined by matching the output of the pyranometer to the standard triad at CUCF. The absolute calibration factor of the broadband pyranometer is determined annually by comparing the output of the broadband sensor in sunlight with that of three collocated UVB-1 standard

pyranometers (triad). The inter-comparison with the triad typically lasts from one to two months in order to obtain sufficient data for the calibration that includes corrections for different amounts of columnar ozone in each zenith angle regime. The standard triad is in turn frequently calibrated for erythemal action spectrum as a function of SZA and total column ozone in the field against a collocated precision spectral radiometer employing the principle described in the literature (Grainger et al., 1993; Lantz et al., 1999; Xu and Huang, 2000; Vijayaraghavan and Goswami, 2002; Xu and Huang, 2003). This practical calibration scheme is supported by the uniformity of the cosine responses of different broadband pyranometers in the UVMRP network. The uncertainty in this calibration is from two sources. One consists of the random and systematic uncertainties of the ozone and SZA dependent erythemal calibration factor. The other is the difference in the scale factor for each pyranometer.

Although the absolute calibration uncertainty of the pyranometers could reach as high as ±10%, relative uncertainties among the pyranometers are more important in certain applications (McKenzie et al., 2006). Differences in spectral response and angular response are the major sources for relative uncertainties. These differences are inherent in the calibration procedure, which is a comparison of the solar signal from the pyranometer to the triad as measured at CUCF. In order to examine the relative accuracy of the instruments, experiments that compared the solar signal from the standard triad to the field site UVB-1 pyranometers were conducted as the instruments cycled through the calibration process. The tests were performed as a function of SZA over 110 two-week periods under various weather conditions. The results indicate the rather remarkable level of consistency amongst the pyranometers in that, on average, the pyranometers differ from the standard triad by 0.1% at an SZA of 20°, and by 2.8% at an SZA of 80° for all 51 tested instruments. Other collocated measurements of the UVB-1 pyranometers also show a good agreement with the broadband pyranometers from other manufacturers, as well as within the tested UVB-1 pyranometers (Seckmeyer et al., 2007). Since a generic factor is applied for ozone-dependent calibration, differences of spectral responses between the pyranometers may introduce uncertainties. In order to more fully characterize the individual pyranometers, their signals are corrected for cosine response, and for the purposes of determining erythemal irradiance, individual characterizations as a function of zenith angle and total column ozone are made as discussed below.

8.4.2.1 Angular (Cosine) Response of the UVB-1 Pyranometer

The erythemal irradiance is almost always supplied as a total horizontal quantity. Thus, the angular response of each UVB-1 instrument must be utilized to correct for imperfect cosine response. The angular response is tested annually by performing a north-south scan and an east-west scan with an interval of one degree zenith angle. The average of the two scans is considered as the cosine response. Figure 8.3 displays the relative angular responses of 10 UVB-1 pyranometers that were

characterized by the CUCF in 2004. The measurements are normalized to 0° SZA. These results have the typical shapes of those reported by previous studies (Grainger et al., 1993; Mayer and Seckmeyer, 1996; Landelius and Josefsson, 2000). The differences of the angular responses from an ideal cosine response have been discussed by Bigelow et al. (1998). Although the departure from the ideal cosine response exceeds 10% beyond 60° SZAs (Bigelow et al., 1998), the variability between different pyranometers is rather small. Figure 8.3 actually displays the cosine response of ten instruments and shows that the agreement is within the width of the plotted line. Figure 8.4 shows the standard deviations of the cosine responses of 20 randomly selected pyranometers. The variances tend to increase with SZA, but the standard deviations are within 0.02% in the zenith angle range of 0° – 89°. This repeatability among the angular responses of the UVMRP broadband pyranometers suggests that a single generic cosine correction may be applied to all pyranometers in the network without introducing significant uncertainties.

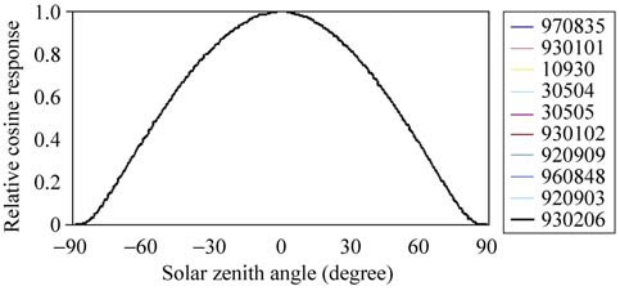

Figure 8.3 Normalized cosine responses of ten UVB-1 pyranometers. Numbers in the legend indicate the serial numbers of the sensors. The 10 curves are overlaid over each other. It is difficult to visibly separate them, which exhibits uniform cosine responses

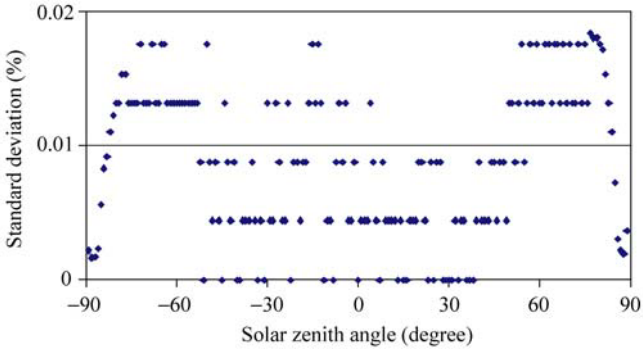

Figure 8.4 Standard deviations of cosine responses of 20 UVB-1 pyranometers as a function of SZA. The results show that the responses are within 0.02% of the mean cosine response and generally within the digitization error of the data logger

8.4.2.2 UVB-1 Spectral Response and Influence of Columnar Ozone

The erythemally weighted irradiance is determined by convolving the CIE action spectrum (McKinlay and Diffey, 1987) shown in Fig. 8.5 with the measured spectral irradiance. Measuring the erythemal UV irradiances requires that the spectral response of the pyranometer is identical with the CIE action spectrum because the spectral distribution of the solar radiation varies with many factors, such as ozone content, SZA, clouds, and other components in the atmosphere. However, the spectral response of the UVB-1 broadband pyranometer does not perfectly simulate the CIE action spectrum (Fig. 8.5), especially in the regions of shorter and longer wavelengths. Therefore, all factors that affect the wavelength distribution of solar irradiance in the erythemal wavelength band will impose potential impacts on the measurements of erythemal UV irradiance. The most significant variables are SZA, total ozone content and aerosol optical properties (Bodhaine et al., 1998; Lantz et al., 1999). Considering the effects of ozone content and SZA, the erythemal calibration factors for the UVB-1 broadband pyranometers are determined by the CUCF as a function of SZA and total ozone, or as a function of SZA with the assumption that the overhead total column ozone is 300 DU. The latter calibration factors are more conveniently applied when ozone measurements are not available at a site. The UVMRP data set provides erythemal UV irradiance data with the calibration factors of SZA dependence that assume overhead column ozone is 300 DU. Due to variable ozone contents and SZA, this assumption may result in an error of up to 25% (Fig. 8.6) for the ozone range of 200 DU − 500 DU for different SZAs. For a more accurate erythemal irradiance data set, however, ozone correction will be necessary. Lantz et al. (1999) detailed

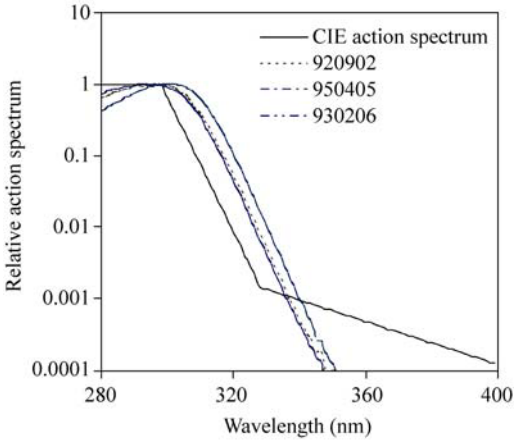

Figure 8.5 CIE action spectrum and spectral responses of three UVB-1 pyranometers. The numbers in the legend indicate the serial numbers of the tested sensors

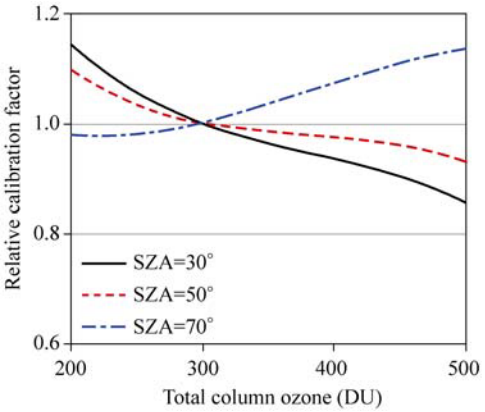

Figure 8.6 Erythemal calibration factors for the UVB-1 as a function of total column ozone for three SZAs normalized by their respective values for total column ozone of 300 DU

an approach to derive erythemal UV irradiance on clear days. This method is also recommended by the World Meteorological Organization/Global Atmosphere Watch (Seckmeyer et al., 2007) for erythemal calibration of broadband pyranometers. In the proposed scheme, the dependence of the calibration factor on ozone is curve-fitted with a third order polynomial for different SZAs from 5° to 80° using a step interval of 5°. Factors between the step intervals can be interpolated using any efficient interpolating technique. In cases where the total column ozone is known to differ significantly from 300 DU, the user may contact UVMRP to obtain erythemally weighted irradiances calibrated at other ozone levels.

8.4.3 Langley Analysis

While the laboratory calibrations and characterizations of the UV-MFRSR instruments were routinely performed, an alternative technique that has been used for many decades in various applications is the Langley plot method (Shaw, 1982; Thomason et al., 1983; Wilson and Forgan, 1995; Slusser et al., 2000). The Langley plot is used to provide more frequent calibrations of both the UV and VIS MFRSRs. The Langley method is based on the Beer-Lambert law, which describes the attenuation of the sun's direct-beam monochromatic radiation passing through the earth's atmosphere and is expressed mathematically (Thomason et al., 1983; Wilson and Forgan, 1995) as:

$$I_\lambda = R^2 I_{0,\lambda} \exp\left(-\sum \tau_{\lambda,i} m_i\right) \tag{8.1}$$

In Eq. (8.1), I_λ is the direct normal irradiance at the ground at wavelength λ, R^2

denotes a correction for the earth-sun distance at the time of measurement, $I_{0,\lambda}$ represents the extraterrestrial irradiance, $\tau_{\lambda,i}$ is the optical depth for the *i*-th air component, and m_i stands for the air mass of the *i*-th air component through the atmosphere. Taking the natural logarithm of both sides, we have

$$\ln I_\lambda = \ln\left(R^2 I_{0,\lambda}\right) - \sum \tau_{\lambda,i} m_i \,. \tag{8.2}$$

Provided that the irradiance is obtained by applying a calibration factor to the voltage output of the radiometer, the Beer-Lambert law can also be applied to the voltage of the instrument measurement. For the raw voltage output of the detector the formula is:

$$\ln V_\lambda = \ln\left(R^2 V_{0,\lambda}\right) - \sum \tau_{\lambda,i} m_i \,. \tag{8.3}$$

In Eq. (8.3), V_λ is the measured voltage at wavelength λ, and $V_{0,\lambda}$ represents the voltage the detector could measure oriented normal to the sun at wavelength λ outside the earth's atmosphere at one Astronomical Unit. Assuming that the optical depth remains constant over a period of time when the air mass, which is a function of SZA, changes significantly, the Langley analysis method determines the $V_{0,\lambda}$ by extrapolating voltage intercept at zero air mass when a linear fit to the logarithm of the measured voltage versus air mass is performed. Since the values of R and $I_{0,\lambda}$ can be accurately estimated (Lean 1991; Lean et al., 1997), a calibration factor (c_λ) to convert the measured voltage at wavelength λ into irradiance can be determined as:

$$c_\lambda = \frac{I_{0,\lambda}}{V_{0,\lambda}} \,. \tag{8.4}$$

The calibrated irradiance, $I_{\lambda,F}$, over the filter pass-band is obtained by multiplying the detector voltage measured at the ground by the calibration factor $c_{\lambda,F}$ (Bigelow et al., 1998). The calibration factor is determined using the filter-weighted integrations of $I_{0,\lambda}$ and $V_{0,\lambda}$ as follows (Slusser et al., 2000):

$$c_{\lambda,F} = \frac{\int I_{0,\lambda} F_\lambda \mathrm{d}\lambda}{V_{0,\lambda} \int F_\lambda \mathrm{d}\lambda}, \tag{8.5}$$

where F_λ is the filter function or spectral response function of the filter. After the direct and diffuse components of the voltage have been corrected for an ideal cosine angular response, the Langley analysis based on the objective algorithms (Harrison and Michalsky, 1994) is performed to determine $V_{0,\lambda}$. Obtaining the correct V_0 is essential in calibration. The V_0 values are generated for morning

and afternoons that supply at least 12 clear-sky measurements to the algorithm. The V_0 values are collected over air mass ranges that depend on the wavelength of the channel. For example, for the 300 nm through the 325 nm channels, the measurements for the direct beam voltages for an air mass range of 1.2 to 2.2 are used, while for the 337 nm and 368 nm channels, an air mass range between 1.5 and 3.0 is used. All the morning V_0 values deemed to be measured under clear sky for a given instrument at a given site are used as the ordinate in a linear regression routine using the air mass as the abscissa. The V_0 for the day is the offset derived from the regression routine.

Comparisons from previous studies of sun photometer calibration using the Langley analysis and the standard lamp in (Schmid and Wehrli, 1995; Schmid et al., 1998; Janson et al., 2004) show that the Langley analysis calibration is superior to the lamp calibration when the analysis is performed under very clear atmospheric conditions. However, the Langley calibration introduces more uncertainties at shorter wavelengths (around 300 nm) because the signals are weak. The Langley method cannot be applied in conditions where the Beer-Lambert law is not applicable such as over broad spectral bandpasses, or where multiple scattering may introduce path radiance into the detector's field of view. Other limitations of the Langley calibration method are discussed in Wilson and Forgan (1995), and Schmid et al. (1998). The combination of both types of calibration serve as an additional means of quality control; long term drifts from lamp calibrations can be detected by comparison with the Langley values whereas unresolved cloudiness in the Langley calibration data may be signaled by comparison with the lamp values. Thus, the use of a combination of both Langley calibration and lamp calibration is recommended to maintain a long term accurate calibration (Schmid and Wehrli, 1995). Figure 8.7 shows the results of the Langley analysis for two UV-MFRSR instruments deployed at Mauna Loa, HI. In the upper plot, 300 nm V_0s are shown, which are characteristically noisy due to a relatively low signal level as compared to the 305 nm channel data displayed in the lower plot.

8.4.4 Data Processing for Other Measurements

The VIS-MFRSR measurements are processed with the same procedures as for UV-MFRSR data with the exception noted above concerning the reliance on Langley calibrations since no recent lamp calibrations are available for the VIS-MFRSR. No out-of-band signals have been detected from the VIS-MFRSR instruments. For the PAR sensors, barometers, and temperature-humidity probes, calibration factors provided by the manufacturers are applied to the raw voltages to derive the final data products.

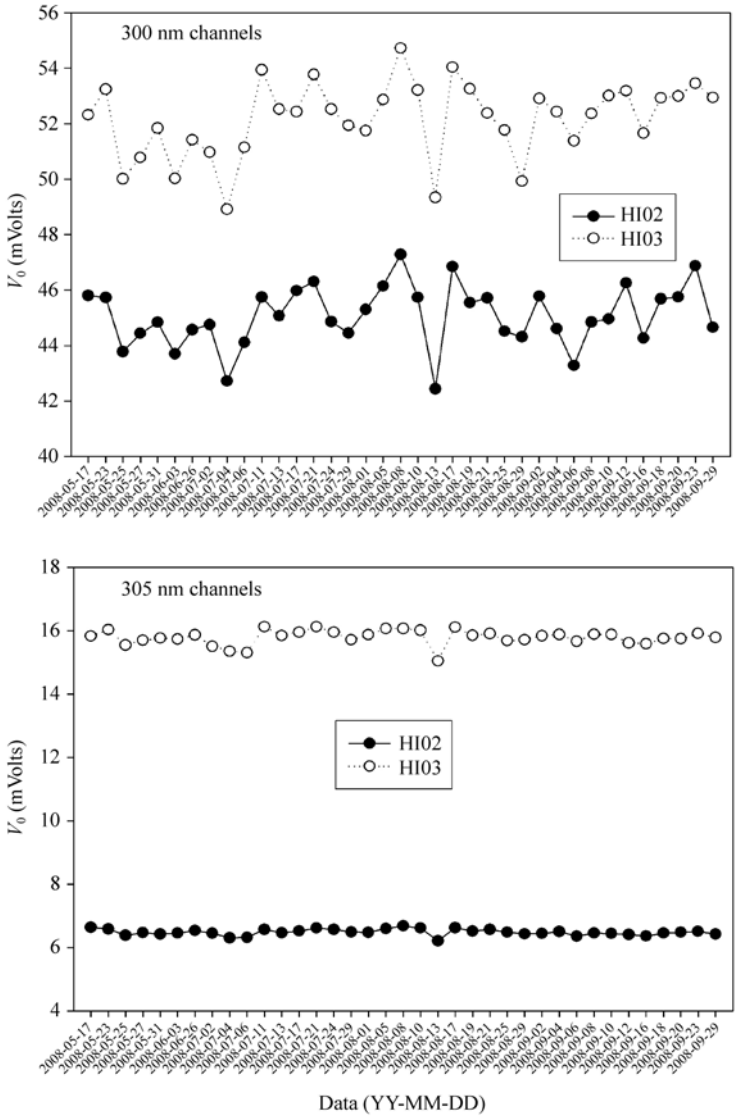

Figure 8.7 Plots of V_0 values from instruments HI02 (climatological site) and HI03 (research site) at Mauna Loa, HI derived from the Langley analysis method for the 300 nm and 305 nm channels from May 17 through September 29, 2008

8.5 Derived Products

By applying the techniques and algorithms developed in recent years to the measurements, various useful products can be derived. Examples of the derived products included in our database are optical depth, daily column ozone, and UV-B

irradiance with 1 nm spectral resolution. Using the synthetic spectrum algorithm discussed below, various agriculturally significant indices are derived, such as the Caldwell and Flint biologically weighted irradiances. An estimate of the vitamin D dosage is available, along with erythemally weighted irradiance and the closely related UV index. In addition to these products routinely available on the UVMRP website, numerous products are processed on demand for users in the agricultural, medical, and industrial materials communities.

8.5.1 Optical Depth

Optical depths are regularly acquired using measured spectral irradiances. These measurements are useful in developing regional aerosol climatology, validating satellite aerosol observations, and offering atmospheric corrections for satellite retrievals. Aerosol optical depth may also serve as a good indicator of surface visibility (Hand et al., 2004).

8.5.1.1 Instantaneous Optical Depth

Total and aerosol plus cloud optical depths are retrieved at 3-min intervals from the measurements of spectral irradiance. The total optical depths are derived using the Beer-Lambert law,

$$\tau_\lambda = \frac{\ln V_{0,\lambda} - \ln V_\lambda}{m}, \tag{8.6}$$

where τ_λ is the total optical depth and m denotes the air mass, which is a function of SZA. V_λ is the measured raw voltage value from the channel centered at wavelength λ. The value of $V_{0,\lambda}$ for each channel and the requested date are determined from a time series of Langley-generated voltage intercepts for morning periods of that day as discussed above. The Langley analysis is performed based on the objective algorithms developed by Harrison and Michalsky (1994), as discussed in Section 8.4.3.

For clear sky data, Rayleigh and ozone optical depths are subtracted from total optical depths to obtain the aerosol optical depths. Methods to accurately estimate Rayleigh optical depths in the atmosphere have been well documented in Fröhlich and Shaw (1980), Young (1981), Teillet (1990), Bucholtz (1995), and Bodhaine et al. (1999). We use the following formula to compute the Rayleigh optical depth for simplicity (Marggraf and Griggs, 1969; Stephens, 1994):

$$\tau_{\mathrm{Ray},z,\lambda} = 0.0088\lambda^{(-4.15+0.2\lambda)}\mathrm{e}^{\left(-0.1188z-0.00116z^2\right)}, \tag{8.7}$$

where $\tau_{\mathrm{Ray},z,\lambda}$ represents the Rayleigh optical depth at the altitude z (in km) and the wavelength is in the units of microns (μm). This formula is valid under the

assumption that the variation of air density with altitude follows the variation of pressure with altitude (Stephens, 1994).

Ozone optical depth is calculated by:

$$\tau_{O_3,\lambda} = \Omega \alpha_{O_3} c_{O_3} \tag{8.8}$$

where Ω is total column ozone in Dobson units, α_{O_3} is the ozone cross section, and $c_{O_3} = 0.001$ is a conversion constant. For UV wavelengths, the effective ozone cross sections are used (Bigelow et al., 1998). For visible wavelengths, the ozone absorption coefficients of Shettle and Anderson (1995) are used. Aerosol optical depth for clear days at 3-min intervals is then calculated by subtracting the Rayleigh optical depth and ozone optical depth from the total optical depth. These calculations are included in the UVMRP database. Note that aerosol optical depths are not available on cloudy days.

8.5.1.2 Average Optical Depth

The averaged optical depths for the mornings and/or afternoons are calculated from the instantaneous results. To ensure the accuracy of the results, time periods included in the averaging process are limited to specific air mass ranges which vary by wavelength: 1.5 – 3.0 for 332 nm and 368 nm, and 2.0 – 6.0 for 415 nm – 860 nm.

8.5.2 Daily Column Ozone

The algorithm for calculating the column ozone of the atmosphere is based on the work of Gao et al. (2001), which uses the direct-beam irradiance for the retrieval. Given spectral measurements of UV-B, the total column ozone Ω in Dobson units is calculated as:

$$\Omega = \frac{N_1 - N_2 - \left[\left(\beta_{305} - \beta_{325}\right) - \left(\beta_{311} - \beta_{332}\right)\right] m_a \left(P/P_0\right)}{\left[\left(\alpha_{305} - \alpha_{325}\right) - \left(\alpha_{311} - \alpha_{332}\right)\right] \mu} \times 10^3, \tag{8.9}$$

where

$$\begin{aligned} N_1 &= \ln \frac{V_{0,305}}{V_{0,325}} - \ln \frac{V_{305}}{V_{325}}, \\ N_2 &= \ln \frac{V_{0,311}}{V_{0,332}} - \ln \frac{V_{311}}{V_{332}}, \\ \mu &= \frac{R + h}{\left[\left(R + h\right)^2 - \left(R + z\right)^2 \sin^2 \theta\right]^{1/2}}, \end{aligned} \tag{8.10}$$

where the notations are:

β_λ Rayleigh scattering optical depth at wavelength λ;

m_a air mass corresponding to the SZA (θ) at the time when the measurement is taken;

P observed station atmospheric pressure;

P_0 mean sea level atmospheric pressure;

α_λ ozone absorption coefficient (base e) at wavelength λ;

$V_{0,\lambda}$ extraterrestrial voltage intercept at zero air mass at wavelength λ;

V_λ direct normal voltage after cosine and dark current bias corrections at wavelength λ;

μ ratio of the actual and the vertical paths of solar radiation through the ozone layer;

R average earth radius (6,371.229 km);

z height of the station above mean sea level;

h height of ozone layer above mean sea level at station location (20 km is assumed);

θ solar zenith angle.

Total column ozone is computed using those 3-min average measurements when the irradiance at 311 nm is greater than 0.002,5 $Wm^{-2}nm^{-1}$ and the condition $\theta > 70^\circ$ holds. Daily total column ozone is then determined by averaging these 3-min results if there are at least five of such 3-min averages.

8.5.3 Synthetic Spectrum Data

The UV-MFRSR instrument, described in Section 8.2.2, makes measurements every three minutes in seven spectral regions, each with a nominal bandwidth of 2 nm. The centers of the bandwidth regions are located at 300, 305, 311, 317, 325, 332 and 368 nm. The measurements are useful in assessing damage to plants and human health, particularly when considered in conjunction with specific Biological Spectral Weighting Functions (BSWFs); see for example Caldwell et al. (1986). The calculation of an index is usually required to indicate the overall magnitude of the effects of the UV-B radiation. The indices are almost always obtained by an integration of the downwelling UV-B total horizontal irradiances, spectrally weighted by the BSWF. Because the UV-B irradiances are measured in discrete spectral regions, some means of interpolating the irradiances at wavelengths appropriate for performing the integrations is required. The estimates of the downwelling UV-B irradiances at each nanometer are currently made using curve fitting techniques, and have come to be known as “synthetic spectra.” The synthetic spectra algorithm provides a functional form which may be used to approximate the spectral, downwelling UV-B irradiances at any wavelength within the wavelength range of the measurements. The current synthetic spectra algorithm, described in

Min and Harrison (1998) with updates by Davis and Slusser (2005), begins with a form of Beer's Law:

$$I_\lambda = I_{0,\lambda} \exp\left\{-\left(mX(\lambda) + C_1\lambda^{-1} + C_2\lambda^{-2} + C_3\lambda^{-3} + C_4\lambda^{-4}\right)\right\}, \qquad (8.11)$$

where I_0 and I are the extraterrestrial and surface spectral irradiance, respectively, at a wavelength λ, m is the atmospheric path, X is the optical depth due to ozone, and the constants C_i are determined by the fitting algorithm. When considering the method to determine the coefficients C_i, one of the first considerations is if the functional form is linear in the undetermined coefficients. In this case, the form requires a non-linear approach; in particular, the non-linear least squares approach of Levenberg and Marquardt is basically used as described in Press et al. (1992). Although taking the natural logarithm of the equation puts it in a form amenable to a linear fitting technique, it has been found through extensive testing at UVMRP, using many different functional representations of the term within the exponential, that the original non-linear form results in superior performance, particularly at the shorter wavelengths where much of the interest lies for agricultural research. Figure 8.8 shows an example of a synthetic spectrum obtained from combined UV and visible MFRSR measurements, and two important BSWFs: (1) the photosynthetically active region (PAR), and (2) the Flint BSWF region.

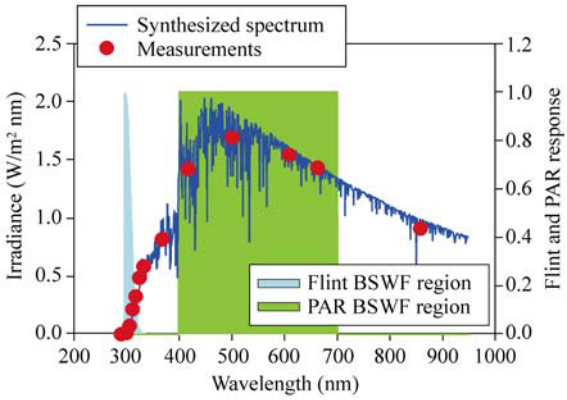

Figure 8.8 An example of a synthetic spectrum, along with the measurements from which it was derived, and the Flint and PAR BSWF regions over which the synthetic spectrum is integrated to produce agriculturally important indices. See Caldwell et al. (1986) for a discussion of the Flint BSWF

The synthetic spectrum has been applied to the data collected by UV-MFRSR instruments deployed at all US UVMRP climatological sites since 2000 to construct a database of daily sums of unweighted UV-A, unweighted UV-B, erythemal, vitamin D, and Flint and Caldwell indices. Figure 8.9 shows the annual average of the daily sum of unweighted UV-A irradiance for 2001 which was derived from

the database. The UVMRP website allows access to the daily sum database to the extent that the user is allowed to find averages of the daily sums over a user specified interval for any of the U.S. UVMRP sites.

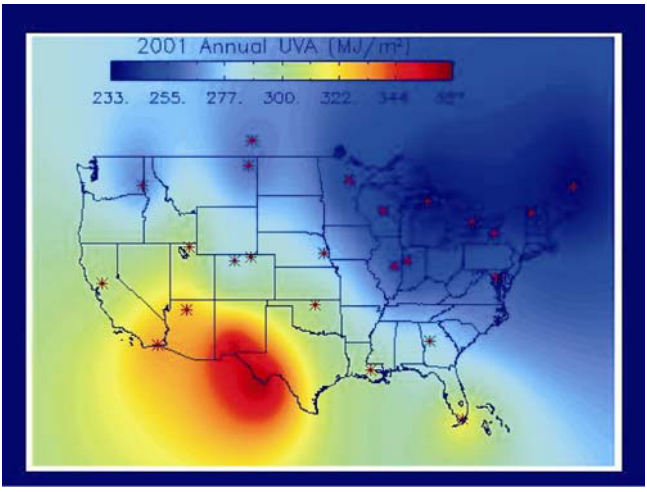

Figure 8.9 Contour map of 2001 annual accumulation of unweighted UV-A irradiance over the continental U.S. in MJ/m^2. The UVMRP station locations are identified by the red asterisks in the figure

8.6 Database Design and Website Interface

The primary objective of the UVMRP database and web design is to provide a user-friendly interface for an end user to search, view, and download data and related descriptions via the Internet. The interface was designed with the client/server paradigm. To prevent loss of data, backups are made with the use of tape, CD, and DVD, some of which are stored off site. The database containing the aforementioned measurements and derived data is implemented using the open source MySQL (DuBois, 2005). Structure Query Language (SQL) and open source Java Server Faces (JSF) are exploited to integrate different parts into this web accessible database. The database is updated daily when new measurements are collected. In this section, we briefly introduce the information that can be viewed and downloaded from the website, the database structure, and the website interface.

8.6.1 The Data

The information contained in the database can be classified into three categories: metadata, measurements, and derived data. As described in Table 8.4, metadata

include site information, instrument history at each site, calibration for each instrument/sensor, and documentation. Raw voltage measurements and calibrated data are recognized as measurements. Derived data are comprised of optical depths, column ozone, and synthetic spectra.

Table 8.4 The structure of the UV-B Database

Data in the UVMRP Database	
Meta Data	Description
Location information	Contains the geography of a location as well as internal location ID and phone number, if a phone line site
Tracking information	Contains the history of a particular instrument. Some instruments are rotated annually through the calibration facility and moved to a different location. A history of this information is maintained for special use
Calibration and angular correction data	All the calibration and angular correction data are stored in a table accessible by calibration date. The calibration factors are interpolated between starting and closing calibration data
Documentation	The quality control flags, historical instrument configurations, web interface error codes, meteorological events at locations, and users of the data are stored in a table to allow dynamic access and change to its structure
Measurements	Description
Raw voltage	Contains raw voltage measurements and quality control codes
Cosine corrected data	Contains cosine corrected data for UV-MFRSR and VIS-MFRSR instruments along with quality control codes
Calibrated data	Data used to calculate both lamp and Langley calibration are stored in tables but the actual calculation is done at the time of the data request
Derived Products	Description
Instantaneous optical depths	Time resolution of 3-min
Average optical depths	Morning and afternoon data
Column ozone	Contains daily column ozone
Synthetic Spectra	Data used to calculate synthetic spectra are stored in tables, but the actual calculation is performed at the time of the data request

To access the link for the data and derived data, go to the UVMRP website (http://uvb.nrel.colostate.edu/UVB). Click on the "Data Access" link at the top of the page where you will access the page shown in Fig. 8.10. On this page, the user can view or download the data desired by clicking on the corresponding self explanatory buttons located in the right hand column. The left hand column contains short descriptions about data from each category. Details regarding data processing and corrections are accessible through the links located at the bottom of the right hand column under "Quality Control."

Figure 8.10 Web interface of USDA UV-B Monitoring and Research Program database

8.7 UVMRP's Role in UV-B Agricultural Effects Studies

The previous sections describe UVMRP's monitoring activities and are limited to the physical aspects of UV radiation. In addition, UVMRP has played a role in the investigation of the biological response or "effects studies" of various plants and animals to UV-B and visible radiation. The goal of these studies is to evaluate the response of plants, forests, ecosystems, and animals to UV-B radiation and other climate stress factors. The program works with agricultural/forest researchers to evaluate the isolated effects of elevated UV-B on agricultural crops, livestock, forests, and range resources. Furthermore, it assesses the combined effects of UV-B radiation and other climate stress factors, such as moisture (drought), temperature, ozone, soil nutrients and CO_2. By understanding both compounding and antagonistic effects of multiple stress factors, the research will help develop solutions that

allow producers to cope with these detrimental effects and ensure quality and productivity for agriculture and livestock into the future. These studies provide a link between the knowledge of the climatology of UV-B radiation and the modeling of crop growth. The effects research is being conducted at a number of universities, and were directed and funded by UVMRP. Excerpts from this research are presented below:

At Colorado State University, Dr. Wei Gao, Dr. Heidi Steltzer, and Dr. Mathew Wallenstein evaluated the counteracting effects of UV-B radiation on litter decomposition. The study was conducted in a controlled greenhouse facility managed by Dr. Jack Morgan, USDA ARS, using aspen litter to determine if the effects of UV-B radiation on litter decomposition vary in relation to water availability and in response to suppressed biotic activity. The UVMRP designed and fabricated the UV-B lighting, control, and measurement hardware used in the study. Another CSU research scientist, Dr. Daniel Milchunas, conducted a three year study to evaluate the influence of UV-B on cattle rangeland grass decomposition and carbon storage. The UVMRP supplied UV-B monitoring instruments as well as data collection and processing services for this outdoor exclosure study.

Other examples of effects research are briefly described below, in no particular order. This list, however, is not meant to be exhaustive of all efforts associated with UVMRP. The work is separated according to the institution of the principal investigator of the study. For a more complete description of this work, the reader is directed to the citations given or to the UVMRP website.

8.7.1 Mississippi State University

Dr. K. Raja Reddy directs a group of researchers concerned with several phenomenological, growth, and physiological parameters influenced by UV-B radiation and other environmental factors. Studies of how UV-B and heat affect plants have been conducted so that cultivars better suited to high-temperature and high UV-B environments can be produced by breeders. Quantitative data on various growth and developmental processes were measured, and algorithms were developed for those processes. Ultraviolet radiation effect modules of crop growth under climate stress scenarios, such as higher temperatures and elevated CO_2 concentrations, have also been produced to incorporate the effects into models assessing the impact of climate change to assist producers and policy decision managers.

8.7.2 Purdue University

At Purdue University, Dr. Richard Grant and his colleagues conducted a number of empirical, field canopy, and greenhouse studies to determine the effects of

UV-B on various plants. Their work included determination of the response of soybean and sorghum to enhanced UV-B, and also its effect on biomass and its distribution. Particular emphasis was placed on the reaction of plant leaf physiology to the UV-B radiation. The group also studied the penetration of UV-B in oak-hickory forest, in a mature maize canopy and into the understory of a leafing-out deciduous forest. Model studies were performed on vegetation exposure, including that of Asian Soybean Rust, for a 3-day trajectory of an actual event in Iowa in September 2007.

8.7.3 Utah State University

Dr. Ron Ryel, Mr. Stephen Flint, and colleagues from Utah State University, combined numerous UV radiation related studies to determine and evaluate various UV-B and UV-A biological weighting functions. Weighted UV doses based on this and other work are routinely calculated and posted on the UVMRP website. Field experiments were conducted on Mauna Kea, HI at approximately 3000 m elevation to test the relative importance of the UV-B and UV-A wavebands under near ambient, no UV-B, and no UV-A or UV-B conditions.

8.7.4 University of Maryland

Dr. Joseph Sullivan (University of Maryland) and Dr. Stephen Britz (USDA Food Components and Health Lab, Beltsville, MD) conducted numerous field, greenhouse and growth chamber studies over the past eight years to determine responses of plants to UV-B radiation. A primary goal of their research was to understand the dose response (e.g., total energy absorbed) and wavelength response (e.g., impact of specific components of the solar spectrum) of plants in terms of damage, and the induction of protective mechanisms by sunlight. These studies, which are focused on important agricultural (e.g., soybean and barley) and forest (e.g., loblolly pine and hybrid poplar) species, utilized the high resolution UV data provided by UVMRP.

8.7.5 Washington State University

Dr. John Bassman and his colleagues conducted studies focused on the effects of enhanced UV-B on secondary chemistry in forage species, and the consequences for nutrition of specialist and generalist mammalian herbivores. The objectives of the studies were to: (1) determine the effects of enhanced solar UV-B radiation on

the concentration of key classes of secondary compounds from both the shikimate acid and mevalonic acid pathways in forage species with inherently different levels of these compounds; (2) identify selected key compounds of potential importance to herbivore nutrition where changes were significant; (3) quantify effects of enhanced UV-B on nutritional quality of these same forage species for a specialist and generalist mammalian herbivore through preference, intake and digestibility; and (4) relate changes in secondary plant chemistry to nutritional responses.

8.7.6 University of Illinois — Chicago

Dr. Katherine Warpeha and Dr. Lon Kaufman used a UVMRP UV-B light source in experiments designed to study the effects of UV-A and UV-B radiation on early development of soybean. The goals of the study were to: (1) quantify the effects of UV radiation on the early development of soybean and to help define ways to evaluate the effects of UV radiation; (2) evaluate the effects of UV radiation on the products of the phenylpropanoid pathway; and (3) initiate experiments to test stable transformation of young soybean seedlings with full length Prephenate Dehydratase1 (PD1) in order to determine if additional PD1 expression confers increased protection from UV radiation.

8.7.7 Highlights of Other Collaborations

In addition to the UVMRP sponsored and funded research efforts described in Sections 8.7.1 through 8.7.6, further research collaborations include:

Cornell University: Dr. Craig N. Austin has focused his research on how UV-B radiation affects the development of powdery mildew on the fruit and foliage of wine grape plants grown in the Finger Lakes Region of New York State. For two summers, the UVMRP supplied a portable UV-B monitoring instrument used in some components of the studies. The objectives of these studies were to: (1) determine the effects of shading versus direct sun exposure on the development of powdery mildew on both fruit and foliage, and investigate the possible mechanisms involved; (2) determine the degree of powdery mildew control provided by exposing fruit and foliage to sunlight via practices such as pruning, training, and leaf pulling; and (3) investigate the interaction of sun exposure and plant water status on powdery mildew development.

USDA Animal and Plant Health Inspection Service: For three consecutive winters from 2001 to 2004, the UVMRP supplied two UV monitoring stations to the USDA APHIS, Veterinary Services, National Animal Health Programs Wildlife Disease group to study the effect of UV radiation on brucellosis persistence in the

Yellowstone National Park ecosystem. The research on the transmission of this potentially devastating disease is a major priority which has involved federal and state agencies, animal health professionals, wildlife professionals and enthusiasts, and cattle ranchers in Montana and Wyoming. Preliminary findings from the study suggest that UV radiation plays a large role in the degradation of Brucella abortus. This finding suggests that continued monitoring of UV radiation levels could be an important tool in managing the disease.

Southern University: Responses of 35 tree species to UV-B radiation are being quantified by Dr. Yadong Qi.

University of California, Davis, Desert Research and Extension Service: Dr. Paul Sebesta is investigating the effect of UV-B and PAR in comparing sugarcane yields for ethanol production in Southern California, Louisiana, and Florida.

University of Nebraska at Lincoln: Dr. Elizabeth Walter-Shea and Dr. Kenneth Hubbard conducted investigations of UV radiation levels within vegetative canopies, and how these levels affect microoganisms.

8.8 Modeling of Agricultural Sustainability

In addition to the monitoring and the effects studies of UV radiation, the UVMRP conducts research on crop growth and production assessment modeling. The goal of the modeling work is to couple a regional climate forecasting model, such as the Climate version-Weather Research and Forecasting Model (CWRF), to crop growth models to assess the role of global climate change on future crop health and crop yields. The main thrust of this effort is to develop an Integrated Agricultural Impact Assessment System (IAIAS) in collaboration with a group at the University of Illinois, Urbana-Champaign, led by Dr. Xin-Zhong Liang. The goal of IAIAS is to develop an integrated system that fully couples the earth's climate, UV-visible solar radiation, and crop growth models, and assimilates satellite and in-situ observations to ultimately predict climate-crop interactions. This effort will facilitate model sensitivity studies thus providing credible information on crop responses to regional climate variability and changes for decision makers to determine optimal cultural practices, assess potential risks, and identify risk management strategies. The coupled model results can be directly validated with the UVMRP UV and PAR measurements, while offering a unique tool to predict crop life cycle processes over the entire U.S. The initial results of the coupled GOSSYM (a cotton growth model) and CWRF models are shown in Fig. 8.11, which displays modeled cotton yields that agree to within ±15% of actual yields at most sites for the 27 years of data accumulated over the entire 14-state region of the Cotton Belt.

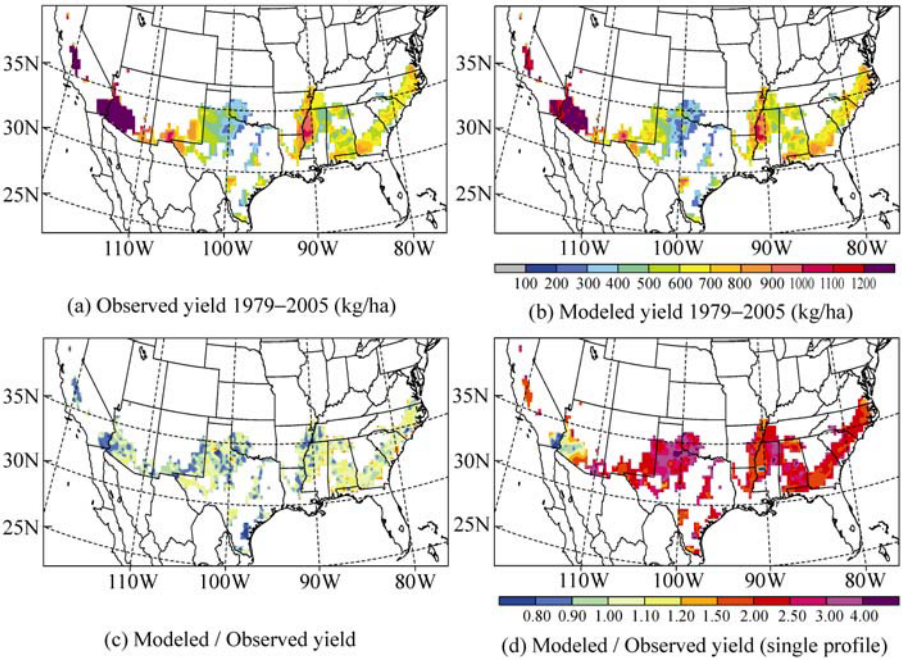

Figure 8.11 Comparison of the long-term observed average of cotton yield in the 14-state Cotton Belt region and that predicted by the coupled GOSSYM-CWRF model. Geographic distributions of the 1979 – 2005 mean cotton yields (kg ha^{-1}): (a) observed and (b) simulated by the new GOSSYM; and of the ratios for the mean cotton yields over observations as simulated by (c) the new and (d) original GOSSYM

8.9 Future Considerations

The USDA UVMRP is constantly reviewing its research goals and evaluating the needs expressed by the stakeholders in USDA research. Although fiscal years 2007, 2008 and 2009 saw budget reductions, the activities at UVMRP are ongoing in a manner as to consistently respond to the needs of the agricultural research community in the best possible manner.

With an eye toward the future, UVMRP also collaborates with developers of UV products from satellite observations. While satellite platforms have a more restrictive temporal sampling program, they offer superior geographic coverage. One challenge to the satellite community is that retrieval of surface UV irradiance requires correction for presence of clouds and aerosols. As an example of how well satellite data can be used at a particular site, data from NASA's CERES SYNI (Clouds and the earth's Radiant Energy System, SYNoptic Interpolated) program is shown in Fig. 8.12. The retrieved UV-A irradiances compare with UV-A irradiance derived from the UVMRP synthetic spectrum to within 0.6 watts/m^2 in the mean with an RMS difference of 5.6 watts/m^2 for this particular case.

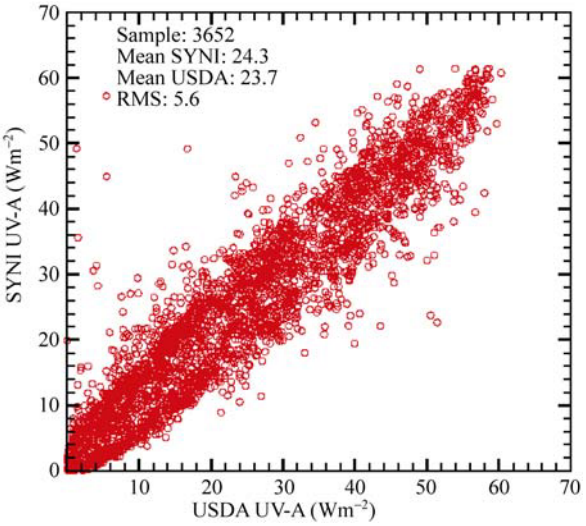

Figure 8.12 Satellite retrieved values of unweighted UV-A total horizontal irradiance compared to the same quantities deduced from a synthetic spectrum fit to UV-MFRSR data measured at the DOE Atmospheric Radiation Monitoring Program's Southern Great Plains site near Ponca City, OK during July 2002 (satellite retrieved data provided by NASA CERES SYNI effort)

Conversely, as an example of the spatial coverage provided by the USDA UVMRP network, the UV Index from the Total Ozone Mapping Spectrometer (TOMS) is compared to gridded values from the UVMRP values (Gao et al., 2009) averaged over the summers from 2000 through 2004. Figure 8.13 shows two examples that demonstrate the level of agreement between the surface and satellite monitoring communities, and lends hope that resources may be focused between the two efforts in obtaining higher quality products useful to agricultural, medical, industrial and meteorological researchers.

8.10 Summary

This chapter has described the data and products of the USDA UVMRP. These datasets are available to the public and can be accessed via the Internet. The monitoring network consists of 37 observation sites covering the continental U.S., along with coverage of Alaska and Hawaii, southern Canada, and southern New Zealand. Multifilter Shadowband Rotating radiometers are deployed to make spectral irradiance measurements in the UV and visible wavelength regions. The erythemally weighted UV radiation is measured by broadband pyranometers. The PAR is also measured for use in agricultural research. The program has been providing quality UV-B radiation data to researchers throughout the agricultural, medical, industrial, and atmospheric research communities since 1993. The primary

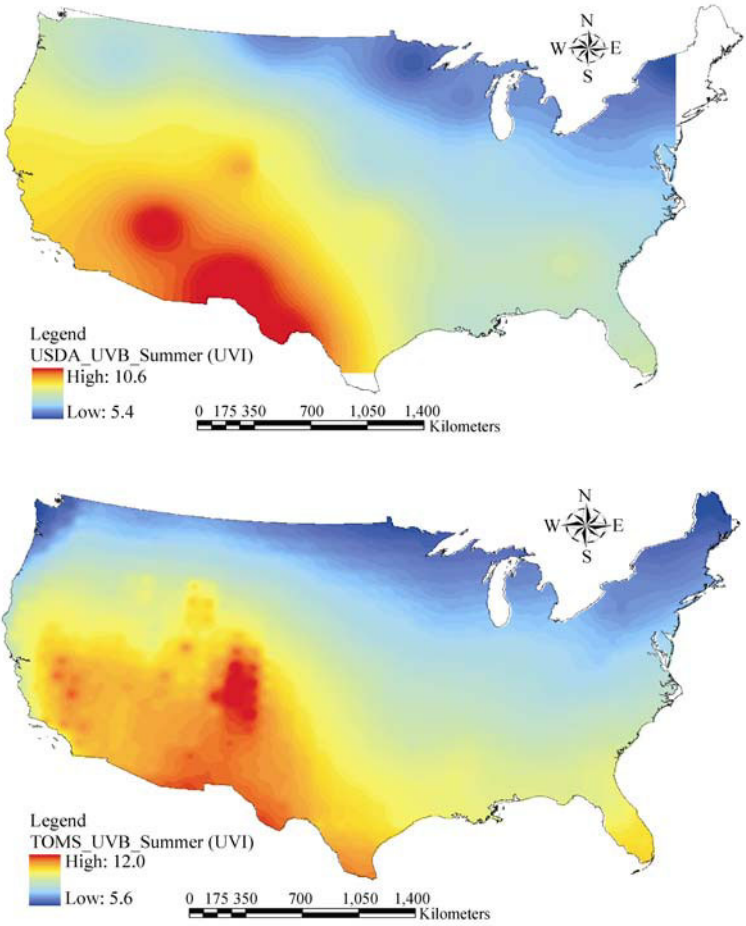

Figure 8.13 Comparison of the UV index from USDA UVMRP (top) averaged over the summers of 2000 – 2004 and the same quantity from NASA TOMS (bottom) as reported in Gao et al. (2009). The UVMRP UV indices span from 5.4 to 9.0 while the TOMS values range from 5.6 to 12.0

raw voltage measurements are available by special request. With our research in instrumentation, correction techniques, system stability, and statistical analysis, high quality calibrated data have been produced as second level products. These data furnish researchers in agriculture, ecology, environment, meteorology, human health, and related specialties with valuable information not available elsewhere. Based on our research results, optical depths, daily column ozone, and synthetic spectra are derived using spectral UV-B measurements, plus spectral irradiances in the visible region. The USDA UVMRP receives numerous requests for its products from researchers in agriculture, atmospheric monitoring, human and animal health, and industrial product quality concerns. The UVMRP is collaborating with the broader scientific community, with an eye toward the future, to focus its activities

and resources to best serve the needs of researchers across a wide spectrum of scientific and social activities.

Acknowledgements

The USDA UVMRP was sponsored during 2007 – 2008 by USDA CSREES under Hatch/Multistate, Contract Number: COL-00-250-W502 and during 2006 – 2007 by USDA CSREES under Contract Number: 2006-34263-16926. The UVMRP effort would not have been possible without the contributions of its staff: Ms. Becky Olson, Mr. Scott Janssen, Mr. Bill Durham and Ms. Rita Deike. A special appreciation is extended to Mr. George Janson for final editing and compilation of figures and to Dr. Xinli Wang for his assistance in the initial drafts of this chapter.

References

Barkstrom BR (1984) The Earth Radiation Budget Experiment (ERBE). Bull. Amer. Meteor. Soc. 65:1170 – 1185

Bassman JH (2004) Ecosystem consequences of enhanced solar ultraviolet radiation: secondary plant metabolites as mediators of multiple trophic interactions in terrestrial plant communities. Photochemistry and Photobiology 79(5): 382 – 398

Bigelow DS, Slusser JR, Beaubien AF, and Gibson JH (1998) The USDA Ultraviolet Radiation Monitoring Program. Bulletin of the American Meteorological Society 79(4): 601 – 615

Bigelow DS, and Slusser JR (2000) Establishing the stability of multifilter UV rotating shadow-band radiometers. Journal of Geophysical Research 105(D4): 4833 – 4840

Blumthaler M, and Ambach W (1990) Indication of increasing solar ultraviolet-B radiation flux in Alpine regions. Science 248(4952): 206 – 208

Bodhaine BA, Dutton EG, McKenzie RL, and Johnston PV (1998) Calibrating broadband UV instruments: ozone and solar zenith angle dependence. Journal of Atmospheric and Oceanic Technology 15(4): 916 – 926

Bodhaine BA, Wood NB, Dutton EG, and Slusser JR (1999) On Rayleigh optical depth calculations. Journal of Atmospheric and Oceanic Technology 16: 1854 – 1861

Bredahl L, Ro-Poulsen H, and Mikkelsen TN (2004) Reduction of the ambient UV-B radiation in the high-arctic increases F_v/F_m in *salix arctica* and *vaccinium uliginosum* and reduces stomatal conductance and internal CO_2 concentration in *salix arctica*. Arctic, Antarctic, and Alpine Research 36(3): 364 – 369

Bucholtz A (1995) Rayleigh-scattering calculations for the terrestrial atmosphere. Applied Optics 34(15): 2765 – 2773

Caldwell MM, Camp CW, Warner CW, and Flint SD (1986) Action spectra and their role in assessing biological consequences of solar UV-B radiation change. In: Worrest RC, Caldwell MM (eds) Stratospheric Ozone Reduction, Solar Ultraviolet Radiation and Plant Life. Springer-Verlag, pp.87 – 111

Caldwell MM, Ballaré CL, Bornman JF, Flint SD, Björn LO, Teramura AH, Kulandaivelu G, and Tevini M (2003) Terrestrial ecosystems, increased solar ultraviolet radiation and interactions with other climatic change factors. Photochemical and Photobiological Sciences 2(1): 29 – 38

Clarke A, and Harris CM (2003) Polar marine ecosystems: major threats and future change. Environmental Conservation 30(1): 1 – 25

Davis JM, and Slusser J (2005) New USDA UVB synthetic spectra algorithm. In: Bernhard G, Slusser JR, Herman JR, Gao W (eds) Ultraviolet Ground- and Space-Based Measurements, Models, and Effects V. Proceedings of SPIE Vol. 5886 (SPIE, Bellingham, WA, 2005), pp. 58860B-1-58860B-7

Disterhoft P (2005) Stability characteristics of 1000 watt FEL-type QTH lamps during the seasoning and screening process. In: Bernhard G, Slusser JR, Herman JR, Gao W (eds) Ultraviolet Ground- and Space-based Measurements, Models, and Effects V, Proceedings of SPIE Vol 5886, SPIE, 58860G

DuBois Paul (2005) MySQL™ The definitive guide to using, programming, and administering MySQL 4.1 and 5.0, Third Edition. Sams Publishing, Indianapolis, IN, USA

Early E, Thompson A, Johnson C, DeLuisi J, Disterhoft P, Wardle D, Wu E, Mou W, Sun Y, Lucas T, Mestechkina T, Harrison L, Berndt J, and Hayes DS (1998a) The 1995 North American interagency intercomparison of ultraviolet monitoring spectroradiometers. Journal of Research of the National Institute of Standards and Technology 103(1): 15 – 62

Early E, Thompson A, Johnson C, DeLuisi J, Disterhoft P, Wardle D, Wu E, Mou W, Ehramjian J, Tusson J, Mestechkina, Beaubian M, Gibson J, and Hayes D (1998b) The 1996 North American interagency intercomparison of ultraviolet monitoring spectroradiometers. Journal of Research of the National Institute of Standards and Technology 103(5): 449 – 482

Farman JC, Gardiner BG, and Shanklin JD (1985) Large losses of total ozone in Antarctica reveal seasonal ClO_x/NO_x interaction. Nature 315: 207 – 210

Flint SD, Ryel RJ, and Caldwell MM (2003) Ecosystem UV-B experiments in terrestrial communities: a review of recent findings and methodologies. Agricultural and Forest Meteorology 120: 177 – 189

Frederick JE, and Snell HE (1988) Ultraviolet radiation levels during the Antarctic spring. Science 241(4864): 438 – 440

Fröhlich C, and Shaw GE (1980) New determination of Rayleigh scattering in the terrestrial atmosphere. Applied Optics 19(11): 1773 – 1775

Gao W, Slusser J, Gibson J, Scott G, Bigelow D, Kerr J, and McArthur B (2001) Direct-Sun column ozone retrieval by the ultraviolet multifilter rotating shadow-band radiometer and comparison with those from Brewer and Dobson spectrophotometers. Applied Optics, 40(19): 3149 – 3155

Gao W, Grant RH, Heisler GM, and Slusser JR (2002) A geometric ultraviolet-B radiation transfer model applied to vegetation canopies. Agronomy Journal 94: 475 – 482

Gao W, Grant RH, Heisler GM, and Slusser JR (2003) UV-B radiation in a row-crop canopy: An extended 1-D model. J. Agric. Forest Meteorol. 120: 141 – 151

Gao W, Gao ZQ, and Chang NB (2009) Comparative analysis of UVB exposure between Nimbus 7/TOMS satellite estimates and ground-based measurements. In: Gao W, Schmoldt D,

Slusser JR (eds) UV Radiation in Global Change: Measurements, Modeling and Effects on Ecosystems. Springer-Verlag and Tsinghua Univ. Press

Gibson JH (ed) (1991) Justification and criteria for the monitoring of ultraviolet (UV) radiation: Report of UV-B measurements workshop (URL: http://uvb.nrel.colostate.edu/UVB/publications/91_workshop.pdf)

Gibson JH (1992) Criteria for status-and-trends monitoring of ultraviolet (UV) radiation: Recommendations of the UV-B Monitoring Workshop (URL: http://uvb.nrel.colostate.edu/UVB/publications/92_report.pdf)

Grainger RG, Basher RE, and McKenzie RL (1993) UV-B Robertson-Berger meter characterization and field calibration. Applied Optics 32(3): 343 – 349

Grant RH (1999) Potential effect of soybean heliotropism on ultraviolet-B irradiance and dose. Agronomy Journal 91: 1017 – 1023

Grant WB (1988) Global stratospheric ozone and UVB radiation. Science 242(4882): 1111

Gröbner J, Blumthaler M, and Ambach W (1996) Experimental investigation of spectral global irradiance measurement errors due to a non ideal cosine response. Geophysical Research Letters 23(18): 2493 – 2496

Hand JL, Kreidenweis SM, Slusser J, and Scott G (2004) Comparisons of aerosol optical properties derived from Sun photometry to estimates inferred from surface measurements in Big Bend National Park, Texas. Atmospheric Environment 38: 6813 – 6821

Harrison L, and Michalsky J (1994) Objective algorithms for the retrieval of optical depths from ground-based measurements. Applied Optics 33(22): 5126 – 5132

Harrison L, Michalsky J, and Berndt J (1994) Automated multifilter rotating shadow-band radiometer: an instrument for optical depth and radiation measurements. Applied Optics 33(22): 5118 – 5125

Herman JR, Bhartia PK, Ziemke J, Ahmad Z, and Larko D (1996) UV-B increases (1979 – 1992) from decreases in total ozone. Geophysical Research Letters 23(16): 2117 – 2120

Janson GT, Slusser JR, Scott G, Disterhoft P, and Lantz K (2004) Long-term stability of UV multifilter rotating shadowband radiometers, part 2: lamp calibrations versus the Langley method. In: Slusser JR, Herman JR, Gao W, Bernhard G (eds) Ultraviolet Ground- and Space-based Measurements, Models, and Effects IV. Proceedings of SPIE Vol 5545, SPIE, 43 – 48

Jaque F, Tocho JO, DaSilva LF, Bertuccelli G, Crino E, Cusso F, DeLaurentis MA, Hormaechea JL, Lifante G, Nicora MG, Ranea-Sandoval HF, Valderrama V, and Zoja GD (1994) Ground-based ultraviolet radiation measurements during springtime in the southern hemisphere. Europhysics Letters, 28(4): 289 – 293

Kakani VG, Reddy KR, Zhao D, and Sailaja K (2003) Field crop responses to ultraviolet-B radiation: a review. Agricultural and Forest Meteorology 120: 191 – 218

Kerr JB (2005) Understanding the factors that affect surface ultraviolet radiation. Optical Engineering, 44(4): 041002-1 – 041002-9

Kerr JB, and McElroy CT (1993) Evidence for large upward trends of ultraviolet-B radiation linked to ozone depletion. Science 262(5136): 1032 – 1034

Kulandaivelu G, and Tevini M (2003) Terrestrial ecosystems, increased solar ultraviolet radiation and interactions with other climatic change factors. Photochemical and Photobiological Sciences 2(1): 29 – 38

Landelius T, and Josefsson W (2000) Methods for cosine correction of broadband UV data and their effect on the relation between UV irradiance and cloudiness. Journal of Geophysical Research 105(D4): 4785 – 4802

Lantz KO, Disterhoft P, DeLuisi JJ, Early E, Thompson A, Bigelow D, and Slusser J (1999) Methodology for deriving clear-sky erythemal calibration factors for UV broadband radiometers of the U.S. Central UV Calibration Facility. Journal of Atmospheric and Oceanic Technology 16: 1736 – 1752

Lantz K, Disterhoft P, Early E, Thompson A, DeLuisi J, Berndt J, Harrison L, Kiedron P, Ehramjian J, Bernhard G, Cabasug L, Robertson J, Mou W, Taylor T, Slusser J, Bigelow D, Durham B, Janson G, Hayes D, Beaubien M, and Beaubien A (2002) The 1997 North American interagency intercomparison of ultraviolet spectroradiometers including narrowband filter radiometers. Journal of Research of the National Institute of Standards and Technology 107(1): 19 – 62

Lantz K, Disterhoft P, Wilson C, Janson G, Slusser J, Bloms S, and Michalsky J (2005) Out-of-band rejection studies of the UV Multi-Filter Rotating Shadow-band radiometers. In: Schäfer K, Comerón A, Slusser JR, Picard RH, Carleer MR, Sifakis N (eds) Remote Sensing of Clouds and the Atmosphere X, Proceedings of SPIE Vol 5979, SPIE, 59791N

Lean J (1991) Variations in the Sun's radiative output. Reviews of Geophysics 29: 505 – 535

Lean JL, Rottman GJ, Kyle HL, Woods TN, Hickey JR, and Puga LC (1997) Detection and parameterization of variations in solar mid- and near-ultraviolet radiation (200 nm – 400 nm). Journal of Geophysical Research 102 (D25): 29939 – 29956

Leszczynski K, Jokela K, Ylianttila L, Visuri R, and Blumthaler M (1998) Erythemally weighted radiometers in solar UV monitoring: results from the WMO/STUK intercomparison. Photochemistry and Photobiology, 67(2): 212 – 221

Li Y, Yue M, and Wang XL (1998) Effects of enhanced ultraviolet-B radiation on crop structure, growth and yield components of spring wheat under field conditions. Field Crops Research 57(3): 253 – 263

LI-COR, Inc. (1991) LI-COR Terrestrial Radiation Sensors, Type SA Instruction Manual. LI-COR, Lincoln, NE, USA

Marggraf WA, and Griggs M (1969) Aircraft measurements and calculations of the total downward flux of solar radiation as a function of altitude. Journal of the Atmospheric Sciences 26: 469 – 476

Mayer B, and Seckmeyer G (1996) All-weather comparison between spectral and broadband (Robertson-Berger) UV measurements. Photochemistry and Photobiology 64(5): 792 – 799

McKenzie R, Bodeker G, Scott G, Slusser J, and Lantz K (2006) Geographical differences in erythemally-weighted UV measured at mid-latitude USDA sites. Photochemical and Photobiological Sciences (5): 343 – 352

McKenzie RL, Aucamp PJ, Bais AF, Björn LO, and Ilyas M (2007) Changes in biologically-active ultraviolet radiation reaching the Earth's surface. Photochemical and Photobiological Sciences 6(3): 218 – 231

McKinlay AF, and Diffey BL (1987) A reference action spectrum for ultraviolet induced erythema in human skin. CIE-Journal 6(1): 17 – 22

Michalsky JJ, Perez R, Stewart R, LeBaron BA, and Larrison L (1988) Design and development of a rotating shadowband radiometer solar radiation/daylight network. Solar Energy 41(6): 577 – 581

Michalsky JJ, Harrison LC, and Berkheiser WE III (1995) Cosine response characteristics of some radiometric and photometric sensors. Solar Energy 54(6): 397 – 402

Min Q, and Harrison LC (1998) Synthetic spectra for terrestrial ultraviolet from discrete measurements. Journal of Geophysical Research 103(D14): 17033 – 17039

Newchurch MJ, Yang E-S, Cunnold DM, Reinsel GC, Zawodny JM, and Russell JM III (2003) Evidence for slowdown in stratospheric ozone loss: First stage of ozone recovery. Journal of Geophysical Research 108(D16): 4507, DOI:10.1029/2003JD003471

O'Hara F, and O'Hara L (eds) (1993) Report. UV-B Critical Issue Workshop, Cocoa Beach, FL, Center for Global and Environmental Studies, Oak Ridge National Laboratory

Press WH, Teukolsky SA, Vetterling WT, and Flannery BP (1992) Numerical Recipes in C: the art of scientific computing. Second Edition, Cambridge University Press

Reddy KR, Kakani VG, Zhao D, Mohammed AR, and Gao W (2003) Cotton responses to ultraviolet-B radiation: experimentation and algorithm development. Agricultural and Forest Meteorology 120: 249 – 265

Reinsel GC, Miller AJ, Weatherhead EC, Flynn LE, Nagatani RM, Tiao GC, and Wuebbles DJ (2005) Trend analysis of total ozone data for turnaround and dynamical contributions. Journal of Geophysical Research 110:D16306, DOI:10.1029/2004JDD004662

Rozema J, van de Staaij J, Björn LO, and Caldwell M (1997) UV-B as an environmental factor in plant life: stress and regulation. Trends in Ecology and Evolution 12(1): 22 – 28

Schmid B, and Wehrli C (1995) Comparison of Sun photometer calibration by use of the Langley technique and the standard lamp. Applied Optics 34(21): 4500 – 4512

Schmid B, Spyak PR, Biggar SF, Wehrli C, Sekler J, Ingold T, and Mämpfer N (1998) Evaluation of the applicability of solar and lamp radiometric calibrations of a precision Sun photometer operating between 300 nm and 1025 nm. Applied Optics 37(18): 3923 – 3941

Science and Policy Associates (1992) Report. UV-B Monitoring Workshop: A review of the science and status of measuring and monitoring programs, Washington, DC, Science and Policy Associates, Inc

Scotto J, Cotton G, Urbach F, Berger D, and Fears T (1988) Biologically effective ultraviolet radiation: surface measurements in the United States, 1974 to 1985. Science 239(4841): 762 – 764

Seckmeyer G, Bais AF, Bernhard G, Blumthaler M, Booth CR, Lantz RL, McKenzie RL, Disterhoft P, and Webb A (2007) Instruments to measure solar ultraviolet radiation. Part 2: Broadband instruments measuring erythemally weighted solar irradiance. WMO/GAW No. 164, World Meteorological Organization, Geneva

Shaw GE (1982) Solar spectral irradiance and atmospheric transmission at Mauna Loa Observatory. Applied Optics 21(11): 2006 – 2011

Shettle EP, and Anderson SM (1995) New visible and near IR ozone absorption cross-sections from MODTRAN. In: Anderson GP, Picard RH, Chetwynd JH (eds) Proceedings of the 17th Annual Review Conference on Atmospheric Transmission Models, Phillips Laboratory, Directorate of Geophyiscs, Hanscom Air Force Base, MA, pp. 335 – 345

Slusser J, Gibson J, Bigelow D, Kolinski D, Disterhoft P, Lantz K, and Beaubien A (2000) Langley method of calibrating UV filter radiometers. Journal of Geophysical Research 105(D4): 4841 – 4849

Smith RC, Préselin BB, Baker KS, Bidigare RR, Boucher NP, Coley T, Karentz D, MacIntyre S, Matlick HA, Menzies D, Ondrusek M, Wan Z, and Waters KJ (1992) Ozone depletion: ultraviolet radiation and phytoplankton biology in Antarctic Waters. Science 255(5047): 952 – 959

Staehelin J, Harris NRP, Appenzeller C, and Eberhard J (2001) Ozone trends: A review. Reviews of Geophysics 39(2): 231 – 290

Stephens GL (1994) Remote Sensing of the Lower Atmosphere: An Introduction. Oxford University Press, New York, p. 253

Stolarski R, Bojkov R, Bishop L, Zerefos C, Staehelin J, and Zawodny J (1992) Measured trends in stratospheric ozone. Science, 256(5055): 342 – 349

Tegelberg R, Aphalo PJ, and Julkunen-Tiitto R (2002) Effects of long-term, elevated ultraviolet-B radiation on phytochemicals in the bark of silver birch (*Betula pendula*). Tree Physiology 22: 1257 – 1263

Teillet PM (1990) Rayleigh optical depth comparisons from various sources. Applied Optics 29(13): 1897 – 1900

Teramura AH, Sullivan JH, and Ziska LH (1990) Interaction of elevated ultraviolet-B radiation and CO_2 on productivity and photosynthetic characteristics in wheat, rice, and soybean. Plant Physiology 94: 470 – 475

Thomason LW, Herman BM, and Reagan JA (1983) The effect of atmospheric attenuators with structured vertical distributions on air mass determinations and Langley plot analyses. Journal of the Atmospheric Sciences 40(7): 1851 – 1854

Turtola S, Rousi M, Pusenius J, Yamaji K, Heiska S, Tirkkonen V, Meier B, and Julkunen-Tiitto R (2005) Clone-specific responses in leaf phenolics of willows exposed to enhanced UVB radiation and drought stress. Global Change Biology 11: 1655 – 1663

Vijayaraghavan S, and Goswami DY (2002) On the calibration of a solar UV radiometer to measure broadband UV radiation from blacklight lamps. Journal of Solar Energy Engineering 124: 317 – 319

Warren JM, Bassman JH, Fellman JK, Mattinson DS, and Eigenbrode S (2003) Ultraviolet-B radiation alters phenolic salicylate and flavonoid composition of *Populus trichocarpa* leaves. Tree Physiology 23: 527 – 535

Wilson SR, and Forgan BW (1995) *In situ* calibration technique for UV spectral radiometers. Applied Optics 34(24): 5474 – 5484

WMO (World Meteorological Organization) (1989) Scientific Assessment of Stratospheric Ozone: 1989. Global Ozone Research and Monitoring Project. Vol. 1, Report No. 20, World Meteorological Organization, Geneva

WMO (2007) Scientific Assessment of Ozone Depletion: 2006. Global Ozone Research and Monitoring Project. Report No. 50, p.572, Geneva, Switzerland

Worrest RC, Smythe KD, and Tait AM (1989) Linkages between climate change and stratospheric ozone depletion. In: White JC (ed) Global Climate Change Linkages, Acid Rain, Air Quality and Stratospheric Ozone. Elsevier Science, pp.67 – 78

Xu G, and Huang X (2000) Characterization and calibration of broadband ultraviolet radiometers. Metrologia 37: 235 – 242

Xu G, and Huang X (2003) Calibration of broadband UV radiometers — methodology and uncertainty evaluation. Metrologia 40: S21 – S24

Yankee Environmental Systems, Inc. (2000) UVB-1 Ultraviolet Pyranometer Installation and User Guide, Version 2.0

Young AT (1981) On the Rayleigh-scattering optical depth of the atmosphere. Journal of Applied Meteorology 20: 328 – 330

9 Radiative Transfer in the Coupled Atmosphere-Snow-Ice-Ocean (CASIO) System: Review of Modeling Capabilities

Knut Stamnes[1], Børge Hamre[2], and Jakob J. Stamnes[2]

[1] Light and Life Laboratory, Department of Physics and Engineering Physics, Stevens Institute of Technology, Hoboken, NJ 07030, USA
E-mail: Knut.Stamnes@stevens.edu
[2] Department of Physics and Technology, University of Bergen, Postboks 7800, 5020 Bergen, Norway
E-mail: Børge.Hamre@ift.uib.no
E-mail: Jakob.Stamnes@ift.uib.no

Abstract A review is provided of ultraviolet (UV) and visible radiative transfer in an atmosphere-sea-ice-ocean system with emphasis on the basic physical principles involved rather than on mathematical/numerical techniques. To illustrate the application of the theory, a few examples are provided. First, we provide a comparison of two different models for radiation penetration into the open ocean, which for a given set of input parameters give identical results. Thus, for a stratified atmosphere-ocean system, our ability to model the transfer of UV radiation and visible light appears to be limited as much by reliable information about the inherent optical properties of marine constituents as by our ability to accurately solve the radiative transfer equation. Second, we discuss a comparison between measured and modeled radiative transfer results in an atmosphere-sea ice-ocean system, which reveals that accurate transmittances as well as accurate values for the radiative energy deposition versus depth can be calculated. Third, we review results of a study showing that multiple scattering in a highly scattering medium such as sea ice gives rise to a marked enhancement of the downward irradiance across the atmosphere-sea ice interface. Finally, we review a recent study in which the modeled radiation field is used to illustrate how the primary production in icy polar waters might be influenced by an ozone depletion. Contrary to previous investigations, this study reveals that a 50% ozone depletion might lead to an increase (~1%) rather than a decrease in primary productivity.

Keywords UV radiation modeling, photolysis, actinic flux, atmospheric warming/cooling rates, UV radiation in aquatic systems

9.1 Introduction

The bulk of the earth's atmosphere (99% by mass) consists of molecular nitrogen and oxygen, which are homonuclear, diatomic molecules that absorb little radiation at wavelengths in the UV and visible spectral ranges. Trace amounts of polyatomic molecules including ozone are responsible for atmospheric absorption. In recent years, ozone loss has been tied to the release of man-made trace gases, mainly chlorofluorocarbons used in the refrigeration industry and as propellants in spray cans. Because ozone provides an effective shield against harmful UV solar radiation, a thinning of the ozone layer due to release of man-made trace gases (Solomon, 1990; Anderson et al., 1991) could have serious biological ramifications (Slaper et al., 1995; Herman et al., 1996; Zerefos and Bais, 1997; Herman et al., 1999).

UV radiation (280 nm – 400 nm) and visible solar radiation determine the concentration of *photochemically active* species through the process of *photolysis*, in which molecules are split up into atoms and smaller molecules. Here we assume for convenience that visible radiation is approximately equal to photosynthetically active radiation (PAR, 400 nm – 700 nm). Ozone is formed when an oxygen atom (O) and an oxygen molecule (O_2) combine to yield O_3. Chemical reactions and photolysis are responsible for the destruction of atmospheric ozone. The bulk content of the ozone gas residing in the stratosphere is determined by a balance between these production and loss processes.

UV radiation penetrating to the troposphere and surface is customarily divided into two spectral ranges: UV-B (280 nm – 320 nm) and UV-A (320 nm – 400 nm). Living organisms are much more susceptible to damage by UV-B radiation than by the more benign UV-A radiation. Fortunately, UV-B radiation is very effectively absorbed by ozone, and therefore very sensitive to the total column amount of O_3.

As a result of stratospheric ozone depletion, UV-B radiation (280 nm – 320 nm) is likely to increase and have adverse effects on both individual marine organisms and marine ecosystems (Worrest, 1986; Holm-Hansen et al., 1993a; Cullen and Neale, 1994; Prézelin et al., 1994; Häder et al., 1998), because UV-B radiation can penetrate to ecologically significant depths in the ocean (Smith and Baker, 1989; Zeng et al., 1993). Many marine organisms are sensitive to UV-B radiation, and it remains uncertain whether or not they will be able to adapt to increases in UV-B radiation exposure (Karentz et al., 1991; 1992). Numerous investigations (Calkins and Thordardottir, 1980; Worrest, 1986; Smith et al., 1992; Holm-Hansen et al., 1993b, Wängberg et al., 1999) have provided indications that UV-B radiation influences phytoplankton productivity. Calkins and Thordardottir (1980) argued that UV radiation is a significant ecological factor, and Jokiel and York (1984) linked long-term growth inhibition to UV radiation. Worrest (1986) found that acute exposure to UV-B radiation significantly depressed primary productivity. Damaging effects on other metabolic processes of phytoplankton and microorganisms have been studied by several groups (Döhler, 1985; Neale et al., 1993; Goes et al., 1995), and recent studies have included effects of UV radiation on pigments and

assimilation of inorganic nitrogen (Döhler and Hagmeier, 1997; Lobman et al., 1998).

Penetration of UV radiation and visible light in the ocean is strongly influenced by small plankton and thus, by biological productivity which provides a close link between biological and optical oceanography (Smith and Baker, 1989). Important aspects of the ozone depletion issue include the effects of increased UV radiation levels on algae, plankton, and fish larvae. Due to air-sea ventilation of dimethylsulfide (DMS), atmospheric sulfur compounds depend on the net production of DMS in the water column, and UV radiation photolysis of DMS represents an important removal process (Deal et al., 2005). Thus, since sources of atmospheric sulfur compounds are involved in cloud formation, the abundance of algae may indirectly affect atmospheric transmission, thereby linking atmospheric radiative transfer with ocean biology.

Major gaps in our present knowledge maybe illustrated by the following questions:

1. Which scattering and absorption agents of biogenic and non-biogenic origin are responsible for the scattering and absorption of UV radiation and visible light in the water column?
2. To what extent are current radiative transfer models able to predict the spectral UV radiation and visible light as a function of depth in the water column?
3. To what extent are current radiative transfer models able to predict the UV and visible spectral radiances emanating from the water column (the so-called water-leaving radiance), and transmitted to the top of the atmosphere?
4. What measurements are needed to test models of radiative transfer in an atmosphere-ocean system that includes an aerosol-loaded or cloudy atmosphere overlying open oceanic water or bodies of turbid water, such as lakes, rivers, and estuarine coastal waters?
5. What light measurements and modeling activities are required to validate remote sensing efforts aimed at characterizing biological productivity of water in the world's oceans as well as water quality of lakes, rivers, and estuarine coastal waters?
6. What is the minimum and what is the ideal number of spectral elements that need to be recorded by remote sensing instruments in order to accurately retrieve water properties in different water regimes?

Questions 1 and 2 are important because they are relevant to our basic understanding of the main drivers of biology in aquatic systems: the UV radiation and visible light fields. Lack of, or an incomplete understanding of, how UV radiation and visible light fields vary in an aquatic ecosystem, and how they relate to scattering and absorption properties of the water constituents, is a major obstacle to the prediction of how an aquatic ecosystem will function in a changing environment, e.g., how it will respond to expected changes, including global warming and ozone depletion. Attempts to assess the impact of UV radiation penetration on aquatic ecosystems have been made by several investigators as discussed by Häder et al. (1998), and efforts are currently underway to address

the effect of stratospheric ozone variations on underwater UV irradiances on a global scale (Vasilkov et al., 2001) by making use of data from the Total Ozone Mapping Spectrometer and the Sea-viewing Wide Field-of-view Sensor (SeaWiFS).

Questions 3 − 6 must be addressed if we are to use the radiation reflected from the atmosphere-ocean system to retrieve information about biological productivity and water quality. The spectral dependence of the water-leaving radiance (i.e., the ocean color) carries information about the optical properties of the water column. If we know how these wavelength (color) dependent optical properties depend on the water constituents, we are in a position to retrieve important information about atmospheric parameters (e.g., aerosol type and optical depth) and marine parameters (e.g., concentrations of chlorophyll, dissolved and particulate organic matter, and suspended inorganic material) from measured water-leaving radiances (Stamnes et al., 2003; Li et al., 2008). Soil material, as well as man-made chemicals and agricultural fertilizing agents, are frequently transported into coastal and estuarine waters by rivers. Knowledge of how the optical properties of water are affected by such river discharges could be used to determine water quality if reliable models were available that related optical properties to water constituents of natural and anthropogenic origin. However, the retrieval of water-leaving radiances from measurements obtained with instruments deployed on earth-orbiting satellites requires accurate removal of the atmospheric component of measured radiances. This task is very difficult because the atmospheric aerosol optical properties vary rapidly, both spatially and temporally. The difficulty is compounded by the fact that 90% of the signal measured by downward-looking sensors in space comes from the atmosphere (Gordon, 1997), which means that accurate removal of the highly varying atmospheric contribution to a measured radiance becomes crucially important.

We start by providing a brief review of how UV radiation and visible light propagate throughout an atmosphere-ocean system. Then we give a few examples to illustrate possible applications of the theory: (1) comparing the results of two different radiative transfer models; (2) comparing measured and modeled radiation fields in sea ice; (3) discussing how multiple scattering in sea ice gives rise to radiation trapping; and (4) discussing how a polar ozone depletion might influence the primary production in icy polar waters.

9.2 Radiative Transfer Modeling

9.2.1 Sun-Earth Geometry

Because the earth moves around the sun in an elliptical orbit, the earth-sun distance, R, varies throughout the year, by about 3.4% from its minimum value on about

January 3 to its maximum value on about July 3. Thus, the variation in R^2 and therefore, in the extraterrestrial solar irradiance, is about 6.9%, which implies that the radiation incident at the top of the atmosphere is almost 7% larger in January (Southern hemisphere) than in July (Northern hemisphere).

The illumination of the earth's surface depends on the solar zenith angle, θ_0, which is the angle between the local zenith and the direction of the center of the solar disk. The solar zenith angle depends on the time of the day, the time of the year, and geographic location.

9.2.2 Spectrum of Solar Radiation

Figure 9.1 shows the incident UV, visible, and near-infrared parts of the spectral solar irradiance (wavelengths shorter than 1,000 nm) measured on board an earth-orbiting satellite (Rottman et al., 1993). Spectra of an ideal blackbody at several temperatures are also shown in Fig. 9.1. Given the requirement that the total solar energy emitted be the same as that emitted by a blackbody, one finds that the sun's effective temperature is 5,778 K. If the radiating layers of the sun had the same temperature at all distances from its center, the solar spectrum would

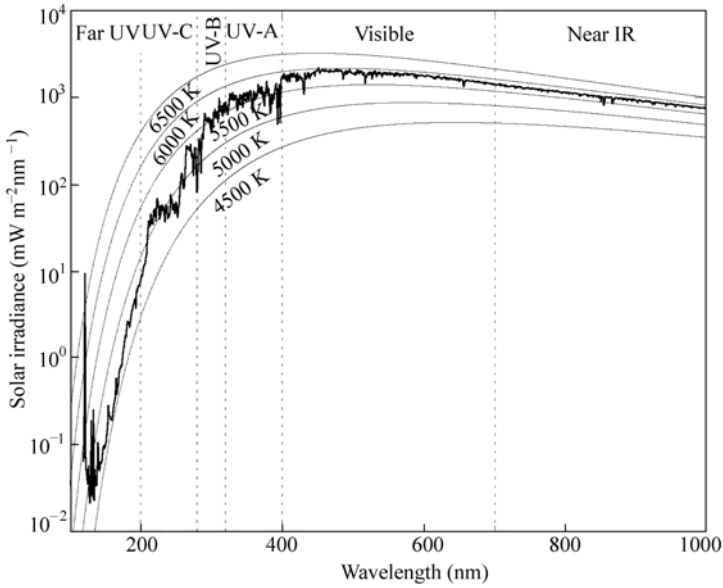

Figure 9.1 Extraterrestrial solar irradiance. The UV spectrum between 119 nm and 420 nm was measured by the SOLSTICE (SOLar STellar Irradiance Comparison Experiment) instrument on the Upper Atmosphere Research Satellite (UARS) (Rottman et al., 1993). The smooth curves are calculated blackbody spectra for several temperatures (adapted from Thomas and Stamnes, 1999)

match one of the theoretical blackbody curves exactly. Thus, the deviations between the measured solar irradiance in Fig. 9.1 and one of the blackbody curves are the result of emission from a non-isothermal solar atmosphere. Most of the solar emission arises within the photosphere where the sun's visible optical depth reaches unity. The fine structure in Fig. 9.1 is due to Fraunhofer absorption by gases in the cooler (more distant) portions of the photosphere. The effective radiating temperature falls to values as low as 4,500 K at wavelengths between 125 nm and 380 nm. Additionally, the UV irradiance is noticeably dependent upon the solar cycle, being more intense at high solar activity than at low solar activity. Thus, the solar illumination varies on diurnal, seasonal as well as the 11-year solar cycle time scales (Thomas and Stamnes, 1999). The 11-year solar cycle is associated with the variation in the number of sunspots.

9.2.3 Atmospheric Vertical Structure

The stratified vertical structure of the bulk properties of an atmosphere is a consequence of hydrostatic balance. For an atmosphere in a state of rest, the pressure, p, must support the weight of the fluid above it. By equating pressure forces and gravitational forces, one finds that $\mathrm{d}p = -g\rho\mathrm{d}z$ where g is the acceleration due to gravity, ρ is the air density, and dp is the differential change in pressure over the small height interval dz. Combining this equation with the ideal gas law $\rho = \bar{M}p / RT = \bar{M}n$, one finds upon integration

$$p(z) = p_0(z)\exp[-\int_{z_0}^{z} \mathrm{d}z' / H(z')] \tag{9.1}$$

where $\bar{M}$ is the mean molecular weight, T the temperature, R the gas constant, and $H = \mathrm{RT}/\bar{\mathrm{M}}\mathrm{g}$ the atmospheric scale height. The ideal gas law allows us to write similar expressions for the density, ρ, and the concentration, n. Clearly, from a knowledge of the surface pressure $p(z_0)$ and the variation of the scale height $H(z)$ with height z, the hydrostatic Eq. (9.1) allows us to determine the bulk gas properties at any height. Equation (9.1) applies to well-mixed gases, but not to short-lived species such as ozone, which is chemically created and destroyed.

The total number of air molecules in a 1 m^2 wide vertical column extending from sea level to the top of the atmosphere is 2.15×10^{29} molecules. In comparison the total column amount of ozone is about 1.0×10^{23} molecules m^{-2}. The height in millicentimeters (10^{-5} m) that the ozone gas in the atmosphere would occupy, if it were compressed to standard pressure (1,013 [hP]; 1 hP (hectoPascal) = 1 $\mathrm{N\cdot m}^{-2}$) at standard temperature (0°C), is called the Dobson unit (DU). Thus, one Dobson unit refers to a layer of ozone that would be 10 μm thick under standard temperature and pressure. The conversion is 1 DU = 2.69×10^{20} molecules m^{-2}. The 1976 US Standard Atmosphere (Anderson et al., 1987) contains about 348 DU of ozone gas.

9.2.4 Light Interaction with Absorbing and Scattering Media

The absorption coefficient $\alpha(\lambda)$, the scattering coefficient $\sigma(\lambda)$, and the scattering phase function $p(\lambda,\Theta)$, can be expressed as:

$$\alpha(\lambda) = \sum_i \alpha_i(\lambda) \tag{9.2}$$

$$\sigma(\lambda) = \sum_i \sigma_i(\lambda) \tag{9.3}$$

$$p(\lambda,\Theta) = \sum_i \frac{\sigma_i(\lambda) p_i(\lambda,\Theta)}{\sigma(\lambda)} \tag{9.4}$$

The subscript *i* is used to denote the various radiatively-active components, i.e., air molecules, aerosols, and liquid water and ice cloud particles in the atmosphere; ice crystals and impurities in the snow; brine pockets and air bubbles in the ice; pure water mixed with air bubbles, chlorophyll, inorganic particles, and yellow substance in the ocean. Here λ is the wavelength, and Θ is the scattering angle, which is related to the polar and azimuthal angles through the cosine law of spherical geometry:

$$\cos\Theta = \cos\theta\cos\theta' + \sin\theta\sin\theta'\cos(\phi - \phi')$$

Here (θ',ϕ') denotes the radiation direction prior to scattering and (θ,ϕ) is the radiation direction after scattering.

9.2.4.1 Absorption and Scattering by Atmospheric Molecules and Pure Water

Absorption by molecules in the earth's atmosphere is due to radiatively-active trace gases. For UV radiation and visible light the most important gas is ozone, but oxides of sulfur and nitrogen may (depending on location) have a significant effect on the UV radiation penetration. In the relatively pristine polar regions, we may assume that for UV radiation and visible light, ozone is the only significant absorbing gas in the atmosphere. Thus, the molecular absorption coefficient becomes:

$$\alpha_m(\lambda) = \alpha_{n,\mathrm{O_3}} n_{\mathrm{O_3}} \tag{9.5}$$

where the subscript *m* stands for molecules, and $\alpha_{n,\mathrm{O_3}}$ and $n_{\mathrm{O_3}}$ are the ozone absorption cross section and number density, respectively (Figs. 9.2(a), (b)). At wavelengths longer than 310 nm, the ozone absorption is due to the Huggins bands, whereas the spectrally-broad but weak absorption between 450 and 700 nm is due to the Chappuis bands (Fig. 9.2(a)).

Scattering by molecules in the atmosphere is proportional to the gas density. Thus, the scattering coefficient due to scattering by air molecules is:

$$\sigma_m(\lambda) = \sigma_{n,\mathrm{Ray}}(\lambda) n_m \tag{9.6}$$

where $\sigma_{n,\mathrm{Ray}}(\lambda) \sim \lambda^{-4}$ is the Rayleigh scattering cross section, and n_m is the total air number density (Fig. 9.2(b)).

Absorption by pure water results from mutual interactions between the intermolecular forces. Calculation of absorption cross sections from first principles is very difficult. Thus, laboratory and *in situ* measurements (Pegau et al., 1995; Pope and Fry, 1997) become essential for establishing the absorption coefficient $\alpha_{n,w}(\lambda)$ for pure water (Fig. 9.2(c)).

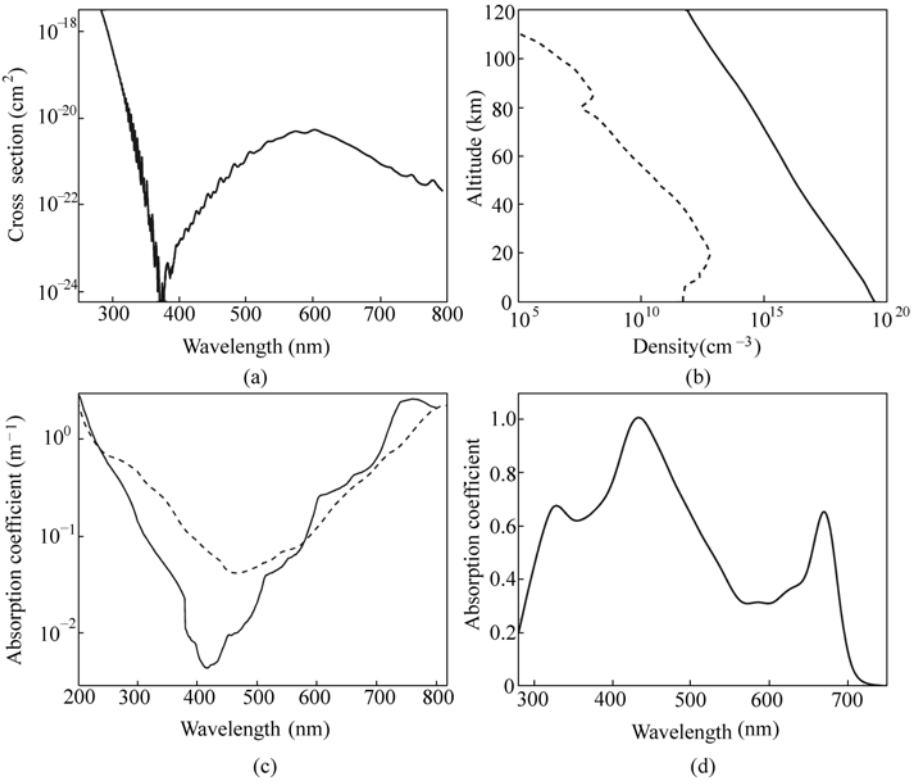

Figure 9.2 (a) Absorption cross section of ozone; (b) number density of atmospheric ozone (dashed line) and total air number density (solid line); (c) absorption spectrum for pure ice (dashed line), and for pure water (solid line; (d) chlorophyll-specific absorption spectrum normalized at 440 nm

Scattering in pure water is due to clusters of molecules and ions, much smaller than the wavelength of light, and from an optical point of view, the clusters are uncorrelated (Thomas and Stamnes, 1999). Thus, the wavelength dependence of the scattering cross section for pure water is $\sigma_{n,w}(\lambda) \sim \lambda^{-4.32}$, similar to the Rayleigh scattering cross section for molecules in the atmosphere. The scattering coefficient for pure water can be approximated by (Morel, 1974):

$$\sigma_w(\lambda) = \left(\frac{129}{\lambda}\right)^{4.32} \qquad \lambda \text{ in [nm].}$$

The phase function for scattering by atmospheric molecules or by pure water is given by:

$$p_w(\Theta) = \frac{3}{(3+x)} \cdot (1 + x\cos^2\Theta)$$

For scattering by air molecules (Rayleigh scattering), the parameter x is set equal to 1, while for scattering by pure water, $x = 0.835$. The latter value of x can be attributed to the anisotropy of the water molecule (Mobley, 1994; Morel and Gentili, 1991).

9.2.4.2 Absorption and Scattering by Particles

In addition to molecules, suspended particulate matter in the atmosphere and ocean has a significant impact on the radiative transfer. This particulate matter consists of aerosols (dust, sulfate particles, soot, smoke particles, cloud water droplets, raindrops, ice crystals, etc.) in the atmosphere, snow grains, air bubbles and brine pockets in ice, and hydrosols (suspended particles of organic and inorganic origin) in the water. Thus, to describe radiative transfer in a medium such as the coupled atmosphere-snow-ice-ocean (CASIO) system, we may think of it as being composed of randomly distributed, radiatively-active 'particles' that absorb and scatter radiation.

We assume that the optical properties of particles (i.e., aerosols, cloud particles, snow grains, brine pockets, etc.) can be approximated by those of spheres. Then, the absorption and scattering coefficients and the scattering phase function can be written as:

$$\alpha_p(\lambda) = \int_{r_{\min}}^{r_{\max}} \pi r^2 Q_\alpha(r) n(r) \mathrm{d}r \tag{9.7}$$

$$\sigma_p(\lambda) = \int_{r_{\min}}^{r_{\max}} \pi r^2 Q_\sigma(r) n(r) \mathrm{d}r \tag{9.8}$$

$$p_p(\lambda,\Theta) = \frac{\int_{r_{\min}}^{r_{\max}} p_p(\lambda,\Theta,r) n(r) \mathrm{d}r}{\int_{r_{\min}}^{r_{\max}} n(r) \mathrm{d}r} \tag{9.9}$$

where $Q_\alpha(r)$ or $Q_\sigma(r)$ is defined as the ratio of the absorption or scattering cross section for a spherical particle of radius r to the geometrical cross section πr^2, $n(r)$ is the particle size distribution, and r is the radius of each individual particle. For a specific value of r, we can compute $Q_\alpha(r)$, $Q_\sigma(r)$, and $p_p(\lambda,\Theta,r)$ using Lorenz-Mie theory, but evaluation of Eqs. (9.7) – (9.9) requires knowledge of the

particle size distribution $n(r)$, which is usually unknown.

Hamre et al. (2004) showed that Eqs. (9.7) – (9.9) can be considerably simplified by making the following assumptions:

- The particle distribution is characterized by an effective radius $r_e = \int_{r_{\min}}^{r_{\max}} n(r) r^3 \mathrm{d}r \Big/ \int_{r_{\min}}^{r_{\max}} n(r) r^2 \mathrm{d}r$, which obviates the need for an integration over r.
- The particles are weakly absorbing, so that $Q_\alpha(r) \approx \frac{16\pi r m_{i,p}}{3\lambda} \cdot \frac{1}{m_{\mathrm{rel}}} \cdot [m_{\mathrm{rel}}^3 - (m_{\mathrm{rel}}^2 - 1)^{3/2}]$, where $m_{i,p}$ is the imaginary part of the refractive index of the particle, λ is the wavelength in vacuum, and $m_{\mathrm{rel}} = m_{r,p} / m_{r,\mathrm{med}}$ is the ratio of the real part of the refractive index of the particle ($m_{r,p}$) to that of the surrounding medium ($m_{r,\mathrm{med}}$).
- The particles are large compared to the wavelength ($2\pi r / \lambda >> 1$), which implies $Q_\sigma(r) = 2$.
- The scattering phase function can be represented by the one parameter Henyey-Greenstein phase function, which depends only on the asymmetry factor $g \equiv \langle \cos\Theta \rangle = \frac{1}{2} \int_{-1}^{1} p(\Theta) \cos\Theta \mathrm{d}(\cos\Theta)$.

With these assumptions, Eqs. (9.7) – (9.9) become:

$$\alpha_p(\lambda) = \alpha(\lambda) \cdot \frac{1}{m_{\mathrm{rel}}} \cdot \left[1 - (m_{\mathrm{rel}}^2 - 1)^{3/2}\right] f_V \tag{9.10}$$

$$\sigma_p(\lambda) = \frac{3}{2} \cdot \frac{f_V}{r_e} \tag{9.11}$$

$$p_p(\lambda, \Theta) = \frac{1 - g^2}{(1 + g^2 - 2g\cos\Theta)^{3/2}} \tag{9.12}$$

where $\alpha(\lambda)$ is the absorption coefficient for the material of which the particle is composed, and $f_V = \frac{4}{3}\pi r^3 n_e$, where n_e is the number of particles per unit volume with radius r_e.

9.2.4.3 Optical Properties of the Ocean

To represent the optical properties of the water beneath the ice, we may use the model of Morel (1991), updated by Morel and Maritorena (2001), according to which the absorption and scattering coefficients and the scattering phase function are given by:

$$\alpha(\lambda) = \alpha_w(\lambda) + \alpha_C(\lambda) + \alpha_Y(\lambda) \tag{9.13}$$

$$\sigma(\lambda) = \sigma_w(\lambda) + \sigma_C(\lambda) \tag{9.14}$$

$$p(\lambda,\Theta) = \frac{\sigma_w(\lambda)p_w(\lambda,\Theta) + \sigma_C(\lambda)p_C(\lambda,\Theta)}{\sigma(\lambda)} \tag{9.15}$$

where the subscript *w* denotes pure water, the subscript *C* denotes chlorophyll-*a* related absorption and scattering, and the subscript *Y* stands for yellow substance. The absorption coefficient for pure water was discussed above (see Fig. 9.2(c)), and

$$\alpha_C(\lambda) = 0.064 A_C(\lambda) C^{0.65}$$

where $A_C(\lambda)$ is the normalized absorption spectrum for the chlorophyll-*a* related absorption displayed in Fig. 9.2(d), and $C(\mathrm{mg \cdot m^{-3}})$ is the chlorophyll-*a* concentration. The absorption by yellow substance is expressed as:

$$\alpha_Y(\lambda) = \alpha_Y(440)\exp[-0.014(\lambda - 440)]$$

where $\alpha_Y(440) = 0.2[\alpha_w(440) + 0.064 A_C(440) C^{0.65}]$, and the chlorophyll-*a* related scattering coefficient is given by:

$$\sigma_C(\lambda) = 0.3\left(\frac{550}{\lambda}\right) C^{0.62}$$

Scattering by pure water was discussed in Section 9.2.4.1.

9.2.4.4 Definitions of Irradiance and Radiance

The spectral net irradiance F_ν is defined as the net energy d^3E crossing a surface element $\mathrm{d}A$ (with unit normal $\hat{n}$) per unit time and per unit frequency (Thomas and Stamnes, 1999):

$$F_\nu = \frac{\mathrm{d}^3E}{\mathrm{d}A\mathrm{d}t\mathrm{d}\nu} \qquad [\mathrm{W \cdot m^{-2} \cdot Hz^{-1}}].$$

Since the irradiance is positive if the energy flow is into the hemisphere centered on the direction $\hat{n}$ and negative if the flow is into the opposite hemisphere, we may define spectral hemispherical irradiances $F_\nu^+ = \mathrm{d}^3E^+ / \mathrm{d}A\mathrm{d}t\mathrm{d}\nu$ and $F_\nu^- = \mathrm{d}^3E^- / \mathrm{d}A\mathrm{d}t\mathrm{d}\nu$. Thus, the spectral net irradiance becomes $F_\nu = F_\nu^+ - F_\nu^-$, and integration over all frequencies yields the net irradiance $F = \int_0^\infty \mathrm{d}\nu F_\nu$ $[\mathrm{W \cdot m^{-2}}]$.

Consider any small subset of the energy d^4E that flows within a solid angle $\mathrm{d}\omega$ around the direction $\hat{\Omega}$ in the time interval $\mathrm{d}t$ and within the frequency range $\mathrm{d}\nu$. If this subset of radiation has passed through a surface element $\mathrm{d}A$ (with unit

normal $\hat{n}$), then the energy per unit area per unit solid angle, per unit frequency, and per unit time, defines the spectral radiance I_ν:

$$I_\nu = \frac{\mathrm{d}^4 E}{\cos\theta \mathrm{d}A \mathrm{d}t \mathrm{d}\omega \mathrm{d}\nu} \qquad [\mathrm{W \cdot m^{-2} \cdot sr^{-1} \cdot Hz^{-1}}].$$

Here θ is the angle between the surface normal $\hat{n}$ and the direction of propagation $\hat{\Omega}$. It is clear from these definitions that $F_\nu^+ = \int_+ \mathrm{d}\omega \cos\theta I_\nu$ and $F_\nu^- = -\int_- \mathrm{d}\omega \cos\theta I_\nu$. Thus, the spectral net irradiance can be expressed as:

$$F_\nu = F_\nu^+ - F_\nu^- = \int_{4\pi} \mathrm{d}\omega \cos\theta I_\nu .$$

Finally, we define the mean intensity as: $\overline{I} = (1/4\pi)\int_{4\pi} \mathrm{d}\omega I_\nu$, which is simply the radiance averaged over the sphere.

9.2.4.5 Absorption, Scattering, and Extinction by Molecules and Particles

A beam of light incident on a thin layer with thickness ds of radiatively-active matter (gases and/or particles) is attenuated so that the differential loss in radiance is proportional to the incident light: $\mathrm{d}I_\nu = -k(\nu,s) I_\nu \mathrm{d}s$, where $k(\nu,s)$ is called the extinction or attenuation coefficient. Integration yields

$$I_\nu(s,\hat{\Omega}) = I_\nu(0,\hat{\Omega}) \exp[-\tau_s(\nu)], \tag{9.16}$$

where $\hat{\Omega}$ denotes the propagation direction of the beam. The dimensionless extinction (or attenuation) optical path (or opacity) along the path s is given by $\tau_s(\nu) \equiv \int_0^s \mathrm{d}s'\, k(\nu,s')$. Attenuation of a light beam can be caused by either absorption or scattering. The extinction (or attenuation) optical path of a mixture of scattering/absorbing molecules and particles is defined as the sum of the scattering and absorption optical paths, $\tau_s(\nu) = \tau_{sc}(\nu) + \tau_a(\nu)$, where $\tau_{sc}(\nu) = \sum_i \int_0^s \mathrm{d}s' \sigma_i(\nu,s')$ and $\tau_a(\nu) = \sum_i \int_0^s \mathrm{d}s' \alpha_i(\nu,s')$. The sum is over all optically active species (each denoted by the subscript i), and $\sigma_i(\nu,s)$ and $\alpha_i(\nu,s)$ [$\mathrm{m^{-1}}$] are the scattering and absorption coefficients, and $k_i(\nu,s) = \alpha_i(\nu,s) + \sigma_i(\nu,s)$ is the extinction or attenuation coefficient. These are defined as $\sigma_i(\nu,s) = \sigma_{n,i}(\nu) n_i(s)$ and $\alpha_i(\nu,s) = \alpha_{n,i}(\nu) n_i(s)$, where n_i [$\mathrm{m^{-3}}$] is the concentration and $\alpha_{n,i}(\nu)$ and $\sigma_{n,i}(\nu)$ [$\mathrm{m^2}$] are the absorption and scattering cross sections of the ith optically active species (molecule or particle).

9.2.5 Equation of Radiative Transfer

If we are interested primarily in energy transfer, rather than the directional dependence of the radiation, it is sufficient to work with the azimuthally-averaged radiance $I_\nu(z,u)$, where z denotes the level in the medium (height in the atmosphere or depth in the ocean), and $u=\cos\theta$, θ being the polar angle. It is convenient to split the radiation field into two parts: (1) the *direct* solar beam, which is exponentially attenuated upon passage through the atmosphere and ocean, and (2) the *diffuse* or scattered radiation.

According to Eq. (9.16), the penetration of the direct solar beam through the atmosphere may be written as $I_{\text{sol}}(s,\hat{\Omega}) = F^s\ \delta(\hat{\Omega}-\hat{\Omega}_0)\,\mathrm{e}^{-\tau_s(\nu)}$. Here $\hat{\Omega}_0=(\theta_0,\phi_0)$ is a unit vector in the direction of the incident solar beam, where $\mu_0=\cos\theta_0$, and θ_0 is the solar zenith angle as illustrated in Fig. 9.3. F^s is the solar irradiance (normal to the solar beam direction $\hat{\Omega}_0$) incident at the top of the atmosphere. In plane-parallel geometry, the vertical optical depth is defined in terms of the optical path $\tau_s(\nu)$ as follows:

$$\tau(\nu,z)\equiv\tau_s(\nu)/\mu_0\equiv\sum_i\int_z^\infty \mathrm{d}z'\,k^i(\nu,z')$$

or

$$\mathrm{d}\tau(\nu,z)=-k(\nu,z)\mathrm{d}z=-\sum_i[\alpha_{n,i}(z)+\sigma_{n,i}(z)]n_i(z)\mathrm{d}z$$

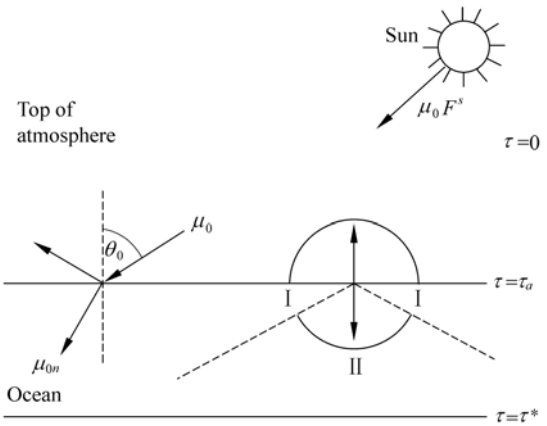

Figure 9.3 Schematic illustration of two adjacent media with a flat interface, such as the atmosphere overlying a calm ocean. Because the real part of the refractive index (m_r) of the atmosphere ($m_{\text{atm},r}\approx 1$) is different from that of the ocean ($m_{\text{ocn},r}\approx 1.33$), radiation distributed over $2\pi\,sr$ in the atmosphere will be confined to a cone less than $2\pi\,sr$ in the ocean (region Ⅱ). Radiation in the ocean within region Ⅰ will be totally reflected when striking the interface from below (Thomas and Stamnes, 1999)

so that for a plane-parallel medium the direct component becomes:

$$I_{\text{sol}}(\tau,u,\phi) = F^s \delta(u-\mu_0)\delta(\phi-\phi_0)\,\mathrm{e}^{-\tau/\mu_0} \tag{9.17}$$

Here $u=\cos\theta$, θ is the polar angle of the observation direction, $\mu=|u|$, and ϕ denotes the azimuth angle of the observation direction.

In a stratified medium, the optical properties vary only in the vertical direction, and the transfer of diffuse radiation through such a medium is described by:

$$u\frac{\mathrm{d}I(z,u)}{\mathrm{d}z} = -k(z)I(z,u) + \sigma(z)\frac{1}{2}\int_{-1}^{1}\mathrm{d}u'\; p(z,u',u)I(z,u') + S^*(z,u) \tag{9.18}$$

where $I(z,u)$ is the azimuthally-averaged diffuse radiance. The term on the left side in Eq. (9.18) is the change in the diffuse radiance $I(z,u)$ along a slant path dz/u. The first term on the right side is the loss of radiation out of the beam due to extinction, and the second term is the gain due to multiple scattering. The third term, $S^*(z,u)$ defined below, is the solar pseudo-source, proportional to the attenuated solar beam, which 'drives' the diffuse radiation. Using the non-dimensional optical depth, $\mathrm{d}\tau(z) = -k(z)\mathrm{d}z$ as the independent variable, we may rewrite Eq. (9.18) as follows:

$$u\frac{\mathrm{d}I(\tau,u)}{\mathrm{d}\tau} = I(\tau,u) - \frac{a(\tau)}{2}\int_{-1}^{1}\mathrm{d}u'\; p(\tau,u',u)\,I(\tau,u') - S^*(\tau,u) \tag{9.19}$$

where the single-scattering albedo is defined as $a(\tau(z)) \equiv \sigma(z)/k(z)$.

9.2.6 Surface Reflection and Transmission

It is necessary to consider two strata for a coupled atmosphere-ocean system; one for the atmosphere with real part of the refractive index $m_{\text{atm},r}$ and another for the ocean with real part of the refractive index $m_{\text{ocn},r}$. The basic radiance, defined as I/m_r^2, where m_r is the real part of the refractive index, is a conserved quantity. Thus, if we neglect reflection losses, the basic radiance will be constant across the interface between the two strata. Assuming for simplicity that the interface is flat and smooth (a calm ocean), then the radiance must satisfy Snell's law and Fresnel's equations. As illustrated in Fig. 9.3, the downward radiation distributed over $2\pi sr$ in the atmosphere will be restricted to a cone less than $2\pi sr$ (referred to as region Ⅱ in Fig. 9.3) after being refracted across the interface into the ocean. Outside the refractive region in the ocean, i.e., in the total reflection region (referred to as region Ⅰ in Fig. 9.3), the radiation is due to in-water multiple scattering. The demarcation between the refractive region and the total reflection region in the ocean is given by the critical angle θ_c given by

$\mu_c \equiv \cos\theta_c = \sqrt{1-1/m_{\text{rel}}^2}$, where $m_{\text{rel}} = m_{\text{ocn},r} / m_{\text{atm},r}$ is the real part of the refractive index in the ocean relative to that in the atmosphere.

Because the radiation field in the ocean is driven by solar radiation passing through the atmosphere-water interface, Eq. (9.19) applies also in the ocean, but the solar pseudo-sources are different in the two media. In the atmosphere we have:

$$S^*_{\text{atm}}(\tau,u) = \frac{a(\tau)}{4\pi} p(\tau,-\mu_0,u)\, \mathrm{e}^{-\tau/\mu_0} + \frac{a(\tau)}{4\pi} \rho_s(-\mu_0;m_{\text{rel}})\, p(\tau,\mu_0,u)\, \mathrm{e}^{-(2\tau_a-\tau)/\mu_0}$$

Here the first term is the usual solar beam pseudo-source, and the second term is due to the reflection occurring at the interface, which is proportional to $\rho_s(-\mu_0;m_{\text{rel}})$, the specular reflectance. The pseudo-source in the ocean is just the attenuated solar beam refracted through the interface:

$$S^*_{\text{ocn}}(\tau,u) = \frac{a(\tau)}{4\pi} \cdot \frac{\mu_0}{\mu_{0m}} T_b(-\mu_0;m_{\text{rel}})\, p(\tau,-\mu_{0m},u)\, \mathrm{e}^{-\tau_a/\mu_0}\, \mathrm{e}^{-(\tau-\tau_a)/\mu_{0m}}$$

Here $T_b(-\mu_0;m_{\text{rel}})$ is the beam transmittance through the interface, and μ_{0m} is the cosine of the solar zenith angle in the ocean, which is related to μ_0 by Snell's law $\mu_{0m} \equiv \mu_{0m}(\mu_0,m_{\text{rel}}) = \sqrt{1-(1-\mu_0^2)/m_{\text{rel}}^2}$. With the use of the appropriate pseudo-sources for the atmosphere [$S^*_{\text{atm}}(\tau,u)$] and ocean [$S^*_{\text{ocn}}(\tau,u)$], Eq. (9.19) can now be solved subject to boundary conditions at the top of the atmosphere and the bottom of the ocean. However, we must also properly account for the reflection from and transmission through the atmosphere-ocean interface by requiring that Fresnel's equations are satisfied.

9.2.7 Radiative Transfer in a Coupled Atmosphere-Snow-Ice-Ocean (CASIO) System

Solar irradiance levels play a key role for energy exchange and primary production in marine polar environments. Because the ocean is typically covered by sea ice and snow for several months of the year, theoretical and experimental knowledge of radiation levels at various depths in the snow, ice, and ocean is essential. The photosynthetically active radiation (PAR, 400 nm$< \lambda <$700 nm) drives the pelagic primary production in general, and the amount of PAR reaching the bottom of the sea ice is of crucial importance for the growth of ice algae, which accounts for between 5% and 30% of the total plankton production in the polar regions (Legendre et al., 1992; Wheeler et al., 1996). The wavelength dependence of UV radiation ($\lambda <$400 nm) is required to assess potential damage and inhibition of primary production induced by UV radiation (Neal et al., 1998). Finally, the amount of radiation that penetrates the snow and ice determines the rate of energy

absorption, melting of sea ice, and warming of the upper ocean (Perovich and Maykut, 1996; Zeebe et al., 1996).

Here we provide a brief description of the CASIO Discrete-Ordinate Radiative Transfer (CASIO-DISORT) model, which treats transfer of solar radiation in the CASIO system based on the theory provided above and its implementation by use of the discrete-ordinate method. Note that in the absence of sea ice, the CASIO system defaults to the CAO (coupled atmosphere-ocean) system.

In summary, the CASIO-DISORT method works as follows:

(1) The atmosphere and the ice-ocean media are treated as two adjacent slabs separated by an interface across which the real part of the refractive index changes from $m_{\mathrm{atm},r} = 1$ in the atmosphere (including a possible snow layer at the bottom, i.e., on top of the ice) to $m_{\mathrm{ocn},r} = 1.31$ (1.33 in the absence of ice) in the ice-ocean medium.

(2) Each of the two slabs is divided into a sufficient number of horizontal layers to adequately resolve vertical variations in their inherent optical properties.

(3) The reflection and transmission through the interface between the atmosphere and the ice-ocean are computed by Fresnel's equations, and the reflection and refraction of a beam at the interface follow the reflection law and Snell's law, respectively.

(4) The radiative transfer equation is solved separately for each layer in the atmosphere and in the ice-ocean using the discrete-ordinate method.

(5) The solution is completed by applying boundary conditions at the top of the atmosphere and the bottom of the ocean, as well as appropriate radiance continuity conditions at each layer interface in the atmosphere, in the ice-ocean media, and at the atmosphere-ice-ocean interface (where Fresnel's equations apply).

9.3 Sample Applications of the Theory

9.3.1 Comparison of Modeled Irradiances in CAO Systems

Gjerstad et al. (2003) undertook a study aimed at comparing two distinctly different methods of solving the radiative transfer equation for coupled atmosphere-ocean systems. One of these methods was the deterministic discrete-ordinate method (Stamnes et al., 1988; 2000), extended to apply to two adjacent slabs with different indices of refraction, such as a coupled atmosphere-ocean (CAO) system (Jin and Stamnes, 1994). The other method was the Monte Carlo (MC) approach, in which the trajectories of individual photons were simulated (Collins et al., 1972; Lenoble, 1985).

Mobley et al. (1993) compared underwater light fields computed by several different methods, including MC methods and the discrete-ordinate method, and showed that different methods give similar results for a limited set of test cases. However, the models included the atmosphere in different ways, which led to a spread in the downward irradiance of 18% just above the water surface and throughout the underwater column. Also, no comparisons of atmospheric irradiances were made. To remedy this shortcoming Gjerstad et al. (2003) performed a detailed quantitative comparison of irradiances simulated with a Monte Carlo method with those computed with a CAO-DISORT model (Jin and Stamnes, 1994; Thomas and Stamnes, 1999).

The CAO-MC and the CAO-DISORT models used by Gjerstad et al. (2003) had precisely the same physical basis, including coupling between the atmosphere and the ocean, and precisely the same atmospheric and ocean input parameters. Computed results for direct and diffuse upward and downward irradiances are shown in Fig. 9.4. The percentage deviation is less than 0.5% for downward irradiances, and less than 1% for upward irradiances. The CAO-MC code has an

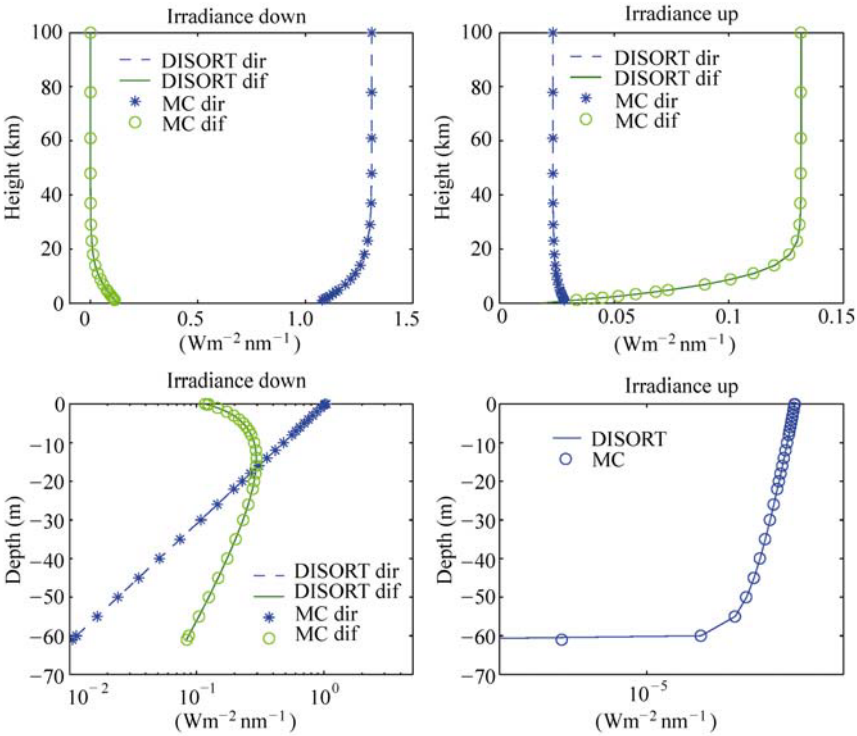

Figure 9.4 Comparison of irradiances computed by a CAO-DISORT code (solid and dashed curves) and a CAO-MC code (circles and asterisks). For details, see Gjerstad et al. (2003)

advantage over the CAO-DISORT (Jin and Stamnes, 1994) code in that it can handle surface waves, but the CAO-DISORT code is computationally much faster. Finally, it should be noted that Jin et al. (2006) recently extended the CAO-DISORT code to include the effects of surface waves.

9.3.2 Measured and Modeled Radiation Fields in Sea Ice

The theory described above was applied to analyze a comprehensive set of measurements taken in Kongsfjorden, Svalbard (Gerland et al., 1999; Hamre et al., 2004). Physical and structural properties (snow and ice thickness, density, *in situ* temperature, and salinity profiles) were measured in addition to irradiances above the surface and under the ice. On the basis of measured snow grain sizes, snow depth, ice temperature, and ice salinity, Hamre et al. (2004) computed the transmittance of first-year sea ice with and without snow cover. These computations were done with a CASIO-DISORT code, and the bubble sizes and the snow grain sizes were estimated by assuming that the absorption by impurities can be neglected at near-infrared wavelengths. Also, it was assumed that the volume fractions of air bubbles and brine pockets (f_V^{bu} and f_V^{br}) could be determined from the salinity, bulk ice density, and temperature (Cox and Weeks, 1983; Jin et al., 1994). The results of this study may be summarized as follows:

- a best fit between measured and computed transmittances was obtained with snow grains that were only 5% larger than the smallest observed values;
- the shape of the impurity absorption spectrum resulting from forcing agreement between modeled and measured transmittances resembled that of ice algae;
- a 2.5 cm-thick layer of snow had the same transmittance for visible light and UV radiation as a 61 cm-thick ice layer;
- UV radiation is removed more efficiently than visible light for snow depths greater than 3 cm − 4 cm implying that algae growing under snow cover may be protected from harmful UV radiation, yet receives sufficient visible light for photosynthesis;
- the CASIO-DISORT model is a useful tool for computing energy deposition in the snow, ice, and ocean, and can be used to investigate the influence of changes in environmental conditions, such as ozone amount, snow thickness, and cloud cover on UV radiation and visible light, and hence, on the aquatic biology in polar regions.

9.3.3 Radiation Trapping in Sea Ice

Comparisons of radiative transfer models used to compute irradiances and radiances in atmosphere-ocean systems have shown that they yield similar results

for identical input, and have clearly demonstrated the influence of the atmosphere/snow-sea ice/ocean interface on the transport of energy across it (Mobley et al., 1993; Gjerstad et al., 2003). Nevertheless, little attention has been paid to the enhanced downward irradiance (EDI) across the atmosphere-sea ice interface due to trapping of light caused by multiple scattering in the sea ice. The EDI is defined as:

$$\Delta F_{\mathrm{d}}(\lambda) \equiv F_{\mathrm{d}}(0^{-},\lambda) - F_{\mathrm{d}}(0^{+},\lambda) \tag{9.20}$$

where $F_{\mathrm{d}}(0^{-},\lambda)$ is the downward irradiance just *below* the interface, and $F_{\mathrm{d}}(0^{+},\lambda)$ is the downward irradiance just *above* the interface. By definition, if the irradiance difference across the interface is positive ($\Delta F_{\mathrm{d}}(\lambda) > 0$), there is an EDI effect across the interface; otherwise, there is no EDI effect.

The irradiance incident on the atmosphere-sea ice interface consists of two components:

$$F_{\mathrm{d}}(0^{+},\lambda) = F_{\mathrm{sol}}(0^{+},\lambda) + F_{\mathrm{diff}}(0^{+},\lambda) \tag{9.21}$$

where $F_{\mathrm{sol}}(0^{+},\lambda)$ is the direct solar beam irradiance and $F_{\mathrm{diff}}(0^{+},\lambda)$ is the downward irradiance due to diffuse skylight. Similarly, the downward irradiance just below the interface consists of three components:

$$F_{\mathrm{d}}(0^{-},\lambda) = F_{\mathrm{trans}}(0^{-},\lambda) + F_{\mathrm{pref}}(0^{-},\lambda) + F_{\mathrm{tref}}(0^{-},\lambda). \tag{9.22}$$

Here $F_{\mathrm{trans}}(0^{-},\lambda) = F_{\mathrm{sol,\,tr}}(0^{+},\lambda) + F_{\mathrm{diff,\,tr}}(0^{+},\lambda)$ is the sum of two downward irradiance components from the atmosphere that are transmitted through the interface, $F_{\mathrm{pref}}(0^{-},\lambda)$ is the downward irradiance due to the upward radiation in the sea ice with directions inside the refraction cone that is partially reflected downwards by the interface, and $F_{\mathrm{tref}}(0^{-},\lambda)$ is the downward irradiance due to the upward radiation in the sea ice with directions outside the refraction cone that is totally reflected downwards by the interface.

Using a radiative transfer model similar to the CASIO-DISORT model described above, Jiang et al. (2005) simulated the EDI effect. Table 9.1 shows all components of the computed downward irradiance just above and just below the atmosphere-sea ice interface for a solar elevation of 30° and for a wavelength of 550 nm under clear sky conditions. The incident downward solar irradiance is 4.21 μ ein $\mathrm{m^{-2}\ s^{-1}\ nm^{-1}}$ (0.92 W $\mathrm{m^{-2}\ nm^{-1}}$). We note that $F_{\mathrm{tref}}(0^{-},\lambda)$ is the main source of the EDI effect. Thus, the EDI effect is primarily due to radiation that is totally reflected by the interface. The dominance of scattering in the ice compared to absorption is the cause of the EDI effect. The biogeophysical significance of the EDI is that the mean intensity just below the interface will be enhanced, and so will the energy available for photolysis and melting of the sea ice.

The third column in Table 9.1 demonstrates that without a jump in the index of refraction, there is no EDI effect ($\Delta F_{\mathrm{d}}(\lambda) = 0$), and the fourth column demonstrates

that in the absence of scattering in the sea ice ($b_{ice} = 0$), there is no EDI effect. In fact, $\Delta F_d(\lambda) < 0$ when $b_{ice} = 0$, which is a consequence of energy conservation, because a fraction of the irradiance incident on the ice is (Fresnel) reflected, and no light can be backscattered from the sea ice when $b_{ice} = 0$.

Table 9.1 Comparison of downward irradiance components (in units of μ ein $m^{-2}\,s^{-1}\,nm^{-1}$) at 550 nm just above and just below the atmosphere-sea ice interface*

Component	$m_{rel} = 1.31$	$m_{rel} = 1$	$b_{ice} = 0$
$F_{sol}(0^+,550)$	2.47	2.47	2.47
$F_{diff}(0^+,550)$	1.20	1.29	1.02
$F_d(0^+,550)$	3.67	3.76	3.49
$F_{sol,tr}(0^-,550)$	2.34	2.47	2.34
$F_{tref}(0^-,550)$	1.32	0	0
$F_{diff,tr}(0^-,550)$	1.08	1.29	0.92
$F_{pref}(0^-,550)$	0.11	0	0
$F_d(0^-,550)$	4.85	3.76	3.26
$\Delta F_d(550)$	1.18	0	−0.23

* The second column shows the EDI effect, the third column shows results obtained with no jump in the index of refraction, and the fourth column shows results when the scattering in the sea ice is ignored (see text above)

9.3.4 Impact of Ozone Depletion on Primary Productivity

Several studies have suggested that a depletion of the ozone layer could lead to a reduction in the primary production of aquatic ecosystems due to an increase in UV-B radiation (Häder, 1997; Häder et al., 1998). Smith et al., (1992) estimated a 6% − 12% reduction in the primary production in the marginal ice of the Southern Ocean for a reduction in the stratospheric ozone from 300 DU − 200 DU. Other studies have indicated that an ozone depletion from 300 DU − 150 DU in Antarctica would lead to a reduction in the primary production of < 3.8% (Holm-Hansen et al., 1993b), and between 8.5% and 0.7% under clear skies (6.5% and 0.8% under cloudy skies).

Many marine organisms are sensitive to UV radiation. The extent to which these marine organisms will be able to adapt to expected increases in UV exposure is uncertain due to a sparcity of measurements. Increased levels of UV-B radiation may impact phytoplankton communities by: (1) initiating changes in cell size and taxonomic structure, (2) reducing the productivity, (3) influencing the protein content, dry weight, and pigment concentration, (4) inducing chloroplast damage, and (5) directly affecting the proteins of the photosynthetic apparatus.

To explore the potential impact of ozone depletions, one may use a simple model, in which marine photosynthesis (or primary production, ignoring respiratory losses)

is parameterized as follows (Cullen et al., 1992; Neal et al., 1998):

$$P = P_s\left(1 - \mathrm{e}^{I_p / I_s}\right)\frac{1}{1 + I^*} \tag{9.23}$$

where P_s is the maximum photosynthesis in the absence of UV radiation inhibition, and I_p is the photosynthetically utilizable radiation (PUR):

$$I_p = \int_{400}^{700} \overline{I}(\lambda) a^*(\lambda) \mathrm{d}\lambda \tag{9.24}$$

Here, $\overline{I}(\lambda)$ is the mean intensity (scalar irradiance), and $a^*(\lambda)$ the normalized algal absorption spectrum. In Eq. (9.23), I_s is the PUR saturation level, and $1/(1 + I^*)$ describes the inhibition caused by UV radiation (UVR), where I^* is given by:

$$I^* = \int_{280}^{400} \varepsilon(\lambda) \overline{I}(\lambda) \mathrm{d}\lambda \tag{9.25}$$

Here, $\varepsilon(\lambda)$ is the action spectrum for UVR-induced inhibition of photosynthesis.

The mean intensity $\overline{I}(\lambda)$ that drives and inhibits primary photosynthesis depends on several environmental factors including the total ozone column amount, solar elevation, and depth in the ocean, as well as the presence of clouds, ice, and snow. Employing the radiative transfer model described above for the coupled atmosphere-sea ice-ocean system, and assuming total ozone column amounts of 400 DU and 200 DU, Hamre et al. (2008) computed $\overline{I}(\lambda)$ at the bottom of the snow-covered sea ice and at various depths of open water, and used the resulting $\overline{I}(\lambda)$-values in Eq. (9.23) to calculate the primary productivity. The results of this study may be summarized as follows:

- an ozone depletion increases not only harmful UVR, but also beneficial PUR;
- at high latitudes, the benefits of increased PUR for phytoplankton under sea ice and below a certain depth in the ocean dominates over the damage caused by increased UVR;
- a large fraction of the primary production in the polar regions is caused by ice algae growing in environments well protected from UVR;
- the primary production in the polar regions could increase by as much as 1% for a 50% ozone depletion.

9.4 Discussion and Conclusions

We have given a review of UV and visible radiative transfer in a CASIO system with an emphasis on basic physical principles. To illustrate applications of the theory we have:

(1) Compared two different models (based on the deterministic discrete-ordinate radiative transfer (DISORT) method and stochastic Monte Carlo simulations)

for radiation penetration into the open ocean, which for a given set of input parameters have been shown to give identical results. Compared measured and modeled radiative transfer in a CASIO system, which reveals that accurate transmittances, as well as accurate values for the radiative energy deposition versus depth, can be calculated using the CASIO-DISORT model.

(2) Discussed results of a study showing that multiple scattering in a highly scattering medium, such as sea ice, gives rise to a marked enhancement of the downward irradiance across the atmosphere-sea ice interface.

(3) Discussed results of a recent study of the primary production in icy polar waters, which, contrary to previous investigations, reveal that a 50% ozone depletion might lead to an increase (~1%) rather than a decrease in primary productivity.

In view of the above, we conclude that:

- for a CAO system, our ability to model the transport of UV radiation and visible light appears to be limited as much by reliable information about optical properties of marine constituents and atmospheric aerosol loading as by our ability to accurately solve the radiative transfer equation;
- multiple scattering in sea ice leads to a significant enhancement of the downward irradiance across the atmosphere-sea ice interface;
- it is important to make field measurements to provide reasonable input to modeling efforts; and
- in icy polar waters, an ozone depletion might lead to an increase rather than a decrease in primary productivity.

Acknowledgements

This work was supported by the US National Science Foundation and the Norwegian Research Council.

References

Anderson GP, Clough SA, Kneizys FX, Chetwynd JH, and Shettle EP (1987) AFGL Atmospheric Constituent Profiles (0-120) km, AFGL-TR-86-0110, AFGL (OPI), Hanscom AFB, MA

Anderson JG, Toohey DW, and Brune WH (1991) Free radicals within the Antarctic vortex: The role of CFCs in Antarctic ozone loss. Science 251: 39 – 46

Calkins J, and Thordardottir C (1980) The ecological significance of solar UV radiation on aquatic organisms. Nature 283: 563 – 566

Collins DG, Blattner WG, Wells MB, and Horak HG (1972) Backwards Monte Carlo calculations of the polarization characteristics of the radiation field emerging from spherical shell atmospheres. Appl. Opt. 11: 2684 – 2705

Cox GF, and Weeks WF (1983) Equations for determining the gas and brine volumes in sea-ice samples. J. Glaciol. 29: 306 – 316

Cullen JL, Neale PJ, and Lesser MP (1992) Biological weighting function for the inhibition of phytoplankton photosynthesis by ultraviolet radiation. Science 258: 646 – 650

Cullen JL, and Neale PJ (1994) Ultraviolet radiation, ozone depletion, and marine photosynthesis. Photosyn. Res. 39: 303 – 320

Deal CJ, Kieber DJ, Toole DA, Stamnes K, Jiang S, and Uzuka N (2005) Dimethylsulfide photolysis rates and apparent quantum yields in Bering Sea seawater. Continental Shelf Research 25: 1825 – 1835

Döhler G (1985) Effect of UV-B radiation (290 – 320 nm) on the nitrogen metabolism of several marine diatoms. J. Plant Physiol. 118: 391 – 400

Döhler G, and Hagmeier E (1997) UV effects on pigments and assimilation of 15N-ammonium and 15N-nitrate by natural marine phytoplankton of the North Sea. Bot. Acta 110: 481 – 488

Gerland S, Winther J-G, Ørbæk JB, and Ivanov BV (1999) Physical properties, spectral reflectance and thickness development of first year fast ice in Kongsfjorden, Svalbard. Polar Res. 18: 275 – 282

Gjerstad KI, Stamnes JJ, Hamre B, Lotsberg JK, Yan B, and Stamnes K (2003) Monte Carlo and discrete-ordinate simulations of irradiances in the coupled atmosphere-ocean system. Appl. Opt. 42: 2609 – 2622

Goes JI, Handa N, Taguchi S, Hama T, and Saito H (1995) Impact of natural ultraviolet radiation on production patterns and composition of dissolved free and combined amino acids in marine phytoplankton. J. Plankton Res. 17: 1337 – 1362

Gordon HR (1997) Atmospheric correction of ocean color imagery in the Earth Observing System era. J. Geophys. Res. 102: 17,081 – 17,106

Häder DP (ed) (1997) The effect of ozone depletion on aquatic ecosystems. R.G. Landes Company, Academic Press, Austin

Häder DP, Kumar HD, Smith RC, and Worrest RC (1998) Effects on aquatic ecosystems. J. Photochem. Photobiol. B: Biology 46: 53 – 68

Hamre B, Winther J-G, Gerland S, Stamnes JJ, and Stamnes K (2004) Modeled and measured optical transmittance of snow covered first-year sea ice in Kongsfjorden, Svalbard. J. Geophys. Res. 109:DOI:10.1029/2003JC001926

Hamre B, Stamnes JJ, Frette Ø, Erga SR, and Stamnes K (2008) Could stratospheric ozone depletion lead to enhanced aquatic primary production in the polar regions? Limnol. Oceanogr. 53: 332 – 338

Herman JR, Barthia PK, Ahmad Z, and Larko D (1996) UV-B radiation increases (1979 – 1992) from decreases in total ozone. Geophys. Res. Lett. 23: 2117 – 2120

Herman JR, McKenzie RL, Diaz SB, Kerr JB, Madronich S, and Seckemeyer G (1999) Ultraviolet radiation at the earth's surface. In: Scientific Assessment of Ozone Depletion: 1998 WMO Rep. 44, World Meteorol. Org., Global Ozone Res. Monit. Proj., Geneva, Switzerland, pp 9.1 – 9.46

Holm-Hansen O, Lubin D, and Helbling EW (1993a) Ultraviolet radiation and its effects on organisms in aquatic environments. In: Young AR, Björn LO, Moan J, Nultsch W (eds) Environmental UV Photobiology, Plenum Press, New York

Holm-Hansen O, Helbling EW, and Lubin D (1993b) Ultraviolet radiation in Antarctica: Inhibition of primary production. Photochem. Photobiol. 58: 567 – 570

Jiang S, Stamnes K, Li W, and Hamre B (2005) Enhanced Solar Irradiance Across the Atmosphere-Sea Ice Interface: A Quantitative Numerical Study. Appl. Opt. 44: 2613 – 2625

Jin Z, and Stamnes K (1994) Radiative transfer in nonuniformly refracting media such as the atmosphere/ocean system. Appl. Opt. 33: 431 – 442

Jin Z, Stamnes K, Weeks WF, and Tsay SC (1994) The effect of sea ice on the solar energy budget in the atmosphere-sea ice-ocean system: A model study. J. Geophys. Res. 99: 25281 – 25294

Jin Z, Charlock TP, Rutledge K, Stamnes K, Wang Y (2006) An analytical solution of radiative transfer in the coupled atmosphere-ocean system with rough surface. Appl. Opt. 45: 7443 – 7455

Jokiel PL, and York RH (1984) Importance of ultraviolet radiation in photoinhibition of microalgae growth. Limnol. Oceanogr. 29: 192 – 199

Karentz D, Cleaver JE, and Mitchell DL (1991) Cell survival characteristics and molecular responses of Antarctic phytoplankton to ultraviolet-B radiation. J. Phycol. 27: 326 – 341

Karentz D, McIntyre S, Matlick HA, Menzies D, Ondrusek M, Wan Z, and Waters KJ (1992) Ozone depletion: Ultraviolet radiation and phytoplankton biology in Antarctic waters. Science 255: 952 – 959

Legendre L, Ackley SF, Dieckmann GS, Gullicksen B, Horner R, Hoshiai T, Melnikov IA, Reeburgh WS, Spindler M, and Sullivan CW (1992) Ecology of sea biota: 2. Global significance. Polar Biol. 12: 429 – 444

Lenoble J (ed) (1985) Radiative Transfer in Scattering and Absorbing Atmospheres: Standard Computational Procedures. A. Deepak, Hampton, VA

Li W, Stamnes K, Spurr R, and Stamnes JJ (2008) Simultaneous retrieval of aerosols and ocean properties: A classic inverse modeling approach. Ⅱ. SeaWiFS Case Study for the Santa Barbara Channel. Int. J. Rem. Sens. DOI: 10.1080/01431160802007632, 29, 5689 – 5698

Lobman M, Döhler G, Huckenbeck N, and Verdini S (1998) Effects of UV radiation of different wavebands on pigmentation, 15N-ammonium uptake, amino acid pools and adenylate contents of marine diatoms. Mar. Biol. 130: 501 – 507

Mobley CD (1994) Light and water: radiative transfer in natural waters. Academic Press, San Diego, CA

Mobley CD, Gentili B, Gordon HR, Jin Z, Kattawar GW, Morel A, Reinersmann P, Stamnes K, and Stavn RH (1993) Comparison of numerical models for computing underwater light fields. Appl. Opt. 32: 7484 – 7504

Morel A (1974) Optical properties of pure sea water. In: Jerlov NG, Nielsen ES (eds) Optical Aspects of Oceanography, Academic Press, pp.1 – 24

Morel A (1991) Light and marine photosynthesis: A model with geochemical and climatological implications. Prog. Oceanogr. 26: 263 – 306

Morel A, and Gentili B (1991) Diffuse reflectance of oceanic waters: Its dependence on sun angle as influenced by the molecular scattering contribution. Appl. Opt. 30: 4427 – 4438

Morel A, and Maritorena S (2001) Bio-optical properties of oceanic waters: A reappraisal, J. Geophys. Res. 106: 7163 – 7180

Neale PJ, Cullen JL, Lesser MP, and Melis A (1993) Physiological bases for detecting and predicting photoinhibition of aquatic photosynthesis by PAR and UV radiation. In: Yamamoto

H (ed) Photosynthetic response to the environment. American Society of Plant Physiology, Rockville, pp.61 – 77

Neale PJ, Cullen JJ, and Davis RF (1998) Inhibition of marine photosynthesis by ultraviolet radiation: Variable sensitivity of phytoplankton in the Weddell-Scotia Confluence during the austral spring, Limnol. Oceanogr. 43: 433 – 448

Pegau WS, Cleveland JS, Doss W, Kennedy CD, Maffione RA, Mueller JL, Trees CC, Weidemann AD, Wells WH, and Zaneveld JRV (1995) A comparison of methods for the measurement of the absorption coefficient in natural waters. J. Geophys. Res. 100: 13,201 – 13,220

Perovich DK, and Maykut GA (1996) Solar heating of a stratified ocean in the presence of a static ice cover. J. Geophys. Res. 95: 18,233 – 18,245

Pope RM, and Fry ES (1997) Absorption spectrum (380 – 700 nm) of pure water, Ⅱ, Integrating cavity measurements. Appl. Opt. 36(33): 8710 – 8723

Prézelin BB, Boucher NP, and Smith RC (1994) Marine primary production under the Antarctic ozone hole. In: Weiler S, Penhale P (eds) Ultraviolet Radiation and Biological Research in Antarctica, Antarctic Research Series 62: 159 – 186

Rottman GJ, Woods TN, and Sparn TP (1993) Solar stellar irradiance comparison experiment I. Instrument design and operation. J. Geophys. Res. 98: 10,667 – 10,678

Slaper H, Velders GJM, Daniel JS, de Gruijl FR, and van der Leun JC (1995) Estimates of ozone depletion and skin cancer to examine the Vienna Convention achievements. Nature 384: 256 – 259

Smith RC, and Baker KS (1989) Stratospheric ozone, middle ultraviolet radiation and phytoplankton productivity. Oceanogr. Mag. 2: 4 – 10

Smith RC, Prezelin BB, Baker KS, Bidigare RR, Boucher NP, Coley, T, Karentz D, Maclntyre S, Matlick HA, Menzies D, Ondrusek M, Wan Z and Waters KJ (1992) Ozone depletion: Ultraviolet radiation and phytoplankton biology in Antarctic waters. Science 255: 952 – 957

Solomon S (1990) Progress towards a quantitative understanding of Antarctic ozone depletion. Nature 347: 347 – 354

Stamnes K, Tsay S-C, Wiscombe WJ, and Jayaweera K (1988) Numerically stable algorithm for discrete-ordinate-method radiative transfer in multiple scattering and emitting layered media. Appl. Opt. 27: 2502 – 2509

Stamnes K, Tsay S-C, Wiscombe WJ, and Laszlo I (2000) DISORT, A General-Purpose Fortran Program for Discrete-Ordinate-Method Radiative Transfer in Scattering and Emitting Layered Media: Documentation of Methodology, Report. ftp://climate1.gsfc.nasa.gov/wiscombe/

Stamnes K, Li W, Yan B, Eide H, Barnard A, Pegau WS, and Stamnes J (2003) Accurate and self-consistent ocean color algorithm: simultaneous retrieval of aerosol optical properties and chlorophyll concentrations. Appl. Opt. 42: 939 – 951

Thomas GE, and Stamnes K (1999) Radiative Transfer in the Atmosphere and Ocean. Cambridge University Press

Vasilkov A, Krotkov N, Herman J, McClain, K. Arrigo C, and Robinson W (2001) Global mapping of underwater UV irradiances and DNA-weighted exposures using Total Ozone Mapping Spectrometer and Sea-viewing Wide Field-of-view Sensor data products. J. Geophys Res. 106: 27202 – 27219

Wängberg S-Aa, Garde K, Gustavson K, and Selmer J (1999) Effects of UV-B radiation on marine phytoplankton communities. J. Plankton Res. 21: 147 – 166

Wheeler PA, Gosselin M, Sherr EE, Thibault D, Kirchman DL, Benner R, and Whitledge TE (1996) Active cycling of organic carbon in the central Arctic Ocean. Nature 380: 697 – 699

Worrest RC (1986) The effect of solar UV-B radiation on aquatic systems: An overview. In: Titus JG (ed) Effects of Changes in Stratospheric Ozone and Global Climate, Overview. U.S. Environmental Protection Agency and United Nations Environmental Program 1, pp.175 – 191

Zeebe RE, Eicken H, Robinson DH, and Wolf-Gladrow D (1996) Modeling the heating of melting sea ice though light absorption by microalgae. J. Geophys. Res. 101: 1163 – 1181

Zeng J, Jin Z, and Stamnes K (1993) Impact of stratospheric ozone depletion on UV penetration into the ocean at high latitudes. In: Underwater Light Measurements. Proc. SPIE 2048: 56 – 63

Zerefos CS, and Bais AF (eds) (1997) Solar Ultraviolet Radiation: Modeling, Measurements and Effects. Springer-Verlag, Berlin

10 Comparative Analysis of UV-B Exposure Between Nimbus 7/TOMS Satellite Estimates and Ground-Based Measurements

Wei Gao[1], Zhiqiang Gao[1,2], and Ni-Bin Chang[3]

[1] USDA UV-B Monitoring and Research Program, Natural Resource Ecology Laboratory, Colorado State University, Fort Collins, CO, USA
E-mail: wgao@uvb.nrel.colostate.edu
E-mail: zgao@uvb.nrel.colostate.edu
[2] Institute of Geographical Sciences and Natural Resources Research, Chinese Academy of Sciences, Beijing, China
[3] Department of Civil and Environmental Engineering, University of Central Florida, Orlando, FL 32816, USA
E-mail: nchang@mail.ucf.edu

Abstract This study describes the patterns of variation in ultraviolet (UV) exposure across time and space, using two continental scale datasets on UV radiation, and conducts a comparative analysis of two sources of noontime UV-B exposure data across the continental U.S. One dataset was collected from 37 ground-based stations equipped with broadband UV-B-1 Pyranometers across North America whereas the other dataset was of synchronous satellite data collected from the Nimbus-7/TOMS sensor. Comparisons of these datasets confirmed agreement between the ground-based measurements and the TOMS satellite estimates with correlation coefficients of 0.87 and 0.95 for daily and monthly Ultraviolet Index (UV-I) time series (i.e., a common metric of UV radiation exposure), respectively. The UV-I value observed by the TOMS sensor is generally greater than that of the USDA ground-based measurements, and the relative error of daily change is, on average, between 5% and 12%. With these two datasets from 1999 to 2005, the trend analyses for daily and monthly UV-I change are statistically summarized at four representative stations distributed across the western U.S as an integral part of the USDA monitoring network. Spatial and temporal features may then be illuminated and retrieved according to UV-I distribution. Overall, the UV-I data acquired by the TOMS sensor can sufficiently detect the effect of spatial variation in topography, whereas continuous measurements through the USDA UV-B

ground-based monitoring network can provide better temporal resolution on holistic changes in UV-I within the last few years.

Keywords UV-B, UV-I, remote sensing, TOMS, U.S.

10.1 Introduction

The sun gives off ultraviolet (UV) radiation that may be divided into three categories based on the wavelength: ultraviolet-A (UV-A, from 320 nm to 400 nm), ultraviolet-B (UV-B, from 290 nm to 320 nm), and ultraviolet-C (UV-C, from 100 nm to 290 nm). It is known that sunlight can impact the skin, causing premature skin aging, skin cancer, and a host of skin changes (Dharmarajan, 2008). Exposure to UV light, such as UV-A or UV-B, from sunlight accounts for 90% of the symptoms of premature skin aging (Dharmarajan, 2008). Ultraviolet light, UV-B in particular, also has the potential to harmfully impact vegetation and livestock. This is especially true at lower latitudes (30.8°S – 30.8°N) during the summer, where the amount of noontime UV radiation is the largest because of smaller solar zenith angles (SZAs). Due to the negative effects of ultraviolet light on humans, livestock, agricultural crops, and forest health, it is critical to be able to assess levels of UV radiation and to estimate its impacts. Many factors affect UV radiation levels and measurements, including extraterrestrial solar irradiance, atmospheric ozone, cloud reflectivity, aerosol amounts, and ground albedo. For example, changes in the earth's atmospheric condition caused by anthropogenic and natural pollutants has led to the well-documented decline in ozone and the corresponding increase in UV irradiance at the earth's surface. Yet the amount of ultraviolet radiation penetrating to the earth's surface with wavelengths shorter than 320 nm (UV-B) can be reduced by tropospheric ozone absorption, aerosols, clouds, and Rayleigh scattering in the atmosphere.

Concerns about increases in surface UV-B have triggered immense scientific and societal interest, especially following the discovery of the ozone hole in the Antarctic and the serious ozone decreases in middle and high latitudes (Herman et al., 2000; 2001; Krotkov et al., 2001). To date, UV has been observed from space for more than 20 years. Early satellite UV measurements were made by the Backscatter Ultraviolet (BUV) sensor onboard the Nimbus 4 platform, which was launched in 1970 and continued functioning for several years. Nimbus 7 provided the longest high-quality space-borne UV observation with the aid of the total ozone mapping spectrometer (Nimbus-7/TOMS) from 1979 – 1993. The National Oceanographic and Atmospheric Administration (NOAA) weather satellites also measured UV radiances for a considerable period with the Solar Backscatter Ultraviolet (SBUV) sensor. TOMS was mainly designed for determining the vertically integrated ozone amount, while SBUV was designed for obtaining ozone profiles. These data are invaluable for studying both ozone and surface UV

radiation. In addition to the Nimbus7, the TOMS instrument was also flown onboard the Russian Meteor 3 from 1991 to 1994, on the Japanese ADEOS for less than a year in 1996－1997, and is currently on the National Aeronautical and Space Administration's (NASA) Earth Probe. Ozone data may also be derived from the TIROS Operational Vertical Sounder (TOVS), the Stratospheric Aerosol and Gas Experiment (SAGE and SAGE Ⅱ), the Global Ozone Monitoring Experiment (GOME) onboard the European ERS-2 satellite, among others. Together, these satellites provide a wealth of data regarding ozone and UV radiation (Wang et al., 2000; Fioletov et al., 2001; 2002; 2003; 2004).

In addition, hundreds of ozone/UV ground-based stations are operating around the globe. Such a long-term, well-established ground-based monitoring network, equipped with the SUV-100 double monochromator instrument, produces consistent UV-B measurements which may be used as the ground-truthing data for satellite data assimilation. These data are well archived by the World Ozone and Ultraviolet Radiation Data Center (WOURDC) of the World Meteorological Organization (WMO) operated by Environment Canada. Stations in the U.S. include the National Science Foundation (NSF) Polar UV Network and the U.S. Department of Agriculture (USDA) UV-B Monitoring and Research Program (UVMRP), which was initiated in 1992 to provide information on the geographical distribution and temporal trends of UV-B radiation in the U.S. The initial network of 12 stations was established in 1994. The network has expanded to 37 climatologic locations plus several research sites. Comparisons of UV-B estimates between Nimbus 7/TOMS satellite data and ground-based measurements may contribute to the potential spatial application of satellite images in the future.

Previous efforts for comparing these two time series laid down the basic foundation of the potential accuracy of the TOMS imageries (Vitali et al., 2002; Ye et al., 2002; Ziemke et al., 2003). Near-to-real time, as well as "archive quality," Brewer UV observations, which are performed with well-maintained and calibrated instruments over the Northern Hemisphere, have been used for the validation of the TOMS imageries. Kaurola (2000) studied the correspondence between the data from: (1) ground-based observations, (2) surface UV Index (UV-I) (i.e., a common metric of UV radiation exposure) determined using TOMS satellite measurements, and (3) reconstructed UV doses using observations of global radiation. Different trend estimates were in very close agreement with each other. Kalliskota (2000) adopted daily UV erythemal doses estimated from Nimbus-7/ TOMS measurements (from 1991 to May 1993) and those calculated from ground-based spectroradiometer data at Ushuaia, Argentina (for 573 days), Palmer, Antarctica (for 450 days), and San Diego, California (for 149 days), and then made comparisons between the datasets. McKenzie (2001) studied the differences between satellite-derived estimates of UV and ground-based measurements at three stations located in northern Europe (Belsk, Norrköping, and Jokioinen) and a clean air site in the Southern Hemisphere. Vitali (2002) found that there are some systematic differences between the measurements of the ground and satellite-

retrieved UV irradiance. The Brewer data are lower than TOMS-estimated UV irradiance by 9% to 10%, on average. Cede (2004) obtained data over a period of more than 4,700 days from 1997 to 1999 at 8 stations of the Argentina UV Monitoring Network to study the major factors that are causing the differences between satellite-derived and ground-based UV erythemal irradiances and doses. Using hourly UV-I values at 45 sites in Canada, Fioletov (2003) made direct comparisons of Brewer measurements and TOMS data showing an agreement within 2% to 3%, except during periods of melting snow when variations in snow albedo yielded higher errors in the UV irradiance derived from both sources. Using long-term monthly mean UV-I values for Canada and the U.S. Fioletov et al. (2004) found that in summer, TOMS UV-I climatology values are 10% to 30% higher than those derived from global solar radiation and other parameters. In this instance, TOMS estimates agree with Brewer measurements. The difference is probably related to aerosol absorption and pollution effects in the lower troposphere which are not currently detected from space. For 21 of 28 mid-latitude Brewer sites, long-term mean summer UV measured values and UV derived from global solar radiation and other parameters agree to within +5% to +7% (Fioletov et al., 2004). The remaining 7 sites are located in "clean" environments where TOMS estimates agree with Brewer measurements, while UV derived from global solar radiation and other parameters is 10% to 13% lower (Fioletov et al., 2004).

Advanced and comprehensive data assimilation methods are essential to model UV radiation from satellite data. These methods span from directly retrieving surface UV (Li et al., 2000), to statistical models (Fioletov et al., 2001), to the Lambert equivalent reflectivity (LER) method (Krotkov et al., 2001), to inversion algorithms (Wang et al., 2000; Ciren et al., 2003). The simple and efficient method for retrieving surface UV (i.e., DISORT-based model) relies on ground-based measurements as ground-truthing to improve the estimation accuracy. The statistical model developed to extend the record of UV back to the early 1960s estimates UV values (at individual wavelengths and spectrally integrated) from global solar radiation, total ozone, dew point temperature, and snow cover (Fioletov et al., 2001).

With such a similarity between the ground-based measurements and satellite data, a suite of trend analyses in regard to the UV variations at differing scales is feasible. By using datasets from the NASA TOMS from 1979 to 1992, Udelhofen (1999) confirmed that statistically significant increases in erythemal UV radiation exposures have occurred during the summer months in the tropics of the Australian continent over multiple decades. These were associated with a simultaneous depletion of ozone and a decrease in cloud cover. Chubarova (2000) analyzed the UV trend with UV irradiance data from Moscow over a 30-year study period. An algorithm was developed to calculate the variability in erythemally weighted (EW) irradiance for the entire period. The analysis of variability in UV 380 and EW irradiance showed a slight increase in UV values since the middle of the 1980s.

Fioletov et al. (2001) explored variations of the UV-I in the context of climatology using both ground-based measurements and satellite data without including spatial analyses. Herman (2001) studied the phenomena of the quasi-biennial oscillation (QBO), and found that it can cause interannual changes of UV-B exposure by 61.5% at 300 nm and 65% at 310 nm at the equator and at middle latitudes.

As seen from the literature review above, major efforts have been devoted to conduct time series and trend analyses of UV radiation. In this chapter, a thorough comparative analysis is conducted between the daily UV-B doses estimated from the Nimbus-7/TOMS data and those calculated from the ground-based spectroradiometer measurements. Ground measurements of daily UV-B data from 2000 to 2005 were collected around noontime (11:00 ~ 13:00) at the 37 ground monitoring stations in the USDA network. The corresponding TOMS data was investigated for the purpose of comparison. To show the statistical relationship between these datasets, an assessment of UV-I climatology was performed based on four representative ground stations.

10.2 Materials and Methods

10.2.1 USDA UV-B Dataset

The UVMRP provides the USDA with the UV-B-1 radiometer information necessary to determine if changing levels of ultraviolet light have an effect on food and fiber production in the U.S. The primary objective of the UVMRP is to provide information to the agricultural community about the geographic and temporal climatology of UV-B irradiance. All data from the network is captured by on-site data loggers and downloaded over phone lines each morning. Data is made available to the scientific community, as well as the general public, for next day retrieval via the network's World Wide Web site at http://uvb.nrel.colostate.edu. Figure 10.1 shows the locations of all 37 ground stations and highlights 4 sites (circled) selected for a detailed statistical analysis, namely, stations WA01, CA01, CO01, AZ01. These 4 stations are geographically well-distributed, with WA01 located in the north, AZ01 in the south, CO01 in the center, and CA01 in the west.

10.2.2 TOMS Dataset

In contrast to the ground-based point measurements, satellite data may provide us with global coverage at a moderate resolution by standard sensors that have been observing UV from space for more than 20 years. The EP/TOMS dataset can be used for monitoring long-term trends in total column ozone as well as the seasonal

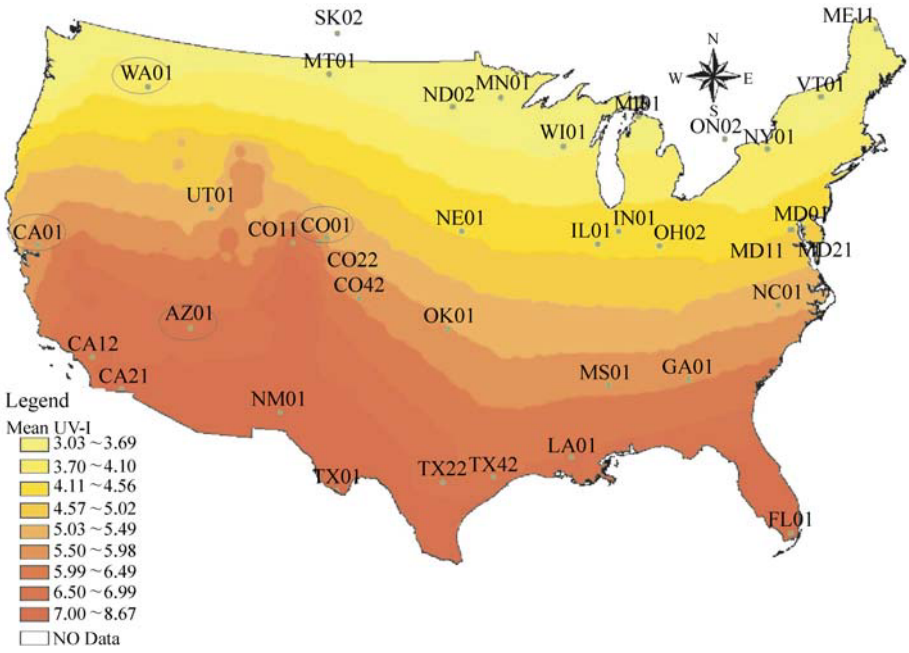

Figure 10.1 Map of the 37 USDA ground stations, 4 of which are circled for statistical analysis

chemical depletions in ozone that occur in both the southern and northern hemisphere polar springs. EP/TOMS also generates the erythemal exposure data product, which is an estimate of the daily integrated UV irradiance, calculated by using a model of the susceptibility of Caucasian skin to sunburn (erythema). This can be interpreted as an index of the potential for biological damage due to solar irradiation, and depends on the column ozone amount and cloud conditions on a given day.

The erythemal exposure was used in this study as a means for UV-B estimation from TOMS satellite data, and is mathematically defined by the following integral,

$$\mathrm{Exp} = \frac{1}{d_{\mathrm{es}}} \int_{280\ \mathrm{nm}}^{400\ \mathrm{nm}} \mathrm{d}_{\lambda} S(\lambda) W(\lambda) \int_{t_{\mathrm{ss}}}^{t_{\mathrm{sr}}} \mathrm{d}_t C(\lambda, \vartheta, \tau_{\mathrm{cl}}) F(\lambda, \vartheta, \Omega) \qquad (10.1)$$

where d_{es} is the distance from the earth to the sun (A.U.); S is the solar irradiance incident on the top of the atmosphere at 1 A.U. (nW m^{-2} nm^{-1}); W is the biological action spectrum for erythemal damage (B.D.); t_{sr} and t_{ss} are the time of sunrise and sunset (radian), respectively; C is the cloud attenuation factor (unitless); τ_{cl} is cloud optical thickness (unitless); ϑ is the SZA that is a function of time (radian); F is the spectral irradiance at the surface under clear skies normalized to unit

solar spectral irradiance at the top of the atmosphere (unitless); and Ω is the total column ozone (DU).

According to McKinlay et al. (1987), the earth-sun distance, times of sunrise and sunset, and the dependence of the SZA on the time of day depend on the latitude and the time of year, and are calculated from standard formulae. The extraterrestrial solar irradiance incident at the top of the atmosphere when the earth is at a distance of 1 A.U. from the sun was measured over the wavelength interval of interest by the UARS/SOLSTICE instrument. The weighting function used to approximate the wavelength-dependent sensitivity of Caucasian skin to erythema-causing radiation followed the model proposed by McKinlay and Diffey (1998a, b) and was adopted as a standard by the Commission Internationale de l'Éclairage (CIE).

10.2.3 UV Index

The term "erythema" refers to the reddening of the skin due to sunburn. For UV-induced erythema, the action spectrum adopted by most international organizations is the CIE, International Commission on Illumination's action spectrum (E), using the method described by McKinlay and Diffey (1987a, b). The erythemal action spectrum is specified over three spectral ranges as: (1) $W(\lambda)=1$ for $250\ \text{nm}<\lambda<298\ \text{nm}$, (2) $W(\lambda)=10^{0.094(298-\lambda)}$ for $298\ \text{nm}<\lambda<328\ \text{nm}$, and (3) $W(\lambda)=10^{0.015(139-\lambda)}$ for $328\ \text{nm}<\lambda<400\ \text{nm}$. The UV-I itself is an irradiance scale computed by multiplying the CIE irradiance in watts m^{-2} by 40. For a fairly wide range of atmospheric conditions, the CIE weighted irradiance changes by approximately 1.2% for a change of 1.0% in the ozone value. Thus the clear sky value at sea level in the tropics would normally be in the range $10-12$ ($250\ \text{nm}-300\ \text{mWm}^{-2}$), with 10 being an exceptionally high value for northern mid-latitudes. This scale has been adopted by the WMO and the World Health Organization (WHO), and is in use in a number of other countries (Environment Canada, 2008). Ultraviolet intensity is also described in terms of UV-I ranges running from low values ($0-2$) to medium ($3-5$), high ($6-7$), very high ($8-10$) and extreme ($11+$). Other irradiance integrals exist which describe other physical and biological effects of UV radiation. However, this one has become the one used most often (Environment Canada, 2008).

10.2.4 Comparative Analysis

Using the 37 USDA point measurements of daily noontime (11:00 AM to 1:00 PM) UV-B time series data from 1999 to 2005, across the continental U.S., the UV-I was generated from an irradiance scale that was computed by multiplying the CIE irradiance in watts m^{-2} by 40 (Environment Canada, 2008). By spatially

interpolating daily and monthly UV-I data, the seasonal and yearly UV-I spatial data were produced. At the same time, synchronous TOMS data were acquired for the purpose of comparison. Finally, a comparison of daily UV doses estimated from Nimbus 7/TOMS measurements and ground-based spectroradiometric data was conducted to examine the agreement of these two sources of data statistically. To present the comparison in detail, several analyses of the daily variation, trends, and spatial distribution characteristics of UV-I are discussed.

10.3 Results and Discussion

10.3.1 UV-I Daily Change Analysis

We produced the daily derived UV-I data from 1999 to 2005 that was associated with the four representative ground-based stations and TOMS data to demonstrate the correspondence between the two data sets by statistical analyses (Table 10.1) and to verify the degree of agreement of the data between these two sources (Fig. 10.2). Table 10.1 provides mean, median, minimum, maximum, std. error, standard deviation, values, and correlation coefficients between the datasets. These summary statistics reveal the degree of correspondence between the two data sources. The maxima of the multi-year time series between these two sources are very close, and the absolute disparity is between 0.2 and 0.8 units. Median values from TOMS were always larger than those from USDA ground-based observations. As for the mean values, TOMS data are 5% to 12% larger than those of the USDA ground-based observations. The standard error of mean at these four stations is between 5.9% and 7.6%. Both standard error of mean and standard deviation are very close at three of the stations—WA01, CA01, and CO01, which shows the

Table 10.1 Daily statistical analysis of UV-I data collected from four ground stations and the TOMS data

	WA01		CO01		CA01		AZ01	
	USDA	TOMS	USDA	TOMS	USDA	TOMS	USDA	TOMS
Minimum	0.12	0.01	0.11	0.35	0.00	0.03	0.00	0.42
Maximum	10.50	10.70	13.08	12.24	11.20	11.63	14.20	12.86
Mean	3.84	4.03	5.20	5.83	5.26	5.83	6.53	6.95
Median	3.08	3.56	4.44	5.47	5.28	5.97	6.02	7.18
Std. error	0.059	0.060	0.073	0.074	0.063	0.066	0.076	0.067
Std. deviation	2.91	2.96	3.38	3.39	3.13	3.26	3.73	3.28
Correlation coefficient	0.94		0.87		0.96		0.87	

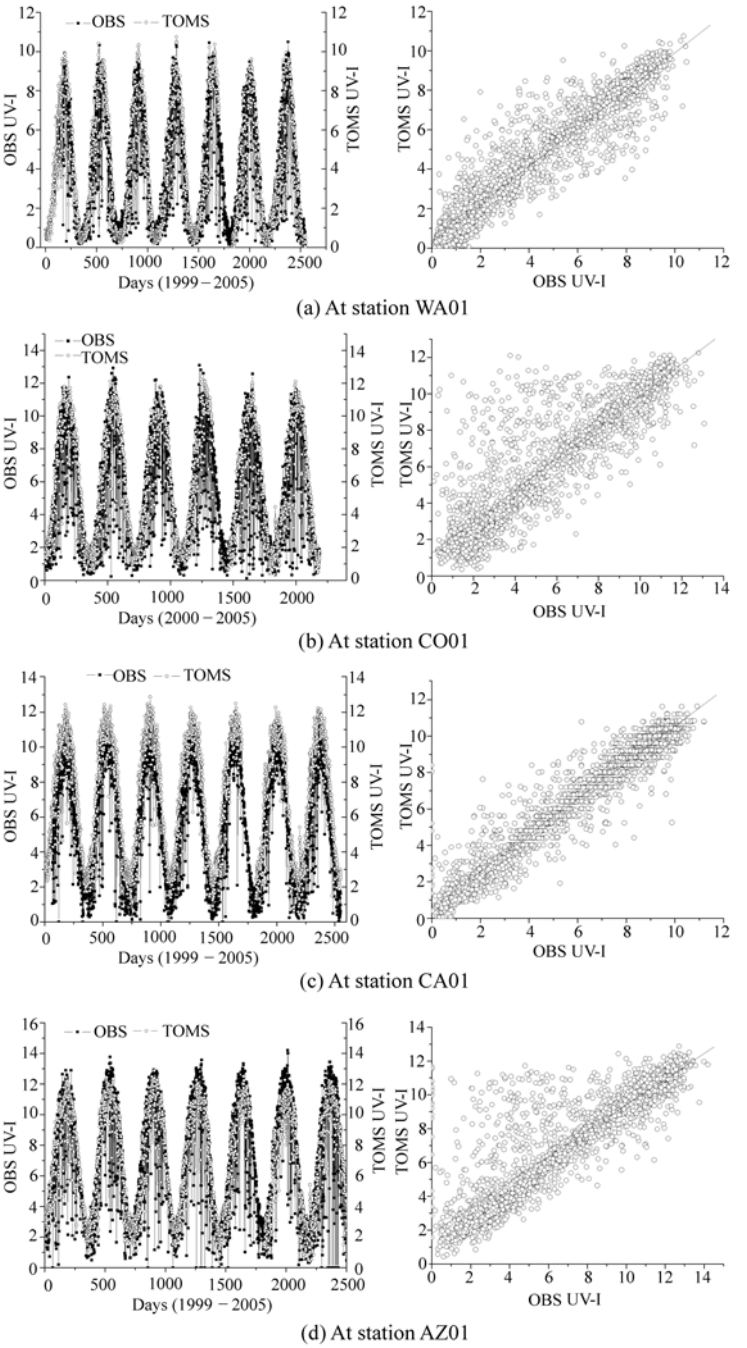

Figure 10.2 Daily UV-I time series variations (left) and the scatter plot along the 45° angle bisector between the TOMS data and the USDA ground-based measurements (right) at 4 stations

similarity in fluctuations. The correlation coefficients associated with WA01 and CA01 are higher than 90% (i.e., significant test $P < 0.0001$), whereas the correlation coefficients associated with stations CO01 and station AZ01 are about 87% (i.e., significant test $P < 0.0001$). Such high agreement can also be seen in Fig.10.2, which plots the time-series of UV-I data and also the UV-I values from each data source against each other for all stations. Although there are some outliers that fall out of the 45° angle bisector (i.e., the one-to-one line), these scatter plots highlight the generally good agreement between the two datasets.

10.3.2 Analysis of UV-I Variability

This section compares trends in the data for monthly differences from the mean value over the six-year period. Positive values indicate greater UV exposure than the mean and negative values indicate reduced UV exposure. Comparing such sequences associated with both data sources may enable us to identify the general trend and can also characterize how the patterns they detect differ. Figure 10.3 summarizes such an analysis as a whole using a series of time series plots. Within each plot, the y axis represents the UV-I difference relative to the mean and the x axis represents the month over the study period. On a monthly time scale, UV-I peak values agree between the two datasets. The mean square values of the UV-I deviation from the monthly means at the WA01 station are 9.75 and 9.69 for the TOMS and ground-based measurements, respectively. Obviously, similar fluctuations of these two data sources are confirmed. Yet the negative slope of TOMS time series data at station WA01 indicates a decrease of the deviation relative to the monthly means of the multi-year UV-I time series trend, which is quite different from the long-term trend of the ground-based measurements at this station. At station CA01, the two datasets differ substantially in terms of both the locations of the peak values and the overall trend. The mean square values of the UV-I deviation from the monthly means at station CA01 are 9.43 and 11.39 for the TOMS and ground-based measurements, respectively. The unique finding is that TOMS data show a decreasing trend in the ground-based measurements. At station CO01, the negative slopes of both deviations relative to the monthly means show a decreasing trend associated with both data sources at this station. The mean square values of the UV-I deviation from the monthly means at station CO01 are 7.43 and 10.61, associated with TOMS and ground-based measurements, respectively. As for the analysis at station AZ01, the deviations relative to the monthly means indicate stronger monthly variation in both data sources. The mean square values of the UV-I deviation from the monthly means at station AZ01 are 11.56 and 18.88, associated with TOMS and ground-based measurements, respectively, which are much larger than those for the three other stations. The small positive slope of deviations relative to the monthly means of ground-based measurements shows an increasing trend but the TOMS data appear to be slightly decreasing at this station.

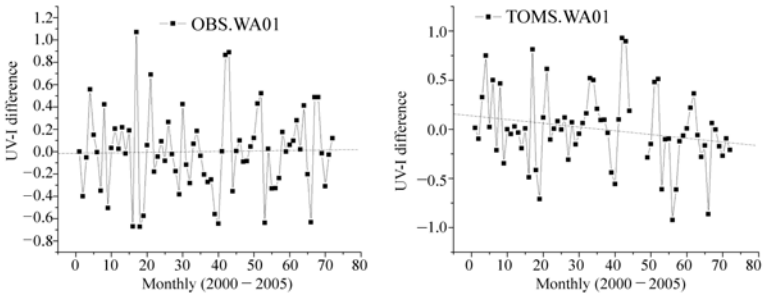

(a) Ground-based measurements at WA01 ;TOMS time series data at WA01

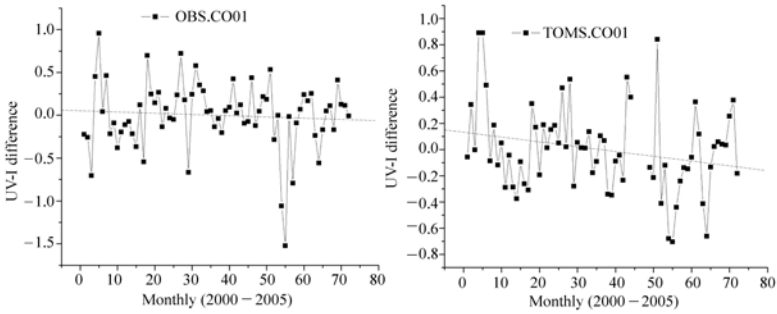

(b) Ground-based measurements at CO01 ;TOMS time series data at CO01

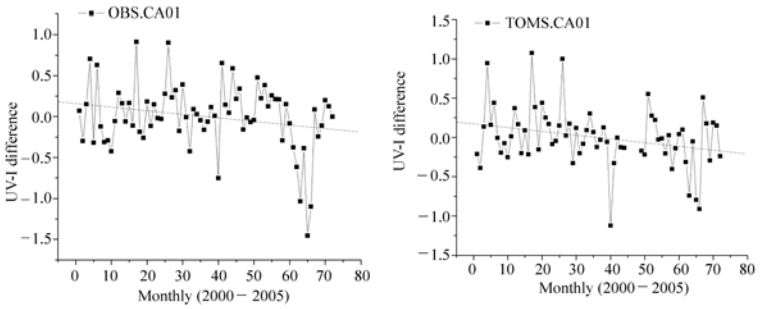

(c) Ground-based measurements at CA01 ;TOMS time series data at CA01

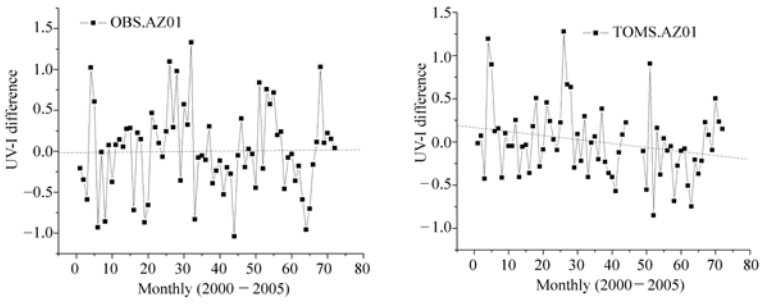

(d) Ground-based measurements at AZ01 ;TOMS time series data at AZ01

Figure 10.3 Trend analysis of the UV-I deviations relative to the monthly means associated with these two data sources at four stations

By comparing the four cases above, it can be concluded that the variability in the TOMS data fluctuations are changing with time at a greater rate than are the fluctuations in the USDA data. Because they are located at high elevation with less impact from clouds, ground-based measurements at stations CO01 (i.e., elevation 1641 m) and AZ01 (i.e., elevation 2073 m) are more consistent with the satellite observations. At the other 2 stations, WA01 (i.e., elevation 804 m) and CA01 (i.e., elevation 18 m), the corresponding impacts from surface clouds and climate factors become obvious. Time series longer than six years might help clarify such discrepancies in the future.

10.3.3 UV-I Spatial Analysis

Spatial patterns of UV-I observed by both data sources were also compared at a 4×4 km spatial resolution. Figures 10.4 – 10.7 collectively delineate the comparison of seasonal UV-I spatial patterns between ground-based measurements and TOMS satellite data. Figure 10.4 first summarizes these spatial patterns of the ground surface UV-I data by season. The two data sources portray very similar spatial distributions of springtime UV-I (Fig. 10.4). The maximum of the UV-I is 9 for the USDA ground-based measurements during spring. The region between the south of New Mexico and Texas and the southern tip of Florida, where the UV-I values exceed 8, accounts for 4.5% of the total study area. However, using the TOMS satellite data, the maximum of the UV-I in spring is 10.3, and the region where the UV-I values exceed 8 accounts for 13.6% of the total study area. This region covers almost all the southern states in the Gulf of Mexico up to the southern Colorado plateau. The minimum UV-I in spring is 3.4. Using the USDA ground-based measurements, the region surrounding the northern states and the Great Lakes, where the UV-I values are less than 4, accounts for 5.4% of the total study area, whereas, using the TOMS data, it accounts for 9.8% of the total study area. Overall, the means of the USDA ground-based measurements and the TOMS data are 5.8 and 6.1, respectively. The lower ground-based measurements could be attributed to the fact that they are interpolated from the point data, and are thus constrained to range between the values observed at the stations. The standard deviations of the UV-I values based on these two data sources are 12.15 and 15.64, respectively. From the minimum and maximum values associated with both data sources, it can be concluded that the TOMS data may exhibit more versatile spatial patterns in response to the terrain complexity. Due to the restrictions of surface observations, the UV-I spatial distribution based on the USDA ground-based measurements, shows less sensitivity in response to topographic features and terrain complexity. This is especially true in the Colorado Plateau.

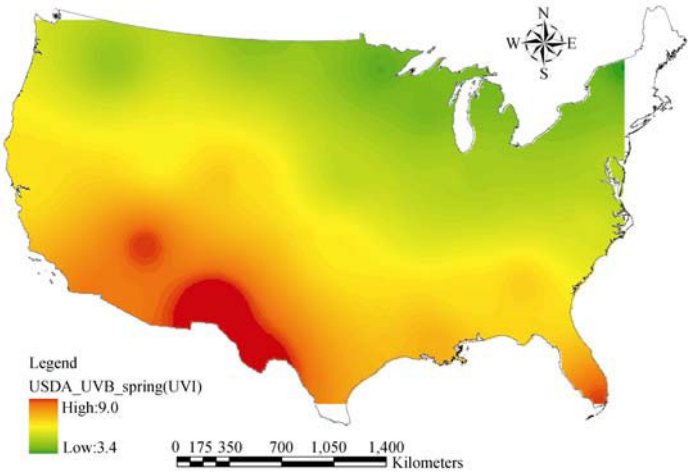

(a) USDA ground-based measurements

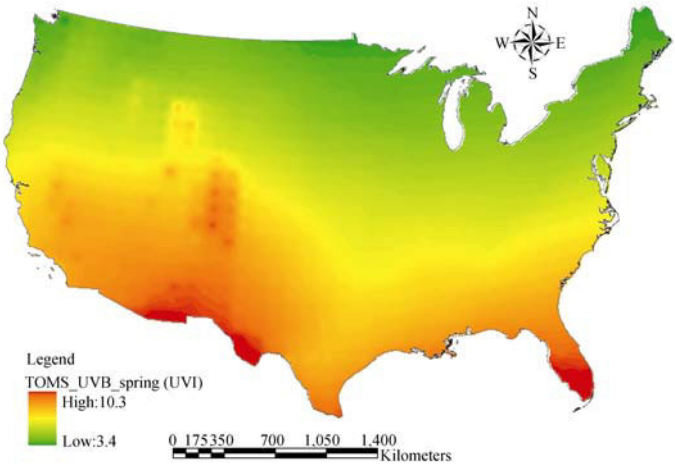

(b) TOMS data

Figure 10.4 Map of the UV-I spatial distributions in spring based on (a) USDA ground-based measurements and (b) TOMS data

In contrast, the UV-I spatial distribution maps associated with the two data sources in summer (see Fig. 10.5) do not portray similar patterns across the continental U.S. In summary, the maximum summertime UV-I is 10.6 with the USDA ground-based measurements. The area where the UV-I values exceed 10 accounts for 3.4% of the total study area. It spreads from the south of New Mexico and Texas, but is absent from the southern tip of Florida. The maximum of the UV-I in summer is 12 with the TOMS satellite data. The area where the UV-I values exceed 10 accounts for 20.9% of the total study area. It spreads from the

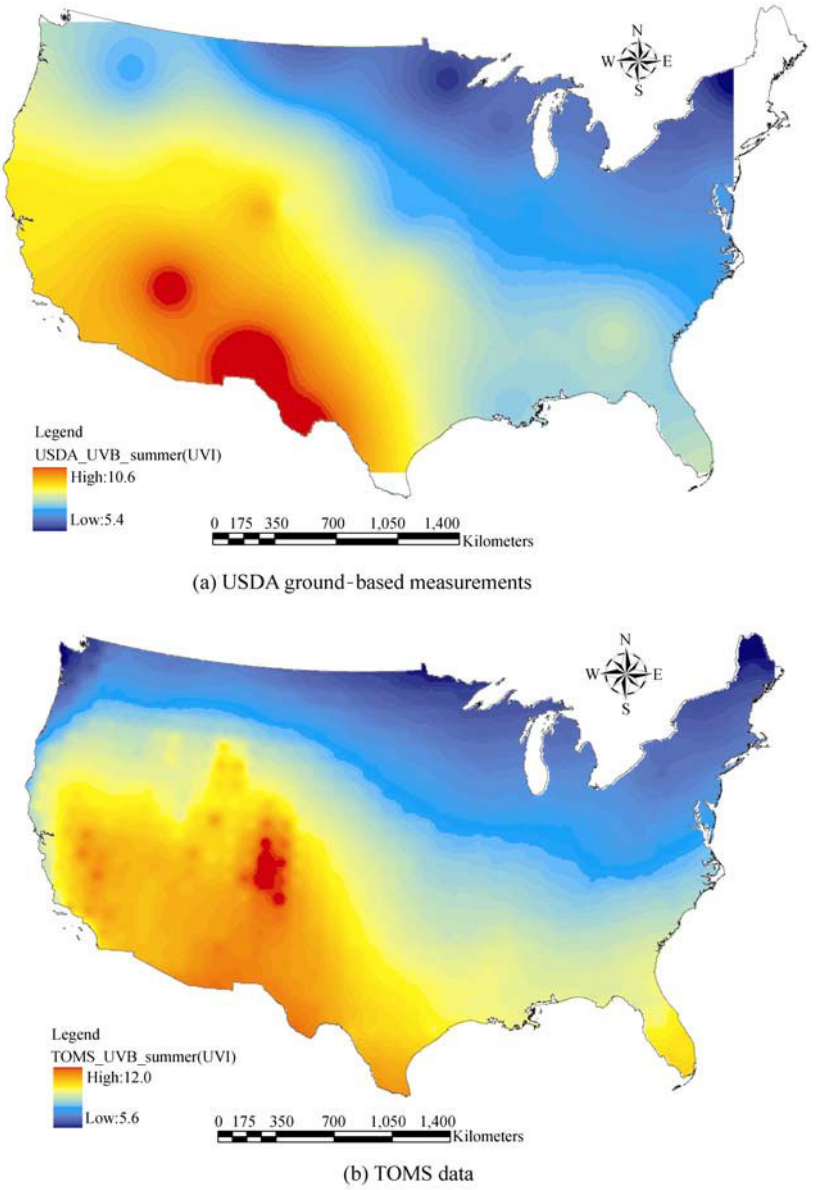

Figure 10.5 Map of the UV-I spatial distributions in summer based on (a) USDA ground-based measurements and (b) TOMS data

Colorado Plateau to southern Texas. The minimum from the USDA ground-based measurements data in summer is 5.4 and the area where the UV-I values are less than 6 accounts for 2.7% of the total study area. On the other hand, the minimum of TOMS satellite data in summer is 5.6 and the area where the UV-I values are less than 6, located mostly in the northern part of Wisconsin, Michigan, and Maine,

accounts for 0.7% of the total study area. Overall, the means of the USDA ground-based measurements and the TOMS data are 7.8 and 8.6, respectively. The standard deviations of the UV-I values based on these two data sources are 11.42 and 13.75, respectively. As in the spring, it can be concluded from the range of values associated with both datasets that the summertime TOMS data may exhibit more versatile spatial patterns in response to the terrain complexity.

The UV-I spatial distribution maps for fall (see Fig. 10.6) portray very similar patterns across the continental U.S. for both data sources (i.e., USDA and TOMS).

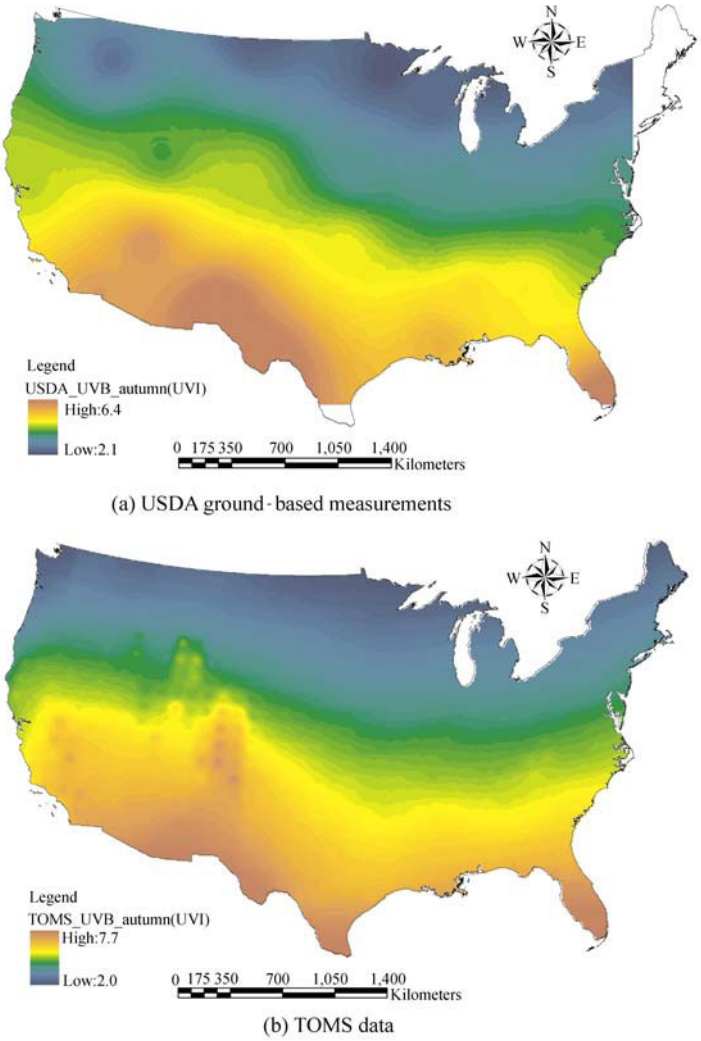

Figure 10.6 Map of the UV-I spatial distributions in fall based on (a) USDA ground-based measurements and (b) TOMS data

In summary, based on the USDA ground-based measurements, the maximum of the UV-I in fall is 6.4. The region spreading from the south of New Mexico, where the UV-I values exceed 6, accounts for 0.8% of the total study area. The maximum of the UV-I in fall is 7.7 based on the TOMS satellite data. The region covering southern Arizona, New Mexico, Texas and Florida, where the UV-I values exceed 6, accounts for 10.1% of the total study area. The minimum of the fall USDA ground-based measurements data is 2.1, and the area where the UV-I values are less than 2.0 accounts for 22.5% of the total study area. On the other hand, the minimum of TOMS satellite data in fall is 2.0, and the area where the UV-I values are less than 2.0 accounts for 18.7% of the total study area, located mostly in the northern part of the continental U.S. Overall, the means of the USDA ground-based measurements and the TOMS data are 3.8 and 4.3, respectively. The standard deviations of the UV-I values, based on these two data sources, are 9.25 and 12.43, respectively. Again, the TOMS data appear to be more sensitive to spatial patterns in response to the terrain complexity.

The two UV-I spatial distribution maps in winter (see Fig. 10.7) are also very similar. In summary, based on the USDA ground-based measurements, the maximum of the UV-I in winter is 4.8. The region located in the south of Texas and Florida, where the UV-I values exceed 4, accounts for 0.6% of the total study area. The maximum of the UV-I in winter is 5.9 with the TOMS satellite data. The region spreading across Arizona, New Mexico, Texas and also southern Florida, where the UV-I values exceed 4, accounts for 2.9% of the total study area. The minimum of USDA ground-based measurements data in winter is 0.9 and the region spreading from Minnesota and Michigan, to New York, where the UV-I values are less than 1.0, accounts for 2.7% of the total study area. On the other hand, the minimum of TOMS satellite data in winter is 0.3 and the region mostly located in the northern part of the continental U.S., where the UV-I values are less than 1.0, accounts for 22.5% of the total study area. Overall, the means of the USDA ground-based measurements and the TOMS data are 2.0 and 2.04, respectively. The standard deviations of the UV-I values based on these two data sources are 6.69 and 10.55, respectively. As with the rest of the year, TOMS data are better able to capture spatial variation in UV-I in response to topography.

Across all seasons, and for both USDA ground-based measurements and TOMS data, the distribution of the UV-I appears to be strongly tied to latitude and topography simultaneously. The higher the latitude, the smaller the UV-I value (Fig. 10.8). The maxima of seasonal and yearly UV-I values are distributed along the latitudes of Arizona, New Mexico, Texas, and southern Florida whereas the minima of the values are distributed across the upper latitudes of the Great Lakes and the Central Plains regions. The UV-I values were also greatly influenced by the topography from east to west. Along the same latitude, the UV-I value in the east is normally smaller due to lower altitudes, while the west is larger due to

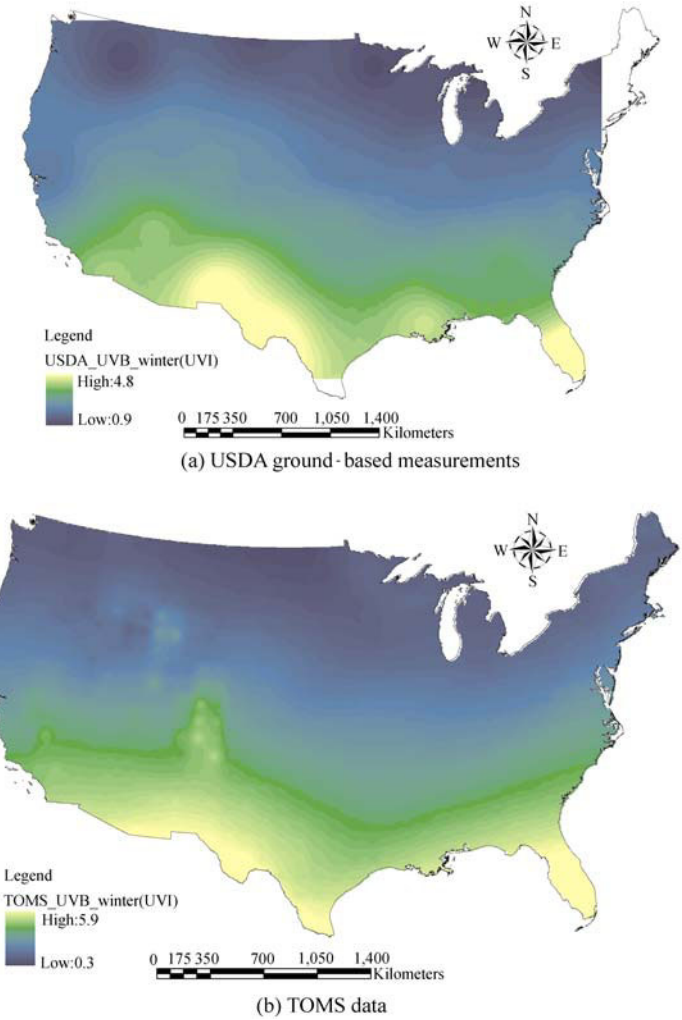

Figure 10.7 Map of the UV-I spatial distributions in winter based on (a) USDA ground-based measurements and (b) TOMS data

higher altitudes. Overall, as a result of the combination of the effects of both latitude and altitude, the UV-I distribution pattern shows a characteristic trend of high values in the southwest and low values in the northeast.

On average, the UV-I values based on TOMS data are 1 – 2 units larger than those based on USDA ground-based measurements. The spatial variation of TOMS data is much more evident and is less generalized than the ground-based counterpart. TOMS data can respond to the topography and latitude remarkably and can easily embody the spatial distribution patterns and characteristics of UV-I. Both types of data accurately depict the macroscopic spatial distribution pattern of UV-I in

the continental U.S., but TOMS better captures the coverage of spatial patterns. In any circumstance, the spatial comparisons described above are not intended to be indicative of the overall accuracy of either dataset.

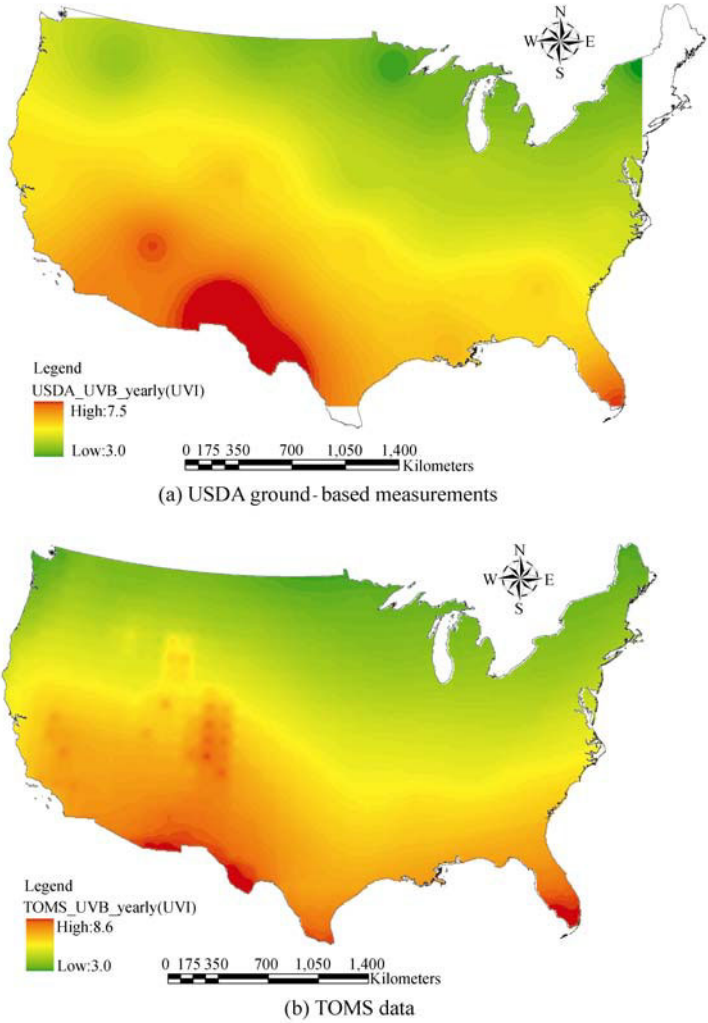

Figure 10.8 Maps of UV-I spatial distributions based on a multi-year average

10.4 Conclusions

This study compares the noontime UV-B data collected by the broadband UV-B-1 Pyranometer measurements against synchronous TOMS data measured over 1999

to 2005 across the continental U.S. These analyses were performed in order to provide insights into how the spatial and temporal patterns of UV-B may be collectively used to identify the UV impacts. For the temporal analysis, we compare trends in the data for monthly differences from the mean value over the five-year period. For the spatial analysis, each TOMS data set is interpolated across the continental U.S. to identify regions with low to high UV exposure for each of the four seasons and across years. However, after describing the patterns of variation in UV exposure across time and space using two continental scale datasets on UV radiation, we conclude that the two approaches are comparable and that the value of each is distinct.

To summarize the trend of daily and monthly changes of UV-I, four specific stations within the USDA network—WA01, CA01, CO01 and AZ01—were chosen for demonstration and comparison. This comparative analysis of UV-I time series data confirmed agreement between the USDA ground-based measurements and the TOMS satellite imageries with correlation coefficients of 0.87 (daily) and 0.95 (monthly). Spatial correlation coefficients between these data sources were as high as 0.93. These observations reveal that both sensors are consistent, reflecting their essential reliability for sensing, modeling, and predictions. Yet the UV-I values observed by the TOMS sensor are generally greater than those of the USDA ground-based measurements by $1-2$ units, on average, with a relative error of daily change between 5% and 12%. In addition, the TOMS data may be better able to represent the essential fluctuations due to latitudinal and topographical features as compared to the USDA ground-based measurements. Although both of these data sources can address the general spatial distribution of the UV-I across the continental U.S., TOMS data can perform relatively better, allowing the more accurate detection of the UV-I distribution pattern that uniquely delineates a transitional change from the high southwest and low northeast UV readings.

Such differences between the two data sources in terms of both spatial and temporal characteristics are mainly due to the fact that the TOMS data are satellite-based and remotely sensed with a resolution of 1×1.25 degree, which receive less impact from cloud cover, rainfall, humidity, ozone, and aerosols in the air. Ultraviolet-B radiation is normally reflected, scattered, and absorbed before reaching the land surface. As a consequence, the USDA ground-based measurement could be significantly affected by climatic factors such as cloud cover, rainfall, and temperature, as well as aerosols, ozone, and numerous other factors. Such findings account for the fact that USDA ground-based measurements are often lower than those of the TOMS data. Nevertheless, the USDA ground-based measurements may be better applied for time series analysis due to the capability to conduct intensive point measurements. The TOMS UV-I data that are often about $1-2$ units larger than the USDA ground-based measurements may be more applicable for exploring the regional patterns of UV-I distribution due to higher spatial resolution and sensitivity to the topography.

Acknowledgements

This research was supported by USDA CSREES under Contract Numbers: 2008-34263-19249 and 2006-34263-16926 and by USDA CSREES under Hatch/ Multistate, Contract Number: COL-00-250-W502. Thanks to Drs. John Davis and Heidi Steltzer for their valuable comments on this chapter.

References

Cede A, Luccini E, Nuñez L, Piacentini RD, Blumthaler M, and Herman JR (2004) TOMS-derived erythemal irradiance versus measurements at the stations of the Argentine UV monitoring network. Journal of Geophysical Research 109(D08109): 1 – 11

Chubarova NY, and Nezval YI (2000) Thirty year variability of UV irradiance in Moscow. Journal of Geophysical Research 105(D10): 25867 – 25876

Chubarova NY, Yurova AY, and Krotkov N (2002) Comparisons between ground measurements of broadband ultraviolet irradiance (300 nm to 380 nm) and total ozone mapping spectrometer ultraviolet estimates at Moscow from 1979 to 2000. Optical Engineering 41(12): 3071 – 3081

Ciren P, and Li Z (2003) Long-term global earth surface ultraviolet radiation exposure. Agricultural and Forest Meteorology 120: 51 – 68

den Outer PN, Slaper H, and Tax RB (2005) UV radiation in the Netherlands: Assessing long-term variability and trends in relation to ozone and clouds. Journal of Geophysical Research 110(D02203): 1 – 11

Dharmarajan TS (2008) Chapter 4 Aging and the Skin: The Geriatrician's Perspective. In: Diagnosis of Aging Skin Diseases. Springer, London 978-1-84628-677-3 (Print) 978-1-84628-678-0 (Online)

Environment Canada (2008) (http://es-ee.tor.ec.gc.ca/e//ozone/uv_index_definition.htm, accessed in Nov. 2008

Fioletov VE, McArthur LJB, Kerr JB, and Wardle DI (2001) Long-term variations of UV-B irradiance over Canada estimated from Brewer observations and derived from ozone and pyranometer measurements. Journal of Geophysical Research 106(D19):23009-23027

Fioletov VE, Kerr JB, Wardle DI, Krotkov N, and Herman JR (2002) Comparison of Brewer ultraviolet irradiance measurements with total ozone mapping spectrometer satellite retrievals. Optical Engineering 41(12): 3051 – 3061

Fioletov VE, Kerr JB, McArthur LJB, Wardle DI, and Mathews TW (2003) Estimating UV index climatology over Canada. Journal of Applied Meteorology 42: 417 – 433

Fioletov VE, Kimlin MG, Krotkov N, McArthur LJB, Kerr JB, Wardle DI, Herman JR, Meltzer R, Mathews TW, and Kaurola J (2004) UV index climatology over the United States and Canada from ground-based and satellite estimates. Journal of Geophysical Research 109(D22308): 1 – 13

Herman JR, Piacentini RD, Ziemke J, Celarier E, and Larko D (2000) Interannual variability of ozone and UV-B ultraviolet exposure. Journal of Geophysical Research 105(D23): 29189 – 29193

Herman JR, Larko D, and Ziemke J (2001) Changes in the earth's global UV reflectivity from clouds and aerosols. Journal of Geophysical Research (Atmospheres) 106: 5353 – 5368

Kalliskota S, Kaurola J, Taalas P, and Herman JR (2000) Comparison of daily UV doses estimated from Nimbus 7/TOMS measurements and ground-based spectroradiometric data. Journal of Geophysical Research 105(D4): 5059 – 5067

Kaurola J, Taalas P, Koskela T, Borkowski J, and Josefsson W (2000) Long-term variations of UV-B doses at three stations in northern Europe. Journal of Geophysical Research 105(D16): 20813 – 20820

Krotkov NA, Herman JR, Bhartia PK, Fioletov V, and Ahmad Z (2001) Satellite estimation of spectral surface UV irradiance 2. Effects of homogeneous clouds and snow. Journal of Geophysical Research (Atmospheres) 106: 11743 – 11759

Li Z, Wang P, and Cihlar J (2000) A simple and efficient method for retrieving surface UV radiation dose rate from satellite. Journal of Geophysical Research 105: 5025 – 5036

McKinlay AF, and Diffey BL (1987a) A reference action spectrum for ultraviolet induced erythema in human skin. CIE Research Note, CIE Journal Commission Internationale de l'Éclairage 6: 17 – 22

McKinlay AF, and Diffey BL (1987b) A reference action spectrum for ultra-violet induced erythema in human skin. In: Passchier WF, Bosnajakovic BFM (eds) Human Exposure to Ultraviolet Radiation: Risks and Regulations. Elsevier, Amsterdam, pp.83 – 87

McKenzie R, Seckmeyer G, Bais AF, Kerr JB, and Madronich S (2001) Satellite retrievals of erythemal UV dose compared with ground-based measurements at northern and southern mid-latitudes. Journal of Geophysical Research (Atmospheres) 106: 24051 – 24062

McPeters RD, Bhartia PK, Krueger AJ, Herman JR, Wellemeyer CG, Seftor CJ, Jaross G, Torres O, Moy L, Labow G, Byerly W, Taylor SL, Swissler T, and Cebula RP (1998) Earth Probe Total Ozone Mapping Spectrometer (TOMS) Data Products User's Guide. NASA Technical Publication 1998-206895. Goddard Space Flight Center Greenbelt, Maryland, 20771, USA

National Aeronautics and Space Administration (NASA) (2008) http://jwocky.gsfc.nasa.gov/, accessed in Nov. 2008

Pubu C, and Li Z (2001) Anisotropic reflection of UV radiation at the top of the atmosphere: Characteristics and models obtained from Meteor 3/TOMS. Journal of Geophysical Research 106(D5): 4741 – 4755

Udelhofen PM, Roy PGC, and Randel WJ (1999) Surface UV radiation over Australia, 1979 – 1992 effects of ozone and cloud cover changes on variations of UV radiation. Journal of Geophysical Research 105(D16): 19135 – 19159

Wang P, Li Z, and Cihlar J (2000) Validation of an UV inversion algorithm using satellite and surface measurements. Journal of Geophysical Research 105(D4): 5037 – 5048

Ziemke JR, Chandra S, Herman J, and Varotsos C (2003) Erythemally weighted UV trends over northern latitudes derived from Nimbus 7 TOMS measurements. Journal of Geophysical Research 105(D6): 7373 – 7382

11 Ultraviolet Radiation and Its Interaction with Air Pollution

William F. Barnard[1] and Brian N. Wenny[2]

[1] North Carolina State University, Department of Marine, Earth, and Atmospheric Sciences, Campus Box 8208
Raleigh, North Carolina 27695-8208, USA
E-mail: SBarn46193@aol.com
[2] MODIS Characterization Support Team (MCST)
Sigma Space Corp.
10210 Greenbelt Road, Suite 500
Lanham, MD 20706
E-mail: brian.wenny@gmail.com

Abstract This chapter contains the methodology, along with study examples, that show the types of interactions that the sun's ultraviolet (UV) spectrum has with the various pollutants in the earth's atmosphere, predominantly those in the troposphere. In the context of this chapter, the absorption of UV by gaseous pollutants (stratospheric ozone is not considered a pollutant) has been observed to present a much smaller problem than originally thought. Additionally, aerosols, particularly black carbon, play a much larger role. One must keep in mind that only two studies are presented here in determining site specific UV transmissions to the surface. Each site has its own variables, not the least of which is the differing combinations of scattering and absorbing aerosols. There is a great need to characterize more sites and identify aerosol types according to their chemical species and by doing so, relate the species to the single scatter albedo and aerosol optical depth. It will then become possible to transfer this ground-based knowledge to satellite observation points so that predictions of surface UV can become more accurate in protecting our environment.

Keywords aerosols, single scatter albedo, black carbon, atmospheric optical depth, particulate scattering and absorption

11.1 Introduction

To attempt to understand this problem, certain concepts and definitions need to be laid out at the beginning to better understand the complexity of this subject.

Air pollution, optics, radiative transfer methodology, information on atmospheric construction, along with models and statistics are all utilized in this chapter to show the complexity of the interaction of ultraviolet UV radiation with air pollution. Because of the nature of UV radiation and its interaction with the atmosphere and its constituents, certain parameters and their known effects on the UV will be explained first so that the reader gets a perspective of the variations that the role of air pollution can play in the earth's UV field. UV radiation, while making up only 1.5% of the total radiation that the earth receives, is the most energetic. Its shorter wavelengths make it highly susceptible for interception by almost anything in its path. Since the earth's climate is constantly changing, the UV that reaches the surface is also changing.

11.1.1 Factors Affecting UV Flux at the Earth's Surface

- Solar zenith angle
- Stratospheric ozone
- Cloud cover
- Atmospheric density
- Air pollution (gases and aerosols)

11.1.1.1 Solar Zenith Angle

If one goes from New York to the Bahamas for a winter vacation, there is a known increase in the UV just from the change in latitude, and thus, the solar zenith angle (SZA) (Fig. 11.1). The same occurs on a summer's day where the solar angle (dependant on latitude) can change dramatically. Ultraviolet radiation around solar noon has its shortest path length to the surface and thus, its greatest intensities. To further increase the UV exposure, one only needs to go to a higher altitude in a lower latitude situation. Here, there is less atmosphere to scatter and absorb the UV and generally, as in the case of Mauna Loa, HI, a very clean environment in which to calibrate the very monitors that measure the surface UV in the more polluted regions of the earth. Ultraviolet-B (UV-B) radiation (280 nm – 320 nm)

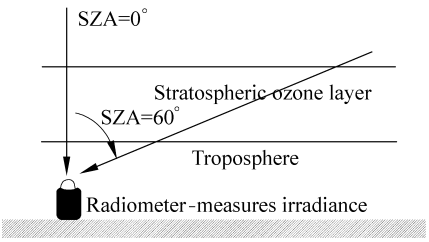

Figure 11.1 Solar zenith angle

comprises roughly 1.5% of the total extraterrestrial solar irradiance and 0.5% of incident irradiance at the earth's surface. Ultraviolet-A (UV-A) radiation encompasses the wavelength region from 320 nm – 400 nm. Ultraviolet radiation has both a daily component that resembles the bell shape distribution curve and a seasonal component that can be expressed with a combination of sine and cosine functions dependant on the Julian date. The daily component's shape is dependant on the wavelength. The shorter wavelengths of 300 nm – 310 nm are generally not observed until the sun has risen past 9:00 a.m. local time in the summer. The longer wavelengths 360 nm – 400 nm exist in the daylight sky from sunrise until sunset.

11.1.1.2 Stratospheric Ozone

The one main absorbing parameter that must be kept constant if the effects of air pollution are being determined is the known interaction of the UV with the stratospheric ozone. The UV absorbed in this layer is the predominant factor affecting the transmission to the earth's surface. Statistical correlations of surface measured UV with variations in this layer of ozone correlate well above the $r = 0.90$ level. The importance of ozone as a regulator of UV stems from strong absorption characteristics over the entire ultraviolet region. Ozone exists in two places in the atmosphere; one is where it is supposed to be to protect life on earth: the stratosphere, and the other, the troposphere, where it is a pollutant that can cause severe health problems. Both ozone areas require high energy UV radiation for creation, but in entirely different ways. In one case it is the primary absorber of UV radiation. In the other, UV creates the tropospheric ozone. Stratospheric ozone is produced by a series of reactions with molecular oxygen and singlet oxygen in the presence of high energy UV radiation, UV-C (200 nm – 280 nm). It is primarily produced over the equatorial regions and is slowly transported poleward. The total column ozone (stratospheric and tropospheric) can comprise a major UV absorber under highly polluted conditions. In the troposphere the UV can create the very gas that helps in its own attenuation. Although in general, as will be shown later, the tropospheric gases play a minor UV absorption role in comparison to other aerosol pollutants.

Stratospheric ozone absorbs all of the UV-C radiation. Tropospheric ozone makes up only a small portion of the total column ozone, usually less than 10%. The path length of the stratosphere is much longer than that of the troposphere, but the higher density of the troposphere and its increasing scattering capabilities are believed to enhance the absorptive powers of this region (Bruhl and Crutzen, 1989). Tropospheric ozone in urban/industrialized regions may reduce the surface UV by 3% to 15% as estimated by Frederick et al. (1993) and Ma and Guicherit (1997). Under clear sky conditions total ozone column variations cause the largest variations in UV transmission and has been the focus of numerous studies (e.g., McKenzie et al., 1991; Kerr and McElroy, 1993; Bojkov et al., 1995; Mims et al., 1995;

Varotsos and Kondratyev, 1995; Fioletov and Evans, 1997). This relationship is demonstrated in Fig. 11.2, which depicts the calculated clear-sky spectral UV irradiance for two total column amounts, 200 Dobson Units (DU) and 400 DU, for Raleigh, NC, during the summer at high solar elevation.

It is apparent that a decrease in the total ozone column substantially increases the surface UV-B irradiance over the erythemally important wavelengths. The human skin has a response curve to solar radiation. The particular portion of the sun's spectral region, which is in the UV, causes redness of the skin and is the erythemal region.

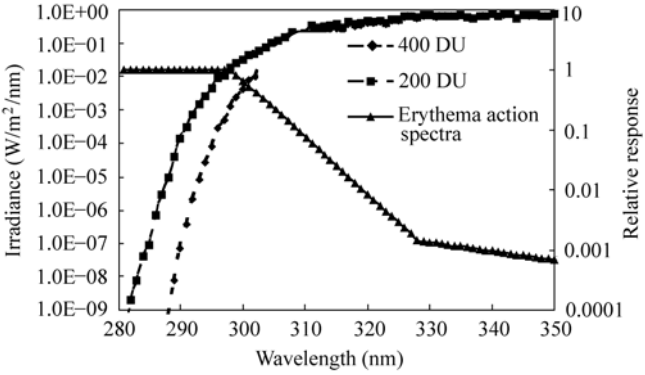

Figure 11.2 UV spectral changes for 200 DU change in stratospheric ozone

11.1.1.3 Cloud Cover

Cloud cover can wreak havoc for making UV measurements. They generally reduce the UV radiation, but it has been shown, Estupinan et al. (1996), and Schafer et al. (1996), that clouds can actually enhance the surface levels by as much as 10%−15%. The physical and chemical makeup of clouds (e.g., thickness, total percent coverage, droplet size distribution, chemical composition, and presence of interstitial absorbing aerosols) causes the cloud's effect on the UV to be highly variable; not only with time, but also with areas of differing pollutant characteristics. Frequently the clouds will act to purge the atmosphere of certain hygroscopic pollutants and in doing so, will alter the atmospheric albedo to reflect UV back to space.

The cloud/physics/chemistry/thermodynamics are not completely understood. Cloud systems vary widely across the world and are dependant upon the cloud type and whether or not they are formed over land or ocean. In one case, they are frequently formed over land where anthropogenic sources have generated thousands of CCN (cloud condensation nuclei) per cubic centimeter, but yet once they are formed (the CCN are hygroscopic, so they collect water vapor as they grow), they become great scavengers of pollution, absorbing the gaseous versions of sulfur

dioxide (SO_2), nitrogen dioxide (NO_2), and ozone (O_3). They may also collect many hydrocarbons, not particularly in solution, but on the droplet surface.

Cloud droplets are formed by condensing water vapor on cloud condensation nuclei. Sizes of these nuclei range from the Aitken nuclei at 0.001 μm up through the large and giant nuclei at 2.0 μm. The smaller nuclei have a much higher concentration in the atmosphere and give rise to clouds with much higher droplet concentrations. These clouds have a higher albedo and provide a cooling effect for the earth's surface by reflecting much of the sunlight back into space. The cloud droplet spectrum broadens as the cloud gets older. For cumulus clouds, this can be caused by collisions and coalescing, condensation and evaporation, turbulence effects, and the mixing of cloud parcels with different histories.

Continental aerosols contain higher concentrations of CCN and thus, cause a different cloud structure over land than over the ocean. The ocean clouds have a broader size distribution of droplet sizes ranging from approximately 6 μm to 45 μm. Droplet counts are in the 35 droplets per cubic centimeter range. However, continental clouds have a narrow size range, 5 μm − 20 μm, but a much higher concentration of approximately 210 droplets/cm^3.

Stratus clouds seem to have the most effect on the radiative transfer and the radiation balance, but don't seem to be studied to the extent that cumulus clouds are. Wind velocities in the two types differ considerably. Cumulus clouds contain updrafts that measure in the meters/second range, while the stratus cloud's wind velocities are in tens of centimeters per second. This is also correlated to the extensive coverage of either type of cloud. Stratus clouds extend coverage over tens of km, while cumulus clouds are generally localized events covering just a few kilometers.

Droplet sizes and growth are different in the two types. Stratus cloud droplets are primarily formed through condensation and their growth processes are largely caused by condensation. The droplets enlarge monotonically with height. The droplet size spectra are narrow as compared to the cumulus. This is caused, in part, by these clouds being contained or height inhibited by an inversion layer just above them. This inhibits further vertical growth of both the cloud and the droplets within.

In the stratus case, there is mixing and partial evaporation at the cloud top causing cooling. Radiative cooling also occurs at the cloud top, as discussed earlier, which causes pockets of colder air to fall through the cloud. These clouds can also contain areas of super cooled droplets. Precipitation is more likely to occur if the cloud is thick and contains ice. The probability of precipitation increases with a combination of cloud age, temperature, and vertical extent. In a cumulus cloud, all three of these exist and are related to cloud thickness. Continental clouds must be thicker than maritime clouds for the same probability of precipitation. The fewer droplets in the maritime clouds are larger and can collide and coalesce with each other more readily than the smaller drops in the continental clouds to form precipitation. Less is known about the stratus clouds. Age, temperature, and thickness are still basic requirements for precipitation.

Empirical relations between cloud coverage and surface UV have been developed by Ilyas (1987), Bais et al. (1993), and Frederick and Steele (1995). Differences in the derived empirical relationships demonstrate a variation in regional cloud characteristics. All of these factors combine to create strong UV variabilities at the surface, thus complicating detection of long-term trends (Madronich et al., 1998). Therefore, clear cloudless days are best when attempting to correlate the effects of UV with air pollution.

11.1.1.4 Atmospheric Density

As previously stated, the path length of the stratosphere is much longer than that of the troposphere, but the higher density of the troposphere and its increasing scattering capabilities are believed to enhance the absorptive powers of this region (Bruhl and Crutzen, 1989). Atmospheric pressure increases dramatically toward the earth's surface and as a result, the mean free path for molecular interaction is greatly reduced from its value in the stratosphere. From 40 km (the approximate center of the stratosphere) to sea level, the pressure increases almost 1,000 times, and the mean free path changes by at least a factor of 10^6. This, combined with the pollution "soup" that is present in the troposphere and especially concentrated in the planetary boundary layer (PBL), make for an interesting array of interaction cases for each UV photon impacting this portion of the atmosphere.

The planetary boundary layer is approximately 1 km thick and extends from the surface to roughly that height. During the morning hours, it can be as small as 400 m – 800 m and can rise to 1,500 m – 2,000 m during the afternoon with the heating of the layer. This area contains the most significant concentration of air pollutants, especially, aerosols. Land use and surface topography can also cause the PBL to have spatial variations in the layer depth and structure. The spatial variations can also be caused by large-scale meteorological variables. Thermal inversions can compress the PBL, and low pressure systems may increase its thickness.

11.1.1.5 Air Pollution (Gases and Aerosols)

Wide varieties of pollutants are emitted to the atmosphere each year by the tons. The Environmental Protection Agency (EPA) has chosen to classify them in two broad categories based on their respective origination points.

1. Primary Pollutants are those classified as being emitted directly from sources and not undergoing any chemical or physical transformation. An example would be the carbon monoxide emitted through the automobile exhaust. Such gases are called non-reactive since they generally do not interact with other gases nor are they altered by solar radiation.

2. Secondary Pollutants are those that are formed in the atmosphere as a result of chemical reactions among primary pollutants and other species, including radiation that may be present in the atmosphere. One of the most notable of these chemiluminescent reactions is that which leads to the formation of tropospheric ozone. Other reactions can lead to the formations of particulate matter (nitrates,

sulfates), acidic droplets, salt particles, and hydrocarbons.

Pollutants can also be broken into two other categories according to their physical properties: (1) gases such as carbon monoxide (CO), O_3, or SO_2, and (2) particulate matter, such as sulfates, nitrates, black carbon, and the heavier hydrocarbons. Particulates, also commonly known as aerosols, include both solid and liquid particles that become airborne. This includes solids that accumulate water and become difficult to assign optical properties to, as will be shown later. Some of the more common air pollution sources are shown below in Table 11.1.

Table 11.1 Sources of air pollution

Anthropogenic			Natural	
Activity	Source	Pollutant	Source/Activity	Pollutant
Transportation	Autos, buses	CO, NO_x, PM *	Erosion	Windblown PM
Industrial	Mining, pulp and paper mills	PM, H_2S, CO_2	Decay	NH_3, methane, H_2S
Construction	Paving, painting	VOCs **	Forest fires	PM, VOCs, NO_x, etc
Open burning	Leaves, Slash burning, fireplaces, etc.	VOCs, particulate matter	Soil processes	N_2O, CO_2, NH_3
Waste	Household waste disposal	CO_2, methane, H_2S	Evaporation	Sea salts
Power generation	Coal and oil fired plants	Hg, PM hydrocarbons,	Volcanoes	SO_2, CO, Fine PM
			Biogenic emissions	VOC's, terpenes, isoprenes, pollen

* PM = Particulate Matter

** VOCs = Volatile organic compounds

3. Gases. In this chapter it will be proposed that due to the short path length of the UV through the polluted portion of the atmosphere and the normally very low concentrations (parts per billion, ppb) of the gaseous pollutants, there will be little to no effect of these gases on the UV reaching the surface. The dry atmosphere is primarily composed of nitrogen (N_2), O_2, and several inert noble gases—argon (Ar), neon (Ne), krypton (Kr), and xenon (Xe). Their relative concentrations have remained essentially fixed over time (Arya, 1999). The concentrations of water vapor (H_2O) are observed to be highly variable, both in time and space. It is one of the most important ingredients of weather and climate in the lower atmosphere, but is not normally considered an air pollutant. Carbon dioxide (CO_2) also has a relatively high concentration, mostly due to emissions as part of the natural carbon cycle. However, the increasing ambient levels of CO_2, at the current rate of 0.5% per year, are clearly due to anthropogenic emissions from fossil fuel burning, slash burning, and deforestation. Even though increasing levels of CO_2 might be beneficial to agriculture and forestry, as some studies have suggested

(Booker, et al., 2007), the potential consequences of climate warming due to increasing levels of CO_2, methane (CH_4), and other greenhouse gases are considered serious enough to put these gases under the category of air pollutants. Most of the other species that are considered to be air pollutants have both natural as well as anthropogenic sources. Their concentrations in polluted atmospheres, such as over large urban and industrial complexes, are found to be several orders of magnitude higher than the "clean" atmospheric values normally measured in the parts per billion (ppb) range.

Tropospheric ozone has seasonal variations that depend on the sun's intensity, and most importantly, on the strength of the UV radiation. In this case, the UV, in conjunction with oxides of nitrogen and varying types of hydrocarbons, produces the tropospheric ozone. This ozone, in turn, absorbs one of its own creators; the UV radiation. Without the UV, there would be no ozone. Anthropogenic precursors, photochemically reacting in the troposphere, result in accumulations of tropospheric ozone in urban and industrialized regions. These reactions give rise to a diurnal ozone pattern in the more urban regions (Fig. 11.3). Tropospheric ozone is produced in more rural areas by naturally emitted precursors. It can also be transported from nearby urban areas.

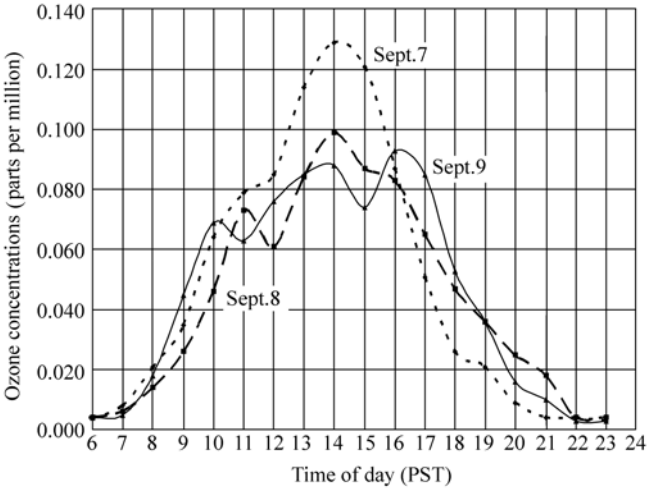

Figure 11.3 Peak ozone concentrations for 3 days in September, Rubidoux, CA

While there are a number of significant gaseous pollutants in the troposphere, only three absorb in the UV region of the spectrum; SO_2, NO_2, and O_3 (Fig. 11.4). As shown in Fig. 11.4, the scattering cross-sections of SO_2 and O_3 are approximately the same magnitude up to about 305 nm, but that of NO_2 is relatively flat in this region and actually surpasses O_3 and SO_2 above 315 nm. Nitrogen dioxide is a precursor for ozone. Its morning peaks can be shown in a daily plot of a polluted urban environment (Fig. 11.5) along with the three peaks of NO_2, UV radiation,

and O_3 (Barnard et al., 2003). As the NO_2 reacts with other pollutants and the incident UV radiation, it produces an afternoon peak of ozone that generally occurs around 14:00 – 16:00 local time. Sulfur dioxide is not a pollutant found during the summer and generally occurs as a result of fossil fuel burning during the winter. Unless found in abnormally high concentrations (greater than 150 parts per billion), the contribution of SO_2 and NO_2 to UV absorption is minimal (less than 1%).

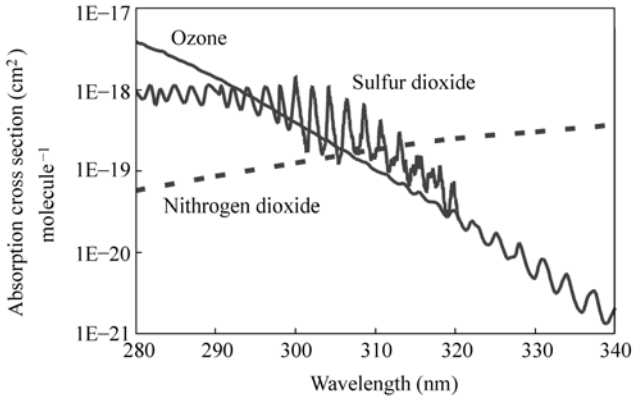

Figure 11.4 Pollutant absorption cross-sections in the UV

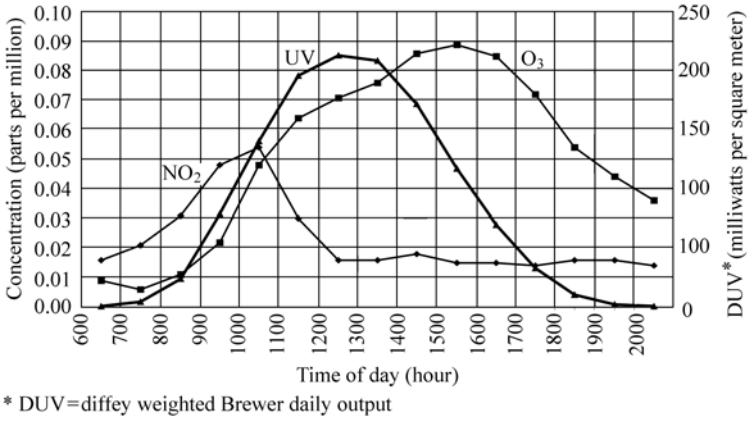

Figure 11.5 Pollution and UV radiation peaks for July 8, 1997. Rubidoux, CA

4. Aerosols. Atmospheric aerosol concentrations provide a complex medium for light scattering and absorption (Ball and Robinson, 1982; Coakley et al., 1983; Charlson et al., 1991; Penner et al., 1992). Coming in all sizes, shapes, hydroscopic, hygroscopic, reflective, refractive, and absorbent, these aerosols create the mathematical soup (mixed and/or layered) through which the UV must pass to get to the earth's surface. They are also present at many altitudes. Volcanic eruptions, such as El Chichon in 1984 and Mt. Pinatubo in 1991, have sent significant

amounts of material into the stratosphere (Stephens, 1995). These materials have reacted with, and depleted the stratospheric ozone. Volcanic gases have reacted at these altitudes to provide fine sulfate particulate matter that is highly reflective. Volcanic materials, gaseous and particulate, have provided the opportunity to assess the climate forcing (Hansen et al., 1997; Kiehl et al., 2000) of stratospheric aerosols (Lacis et al., 1992; Dutton et al., 1994).

Tropospheric aerosol concentrations have increased dramatically since the early 20th century. Anthropogenic emissions have led to increased concentrations over urban areas and have had a significant impact on the air quality east of the Mississippi River valley. Since aerosols have become both positively and negatively implicated in the area of climate change, studies have focused on their radiative properties in the visible and the infrared, but not significantly in the UV region (Flowers et al., 1969). Recently, UV measurements and one of aerosol's main constituents, black carbon (Im et al., 2001), have been implicated in the climate change arena in the southeastern part of the U.S. (Saxena and Menon, 1999). Visible range studies in the eastern United States (Liu et al., 1991) show that biologically active UV reaching the surface has decreased 5%−18% since the industrial revolution. Similar evidence of decreased surface UV-B irradiances attributable to aerosol attenuation has been reported by Seckmeyer and McKenzie (1992), Varotsos et al. (1995), Blumthaler et al. (1996), Mims (1996), and Estupinan et al. (1996). A 14% increase in attenuation of total UV-B irradiance was observed by Lorente et al. (1994), between the highest and lowest turbidity conditions over an urban site. Also observed was an important 27% enhancement of the diffuse UV-B component. For high sun conditions, approximately 50% of UV irradiance was diffuse, and a higher percentage with increasing zenith angle and turbidity. Diffuse radiation, especially for specific species, is very damaging. Frogs laying eggs in what was once thought to be a visibly shady area is now radiated with increased levels of UV, caused by increased aerosols creating a higher percentage of diffuse UV radiation (Blaustein and Wake, 1995; Mims, 1995). The effect of atmospheric aerosols on UV radiation is very complex. It would appear that as opposed to the known adverse effects, increased anthropogenic aerosols have an apparent beneficial effect of reducing surface UV radiation levels, particularly in the presence of increased tropospheric ozone (Bruhl and Crutzen, 1989; Liu et al., 1991).

Black carbon makes up a portion of the aerosol conglomerate in the atmosphere. Concentrations of black carbon in urban areas range up to 13.3 $\mu g/m^3$ (Wolff, 1981), while in the rural areas of western North Carolina, levels can be found in the 0.03 $\mu g/m^3$ range (Bahrmann and Saxena, 1998). It is created in almost all combustion processes, and since it is not degraded under normal atmospheric conditions, wet and dry depositions are its major sinks. Since it occurs primarily in submicron particles (Cadle and Mulawa, 1990), its life in the atmosphere varies from several days to several weeks. It plays an important role in the visibility of the atmosphere through its light extinction properties (Gundel et al., 1984; Cadle

and Mulawa, 1990; Hansen and Rosen, 1990) as well as having catalytic properties that play a role in atmospheric chemistry (Goldberg, 1985). Automotive and diesel exhausts are the prime sources of black carbon.

Particles can also be hydroscopic (absorb water easily) and grow in size. These types frequently reflect radiation due to their outer shell of water, but may also absorb to reradiate at a longer wavelength. Nitrates and sulfates grow from gases in the atmosphere and generally become very good scatterers. Due to the nature of the particle sizes and their ability to retain water, scattering and absorption of light is very wavelength dependent.

11.2 Optics of the Atmosphere

Knowledge of the atmosphere's optical properties is important for radiative transfer modeling studies, remote sensing applications, and climatological studies. In the past, these properties have primarily been studied in the visible and the infrared. Now more attention is being paid to the UV portion to thoroughly understand radiative transfer models. Optical properties of the atmosphere include scattering, emission, and absorption characteristics, which have a strong dependence on wavelength (Reuder and Schwander, 1999). These three processes influence the radiation field in the atmosphere and they each need to be physically and mathematically understood.

11.2.1 Scattering

As one would guess, this denotes a change in the direction in which radiation propagates. Radiation is shifted out of one direction and into another. In general, there can be a shift in frequency upon scattering as well. The wavelength dependence of molecular scattering (i.e., Rayleigh scattering) is proportional to λ^{-4}, so this scattering will be more significant in the UV range than in the visible. The change in direction of radiation associated with scattering is described by the phase function $P(\theta, \phi; \theta', \phi')$ which is dependent upon the size of the particle relative to the wavelength of interest. The phase function describes the probability that an incident photon with incident coordinates (θ', ϕ') is scattered into the direction (θ, ϕ). For molecular scattering the phase function is:

$$P(\Theta) = \frac{3}{4}\left(1 + \cos^2 \Theta\right) \tag{11.1}$$

where Θ is $(\theta - \theta')$. Scattering by larger particles is more complex (Mie scattering), but is generally peaked in the forward direction. This would mean that the left lobe in Fig. 11.6 would be smaller than the right lobe.

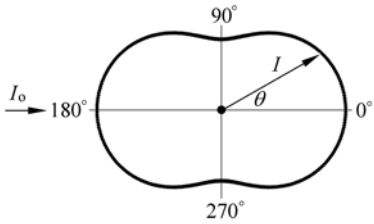

Figure 11.6 Aerosol scattering pattern: Symmetric forward and backward components

Within this category, there are three sub-categories:

1. Rayleigh scattering This type of scattering occurs when the molecules/particles in the atmosphere are smaller than the incident light's wavelength. An example is the blue sky.

Individual air molecules are much smaller than cloud droplets; their diameters are small even when compared with the wavelength of visible light. Each air molecule of O_2 and N_2 selectively scatters the shorter waves of visible light much more effectively than longer wavelengths. As sunlight enters the atmosphere, the shorter visible wavelengths of violet, blue, and green are scattered more effectively by atmospheric gases than are the longer wavelengths of yellow, orange, and especially red. (Violet light is scattered about 16 times more than red light ($\sim 1/\lambda^4$)). As we view the sky, the scattered waves of violet, blue, and green strike the eye from all directions. Since our eyes are more sensitive to blue light, viewing these wavelengths together produces the sensation of blue throughout the sky.

2. Mie Scattering This occurs when the particles are equal to, or larger than, the incident wavelength. In the ambient air pollution realm, there is a peak in the aerosol size distribution near the 2 μm − 3 μm range. Thus, particles in this range would have corresponding Mie scattering wavelengths in the near infrared portion of the spectrum.

Associated with Mie scattering is Mie theory, a system by which electromagnetic wave theory equations are solved using the boundary conditions at the surface of the particle as it interacts with the incoming radiation. It is typically used in a limited realm of spherical particles. By solving the wave equations it is possible to determine the scattered and absorbed electric field around a particle and ascribe an index of refraction to it. This index, being a solution to the wave equation, will have real and imaginary components and characterize the physical properties of the particle. The total solution will also exhibit some phase functions for the scattered field around the particle. These solutions include Bessel and Hankel functions and are beyond the scope of this chapter. Details of these solutions can be found in 'Atmospheric Radiative Transfer' by J. Lenoble (1993).

3. Geometrical scattering This happens when the particulate mater in the air is much larger than the incident wavelength. Rain drops and dust particles fall into this classification.

As a particle increases in size, it scatters light more efficiently. When it reaches

a size that is close to the wavelength of the incident light, it scatters more light than a particle five times its size. These particles remove twice the amount of light intercepted by its geometric cross-sectional area. The laws of geometrical optics may be used to compute the angular distribution of light, which is scattered when a plane electromagnetic wave is incident on a particle much larger than the wavelength of the incident light. Processes involving geometrical optics include rays externally reflected by the particle and rays refracted into the particle; the latter rays may be absorbed in the particle, or they may emerge from it after possibly suffering several internal reflections.

Particles much larger than the incident wavelength also scatter light by means of diffraction, which removes energy from the light wave passing by the particle. The diffraction is concentrated in a narrow lobe around the forward direction, and like geometrical reflection and refraction, it contains an amount of energy equal to that incident on the cross section of the particle. In the far field, the diffracted component of the scattered light may be approximated by the Fraunhofer diffraction theory. The diffraction pattern depends only upon the shape of the cross section of the particle.

We use the term 'ray optics' to describe geometrical reflection and refraction, plus Fraunhofer diffraction. Figure 11.7 illustrates the geometrical configuration for different contributions to light scattered by a large sphere. When hit by radiation, particles can absorb it completely, absorb and reradiate it at a lower, longer wavelength, or completely reflect it. It will generally be a combination of both. The absorption and scattering particle, or molecular cross sections σ_a and σ_s respectively, determine the ability to either absorb or scatter the incoming radiation. Absorption removes photons from the radiation field, whereas scattering changes the photon's direction of propagation. Both functions are particle size/wavelength dependent.

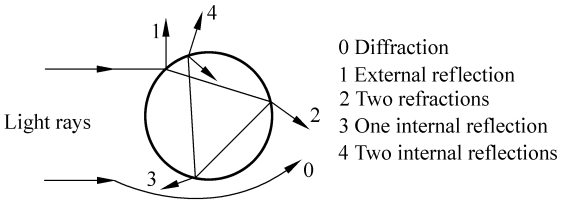

Figure 11.7 Representations of light rays scattered by a sphere according to ray optics, from "An Introduction to Atmospheric Radiation" by K. Liou (1980)

11.2.2 Absorption

Absorption occurs when gas or particulate matter in the air interacts with the UV radiation in such a way as to remove the electromagnetic energy of the UV photon,

and as a result, increases the kinetic energy of the gas or particle. Diesel fuel burning produces a great deal of small black carbon particulate matter. These particles act as very efficient absorbers in the UV region of the spectrum, three times better than in the IR region. This is due to the particle's size (Liousse et al., 1996).

11.2.3 Emission

This is the creation of electromagnetic radiation generally produced as a result of the interactions between the molecules or atoms in the atmosphere with very high energy photons from very short wavelength radiation. These interactions raise either the molecular or atomic state of the gas or particulate matter above its normal ground state and as a result, the gas or particle can emit a longer wavelength of radiation. This emitted radiation is the result of the gas or particle reverting back to its original ground state.

11.2.4 Atmospheric Optical Depth

The optical depth (τ) is the summation of extinction (scattering and absorption) by all the gases and pollutants of the atmosphere:

$$\tau = \int_z^\infty n_j(z)\sigma_j \, \mathrm{d}z \tag{11.2}$$

where n_j is the altitude dependent concentration of the (j) gases and particles that attenuate radiation, each with an effective cross section (scattering and absorption) σ_j. Retrievals of the optical depth from ground-based sensors generally employ two methods: (1) the Langley-plot slope method, and (2) measurements of absolute spectrally-resolved solar flux with a calibrated sun photometer. Each of these methods requires a clear cloudless day to make accurate measurements. The Langley method is a technique based on sun photometry introduced for the first time in November 1725, in France by Pierre Bouguer. This relative measure does not require an absolute calibration of the direct input of the sensor. However, retrievals of optical depths with the Langley method do not provide instantaneous information about the atmospheric optical depth since it requires measurements over a period of time, usually a morning or an afternoon. As a result, it assumes that both total atmospheric optical depth and sensor's sensitivity remain constant during the measurement period. Langley analysis is a linear regression of the natural logarithm (ln) of the signal that is measured vs. air mass (m). A graph of the natural logarithm of the signal vs. air mass falls along a straight line assuming that the atmosphere does not undergo a radical change or the aerosol loading does not change within the measurement time frame. The air mass is defined as

the cosecant of the solar zenith angle for solar angles less than 75°. Above this angle the spherical nature of the atmosphere has to be taken into account, and this involves a more involved calculation (Lenoble, 1993). Extending the straight line to where it crosses the y axis at $m=0$ (zero air mass) yields the extraterrestrial constant, which is the solar flux at the top of the atmosphere. A time averaged extraterrestrial constant is referred to as the characterized Langley intercept for that particular instrument.

Figures 11.8 and 11.9 show two Langley plots derived from Brewer No. 112 during a 1999 summer intensive study at Riverside, California. The data is derived from the PS routine scans taken by the Brewer in the morning and afternoon at 340 nm. The Brewer PS routine looks directly at the sun in the morning and afternoon at various zenith angles to obtain the variables needed to determine the total optical depth. Notice the slight difference in the slopes of the two lines. The slopes are the total optical depths of the atmosphere. The morning slope shows a slightly higher optical depth (OD or ϑ). Since the boundary layer increases with

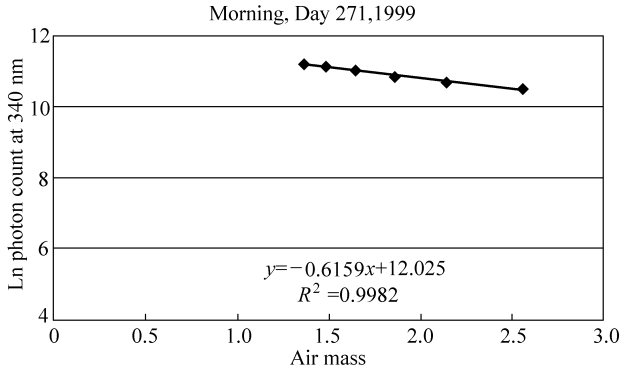

Figure 11.8 Morning Langley plot

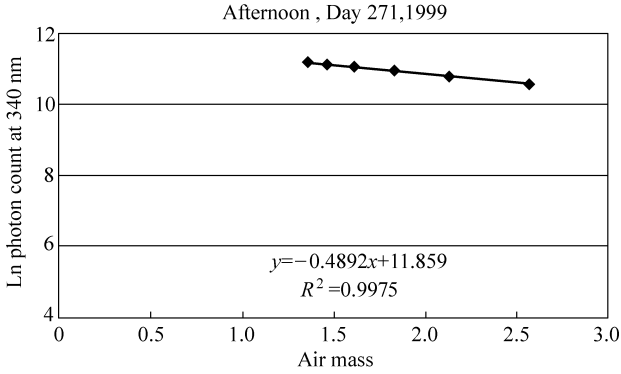

Figure 11.9 Afternoon Langley plot

warming of the atmosphere, the pollutants tend to diffuse as the boundary layer becomes thicker and give a slightly lower OD (ϑ). Other instruments, such as the UV Multi-filter Rotating Shadowband Radiometer (MFRSR), take considerably more data points and can produce Langley plots within an hour or so. This information can be valuable if the atmosphere varies more rapidly than expected.

Measurements taken with a calibrated sun photometer of absolute spectrally-resolved solar flux differ from the standard Langley method in that the extraterrestrial constant is used to directly calculate the total atmospheric optical depth providing instantaneous information about any changes.

Attenuation of a direct solar beam is described by the Beer-Lambert law:

$$I_{\text{dir}} = I_0 \mathrm{e}^{-\tau/\mu_0}$$

I_{dir} is the direct normal irradiance at the surface and I_0 is the extraterrestrial normal irradiance. If this equation is rewritten and applied to the direct solar measurements as taken by the Brewer;

$$\frac{I_\lambda}{I_{0,\lambda}} = -\exp \tau_\lambda m$$

I_λ represents the photon counts measured by the Brewer at wavelength λ and $I_{0,\lambda}$ corresponds to the photon counts that would be measured at the top of the earth's atmosphere. The sum of aerosol and gas extinction is τ_λ and m is the air mass defined as the cosecant of the solar zenith angle. Once the I_0 has been characterized, the total atmospheric optical depth ($\tau_{\text{a},\lambda}$), at a specific wavelength, is calculated using the following:

$$\tau_{\text{a},\lambda} = \left(\frac{1}{m}\right) \ln\left(\frac{I_0}{I_\lambda}\right)$$

I_λ is the Brewer photon count as measured by the PS routine. The natural log of the instrument's photon count (Y-axis) is plotted against the cosecant of the solar zenith angle (X-axis). The slope of the resulting line is the total optical depth.

The total optical depth can be further broken down into its components: (1) the Rayleigh optical depth, (2) the ozone optical depth, and (3) the aerosol optical depth, as shown in Fig. 11.10. One of the objectives for this chapter is to determine the aerosol optical depth (AOD). Anthropogenic aerosols are one of the largest factors affecting surface UV radiation values, but to determine their optical properties is a challenge and one which has many facets. As shown later, the aerosols have a myriad of physical and chemical properties which affect their capabilities to absorb the radiation. Size, chemical composition, and their ability to adsorb or desorb water vapor all contribute to their interaction with the UV.

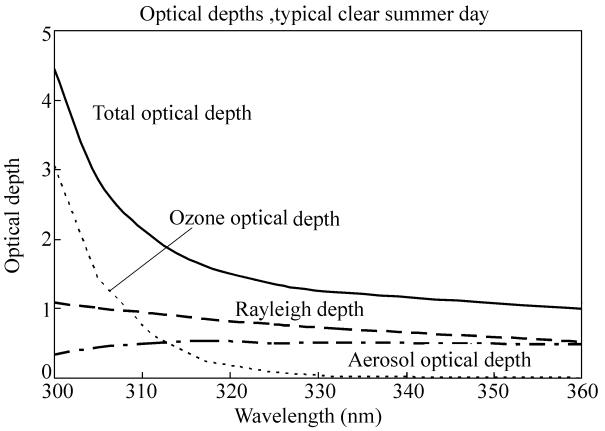

Figure 11.10 The optical depths of the atmosphere

(1) Rayleigh optical depth (Rayleigh scattering): Rayleigh scattering by air molecules is a significant non-pollution contributor to the total optical depth of the atmosphere. It is wavelength dependent, with increased scattering at the shorter UV wavelengths. Rayleigh scattering by the N_2 and O_2 molecules is more significant in the UV portion of the spectra as is shown in the following equation (Dutton et al., 1994).

$$\sigma_{\text{Rayleigh}} = 0.0087 \times \lambda^{-4.05} \times \left(\frac{P_s}{1.013 \times 10^5} \right) \tag{11.3}$$

where λ is wavelength in micrometers and P_s is the atmospheric pressure at the site expressed in Pascals.

(2) Gases: NO_2 and SO_2 also have strong absorption bands in the UV portion of the spectra. The gases can play a small part in determining the total optical depth of the atmosphere, but their concentrations must be extremely high or they must have an extremely long path length. These conditions exist infrequently in the real world. A large SO_2 plume may exist at a soft coal fired power plant or smelter where the concentrations may be very high (much greater than the normal parts per billion normally seen in ambient air). Nitrogen dioxide is normally a by-product of auto emissions, so large concentrations may exist under the right atmospheric conditions (inversions), but even then the path length would be very small, less than a few kilometers.

Total column O_3 is the major absorber of UV radiation due to its relatively large concentration and path length in comparison to other absorbing gases, SO_2 and NO_2. Therefore, measurements of OD obtained from measurements of direct irradiance are directly affected by the total column of O_3 in the atmosphere.

(3) Aerosols: Once the total atmospheric optical depth has been established, the aerosol optical depth (AOD) in the UV is obtained by subtracting the sum of

the Rayleigh and O_3 optical depths. Nitrogen dioxide and SO_2 may contribute to the optical depth in the UV, although their contribution is relatively small (less than 1%). Changes in the total column ozone and the vertical structure of temperature and pressure of the atmosphere have an effect on the retrieved AOD. This effect is small, but non-negligible, in the retrieved AOD for the UV-B ($\lambda < 320$ nm) due to Rayleigh scattering.

Keep in mind though that the UV wavelengths we are talking about generally range between 300 nm and 400 nm. This corresponds to the Rayleigh and the Mie portion of the scattering range described above. Particulate matter found in the atmosphere is generally not found in great quantities below the 1 μ range, but smaller quantities can still be very efficient scatterers.

The selective scattering of blue light by air molecules and very small particles can make distant mountains appear blue, such as the Blue Ridge Mountains of Virginia, North Carolina, and Tennessee. In some remote places, a blue haze may cover the landscape. Hydrocarbon emissions from trees reacting with ozone to produce very small particles selectively scatter blue light and create this haze. When small particles, such as fine dust and salt, become suspended in the atmosphere, the color of the sky begins to change from blue to milky white. Although these particles are small, they are large enough to scatter all wavelengths of visible light fairly evenly in all directions. When our eyes are bombarded by all wavelengths of visible light, the sky appears milky white and when the visibility lowers, we call the day "hazy". If the humidity is high enough, hydroscopic particles will create this haze. Thus, the color of the sky indicates the quantity of the aerosol material suspended in the air. The sky will appear a very deep blue from on top of a very high mountain peak and above the aerosol pollution; a result of Rayleigh scattering.

In a simplified example, for scattering, the luminous flux $=F$, and b is a factor of proportionality; therefore, for a short distance, dl through the atmosphere d$F = -bF$dl. If we integrate both sides we get $F = F_o\, e^{-bl}$. Now if we do the same thing for absorption we get $F = F_o\, e^{-kl}$ where k is another factor of proportionality associated with absorption. If we now combine these two equations, we get $F = F_o e^{-(b+k)l}$ or $F = F_o e^{-\gamma l}$. This last equation is known as the Bouguer/Beer's Law.

Example: In a certain experiment, the luminous flux F is reduced to 36.8% of its original value when a beam of light is passed through an aerosol over a path length of 10 meters. Determine the numerical value of γ in m^{-1}.

From the equation above:

$$F = F_o\, e^{-(b+k)l} = F_o\, e^{-\gamma l} = 0.368$$

$$F/F_o = e^{-\gamma l} = 0.368$$

$$-\gamma l = \ln(0.368) \text{ Since } l = 10 \text{ m}$$

$$-\gamma l = -1.00 \text{ and } \gamma = 0.100 \text{ m}^{-1}$$

These are values that a nephelometer may measure under highly polluted

conditions. A nephelometer measures the ambient light scattering of the atmosphere. This value can be related to the particulate (aerosol) loading of the atmosphere.

11.2.5 Single Scatter Albedo

Absorption and scattering by particles can be simultaneously important, dependent upon the physical-chemical makeup of the particle. The measure of the relative importance of scattering to absorption is the single scatter albedo, ϖ_0, defined as:

$$\varpi_0 = \frac{\sigma_s}{\sigma_s + \sigma_a} \tag{11.4}$$

For purely scattering particles, $\varpi_0 = 1$, and for purely absorbing particles, $\varpi_0 = 0$. Neither extreme will be encountered in the ambient atmosphere where values generally range from 0.55 to 0.95. The single scatter albedo (ω_0) is related to the amount of absorption that is occurring, and is dependent upon particle size, chemical composition, and relative humidity (Kiehl and Rodhe, 1995). Reported values of ω_0 have been primarily restricted to visible and infrared wavelength regions because of the significance to climate change (Hansen et al., 1979; Charlock et al., 1993; Pueschel, 1993). For the UV-B wavelength region, ω_0 is believed to be close to 1.0 for sulfate and marine aerosols and range from 0.5 to 0.7 for desert dust and soot aerosols (Lenoble, 1993; Lacis and Mishchenko, 1995). Madronich (1993) reports a typical ω_0 value at UV wavelengths of 0.8, with a dependence on the levels of chemical impurities in the particles. The amount of moisture available for growth regulates the size of hygroscopic aerosols which in turn affects the scattering efficiency of the aerosol (Charlson et al., 1984). For relative humidities greater than 70%, Waggoner et al. (1981) observed strongly increasing aerosol scattering. When water surrounds an aerosol particle, the particle will not absorb as much, particularly at UV wavelengths since water does not absorb strongly in the UV. Wenny et al. (1998) also found that relative humidity is a controlling factor in the resulting value of ω_0. A larger database encompassing all environmental conditions experienced throughout a year is needed to discern if any seasonal trend exists in ω_0. Based on a short-term study across the Midwest, Ogren and Sheridan (1996) concluded that the dry aerosol ω, for broadband visible radiation is relatively constant in the troposphere both vertically and horizontally, across the U.S. The evidence presented by Wenny et al. (1998) indicates that typically moist climates (such as in the Southeast or Northwest of the U.S) should display larger variations of ω_0 than arid climates (such as in the Midwest and Southwest of the U.S). The magnitude of ω_0 for the dryer atmospheric conditions implies that a fairly substantial portion of aerosol attenuation in the UV is due to absorption. Relative humidities are generally high in the eastern U.S. (typically $> 80\%$), so it is probable that comparatively lower ω_0 values exist in

arid climates and will contribute a significant absorption component to aerosol attenuation of UV-B.

11.2.6 Asymmetry Factor

The asymmetry factor (g) describes the amount of forward or backward scattering by an aerosol particle, and is primarily a function of particle size distribution. The asymmetry factor (g) is a measure of the directionality of scattering, defined as:

$$g = \frac{1}{2}\int_{-1}^{+1} P(\Theta)\cos\Theta \, \mathrm{d}(\cos\Theta) \tag{11.5}$$

and ranges from -1 to $+1$. For symmetric scattering (Rayleigh scattering), $g = 0$. Forward scattering is indicated by $g = +1$ and for backward scattering, $g = -1$. For the UV wavelength region, g typically falls in the range 0.6 to 0.8 (Madronich, 1993). Lacis and Mishchenko (1995) present slight differences in g for aerosols of differing chemical composition. Soot and large desert aerosols generally have $g \approx 0.9$, and for sulfate, marine, and smaller dust aerosols, g ranges from 0.65 to 0.8.

11.2.7 Angstrom's Exponent

Angstrom's formula for spectral extinction has the following form:

$$\tau_a(\lambda) = \beta \times \lambda^{-\alpha} \tag{11.6}$$

where $\tau_a(\lambda)$ is the aerosol optical depth at wavelength λ, β is the extinction at 1 micrometer, α is Angstrom's exponent which is related to the size distribution of the aerosol particles. Cacharro et al. (1989) showed that Angstrom's formula provides a good spectral representation of atmospheric aerosol attenuation. The wavelength to particle diameter ratios is:

- If $\forall = \mathrm{B}\ D/8 << 1$, we will have Rayleigh scattering.
- When particle diameters are between 0.1 and 10 microns we have the case of Mie scattering.
- When $\forall >> 1$, we have the case of geometric optics.

11.3 Models and Measurements

Models can help the researcher determine the UV/pollutant relationships, or the optical properties and physical characteristics of the pollutants utilizing data from numerous sources. Chemical and physical properties can now be retrieved with

regional studies utilizing the newer instrumentation that allows specific ions to be collected and sized. In either case, one must always be aware of the quality of the data that is to be used and must investigate it fully to understand if it will meet the objectives for the accuracy and precision that are being sought. Models are excellent tools for the researcher through which atmospheric optical properties can be determined, but must be tested with real data to insure validity.

Below are two examples of such studies: (1) a statistical study from EPA data banks and a special study carried out by the California Air Resources Board were done to research the pollutant/UV interaction, and (2) an optical properties determination study in which the researchers took their own data from two sites in the mountains of North Carolina. In the second study, the optical properties of various aerosols were researched using models and doing reiterative processes to have the model output coincide with the measured values. Optical properties, such as asymmetry parameter or single scatter albedo, or measured particle sizes and aerosol chemical characteristics, can be determined in this manner. Keep in mind that aerosols are the major contributor to UV absorption in the troposphere and specifically the boundary layer, and ozone is the major absorber of UV in the stratosphere. Additionally, be aware that these studies were done on cloudless days. As mentioned earlier, clouds are major UV absorbers, but their chemical and physical properties and depths are generally not well known.

Study 1:

A study by Barnard (2001) shows that specific air pollutants can reduce the increased surface levels of UV radiation, and offers an explanation for why the expected surface UV increases, caused by decreases in stratospheric ozone, have not been observed, especially in urban regions. Air pollution data (NO_x, O_3, PM-10, SO_2) collected from an EPA UV monitoring site at the University of California at Riverside (UCR), combined with data from a site operated by the California Air Resources Board in Rubidoux, CA, provided the basis of this study. The 1997 South Coast Ozone Study (SCOS) provided three key ingredients: (1) black carbon concentrations, (2) PM-10 concentrations, and (3) collocated radiometric measurements. The Total Ozone Mapping Spectrometer (TOMS) satellite data were used to provide the stratospheric ozone levels that were included in the statistical model. All of these input parameters were used to test this study's hypothesis: "the expected increase of surface UV radiation, caused by decreases in stratospheric ozone, can be masked by increases in anthropogenic emissions." The values for the pollutants were 7:00 a.m. – 5:00 p.m. averages of the instrument's values taken during the summer of 1997. A statistical linear regression model was employed using the stratospheric ozone, black carbon, PM-10, and surface ozone concentrations, and the sin (Θ) and cos (Θ). The angle Θ is defined by: $\Theta = 2\pi$ (Julian date/365). This model obtained a coefficient of determination of 0.94 with an uncertainty level (p-value) of less than 0.3% for all of the variables in the model except ground-based ozone. The final model, regressed against a data set from a

remote, western North Carolina site, resulted in a coefficient of determination of 0.92. The model shows that black carbon can reduce the Diffey weighted UV (DUV) levels that reach the surface by as much as 35%, depending on the season and location.

After review of the various pollutants that absorb in the UV range, only the possibility of PM-10 and a subset of PM-10, the black carbon, and ground-based ozone, were found in high enough concentrations to warrant further investigation. These high concentrations, especially of black carbon, that were found in this urban environment of Riverside-Rubidoux, CA, had not been previously experienced by NC State University personnel who conducted research in the mountains of North Carolina (Im et al., 2001).

Graphs of DUV changes and corresponding stratospheric ozone changes were reviewed for the entire SCOS-97 study. Three days (September 7 – 9), were chosen to study behavioral changes with respect to TOMS ozone, DUV, and black carbon. The graph for this period is shown in Fig. 11.11. Along with the DUV and TOMS, data curves represent the black carbon values for each day of interest. For days 6 – 9, the TOMS ozone value dropped equivalent amounts between days 6 and 7, and between days 8 and 9. However, the DUV increased by over 300 joules m^{-2} from day 6 to day 7, but remained constant from day 8 to day 9, even with a TOMS ozone decrease. In this particular instance, the averaged black carbon for days 6 and 7 is 1.29 μg m^{-3}, while the averaged black carbon for days 8 and 9 is 2.02 μg m^{-3}, a substantial increase. Figure 11.11 also represents the first set of data that are used to relate black carbon and DUV decreases.

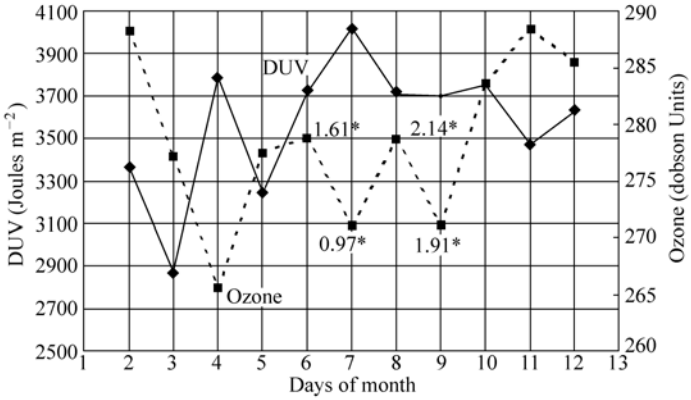

* Numbers on the graph represent black carbon 7:00 a.m. – 5:00 p.m. average in micrograms per cubic meter.

Figure 11.11 Brewer DUV and TOMS Ozone, Sept. 1997

A Statistical Analysis System (SAS) linear regression model was employed that enabled more of the SCOS-97 data to be included. Approximately 63 clear sky days, determined with Brewer DUV readings and the UCR visible data, were investigated.

Ground-based ozone, PM-10, black carbon, and TOMS ozone were used as the independent variables that would be modeled to make up the dependant DUV variable. The model included two other parameters, the sin (Θ) and cos (Θ), to account for DUV seasonal variations caused by the earth's rotation around the sun and the tilt of its axis, where $\Theta = 2\pi$ ((Julian day)$\times(365^{-1})$). Maximum DUV levels at the UC Riverside site occurred during the summer months reaching close to 5,000 joules m^{-2} day^{-1} and minimum levels (781.6 joules m^{-2} day^{-1}) occurred during the winter months.

The results of the SAS linear model are presented below. The final regression developed from this data set is:

$$\begin{aligned}\mathrm{DUV} = {} & 608.91 \sin(\Theta) - 2{,}049\cos(\Theta) - 16.93 \times \mathrm{TOMS} - 7.1 \\ & \times \mathrm{PM\text{-}10} - 148.4 \times \mathrm{Blackcarbon} + 8{,}484. \end{aligned} \tag{11.7}$$

TOMS ozone values are in Dobson units. The units for PM-10 and black carbon are micrograms per cubic meter ($\mu g\ m^{-3}$).

One must be careful at this point in interpreting the results. The *t*-statistics employed here assume a normal distribution, centered on zero with tails in the positive and negative direction. Physically, however, the coefficients for black carbon, PM-10, TOMS, and ground-based ozone must be negative, as all are suspected to be UV radiation absorbers. If positive coefficients had been obtained for any of these independent variables, it would have implied UV radiation had been created, which is not physically possible.

Table 11.2 indicates the sensitivities of each of the parameters used in the model. Table 11.3 was developed using the maxima and minima parameters from this study, and average values based on the author's previous experience in the pollution-monitoring field. The changes noted in Tables 11.2 and 11.3 correlate well with expected physical results. As the Julian day changes from summer (Julian day 180) to winter (Julian day 365), the surface DUV changes dramatically (4,122.3 joules m^{-2}). Likewise, the changes brought about by the TOMS ozone are in line with current literature. A model check done with the radiation amplification factor (RAF) shows excellent agreement with accepted RAF values. This value is known (Madronich et al., 1998) to be between 1.2 and 1.3, and is defined by the percent change in UV divided by the percent change in TOMS ozone. If the change in UV, or in this case DUV, is divided by the mean of the DUV values, a percent change is obtained. Thus, using the appropriate values and the statistical model, the RAF = $16.93 \times 294.5/4{,}036.5 = 1.235$, confirming the relationship between the DUV and TOMS ozone. The surprising factors are the coefficients for the black carbon and the PM-10. Using the values in Table 2, the changes of black carbon and PM-10 encountered in this research account for 46.5% and 58.5%, respectively, of the DUV changes caused by TOMS ozone.

One pollutant, which was not accounted for at all in Eq. (11.1), was the ground-based ozone. Long thought to be one of the significant absorbers of UV-B radiation,

it did not statistically meet the 0.05 significance level in this model. Several trials of the SAS Autoreg procedure, that included non-linear fits of the data and SIN and COS squared terms, did not produce models with coefficients of determination as high as for Eq. (11.1), nor did they produce coefficients that were physically meaningful. When this is carefully analyzed, it makes sense. UV radiation is required to generate the surface measured ozone, but in return, the more ozone, the less UV radiation penetrates to the surface. Also, the more black carbon, the less the UV, and thus the reduction of surface measured ozone.

One factor in the model, which dominates the equation, is the intercept (8,484 joules m^{-2} day^{-1}). This number, much larger than the other terms of the equation, needs some physical explanation. Mathematically, it is the value of the DUV radiation, dependant variable (Y), when all other independent variables (Xs) are zero. Physically it represents a daily averaged DUV value found at the top of the atmosphere. If all the independent variables are removed from the equation, the radiation has no atmospheric constituents to attenuate it and no day-to-day variations caused by the earth's tilting axis and orbit around the sun. If the DUV changes created by these independent variables (Xs) are added to the maximum DUV level from Table 11.2, they sum to 7,994.3 joules m^{-2} day^{-1}. This would approximate a lower boundary level for the daily averaged DUV at the top of the atmosphere. If the same is done for Table 11.3, they sum to 11,481.9 joules m^{-2} day^{-1}. These two numbers represent the range of variations in the DUV values at the top of the atmosphere caused by the maxima and minima values of the factors which alter the radiation as it passes from the top of the atmosphere to the surface. The intercept (8,484 joules m^{-2} day^{-1}) for this model lies within this range. Thus, the intercept could be interpreted as a constant similar to that of the I_0 in the Langley expressions for optical depth.

While this regression was developed utilizing data from a large West Coast experiment in a highly polluted area, it was tested and confirmed in a more pristine, albeit still polluted, East Coast remote site. The Mt. Gibbes site in Mt. Mitchell State Park, NC has been operating for some time with various types of aerosol and radiation equipment. The data from the spring, summer, and fall of 1999 included UV solar radiation and black carbon. TOMS ozone values were obtained from NASA. Since no collocated data were available for the PM-10 concentrations, a yearly averaged value from a neighboring county was used. These were then input into Eq. (11.1) and approximately 30 values of DUV were generated. The values for black carbon at this site ranged from a low of 0.032 μg m^{-3} to a high of 1.545 μg m^{-3}, considerably less than those found at the Riverside site (Table 11.4). UVB-1 data set values, taken at one-minute intervals, were added to obtain a daily (7:00 a.m. – 5:00 p.m.) total UV exposure. This value was then scaled by the CIE (Diffey erythemal curve) factor described in the operations manual for the UVB-1 instrument. The model results were then plotted against these 7:00 a.m. – 5:00 p.m. values.

Table 11.2 Sensitivity tests of DUV in Eq. (11.7) for expected ambient maxima and minima values; the tests consider the parameters of (a) Julian date, (b) TOMS ozone, (c) PM-10, and (d) Black carbon, as the real variables each time, while the others (1999 yearly means) were treated as constants

(a)					
	DUV ($J\ m^{-2}\ d^{-1}$)	Julian Day	TOMS Ozone (DU)	PM-10 ($\mu g\ m^{-3}$)	Black Carbon ($ng\ m^{-3}$)
	777	1			
	3,380	90			
	4,889	180	294	65	1,546
	2,340	270			
	767	365			
Change	4,122				
(b)					
	DUV ($J\ m^{-2}\ d^{-1}$)	TOMS Ozone (DU)	Julian Day	PM-10 ($\mu g\ m^{-3}$)	Black Carbon ($ng\ m^{-3}$)
	3,031	402	183	65	1,546
	5,723	243			
Change	−2,692	159			
(c)					
	DUV ($J\ m^{-2}\ d^{-1}$)	PM-10 ($\mu g\ m^{-3}$)	Julian Day	TOMS Ozone (DU)	Black Carbon ($ng\ m^{-3}$)
	4,164	163	183	294	1,546
	5,271	7			
Change	−1,107	156			
(d)					
	DUV ($J\ m^{-2}\ d^{-1}$)	Black Carbon ($ng\ m^{-3}$)	Julian Day	TOMS Ozone (DU)	PM-10 ($\mu g\ m^{-3}$)
	4,050	7,000	183	294	65
	5,087	10			
Change	−1,037	6,990			

The most striking findings are the results from this testing. As shown in Fig. 11.12, where the modeled data is plotted against the measured UV data from the UVB-1 instrument, there is an excellent correlation, $R^2 = 0.92$. In spite of utilizing one type of instrument to develop the model (Brewer spectrophotometer), and comparing the model's output to that of another type of instrument (Yankee UVB-1), integrated DUV radiation values between the two sites, and the instruments, correlated extremely well. The model (Eq. (11.1)) was applicable for black carbon values ranging from 0.03 $\mu g\ m^{-3}$ to above 4.0 $\mu g\ m^{-3}$, a range of over two decades. It maintained its linearity over this entire range. The Yankee UVB-1 instrument does not have a spectrally resolved output. It measures an entire UV spectrum that includes both the UV-B region and the UV-A region.

Table 11.3 Sensitivity tests for the independent variables of Eq. (11.7) for expected ambient minima and maxima: (a) Julian date, (b) TOMS ozone, (c) PM-10, and (d) Black carbon

(a)					
	DUV	Julian Date	TOMS Ozone	PM-10	Black Carbon
	781.6	0	300 DU	60 μg m^{-3}	1.0 μg m^{-3}
	3,395.3	90			
	4,903.9	180			
	2,355.1	270			
	781.6	365			
Change	4,122.3 joules m^{-2} day^{-1}				
(b)					
	DUV	TOMS Ozone	PM-10	Black Carbon	
	2,364.4	450	60 μg m^{-3}	1.0 μg m^{-3}	
	6,173.6	225			
Change	−3,809.2 joules m^{-2} day^{-1}	225 DU			
(c)					
	DUV	PM-10	TOMS Ozone	Black Carbon	
	3554.9	250	300 DU	1.0 μg m^{-3}	
	5294.4	5			
Change	−1739.5 joules m^{-2} day^{-1}	245 μg m^{-3}			
(d)					
	DUV	Black Carbon	TOMS Ozone	PM-10	
	5,050.8	7.00	300 DU	60 μg m^{-3}	
	4,013.5	0.01			
Change	−1,037.3 joules m^{-2} day^{-1}	6.99 μg m^{-3}			

Table 11.4 Maxima, minima, mean, and standard deviations for the values of the variables used to develop and test the model

	Riverside, CA				Mt. Gibbes, NC			
	Max.	Min.	Mean	Std. Dev.	Max.	Min.	Mean	Std. Dev.
DUV* (J m^{-2} d^{-1})	6,035	2,038	3,698	990	9,677	3,257	6,257	1,764
TOMS (DU)	330	259	285	15	348	270	298	20
PM-10 (μg m^{-3})	132	15	47	20	60**	7	28	12
Black Carbon (ng m^{-3})	4,757	181	1,546	761	1,545	32	395	366
Ozone*** (ppb)	105	25	59	18	na	na	na	na

* UV values obtained from a Brewer spectrophotometer at Riverside, CA and integrated UVB-1 values from Mt. Gibbes, NC.

** PM-10 values from EPA/AIRS database for 1999, yearly average value of 28 used to test model.

*** Ground-based ozone values were used to determine the SAS model, but were not used with the Mt. Gibbes data. Their significance was above the .05 level.

Pollutant concentrations are averages of the hourly averages from 7:00 a.m. – 5:00 p.m.

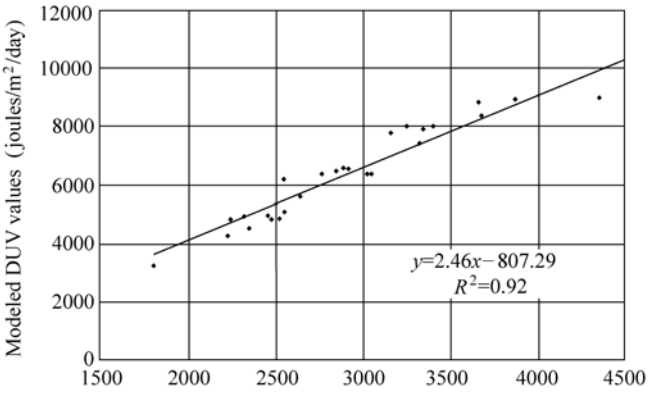

Figure 11.12 UVB-1 Mt. Gibbes daily integrated values

Other studies (Liousse, et al., 1996) have concluded that the black carbon could act to cool the earth, yet UV radiation, being in the shorter end of the spectra, has the highest energy photons. Since the black carbon is absorbing these high-energy photons, and probably re-emitting in the infrared, it would be a logical conclusion that the atmospheric layer in which black carbon resides would be slightly heated. While the UV heating factor would be small, the black carbon absorbs strongly at all wavelengths and can act as a global cooling factor, reducing the available radiation to the earth's surface (Satheesh and Ramanathan, 2000; Yu et al., 2001). The heating of the atmosphere could also impact the photochemical reactions and cloud formations (Ackerman et al., 2000) that occur. There would be a trade-off in this area. The black carbon is reducing the UV that is available to initiate photochemical reactions, but black carbon's presence will also heat the surrounding atmosphere, which tends to speed up these same reactions.

In this particular urban environment, the author found that the black carbon concentrations seem to have little effect on the aerosol optical depth, but did show a relationship with the single scatter albedo. Two papers (Lioussie et al., 1996; Dubovik et al., 1998) that discuss black carbon's optical properties focus on its relationship with the single scatter albedo and not on the optical depth.

In this study statistics and monitoring data led to the formulation of a model that determined an average daily UV dosage at the surface. PM-10 and black carbon were observed to have a significant impact on the UV, but this model still needs to be tested in other regions to refine it with more definitive particulate measurements (chemical composition and size). The research from this study should lead to further investigations that may help develop more quantitative means that would be useful in describing the effects of aerosols on the radiative transfer of UV to the surface. Further work can be done to determine if the long-term increases of automobile and truck emissions are capable of producing the possible effects shown here and to what extent their increases correlate to the decreases of UV radiation. Black carbon's direct and indirect effects on the photochemical

processes in the atmosphere also need to be fully investigated with studies that encompass varied regions.

Study 2:

This study (Wenny et al., 1998) focuses on the attenuation of UV-B that can be attributed to aerosol optical properties. The procedure is to measure UV-B transmission and some aerosol properties in a layer of atmosphere defined by a mountain site and valley site (about 1 km vertically, 6 km horizontally) and analyze the data for aerosol optical effects and aerosol optical properties. The relationship between air mass source region and aerosol optical depth at visible wavelengths and UV-B transmission is investigated. Empirical relations between aerosol optical depth and UV-B transmission are derived to improve predictions of solar noon UV-B transmission, such as done by the U.S. Weather Service (Long et al., 1996). A novel iterative procedure employing Mie scattering and UV-B radiative transfer calculations, in conjunction with actual measurements, is employed to retrieve aerosol optical properties (single scatter albedo (SSA) and asymmetry parameter (AP)) that physically describe the amount of aerosol scattering and absorption occurring, consistent with the observed UV-B transmissions.

The novel approach taken in the present investigation also requires analysis of radiation measurements using Mie theory and radiation transfer calculations; however, the distinction between the present approach and the diffuse/direct method is that the measurement is one of atmospheric irradiance transmission through a layer of atmosphere, determined by the ratio of the irradiance (i.e., diffuse + direct) at the bottom of the layer to the irradiance at the top of the layer, which accurately defines the radiative source illuminating the layer. Moreover, the wavelengths are in the UV region, while the previous investigations were in the visible region.

This study was a step-wise pilot experiment to develop a reliable methodology for gathering an extended set of aerosol information obtained by in situ collections and by confirming the results with measurements and analysis of the radiation field. Long-term measurements are highly desirable for aerosol work because aerosol properties are so variable due to their chemical and spatial inhomogeneous nature; thereby introducing large uncertainties in all radiative and in situ measurement methods of the free atmosphere aerosol.

The aerosol optical depth (τ_λ) was calculated for the three operational wavelength channels of the mountaintop and the valley MFRSR, 415 nm, 500 nm, and 673 nm, using the Langley method. The Langley method assumes that atmospheric attenuation is generally constant throughout the measurement period (airmass length ranging from $m = 2$ to $m = 6$), which is generally true for a clear, stable atmosphere (Lenoble, 1993; Harrison and Michalsky, 1994). Langley plots on all days with clear sky intervals were derived for each instrument's wavelength channels and adjusted to the mean earth-sun distance. Greater variability of the valley instrument was observed and can be attributed to the variability of the atmosphere in the lower layer.

The optical depths for the total column above each respective site, τ_λ, was calculated for each wavelength using an expression of Beer's law

$$\tau_\lambda = -\ln\left(\frac{V_\lambda}{V_{o\lambda}}\right) \times \cos(\theta) \tag{11.8}$$

where τ_λ is the optical depth, V is the instrument output, V_o is the extraterrestrial constant adjusted for earth-sun distance on the day of interest, and θ is the zenith angle. Each τ_λ was calculated as a 12-minute average, centered around the zenith angle of interest.

Wavelength dependent Rayleigh scattering by air molecules was removed from the measurements, as it is a significant non-aerosol contributor to τ_λ. Equation (11.3) was used to estimate the Rayleigh scattering (σ_{Rayleigh}) for each channel. The aerosol optical depth for the layer between the two sites was determined as the subtraction of the Rayleigh-corrected optical depths, $\tau_{\text{valley}} - \tau_{\text{mountain}}$. The absorption optical depth of atmospheric gases, O_3, NO_2, and SO_2 were estimated through calculations using a measured (O_3) or assumed (NO_2, SO_2) column amounts. All three gases were found to have an extremely small contribution to τ_λ, and were thus considered negligible.

The UV-B transmission ($T_{\text{UV-B}}$) for the layer between the two sites was calculated as the ratio of the UV-B measurement at the valley to the UV-B measurement at the mountain. The attenuation of the broadband UV-B irradiance during passage between the sites is assumed to be due to a combination of gaseous and aerosol absorption and scattering.

Aerosol size distributions were measured at the valley site using the Differential Mobility Particle Sizer (DMPS), on nine days coincident with significant clear sky periods. For each of the nine days, an average size distribution was determined from all the distributions collected during the coincident period. Lognormal parameters for the distribution were determined using the fitting software DISTFIT^{TM} provided with the instrument.

A flow chart outlining the method used to derive these aerosol optical properties using a Mie code, similar to the code of Dave (1968), in conjunction with a UV-B radiative transfer code (TUV) (Madronich, 1993) is shown below in Fig. 11.13. The resulting end product is the aerosol optical properties (at UV-B wavelengths) of an atmospheric layer between a mountain valley site and peak site in western North Carolina.

The lognormal parameters derived from the measured aerosol size distributions served as input to the Mie code using a first-guess for the complex index of refraction of $1.5 - 0.08i$ (1.5 is held constant). The Mie code calculations yield first-guess estimates of the asymmetry factor and single scatter albedo at 312 nm, the UVB-1's wavelength of maximum sensitivity to atmospheric UV. These values serve as input into the UV-B radiative transfer model of the UV-B transmission for the spectral response function of the Yankee UVB-1 radiometer. Additional inputs

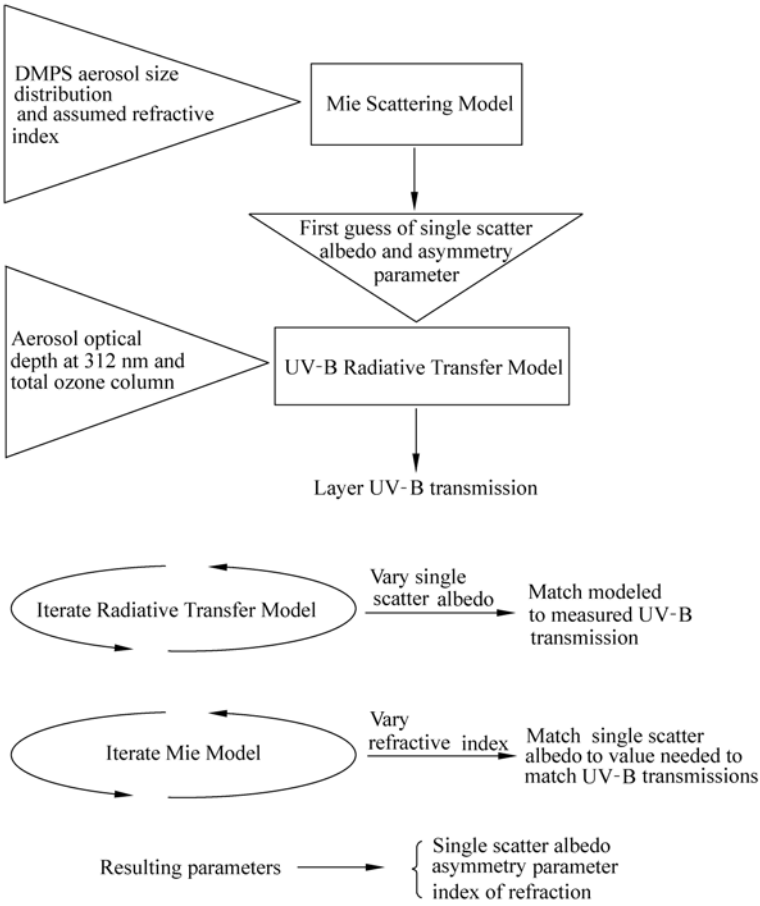

Figure 11.13 Diagram outlining the modeling procedure used to determine single scatter albedo and the asymmetry parameter

are the total ozone column as measured by the valley Brewer spectrophotometer and the aerosol optical depth at 312 nm, extrapolated from the spectral extinction determined from the τ_λ values of the MFRSR. This extrapolation of τ_λ to 312 nm is based on Angstrom's Formula for spectral extinction and has the following form:

$$\tau_a(\lambda) = \beta \times \lambda^{-\alpha} \tag{11.9}$$

where $\tau_a(\lambda)$ is the aerosol optical depth at wavelength λ, β is the turbidity coefficient, α is Angstrom's exponent which is related to the size distribution of the aerosol particles. Cachorro et al. (1989) showed that Angstrom's formula provides a good spectral representation of atmospheric aerosol attenuation. Iteration, varying the single scatter albedo, until the modeled transmission through the layer matched the observed transmission as measured by the UVB-1 instruments and then, varying the imaginary component of the complex index of refraction

until the single scatter albedo matched the value resulting from the radiation code iteration was repeated until convergence was achieved. UV-B transmission is more sensitive to changes in ϖ_0 (compared to g), thus the decision to use it as the varying parameter. The aerosol size distribution acts as a constraint on g, which only changed slightly as the refractive index changed.

Optical depth values were obtained for all clear-sky periods throughout the six month observational period with a mean optical depth for the entire atmosphere as measured from the valley MFRSR at 500 nm of 0.356. The large seasonal variability inherent in optical depth measurements is evident by a standard deviation of 0.329. Past studies of annual turbidity cycles in nearby regions are consistent with this mean value (Flowers et al., 1969).

Clear-sky conditions were present over the two research sites for a large portion of the morning hours on 46 days. Using back trajectory analysis, 18 of these cases were classified as highly polluted air masses, 15 as polluted marine and 13 as polluted continental. Air masses arriving at the site from these sectors have been shown to exhibit differing physio-chemical characteristics (Deininger and Saxena, 1997; Ulman and Saxena, 1997). The MFRSR optical depth measurements for the intervening layer were categorized according to air mass source region. It was found that the τ mean values differed for the three air mass types suggesting that aerosol optical properties vary in relation to air mass. The highest mean value of τ for the highly polluted air mass classification is consistent with an assumption of higher sulfate aerosol concentrations, as this aerosol species has been shown to be an efficient attenuator at visible wavelengths (Whitby, 1978; Hegg et al., 1993; Yuen et al., 1994). The greater standard deviation of the highly polluted air mass cases is indicative of the greater variation in aerosol characteristics arising from differences in source strength, composition, size distribution and age of the aerosol. Two aerosol size distributions (highly polluted classification) displayed a multi-modal shape, which indicates the presence of an accumulation mode (particle diameter between 0.1 μm and 1.0 μm). Assuming that sulfate aerosols are the predominant species in the highly polluted air mass, the presence of a significant accumulation mode is not unexpected and can be explained through condensation and coagulation of sulfate aerosols. The nine clear sky days with DMPS aerosol size distribution measurements permitted a closer examination of the relationship of aerosol and radiative properties using the iterative procedure defined previously.

For the nine days investigated, ϖ_0 at 312 nm varied from 0.75 to 0.93 and showed no discernible dependence on air mass type; however, a dependence on relative humidity was observed. The three days possessing the highest relative humidities have $\varpi_0 > 0.9$, which is consistent with the characteristics of hygroscopic aerosols, which do not absorb strongly in the UV. The remaining six days exhibited ϖ_0 values of 0.75 to 0.82, comparable to the typical value given by Madronich (1993). This relatively narrow range of ϖ_0 for dryer conditions indicates that relative humidity is a controlling factor in the resulting value of ϖ_0.

The small sample size did not allow determination of any seasonal trend in ϖ_0. The evidence from this study indicates that typically moist climates (such as in the Southeast or Northwest U.S.) will display larger variations of ϖ_0 than arid climates (such as in the Midwest and Southwest U.S.). According to our results, the magnitude of ϖ_0 for the dryer atmospheric conditions implies that a fairly substantial portion of aerosol attenuation in the UV is due to absorption. Relative humidities are generally high in the eastern U.S. (typically > 80%), so it is probable that comparatively lower ϖ_0 values exist in arid climates and will contribute a significant absorption component to aerosol attenuation of UV-B. The ϖ_0 values found in this study are in general lower than those used in several UV modeling studies (Liu et al., 1991; Wang and Lenoble, 1994). The nine *g* values determined for our site fall within 0.63 to 0.76. No specific feature based upon air mass is discernible. Angstrom's exponent (α) was determined using the MFRSR spectral aerosol optical depth data and also the volume spectral extinction as calculated by the Mie code. The good agreement for five of the nine cases, evident from the small differences between the two values, gives increased confidence in the modeling procedure results. The larger differences for the remaining four cases can be attributed to greater uncertainty in the aerosol size distribution measurements. The effect of aerosol chemical composition on UV-B transmission is unquantified in this investigation. Future studies should incorporate coupled measurements of aerosol size distribution, aerosol chemical composition characteristics and in-situ aerosol optical properties. Such combined measurements are rarely obtained (Schwartz et al., 1995).

Extrapolation of the spectral extinction curve, determined from $\ln(\tau)$ versus $\ln(\lambda)$ fit with linear regression permits an estimate of τ_{312} for each day. A plot of ln(Solar Noon UV-B Transmission) versus τ_{312} exhibits a strong correlation ($r^2 = 0.904$). The fit is surprisingly good considering the wide range of solar noon zenith angles, 20° to 55°, for the nine days used. The linear regression equation provides a simple expression for determining solar noon UV-B transmission if a value of τ_{312} is known. The regression equation is as follows:

$$\ln(\text{UV-B Transmission at Solar Noon}) = -0.1422 \times (\tau_{312}) - 0.138 \qquad (11.10)$$

The *y*-intercept, i.e. no aerosol attenuation, converts to a transmission of 87.1%.

The average transmission for each clear morning was derived for the UVB-1 measurements. A morning average transmission was determined for the zenith range $65° - 40°$ as the transmission changed by less than 3% over this period for any given day. The highly polluted cases exhibited, on average, the lowest transmission, 77.8% ± 4.6%. The polluted marine cases exhibited an average transmission of 81.9% ± 2.9%, and the polluted continental cases 83.5% ± 2.8%. The observed differences are due both aerosol differences and the abundance of absorbing gases. The mean ozone column for the layer was 12.6 DU (±6 DU), and showed no discernible trend versus air mass type. A change in layer ozone column of 10 DU

resulted in an UV-B transmission change of only 1.5% (decreased transmission for increased ozone and vice versa). The effect of SO_2 and NO_2 absorption on UV-B transmission was modeled and showed a decrease in UV-B transmission of much less than 0.5% for the typically minute layer column amounts of each gas. Differences in gaseous absorption, although small, can account for a portion of the variability between air mass types and also the variability within a given air mass type. Therefore, the remainder of the variability is primarily due to differences in aerosol attenuation properties. Highly polluted air masses, which exhibited the highest aerosol optical depth, also exhibited the greatest attenuation of UV-B. In comparison, the "cleaner" marine and continental air masses had lower average τ_λ values and higher UV-B transmission values. Our observed range of broadband UV-B attenuation for all the days was $14\%-31\%$ for the 1 km layer. This range is quite consistent with the other reported values of an altitude effect, or the percentage decrease per 1,000 meters altitude in the lower troposphere.

An important aspect of this study is the development of an empirical relationship between optical depth and UV-B transmission, useful for calculation of the NOAA UV Index, UV climatology studies, and remote sensing applications. Specific knowledge of aerosol parameters and their effects on UV-B transmission allow for improved accuracy in UV climatology modeling. There is an inherent regionality to optical depth and aerosol optical properties which will in turn cause regional differences in UV-B transmission, and this needs to be considered in such applications as UV forecasts, UV climatology and long term trends. Remote sensing applications that rely upon UV attenuation measurements need to account for any change in aerosol UV attenuation due to changing aerosol properties.

To investigate the effect of aerosols alone, it is necessary to utilize an instrument that measures in wavelength bands where non-aerosol attenuation is minimized, such as the three channels from the MFRSR (415 nm, 500 nm, and 673 nm). Ideally, aerosol optical depths at wavelengths in the UV-B region would yield the best relation. However, optical depths at UV-B wavelengths are more problematic to obtain. Plots of natural logarithm of UV-B transmission versus aerosol optical depth were made for solar zenith angles of 65° to 40° in 2.5° intervals. Individual zenith angle plots were made as opposed to daily averaged plots because global UV-B transmission is slightly dependent upon zenith angle. Each plot was negatively correlated, i.e. increased aerosol optical depth results in decreased UV-B transmission. The correlation coefficient (r^2) values for each plot show that the regressions fit very well, with only 4 of the 33 regressions having an $r^2 < 0.8$. For each wavelength, the slope, or change in ln(UV-B transmission) for a given change in τ, decreases as zenith angle decreases. This implies that as the sun nears solar noon and a shorter atmospheric pathlength, the UV-B transmission becomes less sensitive to τ and also that the UV-B transmission approaches a maximum value. This is of importance in biological terms since the hours surrounding solar noon are the times of maximum irradiance.

For a given zenith angle, the regression slopes increase as the wavelength increases due to the fact that optical depth is proportional to λ^{-1}. The larger range of optical depths at the shorter wavelengths is reflected in a smaller percentage change in UV-B transmission (lesser slope) associated with a given change in aerosol optical depth. Since a given change in aerosol concentration produces a more significant variation in optical depth for shorter wavelengths, the sensitivity of UV-B transmission to aerosol optical depth must be less at these wavelengths. A percentage change in UV-B transmission for a given change in aerosol optical depth can be determined from the regressions. Using the 500 nm plot at 50° solar zenith angle as an example, a change in optical depth of 0.1 predicts a change in the UV-B transmission on the order of 4%. An additional feature of interest is the nearly constant value of the *y*-intercept values. Upon conversion to percent UV-B transmission, the averages of the *y*-intercepts over all zenith angles are $86.8\% \pm 0.7\%$ for the 415 nm channel, $87.0\% \pm 0.8\%$ for the 500 nm channel, and $87.0\% \pm 0.7\%$ for the 673 nm channel. Thus, 87% is the UV-B transmission expected for an aerosol free layer and the 13% attenuation can be ascribed to Rayleigh scattering in addition to the slight absorption by atmospheric gases, i.e., O_3, NO_2, and SO_2, in the layer. This value is consistent with the zero aerosol conditions derived for the nine day case study results discussed previously. Multiple regression analysis using the Statistical Analysis System (SAS) was performed to obtain the full model for prediction of the UV-B transmission versus zenith angle (in degrees) given a set of aerosol optical depth measurements, and the backward elimination procedure was used to identify the most significant variable. Aerosol optical depth at 415 nm (τ_{415}) was determined as the most significant variable for predicting UV-B transmission, with the ability to account for 72.8% of the data variability. Upon including the parameters τ_{500} and zenith angle (the two next most significant parameters) the fit improves to account for 82.0% of the observed variability. All three variables are significant at the 0.0001 level. The empirical regression equation is of the form:

$$\ln(\text{UV-B transmission}) = a_0 + a_1 \times \tau_{415} + a_2 \times \tau_{500} + a_3 \times \text{zenith angle} \qquad (11.11)$$

where the regression coefficients are defined as $a_0 = -0.0935$, $a_1 = -0.8515$, $a_2 = 0.7505$, and $a_3 = -0.0012$. The addition of the two extra terms, resulting in a 10% improvement in fit, was deemed necessary as the inclusion of a zenith angle term enables prediction for UV-B transmission at solar noon, and the use of two optical depth values provides information on the spectral extinction shape. The τ_{673} term was neglected, as inclusion did not significantly improve the quality of the fit (0.1% improvement). The 18% variability unaccounted for can be ascribed to the combined uncertainties of the measurements as well as factors, each individually small, not included in the regression (i.e., variations in ozone, aerosol absorption, chemical composition, and relative humidity). Equation (11.11) is specific to the region surrounding the experiment sites.

11.4 Summary

As previously shown in this chapter, the main constituent of air pollution that affects the transmission of UV to the earth's surface is aerosols. While three gases exhibit strong UV absorption characteristics, their concentrations and path-lengths in the troposphere, and primarily the planetary boundary layer, are both insufficient to produce significantly reduced UV levels at the surface. The physical, chemical and optical properties were studied, and the results strongly indicate that for dryer conditions, the retrieved single scatter albedo was higher in the eastern part of the U.S., and that relative humidity played an important role in determining this level of single scatter albedo. Highly polluted air masses also exhibited larger aerosol optical depths and in turn, the lowest UV transmission.

The second study also showed a novel non-invasive remote sensing procedure. A Mie scattering code and a radiative transfer model were utilized in conjunction with measured parameters to retrieve reasonable values of aerosol single scatter albedo and asymmetry factor using transmission and size distribution measurements. The aerosol single scatter albedo was seen to vary substantially; a probable cause due to the concentrations of black carbon in the atmosphere.

There is an obvious need to initiate an investigation similar to the Wenny study that monitors both the radiation and the aerosol size and speciation at the top of a mountain and in a nearby valley. Recent advances in aerosol instrumentation allow researchers to not only perform real time monitoring of aerosol size distributions, but are also now able to determine aerosol speciation. These data, combined with the procedures presented here, can fully characterize certain aerosol classes within a study area that could be applied throughout the country. Sulfates and nitrates, both thought to be highly scattering media, can each be detected in real time with ion chromatography. An aethalometer can measure black carbon, a DMPS or similar instrument can measure aerosol size distributions, and a good relative humidity or dew point hygrometer, combined with either a Brewer spectroradiometer or a UV MFRSR, should be able to fully characterize the aerosol optical properties in the UV and relate them to the species of aerosols present in the ambient atmosphere.

A recent paper by Petters et al. 2003 describes a methodology that can be used with the UV MFRSR and coupled with a tropospheric UV radiative transfer model to produce values of the single scatter albedo. This study conducted at the same site as the Wenny study has slightly wider variations than previously reported values. The lower values of SSA could indicate that, at least at this site, preferential absorption of UV radiation by black carbon aerosols could be occurring. More SSA data taken in the UV spectrum will allow for better estimation of this parameter for UV radiative transfer modeling and will lessen the modeling error in determining surface UV irradiances.

All of a study's monitoring data must have its quality control factors of precision, accuracy, representativeness, completeness, and comparability known

and documented prior to the beginning of the study. If EPA data are used, the state of the local agency that reports that data to EPA will have a complete set of such documents that will include a Quality Systems Implementation Plan and a systematic approach to provide external system and performance audits. The data quality must be maintained throughout the study. It is a waste of the investigator's time, and more importantly, money, to gather data that cannot be used, simply because its accuracy and precision were not documented. This is true for both the air pollution data and the radiation data.

One must keep in mind that there have only been two studies presented here to show the methodology employed in determining site specific UV transmissions to the surface. Each site will have its own variables, not the least of which will be the differing combinations of scattering and absorbing aerosols. There is a great need to characterize more sites and identify aerosol types according to their chemical species and by doing so, relate the species to the single scatter albedo and the aerosol optical depth. By doing this it will become possible to transfer the ground-based knowledge to satellite observation points so that predictions of surface UV can become a reality.

The reader is referred to the Indian Ocean Experiment (INDOEX), a 1999 international field campaign conducted to study how air pollution affects climate processes over the tropical Indian Ocean, and to the South Coast Ozone Study (SCOS'97) conducted in the Los Angeles Basin during the summer of 1997 where radiation and pollution measurements were taken at the surface and various altitudes. Numerous publications were produced from each of these studies.

References

Ackerman AS, Toon OB, Stevens DE, Heymsfield AJ, Ramanathan V, and Welton EJ (2000) Reduction of Tropical Cloudiness by Soot. Science 288: 1042 – 1047

Arya SP (1999) Air Pollution Meteorology and Dispersion. Oxford University Press, New York, p.301

Bahrmann CP, and Saxena VK (1998) The influence of air mass history on black carbon concentrations in the southeastern US. J. Geophys. Res. 103: 23153 – 23161

Bais AF, Zerefos CS, Meleti C, and Ziomas IC (1993) Spectral measurements of solar UVB radiation and its relation to total ozone, SO_2, and clouds. J. Geophys. Res. 98: 5199 – 5208

Ball RJ, and Robinson GP (1982) The origin of haze in the central United States and its effect on solar radiation. J. Appl. Meteorol. 21: 171 – 188

Barnard WF (2001) Daily Surface UV Exposure and Its Relationship to Surface Pollutant Measurements. PhD. Thesis

Barnard WF, Saxena VK, Wenny BN, and DeLuisi JJ (2003) Daily surface UV exposure and its relationship to surface pollutant measurements, Journal of the Air & Waste Management Association, Vol 53

Blaustein AR, and Wake DB (1995) The puzzle of declining amphibian populations. Scientific American 52 – 57

Blumthaler M, Schreder J, and Grobner J (1996) UV sky radiance influenced by aerosols and tropospheric ozone-measurements and modeling. In: Smith WL, Stamnes K (eds) IRS '96: Current Problems in Atmospheric Radiation. Proc. Int. Radiation Symp., Fairbanks, AK, Deepak Publishing, Hampton, VA, pp.853 – 856

Bojkov RD, Fioletov VE, and Diaz SB (1995) The relationship between solar UV irradiance and total ozone from observations over southern Argentina. Geophysics Research Letters 22: 1249 – 1252

Booker FL, Burkey KO, and Pursley WA (2007) Elevated carbon dioxide and ozone effects in peanut. I. Gas-exchange, biomass, and leaf chemistry. Crop Science 47: 1475 – 1487

Bruhl C, and Crutzen PJ (1989) On the disproportionate role of tropospheric ozone as a filter against solar UV-B radiation. Geophys. Res. Lett. 16: 703 – 706

Cachorro VE, Gonzalez MJ, De Frutos AM, and Casanova JL (1989) Fitting Angstrom's formula to spectrally resolved aerosol optical thickness. Atmos. Environ. 23: 265 – 270

Cadle SH, and Mulawa PA (1990) Atmospheric carbonaceous species measurement methods comparison study: general motors results. Aerosol Science Technology 12: 128 – 141

Charlock TP, Kondratyev K, and Prokofyev M (1993) Review of recent research on the climatic effect of aerosols. In: Jennings SG (ed) Aerosol Effects on Climate, Univ. of Arizona, Tucson, pp.233 – 274

Charlson, RJ, Covert DS, and Larson TV (1984) Observation of the effect of humidity on light scattering by aerosols. In: Ruhnke L, Deepak A (eds) Hygroscopic Aerosols. Deepak Publishing, Hampton, VA

Charlson RJ, Langner J, Rodhe H, Leovy CB, and Warren SG (1991) Perturbation of the Northern Hemispheric radiative balance by backscattering from anthropogenic sulfate aerosols. Tellus 43B: 152 – 163

Coakley JA, Jr, Cess RD, and Yurevich FB (1983) The effect of tropospheric aerosols on the earth's radiation budget: A parameterization for climate models. J. Atmos. Sci. 40: 116 – 138

Dave JV (1968) Subroutines for computing the parameters of electromagnetic radiation scattered by a sphere. IBM Scientific Center, Palo Alto, CA, Rep. No. 320 – 3237

Deininger CK, and Saxena VK (1997) A validation of back trajectories of air masses by principal component analysis of ion concentrations in cloud water. Atmos. Environ. 30: 295 – 300

Dubovik O, Holben BN, Kaufman YJ, Yamasoe M, Smirnov A, Tanre D, and Slutsker I (1998) Single-scattering albedo of smoke retrieved from the sky radiance and solar transmittance measured from the ground. J. Geophys. Res. 103: 31903 – 31923

Dutton EG, Reddy P, Ryan S, and DeLuisi JJ (1994) Features and effects of aerosol optical depth observed at Mauna Loa, Hawaii: 1982 – 1992. J. Geophys. Res. 99: 8295 – 8306

Estupinan JG, Raman S, Crescenti GH, Streicher JJ, and Barnard WF (1996) Effects of clouds and haze on UV-B radiation. J. Geophys. Res. 101: 16807 – 16816

Fioletov VE, and Evans WFJ (1997) The influence of ozone and other factors on surface radiation Ozone Science: a Canadian Perspective on the Changing Ozone Layer. University of Toronto Press, Toronto, pp.73 – 90

Flowers EC, McCormick RA, and Kurfis KR (1969) Atmospheric turbidity over the United States, 1961 – 1966. J. Appl. Meteor. 8: 955 – 962

Frederick JE, Koob EK, Alberts AD, and Weatherhead EC (1993) Empirical studies of tropospheric transmission in the ultraviolet: broadband measurements. J. Appl. Meteor. 32: 1883 – 1892

Frederick JE, and Steele HD (1995) The transmission of sunlight through cloudy skies: an analysis based on standard meteorological information. J. Appl. Meteorol. 34: 2755 – 2761

Goldberg ED (1985) Black carbon in the environment: Properties and distribution. Wiley Interscience

Gundel LA, Dod RL, Rosen H, and Novakov T (1984) The relationship between optical attenuation and black carbon concentration for ambient and source particles. Science Total Environment 36: 197 – 202

Hansen ADA, and Rosen H (1990) Individual measurements of the emission factor of aerosol black carbon in automobile plumes. Journal of Air Waste Management Association 40: 1654 – 1657

Hansen JE, Lacis AA, Lee P, and Lang WC (1979) Climatic effects of atmospheric aerosols. In: Proc. Conf. on Aerosols: Urban and rural characteristics, source and transport studies, 1977. New York Academy of Sciences, pp.575 – 587

Hansen J, Sato M, Lacis A, and Ruedy R (1997) The missing climate forcing. Philosophical Transactions of the Royal Society of London Series B-Biological Sciences 352: 231 – 240

Harrison L, and Michalsky J (1994) Objective algorithms for the retrieval of optical depths from ground-based measurements. Appl. Opt. 33: 5126 – 5132

Hegg DA, Ferek RJ, and Hobbs PV (1993) Light scattering and cloud condensation nucleus activity of sulfate aerosol measured over the Northeast Atlantic Ocean. J. Geophys. Res. 98: 14887 – 14894

Ilyas M (1987) Effect of cloudiness on solar ultraviolet radiation reaching the surface. Atmos. Environ. 21: 1483 – 1484

Im J-S, Saxena VK, and Wenny BN (2001) Temporal trends of black carbon concentrations and regional climate forcing in the southeastern United States. Atmospheric Environment 35: 3293 – 3302

Kerr JB, and McElroy CT (1993) Evidence for large upward trends of ultraviolet-B radiation linked to ozone depletion. Science 262: 1032 – 1034

Kiehl JT, and Rodhe H (1995) Modeling geographical and seasonal forcing due to aerosols. In: Charlson RJ, Heintzenberg J (eds) Aerosol Forcing of Climate. John Wiley & Sons, Chichester, U.K.

Kiehl JT, Schneider TL, Rasch PJ, Barth MC, and Wong J (2000) Radiative forcing due to sulfate aerosols from simulations with the National Center for Atmospheric Research, Community Climate Model, Version 3. J. Geophys. Res.-Atmos. 105: 1441 – 1457

Lacis A, Hansen J, and Sato M (1992) Climate forcing by stratospheric aerosols. Geophys. Res. Lett. 19: 1607 – 1610

Lacis AA, and Mishchenko MI (1995) Climate forcing, cloud sensitivity, and climate response: a radiative modeling perspective on atmospheric aerosols. In: Charlson RJ, Heintzenberg J (eds) Aerosol Forcing of Climate. John Wiley & Sons, Chichester, U.K.

Lenoble J (1993) Atmospheric Radiative Transfer. A Deepak Publishing, Hampton, VA, p.532

Liou K (1980) An introduction to atmospheric radiation Kuo-Nanliou. An International Geophysics Series. Volume 26, Academic Press, San Diego, CA, p.392

Liousse C, Penner JE, Chuang C, Walton JJ, Eddleman H, and Cachier H (1996) A global three-dimensional model study of carbonaceous aerosols. J. Geophys. Res. 101: 19411 – 19432

Liu SC, McKeen SA, and Madronich S (1991) Effect of anthropogenic aerosols on biologically active ultraviolet radiation. Geophys. Res. Lett. 18: 2265 – 2268

Long CS, Miller AJ, Lee H-T, Wild JD, Przywarty RC, and Hufford D (1996) Ultraviolet index forecasts issued by the National Weather Service. Bull. Am. Meteorol. Soc. 77: 729 – 748

Lorente, J, Redano A, and DeCabo X (1994) Influence of urban aerosol on spectral solar irradiance. J. Appl. Meteor. 33: 406 – 415

Ma J, and Guicherit R (1997) Effects of stratospheric ozone depletion and tropospheric pollution on UVB radiation in the troposphere. J. Photochem. Photobio. 66: 346 – 355

Madronich S (1993) The atmosphere and UV-B radiation at ground level. In: Young AR (ed) Environmental UV Photobiology. Plenum Press, New York

Madronich S, McKensie RL, Bjorn LO, and Caldwell MM (1998) Changes in biologically active ultraviolet radiation reaching the earth's surface. J. Photochem. Photobio. B46: 5 – 19

McKenzie RL, Matthews WA, and Johnson PV (1991) The relationship between erythemal UV and ozone, derived from spectral irradiance measurements. Geophys. Res. Lett. 18: 2269 – 2272

Mims FM (1995) Vanishing Frogs. Scientific American 273: 10

Mims FM (1996) Biological effects of diminished UV and visible sunlight caused by severe air pollution. In: Smith WL, Stamnes K (eds) IRS '96: Current Problems in Atmospheric Radiation. Proc. Int. Radiation Symp., Fairbanks, AK, 19-24 August, 1996, Deepak Publishing, Hampton, VA, pp.905 – 908

Mims FM, Barnard WF, Neuendorffer AC, and Labow GJ (1995) Unusually Low Ozone Detected Over South-Central U.S. EOS 76: 113 – 115

Ogren, JA, and Sheriden PJ (1996) Vertical and horizontal variability of aerosol single scattering albedo and hemispheric backscatter fraction over the United States. In: Proceedings of the 14th International Conference on Nucleation and Atmospheric Aerosols, Helsinki, Finland

Penner JE, Dickinson RE, and O'Neill CA (1992) Effects of aerosol from biomass burning on the global radiation budget. Science 256: 1432 – 1434

Petters JL, Saxena VK, Slusser JR, Wenny BN, and Madronich S (2003) Aerosol single scattering albedo retrieved from measurements of surface UV irradiance and a radiative transfer model. J. Geophys. Res. 108(D9):4288, doi:10.1029/2002JD002360

Pueschel RF (1993) Potential climatic effects of anthropogenic aerosols. In: Jennings SG (ed) Aerosol Effects on Climate. Univ. of Arizona, Tucson, 110 – 132

Reuder J, and Schwander H (1999) Aerosol effects on UV radiation in non-urban regions. J. Geophys. Res. 104: 4065 – 4077

Satheesh SK, and Ramanathan V (2000) Large differences in tropical aerosol forcing at the top of the atmosphere and Earth's surface. Nature 405: 60 – 63

Saxena VK, and Menon S (1999) Sulfate-induced cooling in the Southeastern U.S.: An observational assessment. Geophys. Res. Lett. 26: 2489 – 2492

Schafer JS, Saxena VK, Wenny BN, Barnard W, and DeLuisi JJ (1996) Observed influence of clouds on ultraviolet-B radiation. Geophys. Res. Lett. 23: 2625 – 2628

Schwartz SE, Arnold F, Blanchet J-P, Durkee PA, Hoffman DJ, Hoppel WA, King MD, Lacis AA, Nakajima T, Ogren JA, Toon OB, and Wendisch M (1995) Group Report: Connections between aerosol properties and forcing of climate. In: Charlson RJ, Heintzenberg J (eds) Aerosol Forcing of Climate. John Wiley & Sons, Chichester, U.K.

Seckmeyer G, and McKenzie RL (1992) Elevated ultraviolet radiation in New Zealand (45˚S) contrasted with Germany (48˚N). Nature 359: 135 – 137

Stephens GL (1995) Review of atmospheric radiation: 1991 – 1994. Reviews of Geophysics, Supplement, pp.785 – 794

Ulman JC, and Saxena VK (1997) Impact of air mass histories on the chemical climate of Mount Mitchell, North Carolina. J. Geophys. Res. 102: 25451 – 25465

Varotsos CA, and Kondratyev KY (1995) On the relationship between total ozone and solar ultraviolet radiation at St Petersburg, Russia. Geophys. Res. Lett. 22: 3481 – 3484

Varotsos CA, Chronopoulos GJ, Katsikis S, and Sakellariou NK (1995) Further evidence of the role of air pollution on solar radiation reaching the ground. Int. J. Remote Sensing 16: 1883 – 1886

Waggoner AP, Weiss RE, Ahlquist NC, Covert DS, Will S, and Charlson RJ (1981) Optical characteristics of atmospheric aerosols. Atmos. Environ. 15: 1891 – 1909

Wang P, and Lenoble J (1994) Comparison between measurements and modeling of UV-B irradiance for clear sky: a case study. Appl. Opt. 33: 3964 – 3971

Wenny BN, Schafer JS, DeLuisi JJ, Saxena VK, Barnard WF, Petropavlovskikh IV, and Vergamini AJ (1998) A study of regional aerosol radiative properties and their effects on ultraviolet-B radiation. J. Geophys. Res. 103: 17083 – 17097

Whitby KY (1978) The physical characteristics of sulfur aerosols. Atmos. Environ. 12: 135 – 159

Wolff G (1981) Elemental carbon in the atmosphere. J. Air Pollut. Control Assoc. 31: 935 – 938

Yu SC, Zender CS, and Saxena VK (2001) Direct radiative forcing and atmospheric absorption by boundary layer aerosols in the southeastern US: model estimates on the basis of new observations. Atmos. Environ. 35: 3967 – 3977

Yuen P-F, Hegg DA, and Larsen TV (1994) The effects of in-cloud sulfate production on light scattering properties of continental aerosols. J. Appl. Meteorol. 33: 848 – 854

12 Urban Forest Influences on Exposure to UV Radiation and Potential Consequences for Human Health

Gordon M. Heisler

USDA Forest Service Northeastern Research Station,
c/o SUNY ESF, 5 Moon Library, Syracuse, NY 13210, USA
E-mail: gheisler@fs.fed.us

Abstract This chapter explores the literature on ultraviolet (UV) irradiance in urban ecosystems with respect to the likely effects on human health. The focus was the question of whether the health effects of UV radiation should be included in the planning of landscape elements such as trees and shading structures, especially for high use pedestrian areas and school play grounds. Ultraviolet radiation can have a strong effect on humans, primarily as a cause or contributing factor for skin cancer and eye cataracts. It is also a probable factor in the development of immune deficiencies. However, UV can also positively affect human health, primarily because it is essential for photosynthesis of vitamin D in human skin. Vitamin D has long been recognized as a requirement for bone health. Recent epidemiological findings attribute vitamin D for the reduction of many types of non-skin cancers. Moreover, there is evidence that it may reduce mortality for those diagnosed with melanoma skin cancer. Alternatively, some public health authorities, particularly those from countries with a large population of northern European descent, strongly recommend that exposure to UV radiation should be minimized to prevent skin cancer. Other agencies, including the World Health Organization, that take a broader world view, differentiate their recommendations according to skin color. They recommend that humans with darker skin, who are likely deficient in vitamin D and also have little access to vitamin D fortified foods, should have moderate UV exposure. Judging from current knowledge of typical spectra of solar radiation in tree shade and the difference between the action spectra (effectiveness versus radiation wavelength) for vitamin D synthesis and that for sunburn in human skin, tree shade has advantages for moderate exposure to solar radiation. Where trees are separated, as is typical in heavily populated urban areas, the shortest wavelengths of UV radiation are scattered from the sky into shady locations with some sky view, and to a small extent, vitamin-D-promoting

wavelengths are increased over the radiation spectrum that causes sunburn. The sunburn action spectrum includes longer wavelengths that are less readily scattered into direct beam shade. Global climate change, which is expected to increase temperatures, especially at higher latitudes, may have a variety of effects on UV exposure for human populations. For example, warming could lead to greater exposure as people adapt to increased temperatures by wearing less clothing. However, empirical evidence for a temperature influence on human exposure independent of radiation climate does not seem to exist.

Keywords human health, ozone depletion, skin cancer, urban climate, UV-B radiation, vitamin D

12.1 Introduction

The goal of this review is to summarize recent information on the effect of ultraviolet radiation (UV) on human health in urban areas, and the degree to which urban landscapes might be managed to optimize UV exposure for improved health. Considering both the negative and positive health effects of UV exposure, would urban planning to increase tree cover form an effective public health intervention? Can optimum tree arrangements and species selections be prescribed? More specific questions arise; for example, is it important that shade be provided for school play areas?

To propose answers to these questions, a number of more basic questions must be considered. What are the health impacts of UV on particular populations? What is the relationship between climate and the type of dress, which influences the amount of exposure individuals receive during time spent outdoors? How representative are the UV monitoring networks located within the city? What are the urban atmospheric influences on UV irradiance? Are there trends in UV that may change the importance and effectiveness of proposed shade structures during their term of use? If increased radiation shading is deemed desirable, what types are most effective (e.g., trees or constructed shelters)?

Even though the benefits of UV radiation in photosynthesizing vitamin D and also the consequences of vitamin D for bone health have been known for many years, an increased volume of epidemiological literature published since about 1980 suggests that vitamin D, including that photosynthesized in the body from sunlight, is beneficial for human health (Garland and Garland, 1980; Kimlin, 2004; Engelsen et al., 2005; Turnbull et al., 2005). Relative to recent reviews on urban forest influences on UV radiation (Heisler and Grant, 2000a, b), the apparent beneficial influences of UV radiation in reducing the risk for many cancers through vitamin D production (Garland et al., 2002; Grant, 2002b, c; Grant, 2003; Grant and Garland, 2006) are given greater emphasis in this paper.

Although most urban residents can acquire large doses of UV radiation by spending time in open areas near or within their city, most reports on the subject suggest that vegetation and structures within a city, along with the urban atmosphere, modify UV sufficiently over time to affect human health (Heisler and Grant, 2000a, b; Gies and Mackay, 2004). Tree cover differs from city to city, and can also vary within urban areas. In U.S. residential areas with low building density, trees dominate the environment (Nowak and Crane, 1998; Nowak et al., 2002). Tree cover in urban areas can vary with the climate, culture, local income, city infrastructure, and the tree-management programs carried out by local, state, and federal governments (Miller, 1998).

Other important recent changes that have been published include findings of a reduced downward trend in stratospheric ozone (Newchurch et al., 2003; Malanca et al., 2005; Weatherhead and Andersen, 2006). Most papers written during the last two decades that describe UV effects began with a statement regarding the importance of the research due to probable increases in UV-B (here taken to be radiation between 320 nm and 280 nm, unless specified as the alternate definition of 315 nm to 280 nm) radiation resulting from stratospheric ozone depletion. Although it seems too early to declare a reversal in ozone depletion, recent reports suggest that increased downward trends are unlikely.

The first issue to be considered in regard to the effects of UV radiation on health is the epidemiology of diseases.

12.2 Effects of Solar UV on Human Health and Epidemiology

Human diseases that are linked to UV radiation as either the causative agent or as a factor in susceptibility to disease include several types of skin cancer, eye disease, and damage to the immune system. In addition, it is the UV, primarily UV-B, which is responsible for sunburn and skin aging and wrinkling (Weary, 1996). Sunburn itself is a health issue, but more importantly, some cancers are believed to be related to numerous sunburn episodes.

There are also benefits to UV- radiation exposure, including the production and regulation of vitamin D (Holick, 1999), that claims to reduce the risk for many non-cutaneous cancers (Garland et al., 1985; Gorham et al., 1989; Garland et al., 2002; Grant, 2002a, b, c; Grant, 2003). Table 12.1 lists common cancers with their United States population risk in the order of U.S. mortality.

12.2.1 Sunburn

The action spectra for sunburn and tanning were determined using light skinned volunteers who received narrow bands of constant irradiance on a small area of

Table 12.1 Diseases in the United States that have been associated with UV radiation; in order of U.S. deaths per year (usually for 2001). Incidence and mortality are per annum from recent years. (M) male; (F) female; RI = incidence risk increase; RR = risk reduction; MRR = mortality risk reduction

Disease	Incidence/100,000	U.S. Cases	U.S. Deaths	UV Influence	Vitamin D Influence
Colon cancer	39 (U.S. Centers for Disease Control and Prevention, 2005)		53,000 (Centers for Disease Control and Prevention, 2005)	RR (C.F. Garland and Garland, 1980; C.F. Garland et al., 1999; W.B. Grant, 2003), MRR (C.F. Garland et al., 1999)	RR (C.F. Garland & Garland, 1980), MRR (Moan et al., 2005)
Breast cancer	28 (F)(Centers for Disease Control and Prevention, 2005)		41,800 (Centers for Disease Control and Prevention, 2005)	RR (W.B. Grant, 2002a, 2003), MRR (C.F. Garland et al., 1999)	RR (W.B. Grant, 2003)
Prostate cancer	161 (Centers for Disease Control and Prevention, 2005)		30,700 (Centers for Disease Control and Prevention, 2005)	RR (W.B. Grant, 2003), MRR (C.F. Garland et al., 1999)	
Pancreas	11 (Centers for Disease Control and Prevention, 2005)		29,800 (Centers for Disease Control and Prevention, 2005)	RR (W.B. Grant, 2003)	RR (M) (W.B. Grant, 2003)
Non-Hodgkin lymphoma	18 (Centers for Disease Control and Prevention, 2005)		22,300 (Centers for Disease Control and Prevention, 2005)	RR (W.B. Grant, 2003; Smedby et al., 2005)	
Cancer of ovary	13 (Centers for Disease Control and Prevention, 2005)		14,400 (Centers for Disease Control and Prevention, 2005)	RR (W.B. Grant, 2003), MRR (C.F. Garland et al., 1999)	
Cancer of esophagus	5 (Centers for Disease Control and Prevention, 2005)		12,500 (Centers for Disease Control and Prevention, 2005)	RR (W.B. Grant, 2003)	

(Continued)

Disease	Incidence/100,000	U.S. Cases	U.S. Deaths	UV Influence	Vitamin D Influence
Bladder cancer	21 (Centers for Disease Control and Prevention, 2005)		12,200 (Centers for Disease Control and Prevention, 2005)	RR (W.B. Grant, 2002b)	
Kidney cancer	13 (Centers for Disease Control and Prevention, 2005)		12,100 (Centers for Disease Control and Prevention, 2005)	RR (M) (W.B. Grant, 2003)	
Multiple myeloma	5 (Centers for Disease Control and Prevention, 2005)		10,700 (Centers for Disease Control and Prevention, 2005)	RR (W.B. Grant, 2003)*	
Rectal cancer	14 (Centers for Disease Control and Prevention, 2005)		8,500 (Centers for Disease Control and Prevention, 2005)	RR (W.B. Grant, 2003)	
Melanoma	17 (Saraiya et al., 2004)	55,000 (Saraiya et al., 2004)	7,900 (Centers for Disease Control and Prevention, 2005)	RI (Saraiya et al., 2004), MRR (Berwick et al., 2005)	
Uterus (corpus)	23 (Centers for Disease Control and Prevention, 2005)		3200 (Centers for Disease Control and Prevention, 2005)	RR (W. B. Grant, 2002b)	
Squamous cell carcinoma	107 (Hess et al., 2006)		2,500**	High risk	
Cataract		350,000 (Ocampo and Foster, 2004)	Occurs post surgery	UV among many suspected risk factors	
Basal cell carcinoma	475 (M), 250 (F) (Bader, 2008)	900,000	rare	High risk factor	

* UV exposure did not appear as a significant risk reduction in later studies (Pers. comm., William Grant, August 2005).

** From an estimate that appeared in the Squamous Cell Carcinoma website of eMedicine (Hess et al., 2006) before 2006.

exposed skin over different times to create a variance in doses (Parrish et al., 1982; McKinlay and Diffey, 1987). The average time to administer a tanning dose in the UV-B varied from 0.36 min to 7.15 min, depending on the wavelength. Parrish et al. (1982) did not report whether there would be reciprocity between time and irradiance in administering the dose. At some wavelengths, subjects were exposed for considerable lengths of time, up to nearly five hours for longer wavelengths in the UV-A (400 nm – 320 nm). The reciprocity issue may be important in evaluating the effectiveness of shade structures, because presumably there is some level of irradiance below which no damage would occur, even if the subject spent a long time undergoing that irradiance. For more on the reciprocity issue, see the Section 2.10 'Calculation of optimal times for exposure to sunlight' in Chapter 2 (McKenzie and Liley, 2009) of this volume.

12.2.2 Skin Types

The effect of skin color on absorption of light, including the UV, was recently investigated by Nielsen et al. (2004). Skin absorption is largely a function of reflection and absorption by melanosomes. In the visible wavelengths, reflection is greater in light skin, but below the range of 300 nm to 330 nm, reflection is greater in dark skin; a non-intuitive finding with implications for health of dark-skinned populations.

12.2.3 Immune Function

Although UV-B is strongly absorbed in the skin and in the outer layers of the eye and does not penetrate any deeper into the human body, it can affect the human immune system, because part of the immune system is in the outer layers of skin, and the cells of the skin produce mediators that modulate immune responses both locally and throughout the body (De Gruijl, 1995; Longstreth et al., 1998). De Fabo (1994) and Chapman (1995) suggested that UV-B is the probable cause of infectious diseases and cancer, due to its affect on immune systems. Another concern is that excess UV radiation may reduce the effectiveness of immunizations against infectious diseases (Chapman, 1995). De Gruijl (1995) reported that excess UV-B exposure can suppress immune functions even in people with dark skin.

12.2.4 Skin Cancers

It is believed that exposure to UV leads to skin cancers because the UV forms DNA photolesions that induce gene mutations (Pfeifer, 1997). Cutaneous melanoma (CM) and basal cell carcinoma (BCC) seem to be associated with intense intermittent

exposure, whereas squamous cell carcinoma (SCC) seems to be related to cumulative exposure (Melville et al., 1991; Weinstock, 1993; Saraiya et al., 2004).

The importance of urban environmental design and configurations in influencing skin cancers depends on the epidemiology of these diseases. Gathering epidemiological data on non-melanoma skin cancers is difficult, in part because these diseases are not always included in cancer reporting registries (Weinstock, 1993). One indication of the importance of sun as a causative agent is indicated by the fact that incidence rates of all three skin cancers generally increase with decreasing latitude and with average cumulated UV-B irradiance, particularly for BCC (Leffell and Brash, 1996). Incidence of non-melanoma skin cancer in the southern U.S. is about double that in the north (Weinstock, 1993).

12.2.4.1 Non-Melanoma Skin Cancers

Non-melanoma skin cancers (SCC and BCC) are the most frequently diagnosed (Table 12.1) and are the most rapidly rising forms of cancer in white populations (International Agency for Research on Cancer, 1992). Estimates are that in recent years in the U.S., there have been 800,000 cases diagnosed each year, about twice as often in men as in women (Long et al., 1996; Saraiya et al., 2004). In 2004 there were an estimated 2,300 deaths from non-melanoma skin cancers, primarily from SCC (Saraiya et al., 2004). However, the cancer characterized as the most common world-wide is BCC (Chuang et al., 1990; Gailani et al., 1996). Both BCC and SCC are concentrated on the skin surfaces that are most exposed to the sun (Weinstock, 1993).

The estimated lifetime risk of BCC in the white population of the U.S. is 33% to 39% for men and 23% to 28% for women (Bader, 2008). BCC is rarely found in people under 40. Like SCC, BCC skin cancer incidence is a function of average UV-B irradiance in a geographic area, though the relationship is even stronger for BCC (Leffell and Brash, 1996; Heisler and Grant, 2000a).

We might expect average temperature to also be related to skin cancer incidence, because in warmer temperatures, people might wear less clothing to keep cool while outdoors. This could explain the fact that the relatively cool temperatures present in San Francisco result in lower incidence of BCC and SCC than predicted by the average July UV-B dose. However, in a simple regression analysis for the relationship between BCC and SCC incidence, with July UV-B dose and average temperature as predictor variables, temperature did not significantly add to the prediction of cancer incidence after UV-B dose was included (Heisler and Grant, 2000a). The relationship between the dress of pedestrians (skin exposure) and type of climate seems worthy of study. Human thermal comfort models are available that could be used in such studies (Heisler and Wang, 2002).

12.2.4.2 Melanoma

Cutaneous malignant melanoma (CM) is much more life threatening than BCC or SCC. The CM rate increased in the U.S. from 6.8/100,000 in 1973 to 17.4/100,000

in 1999 (Saraiya et al., 2004), and to an average of 19.4/100,000 from 2001 to 2005 (National Cancer Institute, http://seer.cancer.gov/statfacts/html/melan.html). It has been noted for many years that melanoma rates tend to be higher at lower latitudes, following the trend toward a higher incidence of solar radiation with decreasing latitude (Whiteman and Green, 1999).

It has been estimated that 65% to 90% of melanoma cases have been caused by exposure to the sun (Saraiya et al., 2004) with a higher estimated percentage of 95% occurring in Australia (Australian and New Zealand Bone and Mineral Society et al., 2005). One of the remarkable recent findings is that solar elastosis, a histologic indicator of cutaneous sun damage, has been positively associated with melanoma survival (Berwick et al., 2005), suggesting that people with melanoma who have had the most sun exposure have higher survival rates than those with less sun exposure. These observations raise the possibility that high amounts of vitamin D that result from high sun exposure may also increase melanoma survival. However, Berwick et al. (2005) state that other factors could be attributed to the increased survival rate among people with the highest sun exposure; for example, the association between sun exposure and early detection of melanoma.

Some reports suggest that CM is related to intermittent extreme sun exposure (Melville et al., 1991; Weinstock, 1993) rather than to cumulative exposure over long time periods. This is consistent with the fact that melanoma incidence tends to be higher of indoor workers than of outdoor workers (Koh and Lew, 1994), though it could also be consistent with indoor workers having low amounts of vitamin D. People diagnosed with melanoma often do have low vitamin D levels (Egan et al., 2005). Additionally, high exposure to the sun during childhood and early youth seems to positively correlate with CM incidence (Weinstock, 1993), particularly for those who suffered blistering sunburns. If sunburn is the primary cause of melanoma, then higher rates would be expected in mid-latitude U.S. regions where sunburn rates are highest among Caucasians (Saraiya et al., 2002).

An early study suggested that UV-A may be important in CM (Setlow, 1974). If so, there are a number of consequences. Some investigators hypothesize that the risk of melanoma may have increased because until recently, sunscreens blocked only UV-B and not UV-A. The suggestion is that blocking only UV-B is detrimental in part because UV-B causes the body to produce vitamin D, which may protect against melanoma (Garland et al., 1992). If the majority of solar-induced melanomas are caused by UV-A, then malignant melanoma will not be affected to any major extent by stratospheric ozone loss. Additionally, shade would be more important for melanoma prevention, because UV-A penetration is less than UV-B penetration into shaded areas (Grant and Heisler, 2001).

Higher incidence of CM has been assumed to be a result of increased UV due to ozone depletion (Madronich and De Gruiji, 1993). A 1996 examination of the effect of the Montreal Protocol and its amendments (Slaper et al., 1996) concluded that although UV-B would peak near the year 2000, skin cancer rates will continue to increase into the middle of the present century; approximately 10% higher

than in 1976. By 2100, the Slaper study concluded that CM incidence rates would return to the 1976 levels.

12.2.5 Eye Diseases

The most common association between UV radiation and eye disease is the possibility that UV can cause senile cataracts, a clouding of the eye lens. Cataracts are the most common and severe chronic eye disease considered to be the cause for approximately 53% of the cases of blindness across the world (Long et al., 1996). Cataracts are treatable only by surgery in which the natural eye lens is removed and replaced by a plastic lens; the most common surgery in medicine (Belkin, 1994). The use of hats and eyeglasses can greatly reduce eye exposure to UV (Rosenthal et al., 1991), and it is evident that tree shade in urban areas would also reduce exposure. Parisi et al. (2001a) point out that the diffuse component of UV radiation is usually responsible for most eye damage because of the natural aversion people have to looking at the sun. They also measured UV-B and UV-A diffuse fraction in open areas as well as beneath trees (see Section 12.4.3). The epidemiology of cataractogenesis is complicated by the possibility that cataracts increase with higher air temperature (Sliney, 1986)

12.2.6 Sunscreen Effectiveness

The effectiveness of sunscreens is pertinent to the role of UV in urban areas because sunscreens provide an alternative to seeking shade. Sunscreens can clearly provide a high degree of protection against sunburn, dependent on the effectiveness number or sun protection factor (SPF). However, some studies have found a high incidence of sunburn even when there is a high rate of sunscreen use (Davis et al., 2002). There is uncertainty as to whether sunscreens that prevent sunburn can also prevent immunosuppression effects and tumors (Garland et al., 1992; International Agency for Research on Cancer, 1992; Gorman, 1993; Garland et al., 1994; Bestak and Halliday, 1996). Given the uncertainty about sunscreen effectiveness, there is a general concern that those who rely too heavily on sunscreen protection abandon other protective measures (Wright, 1994). Other possible measures of protection could include seeking shade at mid-day and wearing protective clothing.

12.2.7 Positive Impacts

It has long been recognized that some diseases are alleviated by moderate UV-B exposure (van der Leun and de Gruijl, 1993), though the benefits of vitamin D from sun exposure were generally not emphasized.

12.2.7.1 Vitamin D

Although more literature is now available regarding the benefits of UV in the production of vitamin D and the consequent reductions in non-cutaneous cancers, sorting out the risks and benefits of UV exposure is not a simple task. Humans benefit from UV radiation by the production of vitamin-D (e.g., Diffey, 1991; Webb, 1993; Harvard Women's Health Watch, 2004; Webb, 2006). Exposure to UV-B is involved in both synthesis and the breakdown of vitamin D by a complex series of photochemical reactions. These reactions regulate the production of vitamin D so that toxic levels are not reached (Webb, 1993; Webb, 2006).

Balancing the negative influences of exposure to UV radiation against possible benefits from vitamin D production has been termed a conundrum (Webb and Engelsen, 2005), and is indeed considered as such by many in the medical research community. However, some believe there is no conundrum. Their recommendation would be to avoid sun exposure and acquire vitamin D from a proper diet and supplements (Gilchrest, 2007). Others recommend that humans allow for moderate sun exposure, sufficient to photosynthesize adequate vitamin D, yet not to the point where skin damage occurs (Webb, 1993; Garland et al., 2002; Holick and Jenkins, 2003; Dowd and Stafford, 2008). Taking the opinion that a balance of exposure is best, McKenzie and Liley (Chapter 2 this volume) examine the time required to achieve balance in a range of climates. The balance is possible because only low levels of UV-B exposure, far less than one Minimal Erythermal Dose (MED) for the initiation of sunburn in light-skinned individuals, defined as 200 Jm^{-2}, is needed in the vitamin D synthesis process (Webb, 1993), although the time needed for adequate vitamin D varies widely depending on the levels of irradiance and spectrum, skin type, and clothing (Webb and Engelsen, 2005; McKenzie and Liley, Chapter 2, this volume).

Many articles suggest that vitamin D deficiency is currently not a common problem in North America, partly because of fortification of foods (Simard et al., 1991). However, a panel of experts convened by the U.S. Centers for Disease Control and Prevention (U.S. CDC) in 2001 indicated concern about recent rickets cases (Scanlon, 2001). Even though vitamin D supplements have apparently been a general public health benefit, irregular application of the supplements has been noted. Survey results have shown that many samples contained either much less or much more vitamin D than stated on the label (Chen, 1999). During the 1940s in Europe, foods fortified with excess amounts of vitamin D caused intoxication in infants, leading to hypercalcemia and irreversible brain damage (Chen, 1999). A 1995 study reported rickets to be a problem in Mexico City, because UV radiation was greatly reduced by pollution (Galindo et al., 1995). Low vitamin D is much more prevalent in dark-skinned populations in the U.S. In one study, hypovitaminosis D occurred in 40.4% of black women compared to 4.4% among white women (Giovannucci, 2005). Low levels of vitamin D are also common among women in religious groups that require most of the body to be covered (Gannagé-Yared et al., 2000; Glerup et al., 2000). Low vitamin D can also be a

serious problem for those who have medical conditions that require avoidance of sun exposure, such as organ-transplant recipients, those with xeroderma pigmentosum, or people who must take medications that increase sensitivity to UV radiation (Reichrath, 2007).

The 2002 United Nations assessment of the effects of ozone depletion devoted a single paragraph to UV effects on vitamin D. While noting some evidence for high UV exposure or high levels of vitamin D in reducing the risk of some non-cutaneous cancers, it asserted that there is "no simple direct relationship between the vitamin D hormone and UV exposure because of the many regulatory feedback mechanisms," (De Gruijl et al., 2002). The 2006 United Nations assessment (Norval et al., 2007) has a more detailed treatment with about 50 citations dealing with vitamin D benefits for the immune system, internal cancers, autoimmune diseases, and possible infectious diseases.

The action spectrum for the formation of pre-vitamin D by sun exposure in human skin is based on a single study published in Science by MacLaughlin et al. (1982), but there are somewhat differing interpretations of this graphically represented spectrum. The spectrum has an approximate bell-shaped curve with a maximum near 295 nm and tails that approach 0 near 255 nm and between 315 nm and 320 nm. The original spectrum published in Science and republished at a larger size by Chen (1999) is plotted with a linear scale of response over one order of magnitude. It is not clear from the figure that the longer-wavelength end of the response actually reaches an absolute value of 0 by 315 nm, as has been assumed by some users (Webb et al., 1988; Webb, 1993; Kimlin, 2004; Engelsen et al., 2005), or whether it extends to longer wavelengths. A close perusal of the action spectrum curve suggests it approaches 0 in the vicinity of 320 nm asymptotically, and may extend beyond 320 nm. Michael Holick (pers. comm., July 22, 2005), one of the original authors of the Science article, expressed his belief "that the limit of 315 nm is correct." Even a small response at 320 nm could be significant under natural solar radiation because irradiance is typically three orders of magnitude larger at 320 nm than at 295 nm or 296 nm where the vitamin D response apparently peaks. Webb and Engelsen (2005) extrapolated the MacLaughlin relative vitamin D action spectrum to 0.001 at 320 nm, which would somewhat affect the action spectrum convoluted with a solar irradiance spectrum. Figure 2.1 shows the relative action spectrum for vitamin D interpreted from the figure in Chen (1999), with the exception that the Webb and Engelsen (2005) extrapolation to 320 nm is used. The convolution of the action spectrum with a typical solar irradiance spectrum in Fig. 2.1 shows the wavelength most important for vitamin-D to be about 310 nm. A 2006 report by the International Commission on Illumination (CIE) (Bouillon et al., 2006) tabulated a re-interpretation of the vitamin D action spectrum from MacLaughlin et al. (1982) and extrapolated the tail to a value of 0.000,078 at 330 nm. The new interpretation of the vitamin D action spectrum is contrasted to the CIE erythema action spectrum in Fig. 2.5 of McKenzie and Liley (Chapter 2, this volume).

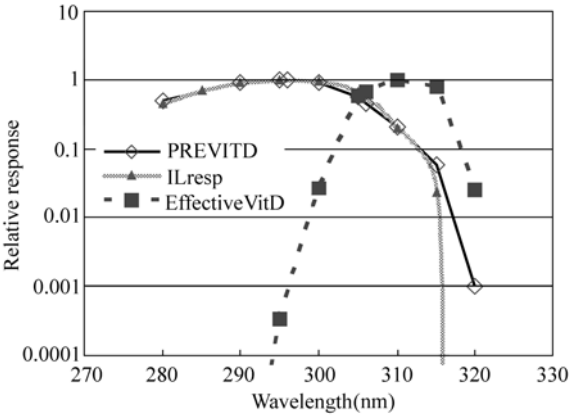

Figure 12.1 Action spectrum of pre-vitamin D_3 formation in human epidermis (PREVITD) from Webb et al. (1988), typical response of International Light UV-B radiometer SED240/UV-B/W (ILresp), and relative effectiveness of typical solar irradiance spectrum in formation of pre-vitamin D_3 (adapted from Heisler, 2005)

Figure 12.1 also shows the typical manufacturer-provided response function of an International Light SED240/UV-B/W filtered vacuum photodiode UV-B sensor (IL)[1]. The response was shown by the manufacturer only for every 5 nm, with a finite response at 315 nm and zero response at 320 nm. Up to 315 nm, the relative IL response is nearly identical to the MacLaughlin et al. (1982) vitamin D action spectrum, and depending upon the interpretation of that action spectrum, the similarity may be even closer between 315 nm and 320 nm than Fig. 12.1 suggests. The IL sensors were used in a series of measurements of tree influences on UV-B irradiance at Purdue University (Grant and Heisler, 1996; Grant, 1997; Grant and Heisler, 2001; Heisler et al., 2003a). Thus, the results of those measurements should relate closely to vitamin D synthesis.

Early evidence that UV-B exposure in mid and high latitudes during winter was limiting for vitamin D photosynthesis was provided by high incidence of rickets in winter (Chen, 1999). A model recently available online (http://zardoz.nilu.no/%7Eolaeng/fastrt/VitD.html) (Engelsen et al., 2005) provides easily obtained estimates of the length of time during a day that UV-B irradiance would be sufficient to photosynthesize pre-vitamin D from 7DHC, which is one of the important roles of UV-B radiation in regulating vitamin D (Holick, 1999).

A CIE standards committee issued a report with a slightly revised interpretation of the MacLaughlin et al. (1982) vitamin D action spectrum (Bouillon et al., 2006). This spectrum is used by McKenzie and Liley (Chapter 2, this volume) to explore diurnal, seasonal, and latitudinal differences between erythemally weighted and pre-vitamin D-weighted irradiances. McKenzie and Liley point out

1 Company names are provided for the convenience of the reader and do not constitute an endorsement of a product by the USDA or the Forest Service.

that because pre-vitamin-D weighting depends more strongly on the shorter UV wavelengths, it is more dependent on ozone and solar zenith angle (SZA) than erythemal weighting.

12.2.7.2 Apparent Anti-Cancer Benefits of UV

Among the vast array of literature recently published on the possible benefits of UV exposure for preventing or reducing the progression of a multitude of cancers are two reviews of special note written by Giovannucci (2005) and Grant and Holick (2005) on the effects of vitamin D, and a report stating that greater exposure actually increases survival among melanoma victims (Berwick et al., 2005; Egan et al., 2005). It has been observed that malignant melanoma is often accompanied by low 1,25-dihydroxyvitamin D_3 (the active form of vitamin D) serum levels (Egan et al., 2005). A study by Smedby et al. (2005) found reduced risk of non-Hodgkin lymphoma in individuals with high exposure to sun.

Although the benefits of sun exposure for cancer reduction were mentioned in Apperly (1941) and Peller and Stephenson (1937), the school of thought that low exposure to UV-B is associated with an increased risk of non-cutaneous cancers apparently began in earnest with Garland and Garland (1980), who suggested that vitamin D reduces the risk of colon cancer. Papers that suggest sunlight reduces the risk for breast cancer are Gorham et al. (1989), Garland et al. (1990), Gorham et al. (1990), and Grant (2002a); papers indicating a reduced risk for other non-cutaneous cancers were written by Grant (2002b, c; 2003) and Lefkowitz and Garland (1994). Grant (2002b, 2003) found inverse associations between regional summer UV-B irradiance and cancer risk for 14 kinds of cancer. Table 12.1 lists current findings and associated references on the effects of UV-B exposure and vitamin D, and the risks of acquiring, and mortality rates for, 15 different cancers. A few studies made direct associations between vitamin D levels of individuals and the risk of cancer, some of which are shown in the last column. These reports are increasingly noted in the popular press, e.g., Newsweek (Cowley, 1991; Raymond and Adler, 2005) and Reader's Digest (Dranov, 2006).

A difficulty in the epidemiology is that there are many possible confounding effects relating to cancer incidence, and the total list of these influences can usually not be included in an analysis. For example, there is a decided trend of increased incidence of breast cancer from south to north in the US (Garland et al., 1990; Sturgeon et al., 1995). This trend has been interpreted as being caused by decreased vitamin D production with the lower UV-B exposure in the north (Garland et al., 1990). However, according to Sturgeon et al. (1995), most of the geographic variations in breast cancer can be explained by demographic patterns. For example, women residing in the southern areas of the U.S. typically give birth to their first child at a younger age, and their breast cancer mortality rate is lower. However, the study by Sturgeon et al. (1995) did not examine environmental factors such as UV exposure. Giovannucci (2005) cited examples that suggest an

inverse relationship between sun exposure and breast cancer, but did not mention incidence of first childbirth at a younger age in the south nor the 1995 Sturgeon et al. paper. Until recently, the potential effect of vitamin D on cancer was often, perhaps usually, not included in cancer epidemiological studies (Giovannucci, 2005).

Although an apparent vitamin D effect in reducing cancer risk and virulence has been deduced for a large range of cancers, individual cancers differ in their response to vitamin D. For example, the relationship between vitamin D and prostate cancer is mixed (Giovannucci, 2005), though there does appear to be a positive relationship between very low 1,25(OH)2 D (the active form of vitamin D) and a higher risk and greater progression of prostate cancer (Giovannucci, 2005).

12.3 UV Climatology

12.3.1 Ozone Trends

Most research reports on UV radiation effects assume continued depletion of ozone, (e.g., Ono et al., 2005). As recently as 2004, a report from the CDC alluded to prospects for additional increases in UV-B as a result of ozone depletion (Saraiya et al., 2004), although, in doing so, they cited Diffey (1991) and Koh et al. (1993), rather than more recent work on stratospheric ozone trends.

Ground level measurements of total column ozone (TOC, includes ozone in the lower atmosphere, the troposphere, and the stratosphere—the major part of total column ozone) are made at about 30 locations In the U.S., with UltraViolet MultiFilter Rotating-Shadowband Radiometer (UV-MFRSR) instruments (Slusser et al., 1999; Gao et al., 2001), which have the advantage of automatically measuring total column ozone under most cloud conditions. Some of these measurements were recorded over the course of a decade, which is sufficient for predicting ozone trends. An examination of operational ozone measurements by UV-MFRSRs at Beltsville and Queenstown, MD since 1999 (data from the USDA UV-B Monitoring and Research Program, http://uvb.nrel.colostate.edu/UVB/index.jsf) indicates that there are cycles of ±10% in the differences in TOC (depth of all ozone in the atmosphere if it could be brought together in a layer, measured in Dobson Units (DU) = 0.001 cm) measured at the two UV-MFRSR sites, but that long-term averages between the ozone records are similar. The ratio of the Beltsville UV-MFRSR ozone to Brewer (Brewer Spectrophotometer, an instrument to measure TOC, SO_2, and UV spectra) measurements of ozone at the National Atmospheric and Space Administration, Goddard Space Flight Center (NASA/GSFC) at nearby Greenbelt, MD (data from Alexander Cede and Gordon Labow) is 0.996 over about four years.

A cursory examination of the TOC records from the Earth Probe Total Ozone Mapping Spectrometer (EPTOMS) satellite for Washington, DC, the UV-MFRSR

sensors at Beltsville and Queenstown, MD, the Brewer sensor at GSFC, and the recent Ozone Monitoring Instrument (OMI, which continues the TOMS satellite ozone measurements) ozone measurements (data from Gordon Labow) suggests that ozone in this locale tended to level off between 2000 and 2005. This conclusion is reached even after making allowance for the observed error in TOMS ozone since 2002 (Gordon Labow, pers. comm.), the cycles in the UV-MFRSR measurements, and the preliminary nature of the OMI measurements. One impression from examining TOC records over a period of years is that variability is large over short periods, and that there is a great need for continued ozone and UV monitoring, improvement of monitoring instrumentation and systems, and characterization of extreme ozone and UV events. Grant and Slusser (2005) point out the importance of extreme ozone events for crops research; the same no doubt applies to human health.

The 1998 United Nations Environment Programme assessment of ozone depletion estimated that since the 1970s, the northern temperate regions have experienced increases in erythemal UV radiation of approximately 4% in summer and fall, and 7% in winter and spring (Madronich et al., 1998). In the Southern hemisphere, the corresponding increase was about 6% year-round. The 1998 assessment indicated that international agreements to limit emissions of ozone depleting substances were showing evidence of success in reducing most, but not all, types of the depleting chemicals, and it suggested that a turnaround in ozone depletion and high levels of UV-B radiation might begin about 2000. By 2003, there was some evidence that the trend of ozone reductions was at least slowing (Newchurch et al., 2003; Malanca et al., 2005). While these studies show a slowing trend in ozone reductions, they do not show ozone increases. The return to the ozone and UV-B conditions that existed prior to the 1980s is apparently still decades away (Weatherhead et al., 2000; McKenzie et al., 2003; World Meteorological Organization (WMO), 2003; Weatherhead and Andersen, 2006). The 2006 WMO assessment estimates that global (60°S – 60°N) ozone will return to pre-1980 levels around the middle of the 21st century, at or before the time when stratospheric abundances of ozone-depleting gases return to pre-1980 levels (WMO, 2007).

The possible effect of greenhouse gases and global temperature change on stratospheric ozone causes additional uncertainty in the recovery process; greenhouse gases may speed ozone recovery because the gases lead to cooling of the stratosphere, which reduces the efficiency of the catalytic ozone destruction processes (WMO, 2007; Dyominov and Zadorozhny, 2008). However, periods of unusually low stratospheric ozone at mid-latitudes correspond with the intrusion of sub-tropical air masses (Bojkov and Balis, 2001; Siani et al., 2002), which further underscores the need for continued monitoring. Climate change will also influence surface UV radiation through changes in cloud formations and the ability of the earth's surface to reflect light (WMO, 2007).

12.4 Urban Structural Influences

The overall impression left by medical literature is that UV radiation in urban areas does have important consequences for human health, but that because little is known about the influence of urban structure on UV exposure, the epidemiological effects of UV radiation in urban areas are not being fully evaluated. Thus, knowledge and methods to predict spatial and temporal distribution of UV would be very beneficial to epidemiology. Such knowledge could also benefit public education and urban planning.

There can be significant differences between reductions of the visible portion of the solar spectrum (that is, the shade pattern we see) and reductions of UV by trees and other structures in urban areas. Large differences may occur in relative irradiance (below/above urban canopy) between the visible and thermal radiation that people see and feel and the ultraviolet spectrum. The differences occur partly because visible and UV radiation differ in the diffuse fraction of total irradiance (Grant and Gao, 2003), in the distribution of sky radiance (Grant, 1985; Grant and Heisler, 1997; Grant et al., 1997a, b) in reflectivity of urban structural surfaces (Heisler and Grant, 2000a), and in optical properties of leaves at different wavelengths (Grant et al., 2003).

12.4.1 Sky Radiance and Diffuse Fraction

It is well known that the atmosphere scatters shorter wavelengths of solar energy much more than longer wavelengths, and that the scattering increases with SZA (Iqbal, 1983). Usually, more than half of the UV-B irradiance arriving on earth is from diffuse radiation from the sky. The greater fraction of radiance from the sky has profound implications for the amount of UV-B irradiance in urban ecosystems.

Not only the sky radiance fraction, but also the distribution of sky radiance, is important in determining irradiance in urban ecosystems where often much of the sky is in view. Models of radiance distributions have been developed for use in predictions of tree and building effects on irradiance (Grant and Heisler, 1996; Grant et al., 1997a, b). The distribution for photosynthetically active radiation (PAR, essentially visible radiation) has a large gradient in radiance in the sun half of the sky and a decided dark portion opposite the sun in the other half of the sky (Grant et al., 1996; Grant and Heisler, 1997). The pattern for UV-A is similar to the pattern for the PAR, though the gradient is smaller. The UV-B distribution has a generally smaller gradient, that is, the irradiance is relatively equal from all parts of the sky, owing to the greater scattering of the energy in this waveband (Grant and Heisler, 1997; Grant et al., 1997a).

12.4.2 UV Reflectivity

The radiation environment in urban areas depends, to a large extent, on the reflectivity of the building materials, paving surfaces, and vegetation. Reflectivities in the UV for many surfaces have been tabulated (Sliney, 1986; Blumthaler and Ambach, 1988; Feister and Grewe, 1995; Heisler and Grant, 2000a). However, reflectivity differences for particular materials within a type (i.e., variances in: (1) color and kind of paint, (2) concretes, (3) building siding, and (4) specialty glass) seldomly seem to be available for the UV, although albedo for total solar radiation is more likely to be available. Almost all surfaces, except snow surface (albedo may be greater than 90%), have UV reflectivities of less than 25%; and only a few materials have UV albedo over 10%. Water and glass have low UV reflectivity at near normal incidence, but may reflect most UV radiation at nearly glazing incidence (Koller, 1965). This means that with high incidence angles, reflection from glass-walled buildings could nearly double the UV-B irradiance on a person standing near the building (Heisler and Grant, 2000a).

A suggestion for making buildings more energy efficient and cities cooler is to increase the albedo of sidewalks, streets, and building surfaces (Akbari et al., 1990; Levinson and Akbari, 2001). Whitening wall or paving surfaces may significantly increase UV-B irradiance on pedestrians and may also increase UV-B loads on vegetation. Heisler and Grant (2000a) estimated that if roof or pavement surfaces were whitened in a sufficient portion of a city so as to increase the general reflectivity of the landscape by 35 percentage points, probably the maximum possible, UV-B reflectivity might be increased up to 20%, again probably the maximum possible, and downward UV radiation at ground level might be increased by about 3%. While some programs have recently been successful for stimulating the lightening of building roof surfaces, the whitening of paving has been limited (http://www.epa.gov/heatisland/strategies/coolpavement.html).

Because the transmission of UV radiation through leaves is negligible for almost all tree species (Yang et al., 1995; Gao et al., 1996; Qi et al., 2002; Grant et al., 2003; Qi et al., 2003a, b; Qi et al., Chapter 18, this volume), leaf optical properties are essentially a matter of reflectivity from the leaf surface. Ultraviolet reflectivity is generally less than 10%; this value is low compared to PAR reflectivity, which is generally in the range of 10% to 30%.

12.4.3 Tree and Building Influences on UV

12.4.3.1 Measurements

Along with protective clothing and sunscreen use, seeking shade is a primary means recommended by public health agencies to avoid excess exposure to UV radiation (Environmental Protection Agency, 1995; Parisi and Kimlin, 1999; Saraiya

et al., 2004). However, tree effects on UV may differ significantly depending on the view of the sky and to some extent, the trees species. Ultraviolet shadows generally differ substantially from the shadows of visible light (Heisler et al., 2003a); with UV shadows being more "fuzzy" and much less sharp edged than visible shadows. Most research on shading structures and trees has been carried out under the premise that minimizing UV exposure at all times is most beneficial to people (Grant, 1997; Moise and Aynsley, 1999; Gies and Mackay, 2004); however, this view may change with increased value placed on the solar production of vitamin D.

The distribution of radiance across the sky for different wavelengths is important for irradiance in urban areas. With distributions such as the PAR, where most of the sky radiance emanates from regions close to the sun, shadows are distinct, and irradiance at points within a shadow is minimally enhanced by radiance from regions of the sky farther from the sun (Grant et al., 1996; Grant and Heisler, 1997). For the UV-A, and more so for the UV-B (Grant and Heisler, 1997; Grant et al., 1997a, b), the radiance is more evenly distributed across the sky, so that in shadows, irradiance may be considerably augmented by sky radiance if large areas of the sky are in view. This effect is enhanced by the greater proportion of total irradiance in the open that comes from the sky in the UV bands (Grant and Gao, 2003).

One effect of shade is the increase in the diffuse fraction (ratio of diffuse to direct-beam radiation). Parisi et al. (1999) found the average full-sun diffuse fraction for UV-B radiation in the open was 0.39, 0.26, and 0.46 during the morning, noon, and afternoon, respectively. In tree shade, the diffuse fractions were increased so that they averaged 0.60 to 0.61 for any of the time periods.

Available information on tree influences on UV irradiance is largely derived from essentially anecdotal measurements under a few trees with broadband sensors (e.g., Grant and Heisler, 1996; Moise and Aynsley, 1999). Spectral measurements at tree and in open have been taken simultaneously because of the limited availability of only one spectroradiometer (Parisi et al., 2001b). Part of the reason for the scarcity of data is the surprising difficulty in finding individual trees located where irradiance near or under the tree is not influenced by buildings or other nearby trees. The possibility for replications of measurements for full-sized trees of the same species is especially unlikely.

Results from a survey of tree influences on UV radiation (shown in Table 12.2) (Grant and Heisler, 1996; Heisler et al., 2003a), illustrate the effect of mature deciduous street trees, typically found in older suburban neighborhoods, on the PAR and UV-B irradiance at points of pedestrian height with significant sky views. Irradiances measured with UV-B and PAR sensors close together on one tripod were averaged over half-hour time periods at a mid-western US location (latitude 40.5°N). The sensor that measured the UV-B (an International Light SED240/UV-B/W) had a response from 280 nm to 320 nm, cutting off sharply before 320 nm, unlike erythemal sensors that extend into the UV-A (Fig. 12.1). Skies

were clear for all measurements. Comparable irradiances measured at a rural field provided an open-condition reference. Upward-facing, hemispherical-view photos from each measurement point (Fig. 12.2) showed that the percent of effective sky view varied from 34% to 60%. The examples include configurations where the shade was provided by trees only (Fig. 12.2(a), (b), (c)), and also by trees and buildings (Fig. 12.2(g)).

In the examples shown in Table 12.2, for in-leaf trees in the shade, PAR was as low as 15% of irradiance in the open (Point b), and UV-B was 44% of open. Conversely, at locations near in-leaf trees, but out of their visible shadow, PAR was not appreciably reduced, while UV-B measured at Point e was only about 59% of that in the open. Trees with only bare branches and twigs can cause substantial reductions in irradiance (Heisler, 1985). Table 12.2 also shows that the 44% of UV-B in the shade of leafless trees was only 7 percentage points more than the relative irradiance in the shade of in-leaf trees. The difference in relative irradiance in the UV-B was much less between shade and sunlit points (averaging 24 percentage points for in-leaf trees vs. 16 percentage points for leafless trees) than in the PAR (averaging 81 percentage points for in-leaf trees vs. 67 percentage points for leafless trees).

The UV-B relative irradiances in Table 12.2 are representative of tree effects, though irradiance will differ somewhat with a greater range of SZA and turbidity of the sky. The important contrast is between the relative irradiance in the UV-B

Table 12.2 Average UV-B and PAR irradiance below a street-tree canopy as a percent of irradiance in the open, away from any obstructions (Grant and Heisler, 1996; Heisler et al., 2003a). Column α is solar zenith angle. Sky views are expressed in percent; they would be converted to decimal fractions (0 to 1) in equations

		Percent of irradiance in open		Percent of view				α
Point		UVB	PAR	Buildings	Trees	Sky	Sky_{eff}*	
In-leaf								
Shade	a	21	16	—	32	68	57	57
	b	44	15	—	46	54	47	47
	c	47	18	—	53	47	52	52
Sunlit	d	74	97	—	45	55	45	45
	e	59	96	—	33	67	51	51
Out-of- leaf								
Shade	f	44	27	—	41	59	34	34
	g	30	53	23	17	60	53	53
Sunlit	h	69	96	—	30	70	36	36
	i	56	96	—	43	57	45	45
	j	41	95	31	13	56	60	60

* Sky_{eff} is sky view weighted according to the proportional contribution to irradiance on the horizontal from each 10º zenithal band of the sky.

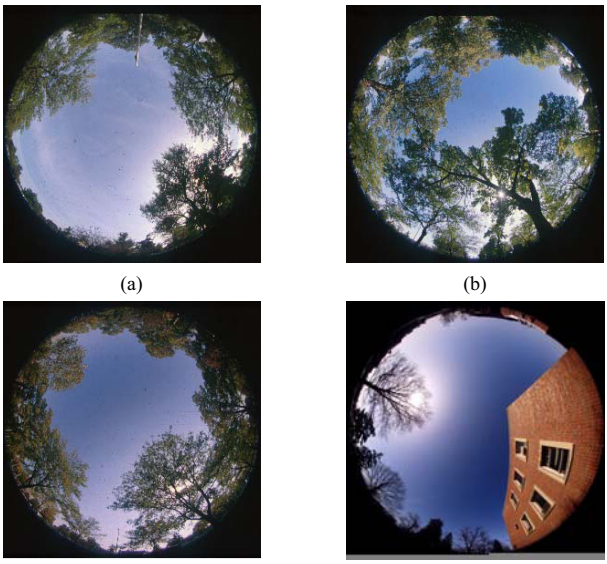

Figure 12.2 Fisheye photos from locations where below-canopy irradiance was measured as listed in Table 12.2. Frames (a), (b), (c), and (g) indicate points listed in the table

and the visible (represented by the PAR band). Most of the in-leaf measurements were made in early September with SZAs ranging from 47° to 57°. Relative irradiances, particularly in the UV-B, would be expected to be smaller because of less scattering with smaller zenith angles and smaller diffuse fractions during mid-day in midsummer.

Differences in sky diffuse fraction are primarily responsible for the differences between UV-B and visible relative irradiance, although differences in reflectance, particularly for sunlit points, can also contribute, especially near building walls. At Point g (Table 12.2 and Fig. 12.2) where a building with a sunlit red brick wall made up 23% of the view, reflection from the wall led to a greater relative irradiance for PAR at a tree-shaded point than when no wall was present. In the UV-B waveband, the wall reduced the relative irradiance because reflection in the UV-B from the brick surface was less than the irradiance that would have come from the sky had the building not been present. Measurements showed that the brick building wall with some windows reflected about 18% of incident visible radiation, whereas according to calculations, it reflected only about 3% of the UV-B.

The effect of reflected radiation from tree crowns on irradiance near the tree is less apparent. As noted in Section 12.4.2, leaf reflectance in the UV-B is about 5% for most species, and PAR reflectivity may be three times larger. Thus, tree crowns contribute little scattered UV-B to adjacent points. However, reflection from trees would be significant in the PAR, and this could partly explain the small reduction of 3% for PAR in sunlit points near trees (Table 12.2).

Other studies have shown results comparable to those in Table 12.2. Where the sun is only obscured by a small tree crown leaving a large portion of the sky in view, the contrast between reductions in the visible and UV wavelengths is even more pronounced. For example, with a tree blocking only 20% of the sky view, UV-B relative irradiance was 63% compared to a visible relative irradiance of about 10% (Grant, 1997).

The potential effect of differences in tree species on UV-B irradiance below their crowns has not been well quantified (Heisler et al., 2003a). This is due to such factors as: (1) the importance of diffuse sky radiation in determining irradiance below tree crowns; (2) the difference in crown density with tree size and pruning regimes, and (3) the considerable difficulty of sampling irradiance effects of individual tree crowns when no other nearby trees and buildings have any influence. These tree and building influences are especially important in the UV-B.

Reductions in UV-B can almost be complete where trees obscure most of the sky. In tropical Australia, UV-B irradiance with clear sky conditions and a range of SZAs was reduced to an average of only 3% by the "dense foliage" of a fig tree, though sky view was not specified (Moise and Aynsley, 1999). This was a greater reduction than provided in seven other urban shade structures that ranged from a school grandstand to a concrete walkway cover. There are also large reductions of UV-B under dense forest canopies. Where the sky is nearly completely obscured and UV-B irradiance is reduced to essentially negligible levels, relative PAR penetration will be greater than UV-B penetration (Lee and Downum, 1991; Brown et al., 1994). This might be expected due to the low transmittance of UV radiation through leaves (Grant et al., 2003). Even in forest canopies with thin but horizontally uniform leaf distributions, UV-B is attenuated more than the PAR (Yang et al., 1993).

In order to more precisely evaluate the influence of tree shade on human health, the tree shade influence on various action spectra for health effects, (i.e., pre-vitamin D and erythema) can be modeled if the irradiance spectra are known. Spectroradiometer measurements at Toowoomba, Australia (27.5°S latitude) showed a linear increase in average relative irradiance with decreasing wavelength from 400 nm to 300 nm in the shade of five Australian trees. Relative irradiance at 300 nm was almost double that at 400 nm (Parisi and Kimlin, 1999). Similar measurements were made by Parisi et al. (2001b) for a camphor tree (*Cinnamomum camphora*) with a "medium dense" canopy that was 6.4 m tall and had a 4.2 m-wide canopy that extended to only 0.4 m from the ground. Interpretation of irradiance ratios in shade to irradiance in the open (see Fig. 12.2, Parisi et al., 2001b) yielded the shade ratios as shown in Fig. 12.3 for irradiance in the shade below the edge of the tree crown. A polynomial (shade ratio $= 1.04 \times 10^{-5} \lambda^2 - 0.0105 \lambda + 2.778$, $\lambda =$ wavelength in nm) fit the interpreted points closely ($R^2 = 0.995$) as shown by the curve in Fig. 12.3. The measurements of Parisi et al. (2001b) below the tree crown, but half way from the edge of the crown to the tree trunk, had similar shade ratios. However, at the trunk, essentially all of the sky was blocked from the

spectroradiometer's view and the shade ratios varied less by wavelength, ranging from about 0.15 at 305 nm to 0.10 at 395 nm. Figure 12.3 also shows a typical UV spectrum in the open for Lauder, New Zealand at 45°S from Fig. 2.5 in McKenzie and Liley (Chapter 2, this volume) and a predicted spectrum in the tree shade by applying the polynomial curve fit to the Parisi et al. (2001b) shade ratios.

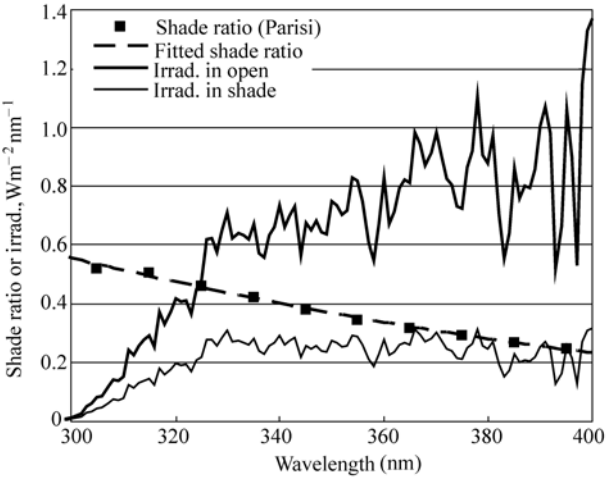

Figure 12.3 Ratio of spectral irradiance on horizontal surfaces in tree shade to irradiance on the horizontal in the open (Parisi et al., 2001b) = square points; polynomial fitted to the shade ratio points = dashed line; spectra of UV irradiance in the open at Lauder, New Zealand on the summer solstice from McKenzie and Liley (Chapter 2, this volume) = heavy black line; and irradiance in tree shade predicted by the Parisi et al. (2001b) shade ratios = thin line

The ratio of vitamin-D-weighted irradiance to erythema-weighted irradiance in tree shade can be higher than in the open. Figure 12.4 shows the irradiances in the open and in the tree shade from Fig. 12.3, but with weighting for erythema (UV_{Ery}) and pre-vitamim D production (UV_{VitD}) using the CIE spectrum for pre-vitamin D (Bouillon et al., 2006). Integrating across wavelength, the ratio of UV_{VitD}/UV_{Ery} is 1.95 in the open and 2.03 in the tree shade. In the example here, the difference is small between UV_{VitD}/UV_{Ery} in the open and in tree shade, and may not be of practical significance, although this ratio will generally be higher in tree shade than in the open. The UV_{VitD}/UV_{Ery} ratio in tree shade would likely be somewhat higher for a location in the shade of a small isolated tree crown, where a large portion of the sky would be in view.

12.4.3.2 Models of Tree Influences on UV-B Irradiance

Traditional methods for modeling solar irradiance below tree canopies have been applied to modeling tree influences on UV. Examples include: (1) use of Beer's law with knowledge of the leaf area index (LAI) for relatively uniform forest

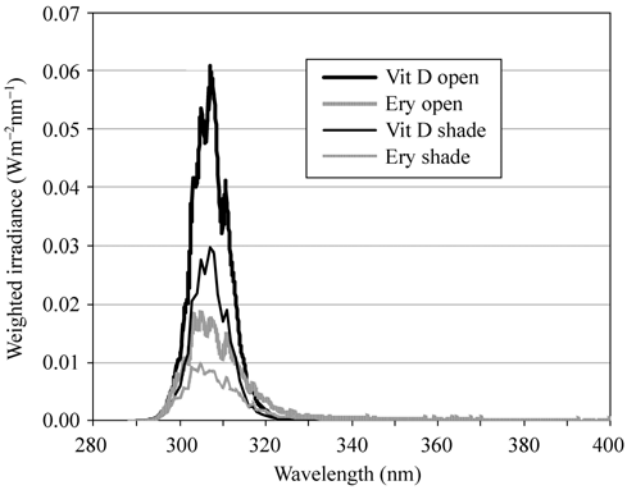

Figure 12.4 The irradiances in Fig. 12.3 for Lauder, New Zealand on the summer solstice from McKenzie and Liley (Chapter 12, this volume) weighted for erythema (grey) and pre-vitamin D production (black) in the open (thick lines) and in tree shade (thin lines) modeled with the shade ratios of Parisi et al. (2001b)

canopies (Yang et al., 1993); (2) models based on fisheye (hemispherical) photos from below the canopy (Grant and Heisler, 1996); and (3) mathematical models that describe the canopy as a series of ellipsoidal shapes of specified porosity (Gao, 1997; Gao et al., 2002).

Beer's law can be used to model the mean UV-B penetration into the forest as a function of LAI for tree influences of a closed uniform forest canopy. Yang et al. (1993) measured the vertical profile of LAI and of broad-band UV-B, PAR, and total global radiation in an oak forest in Pennsylvania. They expressed Beer's law as:

$$t = \mathrm{e}^{-k(\mathrm{LAI})} \tag{12.1}$$

where t is the canopy transmission function for a given wavelength band (UV-B, PAR, and total) at a given depth designated by the cumulative LAI downward from the top of the canopy, and k is the corresponding extinction coefficient for the profile. Yang et al. (1993) measured the profile of LAI and irradiance on the horizontal by moving radiation sensors and a canopy analyzer up and down through the canopy on a telescoping tower with a self-leveling platform for the sensors. Average total LAI of the forest was 1.69; measurements were made in late August, after the forest had been partly defoliated by insects earlier in the summer. By regression analyses, Yang et al. (1993) found k values of 0.86, 0.79, and 0.64 for UV-B, PAR, and total solar radiation, respectively. Thus extinction decreased in the order UV-B, PAR, and total global radiation.

To model irradiance on horizontal surfaces, I_{hor}, at locations below non-uniform

tree canopies, Grant and Heisler (1996) explored some relatively simple methods based on tree and sky view factors determined from hemispherical photographs (Fig. 12.2). The photographs were analyzed manually to estimate sky view by projecting the images onto a grid with radii and concentric zenith angle circles at 10° intervals beginning at 5° of sky zenith and azimuth, and then counting the number of grid intersections that fell on open sky. Measurement results for these sample locations beneath the street trees are presented in Table 12.2.

The modeling methods included use of a "bulk model" with the assumption that:

$$I_{\text{hor}} = I_{\text{dir}}\delta + f_{\text{sky}} I_{\text{dif}}, \tag{12.2}$$

where I_{dir} was the direct beam irradiance above the canopy, δ was 1 if the point was sunlit and 0 if in shade, f_{sky} was the fraction of the sky visible from the point, and I_{dif} was the diffuse irradiance above the canopy. Implicit in Eq. (12.2) is the assumption that there is no transmission through leaves; no reflection from branches, leaves, or buildings; and that sky radiance is uniform for all sky zenith and azimuth angles. The fraction transmitted to the below-canopy point, T_{canopy}, was modeled as:

$$T_{\text{canopy}} = f_{\text{sky}} F_{\text{diff}} + \delta(1 - F_{\text{diff}}), \tag{12.3}$$

where F_{diff} was the diffuse fraction (0 to 1) of total global radiation.

In the UV-B, F_{diff} varies with atmospheric aerosol content, and though Grant and Heisler (1996) assumed aerosols to be a constant average value in their model, they estimated that over the range of possible aerosol content with clear skies, errors in aerosol content could lead to errors in estimated F_{diff} of about 12% for UV-B and 16% for PAR. The TOC could also affect F_{diff}, though Grant and Heisler (1996) estimated that for a SZA of 40°, and TOC ranging from 250 DU to 450 DU (Dobson units), which is about the maximum range for northern mid-latitudes, F_{diff} would vary by approximately 2%.

Because F_{diff} is typically 0.50 or more, the distribution of I_{diff} across the sky may be important for modeling T_{canopy}. The 'bulk model' of Eq. (12.3) assumed a uniform radiance distribution. A "bulk zonal model" assumed a sky radiance distribution that varied with sky zenith and azimuth, as:

$$T_{\text{canopy}} = \sum[f_{\text{sky},\theta} \Psi_\theta F_{\text{diff}} + \delta(1 - \Psi_\theta F_{\text{diff}})], \tag{12.4}$$

where $f_{\text{sky},\theta}$ was the sky view within each 10° band of sky zenith, Ψ_θ was the normalized sky radiance for the band ($\sum \Psi_\theta$ over the nine bands = 1), and the summation of the right side of Eq. (12.4) is over the nine bands. The term Ψ_θ was derived by applying a previous model of UV-B and PAR sky diffuse radiance distributions for clear sky conditions as functions of zenith and azimuth relative to the sun location (Grant et al., 1996; Grant et al., 1997a). For evaluation of the benefit of including the anisotropic sky radiance, T_{canopy} was also modeled with sky radiance assumed to be uniform across the sky.

Grant and Heisler (1996) also used a "generalized" model that included transmission through tree crowns as sun flecks for generally shaded locations. Over the half-hour sampling periods, transmission to a below-canopy was modeled as:

$$T_{\text{canopy}} = \sum(f_{\text{sky},\theta}\Psi_\theta F_{\text{diff}}(1 - P_{\text{dir}}) + [1 - F_{\text{diff}}(1 + f_{\text{sky},\theta}\Psi_\theta)])P_{\text{dir},} \qquad (12.5)$$

where P_{dir} was the sun fleck probability of the crown through which the direct beam penetrated, and again, the summation is over the nine bands. The P_{dir} term was estimated by analysis of hemispherical photographs.

The three different modeling methods showed moderate success in matching measurements. When measured, T_{canopy} was either less than 0.2 or greater than 0.9; the match was within 0.10. The mean bias error was generally low; in the UV-B it was $+0.106$ for the bulk model, -0.04 for the zonal model with anisotropic sky, and -0.012 for the generalized model. However, in the mid-range of measured T_{canopy}, deviations of modeled values from measured values were as large as 0.24 for the generalized model and even larger, up to 0.31, for the bulk model. Some of the modeling error is most likely caused by the rather course 10º photo analysis. Using the Gap Light Analyzer Program (Frazer et al., 1999) to determine sky view would probably increase modeling accuracy. A study using GLA analysis to estimate UV irradiance in below canopy spaces in Baltimore, MD is currently underway (Heisler et al., 2003b). The study will be based on data from hemispherical photos taken from the centers of urban-forest-inventory plots (Nowak et al., 2004).

By using tree cover from urban tree inventories (Nowak et al., 2004), and assuming that tree cover is uniformly distributed, estimates of average UV-B exposure across urban neighborhoods with differing tree cover can be derived from above-canopy irradiance models (Grant and Heisler, 1999) and from the transmission model of Gao et al. (2002) for UV irradiance below canopies of assumed ellipsoidal shaped crowns. Initial estimates indicate that for a mid-latitude city, average UV-B relative irradiance ranges from 0.33 in single-family residential neighborhoods to about 0.60 in parks and neighborhoods with multiple family dwellings (Grant and Heisler, 1999). This method predicted that in Baltimore neighborhoods consisting of high density residential buildings, with mean tree cover of 20%, there would be an average of 5.0 MED of erythemal radiation over the area between the hours of 10:00 to 14:00 during summer months. In mid- and low-building-density neighborhoods with an average tree cover of 32%, only 3.9 MED of erythemal radiation would be available for exposure to pedestrians during that same time period (Grant et al., 2004; Heisler et al., 2004). Average cloud cover was included in the modeling. According to assumptions of Webb and Engelsen (2005), fair-skinned individuals with one-fourth of their body exposed would require about one hour of exposure to acquire a recommended daily 1000 IU of vitamin D.

12.4.4 Human Exposure

In studies of school children's exposure to UV, boys usually have greater exposure than girls (Melville et al., 1991; Ono et al., 2005). Methods of surveying school children for their exposure were recently described (Ono et al., 2005). One reported trend in U.S. elementary schools is the elimination of outdoor recess (DeGregory, 2005), which would remove the option for significant sun exposure for most children for five days of the week during the school year. Policies for outside time vary widely at different schools, ranging from a school in Arizona where on all days without rain, 1st and 2nd graders had outside recess morning and afternoon, during lunch, plus outside physical education twice a week (Sharon Harlan, pers. comm., July 2005), to some inner city Baltimore schools where outside time is unusual (Janie Gordon, pers. comm., 2007), to some Atlanta, GA schools that are being built without outside playgrounds (DeGregory, 2005). Some public schools insist on students wearing hats or sunscreen for outdoor activities whereas others, even in sunny climates, have no such policy (Sharon Harlan, pers. comm., July 2005)

For those schools that do have outside play areas, another recent development pertinent to UV effects on health is the movement to "green school yards, which will most likely lead to greater tree cover and shading of students. The magnitude of this movement is made evident by a search of the internet using the index words "school yard greening," which receives many hits. This raises the issue of the degree to which UV shading is considered in these programs and the guidance that is available for planning and design for UV modification.

Protection of children during the school day is of special concern in Australia and New Zealand because of the large proportion of fair-skinned individuals in the population and the fact that UV irradiance tends to be higher than in equivalent northern latitudes (Gies and Mackay, 2004; Wright et al., 2007). Though there has been some success with inculcating sun protective behaviors in youth in Australia, the provision of shade structures for school yards has been recommended for additional protection (Moise et al., 1999; Gies and Mackay, 2004). The general suggestion in Australia is that these shade structures should provide a UV protection factor (PF = UV in open/UV transmitted) of 15 for "all-day" protection, although a PF of 4 to 8 would be sufficient over the noon hour (Gies and Mackay, 2004). Many structures that have been built at schools, (i.e., verandahs and pavilions) provided PF of at least a 4 to 8 range (Gies and Mackay, 2004). A higher PF could be obtained by adding trees or vines along the open sides of these structures. For tree shade alone, PF could vary widely, ranging from a value of 1.6 for a small-crowned single tree in the open blocking only 20% of sky view (Grant, 1997) to a value of 46 for tree shade in the school-yard study of Gies and MacKay (2004).

Several epidemiological studies (Garland et al., 1990; Grant, 2003) have found that the relationship between solar radiation in a region and the subsequent risk reductions for non-cutaneous cancers is stronger for rural residents than for urban residents. It has been suggested that this is a function of lifestyle differences

(Garland et al., 1990; Grant, 2003). However, more study seems necessary as an alternative hypothesis states that an urban atmosphere may sufficiently reduce UV-B radiation to reduce the benefit of UV-B radiation for adequate vitamin D production.

12.5 Public Health Information

Over the past several years, medical science seems to be developing a trend toward greater valuation of the benefits of UV-B in vitamin D production, and the value of UV radiation for vitamin D regulation has moderated the prevailing philosophy of major public health agencies around the world that reducing sun exposure as much as possible should be the public health goal. For example, in 2004 the internet site for the Cancer Council of Australia (2004) stated: "Deliberate exposure to sunlight does not provide any health benefits. Australians receive more than sufficient sunlight for vitamin D production from just sitting near a window or by as little as two minutes outside during the day." Because transmission of UV-B through glass is negligible (Turnbull et al., 2005), sitting near a window is probably not a significant source of vitamin D, and the two-minute exposure is generally shorter than needed for vitamin D synthesis (Webb and Engelsen, 2005). In March 2005, many health agencies in Australia issued a joint statement that confirmed the hazards of UV radiation for skin cancer, but they also recognized some of the benefits of moderate exposure for vitamin D production (Australian and New Zealand Bone and Mineral Society et al., 2005), and the internet site for the Cancer Council of Australia (http://www.cancer.org.au/home.htm, updated October 2007) now endorses that view in a page on "The Risks and Benefits of Sun Exposure".

In the U.S., public information generally originates from the U.S. CDC (2005) and the U.S. Environmental Protection Agency (U.S. EPA, 2005). A major study on the effectiveness of educational interventions to reduce skin cancer by reducing exposure to solar radiation was published by the CDC (Saraiya et al., 2004). Seeking shade, including tree shade, was prominently mentioned for UV protection in that study, although the subtleties of different UV exposures possible in "shade" were not discussed. The CDC recently re-evaluated the vitamin D issue (Dr. Mona Saraiya, pers. comm., June 27, 2005). It would seem that many of the findings of the study on intervention effectiveness could be translated to the slightly different messages that would be needed if moderate sun exposure for vitamin D photosynthesis were adopted as a goal.

A question arises as to the appropriate education for non-white populations regarding sun exposure. Recommendations for sun exposure are sometimes given by skin type (Cancer Research UK, 2008), although more often the recommendations are for everyone to avoid the sun as much as possible (U.S. CDC, 2005; U.S.

EPA, 2005) without a differentiation of the message on the basis of skin color. This is despite the high percentage of vitamin D deficiency among African-Americans (Giovannucci, 2005). However, recommendations do differ in other countries from those in the U.S. For example, there are no education programs in Japan on reducing sun exposure, even for school children (Ono et al., 2005); which might be anticipated because of the low incidence of skin cancer among Asians.

12.6 Conclusions

All three of the skin cancers, including the most deadly—melanoma, are related to sun exposure, and although action spectra are not clearly defined, the UV-B band is apparently the most responsible for all three cancers. Though use of sunscreens is widely recommended, there remains an uncertainty about the effectiveness of sunscreens in preventing cancer. The incidence rate of skin cancers has been rising rapidly, even though the use of sunscreens has become widespread. Recent studies muddy the picture about the effect of sun exposure on survival of melanoma victims.

The increasing evidence that adequate levels of vitamin D reduce the incidence of many non-cutaneous cancers suggests a role for tree cover in urban areas for pedestrians and for children's playgrounds as an intervention that reduces sun exposure for the erythemal action spectrum somewhat more than for the vitamin D response spectrum. This difference is caused by the greater scattering of the shortest-wavelength radiation and the apparent limit to the vitamin D action spectrum to wavelengths below 320 nm. Determining if this difference is of practical significance requires further study, especially because the interpretations of the vitamin D action spectrum that are currently in use are based on only one study published in 1982. Additional research on the effective spectra in human skin is underway and seems well-justified.

Methods of modeling UV radiation exposure to pedestrians in different urban neighborhoods are being developed. These methods should be verified by additional UV radiation spectral measurements (Webb, 1991) above and below canopy over extended time periods, and by the use of personal dosimeters with volunteers. The dosimeter studies should include school children and structurally different neighborhoods over a range of building structures and tree densities to evaluate human exposure during everyday activities.

Major modifications to the structure of urban areas, including residential neighborhoods, may be accomplished over time with policies for tree management—including tree species selection for planting. Selection for the eventual size and shape of crowns of planted trees, which is generally known, is more important than considerations of tree-crown leaf density, which is less well known.

Studies on above-canopy UV irradiance in urban versus rural areas are also needed. Such research is especially important because epidemiological studies have shown different disease incidences that may be related to differences in exposure to UV radiation caused by different tropospheric atmospheric constituents.

Below typical street trees at mid-latitudes, where the visible solar irradiance is 10% or 15% of irradiance above trees, UV-B relative irradiance is commonly 30% or 40%. For typical solar radiation spectra during mid-day at mid-latitudes in summer, estimates are that Caucasians with medium-skin color may acquire a daily recommended dose of vitamin D from the sun in one-fourth of the time sunburn would occur. Alternatively, when arms, hands, and face are exposed on sunny days, a standard vitamin D dose could be acquired in just 4 or 5 minutes when in the open, and 12 to 15 minutes when in typical tree shade. Dark-skinned individuals would require about 30 minutes in shade of scattered trees where the view of the sky was substantial. Thus tree shade tends to make possible the recommendations that some researchers make for moderate exposure to UV radiation. An advantage of obtaining UV exposure in tree shade is that the reduction of the longer wavelengths of solar radiation will often produce thermal comfort for people when it would be too hot in direct sun.

Global climate change, which is expected to increase temperatures, especially at higher latitudes, may have a variety of effects on UV exposure for human populations; for example, it might be expected that warming would lead to greater exposure as people adapt to the warmer temperatures by wearing less clothing. However, empirical evidence for the influence of temperature on human exposure, independent of radiation climate, does not seem to exist.

Acknowledgements

The following are acknowledged for information provided: Jim Slusser, Alexander Cede, and Gordon Labow for ozone monitoring data and information on procedures; David Nowak for information on urban tree cover, Jeffrey Walton for information on remote sensing of land cover; Sharon Hanlon, Janie Gordon, and Marianne Butler for information on school programs. Some data collection and analysis was supported by National Science Foundation contributions to the Baltimore Ecosystem Study Long-Term Ecosystem Site under Grant no. DEB-9714835. Richard McKenzie generously shared spectral data used in the chapter by McKenzie and Liley in this volume. I thank Germar Bernhard, William B. Grant, Steven Britz, and an anonymous reviewer for helpful suggestions on the manuscript. Contributions of colleagues Richard H. Grant and Wei Gao over years of research on environmental UV radiation were indispensable.

References

Akbari H, Rosenfeld AH, and Taha H (1990) Summer heat islands, urban trees, and white surfaces. ASHRAE Transactions, 96(Part 1), 1381 – 1388

Apperly FL (1941) The relation of solar radiation to cancer mortality in North American. Cancer Research, 1, 191 – 195

Australian and New Zealand Bone and Mineral Society, Osteoporosis Australia, Australasian College of Dermatologists, and The Cancer Council Australia. (2005, 8 March 2005) Risks and Benefits of Sun Exposure Position Statement. Retrieved November 11, 2008, from http://www.dermcoll.asn.au/downloads/ccrisksandbenefitsMarch8.pdf

Bader RS (2008) Basal cell carcinoma, http://www.emedicine.com/med/topic214.htm

Belkin M (1994) Ultraviolet eye damage—the epidemiological evidence. Ultraviolet Radiation Hazards, 2134B, 13 – 18

Berwick M, Armstrong BK, Ben-Porat L, Fine J, Kricker A, and Eberle C (2005) Sun exposure and mortality from melanoma. Journal of the National Cancer Institute, 97(3), 195 – 199

Bestak R, and Halliday GM (1996) Sunscreens protect from UV-promoted squamous cell carcinoma in mice chronically irradiated with doses of UV radiation insufficient to cause edema. Photochemistry and Photobiology, 64(1), 188 – 193

Blumthaler M, and Ambach W (1988) Solar UVB-albedo of various surfaces. Photochemistry and Photobiology, 48(1), 85 – 88

Bojkov RD, and Balis DS (2001) Characteristics of episodes with extremely low ozone values in the northern middle latitudes 1957 – 2000. Annales Geophysicae, 19, 797 – 807

Bouillon R, Eisman J, Garabedian M, Holick M, Klienschmidt J, Suda T, et al. (2006) Action Spectrum for the Production of Pre-vitamin D_3 in Human Skin: CIE 174-2006. Wien, Austria: International Commission on Illumination

Brown MJ, Parker GG, and Posner NE (1994) A survey of ultraviolet-B radiation in forests. Journal of Ecology, 82, 843 – 854

Cancer Council Australia (2004, December 2004) All About Skin Cancer. Retrieved October 18, 2006, from http://www.cancer.org.au/content.cfm?randid = 960742

Cancer Research UK (2008) SunSmart, http://www.cancerresearchuk.org/sunsmart/

Centers for Disease Control and Prevention (2005) United States Cancer Statistics, Web-based Incidence and Mortality Reports 1999 – 2001. Retrieved June 17, 2005, from http://www.cdc.gov/cancer/npcr/uscs/

Chapman RS (1995) Effect of solar UV radiation on the risk of infectious disease in humans: epidemiologic considerations. Photochemistry and Photobiology, 61(3), 243 – 246

Chen TC (1999) Photobiology of Vitamin D. In M. F. Holick (Ed.), Vitamin D: Physiology, Molecular Biology, and Clinical Applications (pp. 17 – 37). Totowa, NJ: Humana Press

Chuang T-Y, Popescu A, Su WPD, and Chutte CG (1990) Basal Cell carcinoma: A population-based incidence study in Rochester, Minnesota. Journal of the American Academy of Dermatology, Vol. 22, No. 3, 413 – 417

Cowley G (1991, December 30) Can sunshine save your life? Newsweek, 56

Davis KJ, Cokkinides VE, Weinstock MA, O'Connell MC, and Wingo PA (2002) Summer sunburn and sun exposure among U.S. youths ages 11 – 18: national prevalence and associated factors. Pediatrics, 110, 27 – 35

De Fabo EC (1994) Effects of UV-B radiation on human and animal health. In R. H. Biggs & M. E. B. Joyner (Eds.), Stratospheric ozone depletion/UV-B radiation in the biosphere (pp. 197 – 198). New York: Springer-Verlag

DeGregory L (2005) Out of play. Saint Petersburg Time Floridian

De Gruijl FR (1995) Impacts of a projected depletion of the ozone layer. Consequences, 1(2), 1-10, http://www.gcrio.org/CONSEQUENCES/summer95/impacts.html

De Gruijl FR, Longstreth J, Morval M, Cullen AP, Slaper H, Kripke ML, et al. (2002) Health effects from stratospheric ozone depletion and interactions with climate change. In J. van der Leun, X. Tang and M. Tevini (Eds.), Environmental Effects of Ozone Depletion and its Interactions with Climate Change: 2002 Assessment (pp. 25 – 53). Nairobi, Kenya: United Nations Environmental Programme (UNEP)

Diffey BL (1991) Solar ultraviolet radiation effects on biological systems. Physics in Medicine and Biology, 36(3), 299 – 328

Dowd JE and Stafford D (2008) The Vitamin D Cure. Hoboken, NY: John Wiley

Dranov P (2006, September) The miracle vitamin. Reader's Digest, 162 – 169

Dyominov IG, and Zadorozhny AM (2008) Greenhouse gases and future long-term changes in the stratospheric temperature and ozone layer. International Journal of Remote Sensing, 29(9), 2749 – 2774

Egan KM, Sosman JA, and Blot WJ (2005) Sunlight and reduced risk of cancer: Is the real story vitamin D? Journal of the National Cancer Institute, 97(3), 161 – 163

Engelsen O, Brustad M, Aksnes L, and Lund E (2005) Daily duration of vitamin D synthesis in human skin with relation to latitude, total ozone, altitude, ground cover, aerosols and cloud thickness. Photochemistry Photobiology, 81(8), 1287 – 1290

Environmental Protection Agency (1995) Health effects of overexposure to the sun (No. EPA 430-F-003). Washington, DC: Environmental Protection Agency

Feister U, and Grewe R (1995) Spectral Albedo Measurements in the UV and Visible Region over Different Types of Surfaces. Photochem. Photobiol., 62(4), 736 – 744

Frazer GW, Canham CD, and Lertzman KP (1999) Gap Light Analyzer (GLA), Version 2.0: Imaging software to extract canopy structure and gap light transmission indices from true-colour fisheye photographs, users manual and program documentation (p.36): http://www.rem.sfu.ca/forestry/index.htm or http://www.ecostudies.org/

Gailani MR, Leffell DJ, Ziegler AM, Gross EG, Brash DE, and Bale AE (1996) Relationship between sunlight exposure and a key genetic alteration in basal cell carcinoma. Journal of the National Cancer Institute, 88(6), 349 – 354

Galindo I, Frenk S, and Bravo H (1995) Ultraviolet Irradiance over Mexico City. Air & Waste Management Association, 45, 886 – 892

Gannagé-Yared MH, Chemali R, Yaacoub N, and Halaby G (2000) Hypovitaminosis D in a sunny country: relation to lifestyle and bone markers. Journal of Bone Mineral Research, 15(9), 1856 – 1862

Gao W (1997) Modeling and Measurement of Ultraviolet Irradiance in Vegetation Canopies. Unpublished Ph.D. thesis, Purdue University, West Lafayette, IN

Gao W, Grant RH, and Heisler GM (1996) Spectral radiative properties of various tree species in ultraviolet wavelengths and irradiance modeling implications. Paper presented at the 22nd Conference on Agricultural and Forest Meteorology, January 28-February 2 1996, Atlanta, Georgia, American Meteorological Society, pp. 417 – 418

Gao W, Slusser J, Gibson J, Scott G, Bigelow D, Kerr J, et al. (2001) Direct-Sun column ozone retrieval by the ultraviolet multifilter rotating shadow-band radiometer and comparison with those from Brewer and Dobson spectrophotometers. Applied Optics, 40(19), 3149 – 3155

Gao W, Grant RH, Heisler GM, and Slusser JR (2002) A geometric ultraviolet-B radiation transfer model applied to vegetation canopies. Agronomy Journal, 94, 475 – 482

Garland CF, and Garland FC (1980) Do sunlight and vitamin D reduce the likelihood of colon cancer. International Journal of Epidemiology, 9(3), 227 – 231

Garland C, Shekelle RB, Barrett-Connor E, Rossof AH, Oglesby P, and Criqui MH (1985) Dietary vitamin D and calcium and risk of colorectal cancer: a 19-year prospective study in men. The Lancet, 307 – 309

Garland CF, Garland FC, and Gorham ED (1992) Could sunscreens increase melanoma risk? American Journal of Public Health, 82(4), 614 – 615

Garland CF, Garland FC, Gorham ED, Kripke ML, Donawho C, Wolf P, et al. (1994) Re: effect of sunscreens on UV radiation-induced enhancement of melanoma growth in mice. Journal of the National Cancer Institute, 86(10), 798 – 800

Garland CF, Garland FC, and Gorham ED (1999) Epidemiology of cancer risk and vitamin D. In M. F. Holick (Ed.), Vitamin D: Physiology, Molecular Biology, and Clinical Applications (pp. 375 – 391). Totowa, NY: Humana Press

Garland CF, Garland FC, Gorham ED, Lipkin M, Newmark H, Raffa JV, et al. (2002) Ultraviolet B, vitamin D and their mechanisms in cancer prevention. Paper presented at the Ultraviolet Ground- and Space-based Measurements, Models, and Effects, July 30 to August 1, 2001, San Diego, CA, The International Society for Optical Engineering, SPIE, pp. 313 – 323

Garland FC, Garland CF, Gorham ED, and Young JF (1990) Geographic Variation in Breast Cancer Mortality in the United States: A Hypothesis Involving Exposure to Solar Radiation. Preventive Medicine, 19, 614 – 622

Gies P, and Mackay C (2004) Measurements of the solar UVR protection provided by shade structures in New Zealand primary schools. Photochemistry and Photobiology, 80, 334 – 339

Gilchrest BA (2007) Sun protection and Vitamin D: Three dimensions of obfuscation. The Journal of Steroid Biochemistry and Molecular Biology, 103(3 – 5), 655

Giovannucci E (2005) The epidemiology of vitamin D and cancer incidence and mortality: A review (United States). Cancer Causes and Control, 16, 83 – 95

Glerup H, Mikkelsen K, Poulsen L, Hass E, Overbeck S, Thomsen J, et al. (2000) Commonly recommended daily intake of vitamin D is not sufficient if sunlight exposure is limited. Journal of Internal Medicine, 247(2), 260 – 268

Gorham ED, Garland CF, and Garland FC (1989) Acid haze air pollution and breast and colon cancer mortality in 20 Canadian cities. Canadian Journal of Public Health, 80, 96 – 100

Gorham ED, Garland FC, and Garland CF (1990) Sunlight and breast cancer incidence in the USSR. International Journal of Epidemiology, 19(4), 820 – 824

Gorman C (1993) Does sunscreen save your skin? Time, May 24, 69

Grant RH (1985) The influence of the sky radiance distribution on the flux density in the shadow of a tree crown. Agricultural and Forest Meteorology, 35, 59 – 70

Grant RH (1997) Biologically active radiation in the vicinity of a single tree. Photochemistry and Photobiology, 65(6), 974 – 982

Grant RH, and Gao W (2003) Diffuse fraction of UV radiation under partly cloudy skies as defined by the Automated Surface Observation System (ASOS). Journal of Geophysical Research, 108(D2), 4046, DOI:4010.1029.2002JD002201

Grant RH, and Heisler GM (1996) Solar ultraviolet-B and photosynthetically active irradiance in the urban sub-canopy: a survey of influences. International Journal of Biometeorology, 39, 201 – 212

Grant RH, and Heisler GM (1997) Obscured overcast sky radiance distributions for the UV and PAR wavebands. Journal of Applied Meteorology, 56(10), 1336 – 1345

Grant RH, and Heisler GM (1999) The adaptation of UV forecasts to typical human environments: the UV shade index [Abstract]. Photochemistry and Photobiology, 69(Special Issue), 56s

Grant RH, and Heisler GM (2001) Multi-waveband solar irradiance on tree-shaded vertical and horizontal surfaces: cloud-free and partly cloudy skies. Photochemistry and Photobiology, 73(1), 24 – 31

Grant RH, and Slusser JR (2005) High UVB exposures in the Continental USA: towards realistic short-term exposure regimes for plant-effects research. Photochemistry and Photobiology, 81, 1038 – 1046

Grant RH, Heisler GM, and Gao W (1996) Photosynthetically-active radiation: sky radiance distributions under clear and overcast conditions. Agricultural and Forest Meteorology, 82, 267 – 292

Grant RH, Heisler GM, and Gao W (1997a) Clear sky radiance distributions in ultraviolet wavelength bands. Theoretical and Applied Climatology, 56, 123 – 135

Grant RH, Heisler GM, and Gao W (1997b) Ultraviolet sky radiance distributions of translucent overcast skies. Theoretical and Applied Climatology, 58, 129 – 139

Grant RH, Heisler GM, and Gao W (2004) Impact of cloud cover on erythemal UV-B exposure under vegetation canopies. Paper presented at the Ultraviolet Ground- and Space-based Measurements, Models, and Effects Ⅳ, 5 – 6 August 2004, Denver, Co, SPIE, Bellingham, WA

Grant WB (2002a) An ecologic study of dietary and solar ultraviolet-B links to breast carcinoma mortality rates. Cancer, 94, 272 – 281

Grant WB (2002b) An estimate of premature cancer mortality in the US due to inadequate doses of solar ultraviolet-B radiation. Cancer, 94, 1867 – 1875

Grant WB (2002c) Health benefits of solar UV-B radiation: cancer risk reduction. Paper presented at the UV Ground- and Space-Based Measurements, Models, and Effects, July 30 to August 1, 2001, San Diego, CA, The International Society for Optical Engineering, SPIE, pp. 324 – 334

Grant WB (2003) Ecologic studies of solar UV-B radiation and cancer mortality rates. Recent Results in Cancer Research, 164, 371 – 377

Grant WB, and Garland CF (2006) The association of solar ultraviolet B (UVB) with reduced risk of cancer: Multifactorial ecologic analysis of geographic variation in age-adjusted cancer mortality rates. Anticancer Research, 26, 2687 – 2700

Grant WB, and Holick MF (2005) Benefits and requirements of vitamin D for optimal health: a review. Alternative Medicine Review, 10(2), 94 – 111

Harvard Women's Health Watch. (2004) Vitamin D's New day in the sun. Harvard Women's Health Watch, 11(6), 6 – 7

Heisler GM (1985) Measurements of solar radiation on vertical surfaces in the shade of individual trees. Paper presented at the Forest-Atmosphere Interaction: Proceedings of Forest Environmental Measurements Conference, October 23 – 28, Oak Ridge, TN, Reidel, pp. 319 – 335

Heisler GM (2005) Health impacts of ultraviolet radiation in urban ecosystems: a review. Paper presented at the Ultraviolet Ground- and Space-based Measurements, Models, and Effects V, San Diego, CA, SPIE — The International Society for Optical Engineering, pp. 5886M-5881-5817

Heisler GM, and Grant RH (2000a) Ultraviolet radiation in urban ecosystems with consideration of effects on human health. Urban Ecosystems, 4, 193 – 229

Heisler GM, and Grant RH (2000b) Ultraviolet Radiation, Human Health, and the Urban Forest (Gen. Tech. Rep. No. NE-268). Newtown Square, PA: U.S. Department of Agriculture

Heisler GM, and Wang Y (2002) Applications of a human thermal comfort model. Paper presented at the Fourth Symposium on the Urban Environment, 20 – 24 May 2002, Norfolk, VA, American Meteorological Society, Boston, MA, pp. 70 – 71

Heisler GM, Grant RH, and Gao W (2003a) Individual- and scattered-tree influences on ultraviolet irradiance. Agricultural and Forest Meteorology, 120, 113 – 126

Heisler GM, Grant RH, Nowak DJ, Gao W, Crane DE, and Walton JT (2003b) Inclusion of an ultraviolet radiation transfer component in an urban forest effects model for predicting tree influences on potential below-canopy exposure to UVB radiation. Paper presented at the Ultraviolet Ground- and Space-based Measurements, Models, and Effects Ⅲ, 4 – 6 August 2003, San Diego, CA, SPIE, pp.228 – 235

Heisler GM, Grant RH, and Gao W (2004) Impact of sky conditions on erythemal UV-B exposure under tree canopies. Paper presented at the 16th Conf. on Biometeorology and Aerobiology, 23 – 26 August 2004, Vancouver, BC, American Meteorological Society

Hess SD, Schmults CD, and Goldman G (2006) Squamous cell carcinoma. eMedicine, http://www.emedicine.com/DERM/topic401.htm

Holick MF (Ed.) (1999) Vitamin D: Physiology, Molecular Biology, and Clinical Applications. Totowa, NY: Humana Press

Holick MF, and Jenkins M (2003) The UV Advantage. New York, NY: Simon & Schuster

International Agency for Research on Cancer. (1992). IARC monographs on the evaluation of carcinogenic risks to humans. Paper presented at the Solar and Ultraviolet Radiation, February 11 – 18, Lyon, France, World Health Organization, p.316

Iqbal M (1983) An Introduction to Solar Radiation. Don Mills, Ontario: Academic Press Canada

Kimlin MG (2004) The climatology of vitamin D producing ultraviolet radiation over the United States. Journal of Steroid Biochemistry & Molecular Biology, 89 – 90, 479 – 483

Koh HK, and Lew RA (1994) Sunscreens and melanoma: implications for prevention. Journal of the National Cancer Institute, 86(2), 78 – 79

Koh HK, Sinks T, Geller A, Miller D, and Lew R (Eds.) (1993) Etiology of melanoma. Boston: Kluwer

Koller LR (1965) Ultraviolet Radiation. New York: John Wiley & Sons

Lee DW, and Downum KR (1991) The spectral distribution of biologically active solar radiation at Miami, Florida,USA. International Journal of Biometeorology, 35, 48 – 54

Leffell DJ, and Brash DE (1996) Sunlight and skin cancer. Scientific American, 275(1), 52 – 59

Lefkowitz E S, and Garland C F (1994) Sunlight, vitamin D, and ovarian cancer mortality rates in US women. International Journal of Epidemiology, 23(6), 1133 – 1136

Levinson R, and Akbari H (2001) Effects of Composition and Exposure on Solar Reflectance of Portland Cement Concrete (No. LBNL-48334). Berkeley, CA

Long CS, Miller AJ, Lee H-T, Wild JD, Przywarty RC, and Hufford D (1996) Ultraviolet Index Forecasts Issued by the National Weather Service. Bull. Am. Met. Soc., 77(4), 729 – 748

Longstreth J, de Gruijl FR, Kripke ML, Abseck S, Arnold F, Slaper H I, et al. (1998) Health risks. Journal of Photochemistry and Photobiology B: Biology, 46, 20 – 39

MacLaughlin JA, Anderson RR, and Holick MF (1982) Spectral character of sunlight modulates photosynthesis of previtamin D_3 and its photoisomers in human skin. Science, 216, 1001 – 1003

Madronich S, and De Gruiji FR (1993) Skin cancer and UV radiation. Nature, 366, 23

Madronich S, McKenzie RL, Bjorn LO, and Caldwell MM (1998) Changes in biologically active ultraviolet radiation reaching the earth's surface. Journal of Photochemistry and Photobiology B: Biology, 46(1 – 3), 5 – 19

Malanca FE, Canziani PO, and Argüello GA (2005) Trends evolution of ozone between 1980 and 2000 at midlatitudes over the Southern Hemisphere: Decadal differences in trends. Journal of Geophysical Research, 110(D05102), DOI:10.1029/2004JD004977

McKenzie RL, and Liley JB (2009) Balancing the Risks and Benefits of UV Radiation. In W. Gao, D. Schmoldt, and J. Slusser (Eds.), UV Radiation in Global Change: Measurements, Modeling and Effects on Ecosystems. New York: Springer-Verlag and Tsinghua University Press, Chapter 2, this volume

McKenzie RL, Björn LO, Bais A, and Ilyasd M (2003) Changes in biologically active ultraviolet radiation reaching the earth's surface. Photochemical & Photobiological Sciences, 2, 5 – 15

McKenzie RL, Liley JB, and Björn LO (2009) UV Radiation: Balancing risks and benefits. Photochemistry and Photobiology, 85(1): 88 – 98

McKinlay AF, and Diffey BL (1987) A reference action spectrum for ultraviolet erythema in human skin. International Illumination Commission [CIE] Journal, 6, 17 – 22

Melville SK, Rosenthal FS, Luckmann R, and Lew RA (1991) Quantitative ultraviolet skin exposure in children during selected outdoor activities. Photodermatology, Photoimmunology, Photomedicine, 8, 99 – 104

Miller RW (1998) Urban Forestry: Planning and Managing Urban Greenspaces (Second ed.). Upper Saddle River, NJ: Prentice Hall

Moan J, Porojnicu AC, Robsahm TE, Dahlback A, Juzeniene A, Tretli S, et al. (2005) Solar radiation, vitamin D and survival rate of colon cancer in Norway. Journal of Photochemistry and Photobiology B: Biology, 78, 189 – 193

Moise AF, and Aynsley R (1999) Ambient ultraviolet radiation levels in public shade settings. International Journal of Biometeorology, 43, 128 – 138

Moise AF, Buttner PG, and Harrison SL (1999) Sun exposure at school. Photochemistry and Photobiology, 70(2), 269 – 274

Newchurch MJ, Yang E-S, Cunnold DM, Reinsel GC, Zawodny JM, and Russell JM (2003) Evidence for slowdown in stratospheric ozone loss: First stage of ozone recovery. Journal of Geophysical Research, 108(D16)

Nielsen KP, Shao L, Juzenaas P, Stamnes JJ, Stamnes K, and Moan J (2004) Reflectance spectra of pigmented and nonpigmented skin in the UV spectral region. Photochemistry and Photobiology, 80, 450 – 455

Norval M, Cullen AP, de Gruijl FR, Longstreth J, Takizawa Y, Lucas RM, et al. (2007) The effects on human health from stratospheric ozone depletion and its interactions with climate change. Photochemical & Photobiological Sciences, 6, 232 – 251

Nowak DJ, and Crane DE (1998) The urban forest effects (UFORE) model: quantifying urban forest structure and functions. In M. Hansen and T. Burk (Eds.), Integrated Tools for Natural Resources Inventories in the 21st Century (pp.714 – 720). St. Paul, MN: USDA Forest Service

Nowak DJ, Crane DE, Stevens JC, and Ibarra M (2002) Brooklyn's Urban Forest (General Technical Report No. NE-290). Newtown Square, PA: USDA

Nowak DJ, Kuroda M, and Crane DE (2004) Tree mortality rates and tree population projections in Baltimore, Maryland, USA. Urban Forestry & Urban Greening, 2, 139 – 147

Ocampo VVD, and Foster CS (2004, Sept. 10, 2004) Senile cataract. Retrieved June 17, 2005, from http://www.emedicine.com/oph/topic49.htm

Ono M, Munkata N, and Watanabe S (2005) UV exposure of elementary school children in five Japanese cities. Photochemistry and Photobiology, 81, 437 – 445

Parisi AV, and Kimlin MG (1999) Comparison of the spectral biologically effective solar ultraviolet in adjacent tree shade and sun. Physics in Medicine and Biology, 44, 2071 – 2080

Parisi AV, Kimlin MG, Wong JCF, and Wilson M (1999) Diffuse component of the solar ultraviolet radiation in tree shade. Paper presented at the Second Internet Conference on Photochemistry and Photobiology, July 16 – September 7, 1999, J. Photochemistry and Photobiology B

Parisi AV, Green A, and Kimlin MG (2001a) Diffuse solar UV radiation and implications for preventing human eye damage. Photochemistry and Photobiology, 73(2), 135 – 139

Parisi AV, Kimlin MG, and Turnbull D (2001b) Spectral shade ratios on horizontal and sun normal surfaces for single trees and relatively cloud free sky. Journal of Photochemistry and Photobiology B: Biology, 65(2 – 3), 151 – 156

Parrish JA, Jaenicke KF, and Anderson RR (1982) Erythema and melanogenesis action spectra of normal human skin. Photochemistry and Photobiology, 36(2), 187 – 191

Peller S, and Stephenson CS (1937) Skin irritation and cancer in the United States Navy. American Journal of Medical Science, 194, 326 – 333

Pfeifer GP (1997) Formation and processing of UV photoproducts: Effects of DNA sequence and chromatin environment. Photochemistry and Photobiology, 65(2), 270 – 283

Qi Y, Bai S, Vogelmann TC, Heisler GM, and Qin J (2002) Methodology for comprehensive evaluation of UV-B tolerance in trees. Paper presented at the Ultraviolet Ground- and Space-based Measurements, Models, and Effects, 30 July – 1 August 2001, San Diego, CA, SPIE — The International Society for Optical Engineering, pp. 367 – 380

Qi Y, Bai S, and Heisler GM (2003a) Changes in ultraviolet-B and visible optical properties and absorbing pigment concentrations in pecan leaves during a growing season. Agricultural and Forest Meteorology, 120, 229 – 240

Qi Y, Bai S, Vogelmann TC, and Heisler GM (2003b) Penetration of UV-A, UV-B blue and red light into leaf tissues of pecan measured by a fiber optic microprobe system. Paper presented at the Ultraviolet Ground- and Space-based Measurements, Models, and Effects, 4 – 6 August 2003, San Diego, CA, SPIE, pp. 281 – 290

Raymond J, and Adler J (2005, January 17, 2005) A neglected nutrient: Are Americans dying from a lack of vitamin D? Newsweek, 47

Reichrath J (2007) Sunlight, skin cancer and vitamin D: What are the conclusions of recent findings that protection against solar ultraviolet (UV) radiation causes 25-hydroxy vitamin D deficiency in solid organ-transplant recipients, xeroderma pigmentosum, and other risk groups? The Journal of Steroid Biochemistry and Molecular Biology, 103(3 – 5), 664

Rosenthal FS, West SK, Munoz B, Emmett EA, Strickland PT, and Taylor H R (1991) Ocular and Facial Skin Exposure to Ultraviolet Radiation in Sunlight: A Personal Exposure Model with Application to a Worker Population. Health Physics, 61(1), 77 – 86

Saraiya M, Hall I, and Uhler RJ (2002) Sunburn prevalence among adults in the United States, 1999. American Journal of Preventive Medicine, 23(2), 91 – 97

Saraiya M, Glantz K, Briss PA, Nichols P, White C, Das D, et al. (2004) Interventions to prevent skin cancer by reducing exposure to ultraviolet radiation. American Journal of Preventive Medicine, 27(5), 422 – 466

Scanlon KS (editor) (2001) Vitamin D Expert Panel Meeting, Final Report. Retrieved June 28, 2005

Setlow RB (1974) The wavelengths in sunlight effective in producing skin cancer: A theoretical analysis. Proc. Nat. Acad. Sci., 71(9), 3363 – 3366

Siani AM, Casale GR, and Galliani A (2002) Investigation on a low ozone episode at the end of November 2000 and its effect on ultraviolet radiation. Optical Engineering, 41, 3082 – 3089

Simard A, Vobecky J, and Vobecky JS (1991) Vitamin D deficiency and cancer of the breast: an unprovocative ecological hypothesis. Canadian Journal of Public Health, 82, 300 – 303

Slaper H, Velders GJM, Daniel JS, de Gruijl FR, and van der Leun JC (1996) Estimates of ozone depletion and skin cancer incidence to examine the Vienna Convention achievements. Nature, Vol. 384, pp. 256 – 258

Sliney DH (1986) Physical factors in cataractogenesis: ambient ultraviolet radiation and temperature. Investigative Ophthalmology & Visual Science, 27(5), 781 – 790

Slusser J, Gibson J, Bigelow D, Kolinski D, Koenig WMG, and Beaubien A (1999) Comparison of column ozone retrievals by use of an UV multifilter rotating shadow band radiometer with those from Brewer and Dobson spectrophotometers. Applied Optics, 38(9), 1543 – 1551

Smedby KE, Hjalgrim H, Melbye M, Torrång A, Rostgaard K, Munksgaard L, et al. (2005) Ultraviolet radiation exposure and risk of malignant lymphomas. Journal of the National Cancer Institute, 97(3), 199 – 209

Sturgeon SR, Schairer C, Gail M, McAdams M, Brinton LA, and Hoover RN (1995) Geographic variation in mortality from breast cancer among white women in the United States. Journal of the National Cancer Institute, 87(24), 1846 – 1852

Turnbull DJ, Parisi AV, and Kimlin MG (2005) Vitamin D effective ultraviolet wavelengths due to scattering in shade. Journal of Steroid Biochemistry and Molecular Biology, 96, 431 – 436

U. S. Centers for Disease Control and Prevention (2005, July 7, 2005) Skin Cancer Primary Prevention and Education Initiative. Retrieved August 10, 2005, from http://www.cdc.gov/cancer/nscpep/index.htm

U. S. Environmental Protection Agency (2005) Sunwise Program. Retrieved August 10, 2005, from http://www.epa.gov/sunwise/

van der Leun JC, and de Gruijl FR (1993) Influences of ozone depletion on human and animal health. In M. Tevini (Ed.), UV-B Radiation and Ozone Depletion (pp. 95 – 123). Boca Raton, Florida: Lewis Publishers

Weary P (1996) An undeclared epidemic of skin cancer. Paper presented at the Symposium on Environmental Applications, Jan. 28 – Feb. 2, Atlanta, GA, American Meteorological Society, p.96

Weatherhead EC, and Andersen SB (2006) The search for signs of recovery of the ozone layer. Nature, 441, 39 – 45

Weatherhead EC, Reinsel GC, Tiao GC, Jackman CH, Bishop L, Hollandsworth Frith SM, et al. (2000) Detecting the recovery of total column ozone. Journal of Geophysical Research, 105, 22,201 – 222,210

Webb AR (1991) Solar ultraviolet radiation in southeast England: The case for spectral measurements. Photochem. Photobiol., 54(5), 789 – 794

Webb AR (1993) Vitamin D synthesis under changing UV spectra. In Young AR, Bjorn LO, Moan J, and Nultsch W (Eds.), Environmental UV Photobiology (pp. 185 – 202). New York: Plenum

Webb AR (2006) Who, what, where and when — influences on cutaneous vitamin D synthesis. Progress in Biophysics and Molecular Biology, 92(1), 17

Webb AR, and Engelsen O (2005) The sunlight conundrum: UV in the 21st century. León 05 Retrieved July 24, 2005, from http://www.ceisp.com/simposium/pdf/simposiumCIE_Leon/ponencias/016thesunlight.pdf

Webb AR, Kline L, and Holick MF (1988) Influence of season and latitude on the cutaneous synthesis of vitamin D_3: Exposure to winter sunlight in Boston and Edmonton will not promote vitamin D_3 synthesis in human skin. Journal of the Endocrinology and Metabolism, 67(2), 373 – 378

Weinstock MA (1993) Ultraviolet radiation and skin cancer: Epidemiological data from the United States and Canada. In Young AR, Bjorn LO, Moan J and Nultsch W (Eds.), Environmental UV Photobiology (pp. 295 – 343). New York: Plenum Press

Whiteman DC, and Green AC (1999) Melanoma and sun exposure: where are we now? International Journal of Dermatology, 38, 481 – 489

World Meteorological Organization (WMO) (2003) Scientific Assessment of Ozone Depletion: 2002 (Global Ozone Research and Monitoring Project No. 47). Geneva, Switzerland

WMO (World Meteorological Organization) (2007) Scientific Assessment of Ozone Depletion: 2006 (Report No. 50). Geneva, Switzerland

Wright B (1994) Sunscreens and the protection racket. New Scientist, 21 – 22

Wright CY, Reeder AI, Dodeker GE, Gray A, and Cox B (2007) Solar UVR exposure, concurrent activities and sun-protective practices among primary schoolchildren. Photochemistry and Photobiology, 83, 749 – 758

Yang X, Miller DR, and Montgomery ME (1993) Vertical distributions of canopy foliage and biologically active radiation in a defoliated/refoliated hardwood forest. Agricultural and Forest Meteorology, 67, 129 – 146

Yang X, Heisler GM, Montgomery ME, Sullivan JH, Whereat EB, and Miller DR (1995) Radiative properties of hardwood leaves to ultraviolet irradiation. International Journal of Biometeorology, 38, 60 – 66

13 Solar UV-B Radiation and Global Dimming: Effects on Plant Growth and UV-Shielding

Ronald J. Ryel[1], Stephan D. Flint[1], and Paul W. Barnes[2]

[1]Department of Wildland Resources and the Ecology Center, Utah State University
Logan, UT 84322-5230, USA
E-mail: ron.ryel@usu.edu
[2]Department of Biological Sciences, Loyola University New Orleans, LA 70118, USA
E-mail: pwbarnes@loyno.edu

Abstract Atmospheric aerosols and other particulates have been linked to reductions in shortwave radiation (global dimming). While much research has focused on the effects on plants caused by ambient and elevated UV-B (290 nm – 320 nm), the direct effects of global dimming, and those mediated by associated changes in UV-B radiation, have not been effectively assessed. We conducted an experiment in the high-UV environment of Mauna Kea, Hawaii to compare the effects of UV-B reduction with a simulation of global dimming (accomplished with 13% shading). Using fava beans, (*Vicia faba*), we found that structural differences due to the treatments were minimal in this high light environment. Most surprising was the minimal effect of UV-B on plant growth given the high UV-B environment. However, both UV-B and shading significantly influenced epidermal UV transmittance, suggesting that changes that occur in secondary chemistry can affect epidermal transmittance for UV. Additional experiments suggest that the change in epidermal transmittance due to shading would most likely occur with foliage in high-shade environments. Such changes in secondary chemistry have the potential to affect herbivory, nutrient cycling, and plant response to pathogens. While there are few experimental studies that specifically address possible reductions in radiation due to global dimming, many UV reduction experiments have been conducted in recent decades. Attempts to generalize latitudinal responses from these studies, however, are frustrated by a number of factors. Chief among them are different methodologies (reduction of different UV wavebands in different experiments) and a lack of reporting UV irradiance levels.

Keywords global dimming, UV-A epidermal transmittance, UV reduction experiment, leaf optical properties, UV-A and UV-B absorbing pigments, UVA-PAM, *Vicia faba*

13.1 Introduction

Total solar radiation reaching the surface of the earth depends on sunlight reaching the top of the atmosphere and the transparency of the atmosphere. Recent research has indicated solar radiation reaching the surface of the earth has decreased globally by 4% − 6% during the period of 1960 − 1990 (Wild et al., 2005) and 10% over the past 50 years (Stanhill and Cohen, 2001). This phenomenon has been termed "global dimming." However, since about 1990, this trend at the global scale has reversed and "global brightening" has been measured at a rate averaging 0.10% per year (Pinker et al., 2005; Wild et al., 2005; Norris and Wild, 2007). These multi-year trends suggest that the total radiation reaching the earth's surface, as affected by changes in atmospheric transparency, can fluctuate over periods of 20 − 50 years (Roderick, 2006).

Sunlight reaching the top of the atmosphere is affected by solar output and earth orientation, while cloudiness and both natural and anthropogenic sources of particulate and aerosol material affect atmospheric transparency. Declines in atmospheric transparency have been linked to volcanic activity (Roderick et al., 2001; Lohmann et al., 2006), increased cloud cover (Cutforth and Judiesch, 2007) and air pollution (Jauregui and Luyando, 1999; Alpert et al., 2005; Ramana and Ramanathan, 2006), while decreased cloudiness related to global warming (Nazarenko and Menon, 2005) and improved air quality (Schiermeier, 2005; Black et al., 2006; Norris and Wild, 2007) have been touted as increasing atmospheric transparency. Potential ecological effects of changes in solar radiation reaching the surface of the earth include changes in plant productivity (Roderick et al., 2001; Stanhill and Cohen, 2001; Black et al., 2006) and alteration of the hydrological cycle (Cohen et al., 2002; Roderick and Farquhar, 2002; Liepert and Romanou, 2005; Brutsaert, 2006; Robock and Li, 2006; Li et al., 2007).

13.1.1 Global Dimming and UV-B: Potential Effects on Plants

Reductions in shortwave radiation with increased atmospheric aerosols and other particulates are well established. This reduction of total shortwave radiation also coincides with an increase in the diffuse portion of the shortwave radiation (Black et al., 2006; Roderick, 2006) as aerosols and particulates increase the scatter of direct beam radiation (Fig. 13.1). Surface ultraviolet radiation (UV; < 400 nm) levels are also influenced by atmospheric aerosols and other pollutants, both causing varying degrees of attenuation and scattering of the radiation. While increased levels of UV-B radiation due to ozone depletion during the latter part of the 20th century are unquestioned (McKenzie et al., 2007), reductions in surface-level UV radiation due to pollution are ubiquitous over some surprisingly large areas of the Northern Hemisphere (McKenzie et al., 2001) and can cancel the increased

UV-B radiation from ozone depletion (Ma and Guicherit, 1997). At present, since stratospheric ozone levels are already showing signs of recovery, UV levels would be expected to decrease in the near future (McKenzie et al., 2007), even without global dimming.

Much is known about the effects of ambient and elevated UV-B (290 nm – 320 nm) on plants (see reviews by Barnes et al., 2005; Caldwell et al., 2007; and others), but the direct effects of global dimming on plants and those mediated by associated changes in UV-B radiation have not been effectively assessed. In particular, experiments specifically designed to assess changes in UV-B under global dimming have not been conducted. Interactions between quantities of photosynthetically active radiation (PAR; 400 nm – 700 nm) and UV on plant performance are known (e.g., Krizek, 2004), but are further complicated by the nature of PAR and UV radiation. Because solar UV radiation has a greater diffuse component than the longer wavelengths of sunlight, the penetration of PAR and UV into plant canopies is different (Flint and Caldwell, 1998). In particular, it has been shown that the ratio of PAR to UV in a canopy differs dramatically depending on whether solar radiation is measured in a sunfleck or the shade (Flint and Caldwell, 1998). Not surprisingly, therefore, generalizations on how total solar radiation changes, as occurs with global dimming and brightening, interact with recovery from ozone depletion are lacking.

Research previously conducted that examined plant responses to changes in total solar radiation, as might be expected under global dimming, involved both modeling and experimental efforts. Modeling studies have generally shown increases in canopy photosynthesis with global dimming as a result of increased penetration of diffuse PAR into the canopy. For example, a substantial increase in the proportion of diffuse radiation following the eruption of Mt. Pinatubo appears to have increased photosynthesis to the same extent that atmospheric CO_2 showed an unexpected decline (Roderick et al., 2001). Experimental studies to assess plant effects resulting from changes in total solar radiation have typically involved manipulation of total sunlight. However, these studies often use substantial amounts of shade (e.g., 30% and 60% shade, Raveh et. al., 2003), which is a much greater change in solar radiation than occurs with global dimming. Therefore, results from these studies make extrapolation to global dimming scenarios tenuous. Results from a limited number of experiments using minimal shading (e.g., 13% used by Fischer, 1975) suggest that some effects can be seen due to even limited shade levels, and may be more affected in plant communities that are light-limited (Black et al., 2006).

13.1.2 Assessing Global Dimming and UV-B Effects on Plant Growth

To provide some insight into the effects of global dimming on plant growth, the

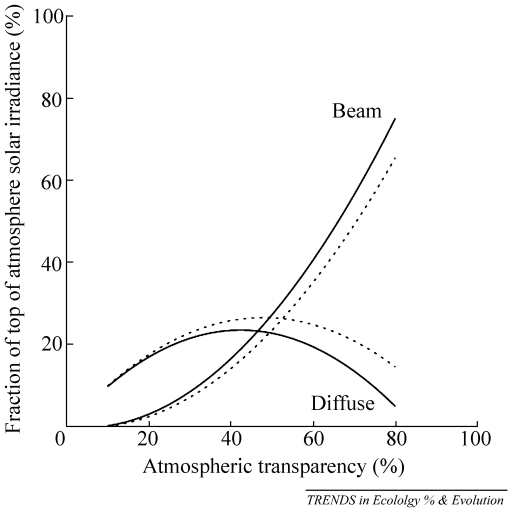

Figure 13.1 Idealized changes in diffuse and direct beam radiation reaching the Earth as a function of atmospheric transparency (reprinted from Roderick 2006). Solid lines represent standard atmospheric conditions; dotted lines show the immediate effect of the Mt. Pinatubo volcanic eruption in June 1991

role of UV-B in this response, and a comparison of the magnitude of the responses to dimming and UV-B, we conducted a field experiment using minimal shading levels approximating the reduction in solar radiation observed under these conditions (e.g., Stanhill and Cohen, 2001). We specifically examined whether there could be direct influences of global dimming and altered solar UV-B on various aspects of leaf development (e.g., leaf optical properties or leaf mass per unit area), which are important traits that influence light penetration into the canopy and which often influence plant responses to UV-B. We further evaluated whether these possible changes in light penetration or other effects of shade could influence overall plant growth in this experiment. These effects were put into perspective with UV-B radiation effects by simultaneously conducting a UV-B screening experiment at the same site (Mauna Kea, Hawaii). This served two purposes: (1) it permitted comparisons between these two global environmental factors, and (2) enabled us to assess whether UV radiation effects are sufficiently large such that a potential reduction in UV accompanied by global dimming could have measurable effects on plants. Finally, we examined whether reports in the literature suggest trends in the effects of UV-B radiation, contrasting UV screening experiments at higher latitudes (lower UV-B) with lower-latitude (higher UV-B) sites, and we compared the responses of other species at high-UV sites with our results.

13.2 Methods

13.2.1 Field Site

Studies were conducted during summer at a field site located on the south slope of Mauna Kea, Hawaii, USA (2,800 m elev.; 19°45'N, 155°27'W). Climate at the study site is Mediterranean, with warm relatively dry summers and cooler, wetter winters. Average summer high temperatures are ca. 20°C – 22°C and annual precipitation is ca. 400 mm. The light climate is characterized by high PAR (max clear day ca. 2,100 μmol m^{-2} s^{-1}) and very high UV-B and UV-A levels (max clear day ca. 5.1 and 69 W m^{-2}, respectively). Additional measurements were conducted at an experimental site located in North Logan, UT, USA (1,408 m elev.; 41°30'N, 111°48'W).

13.2.1.1 Experimental Plots

Vicia faba L. cv. Broad Windsor (fava bean) were grown under horizontal filters with three primary treatments (three replicate filters per treatment) to simulate ambient radiation and dimming conditions: (1) near ambient full spectrum radiation (+UV-B, full sun); (2) full spectrum radiation reduced by 13% (+UV-B, reduced sun); and (3) full spectrum radiation reduced by 13% with UV-B wavelengths removed (-UV-B, reduced sun). A UV-transparent film (Aclar type 22 A, 0.038 mm thick, Honeywell, Pottsville, PA, USA) was used for treatments 1 and 2, and UV-B blocking (<320 nm) film (0.051 mm polyester (Mylar); DuPont Teijin Films U.S., LLP, Hopewell, VA, USA) was used for treatment 3 (Fig. 13.2). Reduced sun treatments were made using three different fine mesh nettings: 4 cm squares, 2.4 cm squares, and mesh with diagonal openings 2 cm per side. A layer of all three mesh nettings was used for treatment 2, while only the 2.4 cm mesh was used for treatment 3 because of the lower transmittance of Mylar. Transmittances for photosynthetically active radiation (PAR, 400 nm – 700 nm) were 92.9%, 81.0% and 80.7% and for broadband UV (UV-A and UV-B) were 88.1%, 74.0% and 50.9% for treatments 1, 2, and 3, respectively, as measured with a quantum sensor (Li-185, Li-COR, Inc., Lincoln, NE, USA) and broadband UV sensor (Skye UV-B; Skye Instruments, Ltd., Powys, UK). Filters and netting were mounted on 1.3 cm diameter electrical conduit in 1.1 m×1.0 m horizontal filter frames and mounted on four metal corner rods 38 cm above the ground. Filters were periodically moved upward to maintain a distance of ca. 15 cm height above growing plants. A fourth treatment (-UV-B, "full" sun) was constructed using only polyester filter material (0.051 mm Mylar); PAR transmittance was 87.2% and broadband UV was 58.8%. Because of the differences in transmittance for PAR, this treatment could not be considered a true -UV-B, full sun treatment for comparing plant growth. This treatment was used only for assessing leaf epidermal transmittance for UV.

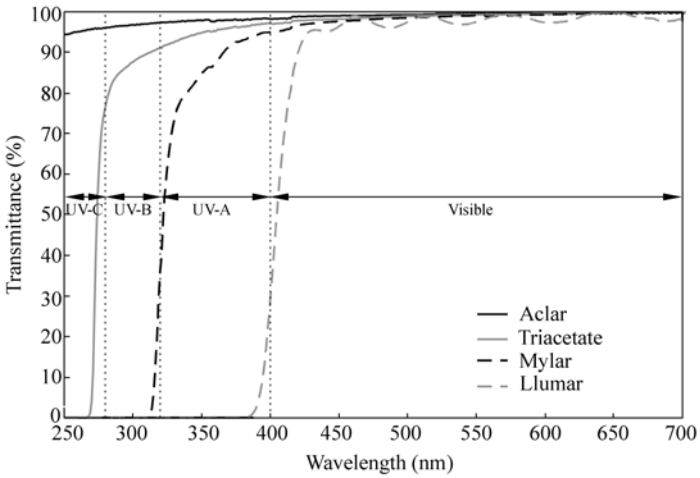

Figure 13.2 Relative spectral transmittance for four commonly used plastic filters used in UV-exclusion experiments. Transmittance is relative to the maximum transmittance (100%) for each filter across the range from 250 nm – 700 nm (see text for filter descriptions)

Vicia faba were grown in cone-shaped pots (Ray Leach Cone-tainers: 0.15 L volume, 205 mm length, 40 mm top diameter; Stuewe and Sons, Corvallis, Oregon, USA) placed in racks holding 49 (7×7) pots with 5 mm edge separation to simulate plants growing in a canopy. This resulted in a plant density of 494 plants m^{-2}. Single seeds were planted (June 2, 2005) at 2 cm – 3 cm depth in each cone-tainer containing organic potting soil and racks of cone-tainers were placed under moderate shade (< 500 μmol m^{-2} s^{-1} max PAR) until emergence 13 days later (June 15). Roughly double the necessary cone-tainers were planted so that seedlings of uniform size could be selected and randomly assigned to treatments. Upon emergence, plants were sorted by size to create three full racks of plants per treatment with similar-sized plants. Each rack of cone-tainers was then placed under a single filter frame. Plants were watered with tap water 1 – 2 times daily to minimize water stress and grown for 30 days (until July 15) under the filters.

13.2.2 Structural and Biomass Measurements

After 30 days of growth, plants were removed from under the filter and taken indoors for structural and epidermal transmittance measurements and then destructively harvested for biomass quantification. Structural measurements included total height (soil surface to top of terminal bud), number of internodes, and height of each internode. Plants were then harvested and sorted into components (leaf, stem, branches), oven dried at 60°C for 24 hours and weighed for dry mass determinations. Leaf mass per area was determined by cutting a leaf

disk (1 cm^2) from a mature leaf at the time of harvest using a cork-borer. The leaf disk was dried at 60˚C and weighed.

13.2.3 UV-A Epidermal Transmittance Measurements

Non-invasive measurements of epidermal UV-A transmittance were made on intact mature leaves of plants at the time of harvest with a field-portable pulse amplitude modulation (PAM) chlorophyll fluorometer (UVA-PAM; Gademann Instruments, Würzburg, Germany). The UVA-PAM provides non-destructive estimates of epidermal UV-A transmittance through fluorescence yields of chlorophyll induced by UV-A (375 nm) and blue (470 nm) radiation pulses (Kolb and Pfündel, 2005). Fluorescence induced by UV-A (F_{UV}) from the mesophyll is compared to fluorescence induced by blue light (F_{BL}). By standardizing the ratio F_{UV}/F_{BL} to unity for an epidermis-free leaf (represented by a blue plastic standard, Heinz Walz GmbH, Effeltrich, Germany), absorbance of UV by the epidermis will proportionately reduce F_{UV} with the resulting ratio equivalent to the transmittance for UV-A. Since UV-A transmittance is a dynamic plant characteristic responding to changing environmental factors (Barnes et al., 2008), these measurements were taken on plants that had been moved indoors.

The UVA-PAM measures the changes in transmittance associated with changes in UV-A absorbing pigments (375 nm peak). To determine the relationship between UV-A and UV-B absorbing compounds in *Vicia faba*, we measured epidermal transmittance and UV-absorbing compounds from additional plants grown in varying light environments in North Logan, Utah. Epidermal transmittance for UV-A was measured on mature intact leaves using the UVA-PAM. The leaves in this study had developed under different densities of shade cloth and under premium cellulose triacetate (0.13 mm thick, Liard Plastics, Salt Lake City, UT, USA) and Llumar (0.13 mm thick, part no. UVCLSRPS, cutoff near 390 nm; CP Films, Inc., Martinsville, VA, USA) to create unfiltered and UV-screened environments (Fig. 13.2), respectively, of different levels of PAR and UV. Subsequently, leaf disks (1 cm^2) were collected from each leaf, dried at 60˚C for 24 hours and weighed. Samples were ground, placed in an acidified methanol solution (5 ml of 70% methanol, 29% H_2O, and 1% HCl) in the dark at 20˚C for 24 hours. Absorbances at 305 nm (approximate midpoint of UV-B spectrum) and 360 nm (midpoint of UV-A spectrum) of the extracts were measured with a scanning UV/visible spectrophotometer (Model DU640; Beckman Coulter, Inc., Fullerton, CA, USA).

13.2.4 Solar UV and PAR Irradiance

Measurements of ambient solar UV and PAR were made using a broadband UV

sensor (Skye UV-B; Skye Instruments, Ltd., Powys, UK) and quantum sensor (LI-185, Li-COR, Inc., Lincoln, NE, USA), respectively, at the Mauna Kea field site during the experiments. Clear-day data during the experiment were regressed against biologically-weighted estimates calculated from solar UV irradiance measured at the USDA UV-B monitoring station UVMFRS radiometer located at the Mauna Loa Meteorological Observatory (3,397 m elevation; ca. 30 km from our field site on Mauna Kea, http://uvb.nrel.colostate.edu/UVB). Biologically effective UV-B irradiances were reported for three generalized spectral weighting functions from Caldwell (1971; UV-BBE71), Flint and Caldwell (2003; UV-BBE03), and McKinlay and Diffey (1987; erythemal). We reported the erythemal (reddening of human skin) weighting as sometimes this is the only weighted irradiance available to researchers and is occasionally reported in plant studies. The UV-BBE data were adjusted for elevation differences between the Mauna Loa station and the Mauna Kea study site using a regression equation generated from data by Nullet and Juvik (1997). Reported integrated UV-A (321 nm − 400 nm) irradiances were not adjusted for elevation, as differences would be minimal.

13.2.5 Statistical Analyses

ANOVA (General Linear Model) was used to test for differences among treatments, and pair-wise comparisons were made using the Tukey-Kramer multiple-comparison test. We initially tested for differences in plant metrics among treatment replicates (three replicates per filter treatment) and found none, but did find highly significant differences among individual plants within container racks due to the red/far-red ratio growth response of plants (tallest plants were in the center of the rack, smallest on the outer margin). Due to this, data were blocked by treatment and by position in the cone-tainer racks (1 − 25); highly significant position effects were found ($p < 0.00001$). Linear regression was used to test for significance of various trends. NCSS Statistical Software (NCSS, 2007; release Aug. 2007; NCSS, Orem, UT, USA) was used for all statistical analyses.

13.3 Results

13.3.1 UV-A Epidermal Transmittance

Epidermal transmittance for UV-A for fava beans grown in a high UV environment on Mauna Kea was found to be significantly affected by both the

dimming treatment and UV-B screening (Table 13.1; Fig. 13.3). On average, measured transmittances increased 6.6% with a 13% reduction in PAR (+UVB full sun vs. +UVB reduced sun). Screening of UV-B further increased epidermal

Table 13.1 Summary of 2-way ANOVA of the global dimming and UV-B reduction experiment conducted with fava bean at the Mauna Kea, HI, USA field station. Dosimetry and meteorological data as described in Fig 13.3. Treatments are described in the text. "mse" refers to mean square error from ANOVA; *n* is the total number measurements per treatment. Not all plants had internodes 7 – 9

Metric	Units	*n*	Treatments			mse	*p*-value
			+UVB full sun	+UVB reduced sun	−UVB reduced sun		
UVA transmittance	%	150	4.521	4.819	5.516	0.097	<0.0001
Total height	cm	75	19.223	19.191	19.309	0.223	0.927
Total biomass	g	75	0.814	0.804	0.803	0.018	0.903
Leaf biomass	g	75	0.402	0.393	0.388	0.014	0.783
Stem biomass	g	75	0.245	0.229	0.227	0.008	0.221
Branch biomass	g	75	0.162	0.177	0.184	0.016	0.609
Leaf mass per area	g cm^{-2}	75	0.0044	0.0044	0.0043	0.0001	0.796
Number of internodes	n	75	7.68	7.91	8.00	0.10	0.081
Number of branch nodes	n	75	2.49	2.56	2.69	0.10	0.330
Number of leaf nodes	n	75	5.19	5.35	5.31	0.08	0.360
Length of 1st internode	cm	75	0.376	0.415	0.324	0.041	0.294
Length of 2nd internode	cm	75	1.420	1.395	1.227	0.094	0.291
Length of 3rd internode	cm	75	2.405	2.273	2.144	0.114	0.272
Length of 4th internode	cm	75	3.020	2.935	2.840	0.107	0.496
Length of 5th internode	cm	75	2.716	2.584	2.761	0.086	0.319
Height of 1st internode	cm	75	0.068	0.088	0.064	0.017	0.547
Height of 2nd internode	cm	75	0.444	0.503	0.388	0.050	0.275
Height of 3rd internode	cm	75	1.864	1.897	1.615	0.131	0.253
Height of 4th internode	cm	75	4.269	4.171	3.759	0.229	0.250
Height of 5th internode	cm	75	7.289	7.105	6.599	0.308	0.262
Height of 6th internode	cm	75	10.005	9.689	9.360	0.316	0.354
Height of 7th internode	cm	73-75	11.991	11.594	11.406	0.282	0.330
Height of 8th internode	cm	41-50	13.238	12.359	12.443	0.316	0.104
Height of 9th internode	cm	10-22	14.101	12.828	13.036	0.551	0.335

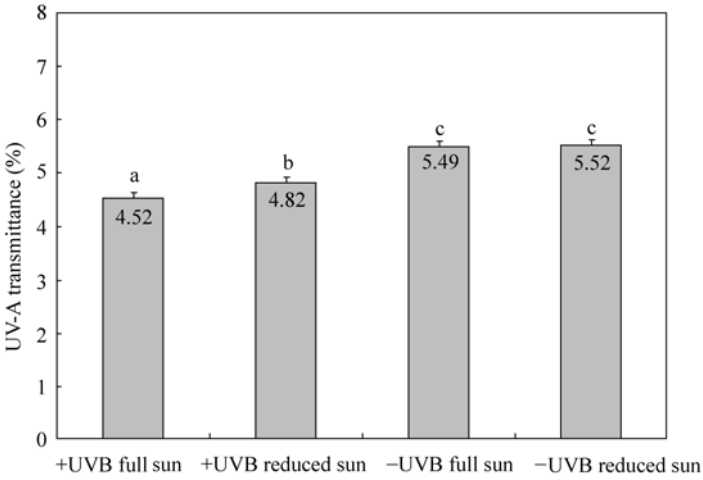

Figure 13.3 Epidermal transmittance for UV-A (375 nm) for mature fava bean leaves grown under simulated global dimming and UV-B exclusion environments at the Mauna Kea, HI field site (see Section 13.2.1). Epidermal transmittance was measured non-destructively with a UVA-PAM fluorometer. Error bars represent 1 standard error. Bars with different letters are significantly different at $p < 0.05$. Average daily biologically weighted UV doses were: erythemal = 8.97 kJ m^{-2} d^{-1} (sd. 1.28, min. 4.90, max. 10.06); UV-BBE71 = 13.8 kJ m^{-2} d^{-1} (sd. 2.0, min. 7.5, max. 15.4); and UV-BBE03 = 37.7 kJ m^{-2} d^{-1} (sd. 5.4, min. 20.6, max. 42.3). Daily total PAR averaged 46.6 mol m^{-2} d^{-1} (sd. 8.3) and daily maximum PAR averaged 2,024 μmol m^{-2} s^{-1} (sd. 332). Daily air temperature averaged 11.8°C (sd. 1.5), daily maximum temperature averaged 17.8°C (sd. 2.0), and daily minimum temperature averaged 5.9°C (sd. 2.1)

transmittance by an additional 14.5% under a 13% reduction in PAR (-UVB reduced sun), and a total 22.1% increase in transmittance from the full sun treatment (vs. +UVB full sun). Screening of UV-B under a 6.1% reduction in PAR resulted in a 21.5% (-UVB, "full" sun) increase in epidermal transmittance for UV-A from the full sun treatment (+UVB full sun).

To determine the relationship between maximum ambient PAR and UV exclusion on leaf epidermal transmittance for UV, we grew fava beans under different PAR and UV environments in Utah. For these plants, relatively small but steady increases in transmittance were observed with declining PAR until maximum daily PAR exposure went below 200 μmol m^{-2} s^{-1} where transmittances were observed to increase rapidly per unit quanta. This pattern was found to be consistent whether UV was present or absent, although leaves not exposed to UV radiation had slightly higher transmittances for all levels of PAR exposure (Fig. 13.4 upper). A similar pattern (Fig. 13.4 lower) was found for quaking aspen (*Populus tremuloides*) leaves grown in Utah under different levels of PAR without UV exclusion.

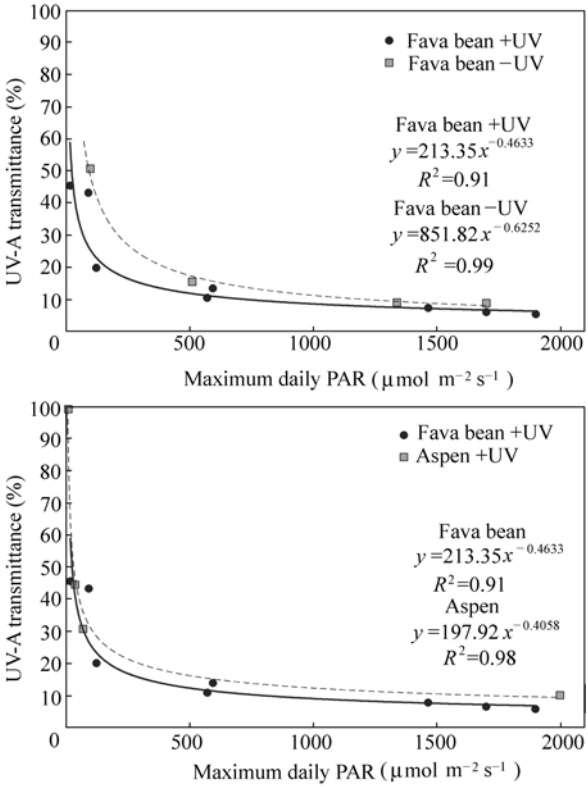

Figure 13.4 Epidermal transmittance for UV-A (375 nm) for mature fava bean (upper and lower panels) and quaking aspen leaves (lower panel only) grown under different PAR intensities in Logan, Utah measured non-destructively with a UVA-PAM fluorometer. Changes in UV exposure were commensurate with changes in PAR. Both UV-A and UV-B were shielded under the UV exclusion treatment (-UV)

The relationship between the concentration of UV absorbing pigments and UV-A epidermal transmittance as measured with the UVA-PAM was also evaluated for the fava beans grown in Utah. Highly significant relationships ($p < 0.0001$) were found among concentrations of extracted UV absorbing pigments and UV-A epidermal transmittance for both UV-A (Fig. 13.5, upper left) and UV-B (Fig. 13.5, lower left) absorbing compounds. In addition, concentrations of UV-A and UV-B absorbing compounds were highly correlated ($R^2 = 0.93$, $p < 0.0001$) and linear in relationship (Fig. 13.5, upper right). The relationship between the concentration of UV-B absorbing compounds and epidermal transmittance were consistent with a relationship (Fig. 13.5, lower right) found for a single quaking aspen growing in Utah.

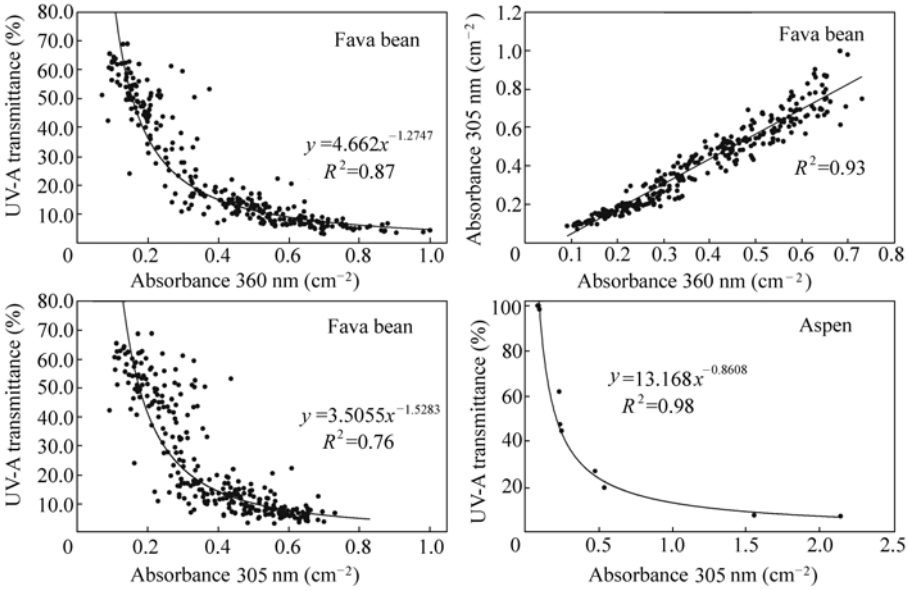

Figure 13.5 Relationship between UV-A transmittance (375 nm) as measured with a UVA-PAM fluorometer and absorbance (at 305 and 360 nm) of flavonoids extracted from same leaves for fava bean (left panels) and quaking aspen growing in Logan, Utah (lower right panel). The relationship between extract absorbance at 305 nm and 360 nm for fava bean is shown in the upper right panel. The quaking aspen relationship was derived from a single tree, while multiple individuals of fava bean were used

13.3.2 Dimming Effects on Biomass and Structure

Changes in structure and biomass of seedling fava beans were assessed with simulated dimming and UV-B exclusion in Hawaii. For total height, internode lengths, specific leaf weight and total, leaf, stem and branch biomass, no statistically significant differences were found between plants grown in full sun and under the dimming treatment, either with or without UV-B exclusion (Table 13.1; Fig. 13.6, upper, middle). Non-significant decreasing trends ($p > 0.05$) from full sun to reduced sun with UV-B exclusion were found for biomass and for many internode heights. One exception to this was a non-significant increase along the same radiation gradient for branch biomass. Evidence that more branching may have been induced with UV-B exclusion were obtained by assessing the number of plants with 8 – 10 internodes and the number of leaf and branch internodes. More plants grown under the dimming treatment with UV-B excluded had 8 – 10 internodes (Fig. 13.6, lower), and more branches per plant and greater branch biomass were measured (although not significant) for this treatment (Fig. 13.7).

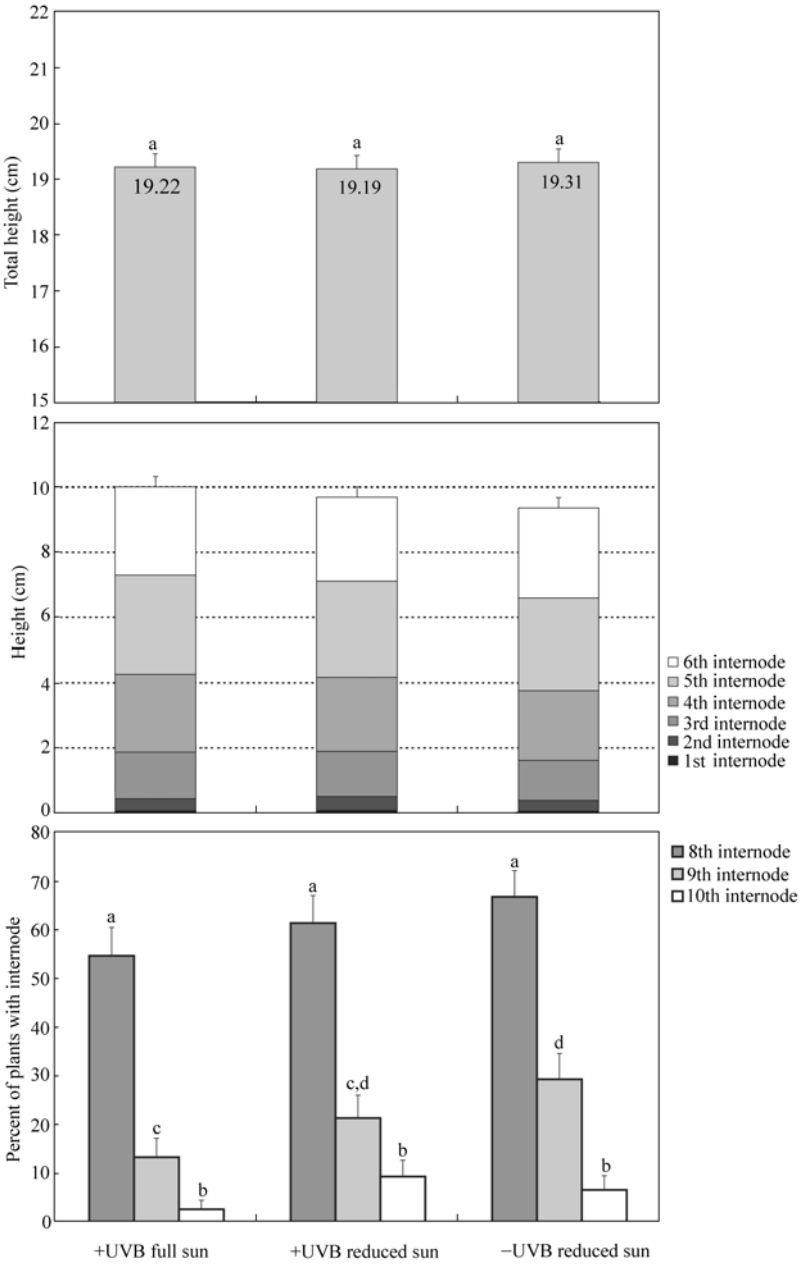

Figure 13.6 Total plant height (upper), height of internodes 1 – 6 (middle) and portion of experimental plants with internodes 8 – 10 (lower) for fava beans grown under simulated global dimming and UV-B exclusion at the Mauna Kea, Hawaii field site. Error bars represent 1 standard error. Values with same letter designation are not significantly different ($p > 0.05$). No significant differences were found among internode heights (middle panel). Dosimetry and meteorological data as in Fig. 13.3

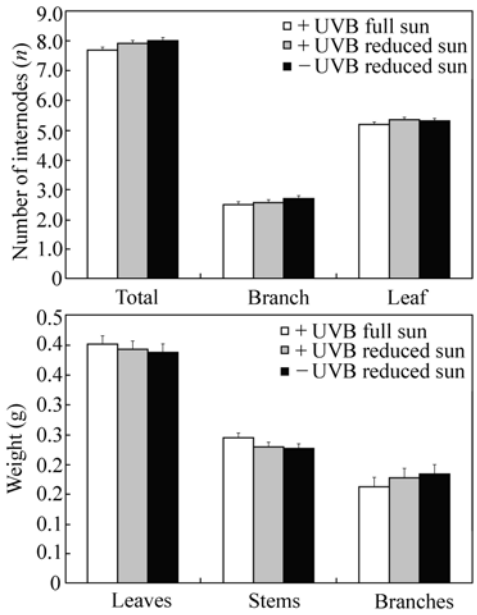

Figure 13.7 Average total number of internodes, number of branches and number of leaf insertions (upper) and weight of leaves, stems and branches (lower) for fava bean plants grown under simulated global dimming and UV-B exclusion at the Mauna Kea, Hawaii field site. Error bars represent 1 standard error. No significant differences ($p > 0.05$) were found among treatments for the number of internodes and weights of plant parts. Dosimetry and meteorological data as in Fig. 13.3

13.4 Discussion

Our results with fava bean (*Vicia faba*) indicated little change in plant structure or biomass under an experimental global dimming environment where ambient PAR was reduced approximately 13%. We also found minimal additional differences with UV-B exclusion in the same environment. However, we found significant changes in leaf optical properties related to UV transmittance in both the reduced PAR and UV-B treatments.

The growth response to UV-B exclusion in this experiment was less than expected for a temperate-latitude crop grown at a high-elevation tropical location with high solar UV. Biologically effective UV radiation increases substantially from high to low latitudes, and there is also an increase with elevation (Caldwell et al., 1980). Because of its elevation and latitude, the study site on Mauna Kea, Hawaii, experiences some of the highest effective UV doses on the planet (Bodhaine et al., 1996). Thus, we were somewhat surprised that attenuation of these high UV fluxes had minimal effect on fava bean growth and morphology. Some small morphological changes in fava bean, without accompanying changes

in above-ground mass, have been reported with UV-B exclusion in the Netherlands (Visser et al., 1997) and in a greenhouse UV-B supplementation experiment (Barnes et al., 1990a). However, under field UV-B supplementation at mid-latitudes, this variety of fava bean showed changes in leaf optical properties, but no changes in photosynthesis (Flint et al., 1985).

13.4.1 Global Dimming and UV-B Effects on Leaf Optical Properties

Small increases of epidermal transmittance for UV in fava bean leaves were found under the 13% reduction in PAR and with UV-B exclusion. These results are consistent with increases in leaf UV-absorbing compounds with increased UV-B exposure (Mazza et al., 2000; Searles et al., 2001; Coleman and Day, 2004). Over a wide range of solar radiation regimes, we found that only small differences in epidermal transmittance occurred over large ranges of PAR ($500 - 2{,}000$ μmol m^{-2} s^{-1}), and that this relationship held even for leaves developed under full UV-B and UV-A exclusion (Fig. 13.4). These findings suggest that the primary effect on changes in leaf epidermal transmittance due to global dimming will likely occur for leaves developed in shaded environments (<200 μmol m^{-2} s^{-1}) where reductions in ambient PAR and UV are related to large changes in epidermal transmittance.

We also observed that changes in levels of whole-leaf UV-absorbing compounds were not linearly correlated with measurements of UV-A transmittance. Rather, this relationship was curvilinear whereby leaves with low UV-A transmittance exhibited a range of whole-leaf absorbance values (Fig. 13.5). In addition, the relationship more closely fit a power function ($y = bx^a$), rather than exponential ($y = be^{ax}$), indicating that the distribution of the absorbing compounds did not approximate a random distribution of particles as in the Beer-Lambert law of light absorbance through particles suspended in a medium (Kostinski, 2001). Krause et al. (2003) also reported constant levels of UV-A transmittance over a wide range of whole-leaf absorbance values in leaves from tropical tree crowns. The non-random distribution of UV-absorbing compounds in the epidermis (Day et al., 1993) may help explain the broad range of whole-leaf absorbance values for a given quantity of epidermal transmittance.

13.4.2 Global Dimming and UV-B Effects on Productivity

The lack of a significant growth response under reduced PAR is not totally unexpected in the high light environment of Mauna Kea where clear sky ambient PAR levels can routinely exceed 2,200 μmol m^{-2} s^{-1}. Light saturation would be expected for many of the leaves of the experimental plants even in early stages of

canopy development. Furthermore, reductions in total available PAR have little effect in the nearly linear portion of the photosynthetic light response curve often observed for C_3 photosynthesis at high levels of PAR (e.g., Lambers et al., 1998). In addition, these results are consistent with those reported by Stanhill and Cohen (2001) for many crops in high-radiation, arid climates. They concluded that there would be minimal negative effects of global dimming on crop productivity due to shade tolerance and anticipated reductions in water stress. Thus, our results did not agree with previous research indicating increased productivity associated with increased diffuse radiation in light-limited canopies (Roderick et al., 2001; Black et al., 2006) under global dimming, and likely reflect a nearly light saturated canopy within the experimental setup. Our results further suggest that reduced leaf photosynthesis resulting from high light exposure (e.g., photoinhibition, Demmig-Adams, 1990) did significantly reduce productivity (Werner et al., 2001).

Many plant responses to a global dimming environment are not necessarily linked to overall plant productivity. In experiments with wheat, Fischer (1975) found that shading reduced dry matter production approximately in proportion to the percent shade, even at the lowest (13%) shade levels used. However, grain production was less influenced by shading, most likely because shading reduced tillering, but enhanced tiller survival (Fischer, 1975). The response of wheat to shade was considerably greater than the growth responses we observed in fava bean, but may relate to higher leaf area and greater canopy self-shading in the wheat experiment. Although not significant, our data suggested a possible increase in branching rate with reduced PAR and UV-B exclusion. Over an entire growing season, such morphological differences might affect productivity as more energy put into branch structures likely results in less energy and carbon allocated to other plant parts.

13.4.3 Ecological Implications

The body of evidence to date indicates that changes in UV effects on plants are often relatively subtle, but these small changes may have important ecological implications, particularly by secondary or indirect effects (Caldwell et al., 2007). The small changes in leaf optical properties and secondary chemistry, and minimal differences in productivity under simulated global dimming and UV-B reduction found in our study, are consistent with this perspective.

Changes in the quantity of UV exposure by plants have been shown to affect morphology in ways that can affect competitive interactions, with changes in biomass among species corresponding to changes in the quantity of UV-B radiation (Barnes et al., 1990b; Ryel et al., 1990; Robson et al., 2003). Changes in yield, as have been observed under small changes in PAR (e.g., Fischer, 1975), and changes in root:shoot allocation (Zaller et al., 2002; Rinnan et al., 2005) may

affect competitive interactions (Rinnan et al. 2006). Exposure to UV-B radiation also may affect herbivory rates (Ballaré et al., 1996; Zavala et al., 2001). Changes in concentrations of UV-B absorbing pigments have also been linked to both negative and positive plant responses to pathogens, (e.g., Raviv and Antignus, 2004). Different levels of secondary compounds related to changes in UV-B absorbing pigments may have additional below-ground effects on soil microorganisms by affecting carbon and other nutrient availability (Robson et al., 2005). All these examples show potential mechanisms for UV-B to influence competitive interactions.

Effects of global dimming on plants may also interact with other environmental changes, including temperature and precipitation patterns, in complex and synergistic ways. These interactive effects include increases in UV-absorbing secondary compounds associated with drought (Milchunas et al., 2004; Yang et al., 2005). These may change plant performance by reducing UV-induced damage, and affecting herbivory rates and soil processes, as discussed above.

13.4.3.1 UV Exclusion Studies

Portions of this study involved using filters to selectively exclude UV-B (and in one experiment all UV) from the incident radiation spectrum. Results from UV exclusion studies have varied widely, and the importance of excluding various portions of the UV spectrum on these biological effects has been debated. At temperate locations, many species often fail to respond to UV-B exclusion (e.g., Cybulski and Peterjohn, 1999). Properly designed UV exclusion experiments at lower latitudes with higher ambient levels of UV-B, but similar levels of PAR, might be expected to show greater effects than similar experiments at higher latitudes. On the other hand, species of low latitudes may be adapted to cope with high levels of ambient solar UV-B and thus, might be expected to show less of a response to solar UV-B exclusion than high latitude species. The examples discussed below show that, while trends of responses to UV exclusion cannot now be easily seen from simple comparisons, improvements in methodology may permit generalizations to be made in the future.

Exclusion studies at low latitudes comprise a small number of the total exclusion studies in literature and show that species exhibit a variety of growth responses to ambient levels of UV-B. An examination of five tropical species at 9ºN latitude in Panama (four tree species and the crop cassava) found substantial growth responses in two species and smaller or no growth responses in others (Searles et. al., 1995). Rice (*Oryza* sp.) exhibited no significant growth responses in four seasons of UV-B exclusion experiments in the Philippines at 15˚N (Dai et al., 1997). However, other crop experiments did show responses. When comparing the responses of maize (*Zea mays*) and the mung bean (*Vigna* sp.) to UV-B removal at New Delhi (28.6˚N), Pal et al. (1997) found the bean to be much more responsive to UV-B than the maize. *Vigna unguiculata* grown under a

similar UV-B exclusion at 10ºN latitude, where we assume UV-B could be more intense, responded to UV-B to a lesser extent (Lingakumar et al., 1999).

The category of UV-absorbing pigments was the most responsive characteristic in a meta-analysis of UV-supplementation studies (Searles et al., 2001) and is a characteristic that often responds in UV exclusion studies. Four of the five species examined by Searles et al. (1995) in Panama showed significant changes in levels of these compounds in response to UV-B exclusion. The only other low-latitude study examining UV-absorbing compounds in response to UV-B exclusion used the bean *Vigna unguiculata* and saw an approximate 60% increase in these compounds under near-ambient radiation compared to the UV-B exclusion (Lingakumar et. al., 1999).

Since UV-exclusion experiments appear less technically complex than lamp-supplementation experiments, it is tempting to use multiple studies at different latitudes or elevations to examine response. One potential comparison uses wheat: Becwar et al. (1982) grew wheat under UV-B exclusion at 3,000 m elevation in the Rocky Mountains at 39.2°N latitude, while Häder (1996) studied several wheat cultivars exposed at 2,400 m elevation in the Andes at 22.8°S latitude. However, the latter study did not use a filter over the ambient UV plants, so the true UV-B effect may be confounded as the lack of a filter induces a host of microclimate differences besides the UV treatment (Flint et al., 2003). A latitudinal gradient study of *Salicornia* along the Atlantic coast of South America (Costa et. al., 2006) had the potential to provide an overview of how this genus responds to varied UV environments, but interpretation is complicated. Experiments in one location lacked filters over the ambient-UV plots, preventing a true evaluation of UV effects as discussed above. In another location in this study, both UV-B and UV-A were removed from the UV exclusion treatment, while all the other sites only excluded UV-B, considerably complicating comparisons (see below).

Selection of different wavebands of interest may complicate comparisons of results between studies. Among the 100 or so published exclusion studies, exclusion has included removing all UV-B wavelengths, removing only a portion of the UV-B waveband, and removing all UV-B and simultaneously some or all of the UV-A. While many studies use polyester (often referred to as Mylar) which removes most UV-B wavelengths (Fig. 13.2), other studies use different techniques or materials to remove more limited wavebands. This is illustrated by experiments with maize at a low-latitude site (28.6°N), where Pal et al. (1997) used the standard polyester filter and saw only some limited change in plant growth with UV-B removal. Several varieties of maize grown further north (38.7°N latitude), under filters that removed only a narrower waveband of UV-B, often seemed to show greater effects (Mark et al., 1996). This is unexpected, both in terms of the direction of the latitudinal response and the larger response to the smaller UV radiation difference between the two treatments.

There is also increasing evidence of the importance of portions of the UV-A

spectrum. Several recent spectral weighting functions extend into the UV-A region (Quaite et al., 1992; Ibdah et al., 2002; Flint and Caldwell, 2003; also see discussion of UV-A exclusion experiments in Flint and Caldwell, 2003). Thus experiments excluding portions of the UV-A spectrum would be expected to produce different results than exclusions of only UV-B and are not directly comparable; in some instances solar UV-A invokes different responses than UV-B (Kotilainen et al., 2008).

Latitudinal comparisons are sometimes further complicated because the latitude of the experiments is not reported. Also, in some studies, the dates of plant growth are not presented. As many UV-exclusion experiments are short-term studies, and UV levels can vary considerably over the course of the growing season in many areas, these two problems make even crude estimates of irradiance levels problematic.

Perhaps the greatest aid for reconciling exclusion experiments in different areas would be the presentation of UV dosimetry integrated over the course of the experiment, although a characterization of representative clear-day radiation would be preferable to a complete lack of dosimetry. Biologically-weighted UV radiation with more than one common weighting function is preferable to unweighted values, as comparisons of weighted and unweighted radiation, or radiation weighted with different spectral weighting functions, are seldom possible. For example, both of the *Vigna* studies referred to above provide dosimetry, but use different weighting functions. Thus, it is not possible to use the available dosimetry to help understand the unexpected response to latitude when these two studies are compared.

13.5 Concluding Remarks

Global dimming, in addition to affecting the amount of visible radiation, will affect the amount of UV radiation reaching the earth's surface. Our experiment using fava beans (*Vicia faba*) grown in the high UV environment of Mauna Kea, Hawaii, was designed to detect whether a 13% reduction in visible radiation (and associated reduction in UV radiation), a level similar to global dimming, could influence plant growth and leaf optical properties for UV-transmittance. We found that structural differences were minimal in this high light environment, but changes that can occur in secondary chemistry can affect epidermal transmittance for UV. Our results, and those of other researchers, suggest that the primary effects of global dimming on plants may be mediated through changes in secondary chemistry, and would be most likely to occur with foliage in high-shade environments. Such changes have the potential to affect herbivory, nutrient cycling, and plant response to pathogens. Future research to further understand global dimming effects on ecosystem function should continue with a focus on secondary compounds of plants.

Experiments involving UV filtration need to have sufficient methodological detail that comparisons can be made between different venues. Methodology need not be ponderous, but needs to include: (1) latitude and elevation of the experimental site, (2) dates of plant growth, (3) dosimetry of UV radiation during the experiment, and (4) filter descriptions. Filter transmittance needs mention if non-standard materials are used, and filter geometry should not be neglected. For example, flat filter sheets permit some radiation to reach plants in the filtered wavelength region while tents or tunnels exclude all filtered wavelengths. With this standardized reporting of experimental conditions, comparisons of experiments between locations will be facilitated and may lead not only to generalizations on plant responses, but may also assist in the evaluation of spectral weighting functions.

Acknowledgements

This research was supported by the US Department of Agriculture UV-B Monitoring and Research Program (USDA-CSREES No. 2004-34263-14270 to Utah State University via subcontract with Colorado State University), the Utah Agricultural Experiment Station, the Loyola University J.H. Mullahy Endowment in Environmental Biology, and a Loyola University Faculty Research Grant. We are grateful to S. Kelly, M. Spriggs and V. Del Bianco for their assistance, and R. Koehler, D. Byrne, A. Teramura, and J. Juvik and the Mauna Kea Support Services for logistical support in Hawaii. Heinz Walz GmbH, Effeltrich, Germany and Gademann Instruments, GmbH, Würzburg, Germany are gratefully acknowledged for their technical assistance and loan of instruments.

References

Alpert P, Kishcha P, Kaufman and YJ, Schwarzbard R (2005) Global dimming or local dimming?: Effect of urbanization on sunlight availability. Geophysical Research Letters 32: L17802

Ballaré CL, Scopel AL, Stapleton AE, and Yanovsky M J (1996) Solar ultraviolet-B radiation affects seeding emergence, DNA integrity, plant morphology, growth rate, and attractiveness to herbivore insects in *Datura ferox*. Plant Physiology 112: 161 – 170

Barnes PW, Flint SD, and Caldwell MM (1990a) Morphological responses of crop and weed species of different growth forms to ultraviolet-B radiation. American Journal of Botany 77: 1354 – 1360

Barnes PW, Beyschlag W, Ryel RJ, Flint SD, and Caldwell MM (1990b) Plant competition for light analyzed with a multi-species canopy model. III. Influence of canopy structure in mixtures and monocultures of wheat and wild oat. Oecologia 82: 560 – 566

Barnes PW, Shinkle JR, Flint SD, and Ryel RJ (2005) UV-B radiation: photomorphogenesis and plant-plant interactions. Progress in Botany 66: 313 – 340

Barnes PW, Flint SD, Slusser JR, Gao W, and Ryel RJ (2008) Diurnal changes in epidermal transmittance of plants in naturally high UV environments. Physiologia Plantarum 133: 363 – 372

Becwar MR, Moore Ⅲ FD, and Burke MJ (1982) Effects of deletion and enhancement of ultraviolet B (280 – 315 nm) radiation on plants grown at 3000 m elevation. Journal of the American Society for Horticultural Science 107: 771 – 774

Black K, Davis P, Lynch P, Jones M, McGettigan M, and Osborne B (2006) Long-term trends in solar irradiance in Ireland and their potential effects on gross primary productivity. Agricultural and Forest Meteorology 141: 118 – 132

Bodhaine BA, McKenzie RL, Johnston PV, Hofmann DJ, Dutton EG, Schnell RC, Barnes JE, Ryan SC, and Kotkamp M (1996) New ultraviolet spectroradiometer measurements at Mauna Loa Observatory. Geophysical Research Letters 23: 2121 – 2124

Brutsaert W (2006) Indications of increasing land surface evaporation during the second half of the 20th century. Geophysical Research Letters 33: L20403

Caldwell MM (1971) Solar ultraviolet radiation and the growth and development of higher plants. In: Giese AC (ed) Photophysiology, Vol 6. Academic Press, New York, pp.131 – 177

Caldwell MM, Robberecht R, and Billings WD (1980) A steep latitudinal gradient of solar ultraviolet-B radiation in the arctic-alpine life zone. Ecology 61: 600 – 611

Caldwell MM, Bornman JF, Ballaré CL, Flint SD, and Kulandaivelu G (2007) Terrestrial ecosystems, increased solar ultraviolet radiation, and interactions with other climate change factors. Photochemical and Photobiological Sciences 6: 252 – 266

Cohen S, Ianetz A, and Stanhill G (2002) Evaporative climate changes at Bet Dagan, Israel, 1964 – 1998. Agricultural and Forest Meteorology 111: 83 – 91

Coleman RS and Day TA (2004) Response of cotton and sorghum to several levels of subambient solar UV-B radiation: a test of the saturation hypothesis. Physiologia Plantarum 122: 362 – 372

Costa C, Armstrong R, Detres Y, Koch EW, Bertiller M, Beeskow A, Neves LS, Tourn GM, Bianciotto OA, Pinedo LB, Blessio AY, and San Roman N (2006) Effect of ultraviolet-B radiation on salt marsh vegetation: trends of the genus *Salicornia* along the Americas. Photochemistry and Photobiology 82: 878 – 886

Cutforth HW and Judiesch D (2007) Long-term changes to incoming solar energy on the Canadian Prairie. Agricultural and Forest Meteorology 145: 167 – 175

Cybulski WJ and Peterjohn WT (1999) Effects of ambient UV-B radiation on the above-ground biomass of seven temperate-zone plant species. Plant Ecology 145: 175 – 181

Dai Q, Peng S, Chavez AQ, Miranda MLL, Vergara BS, and Olszyk DM (1997) Supplemental ultraviolet-B radiation does not reduce growth or grain yield in rice. Agronomy Journal 89: 793 – 799

Day TA, Martin G, and Vogelmann TC (1993) Penetration of UV-B radiation in foliage: evidence that the epidermis behaves as a non-uniform filter. Plant, Cell and Environment 16(6): 735 – 741

Demmig-Adams B (1990) Carotenoids and phytoprotection: A role for the xanthophyll zeaxanthin. Biochimica et Biophysica Acta 1020: 1 – 24

Fischer RA (1975) Yield potential in a dwarf spring wheat and the effect of shading. Crop

Science 15: 607 – 613

Flint SD and Caldwell MM (1998) Solar UV-B and visible radiation in tropical forest gaps: measurements partitioning direct and diffuse radiation. Global Change Biology 4: 863 – 870

Flint SD and Caldwell MM (2003) A biological spectral weighting function for ozone depletion research with higher plants. Physiologia Plantarum 117: 137 – 144

Flint SD, Jordan PW, and Caldwell MM (1985) Plant protective response to enhanced UV-B radiation under field conditions: Leaf optical properties and photosynthesis. Photochemistry and Photobiology 41: 95 – 99

Flint SD, Ryel RJ, and Caldwell MM (2003) Ecosystem UV-B experiments in terrestrial communities: a review of recent findings and methodologies. Agricultural and Forest Meteorology 120: 177 – 189

Häder DP (1996) Effects of solar radiation on local and German wheat seedlings in a Chilean high mountain station. Journal of Photochemistry and Photobiology B: Biology 35: 181 – 187

Ibdah M, Krins A, Seidlitz HK, Heller W, Strack D, and Vogt T (2002) Spectral dependence of flavonol and betacyanin accumulation in *Mesembryanthemum crystallinum* under enhanced ultraviolet radiation. Plant, Cell and Environment 25: 1145 – 1154

Jauregui E and Luyando E (1999) Global radiation attenuation by air pollution and its effects on the thermal climate in Mexico City. International Journal of Climatology 19: 683 – 694

Kostinski AB (2001) Extinction of radiation by a homogeneous but spatially correlated random medium. Journal of the Optical Society of America 18: 1929 – 1933

Kolb CA and Pfündel EE (2005) Origins of non-linear and dissimilar relationships between epidermal UV absorbance and UV absorbance of extracted phenolics in leaves of grapevine and barley. Plant, Cell and Environment 25: 580 – 590

Kotilainen T, Tegelberg R, Julkunen-Tiitto R, Lindfors A and Aphalo PJ (2008) Metabolite specific effects of solar UV-A and UV-B on alder and birch leaf phenolics. Global Change Biology 14: 1294 – 1304

Krause GH, Galle A, Gademann R, and Winter K (2003) Capacity of protection against ultraviolet radiation in sun and shade leaves of tropical forest plants. Functional Plant Biology 30: 533 – 542

Krizek DT (2004) Influence of PAR and UV-A in determining plant sensitivity and photomorphogenic responses to UV-B radiation. Photochemistry and Photobiology 79: 307 – 315

Lambers H, Chapin III FS, and Pons TL (1998) Plant Physiological Ecology. Springer, New York, Berlin, Heidelberg. p.540

Li HB, Robock A, and Wild M (2007) Evaluation of Intergovernmental Panel on Climate Change Fourth Assessment soil moisture simulations for the second half of the twentieth century. Journal of Geophysical Research-Atmospheres 112: D06106

Liepert BG and Romanou A (2005) Global dimming and brightening and the water cycle. Bulletin of the American Meteorological Society 86: 622 – 623

Lingakumar K, Amudha P, and Kulandaivelu G (1999) Exclusion of solar UV-B (280 nm – 315 nm) radiation on vegetative growth and photosynthetic activities in *Vigna unguiculata* L. Plant Science 148: 97 – 103

Lohmann S, Schillings C, Mayer B, and Meyer R (2006) Long-term variability of solar direct and global radiation derived from ISCCP data and comparison with reanalysis data. Solar Energy 80: 1390 – 1401

Ma J and Guicherit R (1997) Effects of stratospheric ozone depletion and tropospheric pollution on UV radiation in the troposphere. Photochemistry and Photobiology 66: 346 – 355

Mark U, Saile-Mark M, and Tevini M (1996) Effects of solar UVB radiation on growth, flowering and yield of central and southern European maize cultivars (*Zea mays* L.). Photochemistry and Photobiology 64: 457 – 463

Mazza CA, Boccalandro HE, Giordano CV, Battista D, Scopel AL, and Ballaré CL (2000) Functional significance and induction by solar radiation of ultraviolet-absorbing sunscreens in field-grown soybean crops. Plant Physiology 122: 117 – 125

McKenzie RL, Seckmeyer G, Bais AF, Kerr JB, and Madronich SA (2001) Satellite retrievals of erythemal UV dose compared with ground-based measurements at northern and southern midlatitudes. Journal of Geophysical Research D 106: 24051 – 24062

McKenzie R, Aucamp P, Bais A, Björn L, and Ilyas M (2007) Changes in biologically-active ultraviolet radiation reaching the Earth's surface. Photochemical and Photobiological Sciences 6: 218 – 231

McKinlay AF, and Diffey BL (1987) A reference action spectrum for ultraviolet induced erythema in human skin. CIE Journal 6: 17 – 22

Milchunas DG, King JY, Mosier AR, Moore JC, Morgan JA, Quirk MH, and Slusser JR (2004) UV radiation effects on plant growth and forage quality in a shortgrass steppe ecosystem. Photochemistry and Photobiology 79: 404 – 410

Nazarenko L and Menon S (2005) Varying trends in surface energy fluxes and associated climate between 1960 and 2002 based on transient climate simulations. Geophysical Research Letters 32: L22704

Norris JR and Wild M (2007) Trends in aerosol radiative effects over Europe inferred from observed cloud cover, solar "dimming" and solar "brightening". Journal of Geophysical Research-Atmospheres 112: D08214

Nullet D and Juvik JO (1997) Measured altitudinal profiles of UV-B irradiance in Hawaii. Physical Geography 18: 335 – 345

Pal M, Sharma A, Abrol Y, and Sengupta U (1997) Exclusion of UV-B radiation from normal solar spectrum on the growth of mung bean and maize. Agriculture, Ecosystems, and Environment 61: 29 – 34

Pinker RT, Zhang B, and Dutton EG (2005) Do satellites detect trends in surface solar radiation? Science 308: 850 – 854

Quaite FE, Sutherland BM, and Sutherland JC (1992) Action spectrum for DNA damage in alfalfa lowers predicted impact of ozone depletion. Nature 358: 576 – 578

Ramana MV and Ramanathan V (2006) Abrupt transition from natural to anthropogenic aerosol radiative forcing: Observations at the ABC-Maldives Climate Observatory. Journal of Geophysical Research-Atmospheres 111: D20207

Raveh E, Cohen S, Raz T, Yakir D, Grava A, and Goldschmidt E (2003) Increased growth of young citrus trees under reduced radiation load in a semi-arid climate. Journal of

Experimental Botany 54: 365 – 373

Raviv M and Antignus Y (2004) UV radiation effects on pathogens and insect pests of greenhouse-grown crops. Photochemistry and Photobiology 79: 219 – 226

Rinnan R, Keinanen MM, Kasurinen A, Asikainen J, Kekki TK, Holopainen T, Ro-Poulsen H, Mikkelsen TN, and Michelsen A (2005) Ambient ultraviolet radiation in the Arctic reduces root biomass and alters microbial community composition but has no effects on microbial biomass. Global Change Biology 11: 564 – 574

Rinnan R, Gehrke C, and Michelsen A (2006) Two mire species respond differently to enhanced ultraviolet-B radiation: effects on biomass allocation and root exudation. New Phytologist 169: 809 – 818

Robock A and Li HB (2006) Solar dimming and CO_2 effects on soil moisture trends. Geophysical Research Letters 33: L20708

Robson TM, Pancotto VA, Flint SD, Ballaré CL, Sala OE, Scopel AL, and Caldwell MM (2003) Six years of solar UV-B manipulations affect growth of *Sphagnum* and vascular plants in a Tierra del Fuego peatland. New Phytologist 160: 379 – 389

Robson TM, Pancotto VA, Scopel AL, Flint SD, and Caldwell MM (2005) Solar UV-B influences microfaunal community composition in a Tierra del Fuego peatland. Soil Biology and Biochemistry 37: 2205 – 2215

Roderick M (2006) The ever-flickering light. Trends in Ecology and Evolution 21: 3 – 5

Roderick ML and Farquhar GC (2002) The cause of decreased pan evaporation over the past 50 years. Science 298: 1410 – 1411

Roderick ML, Farquhar GD, Berry SL, and Noble IR (2001) On the direct effect of clouds and atmospheric particles on the productivity and structure of vegetation. Oecologia 129: 21 – 30

Ryel RJ, Barnes PW, Beyschlag W, Caldwell MM, and Flint SD (1990) Plant competition for light analyzed with a multispecies canopy model. I. Model development and influence of enhanced UV-B conditions on photosynthesis in mixed wheat and wild oat canopies. Oecologia 82: 304 – 310

Schiermeier Q (2005) Cleaner skies leave global warming forecasts uncertain. Nature 435: 135 – 135

Searles PS, Caldwell MM, and Winter K (1995) The response of five tropical dicotyledon species to solar ultraviolet-B radiation. American Journal of Botany 82: 445 – 453

Searles PS, Flint SD, and Caldwell MM (2001) A meta-analysis of plant field studies simulating stratospheric ozone depletion. Oecologia 127: 1 – 10

Stanhill G and Cohen S (2001) Global dimming: a review of the evidence for a widespread and significant reduction in global radiation with discussion of its probable causes and possible agricultural consequences. Agricultural and Forest Meteorology 107: 255 – 278

Visser AJ, Tosserams M, Groen MW, Magendans GWH, and Rozema J (1997) The combined effects of CO_2 concentration and solar UV-B radiation on faba bean grown in open-top chambers. Plant, Cell and Environment 20: 189 – 199

Werner C, Ryel RJ, Correia O, and Beyschlag W (2001) Effects of photoinhibition on whole-plant carbon gain assessed with a photoinhibition model. Plant, Cell and Environment 24: 27 – 40

Wild M, Gilgen H, Roesch A, Ohmura A, Long CN, Dutton EG, Forgan B, Kallis A, Russak V, and Tsvetkov A (2005) From dimming to brightening: Decadal changes in solar radiation at Earth's surface. Science 308: 847 – 850

Yang Y, Yao Y, Xu, G, and Li C (2005) Growth and physiological responses to drought and elevated ultraviolet-B in two contrasting populations of *Hippophae rhamnoides*. Physiologia Plantarum 124: 431 – 440

Zaller JG, Caldwell MM, Flint SD, Scopel AL, Sala OE, and Ballaré CL (2002) Solar UV-B radiation affects below-ground parameters in a fen ecosystem in Tierra del Fuego, Argentina: implications of stratospheric ozone depletion. Global Change Biology 8: 867 – 871

Zavala J, Scopel AL, and Ballaré CL (2001) Effects of ambient UV-B radiation on soybean crops: Impact on leaf herbivory by *Anticarsia gemmatalis*. Plant Ecology 156: 121 – 130

14 Effects of Ultraviolet-B Radiation and Its Interactions with Climate Change Factors on Agricultural Crop Growth and Yield

K. Raja Reddy[1], P.V. Vara Prasad[2], and Shardendu K. Singh[1]

[1]Department of Plant and Soil Sciences, Box 9555, 117 Dorman Hall
Mississippi State University, Mississippi State, MS 39762, USA
E-mail: krreddy@pss.msstate. edu

[2]Department of Agronomy, Kansas State University, Manhattan, KS 66506, USA
E-mail: vara@ksu.edu

Abstract Crops are often exposed to multiple factors of climate change including: (1) enhanced ultraviolet-B (UV-B) radiation, (2) elevated carbon dioxide concentrations (CO_2), and (3) episodes of elevated temperatures and water stress during critical stages of crop development. Our understanding of crop responses to individual climate change stress factors has significantly advanced in recent years. However, crop responses to a combination of stress factors are less understood and need attention. In addition to direct effects on various physiological, growth, and yield traits of plants, the interaction of plants with biotic factors (particularly insects and pathogens) will play an important role in determining crop productivity. The objective of this chapter is to provide a summary of crop responses to UV-B, CO_2, temperature, drought, and a combination of multiple stresses. Exposure to above ambient UV-B radiation decreases crop productivity through negative effects on photosynthesis, growth, dry matter production, yield, and grain quality. Elevated CO_2 often improves photosynthesis, growth, and yield of most crop species. Alternatively, exposure to both above optimum temperatures and water stress significantly decreases crop productivity and quality, particularly when stress occurs during sensitive stages (reproductive phase) of crop development. The positive effects of elevated (CO_2) on photosynthesis and growth do not generally overcome the negative effects of UV-B radiation, elevated temperatures, or water stress on productivity and quality of grain crops. Crop species and cultivars within crop species vary in their responses to both individual and a combination of stress factors, suggesting a scope for genetic improvement. Further research should be focused on breeding for tolerance to multiple stresses of regional and local importance. An increased knowledge of crop responses to multiple stresses and genetics

may also improve crop simulation models resulting in a better understanding, prediction and management of crops in a changing environment.

Keywords climate change, crop growth and yield, drought stress, genetic variability, multiple abiotic stresses, temperature

14.1 Introduction

The growing population of today's world (6.7 billion, U.S. Census Bureau, 2008) faces great challenges due to limited resources for the production of adequate amounts of food, fiber, feed, industrial products, and ecosystem services. As the global population increases by nearly 80 million each year, policies must be developed to ensure the needs of a future population of 8 billion by 2025 and more than 12 billion by 2050 (U.N. Population Division, 2008) are met. About 84% of this growth is expected to occur in developing countries. Since there is essentially no new arable land that can be cultivated, the increased food supply must primarily come from more intensive cultivation of existing arable land. Furthermore, with intensive agriculture, soil degradation will become a major concern. The world's water resource is also finite, and the increased demands will result in reduced availability of water for agriculture. Urban communities do not generally give high priority to the preservation of agricultural resources, such as land and water. In many highly populated countries, food and fiber needs are being met by irrigating up to 75% of the arable land and introducing high yielding cultivars of most grain crops that have higher input use efficiency thus maximizing production. In addition, the benefits humans derive from natural ecosystems, such as marketable products and goods (i.e., timber, fish, pharmaceuticals), recreational opportunities (i.e., camping, boating, hunting, hiking, fishing), maintaining biodiversity, aesthetic and spiritual experiences, and other services (i.e., erosion control, water purification, carbon sequestration, oxygen production), are being threatened by the growing human population through habitat destruction and air and water pollution. In addition to these stresses, there is a threat of global climate change due to increased greenhouse gas concentrations in the atmosphere and the depletion of the ozone layer assumedly due to anthropogenic activities.

Climate change is not a new phenomenon. The planet's climate has changed tremendously over geological time, and the changes are still occurring. However, what appears to be different is the possibility of a new driving force and the cause of the climate change. Changes that were observed over a geological time period now occur over a shorter time span, particularly since the beginning of the industrial revolution. Apparently, human activities are causing climate change. Concentrations of key anthropogenic greenhouse gases, such as carbon dioxide (CO_2), methane (CH_4), nitrous oxide (N_2O), and tropospheric ozone (O_3) have

reached their highest levels ever, primarily due to the combustion of fossil fuels, agriculture, and land-use changes. Pre-industrial concentrations of CO_2, CH_4, and N_2O were about 280 ppm, 700 ppb, and 270 ppb, respectively. Ozone depleting chemicals, such as chlorofluorocarbons (CFC-11) and hydrofluorocarbons (HFC-23), did not exist during that period, and perfluoromethane was about 40 ppt. The current CO_2 concentration is about 380 ppm (increasing at the rate of 1.9 ppm/year), CH_4 is about 1745 ppb (7.0 ppb/year), and N_2O is about 314 ppb (0.8 ppb/year) (IPCC, 2007). Even if we curtail emissions today, these gases will stay in the atmosphere for a long time as the atmospheric lifetimes for these chemicals vary (5 to 200 years for CO_2, 12 years for methane, and 114 years for N_2O). These changes in the atmospheric chemistry are causing the so called "greenhouse" effect (Fig. 14.1(a)).

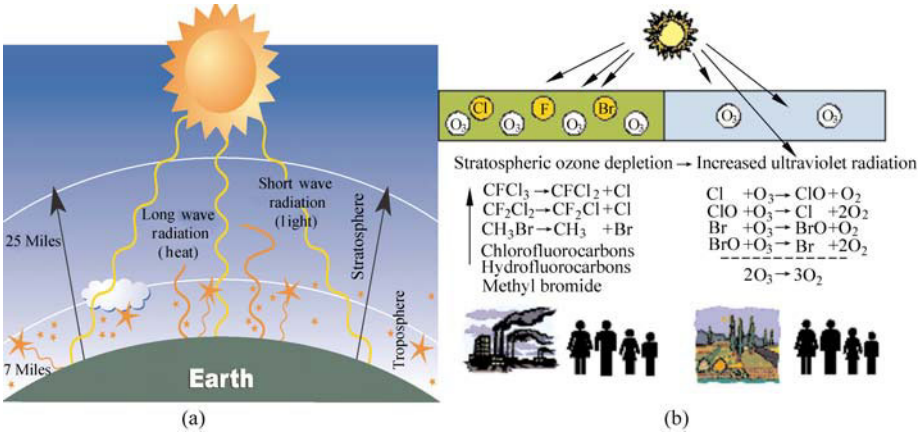

Figure 14.1 Process of global warming (a) and stratospheric ozone depletion (b). Long wave radiation is absorbed by various greenhouse gases in the atmosphere leading to increased temperatures. Anthropogenic emissions of chlorofluorocarbons (CFCs), hydrofluorocarbons, and bromocarbons released in the troposphere move up into the stratosphere. Upon exposure to radiation, atomic chlorine or bromine is released; these react with ozone and convert into oxygen, leading to depletion of ozone. Stratospheric ozone depletion leads to an increase in UV radiation reaching the earth's surface. Adapted with permission from Prasad et al. (2003b)

As the sun's energy passes through the atmosphere and warms the earth's surface, some is reflected back into the atmosphere and dissipates into space. The greenhouse effect refers to accumulation of specific gases that absorb the reflected radiation, effectively trapping heat in the lower atmosphere similar to what occurs in a glasshouse. The most important heat trapping gases are CO_2, water vapor, CH_4, N_2O, CFC-11, and ozone.

If current greenhouse gas emission rates continue, both agricultural and natural ecosystems will face enormous pressure from the stresses caused by these heat trapping gases. Past changes have presumably resulted in an increase in global

temperature of about 0.6°C over the last century. Climate models project even greater warming during the 21st century. The CO_2 concentration is projected to reach 405 ppm to 460 ppm by 2025, 445 ppm to 640 ppm by 2050, and 720 ppm to 1,020 ppm by 2100 (IPCC, 2007). The projected global mean temperature increases (above values in 1990) for those CO_2 stabilization scenarios are 0.4°C – 1.1°C by 2025, 0.8°C – 2.6°C by 2050, and 1.4°C – 5.8°C by 2100. Similarly, the projected mean sea level rise for these same periods is 3 cm – 14 cm, 5 cm – 32 cm, and 9 cm – 88 cm, respectively. These changes in climate were unprecedented during the last 10,000 years. It is also projected that all land areas will warm more rapidly than the global average, particularly at high northern latitudes in the cold season. Projections additionally indicate there will be more hot days, fewer cold days, cold waves, and frost days, and a reduced diurnal temperature range with higher nighttime temperatures. As the world becomes warmer, the hydrological cycle will also become more intense, resulting in more uneven and intense precipitation. This will result in increased summer drying and an associated risk of both droughts and floods. The projected climate change will have both beneficial and adverse effects on environmental as well as socioeconomic systems, but the larger and more abrupt climate changes will cause more adverse effects to be more damaging, particularly on seed-bearing plants.

In addition to the greenhouse effect, another phenomenon known as "ozone hole" is occurring. Ozone, a form of oxygen, plays two roles in the atmosphere. Near the ground, ozone is an air pollutant and a minor greenhouse gas that damages human health and the environment. In the upper atmosphere, known as the stratosphere (10 miles to 30 miles above the earth's surface), ozone forms a layer that helps protect life on earth from the ultraviolet (UV) radiation; sun's harmful rays. The term "ozone hole" refers to the thinning of this layer due to chemical reactions in the stratosphere, especially at higher latitudes, that are caused by the release of ozone-depleting chemicals known as halocarbons (Fig. 14.1(b)). The rate of change in chlorofluorocarbons (CFC) has declined due to the agreement of member countries to the guidelines proposed by the Montreal Protocol. Nonetheless, the concentrations are still high (268 ppb), and other chemicals, such as HFC-23 and perfluoromethane, are present at about 14 ppt and 80 ppt, respectively. Atmospheric concentrations of many of these gases are either decreasing or increasing in response to reduced emissions under the regulations of the Montreal Protocol and its amendments. However, the resident atmospheric times for these chemicals vary greatly (45 years for CFC-11, 260 years for HFC-23, and more than 50,000 years for perfluoromethane), and will have long-term effects on climate systems. Thus, the ozone layer within the stratosphere has thinned substantially, resulting in an increased ground-level UV radiation of about 35% from the pre-industrial period.

There are strong chemical interactions between greenhouse gases and ozone. Ozone and CFCs are minor greenhouse gases. Several gases involved in the ozone depletion chemistry are also greenhouse gases. For example, water vapor,

CH_4, and N_2O can ultimately lead to increases of stratospheric gases (such as NO_2), which can catalytically destroy ozone. It is predicted that increases in greenhouse gases could delay recovery of ozone and may even lead to increased ozone depletion late in the current century (Randeniya et al., 2002; McKenzie et al., 2003). Another chemical feedback is concerned with decreased stratospheric temperatures that could occur as a result of future global warming at the earth's surface. This will tend to slow reactions that destroy ozone at mid-latitudes and thus, may facilitate recovery of the ozone layer (Rosenfield et al., 2002). Ozone depletion at high latitudes proceeds much more rapidly through heterogeneous chemistry on the surfaces of ice and acid crystals that occur when temperatures are below a critical threshold which could be influenced by global warming and delay ozone recovery in the polar region. Several radiative feedback processes also exist (McKenzie et al., 2003). Increases in temperature can lead to changes in cloud cover, rainfall patterns, ice accumulation, and surface albedo. Similarly, radiative changes caused by stratospheric ozone depletion have offset some global warming effects, and could, in the event of future ozone recovery, exacerbate future global warming. Interactions between ozone depletion and global warming are complex. It is suggested that although current ozone depletion is dominated by chlorine and bromine (Fig. 14.1(b)) in the stratosphere, in the longer term (~100 years), the impact of climate change will dominate through the effects of changes in atmospheric dynamics and chemistry (McKenzie et al., 2003).

The main consequence of ozone depletion is increased UV radiation reaching the earth's surface. Ultraviolet radiation is an electromagnetic form of energy that comes from the sun. This energy is classified into several regions based on wavelength, which is measured in nanometers (nm). One nanometer is a millionth of a millimeter. The shorter the wavelength is, the greater the energy of the radiation. The main components of radiation in order of decreasing energy are gamma rays, X-rays, UV, visible light, infrared radiation, microwaves, and radio waves. Ultraviolet radiation is further divided into three categories based on wavelength: UV-A (between 320 nm and 400 nm); UV-B (between 280 nm and 320 nm); and UV-C (between 200 nm and 280 nm). Calculations based on relations with total ozone and total irradiance suggests that UV irradiance has increased since the early 1980s by 6% – 14% in middle and high latitudes of the northern and southern hemispheres. It is projected that every 1% decrease in ozone will increase UV exposure by 2% – 3% in the lower atmosphere.

Shorter wavelength radiation causes more damage to biological systems. UV-A is the least damaging component within the UV spectrum and reaches the earth's surface in large quantities. Both UV-B and UV-C are very harmful. Most UV-C radiation is absorbed by ozone, rarely reaching the stratosphere and never reaching the earth's surface. UV-B radiation is most likely to reach the earth's surface with increased ozone depletion. Factors, such as altitude, latitude, and time of day, influence the amount of UV-B exposure. Current global terrestrial UV-B radiation levels range between 0 and 12 kJ m^{-2} on a given day with near

Equator and mid-latitudes receiving higher doses (Total Ozone Mapping Spectrometer, 2009, http://toms. gsfc. nasa. gov/ery_uv/euv_v8. html). Small increases in solar UV-B radiation can have substantial effects on plants at both the cellular and the whole-plant levels. Relationship and plant responses to various climate change factors are illustrated in Fig. 14.2.

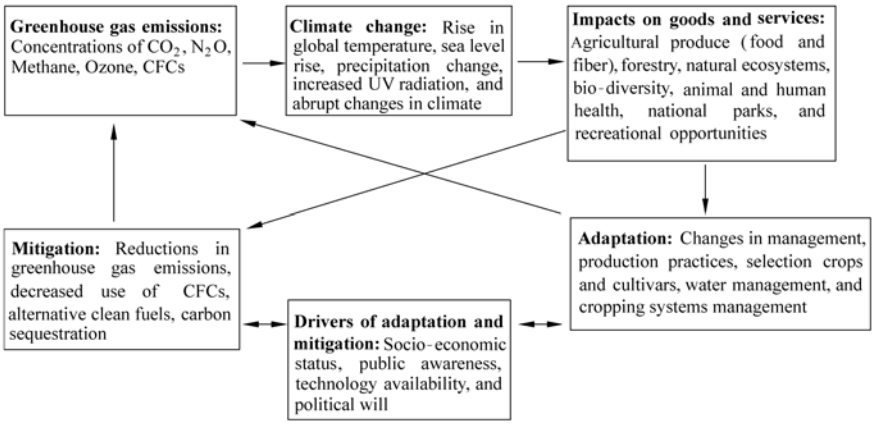

Figure 14.2 Linkages between various facets of greenhouse gas emissions, climate change, ecosystem goods and services, and drivers of adaptations and mitigation

14.2 Abiotic Stress Factors and Crop Yield

Agricultural production and productivity are highly sensitive to changes in climate and weather conditions. Therefore, changes in regional and global climate, particularly climatic variability, affect local as well as global food, fiber, and forest production (Easterling et al., 2007). Atmospheric carbon dioxide, temperature, rainfall patterns, ozone, and UV-B radiation have changed since the dawn of industrial revolution, and the scientific community expects current trends to continue into the future (Houghton et al., 2001; IPCC, 2007). Although crop productivity may benefit from rising CO_2 levels, the increased potential for abiotic stresses, such as increased incidence of drought, flooding, heat waves, and higher UV-B radiation, may challenge community dependence on local agricultural production. Hence, the overall impact of climate change on agriculture will depend on the balance among these climatic factors. These climate change factors have reduced productivity of many crops at both regional and global scales (Teramura, 1983; Lobell and Asner, 2003; Ciais et al., 2005; Lobell et al., 2008). A recent study suggests that, due to climate change, southern Africa could lose production of approximately 30% of its main crop maize (*Zea mays* L.) by 2030, and in southern Asia, production loss of many regional staples, such as rice

(*Orzya sativa* L.), millets (*Pennisetum* sp.), and maize could be up to 10% (Lobell et al., 2008). Similarly, Lobell and Asner (2003) estimated that each degree centigrade of increased temperature during an average growing season may reduce U.S. soybean (*Glycine max* L. Merril) and maize production by 17%. Studies indicate that climate change scenarios that include a combination of factors, such as heat stress, drought, and flooding, reduce crop yields more than a change in a single factor alone (Easterling et al., 2007). Therefore, it is expected that the interaction of abiotic stress factors will influence crop productivity in future climates.

The genotype (thus the genetic background) of a plant defines its range of performance and is determined by a set of heritable traits (Hall, 2001). Consequently, the phenotype produced by a particular genotype results from the interaction of these genotypic traits within the environment where the plant is grown. Therefore, crop yield is determined by genotypic effect, environmental effect, and the effect attributed to the genotype by environmental interaction. In the natural habitat, crop plants are subject to a combination of abiotic conditions that may include one or more stresses, such as heat, drought, and UV-B radiation. Interactions among these factors elicit a variety of responses in plants depending upon the intensity, duration, and timing (developmental stages in a plant species) of the stress. In most cases, abiotic stress conditions reduce crop performance and yield. One important strategy for coping with abiotic stresses is to develop new cultivars with tolerance to the abiotic stress conditions that have minimum yield loss or stable yield under multiple stress conditions. Selection of tolerant cultivars and genetic traits in a population is crucial for developing new cultivars that can adapt to a wide range of environments. This can only be accomplished by subjecting the species of interest to different abiotic stress conditions and determining responses of various growth- and yield-related traits to these stressors. Studies utilizing vegetative and reproductive parameters simultaneously under realistic growth conditions are limited. Therefore, plant processes to a combination of stress factors are not well understood (Rizhsky et al., 2004; Koti et al., 2007; Tegelberg et al., 2008).

14.3 Crop Responses to UV-B and Other Climate Change Factors

Even though UV-B represents a small fraction (0.5%) of total solar radiation, exposure to UV-B at the current and projected levels is known to elicit a variety of responses to all living organisms, including crop plants (Teramura, 1983; Runeckles and Krupa, 1994; Teramura and Sullivan, 1994; Caldwell et al., 1998; Kakani et al., 2003a). Changes in CO_2 and temperature accompanied by emission of ozone-depleting compounds, such as CFCs, CH_4, and N_2O caused by

anthropogenic activities, reduces the thickness and affects distribution of the stratospheric ozone column (IPCC, 2007). The increase in UV-B radiation is closely associated with stratospheric ozone depletion as ozone absorbs the UV-B radiation portion of the solar spectrum (Long, 1991). Relative to the 1970s, the midlatitudes' O_3 column losses for the period of 2002 – 2005 were approximately 3% in the northern and 6% in the southern hemisphere (WMO, 2007). Current global distribution of mean daily doses of UV-B radiation during summer in most crop growing regions ranges from 2 to 9 kJ m^{-2} (McKenzie et al., 2007).

Previous reviews and published studies clearly demonstrate the extent of damage caused by both ambient (Teramura, 1983; Caldwell et al., 1989; Teramura and Sullivan, 1994) and elevated UV-B radiation (Teramura, 1983; Rozema et al., 1997; Krupa, 1998; Searles et al., 2001; Kakani et al., 2003a) on crop growth and yield. Damage varies widely among species and among cultivars of the same species. Teramura (1983) reported that more than 70% of 130 species were significantly affected by elevated UV-B in terms of total biomass production. In a statistical analysis of 77 crop species, mostly based on vegetative growth and a few yield parameters, Krupa (1998) reported sensitivity of more than 50% crop species, including several agriculturally important crops. In a recent review of 129 reports of 35 crop species, including cereals, legumes, oil, sugar, fiber, and tuber crops, enhanced UV-B radiation was shown to directly affect most of the crop growth (Kakani et al., 2003a). Affects included photosynthesis, production of defensive compounds (UV-B absorbing compounds and wax contents), and decreased vegetative growth which led to a myriad of secondary and tertiary effects, including altered crop growth and development. This, in turn, affected light interception which lowered canopy photosynthesis, reduced fruit production and retention, and finally yield.

14.3.1 Specific Effects of UV-B Radiation on Plants

Plants are highly sensitive to UV-B radiation because of their sessile nature. In plants, UV-B radiation damages cell membranes and all organelles within the cell, including the chloroplasts, mitochondria, and deoxyribonucleic acid (DNA) within the nucleus. Damage to these cell organelles directly or indirectly affects basic plant metabolic processes, such as photosynthesis, respiration, growth, and reproduction. Consequently, UV-B damage harms crop yield and quality. An overview of various processes affected by UV-B radiation at cellular and plant levels is presented in Tables 14.1 and 14.2. However, the effect of UV-B radiation varies with intensity and duration of irradiation and stage of plant development. In addition, sensitivity to UV-B radiation varies widely among plant species and cultivars of the same species. Studies on physical or physiological reasons for differences in tolerance to UV-B radiation among species need further attention.

Table 14.1 Effects of exposure to UV-B radiation on various physiological processes in plants. Adapted with permission from Prasad et al. (2003b)

Trait	Decreases	Increases	No Effect
DNA damage		✓	
Protein destruction		✓	
Fatty acid destruction		✓	
Photosynthesis	✓		
Photosystem Ⅰ	✓		
Photosystem Ⅱ	✓		
Rubisco	✓	✓	
Stomata closure			
Chlorophylls	✓		
Flavonoids		✓	
Waxes		✓	
Epidermal hairs		✓	
Cuticle thickness		✓	
Reproduction			
Pollen viability	✓		
Pollen tube growth	✓		
Fertilization	✓		
Cell division	✓		
Cell size			✓

Table 14.2 Effects of exposure to UV-B radiation on various growth and yield parameters in plants. Adapted with permission from Prasad et al. (2003b)

Trait	Decreases	Increases	No Effect
Photosynthesis	✓		
Stomatal conductance	✓		
Phenology			✓
Senescence		✓	
Plant height	✓		
Branching		✓	
Leaf area	✓		
Leaf growth and expansion	✓		
Leaf thickness		✓	
Specific leaf weight		✓	
Dry mater production	✓		
Flowering	✓	✓	
Fruit (grain) number	✓		
Fruit (grain) weight	✓		
Yield	✓		
Quality	✓		
Disease incidence			
Powdery mildew	✓		
Rust		✓	
Insect	✓	✓	

14.3.1.1 Genetic (DNA) and Ultra-Structural Damage

Ultraviolet radiation is efficiently absorbed by most organic substances, which causes many photochemical reactions in the living cells. The nucleus of each cell consists primarily of genetic material in the form of DNA. Nuclear DNA is inherently unstable and can be damaged by spontaneous or metabolically induced changes generated by environment. DNA is highly sensitive to UV-B radiation which can cause damage resulting in heritable mutations if not repaired and thus, can significantly influence various physiological processes. DNA is considered the primary absorbing compound in the cell in the UV-B region of the spectrum. Exposure of DNA to UV-B radiation can result in: (1) breakage of bonds in the DNA and DNA-protein cross links; (2) chromosomal breakage; (3) chromosomal aberrations; and (4) exchange and production of toxic and mutagenic photoproducts (e.g., cyclobutane pyrimidine dimmers (CPDs), 6, 4 pyrimidine- pyrimidone or 6, 4-photoproduct, thymine glycols, and pyrimidine hydrates). These changes in DNA alter transcription, replication, and recombination of genes and cause significant changes in plant metabolic and genetic processes. Proteins, membrane lipids, and other essential substances in the cell can also be altered through exposure to UV-B radiation, resulting in protein degradation and lipid peroxidation. These damages influence genetic makeup and affect protein synthesis, enzyme activities, and gene expression. All cellular life-forms possess DNA repair enzymes that recognize chemically modified bases, including those formed by UV radiation. Furthermore, cells have evolved through a variety of biochemical mechanisms to restore the integrity of the genetic material after DNA damage and retain its stability. These processes are called “DNA repair mechanisms.” There are two main mechanisms of DNA repair of CPDs and 6, 4-photoproduct, photo repair, and dark repair. In photo repair, the enzyme photolyase mediates the repair by forming a complex with the CPDs and 6, 4-photoproducts in a lesion-specific matter that is stable in the absence of light. In dark repair, the 6, 4-photoproducts are removed from the DNA by nucleotide excision of the damaged oligonucleotide, gap-filling DNA synthesis, and restore ligation in the correct pairing order (Sancar, 1994).

Exposure to UV radiation can result in changes in the ultrastructure of various cellular components in many plant species. Ultrastructural changes are generally caused by damage and dilation of the nuclear membrane. UV-B radiation causes damage to chloroplast structure through swelling of chloroplasts, rupture of the chloroplast wall, dilation of thylakoid membranes, disruption of the thylakoid structure, and disintegration of the double membrane that envelops surrounding chloroplasts accompanied by the accumulation of large starch granules (He et al., 1994). It is also known to cause swollen cisternae in the endoplasmic reticulum, damage to the mitochondria and plastids, and vesiculation of plasmalemma and tonoplasts. In addition, UV-B radiation alters cell shape and structure. These changes in ultrastructure can potentially affect various physiological processes, such as cell division, photosynthesis, respiration, and reproduction. However,

plants have some defense and repair mechanisms that help minimize and deal with expected damages at the cellular level by removing or repairing damaged parts, and at the whole-plant level by producing UV-B absorbing compounds and pigments in leaves. These compounds mainly include flavonoids and anthocyanins, which are accumulated in the vacuoles of the epidermal and subepidermal cell layers.

14.3.1.2 Plant Photosynthesis

Photosynthesis is the process by which plants convert carbon dioxide and water into carbohydrate in the presence of sunlight. The photosynthetic apparatus is one of the important target sites of UV-B damage (Vu et al., 1982; 1984; Allen et al., 1997). Direct effects of enhanced UV-B radiation on photosynthesis include: (1) damage to ultrastructure of chloroplasts that are principal sites for photosynthesis; (2) impairment of light energy transfer (i.e., electron transport system of photosystem Ⅱ (PSⅡ) and to a lesser extent, photosystem Ⅰ (PSⅠ); (3) decrease in activity of Ribulose 1, 5-bisphosphate carboxylase/oxygenase (Rubisco); (4) decreased carbon dioxide fixation and oxygen evolution; and (5) decreased starch and chlorophyll content. Components affected in PSⅡ are the water-oxidizing system, light-harvesting complex, and synthesis of chlorophyll a/b-binding proteins. Exposure to UV-B radiation decreases both activity and concentration of Rubisco. UV-B inactivation of Rubisco could mainly be due to modification of the peptide chain, degradation of the protein, and/or diminished transcription of the gene. As indicated previously, almost every facet of photosynthetic machinery can be directly or indirectly damaged by exposure to UV-B radiation. However, electron transport mediated by PSⅡ appears to be the most sensitive (Fiscus and Booker, 1995). Within PSⅡ, all parts from the Mn binding sites to the plastoquinone acceptor sites on thylakoid membrane are sensitive.

In addition to the direct effects of UV-B radiation, photosynthesis may also be indirectly affected by: (1) induction of stomatal closure; (2) decreased individual leaf area and total canopy leaf area; (3) changes in leaf thickness and anatomy; and (4) changes in canopy architecture and morphology. All these changes can potentially decrease light interception and gas exchange, which results in lower canopy photosynthesis. However, the stomatal closure mechanism reduces evapotranspiration water losses and increases water use efficiency, which leads to increased plant growth and yield.

14.3.1.3 Plant Morphology and Architecture

Although UV-B radiation constitutes a small portion of the solar spectrum, it induces a range of strong morphological effects in plants, including leaf thickness, leaf discoloration, cotyledon curling, inhibition of hypocotyl growth, stem and leaf elongation, axillary branching, and shifts in root-shoot ratio (Jansen, 2002). In most plant species, leaves exposed to UV-B radiation initially develop irregular

patches (Fig. 14.3). With continued exposure to UV-B radiation, these chlorotic patches become brown necrotic spots and die (Singh et al., 2008a). The appearance of chlorotic and necrotic patches is generally attributed to decreases in leaf chlorophyll content (Zhao et al., 2003).

Elevated UV-B radiation can result in slower stem extension rates, shorter internode lengths leading to shorter plant height, decreased individual leaf size, fewer leaves leading to less leaf area, and fewer tillers and branch lengths (Kakani et al., 2003b; Reddy et al., 2003; Zhao et al., 2003). Overall, these morphological changes result in a smaller canopy. Plant architecture is modified by UV-B radiation. When exposed to UV-B radiation, both attached and detached tendrils of pea plants form spiral coils. In addition, enhanced UV-B radiation causes increased leaf epicuticular wax and stomatal index, and reductions in thickness of palisade and mesophyll tissues without altering the thinness of the epidermal layers (Kakani et al., 2003b).

(a) Control (b) Chlorotic patches (c) Necrotic patches

Figure 14.3 Typical symptoms of exposure to UV-B radiation on control leaves of cotton plants: (a) No symptoms, (b) Initial chlorotic patches, and (c) Necrotic patches after prolonged exposure. Adapted with permission from Prasad et al. (2003b)

14.3.1.4 Plant Development and Growth

Elevated UV-B radiation can delay flowering time in several different crops (Kakani et al., 2003a; Singh et al., 2008a). However, in some crops, UV-B radiation does not influence early bud or flower development, or the time to first flower (Sinclair et al., 1990). UV-B radiation does affect flower size, anther number, and pollen production, germination, and tube growth in many plant species (Kakani et al., 2003a). Cotton (*Gossypium hirsutum* L.) flowers produced on plants exposed to elevated UV-B were smaller due to reduced petal and bract size, and had fewer anthers (Kakani et al., 2003b). In general, reproductive organs of most plant species (pollen and ovules) are highly protected by sepals, petals, and ovary walls. In these plants, pollen is susceptible after it falls on the stigma. Exposure to UV-B radiation decreases pollen germination and rate of pollen tube growth by 10% – 25% in several crop species (e.g., maize, rye (*Secale cerale* L.) and tobacco (*Nicotiana tabacum* L.); Torabinejad et al., 1998). Increased UV-B radiation decreased total pollen production, pollen germination, and tube growth (Koti et al., 2004).

Consequently, it affects the fertilization process, which results in fewer seeds in sensitive plants. However, once the pollen tube penetrates the stigma surface, the walls of the style and ovary may provide some protection against UV-B radiation.

Growth is the rate of increase in weight and size of plant organs, such as leaf, stem, or root. Dry matter is the total weight of all plant organs. Exposure to UV-B radiation caused decreases in growth of leaves and stems in many plant species in both controlled environment and field studies (Kakani et al., 2003a). However, the effects of UV-B radiation on plant growth and dry matter accumulation were generally smaller under field conditions than under controlled environmental conditions (Caldwell et al., 1994; Olszyk et al., 1996). The decrease in growth of leaves, main stem, and branches is due to reduced cell division rather than decreased cell size. Reduction in plant height from exposure to UV-B is due in part to decreased levels of a growth hormone (indole acetic acid) in plants. The smaller and more compact canopy reduces the amount of UV-B intercepted by the plant, but also reduces the potential or total photosynthetic area essential for growth. The combination of these various factors results in decreased total dry matter or biomass production. In regard to exposure to UV-B radiation, the majority of crop species (60%) show a reduction in dry matter production, a moderate 24% show no change, and only 8% of crop species show an increase in dry matter production (Kakani et al., 2003a).

14.3.1.5 Plant Yield and Quality

Yield is the economic product harvested from plants (e.g., grain from wheat (*Triticum aestivum* L.), seeds from pods of soybean, roots from carrot (*Daucus carota* L.), seed and lint from cotton). Similar to changes in dry matter production, change in yield of crop species from exposure to UV-B varies with species. Some species (e.g., pea (*Pisum sativum* L.), barley (*Hordeum vulgare* L.), and mustard (*Brassica juncea* L.)) show severe reduction; others (e.g., cowpea (*Vigna unguiculata* L.), millets, and tobacco) show less or no yield reduction. The main causes of yield loss are reduced fruit (grain) number due to failure in fertilization, abortion of fruiting structures, and decreased fruit size due to reduced supply of assimilates to the growing sink (fruits). Kakani et al. (2003a) reviewed responses of various crops to UV-B radiation in both controlled environmental and field studies; almost half the studies showed that enhanced UV-B radiation decreased yield, the other half showed no UV-B effect on yield, and a few studies showed increased yields. These differential responses were due to variability in intensity of UV-B radiation. The UV-B radiation in these studies varied and ranged from $2.5-63$ kJ m^{-2} d^{-1} simulating $10\%-50\%$ of stratospheric O_3 depletion. In addition, the variable responses can also be due to differences in responses of cultivar and crop species to UV-B radiation.

Ultraviolet-B radiation also affects the quality of the economic product. For example, seed oil and protein content in soybean are reduced on exposure to UV-B radiation. Enhanced UV-B radiation decreased grain size and increased total

nitrogen and storage protein (glutelin), thus affecting the taste of food products (Hidema et al., 2005). Similarly, Gao et al. (2004) investigated UV-B effects under field conditions and showed that increased UV-B not only decreased dry matter production and grain yield, but also affected grain quality by decreasing protein, sugar, and starch levels while improving lysine levels. Overall, studies conducted to date suggest that climate models predict UV-B radiation will decrease the growth, yield, and quality of crops (Hidema and Kumagai, 2006).

To date, the most comprehensive knowledge on the impact of UV-B radiation on various physiological, growth, and yield components has been developed at Mississippi State University within controlled environmental growth chambers maintained at optimum water, temperature, and nutrient conditions (Reddy et al., 2001; Reddy et al.; 2002, Reddy et al., 2003). Recently, Reddy et al. (2009) used an environmental productivity index to develop functional algorithms to accurately quantify and model impacts of UV-B radiation on the physiology, growth, development, and yield of cotton. On the basis of the critical limit, defined as 90% of optimum or the control, they showed that canopy photosynthesis and total dry weights were most sensitive with lower critical limits of 7 kJ m^{-2} d^{-1} and 7.3 kJ m^{-2} d^{-1}, respectively, compared with stem elongation (8.7 kJ m^{-2} d^{-1} UV-B) or leaf expansion (11.2 kJ m^{-2} d^{-1} UV-B). The identified critical limits and algorithms are currently being incorporated into the mechanistic cotton model GOSSYM to predict yields under present and future climate change conditions across the U.S. cotton belt (Liang et al., 2008). The evaluation and understanding of the impact of UV-B radiation on yield and yield quality of economically important crops requires further study under both field and controlled environmental conditions. The knowledge gained should be incorporated into existing crop simulation models.

14.3.1.6 Pest Damage

The impact of elevated UV-B radiation on plant species is well understood, but knowledge of the effects of UV-B on insect pests and disease-causing pathogens (fungi and bacteria) is limited. Research conducted thus far has shown both a decrease and an increase in disease and pest damage in response to increased UV-B radiation. Effects of UV-B on diseases and insects could be attributed to direct effects on their growth and indirect effects through changes in tissue characteristics and/or composition. Caldwell et al. (2003) summarized the literature and concluded that higher levels of UV-B radiation generally led to less herbivore and/or reduced insect growth compared with lower levels of UV-B. The magnitude of the effects was sizable, with potential ecosystem-level consequences for species composition, organic matter decomposition, and nutrient cycling. Solar UV-B can affect insect herbivores through reduced growth, survivorship, and fecundity (Lindroth et al., 2000) through changes in leaf characteristics (appearance and composition). Insects can perceive UV-B (Mazza et al., 2002), modify their behavior to avoid UV-B radiation, and protect themselves by regulating their cuticular pigmentation to

screen damaging wavelengths (Gunn, 1998). Studies demonstrated that thrips consumed less leaf tissue and Lepidopeteran larvae had lower survivorship in laboratory assay when fed on leaves grown under near-ambient solar UV-B compared with leaves from UV-B excluded plots (Mazza et al., 1999; Zavala et al., 2001). The lower larvae survival was attributed to higher levels of soluble phenolics and lower lignin content in the foliage exposed to UV-B radiation. Similarly, bioassay studies suggested that adult specimens of leaf beetles tend to preferentially feed on plants not exposed to UV-B if given the opportunity to choose between UV-B exposed and unexposed plant materials (Ballare et al., 1996). However, the impact of UV-B radiation on mechanisms of other behavior of adult insects, such as oviposition and breeding, that are more relevant under natural conditions are not well understood and need investigation.

Ultraviolet-B radiation changes the chemistry, morphology, and physiology of plants. This can directly influence pest and disease incidence. For example, UV-B can affect leaf nitrogen content, available carbohydrate, and fiber (Zavala et al., 2001) indirectly influencing insect growth and survival. Plants exposed to UV-B can also stimulate production of secondary metabolites, i.e., phenolics and jasmonic acid (Mazza et al., 2000; Izaguirre et al., 2003; Izaguirre et al., 2007) which can influence insect incidence or behavior by acting as either a deterrent or attractant (Harborne, 1988). Some insects protect themselves from UV-B radiation by feeding on the underside of the leaves where UV-B penetration is lower (Paul et al., 1997) and avoiding areas of plants where defensive chemicals accumulate (McCloud et al., 1992). UV-B radiation effects on insect herbivores can also have consequences on parasitoids by affecting host quality (Soler et al., 2005) which leads to decreased survival and growth of parasitoid larvae (Holton et al., 2003).

Plant pathogen and disease incidence, as well as intensity, are also influenced by exposure to UV-B radiation (Raviv and Antignus, 2004). The effect of UV-B on plant pathogens can occur either through direct effects on various stages of pathogen development, such as spore germination, germ tube extension (Paul et al., 1997; Fourtouni et al., 1998), and sporulation (Ensminger, 1993) or indirectly by influencing host-plant resistance by damaging cells, decreasing plant growth and morphology (decreasing leaf and cuticle thickness), or modifying gene expression (Caldwell et al., 2003). However, it is very difficult to differentiate the effects of UV-B radiation on the host from those on the pathogen itself under field conditions. Stimulated compounds in plants that are localized in epidermis or mesophyll can also function as phytoalexins or antifungal compounds (Keller et al., 2003). Most studies on the effect of UV-B on fungi have focused on reproductive development. Fungal propagules showed high sensitivity (Rotem and Aust, 1991), but some exhibited enhanced sporulation in response to UV-B radiation. However, sensitivity of fungi to UV-B is not always reflected in a reduced infection of the plant (Raviv and Antignus, 2004). In fact, the spread of several disease-causing fungi can be decreased by filtering out UV-B radiation

(Fourtouni et al., 1998). In contrast, several pathogenic fungi (e.g., wheat leaf blotch causing fungi (*Septoria tritici*)) exhibit reduced infection under UV-B (Paul et al., 1997). In general, increasing disease severity primarily involves modification of host plant tissues, whereas decreased severity appears to involve either host plant changes or direct UV-B damage to the pathogen (Caldwell et al., 2003). Despite linkages between plants and herbivores, limited information is available on impacts of UV-B on host plant-insect interactions. A more definite understanding of the effects of UV-B on diseases and insects is needed to accurately predict consequences of ozone depletion on plant ecosystems.

14.3.2 Strategies for Protection against UV-B Radiation

Plants have evolved through several mechanisms by which they protect themselves from the damaging effects of UV-B radiation (Table 14.3).

Table 14.3 Protective mechanisms against damage by UV-B radiation in plants. Adapted with permission from Prasad et al. (2003b)

Repair mechanisms
• DNA repair: photo-reactivation enzymes (photolyase); excision repair by removing damaged part of DNA; bypass damaged DNA and fill gaps later from sister duplex.
Defense mechanisms
• Increase reflectance to avoid entry of UV-B radiation through cuticle wax, leaf hairs, and trichomes.
• Increase absorption of UV-B radiation at epidermal cells by production of pigments, such as flavonoids, carotenoid, and anthocyanins.
• Production of antioxidant enzymes (e.g., superoxide dismutase, ascorbate peroxidase, glutathione reductase) and compounds (ascorbates, alpha-tocopherol, and polyamines) that protect against oxidative stress caused by UV-B exposure.

14.3.2.1 Repair Mechanisms

Plants have constantly been exposed to sunlight, including UV radiation before formation of the ozone layer. In the process of evolution, certain plants developed a tolerance to solar UV-B radiation that limits the amount of DNA damage they suffer. All cellular life-forms possess DNA repair enzymes that recognize chemically modified bases, including those formed because of UV radiation. Furthermore, cells have evolved through a variety of biochemical mechanisms to restore the integrity of the genetic material after DNA damage and thus retain its stability. These processes, called "DNA repair mechanisms," include photo-reactivation, excision repair (nucleotide and base excision repair), and post-replication repair. Photoreactivation mainly involves photolyase, an enzyme responsible for the direct splitting of cyclobutane pyrimidine dimers. Excision repair is done by

nicking the damaged part of DNA, removing the bases in the damaged strand, and synthesis of the gap. In post-replication repair, DNA damage is bypassed during DNA replication and the resulting gaps are filled in later using the information from the sister duplex. Such DNA repair mechanisms are observed in both nuclear and chloroplast DNA. However, different plant species and varieties within a species vary in their ability to repair the damage caused by UV-B.

14.3.2.2 Defense Mechanisms

Plants are exposed to UV-B radiation as it passes through the epidermal layers to reach the sensitive sites. Therefore, the surface structure, physiology, and composition of the epidermal layer play an important role in protecting (shielding) cells from UV-B radiation. The important surface characteristics of the epidermal layer, which reduces penetration of UV-B radiation, include protective structures, such as trichomes and wax coating. These structures have the capacity to attenuate, absorb, and reflect UV-B radiation because of their optimal structure and presence of chemical compounds.

Studies have also shown that UV-B radiation leads to oxidative stress in plant systems as observed in many other abiotic (temperature and light) and biotic (insects and diseases) stress conditions. Therefore, as a result of UV-B exposure, plants increase production of flavonoids and antioxidant enzymes (e.g., superoxide dismutase, ascorbate peroxidase, and glutathione reductase) that provide defense against UV-B radiation. Other chemicals, such as alpha tocopherol (vitamin E), peroxidases, ascorbates, beta carotene, and polyamines, provide protective functions against UV-B damage.

Flavonoids are produced and mainly deposited in epidermal and mesophyll layers and leaf hairs. The presence and distribution of flavonoids at different locations can provide an efficient screen to UV-B radiation. Flavonoids are very effective in screening (absorbing) UV-B radiation and reducing damage to sensitive cell organs (i.e., DNA, chloroplasts, and mitochondria). In addition, anthocyanins and carotenoids could potentially screen UV radiation, particularly in flowers, and provide protection to pollen grains. These compounds attenuate the damaging solar UV-B radiation, but they transmit photosynthetically active radiation through the epidermis. Thus, these compounds do not directly influence photosynthesis and other physiological processes.

UV-B-mediated alterations in plant growth and yield are dependent upon species sensitivity and combined responses to other abiotic and biotic stresses (Teramura and Sullivan, 1994). The inconsistencies may be explained by either genotypic differences in UV-B sensitivity, different environmental conditions under which plants were grown, and/or the intensity of UV-B (Musil et al., 2002; Kakani et al., 2003a). A bulk of these studies conducted in growth chambers, greenhouses, or the field use different types of exposure systems that may be responsible for interpreting the results as intraspecific differential sensitivity of crop species (Runeckles and Krupa, 1994).

14.3.3 Crop Response to Atmospheric CO_2 Concentration

The projected increase in atmospheric CO_2 is expected to enhance growth and production of agricultural terrestrial plants (Easterling et al., 2007). Studies have also shown that the effects of elevated CO_2 on plant growth and yield may depend on photosynthetic pathway, plant species, growth stage, and management practices, such as water and nitrogen applications (Jablonski et al., 2002; Kimball et al., 2002; Ainsworth and Long, 2005). Crops with C_3 photosynthetic pathway respond markedly to increasing CO_2 concentrations compared to C_4 crops. Common C_3 crops are small grain cereals (wheat, rice, barley, oat (*Avena sativa* L.), and rye); grain legume or pulses (soybean, peanut (*Arachis hypogaea* L.), various beans (*Phaseolus* sp.) and peas), root and tuber crops (potato (*Solanum tuberosum* L.), cassava (*Manihot esculenta* L.), sugar beet (*Beta vulgaris* L.), and yams (*Dioscorea* sp.), and most oil, fruit, nut, vegetable, and fiber crops. Common C_4 crops are maize, sugarcane (*Saccharum officinarum* L.), sorghum (*Sorghum bicolor* L. Moench), millet, and many tropical and subtropical zone (warm-climate) grass species. Elevated CO_2 generally increases both above- and belowground biomass, volume and length of roots, and biomass allocation to roots (increased root-shoot ratio). Root and tuber crops tend to have a greater yield response to elevated CO_2 than seed or forage crops. Increased photosynthesis also favors symbiotic nitrogen fixation in legumes. Since legumes can supply nitrogen via symbiotic nitrogen fixation, legumes (both seed and forage) respond relatively more to increased CO_2 than non-legumes. Seed yields generally increase in a nonlinear fashion in response to increased CO_2; however, this increase in not as much as photosynthesis because part of the fixed carbon goes to increased vegetative biomass. Averaged across several species and under unstressed conditions, analysis shows that, compared with the current CO_2, crop yields increased at 550 ppm, CO_2 was 10%−12% for C_3 crops and 0%−10% for C_4 crops (Ainsworth et al., 2004; Gifford, 2004; Long et al., 2004). However, in a recent analysis of the FACE (free-air-carbon-dioxide enrichment) experimental results, Long et al. (2005, 2006) argued that crop responses to elevated CO_2 might be lower than previously thought because of overestimation of responses using crop models. Others have suggested that these new analyses are in fact consistent with previous findings from both FACE and other experimental settings (Tubiello et al., 2007). It is recognized that the models may overestimate the actual field-level responses because of many limiting factors including disease and insects, weeds, soil, water, and nutrient quality, which are neither well understood at large scales nor well implemented into the models (Easterling et al., 2007). In addition, the increase of CO_2 is subjected to a considerable interaction with other climatic factors; therefore, the rising CO_2 can not be assumed to be a single factor because of the associated changes in the temperature and other climatic factors (Giorgi et al., 1998; Prasad et al., 2002; Prasad et al., 2003a, b; Prasad et al., 2005; Zoltán, 2005) that directly affect crop growth and development. The beneficial affects of

elevated CO_2 on seed yields are decreased for several crops under elevated temperatures (Prasad et al., 2002; Prasad et al., 2003a; Prasad et al., 2006a).

14.3.4 Crop Response to Temperature

The inferences from global circulation model simulations indicate that earth's mean surface air temperature warming for a doubling of atmospheric CO_2 is expected to increase by 2°C – 4.5°C (IPCC, 2007). Additionally, it is projected that heat waves will be more intense, more frequent and longer lasting in future warmer climates (Meehl and Tebaldi, 2004). Daily minimum temperatures (nighttime temperature) are projected to increase faster than daily maximum temperature (daytime), leading to decreases in diurnal temperature (IPCC, 2007). For example, in summer 2003, Europe experienced an extreme climate anomaly that caused July temperatures to increase 6°C above the long-term mean and resulted in an approximate 30% reduction in terrestrial gross productivity across Europe (Ciais et al., 2005). Day/night temperatures greater than 36°/30°C commonly occur during a crop's life cycle in most of the world's tropical growing regions where daytime temperatures can occasionally reach up to 45°C (Warrag and Hall, 1983, Ismail and Hall, 1998; Hall, 2004a; National Climate Data Center, 2008). The projected global temperature increase will subject these locations to an even higher temperature regime, particularly for night temperatures (IPCC, 2007).

Temperature is the most important abiotic factor that determines plant adaptation to different climatic zones and seasons of the year. Most annual crops can be described as being adapted to either the cool season or warm season (Hall, 2001; Cutforth et al., 2007) depending on their temperature range of survival ($T_{max} - T_{min}$; Reddy and Kakani, 2007). Temperature also plays an important role in determining the sowing date of a crop species based on seed germination and survival of the seedlings. The minimum threshold for seed germination differs among crop species (e.g., soybean 10°C, cowpea 18°C, upland cotton 16°C, and maize 14°C; Ismail and Hall, 1997; Hall, 2001; Cutforth et al., 2007). Similarly, optimum temperatures depend upon the developmental stage of the plant and species. The optimum temperature for peanut growth and development is between 25°C and 30°C (Williams and Boote, 1995), whereas the optimum temperature for pollen germination and tube growth ranges between 30°C and 34°C (Kakani et al., 2002). The cardinal temperatures for growth and development of a crop species are also process dependant (Reddy et al., 1997a; Reddy and Kakani, 2007; Reddy et al., 2007a). A temperature stress could be anything below and/or above the optimum which influences the functionality and success of the biochemical pathway. This may reduce efficiency of the particular phase of development, resulting in a loss of economic yield (Singh et al., 2008b). Studies on cowpea and common bean have shown that heat stress during floral bud development can reduce fruit set because of damage to the pollen mother cells, resulting in poor anther dehiscence and

reduced pollen number and viability (Warrag and Hall, 1983; Warrag and Hall, 1984; Gross and Kigel, 1994). Peanut (Prasad et al., 1999) and sorghum (Prasad et al., 2008) plants were more sensitive to high-temperature stress during microsporogenesis (just prior to flowering) and at flowering. High-temperature stress during pre-flowering stages mainly influences viability of male or female gametes, whereas at flowering, high-temperature stress decreases pollen dehiscence, germination, and tube growth, resulting in decreased fruit set and grain numbers. A negative association between increased daily mean temperature and reduction in yield has been reported in many crops (Ismail and Hall, 1998; Walton et al., 1999). Lobell and Asner (2003) projected an approximate 17% yield reduction in corn and soybean for each degree centigrade increase in average growing season temperature above the optimum in the U.S.. Most grain crops (i.e., peanuts, rice, wheat, soybean, and maize) are already being grown above optimum growth temperature; further increases in temperature due to climate change or increased frequencies of high-temperature stress during sensitive periods of reproduction will decrease crop yields (Reddy et al., 1997b; Lobell and Asner, 2003; Prasad et al., 2003a; Boote et al., 2005; Prasad et al., 2006a; Prasad et al., 2009).

14.3.5 Crop Response to Drought

Climate change is predicted to bring regional-scale precipitation extremes, causing both flooding and drought in certain areas (Giorgi et al., 1998). Most model simulations predict decreased precipitation by the end of the 21st century in subtropical regions (IPCC, 2007). Increased precipitation extremes are also likely in major agricultural production areas, e.g., southern and eastern Asia, eastern Australia, and northern Europe (Christensen et al., 2007). The 2003 summer drought in Europe caused a severe reduction in corn yield in eastern Europe (Ciais et al., 2005) and in forest biomass productivity in southern Europe (Gobron et al., 2005).

Water shortage is one of the most important factors limiting crop production worldwide due to geographic limited availability of irrigation water or the occurrence of drought mainly caused by reduced rainfall. Demand for drought-tolerant genotypes will increase due to diminishing water resources and alteration in precipitation patterns under climate change scenarios (Longenberger et al., 2006; Christensen et al., 2007). Understanding the detrimental effects of drought on plant processes and identifying the tolerance mechanisms will help breeders to develop tolerant genotypes.

Drought stress induces several changes in various physiological, biochemical, and molecular components of photosynthesis. Drought can influence photosynthesis through either pathway regulation by stomatal closure and decreasing flow of CO_2 into mesophyll tissue or by directly impairing metabolic activities. The main metabolic changes are declines in regeneration of Ribulose bisphosphate (RuBP) and Rubisco protein content, decreased Rubisco activity, impairment of ATP

synthesis and photophosphorylation, and decreased inorganic phosphorus. Effects of drought on whole plant processes are manifold and can influence germination, emergence, leaf, root, tillers, stem development and growth, dry matter production, floral initiation, panicle exertion, pollination, fertilization, seed growth, seed yield, and seed quality. For most crop plants seed is the starting point of the growth cycle. Seeds begin biochemical changes shortly after imbibing water. Water uptake and imbibition of water by seed are dependent upon the soil water availability. Drought delays imbibition and thus can lead to decreased germination rates and total germination percentage. Leaf expansion is one of the growth processes most sensitive to drought (Alves and Setter, 2004; Reddy et al., 2009). This sensitivity is expressed in terms of smaller cells and reductions in the number of cells produced by leaf meristems (Randall and Sinclair, 1988; Tardieu et al., 2000). Drought stress can also influence total leaf area through its effect on the initiation of new leaves, which decreases under drought stress. Drought and heat stress alter the initiation and duration of developmental phases. In most cases, the length of time from floral initiation to anthesis is decreased by moderate drought and/or temperature stress, but is increased by severe stress. Drought stress during panicle development inhibits the conversion of vegetative to reproductive phase, and plants remain vegetative until this stress is relieved. Panicle initiation in sorghum was delayed by as many as 2 to 25 days and flowering by 1 to 59 days under drought stress, with more severe effects when drought was imposed at both early and late stages of panicle development (Craufurd et al., 1993). Drought stress inhibits pollen development and causes sterility. It also shortens the spike development duration (period during which potential kernel or seed numbers are determined) and the grain filling duration (during which the grain or seed weight is determined). Drought stress during later stages of panicle or flower development decreases seed numbers and can also increase the duration from seed set to full seed growth. Drought affects yield by limiting seed numbers caused by either influencing the amount of dry matter produced by the time of flowering (this is particularly true for determinate plant types), or by directly influencing pollen or ovule function which leads o a decreased seed set. Secondarily, drought influences seed filling by limiting the assimilate supply, leading to smaller seed size and lower yields.

Past difficulties have been associated with the identification of physiological traits that could be used as indicators of drought tolerance (Longenberger et al., 2006). However, various plant characteristics such as water use efficiency (Condon et al., 2002), root characteristics (Basal et al., 2003), canopy temperature (Patel et al., 2001), leaf water potential and leaf relative water content (Chiulele and Agenbag, 2004), and stomatal conductance (Bota et al., 2001; Flexas et al., 2002; Medrano et al., 2002) have been used as possible indicators to assess drought tolerance in crop species. Understanding the mechanisms of drought tolerance in crop species, particularly those adapted to dry conditions, will help plant breeders

improve agronomic performance of these species by incorporating the superior traits into new species or cultivars (Clavel et al., 2005).

14.3.6 Crop Response to Multiple Abiotic Stress Factors

In natural habitats, plants are routinely subjected to a combination of abiotic factors. Under climate change scenarios, plants will be exposed to CO_2, UV-B radiation, temperature, and water stress simultaneously and their performance can be assessed only when grown under these multiple abiotic stress conditions. Many recent studies suggest that temperature and precipitation changes in future decades will modify, and often limit, the direct effect of CO_2 enrichment on plants (Easterling et al., 2007). For instance, high temperature during flowering may lower positive CO_2 effects by reducing reproductive traits such as grain number, size, and quality in several crops (Reddy et al., 1997b; Prasad et al., 2002; Prasad et al., 2003a,b; Baker, 2004; Prasad et al., 2006a; Caldwell et al., 2005). Prasad et al. (2006a) showed that adverse effects of high temperature on reproductive processes (seed set and harvest index) of sorghum were more severe at elevated CO_2 than at ambient CO_2. Similarly, for rice (Matsui et al., 1997) and red kidney bean (Prasad et al., 2002), the ceiling temperature for a seed set was 2˚C cooler for plants grown at elevated CO_2 than at ambient CO_2. Increased temperatures may also reduce CO_2 effects indirectly by increasing water demand. Rainfed wheat grown at 450 ppm CO_2 demonstrated yield increases with temperature increases of up to 0.8˚C, but declines with temperature increases beyond this point (Xiao et al., 2005). Future CO_2 levels may favor C_3 over C_4 plants (Ziska, 2003; Ainsworth et al., 2004; Gifford, 2004; Long et al., 2004); however, the opposite is also expected because of coupled increases in temperature, UV-B radiation, and drought (Reddy et al., 1997b; Xiao et al., 2005; Koti et al., 2007).

Interactive studies on a combination of elevated CO_2 and UV-B radiation have shown counteractive effects (i.e., responses in opposite directions). The positive effects of elevated CO_2 on plant photosynthesis, growth, and yield were apparent under ambient (normal) UV-B radiation. Under enhanced UV-B radiation, the stimulated effects of elevated CO_2 were decreased. In cotton, elevated CO_2 significantly increased photosynthesis, growth, and dry matter production under no UV-B or near-ambient UV-B conditions. These responses to CO_2 were reflected in significantly higher concentrations of carbohydrates in leaves (Zhao et al., 2003). However, the detrimental effects of high UV-B on cotton photosynthesis and growth, particularly on reproductive growth, could not be alleviated by elevated CO_2. This suggests that breeding for UV-B radiation-tolerant cultivars is important in future climates with elevated CO_2. Apart from plant growth and related responses like photosynthesis, the attractiveness of plant foliage to insect herbivores may vary under combinations of elevated CO_2 and enhanced UV-B (Caldwell et al., 2003). Lavola et al. (1998) found that insects preferred plants grown with enhanced

UV-B, and the combination of high CO_2 and enhanced UV-B increased the tendency of the insects to consume more foliage.

Sullivan and Teramura (1990) studied the combined effects of enhanced UV-B radiation and drought. Both drought and UV-B radiation altered biochemical and photochemical processes of photosynthesis and independently elicited similar reductions in growth. However, no additive affects were observed on photosynthesis, growth, or yield. Their results suggested that UV-B radiation may significantly affect soybean growth and photosynthesis primarily when water is readily available and that these effects may be obscured by drought when growth and yield are already reduced. In cowpea, for example, the combination of enhanced UV-B and drought stress elicited beneficial effects on morphological and growth characteristics (Balakumar et al., 1993).

Plant response to enhanced UV-B radiation might also be influenced by nitrogen fertilization. Hunt and McNeil (1998) reported that when plants received more nitrogen, their growth was more depressed by exposure to enhanced UV-B, whereas nitrogen-deficient plants were not responsive to UV-B. Similarly, the response of elevated CO_2 is achieved only when plants are sufficiently supplied with nitrogen. Moreover, the requirement of nitrogen under elevated CO_2 may be greater because of increased growth and biomass production. Interactive effects of elevated CO_2 and potassium (K) supply on cotton showed that elevated CO_2 significantly increased photosynthesis, leaf area, and biomass production of K sufficient plants, but did not affect K concentration (Reddy and Zhao, 2005). There were significant interactive effects of CO_2 and K on leaf area, canopy photosynthesis, and biomass accumulation and partitioning. The stimulation of physiological and growth parameters observed because of elevated CO_2 was lost under severe K deficiency. Interactive effects of climate change factors and soil fertility have received far less attention and need investigation. As several climate change factors can directly influence crop growth and yields, crops grown in future climate would require changes in fertilizer management practices.

Ultraviolet radiation also interacts with temperature stress (both low and high temperatures). Temperature above and below optimum can negatively influence crop growth and yield, and interaction among factors can alter limits of temperature tolerance. Beerling et al. (2001) reported that frost sensitivity of subarctic plant species was enhanced under elevated UV-B. They also showed that elevated CO_2 led to an increase in frost sensitivity of these species and if both elevated CO_2 and enhanced UV-B were imposed, there was a further increase in frost sensitivity. At high temperatures, some synergistic effects of enhanced UV-B and the elevated temperature were observed (Caldwell et al., 2003). In some tropical legumes, enhanced UV-B reduced growth of the plants at moderate temperatures (20℃ − 30℃); but at 40℃, chloroplasts in leaves were modified and thus masked the UV-B depressions of growth (Kulandaivelu and Nedunchezhian, 1993; Nedunchezhian and Kulandaivelu, 1996). Recent studies on cotton showed that of various growth and developmental processes, square and boll retention were

most sensitive to high temperature and UV-B radiation (Reddy et al., 2004). Positive interactions were found on the number of main stem nodes, total leaf area, and total fruiting sites. Leaf photosynthesis increased with higher temperatures, but was reduced only by extreme UV-B radiation at high temperatures. The interaction between temperature and UV-B was additive on boll retention causing severe boll loss. Reddy et al. (2004) concluded that in current and future climates, severe yield losses would occur in the presence of high temperatures and UV-B radiation. Both these environmental factors stress plants by reducing reproductive mechanisms as well as vegetative growth.

Drought and high-temperature stress often occur simultaneously, but they can have very different effects on various physiological, growth, developmental, and yield processes. Few studies that examined the impact of combined effects of drought and high-temperature stress suggested that this combination produced a significantly higher detrimental effect on crop growth and productivity compared with each stress applied individually (Craufurd and Peacock, 1993; Savin and Nicolas, 1996). In addition, combinations of drought and heat stress were found to alter physiological processes, such as photosynthesis, accumulation of lipids, and transcript expression (Jagtap et al., 1998; Jian and Huang, 2001; Rizhsky et al., 2004). The interactive or combined effects of drought and high-temperature stress on reproductive processes of crop plants have not been well defined or quantified for any crop species and require further investigation. There might be differences in the response of reproductive function to these stresses. For example, in corn, both drought and heat stress have a direct influence on seed set or seed formation (Westgate, 1994). However, the cause is a result of effects on different processes. Heat stress decreases pollen viability, whereas drought stress (as measured for low leaf water potential) inhibits pistillate flower development and function.

Experiments designed to explore the interaction among these factors are useful for determining the potential effect of these abiotic stresses on crop plants (Caldwell et al., 2007). In a modeling approach, Runeckles and Krupa (1994) suggested that there may be no interaction between these stress factors as a whole, or to certain plant processes, and that the major variable will override the plant response. Otherwise, there may be an additive effect or greater-than-additive effect when the plant response is greater than the sum of responses to the individual factors. Additionally, there is a possibility of a less-than-additive interaction; for example, if CO_2 and/or temperature would stimulate more plant dry matter production and repair processes in UV-B sensitive plants (as shown in sunflower (*Helianthus annuus* L.) and maize seedlings in one of the earliest interactive studies involving CO_2, temperature), and UV-B radiation (Mark and Tevini, 1997).

In a recent study, Tegelberg et al. (2008) reported no significant interaction between elevated CO_2, temperature, and UV-B for the activity of defensive enzymes, growth-regulating polyamines, photosynthetic pigments, and soluble

protein in silver birch (*Betula pendula* L. Roth). In contrast, there were significant interactions between these abiotic stresses for most of the vegetative and reproductive parameters in soybean (Koti et al., 2005; Koti et al., 2007). However, studies that simultaneously evaluate both vegetative growth and yield attributes under multiple stress conditions are limited. In a recent study, Singh (2008) demonstrated that vegetative and reproductive processes in cowpea respond differently under multiple abiotic stress conditions, including UV-B radiation. Therefore, given the changing climate, it will be useful to study the relative response of vegetative and reproductive plant attributes for important grain and legume crops.

The interaction between abiotic stresses can drastically alter the response mechanisms in plants. This interaction may cause either a positive or negative effect, or can even counteract (neutralize) the effects of individual stresses depending upon the species. Elevated temperatures alleviated the damaging effects of UV-B radiation on various growth parameters in sunflower and corn (Mark and Tevini, 1997), whereas high temperatures in combination with UV-B resulted in an increased reduction in the growth of soybean (Koti et al., 2007). The response of plants to multiple abiotic stresses is unique and should be treated as a new state of abiotic stress rather than a combination of two or more stress factors (Mittler, 2006). One abiotic stress factor evokes a chain of complex metabolic processes in plants in the presence of other stress factors. Developing new crop genotypes of a species with enhanced tolerance to a given stress factor may fail to withstand in the presence of another abiotic stress. Therefore, plant breeders must consider the variable effects of possible climate change when developing breeding programs or transgenic plants for abiotic stress tolerance (Hall and Ziska, 2000; Mittler, 2006).

14.4 Abiotic Stress Tolerance and Cultivar Screening Tools

There is a large variation in tolerance or susceptibility to abiotic stresses, particularly to different climate change factors including UV-B radiation (Reddy et al., 2005; Singh et al., 2008a), high temperature stress (Craufurd et al., 2003; Prasad et al., 2006b; Ristic et al., 2008), and water stress (Foulkes et al., 2002; Upadhyaya, 2005; Bakheit, 2008; Singh, 2008). This variation can provide an opportunity for genetic improvement of plant species through either traditional plant breeding techniques (selection and crossing) or modern molecular biology techniques, such as plant transformation. Screening wide germplasm from various locations and origins including native wild relatives of crop plants and landraces for single and multiple abiotic climate change factors may prove useful for identifying tolerant traits and in developing climate-ready species or cultivars for a given region.

The available genotypic variability of a species offers an opportunity for breeders to design and develop specific plant types to suit different agro-ecological environments. Effectiveness of selection for a trait depends on the magnitude of

genetic and nongenetic causes in the expression of phenotypic differences among the genotypes in a population and is expressed as heritability of the trait (Thiaw and Hall, 2004). A thorough understanding of the physiological basis of differences in stress tolerance could be used to select or create new cultivars of crops that have increased productivity under such conditions (Wentworth et al., 2006). The genetic association of a trait with a higher level of physiological and/or developmental attributes facilitates adaptation of a crop to a stress condition and has proven useful for breeding purposes and developing improved lines of a crop species (Singh and Sharma, 1996). Several screening methods, such as cell membrane thermostability in soybean (Martineau et al., 1979; Blum et al., 2001) and cowpea (Ismail and Hall, 1999), in vitro pollen germination in canola (Singh et al., 2008b), cotton (Kakani et al., 2005), peppers (*Capsicum spp.*; Reddy and Kakani, 2007), and soybean (Koti et al., 2004; Salem et al., 2007), chlorophyll fluorescence in *Arabidopsis* (Barbagallo et al., 2003), photosynthesis and stomatal conductance in cotton (Lu et al., 1998), and intrinsic water use efficiency and associated gas exchange parameters in almond (*Prunus dulcis* L.), wheat, and cowpea (Brodribb, 1996; Condon et al., 2002; Singh, 2008), have been used at field and laboratory scales to identify tolerant traits and genotypes to abiotic stresses.

Abiotic stresses adversely affect various cellular functions, but photosynthesis is particularly sensitive to heat and drought stress (Berry and Bjorkman, 1980; Brodribb, 1996; Haldimann and Feller, 2005). Fluorescence parameters have been shown to relate directly to the photosynthetic rates of leaves (Genty et al., 1990; Edwards and Baker, 1993) and have been widely used to study leaf photosynthetic performance (Maxwell and Johnson, 2000). Consequently, any small perturbation in photosynthetic metabolism significantly modifies the fluorescence characteristics of plants. The sensitivity of chlorophyll fluorescence to the stress-induced perturbation in plant metabolism can potentially make it useful for screening genotypes with differential responses to abiotic factors (Brodribb, 1996; Barbagallo et al., 2003). Previous studies suggest significant changes in the photochemical activities of cowpea leaves subjected to heat (Costa et al., 2003; Costa et al., 2004), UV-B (Premkumar and Kulandaivelu, 1996; Lingakumar et al., 1999), and drought conditions (Lopez et al., 1987; Souza et al., 2004).

Hall (2004b) proposed a yield component model that can be incorporated for selection of most legumes, including cowpea cultivars in the high-temperature-limited production zones. Four yield components (number of flowers per unit area, number of pods per flower, number of seeds per pod, and weight of individual seeds) that contribute to yield reduction were recognized. In a simple screening approach for heat tolerance, Ismail and Hall (1999) found an association between reproductive-stage heat tolerance and higher cell membrane thermostability measured as electrolyte leakage from leaves subjected to high-temperature treatment. In an extremely hot field environment, negative correlations were observed between grain yield and electrolyte leakage ($r = -0.79$, $n = 9$), and pod set and electrolyte leakage ($r = -0.89$, $n = 9$) among nine cowpea breeding lines.

A similar approach could also be used to assess variable differences among species and cultivars of the same species under UV-B radiation.

An increased concern in regard to abiotic stress effects on crop plants has prompted screening for tolerance in crop populations (Hall, 2001). Many crops have been screened by using various abiotic stress response indices derived from the different stages of plant growth in response to single or multiple abiotic stresses (Dai et al., 1994; Saile-Mark and Tevini, 1997; Koti et al., 2004; Hubbard and Wu, 2005). Several crops, including rice (Dai et al., 1994), wheat (Yuan et al., 2000), bean (Saile-Mark and Tevini, 1997), and corn (Hubbard and Wu, 2005), have been screened by using several UV-B and drought response indices derived from plant growth responses under UV-B or drought conditions. In addition, multivariate analyses, such as principal component analyses and factor analysis, have been used for efficiently characterizing the stress responsiveness of a population under study and the associated plant attributes (Hofmann et al., 2001; Kaspar et al., 2004; Singh et al., 2008a).

Simultaneous occurrences of different abiotic stresses are common in natural plant habitats, which greatly modify the individual stress effect. This modification in the degree of response mechanisms could have been caused because of co-activation of different response pathways by simultaneous exposure of plants to different abiotic stresses leading to synergistic or antagonistic effects (Mittler, 2006). Developing a crop plant with enhanced tolerance to a stress combination, including UV-B radiation by either traditional breeding or genetic engineering, requires an understanding of the complex cross-communication between different signaling pathways and their direct or indirect effects on plant growth and metabolism (Hall, 2004a; Mittler, 2006).

Hall and Ziska (2000) recommended that plant breeders should consider possible climate change when developing a breeding strategy. Grain yield in legumes, such as cowpea, can be enhanced by selection of greater reproductive sinks under high temperatures, which will minimize the feedback effect that down regulates the photosynthetic mechanisms (Ahmed et al., 1993; Hall and Allen, 1993). However, yield has less importance in a trait-based breeding program particularly for high-temperature and drought tolerance. The yield reduction caused by abiotic stresses is a consequence of several first-order effects, such as photosynthetic performance (photosynthesis and fluorescence reduced water use efficiency), morphogenesis (differentiation and developmental rate), and production of defense compounds (phenolic compounds, and free amino acids and waxes) affecting overall vegetative growth and dry matter production. Therefore, survival capacity and maintenance of normal metabolic activity in the presence of stress conditions are key features for sustaining higher yields and should be considered an important component of breeding programs.

Molecular genetic mapping of the plant genome has facilitated identification of biomarkers that are closely linked to known resistance genes such that their isolation is clearly feasible in the future (Easterling et al., 2007). Temperature

and drought stress resistance are especially relevant to climate change. Earlier studies have demonstrated genetic modifications to major crop species (e.g., maize and soybean) that increased their water deficit tolerance (Drennen et al., 1993; Kishor et al., 1995; Cheikh et al., 2000), although this may not extend to a wider range of crop plants. Little is known about how the desired traits achieved by genetic modification will perform under multiple abiotic conditions that commonly occur in the natural environment. The genomic approach offers new germplasm and understanding, but the emergent nature of yield from physiological processes demands that all components contributing to the yield be considered. It is important to understand the interactions of various regulatory pathways within plants, and between plants and environments, to understand key links between gene activity and crop yield (Sinclair and Purcell, 2005). Biotechnology is not expected to replace conventional agronomic breeding (Easterling et al., 2007); however, it will be a crucial adjunct to conventional breeding because both will be needed to meet future environmental challenges, including climate change (Cheikh et al., 2000; FAO, 2004).

14.5 Climate Change and Aerobiology and Public Health

In recent years, concerns regarding possible links among climate, plant biology, aerobiology, and public health (Ziska et al., 2008) have increased. Atmospheric CO_2, the main input needed for photosynthesis, stimulates plant growth; however, the rate of stimulation depends on the species. Plants with an indeterminate growth habit will benefit immensely because additional carbon can increase the production of branches/tillers and result in more nodes/fruiting sites on all branches, thus adding more potential for flowers to produce additional pollen (Reddy and Hodges, 2000; Ziska and Caulfield, 2000; Jablonski et al., 2002; Kimball et al., 2002; Long et al., 2005; Long et al., 2006; Easterling et al., 2007). In addition, plants grown in elevated CO_2 can also stimulate earlier flowering and sustained growth due to additional carbon, which will lead to a longer flowering period and pollen production range. Higher temperatures, on the other hand, will increase the rate of development, and in most cases promote early flowering and also a greater number of flowers and pollen if the change in temperature is small. If the change in temperature is large, flower and pollen vitality (production, viability and germination) will be curtailed regardless of other factors such as elevated CO_2. Other climate change factors, such as elevated UV-B, normally suppress flower and pollen production. However, the effects vary depending on the species and cultivars within a species (Teramura, 1983; Caldwell et al., 1989; Teramura and Sullivan, 1994; Rozema et al., 1997; Krupa, 1998; Searles et al., 2001; Kakani et al., 2003a).

The influence of multiple climatic variables (e.g., UV-B radiation, CO_2, and temperature) is limited, and a definite conclusion regarding the combined effects

of these variables on plant pollen is harder to assess at this time. Studies conducted across natural gradients in climatic factors from rural to urban areas indicate that increasing levels and temporal shifts in aeroallergen production and allergenicity are linked to rising temperatures and/or CO_2 (Ziska et al., 2003; Ziska and George, 2004; Mohan et al., 2006; Rogers et al., 2006; Ziska et al., 2008). However, quantity and seasonality of pollen production depend on the plant response to environmental conditions. As previously indicated, several climate change factors influence pollen production of not only crop plants, but also several weed species (Ziska and Caulfield, 2000; Ziska et al., 2003) and allergenic pollen-producing tree species (Emberlin et al., 2002; Wan et al., 2002). Allergenic tree pollen from birch showed earlier spring floral initiation and pollen release in response to spring warming (Emberlin et al., 2002). Similarly, a simulated increase of summer temperature (+4°C) increased growth and re-growth following cutting, with an 85% increase in overall pollen production (Wan et al., 2002). Research on loblolly pine (*Pinus taeda* L.) also showed that elevated CO_2 resulted in early pollen production from younger trees and greater seasonal pollen production (LaDeau and Clark, 2006). Recent research also suggested that algernicity associated with poison ivy will increase with rising CO_2 (Mohan et al., 2006). As described in the previous section, climate change factors can also influence fungal spore production, which can influence allergen production. Increased exposure to allergic fungal spores can also influence human diseases, such as asthma (Dales et al., 2004). The linkage between aeroallergen production and alergenicity and the incidence of asthma intensity and incidence needs further investigation.

14.6 Concluding Remarks

Increased UV-B radiation and its interaction with other climate change factors, such as temperature, water stress, and elevated CO_2, can influence various physiological, growth, and yield traits of plants. In addition to direct effects on crop plants, these factors can also influence the interaction of plants with biotic factors (particularly with insect pests and plant pathogens). A comprehensive understanding of these interactions will be critical for evaluating the impact of climate change and climate variability on crop production and its long-term impact on crop ecology. Crop species and cultivars within species vary in their responses to both individual and a combination of stresses, suggesting a scope for genetic improvement. Thus, research should be more focused on breeding for tolerance to multiple stresses of regional or local importance. Sufficient care should be taken while evaluating and imposing stress treatments both in controlled environment and field conditions, particularly with respect to distribution of wavelength in the UV range for UV-B stress, diurnal differences and patterns between day and night temperatures for heat stress, time and intensity for moisture stress, and also acclimation response of plants to stressed environments. Experimentalists (molecular

biologists and crop physiologists) should also consider light regimes that mimic filed-level solar radiation regimes while studying effects of stress factors on plants. The method of the imposition of stress could influence the quantitative response of any trait. As our knowledge of crop responses to multiple environmental stresses increases, it might be important to incorporate these algorithms, including genetic responses, into existing crop simulation models to develop better predictions of crop production and available management options in future climates.

Acknowledgements

We thank Drs. Harry Hodges and Mary Beth Kirkham for their comments and suggestions. Part of this work was supported by the US DOE, the USDA-UV-B Monitoring and Research Program, and the USDA-ARS 58-6402-7-241. Contributions were also made by the Department of Plant and Soil Sciences, Mississippi State University; Mississippi Agricultural and Forestry Experiment Station (BC-11471), MS, the Agronomy Department, Kansas State University, and the Kansas Agricultural Experiment Station Contribution No: KAES 09-129-B.

References

Ahmed FE, Hall AE, and Madore MA (1993) Interactive effects of high temperature and elevated carbon dioxide concentration on cowpea (*Vigna unguiculata* (L.) Walp.). Plant Cell Environ. 16: 835 – 842

Ainsworth EA and Long SP (2005) What have we learned from 15 years of free-air CO_2 enrichment (FACE)? A meta-analytic review of the responses of photosynthesis, canopy properties and plant production to rising CO_2. New Phytol. 165: 351 – 372

Ainsworth EA, Rogers A, Nelson R, and Long SP (2004) Testing the "source-sink" hypothesis of down-regulation of photosynthesis in elevated (CO_2) in the field with single gene substitutions in *Glycine max*. Agric. For. Meteorol. 122: 85 – 94

Allen DJ, Mckee IF, Farage PK, and Baker NR (1997) Analysis of limitations to CO_2 assimilation on exposure of leaves of two *Brassica napus* cultivars to UV-B. Plant Cell Environ. 20: 633 – 640

Alves AAC and Setter TL (2004) Response of cassava leaf area expansion to water deficit: Cell proliferation, cell expansion and delayed development. Ann. Bot. 94: 605 – 613

Baker JT (2004) Yield responses of southern U.S. rice cultivars to CO_2 and temperature. Agric. For. Meteorol. 122: 129 – 137

Bakheit BR (2008) Variability and correlations in grain sorghum genotypes (*Sorghum bicolor* (L.) Moench) under drought conditions at different stages of growth. J. Agron. Crop Sci. 165: 355 – 360

Balakumar T, Vincent VHB, and Paliwal K (1993) On the interaction of UV-B radiation (280 nm – 315 nm) with water stress in crop plants. Physiol. Plant. 87: 217 – 222

Ballare CL, Scopel AL, Stapleton AE, and Yanovsky MJ (1996) Solar ultraviolet-B radiation affects seedling emergence, DNA integrity, plant morphology, growth rate, and attractiveness to herbivore insects in *Datura ferox*. Plant Physiol. 112: 161 – 170

Barbagallo RP, Oxborough K, Pallett KE, and Baker NR (2003) Rapid, noninvasive screening for perturbations of metabolism and plant growth using chlorophyll fluorescence imaging. Plant Physiol. 132: 485

Basal H, Bebeli P, Smith CW, and Thaxton P (2003) Root growth parameters of converted race stocks of upland cotton and two BC_2F_2 populations. Crop Sci. 43: 1983 – 1988

Beerling DJ, Terry AC, Mitchell PL, Callaghan TV, Jones DG, and Lee JA (2001) Time to chill: effects of simulated global change on leaf ice nucleation temperature and subarctic vegetation. Am. J. Bot. 88: 628 – 633

Berry J and Bjorkman O (1980) Photosynthetic response and adaptation to temperature in higher plants. Ann. Rev. Plant Physiol. 31: 491 – 543

Blum A, Klueva N, and Nguyen HT (2001) Wheat cellular thermotolerance is related to yield under heat stress. Euphytica 117: 117 – 123

Boote KJ, Allen Jr LH, Prasad PVV, Baker JT, Gesch RW, Synder AM, Pan D, and Thomas JMG (2005) Elevated temperature and CO_2 impacts on pollination, reproductive growth and yield of several globally important crops. J. Agric. Meteorol. 60: 469 – 474

Bota J, Flexas J, and Medrano H (2001) Genetic variability of photosynthesis and water use in Balearic grapevine cultivars. Ann. Appl. Biol. 138: 353 – 361

Brodribb T (1996) Dynamics of changing intercellular CO_2 concentration (C_i) during drought and determination of minimum functional C_i. Plant Physiol. 111: 179 – 185

Caldwell CR, Britz SJ, and Mirecki RM (2005) Effect of temperature, elevated carbon dioxide, and drought during seed development on the isoflavone content of dwarf soybean (*Glycine max* (L.) Merrill) grown in controlled environments. J. Agric. Food Chem. 53: 1125 – 1129

Caldwell MM, Teramura AH, and Tevini M (1989) The changing solar ultraviolet climate and the ecological consequences for higher plants. Trends Ecol. Evol. 4: 363 – 367

Caldwell MM, Flint SD, and Searles PS (1994) Spectral balance and UV-B sensitivity of soybean: a field experiment. Plant Cell Environ. 17: 267 – 276

Caldwell MM, Teramura AH, Tevini M, Bornman JF, Björn LO, and Kulandaivelu G (1998) Effects of increased solar ultraviolet radiation on terrestrial ecosystems. J. Photochem. Photobiol. B: Biol. 46: 40 – 52

Caldwell MM, Ballare CL, Bornman JF, Flint SD, Bjorn LO, Teramura AH, Kulandaivelu G, and Tevini M (2003) Terrestrial ecosystems, increased solar ultraviolet radiation and interactions with other climate change factors. Photochem. Photobiol. Sci. 2: 29 – 38

Caldwell MM, Bornman JF, Ballaré CL, Flint SD, and Kulandaivelu G (2007) Terrestrial ecosystems, increased solar ultraviolet radiation, and interactions with other climate change factors. Photochem. Photobiol. Sci. 6: 252 – 266

Cheikh N, Miller PW, and Kishore G (2000) Role of biotechnology in crop productivity in a changing environment. In: Reddy KR, Hodges HF (eds) Climate Change and Global Crop Productivity. CAP International, Oxon, UK, pp.425 – 436

Chiulele RM and Agenbag GA (2004) Plant water relations and proline accumulation on two cowpea (*Vigna unguiculata* (L.) Walp.) cultivars as a response to water stress. S. Afr. J. Plant and Soil 21: 109 – 113

Christensen JH, Hewitson B, Busuioc A, Chen A, Gao X, Held I, Jones R, Kolli RK, Kwon WT, Laprise R, Rueda VM, Mearns L, Menendez CG, Raisanen J, Rinke A, Sarr A and Whetton P. (2007) Regional climate projections. In: Solomon S, Qin D, Manning M, Marquis M, Averyt K, Tignor MMB, Miller HL and Chen Z (eds) Climate Change 2007: Contribution of Working Group I to the Fourth Assessment Report of the Intergovernmental Panel on Climate Change. Cambridge University Press, Cambridge, UK, pp.847－940

Ciais P, Reichstein M, Viovy N, Granier A, Ogee J, Allard V, Aubinet M, Buchmann N, Bernhofer C, Carrara A, Chevallier F, De Noblet N, Friend AD, Friedlingstein P, Grunwald T, Heinesch B, Keronen P, Knohl A, Krinner G, Loustau D, Manca G, Matteucci G, Miglietta F, Ourcival JM, Papale D, Pilegaard K, Rambal S, Seufert G, Soussana JF, Sanz MJ, Schulze ED, Vesala T, and Valentini R (2005) Europe-wide reduction in primary productivity caused by the heat and drought in 2003. Nature 437: 529－533

Clavel D, Drame NK, Roy-Macauley H, Braconnier S, and Laffray D (2005) Analysis of early responses to drought associated with field drought adaptation in four Sahelian groundnut (*Arachis hypogaea* L.) cultivars. Environ. Exp. Bot. 54: 219－230

Condon AG, Richards RA, Rebetzke GJ, and Farquhar GD (2002) Improving intrinsic water-use efficiency and crop yield. Crop Sci. 42: 122－131

Costa ES, Bressan-Smith R, Oliveira JG, and Campostrini E (2003) Chlorophyll a fluorescence analysis in response to excitation irradiance in bean plants (*Phaseolus vulgaris* L. and *Vigna unguiculata* L. Walp) submitted to high temperature stress. Photosynthetica 41: 77－82

Costa JW, Hasenfratz-Sauder MP, Pham-Thi AT, Lima MDS, Dizengremel P, Jolivet Y, and de Melo DF (2004) Identification in *Vigna unguiculata* (L.) Walp. of two cDNAs encoding mitochondrial alternative oxidase orthologous to soybean alternative oxidase genes 2a and 2b. Plant Sci. 167: 233－239

Craufurd PQ and Peacock JM (1993) Effect of heat and drought stress on sorghum. Exp. Agr. 29: 77－86

Craufurd PQ, Flower DJ, and Peacock JM (1993) Effect of heat and drought stress on sorghum. I. Panicle development and leaf appearance. Exp. Agr. 29: 61－76

Craufurd PQ, Prasad PVV, Kakani VG, Wheeler TR, and Nigam SN (2003) Heat tolerance in groundnut. Field Crop Res. 80: 63－77

Cutforth HW, McGinn SM, McPhee KE, and Miller PR (2007) Adaptation of pulse crops to the changing climate of the Northern Great Plains. Agron. J. 99: 1684－1699

Dai Q, Peng S, Chavez AQ, and Vergara BS (1994) Intraspecific response of 188 rice cultivars to enhanced UV-B radiation. Environ. Exp. Bot. 34: 433－442

Dales RE, Cakmak S, Judek S, Dann T, Coates F, Brook JR, and Burnett RT (2004) Influence of outdoor aeroallergens on hospitalization for asthma in Canada. J. Allergy Clin. Immunol. 113: 303－306

Drennen PM, Smith M, Goldsworthy D, and van Staten J (1993) The occurrence of trahaolose in the leaves of the desiccation-tolerant angiosperm *Myronthamnus flabellifoliius* Welw. J. Plant Physiol. 142: 493－496

Easterling WE, Aggarwal PK, Batima P, Brander KM, Erda L, Howden SM, Kirilenko A, Morton J, Soussana JF, Schmidhuber J, and Tubiello FN (2007) Food, fibre and forest

products. In: Parry ML, Canziani OF, Palutikof JP, van der Linden PJ, Hanson CE (eds) Climate Change 2007: Impacts, Adaptation and Vulnerability. Contribution of Working Group Ⅱ to the Fourth Assessment Report of the Intergovernmental Panel on Climate Change. Cambridge University Press, Cambridge, UK, pp.273－313

Edwards GE and Baker NR (1993) Can CO_2 assimilation in maize leaves be predicted accurately from chlorophyll fluorescence analysis? Photosynthesis Res. 37: 89－102

Emberlin J, Detandt M, Gehrig R, Jaeger S, Nolard N, and Rantio-Lehtimaki A (2002) Responses in the start of *Betula* (birch) pollen seasons to recent changes in spring temperatures across Europe. Int. J. Biometeorol. 47: 113－115

Ensminger PA (1993) Control of development in plants and fungi by far-UV radiation. Physiol. Plant. 88: 501－508

FAO (2004) The state of food and agriculture 2003－2004. Agricultural Biotechnology: Meeting the Needs of the Poor, Food and Agriculture Organization of the United Nations, Rome, Italy, p.208

Fiscus EL and Booker FL (1995) Is increased UV-B a threat to crop photosynthesis and productivity? Photosyn. Res. 43: 81－92

Flexas J, Bota J, Escalona JM, Sampol B, and Medrano H (2002) Effects of drought on photosynthesis in grapevines under field conditions: An evaluation of stomatal and mesophyll limitations. Funct. Plant Biol. 29: 461－471

Foulkes MJ, Scott RK, and Bradley RS (2002) The ability of wheat cultivars to withstand drought in UK conditions: Formation of grain yield. J. Agr. Sci. 138: 153－169

Fourtouni A, Manetas Y, and Christias C (1998) Effects of UV-B radiation on growth, pigmentation and spore production in the phytopathogenic fungus *Alternaria solani*. Can. J. Bot. 76: 2093－2099

Gao W, Zheng Y, Slusser JR, Heisler GM, Grant RH, Xu J, and He D (2004) Effects of supplementary ultraviolet-B radiation on maize yield and qualities: A field experiment. Photochem. Photobiol. 80: 127－131

Genty B, Briantais JM, and Baker NR (1990) Relative quantum efficiencies of the two photosystems of leaves in photorespiratory and not photorespiratory conditions. Plant Physiol. Biochem. 28: 1－10

Gifford RM (2004) The CO_2 fertilizing effect does it occur in the real world? New Phytol. 163: 221－225

Giorgi R, Meehl GA, Kattneberg A, Grassl H, Mitchell JFB, Stouffer RJ, Tokioka T, Weaver AJ, and Wigley TML (1998) Simulation of regional climate change with global coupled climate models and regional modeling techniques. In: Watson RT, Zinyowera MC, Moss RH (eds) The Regional Impacts of Climate Change: An Assessment of Vulnerability. Cambridge University Press, New York, NY, pp.427－437

Gobron N, Pinty B, Melin F, Taberner M, Verstraete MM, Belward A, Lavergne T, and Widlowski JL (2005) The state of vegetation in Europe following the 2003 drought. Int. J. Remote Sens. 26: 2013－2020

Gross Y and Kigel J (1994) Differential sensitivity to high temperature of stages in the reproductive development in common bean (*Phaseolus vulgaris* L.). Field Crops Res. 36: 201－212

Gunn A (1998) The determination of larval phase coloration in the African armyworm *Spodoptera exempta* and its consequences for thermoregulation and protection from UV light. Entomol. Exp. Appl. 86: 125－133

Haldimann P and Feller U (2005) Growth at moderately elevated temperature alters the physiological response of the photosynthetic apparatus to heat stress in pea (*Pisum sativum* L.) leaves. Plant Cell Environ. 28: 302－317

Hall AE (2001) Crop response to environment. CRC Press, New York, NY, p.248

Hall AE (2004a) Breeding for adaptation to drought and heat in cowpea. Eur. J. Agron. 21: 447－454

Hall AE (2004b) Comparative ecophysiology of cowpea, common bean, and peanut. In: Henry TN, Abraham B (eds) Physiology and Biotechnology Integration for Plant Breeding. Marcel Dekker, New York, NY, pp.271－385

Hall AE and Allen LH (1993) Designing cultivars for climatic conditions of the next century. In: Buxton DR, Shibles R, Forsberg RA, Blad BL, Asay KH, Paulsen GM, Wilson RF (eds) International Crop Science I. Madison: Crop Sciences Society of America, WI, pp.291-297

Hall AE and Ziska LH (2000) Crop breeding strategies for the 21st century. In: Reddy KR, Hodges HF (eds) Climate Change and Global Crop Productivity. CAB International, Oxon, UK, pp.407－423

Harborne JB (1988) The flavanoids. Advances in research since 1980. Chapman and Hall, New York, NY, p.676

He J, Huang LK, and Whitecross MI (1994) Chloroplast ultrastructure changes in *Pisum sativum* associated with supplementary ultraviolet (UV-B) radiation. Plant Cell Envrion. 17: 771－775

Hidema J and Kumagai T (2006) Sensitivity of rice to ultraviolet-B radiation. Ann. Bot. 97: 933－942

Hidema J, Zhang WH, Yamamoto M, Sato T, and Kumagai T (2005) Changes in grain size and grain storage protein of rice (*Oryza sativa* L.) in response to elevated UV-B radiation under outdoor conditions. J. Radiation Res. 46: 143－149

Hofmann R, Campbell B, Fountain D, Jordan BR, Greer DH, Hunt D, and Hunt C (2001) Multivariate analysis of intraspecific responses to UV-B radiation in white clover (*Trifolium repense* L.). Plant Cell Environ. 24: 917－927

Holton MK, Lindroth RL, and Nordheim EV (2003) Foliar quality influence tree-herbivore-parasitoid interactions: Effects of elevated CO_2, O_3, and plant genotype. Oecologia 137: 233－244

Houghton JT, Ding Y, Griggs DJ, Noguer M, van der Linden PJ, Dai X, Maskell K, and Johnson CA (2001) Climate Change 2001: The Scientific Basis. Contribution of Working Group to Third Assessment Report to the Intergovernmental Panel on Climate Change (IPCC). Cambridge University Press, Cambridge, UK, p.892

Hubbard KG and Wu H (2005) Modification of a crop-specific drought index for simulating corn yield in wet years. Agron. J. 97: 1478－1484

Hunt JE and McNeil DL (1998) Nitrogen status affects UV-B sensitivity of cucumber. Aust. J. Plant Physiol. 25: 79－86

IPCC (2007) Climate Change 2007: The Physical Science Basis. Contribution of Working Group I to the Fourth Assessment Report of the Intergovernmental Panel on Climate Change. Cambridge University Press, Cambridge, UK and New York, NY, p.996

Ismail AM and Hall AE (1997) Chilling tolerance during emergence of cowpea associated with a dehydrin and slow electrolyte leakage. Crop Sci. 37: 1270

Ismail AM and Hall AE (1998) Positive and potential negative effects of heat-tolerance genes in cowpea. Crop Sci. 38: 381－390

Ismail AM and Hall AE (1999) Reproductive-stage heat tolerance, leaf membrane thermostability and plant morphology in cowpea. Crop Sci. 39: 1762－1768

Izaguirre MM, Scopel AL, Baldwin IT, and Ballare CL (2003) Convergent responses to stress: Solar ultraviolet-B radiation and *Manduca sexta* herbivory elicit overlapping transcriptional responses in field-grown plants of *Nicotiana longiflora*. Plant Physiol. 132: 1755－1767

Izaguirre MM, Mazza CA, Svotos A, Baldwin IT, and Ballare CL (2007) Solar ultraviolet-B radiation and insect herbivory trigger partially overlapping phenolic responses in *Nicotiana attenuate* and *Nicotiana longiflora*. Ann. Bot. 99: 103－109

Jablonski LM, Wang X, and Curtis PS (2002) Plant reproduction under elevated CO_2 conditions: A meta-analysis of reports on 79 crop and wild species. New Phytol. 156: 9－26

Jagtap V, Bhargava S, Streb P, and Feierabend J (1998) Comparative effect of water, heat and light stresses on photosynthetic reactions in *Sorghum bicolor* (L.) Moench. J. Exp. Bot. 49: 1715－1721

Jansen MAK (2002) Ultraviolet-B radiation effects on plants: Induction or morphogenic responses. Physiol. Plant. 116: 423－429

Jian Y and Huang B (2001) Drought and heat stress injury to two cool-season turf grass in relation to antioxidant and lipid peroxidation. Crop Sci. 41: 436－442

Kakani VG, Prasad PVV, Craufurd PQ, and Wheeler TR (2002) Response of *in vitro* pollen germination and pollen tube growth of groundnut (*Arachis hypogaea* L.) genotypes to temperature. Plant Cell Environ. 25: 1651－1661

Kakani VG, Reddy KR, Zhao D, and Sailaja K (2003a) Field crop responses to ultraviolet-B radiation: A review. Agric. For. Meteorol. 120:191－218

Kakani VG, Reddy KR, Zhao D, and Mohammed AR (2003b) Ultraviolet-B radiation effects on cotton (*Gossypium hirsutum* L.) morphology and anatomy. Ann. Bot. 817－826

Kakani VG, Reddy KR, Koti S, Wallace TP, Prasad PVV, Reddy VR, and Zhao D (2005) Differences in *in vitro* pollen germination and pollen tube growth of cotton cultivars in response to high temperature. Ann. Bot. 96: 59－67

Kaspar TC, Pulido DJ, Fenton TE, Colvin TS, Karlen DL, Jaynes DB, and Meek DW (2004) Relationship of corn and soybean yield to soil and terrain properties. Agron. J. 96: 700－709

Keller M, Rogiers SY, and Schulz HR (2003) Nitrogen and ultraviolet radiation modifies grapevines susceptibility to powdery mildew. Vitis 42: 87－94

Kimball BA, Kobayashi K, and Bindi M (2002) Responses of agricultural crops to free-air CO_2 enrichment. Adv. Agron. 77: 293－368

Kishor PBK, Hong Z, Miao G, Hu C, and Verma D (1995) Over expression of Δ^1-pyrroline-5-carboxylase synthase increases proline production and confers osmotolerance in transgenic plants. J. Plant Physiol. 108: 1387－1394

Koti S, Reddy KR, Kakani VG, Zhao D, and Reddy VR (2004) Soybean (*Glycine max*) pollen germination characteristics flower and pollen morphology in response to enhanced ultraviolet-B radiation. Ann. Bot. 94: 855－864

Koti S, Reddy KR, Reddy VR, Kakani VG, and Zhao DL (2005) Interactive effects of carbon dioxide, temperature, and ultraviolet-B radiation on soybean (*Glycine max* L.) flower and pollen morphology, pollen production, germination, and tube lengths. J. Exp. Bot. 56: 725－736

Koti S, Reddy KR, Kakani VG, Zhao D, and Gao W (2007) Effects of carbon dioxide, temperature and ultraviolet-B radiation and their interactions on soybean (*Glycine max* L.) growth and development. Environ. Exp. Bot. 60: 1－10

Krupa SV (1998) Elevated UV-B radiation and crop. In: Krupa SV, Kickert RN, Jäger HJ (eds) Elevated Ultraviolet (UV)-B Radiation and Agriculture. Springer-Verlag, Heidelberg and Landes Bioscience, Georgetown, TX, pp.105－131

Kulandaivelu G and Nedunchezhian N (1993) Synergistic effects of ultraviolet-B enhanced radiation and growth temperature on ribulose 1, 5-bisphosphate carboxylase and $^{14}CO_2$ fixation in *Vigna sinensis* L. Photosynthetica 29: 377－383

LaDeau SL and Clark JS (2006) Pollen production by *Pinus taeda* growing in elevated CO_2. Funct. Ecol. 10: 1365－1371

Lavola A, Tiitto RJ, Roininen H, and Aphalo P (1998) Host-plant preference of an insect herbivore mediated by UV-B and CO_2 in relation to plant secondary metabolites. Biochem. Syst. Ecol. 26: 1－12

Liang X, Xu M, Gao W, Reddy KR, Kunkel K, and Schmoldt DL (2008) Physical modeling of U.S. cotton yields and climate stresses during 1979－2005. J. Geo. Res., Atmospheres (in press)

Lindroth RL, Hofmann RW, Campell BD, McNabb WC, and Hunt DY (2000) Population differences in *Trifolium repens* L-response to ultraviolet-B radiation: Foliar chemistry and consequences for two lepidopteran herbivores. Oecologia 122: 20－28

Lingakumar K, Amudha P, and Kulandaivelu G (1999) Exclusion of solar UV-B (280 nm－315 nm) radiation on vegetative growth and photosynthetic activities in *Vigna unguiculata* L. Plant Sci. 148: 97－103

Lobell DB and Asner GP (2003) Climate and management contributions to recent trends in U.S. agricultural yields. Science 299: 1032

Lobell DB, Burke MB, Tebaldi C, Mastrandrea MD, Falcon WP, and Naylor RL (2008) Prioritizing climate change adaptation needs for food security in 2030. Science 319: 607－610

Long SP (1991) Modification of the response of photosynthetic productivity to rising temperature by atmospheric CO_2 concentrations: Has its importance been underestimated? Plant Cell Environ. 14: 729－739

Long SP, Ainsworth EA, Rogers A, and Ort DR (2004) Rising atmospheric carbon dioxide: Plants FACE the future. Annu. Rev. Plant Biol. 55: 591－628

Long SP, Ainsworth EA, Leakey ADB, and Morgan PB (2005) Global food insecurity. Treatment of major food crops with elevated carbon dioxide or ozone under large-scale fully open-air conditions suggests recent models may have overestimated future yields. Philos. Trans. R. Soc. Lond., Ser. B: Biol. Sci. 360: 2011－2020

Long SP, Ainsworth EA, Leakey ADB, Nosberger J, and Ort DR (2006) Food for thought: Lower-than-expected crop yield stimulation with rising CO_2 concentrations. Science 312: 1918－1921

Longenberger PS, Smith CW, Thaxton PS, and McMichael BL (2006) Development of a screening method for drought tolerance in cotton seedlings. Crop Science 46: 2104－2110

Lopez FB, Setter TL, and McDavid CR (1987) Carbon dioxide and light responses of photosynthesis in cowpea and pigeonpea during water deficit and recovery. Plant Physiol. 85: 990－995

Lu Z, Percy RG, Qualset CO, and Zeiger E (1998) Stomatal conductance predicts yields in irrigated pima cotton and bread wheat grown at high temperatures. J. Exp. Bot. 49: 453－460

Mark U and Tevini M (1997) Effects of solar ultraviolet-B radiation, temperature and CO_2 on growth and physiology of sunflower and maize seedlings. Plant Ecol. 128: 224－234

Martineau JR, Williams JH, and Specht JE (1979) Tolerance in soybean. Ⅱ. Evaluation of segregating populations for membrane thermostability. Crop Sci. 19: 79－81

Matsui T, Namuco OS, Ziska LH, and Horie T (1997) Effects of high temperature and CO_2 concentration on spikelet sterility of indica rice. Field Crop. Res. 51: 213－219

Maxwell K and Johnson GN (2000) Chlorophyll fluorescence: A practical guide. J. Exp. Bot. 51: 659－668

Mazza CA, Zavala J, Scopel AL, and Ballare CL (1999) Perception of solar UVB radiation by phytophagous insects: Behavioral responses and ecosystem implications. Proc. Natl. Acad. Sci. USA. 96: 980－985

Mazza CA, Boccalandro HE, Giordano CV, Battista D, Scopel AL, and Ballare CL (2000) Functional significance and induction by solar radiation of ultraviolet—absorbing sunscreens in field-grown soybean crops. Plant Physiol. 122: 117－125

Mazza CA, Izaguirre MM, Zavala J, Scopel AL, and Ballare CL (2002) Insect perception of ambient ultraviolet-B radiation. Ecol. Lett. 5: 722－726

McCloud ES, Berenbaum MR, and Tuveson RW (1992) Furanocoumarin content and phototoxicity of rough lemon (*Citrus jambhiri*) foliage exposed to enhanced ultraviolet-B (UVB) radiation. J. Chem. Ecol. 18: 1125－1137

McKenzie RL, Bjorn LO, Bais A, and Ilyasd M (2003) Changes in biologically active ultraviolet radiation reaching the Earth's surface. Photochem. Photobiol. Sci. 2: 5－15

McKenzie RL, Aucamp PJ, Bais AF, Björn LO, and Ilyas M (2007) Changes in biologically active ultraviolet radiation reaching the Earth's surface. Photochem. Photobiol. Sci. 6: 218－231

Medrano H, Escalona JM, Bota J, Gulias J, and Flexas J (2002) Regulation of photosynthesis of C_3 plants in response to progressive drought: Stomatal conductance as a reference parameter. Ann. Bot. 89: 895－905

Meehl TGA and Tebaldi C (2004) More intense, more frequent, and longer lasting heat waves in the 21st century. Science 305: 994－997

Mittler R (2006) Abiotic stress, the field environment and stress combination. Trends Plant Sci. 11: 15－19

Mohan JE, Ziska LH, Thomas RB, Sicher RC, George K, Clark JS, and Schlesinger WH (2006) Biomass and toxicity responses of poison ivy (*Toxicodendron radicans*) to elevated atmospheric CO_2. Proc. Natl. Acad. Sci.103: 9086－9089

Musil CF, Björn LO, Scourfield MWJ, and Bodeker GE (2002) How substantial are ultraviolet-B supplementation inaccuracies in experimental square-wave delivery systems? Environ. Exp. Bot. 47: 25－38

National Climate Data Center. http://www.ncdc.noaa.gov/oa/ncdc.html

Nedunchezhian N and Kulandaivelu G (1996) Effect of ultraviolet-B enhanced radiation and temperature on growth and photochemical activities in *Vigna unguiculata*. Biol. Plant. 38: 205－214

Olszyk D, Dai QJ, Teng P, Leung H, Luo Y, and Peng SB (1996) UV-B effects on crops: Response of irrigated rice ecosystem. J. Plant Physiol. 148: 26－34

Patel NR, Mehta AN, and Shekh AM (2001) Canopy temperature and water stress quantification in rainfed pigeonpea (*Cajanus cajan* (L.) Millsp.). Agric. For. Meteorol. 109: 223－232

Paul ND, Rasanayagam S, Moody SA, Hatcher PE, and Ayres PG (1997) The role of interactions between trophic levels in determining the effects of UV-B on terrestrial ecosystems. Plant Ecol. 128: 296－308

Prasad PVV, Craufurd PQ, and Summerfield RJ (1999) Sensitivity of peanuts to timing of heat stress during reproductive development. Crop Sci. 39: 1352－1357

Prasad PVV, Boote KJ, Allen Jr LH, and Thomas JMG (2002) Effects of elevated temperature and carbon dioxide on seed-set and yield of kidney bean (*Phaseolus vulgaris* L.). Global Change Biol. 8: 710－721

Prasad PVV, Boote KJ, Allen Jr LH, and Thomas JMG (2003a) Super-optimal temperatures are detrimental to reproductive processes and yield of peanut under both ambient and elevated carbon dioxide. Global Change Biol. 9: 1775－1787

Prasad PVV, Kakani VG, and Reddy KR (2003b) Plants and environment: Ozone depletion. In: Thomas B, Murthy DJ, Murray BG (eds) Encyclopedia of Applied Plant Sciences. Elsevier, London, UK, pp.749－756

Prasad PVV, Allen LH, and Boote KJ (2005) Crop responses to elevated carbon dioxide and interaction with temperature: Grain legumes. In: Tuba Z (ed) Ecological Responses and Adaptations of Crops to Rising Carbon Dioxide. Harworth Press, USA, pp.113－155

Prasad PVV, Boote KJ, and Allen Jr. LH (2006a) Adverse high temperature effects on pollen viability, seed-set, seed yield and harvest index of grain sorghum (*Sorghum bicolor* (L.) Moench) are more severe at elevated carbon dioxide due to higher tissue temperatures. Agric. Forest Meteorol. 139: 237－251

Prasad PVV, Boote KJ, Allen Jr LH, Sheehy JE, and Thomas JMG (2006b) Species, ecotype and cultivar differences in spikelet fertility and harvest index of rice in response to high temperature stress. Field Crop Res. 95: 398－411

Prasad PVV, Pisipati SR, Mutava RN, and Tuinstra MR (2008) Sensitivity of grain sorghum to high temperature stress during reproductive development. Crop Sci. 48: 1911－1917

Prasad PVV, Staggenborg SA, and Ristic Z (2009) Impacts of drought and/or heat stress on physiological, developmental, growth and yield processes of crop plants. In: Ahuja LH, Reddy VR, Saseendran SA and Yu Q (eds) Responses of Crops to Limited Water: Understanding and Modeling Water Stress Effects on Plant Growth Processes. Advances in Agricultural Modeling Series 1. ASA-CSSA, Madison, WI. pp.301－355

Premkumar A and Kulandaivelu G (1996) Influence of ultraviolet-B enhanced solar radiation on growth and photosynthesis of potassium deficient cowpea seedlings. Photosynthetica 32: 521－528

Randall HC and Sinclair TR (1988) Sensitivity of soybean leaf development to water deficits. Plant Cell Environ 11: 835－839

Randeniya LK, Vohralik PF, and Plumb IC (2002) Stratospheric ozone depletion at northern and mid latitudes in the 21st century: The importance of future concentrations of greenhouse gases nitrous oxide and methane. Geophys. Res. Lett. 29: 101－104

Raviv M and Antignus Y (2004) UV radiation effects on pathogens and insect pests of greenhouse-grown crops. Photochem. Photobiol. 79: 219－226

Reddy KR and Hodges HF (2000) Climate Change and Global Crop Productivity. CAB International, Oxon, UK, p.448

Reddy KR and Zhao D (2005) Interactive effects of elevated CO_2 and potassium deficiency on photosynthesis, growth and biomass partitioning of cotton. Field Crop Res. 94: 201－213

Reddy KR and Kakani VG (2007) Screening *Capsicum* species of different origins for high temperature tolerance by *in vitro* pollen germination and pollen tube length. Sci. Hortic. 112: 130－135

Reddy KR, Hodges HF, and McKinion JM (1997a) Crop modeling and applications: A cotton example. Adv. Agron. 59: 225－290

Reddy KR, Hodges HF, and McKinion JM (1997b) A comparison of scenarios for the effect of global climate change on cotton growth and yield. Aust. J. Plant Physiol. 24: 707－713

Reddy KR, Read JJ, Baker JT, McKinion JM, Tarpley L, Hodges HF, and Reddy VR (2001) Soil-Plant-Atmosphere-Research (SPAR) facility—A tool for plant research and modeling. Biotronics 30: 27－50

Reddy KR, Kakani VG, McKinion JM, and Baker DN (2002) Applications of a cotton simulation model, GOSSYM, for crop management, economic and policy decisions. In: Ahuja LR, Ma L and Howell TA (eds) Agricultural System Models in Field Research and Technology Transfer. CRC Press, LLC, Boca Raton, FL, pp.33－73

Reddy KR, Kakani VG, Zhao D, Mohammed AR, and Gao W (2003) Cotton responses to ultraviolet-B radiation: Experimentation and algorithm development. Agric. For. Meteorol. 120: 249－265

Reddy KR, Kakani VG, Zhao D, Koti S, and Gao W (2004) Interactive effects of ultraviolet-B radiation and temperature on cotton physiology, growth, development and hyperspectral reflectance. Photochem. Photobiol. 79: 416－427

Reddy KR, Koti S, Kakani VG, Zhao D, and Gao W (2005) Genotypic variation of soybean and cotton crops in their response to UV-B radiation for vegetative growth and physiology. In: Bernhard G, Slusser JR, Herman JR, Gao W (eds) Ultraviolet Ground- and Space-based Measurements, Models, and Effects. Proc. SPIE, pp.156－168

Reddy KR, Kakani VG, and Hodges HF (2009) Exploring the use of environmental productivity index concept for crop production and modeling. In: Ahuja LH, Reddy VR, Saseendran SA and Yu Q (eds) Recent Advances in Understanding and Modeling of Water Stress Effects on Plant Growth Processes, Crop Science Society of America, Madison, WI. pp.387－410

Ristic ZR, Bukovnik U, Momcilovic I, Fu JM, and Prasad PVV (2008) Heat-induced accumulation of chloroplast protein synthesis elongation factor, EF-Tu, in winter wheat. J. Plant Physiol. 165: 192－202

Rizhsky L, Liang H, Shuman J, Shulaev V, Davletova S, and Mittler R (2004) When defense pathways collide. The response of *Arabidopsis* to a combination of drought and heat stress. Plant Physiol. 134: 1683－1696

Rogers CA, Wayne PM, Macklin EA, Muilenberg ML, Wagner CJ, Epstein PR, and Bazzaz FA (2006) Interaction of the onset of spring and elevated atmospheric CO_2 on ragweed (*Ambrosia artemisiifolia* L.) pollen production. Environ. Health Perspect. 114: 865－869

Rosenfield JE, Douglass AR, and Considine DB (2002) The impact of increasing carbon dioxide on ozone recovery. J. Geophys. Res. 107: 4049

Rotem J and Aust HJ (1991) The effect of ultraviolet and solar radiation and temperature on survival of fungal propagules. J. Phytopathol. 133: 76－84

Rozema J, van de Staaij J, Björn LO, and Caldwell M (1997) UV-B as an environmental factor in plant life: Stress and regulation. Trends Ecol. Evol. 12: 22－28

Runeckles VC and Krupa SV (1994) The impact of UV-B radiation and ozone on terrestrial vegetation. Environ. Pollut. 83: 191－213

Saile-Mark M and Tevini M (1997) Effects of solar UV-B radiation on growth, flowering and yield of central and southern European bush bean cultivars (*Phaseolus vulgaris* L.). Plant Ecol. 128: 115－125

Salem MA, Kakani VG, Koti S, and Reddy KR (2007) Pollen-based screening of soybean genotypes for high temperatures. Crop Sci. 47: 219－231

Sancar A (1994) Structure and function of DNA photolyase. Biochemistry 33: 2－9

Savin R and Nicolas ME (1996) Effect of short episodes of drought and high temperature on grain growth and starch accumulation of two malting barley cultivars. Aust. J. Plant Physiol. 23: 201－210

Searles PS, Flint SD, and Caldwell MM (2001) A meta-analysis of plant field studies simulating stratospheric ozone depletion. Oecologia 127: 1－10

Sinclair TR and Purcell LC (2005) Is a physiological perspective relevant in a 'genocentric' age? J. Exp. Bot. 56: 2777－2782

Sinclair TR, N'Diaye O, and Briggs RH (1990) Growth and yield of field-grown soybean in response to enhanced exposure to ultraviolet-B radiation. J. Environ. Qual. 19: 478－481

Singh BB and Sharma B (1996) Restructuring cowpea for higher yield. Indian J. Genet. Plant Breed. 56: 389－405

Singh SK (2008) Developing screening tools for abiotic stresses using cowpea (*Vigna unguiculata* (L.) Walp.) as a model crop. Ph.D. Dissertation, Mississippi State University, MS

Singh SK, Surabhi GK, Gao W, and Reddy KR (2008a) Assessing genotypic variability of cowpea (*Vigna unguiculata* (L.) Walp.) to current and projected ultraviolet-B radiation. J. Photochem. Photobiol. B: Biology 93: 71－81

Singh SK, Kakani VG, Brand D, Baldwin B, and Reddy KR (2008b) Assessment of cold and heat tolerance of winter-grown canola (*Brassica napus* L.) cultivars by pollen-based parameters. J. Agron. Crop Sci. 194: 225－236

Soler R, Bezemer TM, Van der Putten WH, Vet LEM, and Harvey JA (2005) Root herbivore effects on above-ground herbivore, parasitoid and hyperparasitoid performance via changes in plant quality. J. Anim. Ecol. 74: 1121－1130

Souza RP, Machado EC, Silva JAB, Lagôa AMMA, and Silveira JAG (2004) Photosynthetic gas exchange, chlorophyll fluorescence and some associated metabolic changes in cowpea (*Vigna unguiculata*) during water stress and recovery. Environ. Exp. Bot. 51: 45－56

Sullivan JH and Teramura AH (1990) Field study of the interaction between solar ultraviolet-B radiation and drought on photosynthesis and growth in soybean. Plant Physiol. 92: 141－146

Tardieu F, Reymond M, Hamard P, Granier C, and Muller B (2000) Spatial distribution of expansion rate, cell division rate and cell size in maize leaves: A synthesis of the effects of soil water status, evaporative demand and temperature. J. Exp. Bot. 51: 1505－1514

Tegelberg R, Julkunen-Tiitto R, Vartiainen M, Paunonen R, Rousi M, and Kellomäki S (2008) Exposures to elevated CO_2, elevated temperature and enhanced UV-B radiation modify activities of polyphenol oxidase and guaiacol peroxidase and concentrations of chlorophylls, polyamines and soluble proteins in the leaves of *Betula pendula* seedlings. Environ. Exp. Bot. 62: 308－315

Teramura AH (1983) Effects of ultraviolet-B radiation on the growth and yield of crop plants. Physiol. Plant. 58: 415－427

Teramura AH and Sullivan JH (1994) Effects of UV-B radiation on photosynthesis and growth of terrestrial plants. Photosynthesis Res. 39: 463－437

Thiaw S and Hall AE (2004) Comparison of selection for either leaf-electrolyte-leakage or pod set in enhancing heat tolerance and grain yield of cowpea. Field Crops Res. 86: 239－253

Total Ozone Mapping Spectrometer (TOMS) (2009) Atmosphere Chemistry and Dyna mics Brach (Online). Available at http://toms. gsfc.nasa. gov/ery_uv/euv_v8. html (verified 3 June 2009)

Torabinejad J, Caldwell MM, Flint SD, Durham S (1998) Susceptibility of pollen to UV-B radiation assay of 34 taxa. Am. J. Bot. 85: 360－369

Tubiello FN, Amthor JS, Boote KJ, Donatelli M, Easterling W, Fischer G, Gifford RM, Howden M, Reilly J, and Rosenzweig C (2007) Crop response to elevated CO_2 and world food supply: A comment on "Food for Thought..." by Long et al., Science 312: 1918－1921, 2006. Eur. J. Agron. 26: 215－223

U.N. Population Division (2008) Webpage http://www.un.org/esa/population/unpop.htm

U.S. Census Bureau, (2008) U.S. and World Population Clocks—POPClocks. http://www.census.gov/main/www/popclock.html

Upadhyaya HD (2005) Variability for drought resistance related traits in the mini core collection of peanut. Crop Sci. 45: 1432－1440

Vu CV, Allen LH, and Garrard LA (1982) Effects of UV-B radiation (280 nm－320 nm) on photosynthetic constituents and processes in expanding leaves of soybean (*Glycine max* (L.) Merr.). Environ. Exp. Bot. 22: 465－473

Vu CV, Allen LH, and Garrard LA (1984) Effect of UV-B radiation (280 nm－320 nm) on ribulose-1, 5-bisphosphate carboxylase in pea and soybean. Environ. Exp. Bot. 24: 131－143

Walton GH, Si P, and Bowde B (1999) Environmental impact on canola yield and oil. In: Wratten N, Salisbury PA (eds) Proceedings of the 10th International Rapeseed Congress (CD-ROM). The Regional Institute Ltd, Canberra, Australia

Wan S, Yuan T, Bowdish S, Wallace L, Russell SD, and Luo Y (2002) Response of an allergenic species *Ambrosia psilostachya* (Asteraceae), to experimental warming and clipping: Implications for public health. Am. J. Bot. 89: 1843－1846

Warrag MOA and Hall AE (1983) Reproductive responses of cowpea to heat stress: Genotypic differences in tolerance to heat at flowering. Crop Sci. 23: 1088－1092

Warrag MOA and Hall AE (1984) Reproductive responses of cowpea (*Vigna unguiculata* (L.) Walp.) to heat stress. Ⅱ. Responses to night air temperature. Field Crops Res. 8: 17－33

Wentworth M, Murchie EH, Gray JE, Villegas D, Pastenes C, Pinto M, and Horton P (2006) Differential adaptation of two varieties of common bean to abiotic stress: Ⅱ. Acclimation of photosynthesis. J. Exp. Bot. 57: 699－709

Westgate ME (1994) Water status and development of the maize endosperm and embryo during drought. Crop Sci. 34: 76－83

Williams JH and Boote KJ (1995) Physiology and modeling predicting the unpredictable legume. In: Patte HE, Stalker HT (eds) Advances in peanut science. APRES, Stillwater, OK, pp.301－335

WMO (2007) Scientific Assessment of Ozone Depletion: 2006. Global Ozone Research and Monitoring Project 50. Geneva, Switzerland

Xiao G, Liu W, Xu Q, Sun Z, and Wang J (2005) Effects of temperature increase and elevated CO_2 concentration, with supplemental irrigation, on the yield of rain-fed spring wheat in a semiarid region of China. Agric. Water Manage. 74: 243－255

Yuan L, Yanqun Z, Haiyan C, Jianjun C, Jilong Y, and Zhide H (2000) Intraspecific responses in crop growth and yield of 20 wheat cultivars to enhanced ultraviolet-B radiation under field conditions. Field Crops Res. 67: 25－33

Zavala JA, Scopel AL, and Ballare CL (2001) Effect of ambient UV-B radiation on soybean crops: Impact on leaf herbivory by *Anticarsia gemmatalis*. Plant Ecol. 156: 121－130

Zhao D, Reddy KR, Kakani VG, Reed J, and Sullivan J (2003) Growth and physiological responses of cotton (*Gossypium hirsutum* L.) to elevated carbon dioxide and ultraviolet-B radiation under controlled environment conditions. Plant Cell Environ. 26: 771－782

Ziska LH (2003) Evaluation of yield loss in field sorghum from a C_3 and C_4 weed with increasing CO_2. Weed Sci. 51: 914－918

Ziska LH and Caulfield FA (2000) Rising CO_2 and pollen production of common ragweed, a known allergy-inducing species: Implications for public health. Aust. J. Plant Physiol. 27: 893－898

Ziska LH and George K (2004) Rising carbon dioxide and invasive, noxious plants: Potential threats and consequences. World Resource Rev. 16: 427－447

Ziska LH, Gebhand DE, Frenz DA, Faulkner S, Singer BD, and Straka JG (2003) Cities as harbingers of climate change: Common ragweed, urbanization, and public health. J. Allergy Cli. Immunol. 111: 290－295

Ziska LH, Epstein PR, and Rogers CR (2008) Climate change, aerobiology, and public health in the northeastern United States. Mitig. Adapt. Glob. Change 13: 607－613

Zoltán T (2005) Is the long-term elevated air CO_2 environment beneficial for plants, crops and vegetation? In: Tuba Z (ed) Ecological Responses and Adaptations of Crops to Rising Atmospheric Carbon Dioxide. Haworth Press, Inc., New York, NY, pp.1－6

15 Assessment of DNA Damage as a Tool to Measure UV-B Tolerance in Soybean Lines Differing in Foliar Flavonoid Composition

Joseph H. Sullivan[1], Linda C. Pope, Betsy M. Sutherland[2], Paula V. Bennett[2], James E. Blum[3], Ann E. Stapleton[4], and Dennis C. Gitz III[5]

[1] Department of Plant Science and Landscape Architecture, 2122 Plant Sciences Building
University of Maryland, College Park, MD 20742, USA
E-mail: jsull@umd.edu
[2] Brookhaven National Laboratory, P.O. Box 5000, Upton, NY 11973-5000, USA
E-mail: bms@bnl.gov
[3] Department of Mathematics and Statistics
University of North Carolina at Wilmington, Wilmington, NC 28403, USA
E-mail: blumj@uncw.edu
[4] Department of Biology and Marine Biology
University of North Carolina at Wilmington, Wilmington, NC 28403, USA
E-mail: stapletona@uncw.edu
[5] USDA-ARS, 3810 4th Street, Lubbock, Texas 79415,USA

Abstract Damage to DNA, in the form of cyclobutane pyrimidine dimers (CPD), may occur in soybean (*Glycine max* (L.) Merr) plants when they are exposed to increasing levels of ultraviolet-B (UV-B) radiation. Flavonoids and other phenolics accumulate in the epidermal layer of leaves and may provide protection for sensitive tissues including DNA molecules. We evaluated the steady state levels of accumulated damage and the protection afforded by flavonoids in two soybean isolines: Clark producing high levels of flavonoids, and Clark-magenta producing extremely low flavonoid levels. Both cultivars were grown in the field under ambient and supplemental UV-B radiation. Leaf tissue was harvested in a diurnal sequence, and the samples were analyzed. Two methods of analysis were used in order to develop a common reference point between the two. In one method, DNA was isolated and treated with UV endonuclease, and the DNA fragments were separated using unidirectional pulsed field electrophoresis and quantified through electronic imaging. In the alternate method, a western blotting procedure, immobilized DNA was reacted with monoclonal antibodies specific to CPD DNA damage. Results were similar in both techniques and show lesion frequency to be low in both isolines. However significant differences

were found between cultivars, UV treatments, time of day collected, and levels of PAR. The average level of dimers per megabase for the isoline Clark was ~4 (with or without supplemental UV), and for Clark-magenta, ~4 for samples with no supplemental UV and ~6 for those exposed to supplemental UV radiation. Diurnally, dimer levels were frequently higher in the Clark-magenta isoline, especially when exposed to supplemental UV-B. Both isolines appear to be either well-protected from DNA damage, or repair is efficient enough to minimize biologically significant accumulation of DNA damage. This suggests that protection mechanisms, other than flavonoids alone, contribute to maintenance of DNA integrity in soybean.

Keywords Glycine max, soybean, DNA damage, pyrimidine dimers, UV-B radiation, stratospheric ozone depletion

15.1 Introduction

Continued stratospheric ozone depletion and the resultant increase in ultraviolet-B radiation (UV-B) raises a concern for a potential decrease in crop yields and impacts on agricultural and natural ecosystems. Although the implementation of regulations that minimize inputs of chlorofluorocarbons into the stratosphere is resulting in recovery of the ozone layer, there is still uncertainly about the stability of future ozone levels (WMO, 2003). For example, the link between global warming and ozone depletion is not fully understood and warrants further investigation.

Warming trends in the Pacific Ocean affect the strength of the vortex at the South Pole allowing the photochemical reactions that deplete ozone to persist longer in the spring (Kerr, 1995). As CO_2 levels increase and the troposphere warms, the associated cooling of the stratosphere leads to increased transport of water vapor to the stratosphere (Kirk-Davidoff et al., 1999). This water vapor is the basis for the formation of the polar stratospheric clouds (PSCs) that provide a surface on which ozone destruction takes place. Persistence of PSCs into the Antarctic spring due to stratospheric cooling may lead to enhanced rates of catalytic ozone destruction. This may be further exaggerated by atmospheric denitrification that reduces the effectiveness of nitric acid to combine with free chlorine and prevent ozone destruction (Salawich et al., 2002). Thirty-five percent of the ozone lost in the Arctic winter of 1994 – 1995 was attributable to stratospheric denitrification (Waibel et al., 1999). Concerns such as these suggest that the possible implications of continued ozone depletion and concomitant increases in solar UV-B radiation (between 290 nm and 315 nm) need further evaluation.

Although it represents only a fraction of the total solar electromagnetic spectrum, UV-B may exert substantial photobiological effects when absorbed by important macromolecules such as proteins and nucleic acids (Giese, 1964). The highly energetic photons of UV-B radiation may reduce photosynthesis, alter

stomatal development and functioning, damage proteins and membranes, and induce DNA lesions if absorbed in sufficient quantity (e.g., Caldwell et al., 2003; Sullivan, 2005). However, sensitivity to UV-B varies greatly among plant species. Some plants are quite tolerant to high fluences of UV-B (Sullivan et al., 1992; Ziska et al., 1992), while others are sensitive to present ambient fluences (Bogenrieder and Klein, 1982; Krizek et al., 1998). This variation in response to UV-B makes it difficult to generalize about UV-B effects, but overall meta-analysis of UV studies through the end of the Century suggested that major reductions in growth or biomass were rare in realistic field studies (Searles et al., 2001). This infers the importance of UV-B throughout the evolution of land plants that has led to well-developed UV protection mechanisms in many plant species (Beggs et al., 1986).

One of the protective responses that have generally been considered adaptive is the accumulation of epidermal UV-screening compounds that serve as UV filters. The accumulation of phenolics, and flavonoids in particular, has been frequently reported in response to UV-B radiation (e.g., Robberecht and Caldwell, 1978; Caldwell et al., 1983; Sullivan and Teramura, 1989; Tevini et al., 1991). In fact, Searles et al. (2001) found through a meta-analysis of 103 published articles that the most common response of plants to UV-B is an increase in UV-screening compounds. Flavonoids and other phenolics, especially hydroxycinnamic acids (Sheahan, 1996), absorb strongly in the UV-B range. The accumulation of these compounds in the epidermis has been shown to reduce UV-B radiation transmittance and hypothesized to protect sensitive targets (Robberecht and Caldwell, 1978; Robberecht and Caldwell, 1983; Beggs et al. 1986; and many others). The accumulation of these compounds is dependent upon a number of factors, including both visible and UV fluence (Mohr and Drumm-Herrel, 1983; Wellman, 1983) and many other environmental factors (McClure, 1986). The mechanistic basis of light or UV-induced accumulation lies at the gene level as several key enzymes in the flavonoid biosynthetic pathway, such as, phenylalanine ammonia lyase (PAL) and chalcone synthase (CHS), are induced by UV radiation (Chappell and Hahlbrock, 1984; Beerhues et al., 1988; Liu and McClure, 1995; Schnitzler et al., 1997). There is little doubt that phenolics accumulate in leaf tissue in response to UV-B radiation, and that they are important in conferring photoprotection to "target" molecules that may be damaged by UV-B radiation.

One of the best methods utilized to date to evaluate the screening effectiveness of phenolics has been to actually measure UV-B penetration inside a leaf and compare this to expected values based on soluble phenolic levels. The research by Day et al. (1994), and other related studies (see Vogelmann, 1994, and references therein), have shown that the penetration of UV-B through the epidermis is quite variable and may be related to plant life form and growth habit. However, a rather poor correlation ($r^2 = 0.21$) was found between epidermal transmittance of UV-B at 300 nm and absorbance of soluble phenolics (Day, 1993). Also, Day et al. (1994) measured epidermal transmittance of both UV-B at 300 nm and total

UV-B weighted with one of several weighting functions. They found that the expected extinction rates based on absorbance values across a wide range of species within a life-form group followed the theoretical expectation in only 1 of 42 species. In other words, "Beer-Lambert" type extinction was rarely observed, based on concentrations of soluble UV-absorbing compounds alone. The presence of bound phenolics in the epidermis that are not extracted, but alter epidermal transmittance, could contribute to this relationship.

Even when the concentration or screening ability of soluble and bound phenolics are considered, these parameters do not always correlate well with UV tolerance (e.g., Barnes et al., 1987; Dillenburg et al., 1994; Sullivan et al., 1996), and simple correlations may not exist between the apparent concentrations of soluble UV-absorbing compounds and UV-sensitivity. Barnes et al. (1987) suggested that some species adapted to high ambient UV-B fluxes were inherently tolerant to UV-B radiation, but we do not yet have a complete understanding of all tolerance mechanisms.

In addition to their role as sunscreens, phenolics are involved in numerous aspects of plant growth and development, such as serving as antioxidants (Sheahan, 1996), involvement with auxin-mediated responses (Stafford, 1991), cell wall extension (Dale, 1988; Liu et al., 1995), and lignification (Raven, 1977). Phenolic concentrations and composition also have important ecological implications for decomposition rates and nutrient cycling, as well as for plant-insect and plant-pathogen interactions. Therefore, the physiological and ecological roles of phenolics in plants, and the role that solar UV radiation plays in regulating the composition and concentration of them, needs further evaluation. For example, the specific dose response of accumulation of protective compounds, the action spectrum for this response, and the contribution of environmental factors other than UV-B to this response, have not been clearly resolved in field studies.

Soybean has been intensively studied for UV-B responses for the past quarter century and its production of primary flavonols in response to UV-B radiation has frequently been reported (Murali and Teramura, 1986; Sinclair et al., 1990; Mazza et al., 2000). Therefore, since its chemistry and response to UV-B are rather well-known, soybean is a good candidate for a model system to evaluate the protective role of phenolics, flavonoids in particular, in response to UV radiation. This chapter assesses the protective role of flavonoids in protecting soybean DNA from damage due to exposure to high levels of UV-B radiation in the field. DNA damage, primarily cyclobutane pyrimidine dimers (CPDs) caused by UV-B exposure in plants, has been studied in a variety of plant systems, including soybean (Sutherland et al., 1996; Mazza et al., 2000; Bennett et al., 2001; and others). In addition, it is known that DNA damage may accumulate in some species. However, it is not clear whether the absence of flavonoids as screening compounds would alter the diurnal progression of CPD formation.

In this study, we utilized soybean lines that differ in flavonoid quantity and composition in order to evaluate the protective role of flavonoids against UV-B

damage. These cultivars included: (1) the Clark cultivar, a moderately tolerant cultivar that produces primarily the flavonols quercetin and kaempferol for putative UV-screening; and (2) an isoline of Clark, Clark-magenta (Buzzell et al., 1977) that produces essentially no flavonols, but accumulates cinnamic acids in response to UV radiation. Two of three goals of this research were to determine if: (1) CPDs accumulate over the course of the day; and (2) the absence of flavonol glycosides lead to the formation of more photoproducts in the DNA.

A third goal was to compare two methods of CPD analysis. One method previously utilized to evaluate CPDs uses a gel electrophoresis and imaging system to quantify dimers, while many researchers employ an alternate method using a western blotting procedure, in which immobilized DNA is reacted with monoclonal antibodies specific to CPD DNA damage (Mori et al., 1991; Stapleton et al., 1993; Stapleton and Walbot, 1994; Mazza et al., 2000). As previous research has rarely used both methods of dimer quantification, a comparison of these two methods will lend perspective and increase the interpretive power of past and future studies that may utilize one method or another.

15.2 Materials and Methods

15.2.1 Plant Growth and UV Irradiation

Soybean seeds (Glycine max L., cultivars Clark and Clark-magenta) were planted in plots (4.5 m×2.5 m) at the USDA Agricultural Research Center (ARS), South Farm, Beltsville, MD, with a spacing between rows of 0.4 m, and a density of ~35 seeds m^{-1}. One row (4.5 m) of Clark seed was planted next to one row of Clark-magenta seed, and bordered by additional rows of soybeans to simulate field-crowding conditions and to create even sunlight exposure and shading. After germination, plants were thinned to ~25 plants m^{-1} (see (Teramura et al., 1990) for additional information regarding the field sites). In order to reduce water or nutrient stress that can mask the response to UV-B radiation, the plants were watered daily when natural precipitation did not occur, and the plots were fertilized before planting according to recommendations from the Maryland Soil Testing Laboratory.

Ultraviolet-B radiation was provided in a squarewave system by Q-Panel (Cleveland, OH) with UVB-313 sunlamps (12 lamps per plot, 30 cm apart) suspended over and perpendicular to the rows of soybean plants (Teramura et al., 1990). Lamps suspended over the supplemental UV-B plants were wrapped with either cellulose diacetate (CA) which transmits UV-B radiation down to 290 nm, or with polyester filters that block almost all UV-B below 316 nm. Therefore, plants received similar levels of PAR and UV-A radiation, but differed in

exposure to UV-B radiation. Spectral irradiance beneath the lamps was measured with an Optronic Laboratories Inc. (Orlando, FL) Model 754 spectroradiometer. The height of the lamps above the plants was maintained at approximately 75 cm.

All filters were presolarized for eight hours, and changed weekly for CA and every two weeks for polyester to compensate for filter degradation. Plants in the field received either ambient UV-B (polyester) or ambient UV-B plus a maximum of 5 kJ m^{-2} d^{-1} UV-B_{BE} (Biologically Effective UV-B when weighted with the action spectrum of Caldwell (1971)). This represented the maximum supplemental level of UV-B radiation that would be received at College Park, MD, during a cloudless day at the summer solstice, with a 25% reduction in ozone, according to the model derived by Green et al. (1980), with later derivations by Björn and Murphy (1985).

15.2.2 Field Sampling

Samples were collected on two days, July 9 and July 22 (2000) from the newest, fully-expanded leaves. Average daily UV-B radiation values and climatological data were obtained from the USDA UV-B Monitoring and Research Program website (http://uvb.nrel.colostate.edu/UVB/index.jsf) for the Beltsville, MD station, located approximately 300 m from the study site. Overall average daily radiation was 68.9 kW/m^2 at 300 nm on July 9th and 46.7 kW/m^2 at 300 nm on July 22nd. This led to ambient daily weighted (Caldwell, 1971) UV-B levels of 4.2 and 3.1 kJ m^{-2} on the two days respectively, and 9.2 and 8.1 kJ m^{-2} respectively of UVB_{BE} when ambient and supplemental levels were combined. Relative humidity ranged from 27% to 94.7% on July 9 and between 56% and 100% on July 22. Daily average temperature was 81.7°F (27.6°C) on July 9 and 80.7°F (27.0°C) on July 22. Plants were watered daily.

Sampling in the field began at dawn, (4:00 Solar time) on July 9th and continued at two hour intervals until after dark (22:00 Solar time). At each time point, at least six samples were collected from each cultivar, UV treatment, and replicate block. A second set of samples was collected using approximately the same method on July 22, 1999. The weather on July 22nd was overcast with light rain. In all cases, samples (two leaf disks, 1 cm in diameter) were taken from the newest, fully expanded trifoliate in the upper canopy, immediately wrapped in a labeled foil packet, dropped into liquid nitrogen (LN_2), and stored over dry ice (CO_2, −78.5°C). In order to avoid variation from plant to plant and leaf to leaf, the same trifoliate was sampled five times over the course of the day. However, to reduce the chance that wounding affected dimer levels, at least one leaf was sampled for the first time in each sampling period, and a rotation of leaves sampled was implanted such that each measurement period (after the fifth each day) included leaves that had been previously sampled from one to five times.

15.2.3 Analysis of Phenolics

Leaf samples were collected on plants at predetermined times following the commencement of irradiation in order to verify their chemical composition and to assess their response to UV-B radiation. Leaf disks (1.13 cm^2) were made on the first true leaf of the plants for studies on emerging plants and on the most recently mature leaf on mature plants. These were placed on ice and taken to the laboratory where they were placed in 20 ml high density polyethylene (HDPE) scintillation vials covered with 10 ml of slightly acidified aqueous methanol (MeOH:H_2O:AcOOH, 50:50:1, v:v:v), tightly capped, and held in the dark at room temperature with gentle agitation (50 rpm) on a G10 Gyrotory Shaker (New Brunswick Scientific, Edison, NJ, USA) for 48 hrs. − 72 hrs. During extraction, vials were sealed with polyethylene lined caps; since it was found that foil lined caps would occasionally corrode and contaminate the extracts leading to the non-uniform formation of metal-flavonol complexes and bathochromic shifting of the absorbance spectra. The extract absorbance was determined from 260 nm − 760 nm at 1 nm intervals with a Shimadzu UV-1601 dual beam spectrophotometer (Shimadzu Scientific Corp., Columbia, MD, USA), and data were expressed as absorbance units per unit leaf area (A cm^{-2}). Since UV level did not lead to qualitative differences in spectra within a species or cultivar, absorbance values at 300 nm were used for comparative purposes between the treatment and controls.

In order to verify presence or absence of flavonoids in the Clark and Clark-magenta isoline of soybean, High Performance Liquid Chromatography (HPLC) separation and determination of flavonoids were conducted. Leaf disks were milled under liquid nitrogen in microcentrifuge tubes, hydrolyzed in 1 N H_2SO_4 in 1 ml 50% aqueous methanol at 80° for 30 minutes under nitrogen, brought to 5 ml, and filtered. Forty µL of the filtrate was directly injected onto a 250×4.6 mm column packed with 7 µ spherical C8 stationary phase with gradient elution by 20% solvent B (aqueous 1% orthophosphoric acid) in solvent A (acetonitrile in 1% orthophosphoric acid) increased to 60% B over 20 min at a flow rate of 1.5 ml min^{-1}. Detection at 370 nm was accomplished using a Waters 490E programmable multiwavelength detector. Naringenin (5µL) in 50% aqueous methanol (1 mg ml^{-1}) was coinjected at the beginning of each run as a standard.

15.2.4 Determination of DNA Lesions—Gel Electrophoresis Method

1. Leaf tissue processing: Unless otherwise noted, all procedures were performed under dim yellow light (General Electric, fluorescent; >~500 nm) to reduce the possibility of undesired photoreactivation of the samples during processing. Leaf tissue was processed according to the methods outlined by several researchers (Quaite et al., 1992; Quaite et al., 1994; Sutherland et al., 1996; Kang et al., 1998;

Bennett et al., 2001). Leaf disks were chopped and ground to a fine, light green powder in liquid nitrogen (LN_2), dropped into Lysis Buffer #1 (10 mM Tris-HCl, pH 8.0, 0.83 M EDTA, 13% mannitol, 2% sarcosyl, and 1 mg/ml Proteinase K (Boehringer Mannheim, Indianapolis, IN), 40°C – 45°C) and vacuum-infused. Agarose Sea Plaque (2-1/2% w/v, FMC, Rockland, ME) in TE buffer (10 mM Tris-HCl, pH 8.0, 1 mM EDTA, heated to 70°C – 75°C) was added and the mixture pipetted into chilled molds (GeNunc Module, Nalge Nunc, catalog no. 2-32549). The solidified samples were covered with Lysis buffer #2 (10 mM Tris-HCl pH 8.0, 0.83 M EDTA, 2% sarcosyl, and 1 mg/ml Proteinase K), wrapped with aluminum foil, and incubated 24 hours at 45°C. Lysis buffer #2 was replaced with Lysis buffer #3 (10 mM Tris-HCl pH 7.8 – 8.0, 0.1 M EDTA, 20 mM NaCl, 1% sarcosyl, and 1 mg/ml Proteinase K), rewrapped in foil, and incubated for 24 to 48 hours at 45°C. Lysis buffer #3 was refreshed, and the plugs incubated for an additional 24 to 48 hours at 45°C (total of 72-hour minimum in Lysis buffer #3).

2. Plug processing: Plugs were soaked in TE (pH 7.6) in the dark and over ice. Plugs were subsequently soaked in TE and phenylmethyl sulfonyl fluoride (PMSF) (2.2 μL/ml) 2X at room temperature, with a final cold TE rinse. Samples were soaked 3X in UV endonuclease buffer (30 mM Tris-HCl, pH 7.6, 40 mM NaCl, 1 mM EDTA) over ice. Two similar plugs were placed in a single labeled Eppendorf centrifuge tube, placed in a water bath (70°C – 72°C) and the re-melted DNA-agarose mixture pipetted (7 μL) to form new plugs. The new plugs were covered with UV endonuclease buffer and stored overnight (4°C). The buffer was replaced with 20 μL Reaction Mix (UV endonuclease buffer containing 1 mM dithiothreitol (DTT) and 0.1 mg ml^{-1} bovine serum albumin (BSA)), and the samples were kept on ice.

3. Plug preparation: Plugs were divided into two groups: the "Minus" plugs and the "Plus" plugs. The Reaction Mix was refreshed in the "Minus" plugs, removed from the "Plus" plugs, and then replaced with a solution of Reaction Mix and sufficient *Micrococcus luteus* UV endonuclease (MLE) enzyme to cut the DNA at all dimer locations. The preparation of MLE used in these experiments cleaved approximately 4×10^{15} CPDs $\mu L^{-1}h^{-1}$. The relative numbers of DNA fragments in each "Plus" plug (sample cut with MLE) and "Minus" plug (sample not exposed to the enzyme) were determined. All plugs were kept on ice for 30 minutes and then incubated at 37°C for 60 minutes. Additional Reaction Mix (2 μL) was added to the "Minus" plugs, and an equal volume of Reaction Mix with 50% MLE was added to the "Plus" plugs. Samples were incubated at 37°C for 30 minutes and held on ice until processed. All plugs were rinsed 2X with TE, covered with alkaline stop (0.5 M NaOH, 50% (vol/vol) glycerol and 0.25% (wt/vol) bromocresol green), and stored on ice at 4°C. The gels (agarose (SeaKem LE; FMC, Rockland, ME) (0.4% wt/vol) in 1 mM EDTA, 50 mM NaCl) were prepared and equilibrated with alkaline electrophoresis solution (2 mM EDTA, 30 mM NaOH), at room temperature. The molecular length standards from bacteriophages

G (750kb), T4 (170 kb), λ (48.5 kb), the HindIII digest of λ (23, 9.4, 6.6, 4.3, 2.1 kb) and BioLow (1.0, 0.5, and 0.2 kb) (BioMarker Low, BioVentures, Inc., Murfreesboro, TN) were prepared, and treated with alkaline stop for 60 minutes. All sample plugs were placed in a water bath (at 37°C) for 60 minutes to denature the DNA, rinsed with cold alkaline electrophoresis solution (30 mM NaOH, 2 mM EDTA), and the companion pair of "Plus" and "Minus" samples were loaded into adjacent gel wells.

4. Static field electrophoresis: The gel rig was placed in a 10°C water bath to provide temperature stability. The gel was subjected to a static field electrophoresis for 15 minutes at 3 volts/cm. Recirculation of the electrophoresis solution was begun, and the gel electrophoresed for an additional 25 minutes at 3 volts/cm.

5. Unidirectional pulsed-field electrophoresis (UPFE): This method improves the resolution of DNA molecules longer than 100 kilobases (kb), and increases the ability to measure low frequencies of lesions (Sutherland et al., 1987; Quaite et al., 1992; Quaite et al., 1994) that can occur in DNA exposed to ultraviolet light. Electrophoresis resumed with UPFE (15 volts/cm; 0.3 second pulse with 10 second interpulse period, 10°C with buffer recirculation) for 7 hours ±1 hour. The DNA plugs were removed, and the electrophoresis continued for a total of 24 hours. The DNA fragments were dispersed in the gel according to their single-strand molecular lengths. The gel was rinsed, neutralized 2X with 0.1 M Tris-HCl pH 8.0, and stained with ethidium bromide (0.67 μg/mL). Gels were stored at 4°C until imaged.

6. Electronic imaging: A quantitative (digital) electronic image was obtained using a charge-coupled device-based (CCD) system designed and built by J. C. Sutherland (Sutherland et al., 1987). The dual-camera system gave a linear response to the DNA-bound ethidium fluorescence. By obtaining the optical density profile in digital form of the DNA in each lane within the gel, median migration distances were calculated by the computer (Sutherland et al., 1990). The distribution of fluorescence was measured. Results were proportional to the quantity of DNA at each position within the lane (Sutherland et al., 1990).

7. Analysis and dimer quantification: The number of breaks in the DNA molecule was derived from the total number of DNA molecules in the MLE treated sample, less the number of molecules in the untreated sample. In general, molecules in the "Plus" sample are shorter than those in the "Minus" sample (Freeman et al., 1986). The standard sensitivity using this method is approximately 1 lesion/Mb, with a current limit sensitivity of about 1 lesion/5 Mb. In a preliminary action spectrum using very high irradiance levels (0 kW m^{-2} – 15 kW m^{-2}), nearly 120 dimers were measured (data not shown), showing that these isolines are capable of accumulating a very large amount of DNA damage (Pope, 2001). Samples containing a known quantity of dimers (~30 CPDs – 60 CPDs) were periodically run with the test samples to verify the analytic procedures, providing a positive control.

15.2.5 Determination of DNA Lesions—Monoclonal Antibody Method

Plant material was collected simultaneously with the gel-electrophoresed samples (samples collected in July 1999) and stored at −80°C until processed. Samples were shipped on dry ice to the University of Tennessee at Chattanooga, Chattanooga, TN for processing. As described in A. E. Stapleton (1999) and the references therein, DNA was isolated from leaf tissue powdered in liquid nitrogen. Samples were processed by adding ~500 ng of DNA to TE buffer, followed by denaturation and slot-blotting to the membrane. CPDs were detected using a TDM-2 monoclonal antibody. This method detects the primary-bound antibody by an alkaline phosphatase-conjugated secondary antibody. By using a chemiluminescent substrate (CSPD), chemiluminescence was detected with autoradiographic film (or with a cooled CCD camera), and the counts were plotted as a function of time.

15.2.6 Experimental Design and Statistical Analysis

The experimental design was a completely randomized split plot design with two UV-B treatments (main plot) and two cultivars within each treatment as the subplot. Each treatment was replicated twice. Samples were analyzed using the mixed procedure of the Statistical Analysis System (SAS, Cary, NC), with separate models used for the ESS gel data, CPD antibody data, and for the methanol extract absorbance, as each of these used different samples, thus precluding a global multivariate analysis. The models tested for main effects of cultivar, UV-B treatment, sampling day and sampling hour, and their interactions. As several samples were measured on the gel system more than once, a nested term for gel within plant was included in the ESS data analysis. The SAS GLM procedure was used to estimate variance components for the ESS data that contained the nested term.

15.3 Results and Discussion

15.3.1 Leaf Phenolics

The first sampling collection day (July 9) was a clear, sunny day, while the second sampling day (July 22) was primarily overcast and rainy. This provided an opportunity to observe the occurrence of DNA damage and the levels of UV-absorbing compounds under contrasting conditions of PAR and UV radiation.

The absorption spectrum in the UV region of the extracts from the Clark-soybean line was typical of a common flavonoid spectrum (e.g., Mabry et al.,

1970). However, the spectrum from the magenta isoline was suggestive of a lack of flavonoids. The absorption peak in the 280 nm – 290 nm range did not exhibit the classic bathochromic shift indicative of flavonoids (data not shown). It is likely that the UV absorbance in the magenta line was due to the presence of hydroxycinnamates (HCAs) which also strongly absorb in the UV-B waveband. Analysis with HPLC confirmed that the primary flavonoids accumulating in the Clark cultivar were the flavonols quercetin and kaempferol, with quercetin accounting for a large proportion of the total flavonols present (Fig. 15.1). Only minute traces of quercetin were observed in the extract from the Clark-magenta plants.

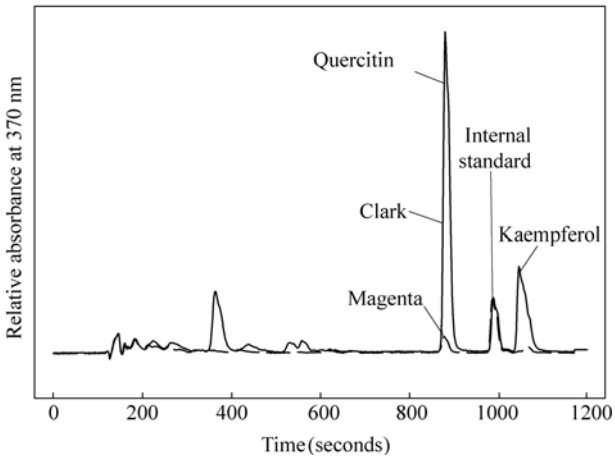

Figure 15.1 HPLC trace from methanol extracts of Clark and Clark-magenta soybean lines grown in the field under ambient levels of UV radiation. The primary flavonol in Clark was found to be quercetin, and only trace amounts of this compound were found in the magenta line

The absorbance at 300 nm of the methanol extracts varied between the two sampling days with higher absorbance values found on the sunny day compared to the cloudy day ($P = 0.02$). There was also a significant difference between the Clark and the Clark-magenta lines on the sunny, but not the cloudy, day. Overall, however, there was little response in these measurements to supplemental UV-B radiation (Fig. 15.2).

It has been suggested (e.g., Searles et al., 2001) that the most common response to increasing levels of UV-B radiation is the increase in UV-absorbing compounds. Several studies with soybean have found that this is a common response (Murali and Teramura, 1986; Sullivan and Teramura, 1990; Gitz et al., 2005). Since the levels were higher on the sunny compared to the cloudy day, the short-term (day-to-day) variations observed in this study may have been linked with ambient levels of UV-B, UV-A, and/or PAR. However, Cosio and McClure (1984) found

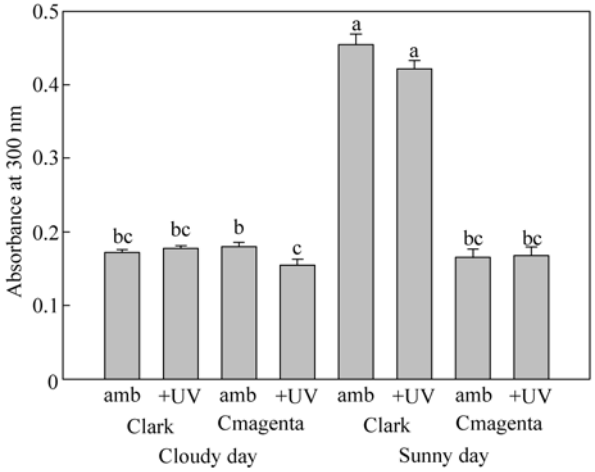

Figure 15.2 The absorbance at 300 nm of a methanol extract from soybean grown in the field under either ambient or ambient plus supplemental levels of UV-B radiation. Each bar is the mean of 5 replicate samples from 2 treatment replicates plus 1 SD. Different letters over a bar indicate a significant difference between the bars

that activities of key enzymes in the flavonoid biosynthetic pathway were greatly reduced following the completion of leaf expansion. Only exposure to UV-C, not found in sunlight reaching the earth's surface, resulted in renewed enzyme activity. Therefore, it seems unlikely that new synthesis of flavonoids on the sunny day would have explained the differences. It is more likely to have been due to environmental conditions (self shading, ambient UV levels, etc.) present during the development of these particular leaves, which led to leaf-to-leaf variations in flavonoid levels. Sullivan et al. (2007) found that soybean responded to short-term changes in ambient levels of both UV-A and UV-B during the initial phases of leaf development and that the spectral sensitivity varied with the species and soybean cultivar. Ultraviolet-A also had a greater effect than did UV-B in soybean lines that were lacking flavonoids. Therefore, it is unclear just how flavonoid synthesis is regulated and further studies on the spectral and fluence response are needed before we have a complete understanding of this process. It is important that we understand the regulation of this process in order to fully understand how plants have adapted to UV-B radiation and how plants and ecosystems will respond to potential changes in solar UV radiation reaching the earth's surface.

15.3.2 DNA Damage

An assessment of how plants differing in flavonoid composition and quantities are affected at the DNA level may provide key information regarding UV tolerance mechanisms and the importance of flavonoids in this process. No significant

difference was noted between blocks on July 9th, and the data were combined for all further analysis. Replicate blocks were also sampled on July 22, but only samples from block 1 were processed using the gel electrophoretic method. Samples taken from both blocks were processed with the monoclonal antibody method.

Statistically significant differences in DNA integrity were observed using both methods of analysis. In the gel method, a significant effect was found for cultivar ($P = 0.0064$), UV treatment ($P = 0.0103$), day ($P = 0.002$), and the interaction between UV treatment and cultivar ($P = 0.0293$). On the cloudy day, supplemental UV-B induced more DNA dimers in the Clark-magenta line than in the ambient UV-treatment, and more than in either treatment in the Clark wild type with a normal flavonoid complement (Fig. 15.3). The Clark-magenta line showed a trend of increasing dimers on the sunny day, but this was not statistically significant. In the CPD analysis, significant effects were cultivar ($P = 0.0001$), time of day ($P = 0.015$), and sunny vs. cloudy day ($P = 0.0001$). Also, when considering the diurnal changes in CPDs, the Clark-magenta line had increased CPD amounts at 13:00 h on the cloudy day (Fig. 15.4). Overall, the Clark line generally had less DNA damage than the Clark-magenta line, but the difference was only significant on the cloudy day (Fig. 15.5).

The level of dimers tended to increase early in the day and then subside in the afternoon. This suggests that at some points, the number of dimers formed over the course of the day exceeds the capacity of repair mechanisms. This short term accumulation of damage might be responsible for some of the deleterious responses of plants to increased levels of UV-B radiation.

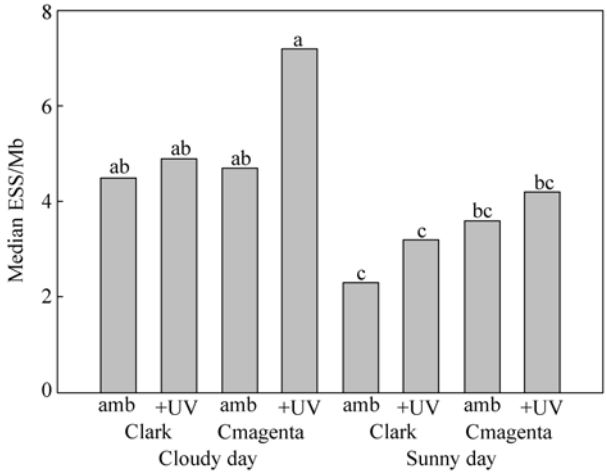

Figure 15.3 The number of ESS (measure of DNA lesions formed) in soybean grown in the field under either ambient or ambient plus supplemental levels of UV-B radiation. Each bar is the mean of 5 replicate samples from 2 treatment replicates plus 1 SD. Different letters over a bar indicate a significant difference between the bars

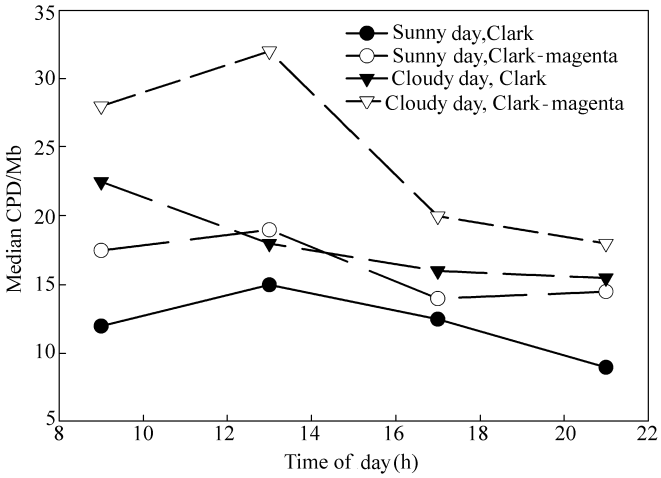

Figure 15.4 Diurnal changes in the number of CPDs formed in 3 soybean lines grown under ambient or ambient plus supplemental levels of UV-B radiation. Each point is the mean of 5 samples collected each 2-hour period (see text for details on sampling protocols)

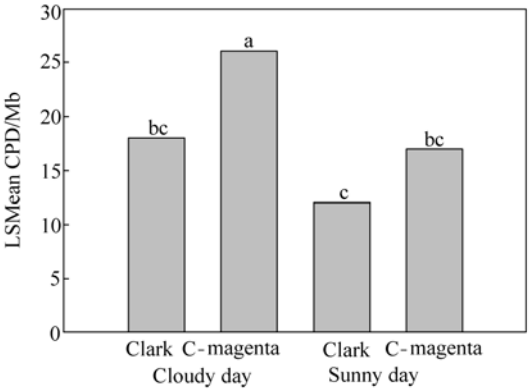

Figure 15.5 CPDs found in two soybean lines grown in the field under either ambient or ambient plus supplemental levels of UV-B. LSMeans of CPDs formed over the course of the day. UV-B treatments are combined since there was no statistical difference between treatments. Each bar is the mean of 5 samples collected each 2-hour period (see text for details on sampling protocols). Different letter over a bar indicates a statistically significant difference in the means at $P = 0.05$

Damage to DNA by UV-B radiation is one factor that could lead to abnormal plant growth and development, altered biochemical pathways and metabolism, inability to reproduce successfully, and even death. Therefore, plants have developed a suite of photorepair and dark repair processes. Ultraviolet-screening mechanisms, such as that afforded by flavonoids, is another protective response. In this study, minimal DNA damage was observed in all cases, but there was some indication

that the absence of flavonoids increased damage at certain times. It is also possible that screening by compounds other than flavonoids, per se (e.g., HCAs), may also be important. The minimal damage that occurred on the cloudy day in Clark-magenta did not persist at the end of the day (20:00 h), so we may assume that the repair of lesions was sufficient to mitigate the majority of damage.

Several studies have shown that the repair of UV-induced damage is mediated by photolyase in mature leaves (Dany et al., 2001). Since photolyase requires a photon of light, preferentially UV-A or blue light (Stapleton et al., 1997) to reverse the damaged DNA, this process must be completed before the energy from the sun dissipates late in the evening, as was the case in our samples. It was primarily on the cloudy day that lesions accumulated in the afternoon in Clark-magenta. The higher ratio of UV-B to PAR was such that minor increases in CPDs occurred periodically. Perhaps PAR levels were not sufficiently high enough to prevent these accumulations. Alternatively, it is possible that the absence of flavonoids, which are more efficient in the absorption of UV-A (Mabry et al., 1970) may lead to increased penetration of UV-A into the leaf mesophyll and therefore, lead to more effective repair systems.

These measurements quantify net dimer levels, and an increased rate of dimer formation might possibly have been countered by enhanced repair capability. Xu et al. (2008a) also noted that the rate of oxidant production appeared to be increased in these same soybean lines in ambient compared to reduced UV-B levels, but observed an increase in the antioxidant system in the magenta soybean line. It is well-known that the balance of repair mechanisms vs. those that provide protection is important (Jansen et al., 1998; Frohnmeyer and Staiger, 2003), and that an increase in UV-absorbing compounds is a common response to UV-B radiation (Searles et al. 2001). However, the results of this study do not allow us to quantify if it was protection (in the case of Clark) and repair (in the case of Clark-magenta) that maintained the low levels of CPDs. Clearly, the effects of UV-A on plant metabolism and the interactions between PAR, UV-A, and UV-B, is not fully understood. This is an area in which continued research may lead to a better understanding of how plants are affected by the various components of sunlight.

When dimer levels from this experiment were compared to maximum levels reached in a exposure response study (~120 CPD's/Mb, data not shown), it was clear that although there was a significant difference in dimers produced by the two cultivars, UV treatments, and irradiance levels, the difference was not biologically significant. Although Clark had fewer dimers on both days (3.46 ± 0.91 and 5.20 ± 1.67) as compared to Clark-magenta (4.39 ± 1.07 and 6.65 ± 1.66), the effects of the small size differences on the plants is probably minimal. This indicates that although flavonoids and phenolics do protect plants from UV-B exposure, in cases where they are not present, plants must provide protection to DNA integrity through other pathways. For example, additional repair enzymes may be produced in plants lacking phenolic protection.

15.4 Conclusions

In the meta-analysis of Searles et al. (2001), UV-induced changes in foliar chemistry, particularly that of production of epidermal screening compounds, were cited as one of the most common responses to UV-B radiation. In this and several related studies (Sullivan et al., 2007; Xu et al., 2008a, b), we evaluated the consequences of removal of one part of the screening system; namely, the flavonols of soybean, and found that they were important screening compounds. This attests to the role of these compounds in providing protection or at least minimizing damage. However, hypersensitivity was not found in the magenta line which suggests the existence of multiple screening pigments and repair processes that may be present in soybean and other plant species. In fact, studies have shown that although a wide range of plant responses to changes in UV-B levels may be observed, the fact remains that total plant growth is rarely severely impacted by small or moderate levels of UV-B when received under realistic field conditions (e.g., see Searles et al., 2001).

There is no question, however, that photons in this highly energetic waveband are quite biologically damaging, yet repair and protective process prevent much of the potential damage. For example, when evaluating the growth and morphology of these soybean lines (Table 15.1), there were some detrimental effects on growth and morphology, but survival and reproductive success were not compromised. Similar results were also obtained on studies with another soybean line, Harosoy, which also has a non-flavonoid isoline (Sullivan et al., unpublished data). In this case, Harosoy showed greater sensitivity which could have been related to differing flavonol composition. The Harosoy line primarily produces the flavonol kaempferol and only trace quantities of quercetin. This indicates that flavonoid composition, in addition to quantities and localization, may contribute to differing levels of UV protection. The importance of flavonoids as antioxidants, in addition to UV-screens, needs further evaluation (Xu et al., 2008b). Appreciable absorbance by the putative HCAs in the magenta lines may provide some UV protection as well. Finally, and for DNA damage in particular, the results of these and other studies indicate net dimer levels that are modulated by ongoing damage and repair processes. We still have a limited understanding of the induction of these repair processes. Clearly, if UV-screening by flavonoids was the only protection method, the results of this study would have been very different, and damage to the magenta line would have been severe at best. Therefore, the quantity and type of screening compounds, the localization and degradation of them, and other factors such as DNA repair processes, determine the sensitivity of plants to UV-B radiation. This aspect of the perception and response of plants to UV-B radiation needs further evaluation. Important topics for continued research are the evaluation of the spectral sensitivity and regulation of the induction and catalysis of these pigments and of the indirect effects of these photomorphogenic changes in leaf chemistry on plant development and ecological processes.

Table 15.1 The effects of supplemental UV-B radiation on the growth and morphology of soybean lines differing in flavonoid levels. Plants received either ambient levels of UV-B radiation (Controls or C) or ambient plus a daily maximum of 5.0 kJ of UV-B when weighted with the action spectra of Caldwell, 1971. An asterisk indicates a significant statistical difference ($P < 0.05$) between UV treatments as determined by the Student Newman-Keuls Multiple Range Test (SAS manual, 2000)

Cultivar	UV Treatment	Height (cm)	Plant Leaf Area (cm^2)	Plant Dry Weight (g)	RSR (root:shoot)
Clark	Control	153± 15	2960± 197	34.9± 3.5	0.241± 0.02
Clark	+UV	130± 12	2400± 210	32.0± 3.7	0.301± 0.03
$Clark_{wm}$	Control	139± 13	2369± 245	31.5± 3.2	0.258± 0.03
$Clark_{wm}$	+UV	106± 11 *	1930± 167	28.2± 3.4	0.333± 0.04

Acknowledgements

This work has been supported in part by the USDA UV-B Monitoring and Research Program, Colorado State University, Fort Collins, CO and the University of Maryland Agricultural Experiment Station. The authors thank Bruce Hundermark for assistance with UV data and Mr. Roman Mirecki and Mr. Darren DeStefano for assistance with care of the plants and UV-B treatments.

References

Barnes PW, Flint SD and Caldwell MM (1987) Photosynthesis damage and protective pigments in plants from a latitudinal arctic/alpine gradient exposed to supplemental UV-B radiation in the field. Arctic and Alpine Research 19: 21 – 27

Beerhues L, Robenek H and Wiermann R (1988) Chalcone synthesis from spinach (Spinacia oleracea L.) Ⅱ. Immunofluorescence and immunogold localization. Planta 173: 544 – 553

Beggs CJ, Schneider-Ziebert U and Wellmann E (1986) UV-B radiation and adaptive mechanisms in plants. pp.235 – 250 In Stratospheric Ozone Reduction, Solar Ultraviolet Radiation and Plant Life. R.C. Worrest and M.M. Caldwell (eds) Springer-Verlag. Berlin, Heidelberg

Bennett PV, Hada M, Hidema J, Lepre AM, Pope LC, Quaite FE, Sullivan JH, Takayanagi S, Sutherland JC and Sutherland BM (2001) Isolation of High Molecular Length DNA: Alfalfa, Pea, Rice, Sorghum, Soybean and Spinach. Crop Science 41: 167 – 172

Björn LO, and Murphy TM (1985) Computer calculation of solar ultraviolet radiation at ground level. Physiologia Vegetatio 23: 555 – 561

Bogenrieder A and Klein R (1982) Does solar UV influence the competitive relationship in higher plants? In Calkins J, (ed.). The role of solar ultraviolet radiation in marine ecosystems. pp.641 – 649. Plenum Press, New York

Buzzell RI, Buttery BR and Bernard RI (1977) Inheritance and linkage of a magenta flower gene in soybeans. Can. J. Genet. Cytology. 19: 749 – 751

Caldwell MM (1971) Solar ultraviolet radiation and the growth and development of higher plants, pp.131 – 177, *In* A. C. Giese, ed. Photophysiology, Vol. 6. Academic Press, New York

Caldwell MM, Robberecht R and Flint SD (1983) Internal filters: prospects for UV-acclimation in higher plants. Physiol. Plant. 58: 445 – 450

Caldwell MM, Ballare CL, Bornman JF, Flint SD, Bjorn LO, Teramura AH, Kulandaivelu G, and Tevini M (2003) Terrestrial ecosystems, increased solar ultraviolet radiation and interactions with other climatic change factors. Photochemistry. Photobiology. Science. 2, 29 – 38

Chappell J and Hahlbrock K (1984) Transcription of plant defense genes in response to UV light or fungal elicitor. Nature (London) 311: 76 – 78

Cosio EG, and McClure JW (1984) Kaempferol glycosides and enzymes of the flavonol biosynthesis in leaves of a soybean strain with low photosynthetic rates. *Plant Physiol.* 74, 877 – 881

Dale JE (1988) The control of leaf expansion. Ann. Rev. Plant Physiol. Plant Molec. Biol. 39: 267 – 295

Dany A-L, Douki T, Triantaphylides C and Cadet J (2001) Repair of the main UV-induced thymine dimeric lesions within *Arabidopsis thaliana* DNA: evidence for the major involvement of photoreactivation pathways. Journal of Photochemistry and Photobiology 65: 127 – 135

Day TA (1993) Relating UV-B radiation screening effectiveness of foliage to absorbing-compound concentration and anatomical characteristics in a diverse group of plants. Oecologia 95: 542 – 550

Day TA, Howells BW and Rice WJ (1994) Ultraviolet absorption and epidermal-transmittance spectra in foliage. Physiol. Plant. 92, 207 – 218

Dillenburg LR, Sullivan JH and Teramura AH (1994) Leaf expansion and development of photosynthetic capacity and pigments in Liquidambar styraciflua — Effects of UV-B radiation. Amer. J. Bot. 82: 878 – 885w

Freeman SE, Blackett AD, Monteleone DC, Setlow RB, Sutherland BM and Sutherland JC (1986) Quantitation of radiation-, chemical-, or enzyme-induced single strand breaks in nonradioactive DNA by alkaline gel electrophoresis: application to pyrimidine dimers. Analytical Biochemistry 158: 119 – 129

Frohnmeyer H, and Staiger D (2003) Ultraviolet-B Radiation-Mediated Responses in Plants. Balancing Damage and Protection. Plant Physiology 133: 1420 – 1428

Giese AC (1964) Studies on ultraviolet radiation action upon animal cells. In Photophysiology. Vol 2 (Edited by A.C. Giese), pp.203 – 245. Academic Press, New York

Gitz DC, Liu-Gitz L, Britz SJ and Sullivan JH (2005) Ultraviolet-B effects on stomatal density, water use efficiency and stable carbon isotope discrimination in four glasshouse-grown soybean (Glycine max) cultivars. Env. Exp. Bot. 53: 343 – 355

Green AES, Cross KR, and Smith LA (1980) Improved Analytical characterization of ultraviolet skylight. Photochemistry Photobiology 31: 59 – 65

Jansen MAK, Gaba V, and Greenberg BM (1998) Higher plants and UV-B radiation: balancing damage, repair and acclimation. Trends in Plant Science 3: 131 – 135

Kang HS, Hidema J, and Kumagai T (1998) Effects of light environment during culture on UV-induced cyclobutyl pyrimidine dimers and their photorepair in rice (*Oryza sativa* L.). Photochemistry Photobiology 68: 71 – 77

Kerr RA (1995) At quadrennial geophysics fest, Earth scientists think globally. Science 269: 477 – 478

Kirk-Davidoff DB, Hintsa EJ, Anderson JD, and Keith DW (1999) The effect of climate change on ozone depletion through changes in stratospheric water vapour. Nature 402: 399 – 401

Krizek DT, Britz SJ and Mirecki RM (1998) Inhibitory effects of ambient levels of solar UV-A and UV-B radiation on growth of cv. New Red Fire lettuce. Physiologia Plantarum 3: 1 – 7

Liu L and McClure JW (1995) Effects of UV-B on activities of enzymes of secondary phenolic metabolism in barley primary leaves. Physiologia Plantarum 93: 734 – 739

Liu L, Gitz DC and McClure JW (1995) Effects of UV-B on flavonoids, ferulic acid, growth and photosynthesis in Barley primary leaves. Physiol. Plant. 93: 725 – 733

Mabry TJ, Markham KR and Thomas MB (1970) The systematic identification of flavonoids. Springer-Verlag, Berlin

Mazza CA, Boccalandro H, Giordano CV, Battista D, Scopel AL, and Ballaré CL (2000) Functional significance and induction by solar radiation of ultraviolet-absorbing sunscreens in field-grown soybean crops. Plant Physiology 122: 117 – 125.Sumere, (eds.). Plenum Press. New York and London. pp. 525 – 556

McClure JW (1986) Physiology of flavonoids in plants. pp. 77 – 85. In (V. Cody, E. Middleton and J.B. Harborne, eds) Plant Flavonoids in Biology and Medicine: Biochemical, Pharmacological, and Structure-activity Relationships. Alan Risws, Inc.

Mohr H and Drumm-Herrel H (1983) Coaction between phytochrome and blue/UV light in anthocyanin synthesis in seedlings. Physiol. Plant. 58: 408 – 414

Mori T, Nakane M, Hattori T, Matsunaga T, Ihara M, and Nikaido O (1991) Simultaneous establishment of monoclonal antibodies specific for either cyclobutane pyrimidine dimer or (6,4) photoproduct from the same mouse immunized with ultraviolet-irradiated DNA. Photochemistry and Photobiology 54: 225 – 232

Murali NS and Teramura AH (1986) Effects of supplemental ultraviolet-B radiation on the growth and physiology of field-grown soybean. Environmental and Experimental Botany 26: 233 – 242

Pope LC (2000) Ultraviolet-B radiation effects on two soybean isolines that differ in flavonoid concentration. M.S. Thesis. University of Maryland. 111

Quaite FE, Sutherland BM, and Sutherland JC (1992) Quantification of pyrimidine dimers in DNA from UV-B irradiated alfalfa (Medicago sativa L.) seedlings. Applied and Theoretical Electrophoresis 2: 171 – 175

Quaite FE, Sutherland JC, and Sutherland BM (1994) Isolation of high molecular weight plant DNA for DNA damage quantification: relative effects of solar 297 nm UVB and 365 nm radiation. Plant Molecular Biology 24: 475 – 483

Raven JA (1977) Evolution of vascular land plants. Adv. Bot. Res. 5: 154 – 219

Robberecht R and Caldwell MM (1978). Leaf epidermal transmittance of ultraviolet radiation and its implications for plant sensitivity to ultraviolet-radiation induced injury. Oecologia (Berl.) 32: 277 – 287

Robberecht R and Caldwell MM (1983) Protective mechanisms and acclimation to solar ultraviolet-B radiation in Oenothera stricta. Plant Cell Environ. 6: 477 – 485

Schnitzler JP, Jungblut TP, Feicht C, Kofferlein M, Langebartels C, Heller W and Sandermann Jr. H (1997) UV-B induction of flavonoid biosynthesis in Scots pine (Pinus sylvestris L.) seedlings. Trees Structure and Function 11: 162 – 168

Statistical Analysis System, Inc. (2000) SAS Users Guide: Statistics. SAS Institute, Inc., Cary, N.C. 584

Salawitch RJ, Margitan JJ, Sen B, Toon GC, Osterman GB, Rex M, Elkins JW, Ray EA, Moore FL, Hurst DF, Romashkin PA, Bevilacqua RM, Hoppel KW, Richard EC and Bui TP (2002) Chemical loss of ozone during the Arctic winter of 1999 – 2000: An analysis based on balloonborne observations, Journal of Geophysical Research 107: 8269

Schnitzler JP, Jungblut TP, Feicht C, Kofferlein M, Langebartels C, Heller W and Sandermann Jr. H (1997) UV-B induction of flavonoid biosynthesis in Scots pine (Pinus sylvestris L.) seedlings. Trees Structure and Function 11: 162 – 168

Searles PS, Flint SD and Caldwell MM (2001) A meta-analysis of plant field studies simulating stratospheric ozone depletion. Oecologia 127: 1 – 10

Sheahan JJ (1996) Sinapate esters provide greater UV-B attenuation than flavonoids in Arabidopsis thaliana (Brassicaceae). Amer. J. Bot. 83: 679 – 686

Sinclair TR, N'Diaya O and Biggs RH (1990) Growth and yield of field-grown soybean in response to enhanced ultraviolet-B radiation. J. Environ Qual. 19: 478 – 481

Stafford HA (1991) Flavonoid evolution: An enzymatic approach. Plant Physiol. 96: 680 – 685

Stapleton AE (1999) Measurement of UV Radiation-Induced DNA Damage Using Specific Antibodies, In E. D. S. Henderson, ed. DNA Repair Protocols: Eukaryotic Systems, Vol. 113. Humana Press Publishing Agencies, Totowa, NJ

Stapleton AE and Walbot V (1994) Flavonoids can protect maize DNA from the induction of ultraviolet radiation damage. Plant Physiology 105: 881 – 889

Stapleton AE, Mori T, and Walbot V (1993) A simple and sensitive anti-body-based method to measure UV-induced DNA damage in *Zea mays*. Plant Molecular Biology Reporter 11: 230 – 236

Stapleton AE, Thorner CS and Walbot V (1997) UV-B component of sunlight causes measurable damage in field-grown maize (*Zea mays L.*): developmental and cellular heterogeneity of damage and repair. Plant Cell and Environment 20: 279 – 290

Sullivan JH (2005) Possible impacts of changes in UV-B radiation on North American trees and forests. Invited Review. Env. Pol. 137: 380 – 389

Sullivan JH and Teramura AH (1989) The effects of ultraviolet-B radiation on loblolly pines I. Growth, photosynthesis and pigment production in greenhouse grown saplings. Physiol. Plant. 77: 202 – 207

Sullivan JH and Teramura AH (1990) Field studies on the interaction between supplemental ultraviolet-B radiation and drought on soybean growth and physiology. Plant Physiology 92: 141 – 146

Sullivan JH, Teramura AH and Ziska LH (1992) Variation in UV-B sensitivity in plants from a 3,000 m elevational gradient in Hawaii. Amer. J. Bot. 79: 737 – 743

Sullivan JH, Howells BW, Ruhland C and Day TA (1996) Influence of leaf age and enhanced UV-B radiation on epidermal penetration by UV-B radiation in loblolly pine and sweetgum. Physiologia Plantarum 98: 349 – 357

Sullivan JH, Gitz DC, Liu-Gitz L, Xu C, Gao W and Slusser J (2007) Coupling short-term changes in ambient UV-B levels with induction of UV-screening compounds. Photochemistry and Photobiology. 83: 863 – 870

Sutherland BM, Takayanagi S, Sullivan JH, and Sutherland JC (1996) Plant responses to changing environmental stress: cyclobutyl pyrimidine dimer repair in soybean leaves. Photochemistry Photobiology 64: 464 – 468

Sutherland JC, Monteleone DC, Mugavero JH, and Trunk JG (1987) Unidirectional pulse-field electrophoresis of single- and double-stranded DNA in agarose gels: analytical expressions relating mobility and molecular length and their application in the measurement of strand breaks. Analytical Biochemistry 162: 511 – 520

Sutherland JC, Chen CZ, Emrick A, Hacham H, Monteleone DC, Ribeiro E, Trunk JG, and Sutherland BM (1990) Lesion measurment in non-radioactive DNA by quantitative gel electrophoresis, pp. 45 – 61, In Sutherland BM and Woodhead AD (eds). DNA Damage and Repair in Human Tissues. Plenum Press, New York

Teramura AH, Sullivan JH, and Lydon J (1990) Effects of UV-B radiation on soybean yield and seed quality: A 6-year field study. Physiologia Plantarum 80: 5 – 11

Tevini M, Braun J and Fieser F (1991) The protective function of the epidermal layer of rye seedlings against ultraviolet-B radiation. Photochem. Photobiol. 53: 329 – 333

Vogelmann TC (1994) Light within the plant. In: Photomorphogenesis in Plants. 2nd. Ed. (Kendrick RE and Kronenburg GHM, eds.). Kluwer Academic Publishers, Dordecht, The Netherlands. pp. 491 – 535

Waibel AE, Peter T, Carslaw K, Oelhaf H, Wetzel G, Crutzen PJ, Pöschl U, Tsias A, Reimer E, and Fischer H (1999) Arctic ozone loss due to denitrification. Science 283: 2064 – 2069

Wellman E (1983) UV radiation: Definitions, characteristics and general effects. In Encyclopedia of Plant Physiology, New Series. Vol. 16B. (Shropshire W & Mohr H, ed,), pp.745 – 756, Springer Verlag, Berlin

WMO (World Meteorological Organization) (2003). Scientific Assessment of Ozone Depletion: 2002. Global Ozone Research and Monitoring Project—Report No, 47 Ajavon AN, Albritton DL, Megie G, Watson RT (eds). World Meteorological Organization. Geneva

Xu C, Natarajan S and Sullivan JH (2008a) Impact of Solar Ultraviolet-B radiation on the antioxidant defense system in soybean lines differing in flavonoids biosynthesis. Environmental and Experimental Botany 63: 39 – 48

Xu C, Sullivan JH, Garrett WM, Caperna TJ, Natarajan S (2008b) Impact of solar ultraviolet-B radiation on the proteome in soybean lines differing in flavonoid contents. Phytochemistry 69: 38 – 48

Ziska LE, Teramura AH and Sullivan JH (1992) Physiological sensitivity to plants along an elevational gradient to UV-B radiation. American Journal of Botany 79: 863 – 871

16 Physiological Impacts of Short-Term UV Irradiance Exposures on Cultivars of Glycine Max

Richard H. Grant[1], Kent G. Apostol[2], and Hans F. Schmitz[1]

[1] Department of Agronomy, Purdue University, West Lafayette, IN 47907-2054, USA
E-mail: rgrant@purdue.edu
E-mail: hschmitz@purdue.edu
[2] Department of Biological Sciences, Bethel University, St. Paul, MN 55112, USA
E-mail: k-apostol@bethel.edu

Abstract Solar ultraviolet-B (UV-B) radiation affects the growth and physiology of different cultivars of soybean (*Glycine max* (L.) Merr.) in different ways. Consequently chronic exposure studies of various cultivars have indicated the full range of biomass productivity sensitivities to UV exposure: from highly sensitive and detrimental to tolerant and advantageous. Since most current and future exposures to UV radiation in mid-latitudes come as alternating periods of intense UV followed by periods of low UV, soybean sensitivity to UV should be studied as transient events. The effects of transient UV exposure on stomatal conductance (g_s), UV-B absorbing compounds, pigment concentrations, photosynthesis (A), transpiration (E), and photosystem Ⅱ efficiency on two soybean cultivars were evaluated. Soybean cultivars "Essex" and "Williams 82" were studied in a number of experiments under greenhouse conditions and in one study that was conducted in the field. Essex and Williams 82 cultivars responded differently to transient UV-B effects. In Essex, UV exposure initially resulted in increased g_s and E, which over time became a decreased g_s and E. Ultraviolet exposure initially resulted in decreased g_s, which over time resulted in no change or increase in g_s in Williams 28 after the first day. The UV exposure of Williams 82 plants had no statistically-supported effect on E. UV exposures and changes in g_s did not affect A for either cultivar. The concentrations of carotenoids and chlorophyll *a* were not influenced by UV exposure in Essex, but increased significantly in Williams 82 in a short term exposure. UV-B absorbing compounds were substantially higher in Essex compared to Williams 82. After the initial responses to UV exposure, both Williams and Essex had reduced responses to additional UV exposures. This suggests that the overall long-term plant response to UV exposure is triggered by high levels of short term UV exposure.

Keywords soybean, transpiration, plant physiology, short-term exposure

16.1 Introduction

Stratospheric ozone decreases have heightened the concern over the ecological implications of increasing solar ultraviolet-B (UV-B; 280 nm – 320 nm) radiation on agricultural production (Caldwell et al. 1998). Biologically effective UV ($UV\text{-}B_{BE}$) varies seasonally, geographically, and with changes in cloud cover. While long periods of low stratospheric ozone and corresponding high UV-B are unlikely, short-term events of 70 kJ m^{-2} – 80 kJ m^{-2} are likely to occur during the summer. This extremely high UV-B intensity, consisting of 2 to 4 days of sequential high exposure (Grant and Slusser, 2003), may affect large portions of cropland (Grant and Slusser, 2002).

The effects of solar UV-B on plants involve both acute and chronic exposures to moderate to high levels of UV-B radiation (Grant and Slusser, 2003). Depending on species, experimental conditions, and duration of UV-B exposure (Gwynn-Jones et al., 1999), there appears to be a variety of mechanisms through which UV-B affects growth and physiology of plants. Long-term exposure of plants to UV-B is known to inhibit photosynthesis (Nogués et al., 1998) through the inhibition of reaction centers in photosystem Ⅱ which results in decreased plant productivity. Ultraviolet-B is also reported to inhibit ribulose 1,5-bisphosphate carboxylase/ oxygenase (rubisco) activity, ATP hydrolysis, and reduce thylakoid membrane proteins (Bornman, 1989; Jordan et al, 1991; Jordan et al., 1992). In a few cases, UV-B increased stomatal conductance in some Ericaceae (Musil and Wand, 1993), but not in others (Teramura et al., 1983).

Different plant species and crop cultivars vary in their tolerance to UV-B and appear to respond to UV-B stress in a variety of ways (Murali et al., 1988; Kankani et al., 2003). Some plants tolerate UV-B through the production of photosynthetic and protective pigments and through changes in electron transport capability (Teramura, 1983; He et al., 1994; Teramura and Sullivan, 1994). Some long-term UV-B effects on plants are known; however, little work has been done to examine the transient UV-B effects on plants, in particular on soybeans. Studying the immediate responses of plants during short-term UV-B exposure may further our understanding of the mechanisms of UV-B damage and tolerance in plants. Soybean cultivars responded differently to prolonged UV-B exposure, with Essex being the most sensitive to UV-B while Williams 82 was the least affected (Murali et al., 1988).

Pigments are integrally related to the physiological function of leaves. Recently, leaf reflectance has been regarded as a good measure of pigment contents (Gamon and Surfus, 1999; Sims and Gamon, 2002). Changes in leaf reflectance due to stress factors are likely due to metabolic disturbance on chlorophyll concentrations (Knipling, 1970; Gamon and Surfus, 1999). Leaf reflectance measurements have been used in several UV-B studies (Bornman and Vogelmann, 1991; Visser et al., 1997; Qi et al., 2003; Kakani et al., 2004). However, little is known about how

these different levels of UV-B and duration of exposure affect leaf spectral reflectance in soybeans.

Most plant species are thought to have photoreactivation or photorepair mechanisms to deal with elevated UV-B intensity (Beggs et al., 1986). These mechanisms include production of UV-B absorbing compounds (Murali and Teramura, 1986) and photosynthetic pigments (Bornman and Vogelman, 1991) that are correlated with UV-B tolerance. The UV-B absorbing compounds are known to reduce the level of damaging effects of UV-B radiation reaching the sensitive organelles in mesophyll tissues (Tevini et al., 1991; Teramura and Sullivan, 1994). The production of UV- protective compounds in plants is dependent on the availability of carbohydrates from photosynthesis and storage (Matsuki, 1996). Therefore, provision of resources may be crucial to maintain protection from, and repair following, UV-B exposure.

It has been reported that the effects of UV-B on soybeans are more injurious during early stages of seedling growth (Murali and Teramura, 1986). Additionally, the synthesis of UV-B absorbing compounds and alterations in photosynthetic pigments are one of the immediate responses to UV-B exposure (Jordan et al., 1994; Battaglia and Brennan, 2000). Essex and Williams 82 cultivars were chosen in the present study because they have shown contrasting UV-B sensitivities in many studies (Tevini, 1993). We hypothesized that UV-B tolerance in Williams 82 is conferred by its ability to accumulate UV-B absorbing compounds and photosynthetic pigments.

The present study examined the short-term effects of UV exposure on stomatal conductance (g_s), concentrations of photosynthetic pigments and UV-B absorbing compounds, photosynthetic carbon fixation (A), transpiration (E), and photosystem Ⅱ quantum efficiency (Φ_{PSII}) in William 82 and Essex cultivars (Table 16.1) growing under greenhouse and field conditions. This study is one of the few documenting short-term effects of UV radiation on the physiology of soybean cultivars. Our objective was to build on the work of Bawhey et al. (2003) regarding the mechanisms of injury and tolerance of soybeans to UV-B exposures.

Table 16.1 Experimental conditions and physiological measurements

Experiment	Mean exposure rates at plant leaf height	Exposure duration	Cultivar(s) and phonological stage*	Physiological measurements made
Greenhouse, Spring 2004	UV exposure UV-B_{BE}: 7.8 kJ m^{-2} d^{-1} UV-A: 4.1 MJ m^{-2} d^{-1} PAR: 18.7 mol $m^{-2}d^{-1}$ Control UV-A: 0.45 MJm^{-2} d^{-1} PAR: 25.3 mol $m^{-2}d^{-1}$	6h/d for 3 days	W82 and Essex at V2	g_s, Pigments and UV-absorbing compounds

(Continued)

Experiment	Mean exposure rates at plant leaf height	Exposure duration	Cultivar(s) and phonological stage*	Physiological measurements made
Greenhouse, Winter 2007	UV exposure UV-B_{BE}: 12 kJ m^{-2} d^{-1} UV-A: 6.3 MJ m^{-2} d^{-1} PAR: 17.4 mol m^{-2} d^{-1} Control UV-A: 0.54 MJ m^{-2} d^{-1} PAR: 22.7 mol m^{-2} d^{-1}	8 h/d for 3 days	Essex, W82 at R2-R4	g_s, E, A, PSII efficiency
Greenhouse, Winter 2008	UV exposure UV-B_{BE}: 12 kJ m^{-2} d^{-1} UV-A: 6.3 MJ m^{-2} d^{-1} PAR: 15.9 mol m^{-2} d^{-1} Control UV-A: 0.57 MJ m^{-2} d^{-1} PAR: 19.7 mol m^{-2} d^{-1}	8 h/d for 6 days	Essex at VC, V1, V2, V3, V4	g_s, E, A, PSII efficiency
Field, Summer 2004	UV exposure UV-B_{BE}: 4.6 kJ m^{-2} d^{-1} UV-A: 2.5 MJ m^{-2} d^{-1} PAR: 62 mol m^{-2} d^{-1} Control UV-A: 13.5 MJ m^{-2} d^{-1} PAR: 62 mol m^{-2} d^{-1}	ambient	Essex, W82	g_s, E, A, Pigments and UV-absorbing compounds

* The following growth and development stages are described in detail in the measurement section.

16.2 Materials and Methods

A number of experiments were conducted to determine the short-term effects of UV radiation on A, E, g_s, photosystem II efficiency, concentrations of leaf pigments, and bulk UV-B absorbing compounds in Essex and Williams 82 cultivars.

16.2.1 Plant Material and Greenhouse Growth Conditions

Greenhouse studies

Two cultivars of soybean (*Glycine max* (L.) Merr. cvs. Essex and Williams 82) were grown from seeds in pots (7.5-L) filled with a mixture of sand and soil (1:2 by volume in 2004 and 3:5 by volume in 2007 and 2008) in the greenhouse at Purdue University, West Lafayette, IN (40.5°N, 87°W). The greenhouse was set to have day/night air temperatures of 26°C/20°C respectively; relative humidity (RH) of

70%, an 18 hour photoperiod with photosynthetic photon flux density (PPFD) measured during solar noon at the seedling top height of at least 180 μmol m^{-2} s^{-1} when only the sodium lamps provided PPFD in the early morning and late afternoon during the winter.

Plants were watered with tap water three to four times a week in 2004 and 2007 and five times a week in 2008. No fertilizer was applied to the soil medium. In 2004, whiteflies infested the greenhouse. Plants were periodically sprayed with Conserve SC (Dow AgroSciences, Indianapolis, IN) to minimize herbivory.

Field study

Plants of the two cultivars (Essex and Williams 82 cv.) were planted in 2004 at the Purdue Agronomic Center for Research and Education at West Lafayette, IN (40.5°N, 87°W) with 15 in. spacing in 40 ft long rows, buffered on either side by eight rows of a commercial variety. The plants were allowed to emerge and develop for 14 days prior to the establishment of the filter treatments. Plants used in the experiment were grown near the center of each filtered radiation plot. The plants were watered solely from precipitation.

16.2.2 UV Treatment

Greenhouse studies

After two weeks, plants in the 2004 experiment were randomly split into two groups with six plants for each cultivar placed on a bench with unpowered UV lamps overhead (no UV), termed the "control" treatment. Another six plants on a bench with identical powered UV lamps overhead were termed the "UV" treatment. Plants were exposed to UV-B soon after reaching the V2 stage (first fully developed trifoliate leaf at the node above the unifoliate node; Fehr and Caviness, 1977). Plants were irradiated for six hours each day, cantered at solar noon from 9:45 – 15:45 (local time (LT)) for a total of three days. Measurements were made for three days. The experimental conditions (temperature, relative humidity (RH), and photoperiod) were the same as for the growth conditions except for the PPFD, which was approximately 300 μmoles m^{-2} s^{-1} – 400 μmoles m^{-2} s^{-1} at seedling height in the control and UV exposure areas. Plants were well-watered throughout the experiment; there was no evidence of over-watering or water stress on any of the plants.

In the 2007 experiment, two plants per pot, one of Essex and one of Williams 82 and/or Beck's 367NRR, were grown in the control (bank) area. Those to be exposed transferred to the experimental exposure area in a random design when the plants were at R2 (full bloom-an open flower at one of the two uppermost nodes on the main stem with a fully developed leaf) to R4 (full pod elongation-pod 2 cm (3/4 inch) long at one of the four uppermost nodes on the main stem with a fully developed leaf) stage. Twelve pots (eight plants of each cultivar) were in

the exposure area while twelve pots were in the control (bank) area. Plants were randomly distributed, both longitudinally and laterally under the UV lamp bank. Measurements were made on the top trifoliate for three days following the initial exposure. The experimental conditions (temperature, RH, PPFD, and photoperiod) were the same as for the growth conditions. Plants were well-watered throughout the experiment: there was no evidence of over-watering or water stress on any of the plants.

In the 2008 experiment, 15 plants, 2 per pot, of Essex were grown in the control (bank) area while 15 plants, 2 per pot, of Essex were grown under the UV lamps. Plants were randomly distributed both longitudinally and laterally, under the UV lamp bank. Experiments were conducted on intact leaves at VC, V1, V2, V3, and V4 stages. Leaf trifoliates of each stage were measured once fully expanded and on subsequent days until the leaves above shaded the trifoliate. The experimental conditions and watering regime were the same as in the 2007 experiment.

Field study

The UV-exposure treatment consisted of plants grown under a polyethylene plastic filter that allowed 84% penetration of the UV-B_{BE} solar radiation, an 87% penetration of UV-A (320 nm – 400 nm) solar radiation, and a 90% penetration of photosynthetically active radiation (PAR) (400 nm – 700 nm). The Llumar plastic allowed below 1% penetration of UV-B_{BE} solar radiation, 16% penetration of UV-A solar radiation, and an 88% penetration of PAR.

16.2.3 UV Exposure Regimes

Greenhouse studies

The greenhouse UV-B treatment was based on the exposures found in the conterminous United States. Analysis of the probability of having four hours in a day with an upper 5% daily exposure of 8 kJ m^{-2} UV-B_{BE} (based on the action spectrum of Caldwell, 1971) occurs approximately 5% of the days in June and July (Grant and Slusser, 2002). During the early part of June, the soybean crops are in early vegetative stages. A 3-day sequence of such exposure levels occurs approximately 1% of the time (Grant and Slusser, 2002). An 8 kJ m^{-2} UV-B_{BE} exposure, when distributed over 6 hours of the day as a square wave exposure, corresponds with an exposure of 1.33 kJ m^{-2} h^{-1} UV-B_{BE}. The use of short-term exposures minimizes the problems surrounding variability in exposure relative to outside solar radiation levels as reported by Musil et al. (2002), although a few of the days during these experiments were heavily overcast and therefore had relatively little solar radiation incoming through the greenhouse glass. These days will be mentioned below.

Since the response of plants to UV-B irradiance is influenced by the amount of

UV-A irradiance, greenhouse experiment exposures were made using a UV lamp array composed of eight UV-A lamps (UV-340, Q Panel Lab Products, Cleveland, OH) and eight UV-B lamps (UV-B-313, Q Panel Lab Products) alternately arranged on a frame positioned 0.6 m above the seedlings. The UV-C radiation was screened out by placing two layers of 0.08 mm CA films below the frames (Fig. 16.1). The CA films were solarized for six hours prior to use and replaced every three to four days to maintain the appropriate spectral irradiance. Ultraviolet-B exposures were determined from prior measurements of the irradiance with distance from the lamp.

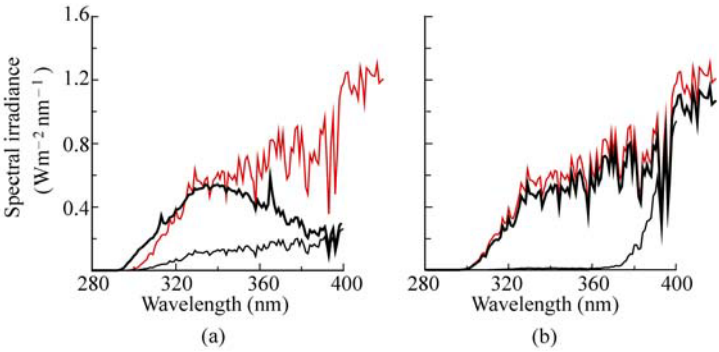

Figure 16.1 Approximate spectral exposure distributions for experimental schemes. Panel (a): Spectral distribution of above-greenhouse solar irradiance (red solid line), irradiance in the control area (light black solid line), and irradiance at plant height in experimental setup (dark black solid line). Values derived from lamp manufacturer-provided spectra for the UV-B-313 and UV-340 lamps, laboratory-measured cellulose acetate filter, and solar spectrum from a TUV model run for solar zenith angle of 30° and total ozone column depth of 320 DU. Panel (b): Spectral irradiance above exclosure plastic filter (red solid line), under UV exposure filter (dark black solid line), and under the control filter (light black solid line)

Ultraviolet-A exposures were a result of both lamp enhancement and ambient solar radiation penetration to the plants. The lamp enhancement of UV-A was determined from the ratio of UV-A to UV-B emitted by the lamps times the UV-B exposure. The ambient UV-A reaching the plants was calculated from the ambient measurement of spectral irradiance at 368 nm made at the W. Lafayette, IN UV-B Climate Monitoring Station located within 8.5 km of the greenhouse. The UV-A irradiance was calculated from the 368 nm irradiance according to Grant and Slusser (2005). Ultraviolet-A radiation penetrates the greenhouse glass. The measured light transmittance through the greenhouse glass panels was above 80% for wavelengths above 350 nm; below 350 nm the transmittance rapidly reduced to 10% at 320 nm and less than 1% at 310 nm. When the bank of UV lamps is overhead, the UV-A penetration is only 25% of that above the greenhouse (Fig. 16.1). When there is no bank of lights overhead, the penetration of UV-A is 48% of that overhead. The

relatively low apparent penetration of UV-A is due to the wall influences or adjacent greenhouse rooms and protective plastic shields for people walking through the greenhouse of the UV lamp irradiance.

Since the response of plants to UV-B irradiance is influenced by the simultaneous receipt of PPFD, greenhouse experiments also measured and controlled the PPFD. Photosynthetically active radiation exposure during the experiments was a result of both lamp enhancement and ambient solar radiation penetration to the plants. Photosynthetic photon flux density levels for plants in both the control and UV areas were supplemented by three 400-W high pressure sodium lamps that provided 180 μmoles m^{-2} s^{-1} at plant height. The ambient PPFD reaching the plants was calculated from ambient measurement made at the W. Lafayette, IN UV-B Climate Monitoring Station. When the bank of UV lamps is overhead, the PPFD penetration is only 25% of that above the greenhouse. When there is no bank of lights overhead, the penetration of PPFD is 48% of that overhead.

Exposures varied with the experiment. In the 2004 experiment, the lamp banks were positioned to provide 1.3 kJ m^{-2} h^{-1} UV-B_{BE} and 0.65 MJ m^{-2} h^{-1} UV-A for 6 hours as a square wave centered on solar noon, while in the 2007 and 2008 experiments, the lamps were positioned to provide 1.5 kJ m^{-2} h^{-1}UV-B_{BE} and 0.75 MJ m^{-2} h^{-1} UV-A for 8 hours as a square wave cantered on solar noon (Table 16.1).

The response of plants to UV irradiance depends on the amount of UV received which can vary over the day as the soybean plants adjust their leaf orientation in response to the position of the sun (Rosa and Forseth, 1995; Bawhey et al., 2003). Leaf orientations were modelled according to Bawhey et al. (2003), and the leaf exposures to both UV radiation and PAR were calculated assuming the lamp bank represented a diffuse radiation source. The orientation of leaves influences the exposure of plants to UV radiation. In these studies, we calculated the daily fractional UV-B exposure using the assumption of isotropic sky radiance distributions (ISO) as described in Bawhey et al. (2003). It was estimated that Essex received 7% greater UV-B exposure than Williams 82 over the UV treatment exposures.

Field study

The 2004 field study utilized plastic filters mounted on 1.2 m by 3.7 m frames to prevent UV radiation from reaching plants grown under the plastic. Plants were grown around the experimental plot in identical planting density to limit the solar radiation penetration to the experimental plots from the side. The control exposure was that under a Llumar filter plastic while the ambient "treatment" exposure was that under a polyethylene filter plastic. Since ambient exposure conditions prevailed, the UV-A exposures were determined from the measurement record of the USDA UV-B Monitoring and Research Station's Ultraviolet Multifilter Rotating Shadowband Radiometer (UV-MFRSR) measuring the 368 nm solar radiation according to Grant and Slusser (2005). The UV-B_{BE} exposures were based on column ozone, solar zenith angle (SZA), and measured erythema irradiance

determined from the measurement record of the USDA UV-B Monitoring and Research Station's Yankee Scientific Incorporated UV-B-1 radiometer. The mean daily exposure of UV-B_{BE} under the Llumar (control) averaged 27 $Jm^{-2}d^{-1}$, while that under the polyethylene averaged 4.6 $kJm^{-2}d^{-1}$. The mean daily exposure of UV-A under the Llumar (control) was 2.49 $MJm^{-2}d^{-1}$, while that under the polyethylene was 13.5 $MJm^{-2}d^{-1}$. The PAR exposure under the two plastic filters was nearly identical; under Llumar it was 61.7 mol $m^{-2}d^{-1}$ and under polyethylene it was 61.7 mol $m^{-2}d^{-1}$.

Since the exposure to the plant depends on leaf orientations, we calculated the fractional UV-B exposure over the course of the experiment using the assumption of anisotropic sky radiance distributions as described in Bawhey et al. (2003). It was estimated that Essex received only 2% greater UV-B exposure than Williams 82.

16.2.4 Stomatal Conductance Measurements

In the 2004 greenhouse study, stomatal conductance (g_s) measurements were performed on the center leaflet adaxial surface of the highest (youngest) fully-expanded leaf on six seedlings ($n=6$). Leaves were oriented to maximize solar irradiance and allowed to acclimize to the radiation level until measurements stabilized (approximately 5 – 7 minutes). In 2004, measurements were made with a closed chamber steady-state porometer (LI-600, Li-Cor Inc., NE, USA) after 1, 3, 6, 12 and 18 hours of UV exposure. Again, the 6, 12, and 18 hour measurements represented measurements at the end of each day's UV exposure period and the 1 and 3 hour measurements were made partway through the first 6 hours of UV exposure. In the 2004 field study, g_s was measured on 9 replicates in each treatment. Measurements were made using a LI-6200 (Li-Cor Inc., NE, USA) closed photosynthesis system.

In 2007 and 2008, g_s was measured on the center leaflet of the highest fully-expanded leaf with 3 and 16 replicates (respectively) of each treatment using the open chamber CI-340 portable photosynthesis system at the same times as the transpiration and photosynthesis. Leaves were kept as close to their natural angle as possible (nearly horizontal) while maximizing solar irradiance. In 2007, measurements were made at 1, 4, 6, and 8 hours (Day 1), 22, 24, 27, 29, and 31 hours (Day 2), and 46, 48, 51, 53, and 55 hours (Day 3) after the beginning of the experiment. In 2008, the measurements were made at 6 hours (Day 1), 30 hours (Day 2), 52 hours (Day 3), and 77 hours (Day 4) after the start of the experiment.

For the 2004 field study, leaves used for gas exchange measurements were placed in sample bags with moist paper towel and kept in a cooler prior to leaf area analysis. Leaf area was determined using a LiCor LI-3100 Leaf area meter. Leaves were then flash-frozen in liquid nitrogen and stored in −85°C immediately following leaf area determination. Leaf area measurements in the 2007 and 2008 studies were not needed since the measured leaf filled the entire domain of the leaf chamber.

16.2.5 Photosynthesis and Transpiration Measurements

In 2007 and 2008, A and E were measured on the highest fully-expanded leaf of 3 and 16 replicates, respectively, in each treatment. Leaves were kept as close to their natural angle as possible (nearly horizontal) while maximizing solar irradiance. In both experiments, A and E were measured at the same times as the g_s measurements (see Section 16.2.4) using a portable open photosynthesis system (CI 340, CID, Inc., Camas, WA, USA). In 2004, A and E were measured on 9 replicates in each treatment using a closed photosynthesis system (LiCOR LI-6200, LiCor, Inc, Lincoln, NE, USA).

Photosystem (PS) Ⅱ quantum efficiency ($\Phi_{PSII}=(F_m\text{-}F_o)/F_m$; F_o = minimum fluorescence yield of dark-adapted leaves, F_m = maximum fluorescence of dark-adapted leaves) was estimated during the 2007 experiment before dawn (700 LT) and after dusk (2100 LT) of each day of exposure. Photosystem Ⅱ yield ($\Psi_{PSII}=(F_{ms}\text{-}F_o)/F_{ms}$; F_s = steady state after exposure to a light source that drives photosynthesis, F_{ms} = maximum fluorescence of leaves after exposure to a light source that drives photosynthesis) was estimated during the 2008 experiment at 6 hours (Day 1), 30 hours (day 2), 52 hours (Day 3), and 77 hours (Day 4) after the start of the experiment. Maximal fluorescence with all PSⅡ reaction centers in the closed state was induced by a 0.8 s saturating pulse of white light (3,000 μmol m^{-2} s^{-1}). After 10 s, the actinic light was turned on and the same saturating pulse described previously was applied every 1 s, until steady-state photosynthesis was reached in order to obtain F_s or F_m. Measurements were made using the CI-340 portable photosynthesis system with a pulse-modulated CI-510CF Chlorophyll Fluorescence Module (CID, Inc., Camas, WA, USA).

16.2.6 Pigment Analyses

In the 2004 field and greenhouse experiments, leaf pigments were determined on the same leaflet used in the g_s ($n=6$). Ten leaf discs (total leaf area of 5 cm^2) were cut using a puncher from a single leaf of individual control plants and plants treated with UV-B, then macerated with a few drops of 80% acetone in a pestle and mortar as described by Apostol and Zwiazek (2004). The extract was centrifuged at 1,500 g for 5 minutes. The supernatant was diluted with 10 mL of 80% acetone. Leaf pigments were estimated from absorbance measurements of the supernatant made on a Lambda 1 UV/Visible Spectrophotometer (Perkin-Elmer Corp., Wilton, CT). The chlorophyll concentrations were determined from absorbance at 664 nm and 647 nm (Graan and Ort, 1984). Carotenoid concentrations were determined from absorbance at 483, 663 and 638 nm following the procedure of Davies (1976). Anthocyanins were estimated from absorbance measurements at 534, 643, and 661 nm, as previously described by Lichtenthaler (1987).

16.2.7 UV-B Absorbing Compounds

In the 2004 field and greenhouse experiments, 4 leaf discs (1.0 cm^2) were excised from the same leaf samples used for the g_s measurements described above ($n = 6$). Leaf discs were frozen in liquid nitrogen and stored in -80°C for one week. Ultraviolet-B absorbing pigments were extracted with 5 mL of a mixture of methanol:water:HCl solution (79:20:1 v/v) at 90°C for 90 minutes until the leaf discs were completely bleached. The extract was centrifuged at 2,500 rpm for 5 minutes. The absorbance (per cm^2 of leaf area) of the supernatant was measured at 1 nm increments between 280 nm and 320 nm with a Perkin-Elmer Lambda 1 UV/Visible Spectrophotometer (Perkin-Elmer Corp., Wilton, CT).

Bulk absorbance was determined by both a direct summation of the spectral absorbance across the 280 nm – 320 nm bandwidth and a weighted summation of the spectral absorbance across the 280 nm – 320 nm bandwidth. The spectral weighting factors for the UV-exposed leaves in the 2004 greenhouse study were based on the combined spectral irradiance of the UV lamp bank at 0.6 m and the predicted greenhouse-transmitted solar spectral irradiance with the waveband irradiance normalized to one. The spectral weighting factors for the control leaves were based on the predicted greenhouse-transmitted solar spectral irradiance with the waveband irradiance normalized to one. The difference in spectral irradiance between the UV exposure area and the control area was likewise normalized to one and used as weighting factors for the difference in spectral absorbance between the UV-exposed and control plants. The predicted greenhouse-transmitted solar spectral irradiance was approximated from a ratiometric correction for cloud cover of the clear sky spectral solar irradiance as determined from the TUV UV irradiance model (http://cprm.acd.ucar.edu/Models/TUV/Interactive_TUV/) using a nominal 40° SZA, an ozone column thickness equal to the measurement period mean value, a site altitude of 0.5 km, and a nominal 0.02 albedo. The mean 3-d ozone column thickness was 317 Dobson units (DU) based on the National Aeronautical and Space Administration (NASA) "Earth Probe" satellite total ozone mapping spectrometer (TOMS) measurements: http://toms.gsfc.nasa.gov/eptoms/ep_v8.html). The ratiometric correction for cloudiness was estimated by a ratio between the modelled and clear-sky above-greenhouse UV-A irradiance. For the 2004 greenhouse study period, the measured UV-A irradiance was 81% of the modelled at the times when the SZA was 40°.

The spectral weighting factors for the UV-exposed leaves in the 2004 field study were based on the predicted Llumar and polyethylene plastic-transmitted solar spectral irradiance with the waveband irradiance normalized to one. The difference in spectral irradiance, between the UV-exposed (under polyethylene filters) and control plants (under Llumar filters) was likewise normalized to one and used as weighting factors for the difference in spectral absorbance between the UV-exposed and control plants. The predicted solar spectral irradiance was approximated from clear sky spectral solar irradiance determined from the TUV

UV irradiance model using a nominal 40° SZA, an ozone column thickness equal to the measurement period mean value, a site altitude of 0.5 km, and a nominal 0.02 albedo. The mean ozone column thickness over the period of the study was 320 DU (NASA "Earth Probe" TOMS measurements).

16.3 Results and Discussion

Measurements of leaf physiology and pigment composition are often highly variable leaf-to-leaf and over time, and limit the ability to delineate plant responses, specifically as a result of UV exposure. Variability was minimized by measuring only the central soybean leaflets of fully-expanded, sunlit (when possible) leaves at similar times during each day of the experiment. All plants in the greenhouse studies were well-watered throughout their development to minimize confounding water stress effects on the plant's physiological activity. However, variability in measurements remains due to other genetic differences in plants, variability in stomatal openings across the leaf, and environmental conditions, such as cloud cover or UV obstruction of direct radiation due to the UV light bank on a given day for a given leaf.

16.3.1 Stomatal Conductance

The 2004 g_s measurements of the control plant leaves at V2 stage were significantly higher than that of the R2 through R4 stages in 2007 (Fig. 16.2(a)), but were comparable to the measurements of the control plant leaves at V2 stage in 2008 (Fig. 16.2(c)). The g_s of Essex leaves at VC stage consistently increased with time into the experiment while that of the other stages showed no trend over the experimental time period (Fig. 16.2(c)). The Williams 82 and Essex control plant g_s measurements were relatively insensitive to the PPFD in 2004 and 2008 (Fig. 16.2(b)). The Essex control plant g_s measurements in 2007 were similarly relatively insensitive to PPFD, but showed a greater range of g_s for the same range in PPFD (Fig. 16.2(d)). Even though four to five g_s measurements were made during daylight hours on each plant in 2007, there was no evident diurnal periodicity in the measurements. Measurement variability, limiting the ability to determine treatment effects, is partly a result of variability in stomatal openings across the leaf.

In the 2004 study, the g_s measurements on V2 leaves were only significantly different from the control (students t-test, hereafter referred to as "t-test" at $P = 0.10$) on the first day of exposure (Fig. 16.3(a)). Note that the PPFD over the UV-exposed plants was only 10 μmol $m^{-2}s^{-1}$ – 40 μmol $m^{-2}s^{-1}$ less than that over the control plants. Starting at 3 hours into the UV exposure, the g_s of UV-exposed Essex was greater, yet not significantly, than those of the control plants. Similarly,

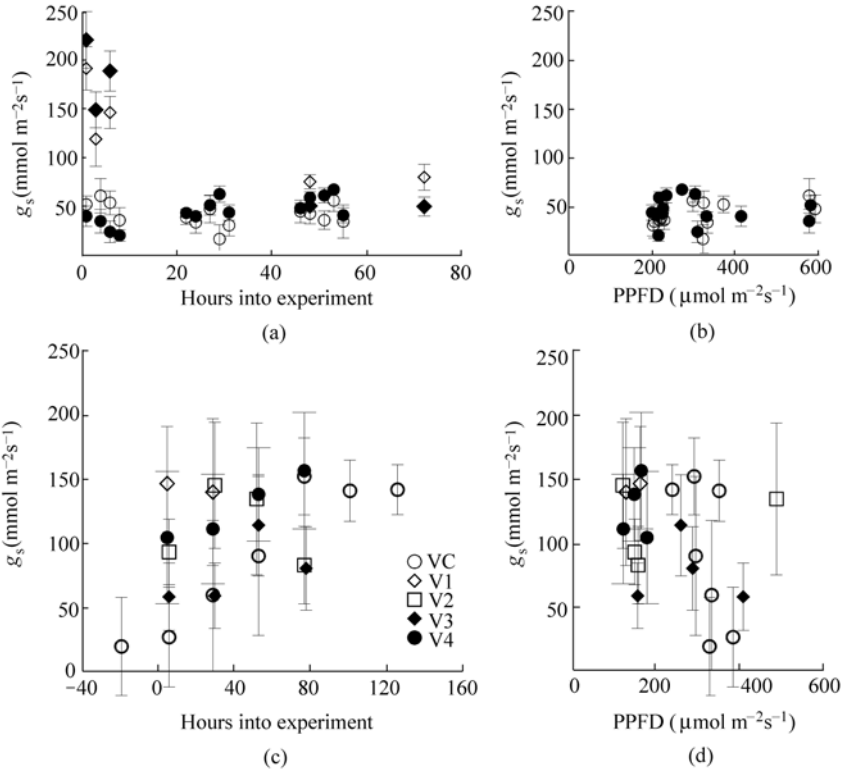

Figure 16.2 Influence cultivar and leaf node on leaf stomatal conductance. Essex and Williams stomatal conductances at R2-R4 stage (circles indicating 2007 measurements) in panel (a), and V2 stage (diamonds indicating 2004 measurements and squares indicating 2008 measurements). The relationship between the PPFD and stomatal conductance of the control leaves in 2007 are indicated in panel (b). Filled symbols represent Williams 82 while open symbols represent Essex cv. Essex leaf stomatal conductances at development stages VC through V4 (2008) are illustrated in panel (c) with corresponding relationship between the PPFD and stomatal conductance of the control leaves in 2007 are indicated in panel (d). Error bars are standard error of the difference. All measurements were made in greenhouse experiments

the g_s of the UV-exposed Williams 82 was significantly lower (t-test at $P=0.10$) than the control plants only after 6 hours of exposure (the end of the first day). As the UV exposure increased beyond the first day, the exposure to UV had less effect on g_s (Fig. 16.3(a)). Solar irradiance on the third day of measurements (120 μmol $m^{-2}s^{-1}$ – 140 μmol $m^{-2}s^{-1}$) was less than the prior days (120 μmol $m^{-2}s^{-1}$ – 200 μmol $m^{-2}s^{-1}$), but did not appear to influence the plant response.

In the 2007 study, many of the g_s measurements of UV-exposed Essex leaves from reproductive R2 through R4 stages had slightly greater, but non-significant, differences (t-test at $P=0.10$) from the control plants mostly occurring after 31 hours into the experiment (end of the second day of exposure). The increased

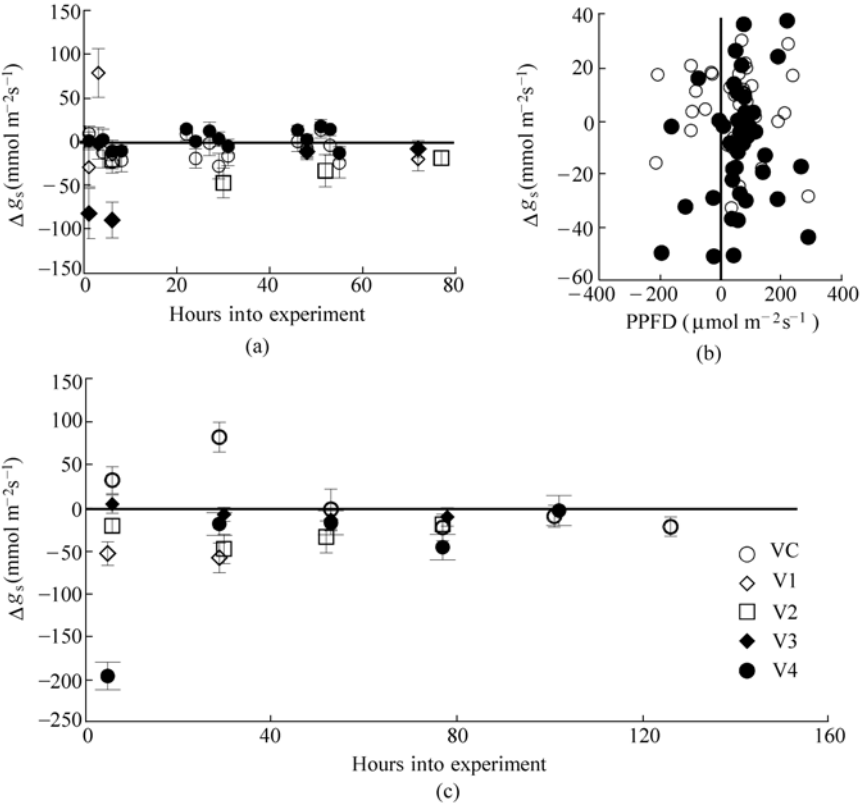

Figure 16.3 Influence of UV exposure on leaf stomatal conductance. Essex and Williams stomatal conductances at R2-R4 stage (circles indicating 2007 measurements), and V2 stage (diamonds indicating 2004 measurements and squares indicating 2008 measurements). The relationship between the difference in PPFD and stomatal conductance between UV and control leaves in 2007 are indicated in panel (b). Filled symbols represent Williams 82 while open symbols represent Essex cv. Essex leaf stomatal conductances at development stages VC through V4 (2008) are illustrated in panel (c). Difference is indicated as UV-Control. Error bars are standard error of the difference. All measurements were made in greenhouse experiments

g_s associated with UV exposure on Williams 82 leaves at R2 through R4 was not significant at $P = 0.10$. As a pooled sample of all hours of measurement, the UV exposure resulted in a statistically significant decrease in g_s at R2 through R4 in Williams 82 (t-test at $P = 0.05$), but not a statistically significant increase in Essex. In the 2008 study, the UV-exposed Essex plants at the VC stage had a tendency for greater g_s (t-test at $P = 0.10$) than the controls for the first 2 days (corresponding to low g_s values for control leaves); however, the differences between exposed and unexposed leaves disappeared by the third day (Fig. 16.3(c)). At all subsequent vegetative stages (V1 though V4), the Essex leaves exposed to UV had an increased or similar g_s as the controls (Fig. 16.3(c)). As a pooled sample of all

hours of measurement, the UV exposure resulted in a statistically significant increase in g_s at VC (t-test $P = 0.01$) and statistically significant decreases at V1, V2, and V4 (t-test $P = 0.01$), but not at V3.

In the 2004 field study both, cultivars showed non-significant differences in g_s between the UV-exposed and control plants at V5 (Table 16.2). Although such results might be expected given the trend of decreasing impact of UV exposure on g_s as the plants have increased UV exposure indicated in the greenhouse experiments (Fig. 16.3(a)), the wide variability of measured g_s in the replicates prevents any definitive statement.

Table 16.2 2004 field study results

		UV-Control			
		V5 Stage		R3 Stage	
Cultivar	Measurement	Mean	SE	Mean	SE
Essex	g_s (mmol m^{-2} s^{-1})	−140	158.1	52.9	187.5
	E (mmol m^{-2} s^{-1})	−1.35	0.558	0.859	0.830
	A (μmol m^{-2} s^{-1})	−2.33*	1.28	−1.15	2.25
	WUE ($\times 10^{-4}$)	2.28	3.29	−4.12	3.07
Williams 82	g_s (mmol m^{-2} s^{-1})	−23.6	142	322	367
	E (mmol m^{-2} s^{-1})	−1.44	0.863	0.395	1.06
	A (μmol m^{-2} s^{-1})	−2.07	1.91	0.204	1.21
	WUE($\times 10^{-4}$)	3.89	2.95	0.0268	2.39

* = statistically significant difference at $P = 0.10$.

In general, the effects of UV exposure on Essex corresponded to an increase in g_s at the beginning of an exposure with the plants (at V1 through V4 and R2 through R4) compensating to some degree as the exposure duration increased. This is consistent with the field study results of no significant difference in g_s at V5 or R3. Williams 82 at V2 and R2-4 initially appeared to have a decreased g_s which changed to a non-significant (t-tests at $P = 0.1$) increase throughout the duration of exposures in the greenhouse. The field study showed negligible changes in g_s at V5 and R3. Several studies have demonstrated reduced g_s in response to UV-B radiation (Middleton and Teramura, 1993; Dai et al., 1995), while others revealed an increase in g_s (Musil and Wand, 1993). Eisinger et al. (2000) have shown that UV exposure caused stomatal opening in broad bean at two major peaks, which are in 280 (UV-B) nm and 360 (UV-A) nm. Negash (1987) showed that UV radiation from 255 nm − 295 nm caused rapid stomatal closure in *Eragrostis tef* after 15 and 45 minutes of UV exposure. Battaglia and Brennan (2000) observed a decrease in stomatal aperture following brief UV-B exposure in the cotyledons of cucumber (*Cucumis sativus L. cv. Poinsett*), but not in sunflowers (*Helianthus annuus L cv.* Gray Stripe). Some studies suggest that the g_s in plants vary greatly because of the difference in their light requirement

(Kozlowski and Pallardy, 1997). The 2004, 2007, and 2008 greenhouse studies showed no evidence of influence of PPFD on g_s (Figs. 16.2(b), (d)). The difference in the amount of UV-B received between the cultivars, with Essex receiving 7% greater UV exposure than Williams 82, may have partly contributed to the differences in plant response found in this study and could be an important factor under prolonged UV-B exposure.

Stomatal conductance generally exhibited a response pattern similar to that of reductions in guard cell length (Gitz et al., 2005). Nogués et al. (1998) found that reductions in conductance in pea (Pisum sativum) exposed to high levels of UV-B were largely the result of altered guard cell. We have shown that UV caused an increase in guard cell length in Williams 82, while a reduction in guard cell length was observed in Essex (unpublished data). It remains to be conclusively shown whether the observed alteration in guard cell length are the result of UV damage to developing stomatal initials or the result of developmental process as Essex and Williams 82 exhibit differential morphological responses.

16.3.2 Transpiration

The E of the control plants in the 2007 and 2008 experiments varied between 0.5 and 2.6 mmol $H_2O\ m^{-2}s^{-1}$ (Figs. 16.4(a) and 16.5(a)). At VC stage, the Essex control leaves increased transpiration over the course of the experiment which corresponded to the increases in g_s (Fig. 16.2(c)). There was no trend evident in the E of the 2007 or 2008 experimental control leaves with increasing PPFD (Fig. 16.5(b)). Although four to five E measurements were made on each plant during daylight hours in 2007, there was no evident diurnal periodicity in the measurements. Measurement variability, limiting the ability to determine treatment effects, is partly a result of the variability in stomatal openings across the leaf.

In the 2007, E measurements on plants in reproductive stages R2 through R4 showed non-significant (t-test at $P=0.10$) increases for both cultivars under UV exposure (Fig. 16.4(b)). For Williams, E increased less than 27 hours into the experiment. For Essex, E increased after the first day of exposure. The UV-exposed leaves of Essex cv. transpired more than control plants on the first two days of the experiment when the sky was clear, but less than the control plants on the third day of exposure (around hour 50 in Fig. 16.4(b)) when the sky was overcast. The control plants had lower average E (Fig. 16.4(a)) on the overcast day than the clear days. The sky cover however did not affect g_s (Fig. 16.2(a)). As a pooled sample of all hours of measurement, the UV exposure resulted in a statistically significant increase in E at R2 through R4 in Essex (t-test at $P=0.10$), but did not indicate a statistically significant increase in Williams 82. Similarly the 2008 greenhouse experiment on Essex leaves at vegetative stages VC through V4 showed that E was initially significantly decreased by UV exposure at the V1 and V2 stages, but not at the V3 stage (Fig. 16.5(c)). Leaves at VC had significantly

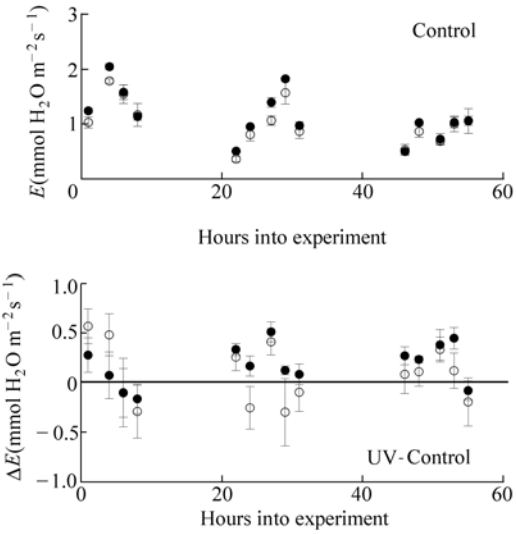

Figure 16.4 Influence of UV exposure on Essex and Williams 82 leaf transpiration at development stages R2-R4. Difference is indicated as UV-Control. Essex cv is indicated by the open circle. Williams 82 is indicated by the filled circle. Error bars are standard error of the difference. All measurements were made in greenhouse experiments

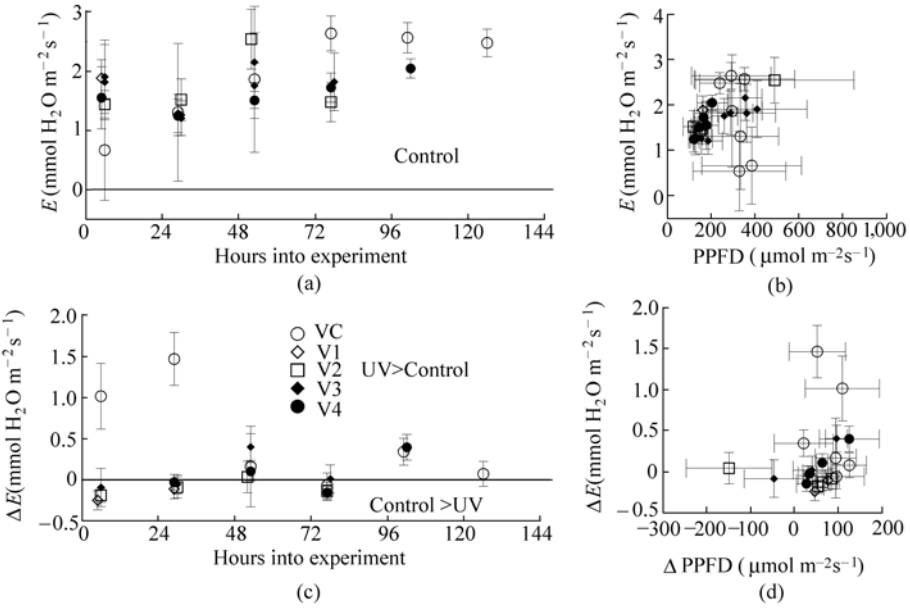

Figure 16.5 Influence of UV exposure on Essex leaf transpiration at development stages VC through V4. Transpiration of control plant leaves are indicated in panel (a) with the corresponding relationship between PPFD and transpiration in panel (b). Difference in transpiration due to UV exposure is indicated as UV-Control in panels (c) and (d). Error bars are standard error of the difference. All measurements were made in greenhouse experiments

greater transpiration under the UV exposure than those unexposed; however, this effect decreased with days of exposure (Fig. 16.5(c)). As a pooled sample of all hours of measurements, the UV exposure resulted in a statistically significant increase in g_s at VC (t-test $P=0.01$), and statistically significant decreases in g_s at V1 (t-test $P=0.1$) and V4 (t-test $P=0.01$), but not at V2 or V3. This suggests that the plant does not initially have a mechanism for UV-B protection, but develops this protective mechanism by the third day of exposure at VC stage. For all other stages, it appears that the plant reduces transpiration under increased UV exposure. This is in agreement with the results of Teramura et al. (1980) in a greenhouse study of Hardee cv. after at least two weeks of UV exposure.

The temperature difference between the leaf and the air (ΔT) was significantly less for the UV-exposed plants than the control plants for all but a few measurements over the growth stages VC through V4 (Fig. 16.6(a)). The ΔT was significantly less because the leaf temperature was significantly higher for the UV-exposed leaves

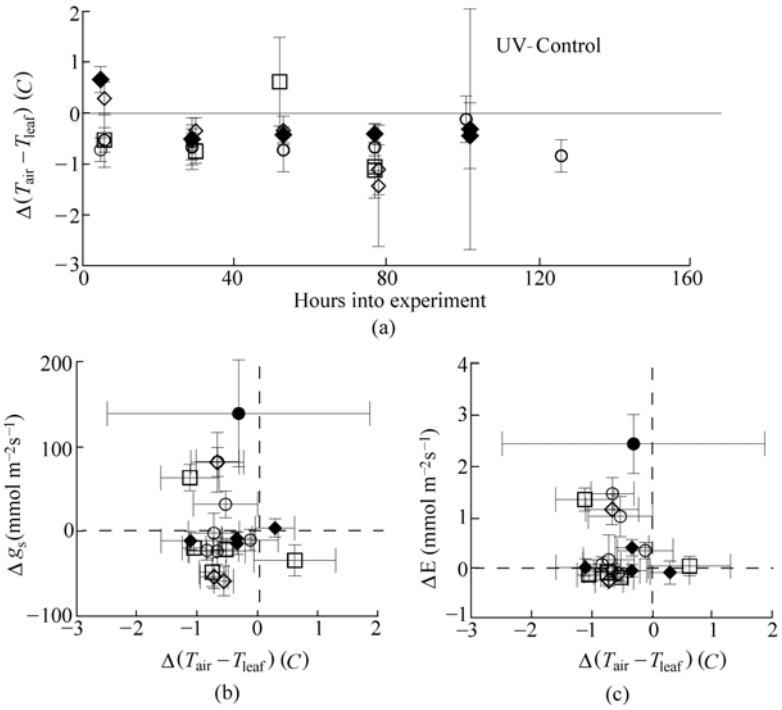

Figure 16.6 Influence of UV exposure on Essex temperature difference between the leaf and the air. The difference between the control and UV-exposed leaves is indicated as UV-Control. The difference between air and leaf temperature with UV exposure is indicated in panel (a). The relationship between the differences in leaf stomatal conductance and transpiration due to UV exposure are indicated in panels (b) and (c) respectively. Symbols are indicated in Fig. 16.5. Error bars are standard error of the difference. All measurements were made in greenhouse experiments

than the control leaves. However, the ΔT did not correspond with differences in either g_s or E between the UV-exposed and control plant leaves (Fig. 16.6(b), (c)). This suggests that the UV-exposed plants could not entirely compensate for elevated leaf temperatures through the normal process of increasing E through decreased g_s.

Transpiration measurements made in the field in 2004 showed non-significant (t-test at $P=0.10$) decreases in Essex at V5 and non-significant differences at R3 (Table 16.2). Similarly, transpiration of Williams 82 leaves indicated non-significant decreases at V5 and non-significant differences at R3 (Table 16.2). This tendency was in contrast to the 2007 greenhouse study of Williams 82 (under a much higher exposure rate) that showed an enhanced E (non-significant) with UV exposure. In general, the magnitudes of the transpiration differences due to short term UV exposures in the greenhouse were smaller than those for longer term exposures in the field. These results suggest that the response of both cultivars to UV exposure was decreased transpiration in the vegetative stage. Essex showed a decrease in transpiration with UV exposure shortly after UV exposure begins. Williams 82 showed a decrease in transpiration that develops over time.

16.3.3 Photosynthesis

Leaf photosynthetic rates of the control plants typically varied from 1 to 11 mmol $m^{-2}s^{-1}$ (Fig. 16.7(a), Table 16.2) and were not significantly different over the course of the experiment (Fig. 16.7(a)). Four or five photosynthetic rate measurements were made on each plant during daylight hours in 2007. A diurnal periodicity was suggested in the measurements, but was not conclusive. Measurement variability, limiting the ability to determine treatment effects, is partly a result of variability in stomatal openings across the leaf.

Photosynthetic rates of both Williams 82 and Essex cv. were not significantly affected (t-test at $P=0.10$) by the UV exposures within a given measurement period or as a pooled sample in the 2007 study. In the 2008 study, A of the fully-expanded leaves from the VC was non-significantly (t-test at $P=0.10$) higher than the control leaves for the first four days of the exposure. Plants at V1, V2, V3, and V4 stages, however, showed a non-significant trend of decreasing A with increasing exposure (also showed no effect of UV exposure (Fig. 16.7(b)). As a pooled sample of all hours of measurements, the UV exposure resulted in a statistically significant increase in A at VC (t-test $P=0.01$) and no statistically significant change at V1, V2, V3 or V4. This is in agreement with recent studies showing no reductions in photosynthesis under current or future UV-B exposures in the presence of ambient PPFD (Fiscus and Booker, 1995; Allen et al., 1998).

In the 2007 study on leaves from R2 through R4, $\Phi_{PS\,II}$ was not significantly different relative to the control (t-test at $P=0.10$) for both cultivars. Initially the $\Phi_{PS\,II}$ was higher than the control for Essex and lower than the control for

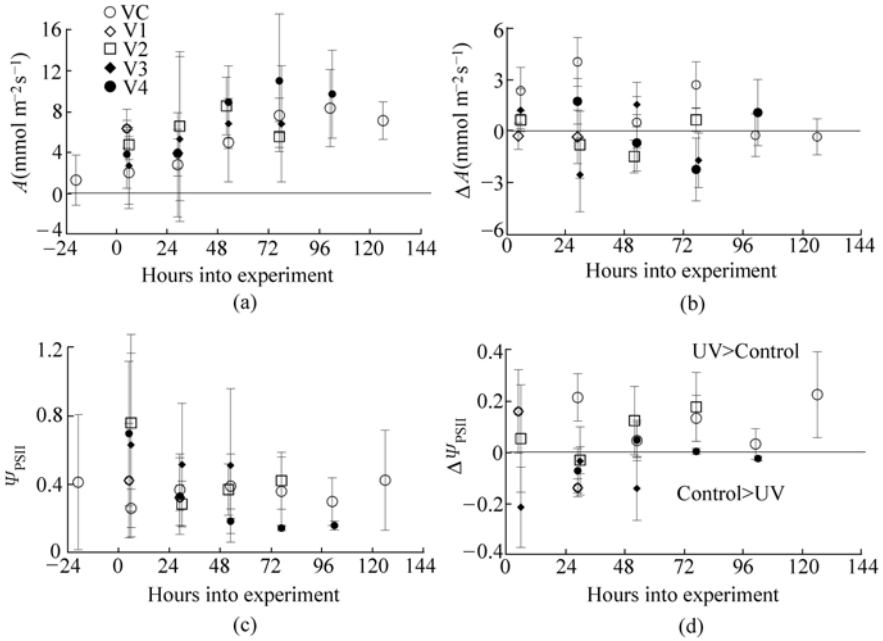

Figure 16.7 Influence of UV exposure on Essex leaf photosynthesis at development stages VC through V4. Measurements of the efficiency of photosystem Ⅱ (PSⅡ) are indicated in panel (a) while measurements of photosynthetic rate (a) are indicated in panel (b). Differences indicated are UV-Control. Error bars are standard error of the difference. All measurements were made in greenhouse experiments

Williams 82 after the first day of exposure, but showed no significant affect at the end of the first night and in the subsequent two days of exposure. This suggests that initial exposures to UV radiation may result in a response by the plant that is compensated for by the second day through metabolic responses to the initial exposure.

The Williams 82 A, during the first day of exposure in the 2007 experiment, were greater for the control than the UV-exposed leaves while $\Phi_{PS\text{Ⅱ}}$ was greater for the UV-exposed plants than the controls. Subsequent UV exposure did not show effects on A. The Essex leaves had the exact opposite relationship during the first two hours of exposure, yet responded like the Williams 82 leaves by the end of the first exposure period.

The $\Psi_{PS\text{Ⅱ}}$ of leaves of Essex during vegetative growth stages was examined in 2008 to determine if there is evidence of decreased efficiency under UV exposure. There was no discernible difference in the control plant leaf $\Psi_{PS\text{Ⅱ}}$ measurements over the course of the experiment (Fig. 16.7(d)). During VC stage, the UV-exposed plants were uniformly, but not significantly, more efficient than the control (Fig. 16.7(c)). This tendency continued for the leaves at V1 and V2 stages. At V3 and V4 stages, the UV-exposed leaves were negatively affected by the first

exposure day, with exposure during the subsequent days having less effect on the efficiency (Fig. 16.7(c)). This suggests that the plant has responded to the exposure by changing metabolic pathways that protect the plant from further damage with additional exposure. If true, this might explain why the decreased Φ_{PSII} at R2 through R4 did not appear to affect A in Essex. The general finding of insensitivity of Ψ_{PSII} and Φ_{PSII} to UV exposure extending beyond one day is consistent with the lack of A response to the UV exposure described above.

16.3.4 Water Use Efficiency

The lack of photosynthetic response to UV exposure in combination with the increased or no transpiration response suggests that the water use efficiency (WUE) of the plants may change due to UV exposure. The mean WUE of the field study Essex control plants (under Llumar) was 0.0023 (SD = 0.0005) at V5 stage and 0.0026 (SD = 0.0008) at R3. The mean WUE of the field study Williams control plants was 0.0021 (SD = 0.0005) at V5 stage and 0.0023 (SD = 0.0004) at R3. The mean WUE of the 2007 Essex and Williams control plants at R2 through R4 was 0.0074 (SD = 0.0026) and 0.0064 (SD = 0.0034) respectively, higher than those at R3 in the field. The mean WUE of the Essex plants at VC through V4 ranged from 0.0019 to 0.0065. The WUE of four to five pairs of photosynthetic rate and E measurements made on each plant during daylight hours in 2007 suggested a diurnal periodicity, but the pattern was not consistent for all days and cultivars.

Results are not conclusive, but indicate that the WUE of Essex was not affected by UV exposure (Fig. 16.8(a)), while that of Williams 82 was affected by UV exposure. The 2007 study showed the UV exposure did not significantly affect (t-test at $P = 0.10$) the WUE in Essex within a given measurement period or as a pooled sample. The UV exposure in 2007 did not significantly (t-test at $P = 0.10$) affect WUE in Williams 82 within a given measurement period or as a pooled sample, although there was a tendency for reduced WUE associated with UV exposure (Fig. 16.8(a)).

The WUE of Essex plants at VC stage increased with UV exposure until after the second day of exposure. The relationship between UV exposure and WUE of Essex plants at the V1 through V4 stages was ambiguous. Generally it appears that the WUE is unaffected by UV exposure, but plants at V4 stage may have reduced WUE under exposure for the duration of the measurements (Fig. 16.8(b)).

16.3.5 UV-B Absorbing Compounds and Leaf Pigments

The 2004 greenhouse study evaluated UV-B absorbing compounds and leaf pigment concentrations after 23.4 kJ m^{-2} UV-B_{BE} of exposure. The initial content of UV-B absorbance of acidified methanolic leaf extracts of Essex at 300 nm – 320 nm

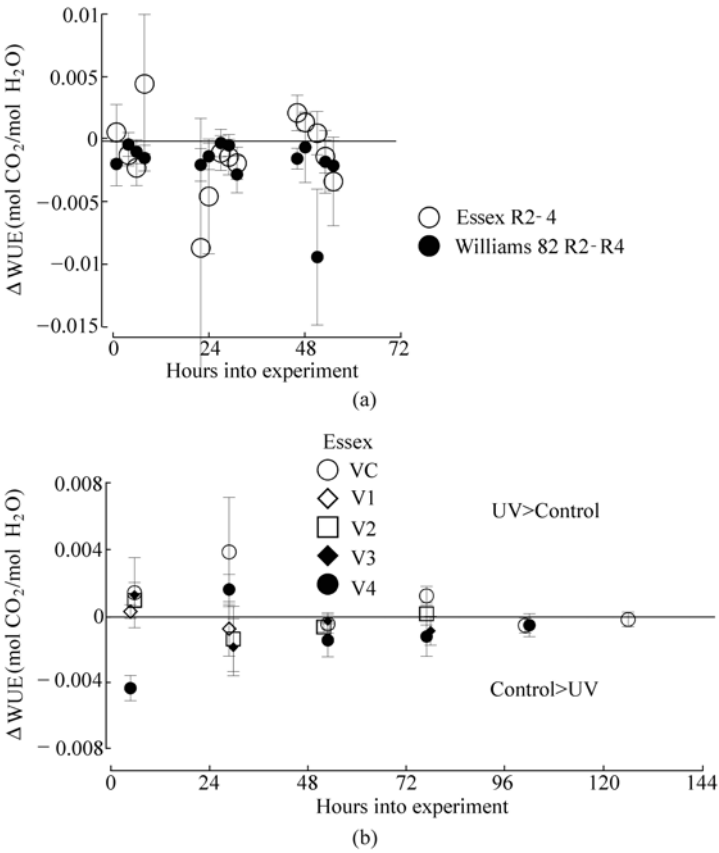

Figure 16.8 Changes in water use efficiency with UV exposure. Differences indicated are UV-Control. Error bars are standard error of the difference. All measurements were made in greenhouse experiments

was higher than in Williams 82 and Essex had significantly higher UV-B absorbance than Williams 82 after UV-B exposure. The UV-B absorbance of Essex and Williams 82 cultivars showed a peak spectral absorbance at the minimum wavelength of measurement (280 nm) after 18 hours of UV-B exposure. The difference in bulk UV-B absorbance of leaf extracts of UV exposed plants and unexposed control plants of Essex was higher than those of Williams 82 (4.36 and 1.80 respectively). Essex plants had an average of 2.4 times the absorbance of Williams 82. This is in contrast to the greenhouse study results of Murali et al. (1988) who found that Williams plants had a greater concentration of UV-absorbing compounds than Essex plants after a much longer period of 34 days at 11.5 kJ m^{-2} d^{-1} $UV\text{-}B_{BE}$. Since the spectral irradiance distribution of the lamps differed from natural solar radiation, the change in bulk UV-B absorbance with exposure was weighted according to the spectral irradiance distribution of the lamps. The

spectrally-weighted difference in bulk absorbance between UV-exposed and control plants of Essex (3.57) was 3.5 times that of Williams 82 (1.02).

The 3 days of UV exposure (totaling 23.4 kJ m^{-2} UV-B_{BE}) resulted in an increase in the concentration of several leaf pigments in Williams 82 and Essex (Table 16.3). The chlorophyll *a* and carotenoid concentrations were significantly higher (t-test at $P = 0.10$) for the UV-exposed Williams 82 plants compared to control plants. In contrast, UV did not significantly affect chlorophyll *b* concentrations in both cultivars (Table 16.3). Chlorophyll *a* is the most widely distributed photosynthetic pigment in plants and is mainly responsible for the absorption of light that powers photosynthesis. Similar to the results of our present study, chlorophyll *a* has been observed to be more affected than chlorophyll *b* (Teramura 1983; Strid et al., 1990). Williams 82 also responded to the exposure to UV radiation by increased production of carotenoids while Essex did not (Tables 16.3 and 16.4). Carotenoids play an essential role in both light harvesting and photoprotection (Taiz and Zeigler, 2002). Similarly, Steel and Keller (2000) observed an increase in carotenoid concentrations in *Vitis vinifera* following UV-B exposure.

Table 16.3 Leaf pigment concentrations at V2 stage in 2004 greenhouse study

		UV-Control			
	CV	Carotenoids (mg/cm^2)	Chlorophyll a (mg/cm^2)	Chlorophyll b (mg/cm^2)	Anthocyanins (mg/cm^2)
Essex	Mean	0.008	1.29	−0.22	0.00012
	SE	0.054	1.07	0.35	0.00068
Williams 82	Mean	0.121*	4.22*	0.20	−0.00017
	SE	0.043	1.88	0.57	0.00063

* = statistically significant difference at $P = 0.10$.

Table 16.4 Leaf pigment concentrations at V5 in 2004 field study

		UV-Control		
	CV	Carotenoids (mg/cm^2)	Chlorophyll a (mg/cm^2)	Chlorophyll b (mg/cm^2)
Essex	Mean	−0.014	−0.23	−0.26
	SE	0.046	1.45	0.49
Williams 82	Mean	0.017	0.57	0.18
	SE	0.034	1.10	0.40

Ultraviolet exposure did not appear to alter anthocyanin concentrations in either the Essex or Williams 82 cultivars (Table 16.3). Consequently, the enhanced UV absorbing compounds do not apparently include the anthocyanins. While

Chalker-Scott (1999) suggests that anthocyanins are linked to UV-B tolerance in some cultivars, our results did not indicate that anthocyanins were produced in plants of the studied cultivars at the V2 stage in the presence of UV-B radiation.

The 2004 field study evaluated UV-B absorbing compounds and leaf pigment concentrations at V5 after approximately 150 kJ m^{-2} UV-B_{BE} (35 days from planting) of exposure and R3 after approximately 488 kJ m^{-2} UV-B_{BE} (84 days from planting) of exposure. As in the greenhouse experiment, the UV-B absorbance of Essex and Williams 82 cultivars showed a peak spectral absorbance at the minimum wavelength of measurement (280 nm) at V5 as well as R3. At the V5 stage, the difference in bulk UV-B absorbance of leaf extracts between UV exposed plants and unexposed control plants of Essex was 4.7 times higher than the Williams 82 (2.35 and 0.50 respectively), while at the R3 stage, there was no significant difference in this same comparison (-0.10 and -0.03, respectively). The spectrally-weighted difference between leaf absorbances of the UV-exposed and control plants of Essex was 2.6 times greater than that of Williams at V5 and 4.3 times smaller than that of Williams at R3. The tendency for greater spectrally-weighted UV-B absorbance in Essex than Williams leaves at V5 is similar to the results at V3 in the 2004 greenhouse study. The change in cultivar with the greatest UV-B absorbing compound amount with development is a result of a decrease in weighted UV-B absorbance in Essex leaves with UV exposure at R3 (0.007) compared to at V5 (0.065), while the change in weighted UV-B absorbance in Williams leaves at R3 (0.27) was similar to that at V5 (0.25). It appears that by the time the plants are in reproductive phases, the earlier differences in UV absorbing compounds may be less important.

The control plants in the 2004 field study had lower concentrations of all pigments than the plants in the 2004 greenhouse study. Differences in chlorophyll content between greenhouse and field studies are consistent with commonly reported responses to increased blue and UV-A radiation in the greenhouse study relative to the field. This reduction may also have been a result of additional stresses on the plants in the field. Plants in the field were not supplementally watered beyond natural precipitation. In a comparison with the control plants, the UV-exposed plants did not have significantly different concentrations of carotenoids, chlorophyll *a*, or chlorophyll *b* (Table 16.4). The lack of statistical significance was not a result of greater variability in the field plants as the coefficient of variation of chlorophyll *a* and *b* in the field study was very similar to that of the greenhouse study. Variability in leaf carotenoid concentration in the field study was greater than that in the greenhouse study.

16.4 Summary and Conclusions

Essex and Williams 82 cultivars respond differently to UV exposure. Ultraviolet-exposed Williams 82 exhibited greater g_s after the initial exposure response of

reduced g_s compared to the control plants that did not correspond with changes in *E*. Essex initially showed an increase in g_s and *E* with UV exposure which then decreased after one day of UV exposure, or 8 kJ m^{-2} – 12 kJ m^{-2} UV-B_{BE} exposure. The exposure of Essex and Williams to UV radiation showed no affect on photosynthesis (*A* or PSⅡ efficiency), consistent with many other studies.

Plant tolerance to UV-B exposure involves many different strategies including radiation avoidance, changes in leaf structure, enhanced production of UV-B absorbing pigments, enhanced production of photosynthetic pigments, and dimer repair (Caldwell et al., 1983; Day et al., 1992; Vogelmann, 1993). The 2004 greenhouse and field experiments showed that the production of secondary compounds in the presence of UV radiation differed between Essex and Williams 82 cultivars. Williams 82 showed no significant increase in UV-B absorbing compounds after 18 hours of UV-B radiation exposure. Essex, on the other hand, accumulated UV-B absorbing compounds while UV-B exposed Williams accumulated chlorophyll *a* and carotenoids compared to control plants. The lack of UV exposure effects on pigments in some plants was related to higher UV-B screening compounds (Day et al., 1992; Sullivan et al., 2000). This may explain why UV-B did not significantly alter photosynthetic pigment concentrations in Essex.

The production of secondary compounds depends on the amount of photosynthetically fixed carbon partitioned to growth or defense (Herms and Mattson, 1992). Photosynthetic rates and Φ_{PSII} of both Essex and Williams 82 were not significantly affected by the UV exposures. Initially it appears that carbon fixed by Essex was preferentially directed towards the production of UV-B absorbing compounds, while that of Williams 82 was preferentially directed to compounds enhancing photosynthesis. Therefore, it appears that Williams 82 has significant UV tolerance mechanisms other than UV-B absorbing pigments for UV-B protection. The results of the present work have suggested that Essex and Williams 82 have different mechanisms to control injury and increase tolerance that appear to be activated after brief exposures to UV-B.

In Essex, chlorophyll concentrations were unaffected by UV exposure in both the short-term greenhouse study and the longer term field study, while in Williams 82, chlorophyll concentrations increased with UV exposure in the greenhouse. Chlorophyll concentrations are often highly correlated with photosynthetic capacity (Dillenburg et al., 1995). Since Φ_{PSII} was also not affected by the UV exposure, the observed increase in chlorophyll *a* concentrations in Williams 82 (Table 16.2) was not readily explicable. The lack of UV exposure effects on the photosynthetic rate of Essex and Williams 82 plants, even though other physiological responses are affected, supports the growing evidence that biomass reductions and yield losses are associated with changes in plant morphology more than function (Day, 2001; Kakani et al., 2003). Additionally, alterations in gene expression before there is any UV-B induced injury (RNA levels for chloroplast proteins and other biochemical composition) cannot be discounted.

Comparisons between greenhouse and field studies are always fraught with complications. As found in this study for g_s and E, differences in plant responses to UV exposure commonly found in greenhouse studies are not found in field studies. This may be a result of the influence of water stress, temperatures, plant competition, available PPFD, and a host of other environmental conditions. Of interest is the evidence for similar relationships between Essex and Williams of UVB-absorbing compounds in early vegetative leaf stages. This suggests that the effects of UV exposure on these cultivars may at least be somewhat similar between greenhouse and field studies.

Although efforts were made to minimize the differences in PPFD between UV-exposed and control plants, the disparity between PAR exposures may influence the results discussed. Furthermore, the ratio of PPFD to UV-A and UV-B irradiance varied to some degree. Since plants are known to have complex responses to spectral irradiance, the variation in these ratios may have exclusively masked UV effects on plant physiology. The variability in physiological measurements both in the greenhouse and in the field studies limited the ability to differentiate effects due to UV exposure, PPFD, and these irradiance ratios between PAR, UV-A and UV-B radiation. Further work should be conducted where the UV-exposed and the control plants have more similar and higher PAR exposures, and similar irradiance ratios to assess what the UV-protective mechanisms initialized within the first day of exposure are, and how they are regulated. In addition, further understanding is needed to determine how decreases in daily exposures due to cloud cover vary the cumulative longer-term plant response.

Acknowledgements

The authors gratefully acknowledge partial funding for this study from the USDA UV-B Monitoring and Research Program, Colorado State University, Fort Collins, Colorado. The assistance of Laura Grossman and Dr. Tom Housley is also appreciated. We also acknowledge Drs. Jeffrey Volenec and Cliff Johnston of the Department of Agronomy, Purdue University for allowing us to use their laboratory facilities, Dr. Robert Joly of the Department of Horticulture and Landscape Architecture for lending us the steady-state pyrometer, and Ms. Judy Santini of the Department of Agronomy, Purdue University for valuable advice concerning statistical analyses.

References

Allen DJ, Nogúes S, and Baker NR (1998) Ozone depletion and increased UV-B radiation: is there a real threat to photosynthesis? J. Exp. Bot. 49, 1775 − 1788

Apostol KG and Zwiazek JJ (2004) Boron and water uptake in jack pine (*Pinus banksiana*) seedlings. Env. Exp. Bot. 51, 145 – 153

Battaglia PR and Brennan TM (2000) Differential effects of short-term exposure to ultraviolet-B radiation upon photosynthesis in cotyledons of a resistant and a susceptible species. Int. J. Plant Sci. 161, 771 – 778

Bawhey CI, Grant RH, and Gao W (2003) Digital measurement of heliotropic leaf response in soybean cultivars and leaf exposure to solar UV-B radiation. Agric. Forest Meteorol. 120, 161 – 175

Beggs CJ, Schneider-Ziebert U, and Welman E (1986) UV-B radiation and adaptive mechanisms in plants. In: Worrest, R.C., Caldwell, M.M. (Eds.), Stratospheric Ozone Reduction, Solar Ultraviolet Radiation and Life. Vol. 1 Springer-Verlag, Berlin. pp. 235 – 250

Bornman JF (1989) Target sites of UV-B radiation in photosynthesis of higher plants. J. Photochem. Photobiol. B Biol. B4, 145 – 158

Bornman JF and Vogelmann TC (1991) Effect of UV-B radiation on leaf optical properties measured with fiber optics. J. Exp. Bot. 42, 547 – 554

Caldwell MM (1971) Solar ultraviolet irradiation and the growth and development of higher plants. In: Giese, A.C. (Ed.), Photophysiology. Academic Press. New York. Vol. 6 pp. 131 – 177

Caldwell MM, Robberecht R, and Flint SD (1983) Internal filters: prospects for UV acclimation in higher plants. Phys. Plant. 58, 445 – 450

Caldwell MM, Björn LO, Bornman JF, Flint SD, Kulandaivelu G, Teramura AH, and Tevini M (1998) Effects of increased solar ultraviolet radiation on terrestrial ecosystems. J. Photochem. Photobiol. B Biol. 46, 40 – 52

Chalker-Scott L (1999) Environmental significance of anthocyanins in plant stress responses. Photochem. Photobiol. 70, 1 – 9

Dai Q, Peng S, Chavez A, and Vergara BS (1995) Effects of UV-B radiation on stomatal density and opening in rice (*Oryza sativa* L.). Ann. Bot. 76, 65 – 70

Davies BH (1976) Carotenoids. In: Goodwin TW (Ed.), Chemistry and Biochemistry of Plant Pigments. Academic Press, New York. Vol. 1. pp.38 – 155

Day TA (2001) Ultraviolet Radiation and plant ecosystems. pp.80 – 117 In: Cockell, CS and Blaustein AR (Eds.), Ecosystems, Evolution, and Ultraviolet Radiation. Springer Verlag, NY. p.221

Day TA, Vogelmann TC, and DeLucia EH (1992) Are some plant life forms more effective than others in screening out ultraviolet-radiation? Oecol. 92, 513 – 519

Dillenburg LR, Sullivan JH, and Teramura H (1995) Leaf expansion and development of photosynthetic capacity and pigments in *Liquidambar styraciflua* (Hamamelidaceae)—Effects of UV-B Radiation. Am. J. Bot. 82, 878 – 885

Eisinger W, Swartz TE, Bogomolni RA, and Taiz L (2000) The ultraviolet action spectrum for stomatal opening in broad bean. Plant Physiol. 122, 99 – 105

Fehr WR and Caviness CE (1977) Stages of soybean development. Iowa State University Cooperative Extension Service. Special Rep. 80, 1 – 12

Fiscus EL and Booker FL (1995) Is UV-B a hazard to crop photosynthesis and productivity? Results of an ozone-UV-B interaction study and model predictions. Photosyn. Res. 43, 81 – 92

Gamon JA and Surfus JS (1999) Assessing leaf pigment content and activity with a reflectometer. New Phytol. 143, 105 – 117

Gitz Ⅲ DC, Liu-Gitz L, Britz SJ, and Sullivan JH (2005) Ultraviolet-B effects on stomatal density, water-use efficiency, and stable carbon isotope discrimination in four glasshouse-grown soybean (*Glyicine max*) cultivars. Env. Exp. Bot. 53: 343 – 355

Graan T and Ort D (1984) Quantification of the rapid electron donors to P700, the functional plastoquionone pool, and the ratio of the photosystems in spinach chloroplasts. J. Biol. Chem. 259, 14003 – 14010

Grant RH and Slusser JR (2002) Spatial correlations of daily exposure and weekly maximum day exposure of solar UV radiation in the continental United States: In: Slusser, J.R., Herman, J.R., Gao, W. (Eds.). Ultraviolet ground-and spaced-based measurements, models and effects, II. Proceedings of SPIE, Vol. 4896: 52 – 61

Grant RH and Slusser JR (2003) Defining the probabilities of solar UV event exposures for plant effects research. In: Slusser JR, Herman JR, Gao W (Eds.) Symposium on Ultraviolet ground-and spaced-based measurements, models and effects. Proceedings of SPIE — The International Society for Optical Engineering. Vol. 5156, 5156 – 28

Grant RH and Slusser JR (2005) Estimation of ultraviolet-A irradiance from measurements of 368-nm spectral irradiance. J. Atmos. & Ocean. Technology 22: 2853 – 2863

Gwyn-Jones D, Johanson U, Phoenix GK, Callaghan TV, Sonesson M and Lee JA (1999) The responses of plant functionally types to enhanced UV-B. In: Rozema J. (Ed.) Stratospheric ozone depletion. The effects of enhanced UV-B radiation on terrestrial ecosystems. Backhuys Publishers, Leiden. pp. 187 – 201

He J, Huang LK, and Whitecross MI (1994) Chloroplast structure changes in *Pisum sativum* associated with supplementary ultraviolet (UV-B) radiation. Plant Cell Environ. 17, 771 – 775

Herms DA and Mattson WJ (1992) The dilemma of plants: to grow or to defend. Q. Rev. Biol. 67, 283 – 335

Jordan BR, Chow WS, Strid A, and Anderson JM (1991) Reduction in cab and psb A RNA transcripts in response to supplementary ultraviolet-B radiation. FEBS Lett 284, 5 – 8

Jordan BR, He J, Chow WS, and Anderson JM (1992) Changes in mRNA levels and polypeptide subunits of ribulose-1,5-biphosphate carboxylase in responses to supplementary ultraviolet-radiation. Plant Cell Environ. 15: 91 – 98

Jordan BR, James PE, Strid A, and Anthony RG (1994) The effect of ultraviolet-B radiation on gene expression and pigment composition in etiolated and green pea leaf tissue: UV-B-induced changes are gene specific and dependent upon the developmental stage. Plant Cell Environ. 17, 45 – 54

Kakani VG, Reddy KR, Zhao D, and Sailaja K (2003) Field crop responses to ultraviolet-B radiation: a review. Agric. For. Meteorol. 120, 191 – 218

Kakani VG, Reddy KR, Zhao D, and Gao W (2004) Senescence and hyperspectral reflectance of cotton leaves exposed to ultraviolet-B radiation and carbon dioxide. Physiol. Plant. 121, 250 – 257

Kozlowski TT and Pallardy SG (1997) Physiology of Woody Plants, second ed. Academic Press. San Diego, p.411

Knipling EB (1970) Physical and physiological basis for the reflectance of visible and near-infrared radiation from vegetation. Rem. Sens. Env. 1, 155 – 159

Lichtenthaler HK (1987) Chlorophylls and carotenoids: pigments of photosynthetic biomembranes. Meth. Enzymol. 148, 350 – 382

Matsuki M (1996) Regulation of plant phenolic synthesis: from biochemistry to ecology and evolution. Aus. J. Bot. 44, 613 – 634

Middleton EM and Teramura AH (1993) The role of flavonol glycosides and carotenoids in protecting soybean from ultraviolet B damage. Plant Physiol. 103, 741 – 752

Murali NS and Teramura AH (1986) Effects of supplemental Ultraviolet-B radiation on the growth and physiology of field-grown soybean. Env. Exp. Bot. 26, 233 – 242

Murali NS, Teramura AH, and Randall SK (1988) Response differences between two soybean cultivars with contrasting UV-B radiation sensitivities. Photochem. Photobiol. 48, 653 – 657

Musil CF and Wand SJE (1993) Responses of sclerophyllous Ericaceae to enhanced levels of ultraviolet-B radiation. Env. Exp. Bot. 33, 233 – 242

Musil CF, Bjorn LO, Scourfield MWJ, and Bodeker GE (2002) How substantial are ultraviolet-B supplementation inaccuracies in experimental square-wave delivery systems? Env. Exp. Bot. 47, 25 – 38

Negash L (1987) Wavelength-dependence of stomatal closure by ultraviolet radiation in attached leaves of *Eragrostis tef*: action spectra under backgrounds of red and blue lights. Plant Physiol. Biochem. 25, 753 – 760

Nogués S, Allen DJ, Morison JIL, and Baker NR (1998) Ultraviolet-B radiation effects on water relations, leaf development and photosynthesis in droughted pea plants. Plant Physiol. 117, 173 – 181

Qi Y, Bai S, and Heisler GM (2003) Changes in ultraviolet-B and visible optical properties and absorbing pigment concentrations in pecan leaves during a growing season. Agric. Forest Meteorol. 120, 229 – 240

Rosa LM and Forseth IN (1995) Diurnal patterns of soybean leaf inclination angles and azimuthal orientation under different levels of ultraviolet-B radiation. Agric. For. Meteorol. 78, 107 – 119

Sims DA and Gamon JA (2002) Relationships between leaf pigment content and spectral reflectance across a wide range of species, leaf structures and developmental stages. Rem. Sens. Environ. 81, 337 – 354

Steel CC and Keller M (2000) Influence of UV-B irradiation on the carotenoid content of *Vitis vinifera* tissues. Biochem. Soc. Trans. 28, 883 – 885

Strid Å, Chow WS, and Anderson JM (1990) Effects of supplementary ultraviolet-B radiation on photosynthesis in *Pisum sativum*. Biochim. Biophys. Acta. 1020, 260 – 268

Sullivan JH, Howells BW, Ruhland CT, and Day TA (2000) Changes in leaf expansion and epidermal screening effectiveness in *Liquidambar styraciflua* and *Pinus taeda* in response to UV-B radiation. Physiol. Plant. 98, 349 – 357

Taiz L and Zeiger E (2002) Plant Physiology. Third edition, Sinauer Associates, Inc. Publishers. p.690

Teramura AH (1983) Effects of ultraviolet-B radiation on the growth and yield of crop plants. Physiol. Plant. 58, 415 – 427

Teramura AH and Sullivan JH (1994) Effects of UV-B radiation on photosynthesis and growth of terrestrial plants. Photosynth. Res. 39, 463 – 473

Teramura AH, Biggs RH, and Kossuth S (1980) Effects of Ultraviolet-B irradiance on soybean: II. Interactions between ultraviolet-B and photosynthetically-active radiation on net photosynthesis, dark respiration, and transpiration. Plant Physiol. 65, 483 – 488

Teramura AH, Tevini M, and Iwanzik W (1983) Effects of ultraviolet-B irradiation on plants during mild water stress. 1. Effects on diurnal stomatal resistance. Physiol. Plant. 57, 175 – 180

Tevini MJ, Braun G, and Fieser G (1991) The protective function of the epidermal layer of rye seedlings against ultraviolet-B radiation. Photochem. Photobiol. 53, 329 – 333

Tevini M (1993) Effects of enhanced UV-B radiation on terrestrial plants. In: Manfred T. (Ed.). UV-B Radiation and Ozone Depletion. Effects on humans, animals, plants microorganisms, and materials. pp. 125 – 154

Visser AJ, Tosserams M, Groen MW, Kalis G, Kwant R, Magendans GWH, and Rozema J (1997) The combined effects of CO_2 concentration and enhanced UV-B radiation on faba bean. 3. Leaf optical properties, pigments, stomatal index and epidermal cell density. Plant Ecol. 128, 209 – 227

Vogelmann TC (1993) Plant tissue optics. Ann. Rev. Plant Physiol. Plant Mol. Biol. 44 231 – 251

17 UV-Effects on Young Seedlings of Soybean: Effects in Early Development and Long-Term Effects

Katherine M. Warpeha and Lon S. Kaufman

Department of Biological Sciences m/c 567
University of Illinois at Chicago 900 S. Ashland Ave
Chicago, IL 60607, USA
E-mail: kwarpeha@uic.edu
E-mail: lkaufman@uic.edu

Abstract Young plants are the most susceptible to ultraviolet (UV) radiation, due to the large number of growing and dividing cells. Incident UV radiation to earth has increased, even at temperate latitudes. Chronic exposure to UV light, especially UV-B (290 nm − 320 nm) radiation, causes damage to land plants including reduced photosynthetic capacity, biomass yield, nutritional quality of the seed, altered patterns of species competition, plant ultrastructure and pigment production, and increased incidence of disease. Hence it is important to know how exposures early in the life cycle of the plant affect the establishment of the seedling and the production of viable seed. We found that the greatest affects of UV-B occurred very early in the plant's life cycle, notably in the first week post planting. Aside from increased mortality with increasing UV energy, UV-B treated seedlings had increased deformity, decreased ability to produce viable seeds and dysregulation of phenylpropanoid synthesis, which is dependent upon phenylalanine. Responses to high energy UV-B cause noticeably different effects in different varieties of soybean. If soybean experience higher energy UV in the early stages of growth, the effects can cause heritable changes, which will in turn effect yield and impact the viability of the next generation of seed.

Keywords phenylalanine, photoreceptor, stress, soybean, phenylpropanoids

17.1 Introduction

Phenylpropanoids are secondary metabolites ultimately synthesized from the aromatic amino acid phenylalanine (Phe; Gilchrist and Kosuge, 1980). It has been reported that adequate induction of the phenylpropanoid pathway within the first three weeks post-germination can influence a plant's ability to respond to or

protect itself from stresses occurring later in the life cycle (Liu et al., 1995; Bilger et al., 2001; Sullivan et al., 2003), but until recently, there were few clues as to how this actually was achieved or how it was regulated. Cosio and McClure (1984) reported that key enzymes of the flavonoid biosynthetic pathway were greatly reduced in activity by completion of leaf expansion, confirmed by recent work in assessing impact of ultraviolet-B (UV-B) on seedlings (Sullivan et al., 2007). Warpeha et al. (2008) reported that the developmental state and adequate Phe synthesis was critical for protection from UV radiation in the genetic model of Arabidopsis. Hence, it is important to fully investigate and understand how seedlings in general perceive and prepare for stress in the process of germination and exposure to UV. Herein we discuss how soybean seedlings respond to small doses of UV-B radiation in the first few weeks of growth, and assess some of the qualitative responses.

Environmental assessments over the last ten years indicate incident UV radiation has increased, even at temperate latitudes (Ajavon et al., 2003). Chronic exposure to UV light, especially UV-B (290 nm – 320 nm) radiation, causes a number of deleterious effects to land plants which have been documented in crops and uncultivated species, including reduced photosynthetic capacity, biomass yield, nutritional quality of the seed, altered patterns of species competition, plant ultrastructure and pigment production, and increased incidence of disease (reviewed in Caldwell and Flint, 1994; Stapleton et al., 1997; Grammatikopoulos et al., 1998; Sullivan and Rozema, 1999; Ries et al., 2000; Caldwell et al., 2003; reviewed in Frohnmeyer and Staiger, 2003; Sullivan, 2005; Jenkins and Brown, 2007; reviewed in Caldwell et al., 2007).

Understanding how young seedlings respond to initial exposure to UV is very important to understanding this stress. There is a wide variation in sensitivity to UV between species and among varieties of the same species (Sato et al., 1994; Torabinejad and Caldwell, 2000; Cartwright et al., 2001; Li et al., 2003; Koti et al., 2005; Rozema et al., 2005; Koti et al., 2007; Sullivan et al., 2007). It is unknown what mechanisms of perception and signal transduction determine the level of sensitivity to UV-B. The pathways that invoke “protective” responses also remain largely unstudied and undetermined (Ulm and Nagy, 2005; Sullivan et al., 2007), although G proteins are involved in the early sensing mechanism of both low fluencies of UV-A and UV-B in the genetic model Arabidopsis (Warpeha et al., 2008).

Ultraviolet radiation elicits several types of responses in higher plants. One is to initiate repair of negative alterations after the absorption and damage to DNA by UV, where UV-B exposure is followed by the repair of UV-induced thymidine dimers, as assisted by blue light (BL) (reviewed in Jansen et al., 1998; Frohnmeyer and Staiger, 2003). Plants can also prevent injury from exposure to UV-B by synthesizing and / or deploying UV screening pigments that are originally made from Phe in a pathway called the phenylpropanoid pathway. In most plants,

exposure to UV-B results in the increased accumulation or new synthesis of pigments capable of directly screening UV wavelengths (Robberecht and Caldwell 1978; Li et al., 1993; Stapleton and Walbot, 1994; Caldwell et al., 1995; Landry et al., 1995; Christie and Jenkins, 1996; Gonzalez et al., 1996; Reuber et al., 1996; Rozema et al., 1997; Burchard et al., 2000; Mazza et al., 2000; Tattini et al., 2000; Bieza and Lois, 2001; Rozema et al., 2002; Weinig et al., 2004; Casati and Walbot, 2005). Ultraviolet-B can also regulate a number of gene families, particularly those associated with the phenylpropanoid pathway, including enzymes directing the production of screening pigments like chalcone synthase (CHS) (Strid et al., 1994; Liu and McClure, 1995; reviewed in Frohnmeyer and Staiger, 2003; Oravecz et al., 2006; Blanding et al., 2007; Kaiserli and Jenkins, 2007).

Additional phenylpropanoids important for protection include materials such as suberin and other structural products that are deployed by plants to build and fortify the cuticle (Bird and Gray, 2003). Exposure to UV irradiation results in an increase in the quantity of wax occurring on the surface of leaves (Gonzalez et al., 1996; Long et al., 2003). Waxes and other cuticular materials can provide protection from UV radiation (Sieber et al., 2000; Long et al., 2003) and other stresses (Kim et al., 2007; reviewed in Nawrath, 2006) in higher plants, but do depend upon attaining a particular developmental state of the seedling. Seedlings that are null mutants for the prephenate dehydratase1 (PD1 or called ADT3 for arogenate dehydratase3) gene in Arabidopsis are unable to synthesize and deploy normal wax materials on the cotyledon, and do not form a proper cuticle. Inability to form proper cuticle and normal cuticular structures is correlated with sensitivity to UV radiation (Sieber et al., 2000; Long et al., 2003; Warpeha et al., 2008). It is also interesting to note that PD1 mutants had considerable delay in development of the chloroplast—a key difference compared to wild type seedlings. The PD1 mutants could not be induced to make Phe by the normal mechanisms (i.e., BL or UV).

Phe is an aromatic amino acid required for protein synthesis in primary metabolism, but is also the precursor to the thousands of secondary metabolites produced from the phenylpropanoid pathway (Hahlbrock and Scheel, 1989; Chapple et al., 1994; Kliebenstein 2004). Exposure to UV-B can result in the induction of genes encoding enzymes in the phenylpropanoid pathway (e.g., phenylalanine ammonia lyase (PAL) or CHS) which can affect the levels of various pigments. Expression of these genes and the activity of the encoded enzymes depend on intensity and the wavelengths of the incident UV (Margna, 1977; Chappell and Hahlbrock, 1984; Beerhues et al., 1988; Ohl et al., 1989; Li et al., 1993; Christie et al., 1994; Leyva et al., 1995; Liu and McClure, 1995; Fuglevand et al., 1996; Frohnmeyer et al., 1997; Wade et al., 2001; Brown et al., 2005; Kaiserli and Jenkins, 2007; Brown and Jenkins, 2008). For years it was unclear what controlled the synthesis of phenylpropanoids, but more recent data clearly indicate that the synthesis of Phe appears to be the rate-limiting step; i.e., the bottleneck for all downstream compounds produced in this pathway. Warpeha

et al. (2006; 2008; 2009) demonstrated that in response to BL, abscisic acid, or UV, Phe is the rate-limiting step for phenylalanine-derived pigment synthesis in etiolated seedlings of Arabidopsis, and also appears to be important in soybean (Warpeha et al., 2006; 2008; 2009). Phe can account for a significant proportion of the dry mass of a plant (Lewis and Yamamoto, 1989; Margna et al., 1989; Davin and Lewis, 1992; Van Heerden et al., 1996). There is generally a small pool of Phe in seeds and in the developing young seedlings. The actual process of germination and establishment of the seedling places a heavy demand on this pool (Margna, 1977; Margna et al., 1989), whereby incidents of stress or the actual growth process necessitate an even greater demand.

Studies on Phe synthesis and the effects on primary and secondary metabolites early in development are very rare. In Arabidopsis, where the process has been examined, BL and UV induce synthesis of Phe in etiolated Arabidopsis seedlings, occurring within minutes through the activation of a signal transduction chain consisting of GCR1 (a putative G-protein coupled receptor), and GPA1 (the sole Gα-subunit coded for in the Arabidopsis genome). This activation results in the activation of PD1 (aka ADT or AT3; one of six members of the PD gene family coded for in the Arabidopsis genome and the only member expressed in the etiolated seedling). Phe production occurs as a direct result of the activation of PD1 via its physical interaction with activated GPA1 (Warpeha et al., 2006). We do not know if other plants have the same sort of dependence on Phe early in development as Arabidopsis, the model system, but it is possible that rice and soybean may have a highly similar system of regulation (Yamada et al., 2008; Warpeha et al., 2009, respectively).

Given that Phe is very important for early synthesis of primary growth of young seedlings, and given that Phe is the first metabolite required for the activation of the phenylpropanoid pathway, a priority in research is to analyze the effects of UV radiation quality on the very early stages of seedling growth and to develop a stress model to understand how crop plants use Phe early in development.

Soybean has tremendous economic importance both as a domestic, and as an export crop. It is a potent source of oil and protein, and since it can fix atmospheric nitrogen and thereby add nitrogen to the soil, it is the ideal rotation crop for maize or wheat. However, soybean is susceptible to injury by UV radiation (Biggs et al., 1981; Teramura and Murali, 1986; Teramura et al., 1990; Teramura and Sullivan, 1991; Reed et al., 1992; Mazza et al., 2000; Li et al., 2003; Gritz et al., 2005; Koti et al., 2005; Middleton et al., 2005; Koti et al., 2007; Warpeha et al., 2009). Responses to UV can vary among plant species intraspecifically, and dependent on the developmental stage of growth when UV was received (Biggs et al., 1981; Teramura and Murali, 1986; Teramura and Sullivan, 1987; Sullivan and Teramura, 1988; Reed et al., 1992; Sullivan et al., 2007). Atmospheric ozone levels are not expected to improve in the next decade(s), and the levels of incident UV radiation may thus continue to increase.

Main Objectives

The main objective of this UV-B study was to examine the qualitative effects of UV radiation on the early development of soybean (*Glycine max*), using two varieties Williams and Forrest. The goals of the study were to: (1) evaluate the initial responses to low dose UV radiation in newly emerging plants up to 28 days post-germination; (2) evaluate effects of UV radiation on the seed production and viability of seed by examining the viability of the seeds produced from plants receiving a low dose UV radiation at germination (Day 3 after planting); and (3) examine the effects of UV-B on some of the products of the phenylpropanoid pathway.

17.2 Results and Discussion

17.2.1 UV Effects on Early Development and Survival of Young Soybean

Soybeans are generally planted close to the surface of soil; however, little UV radiation is said to penetrate any soil type. Organisms are most prone to cell and genetic alteration during periods of rapid call division and growth, as would be the case for plants in the first 3 to 4 days after planting, when the seed is germinating. We have been intrigued by the reports that plants appear to be the most affected by UV radiation in the first 3 weeks of growth, particularly in terms of the leaf's ability to synthesize screening compounds and in the activities of key enzymes in the phenylpropanoid pathway (Cosio and McClure, 1984; Liu and McClure, 1995; Sullivan et al., 2007). As our primary work is evaluating the photobiological responses of very young seedlings in response to different qualities of light (i.e., photoinduction of various pathways), we treated germinating seeds with very small doses of different qualities of UV to follow the early (first 3 to 4 weeks) seedling responses, from germination out to 28 days post-treatment, in a number of experiments designed to look at the development of critical tissues in a young seedling.

On Day 3 after planting Williams and Forrest seeds in darkness, sets of germinating seeds were given either a single dose of UV radiation (total dose 10^4 μmol m^{-2}, equivalent in dose to the strength of 1 sec of sunlight at midday (Warpeha et al., 2008)) at various wavelengths between 300 nm and 368 nm or a mock pulse of UV (Untreated = Control). The germinating seedlings were then transferred to a light growth chamber (14 h light: 10 h dark, i.e., 14:10; maintained at 23°C (Warpeha et al., 2009)). At 7 days post-planting (4 days post-germination), we scored seed germination. We observed that 20% − 30% of planted seeds had

mortality during the germination process; i.e., cessation of growth processes and decomposition, after treatment with 300 nm, 305 nm, or 311 nm in both varieties (Table 17.1).

Table 17.1 Survival of germinating seed post UV-irradiation at 7 days after planting. Germinating seeds were treated with UV-B radiation (Untreated = mock pulse; UV treatments = total dose 10^4 μmol m^{-2} (Warpeha et al., 2008)) wavelengths as shown on Day 3 after planting, and scored for germination and survival 4 days later

Variety	300 nm	305 nm	311 nm	317 nm	Untreated
Forrest	73%	79%	80%	81%	100%
Williams	68%	71%	78%	78%	100%

A number of Forrest and Williams seedlings died within the first week post-treatment, as shown in Table 17.1. This phenotype of severe damage after exposure to UV radiation may be due to epigenetic factors. For other abiotic stresses experienced in germinating seedlings/young plants, the structure of the shoot apical meristem may be adversely affected or development of the photosynthetic apparatus is impaired. Structural damage to the shoot apical meristem appears to be a major reason for death and decline in the growth of very young plants in both Arabidopsis and crop plants of interest in the case of salinity stressors (Sacks et al., 1997; West et al., 2004; Mahmoodzadeh, 2007), but is still poorly investigated for other stressors.

In order to understand what happens to seedlings surviving the 4-day milestone as shown in Table 17.1, we assessed young seedling responses to brief doses of UV administered at the time of germination. On Day 3 after planting Williams and Forrest seed in darkness, at least 3 sets of germinating seeds were given a single dose of UV radiation (total dose 10^4 μmol m^{-2} (Warpeha et al., 2008)) at 300 nm, 317 nm, or 368 nm, or were left Untreated (Controls). Immediately post-irradiation, at least 3 replicated sets of 20 seedlings were transferred to soil in order to follow growth effects under "summer" growth conditions (14 h light: 10 h dark; 23°C (Warpeha et al., 2009)). Surviving seedlings were observed up to 28 days after planting, and a representative example of each is depicted in Fig. 17.1. The seedlings that were given a 368 nm treatment appeared no different than those which were not treated (Controls) with UV. Seedlings treated by 300 nm or 317 nm did have surviving plants that grew at a much smaller rate in the first week (one example each of Williams is shown in Fig. 17.1), but then appeared to "recover" and grow at a steady rate as can be observed by seedling heights (Fig. 17.2). The 300 nm-treated seedlings in particular had smaller leaves and thickened stems at the very base; however, not all seedlings displayed these characteristics.

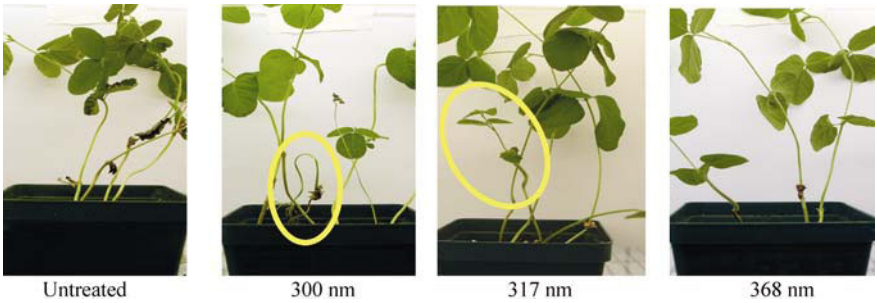

Figure 17.1 Photographs of Williams, 21 days after planting. Growth characteristics were observed for seedlings that were Untreated, or treated with a UV wavelength: 300 nm, 317 nm, and 368 nm. Plants were grown as described in Methods for seedling growth. Depicted above are some of the surviving seedlings. Delay and abnormal growth shown for example, by the yellow outline on the photographs. Treatments with 368 nm appeared highly similar to Untreated seedlings, same age (above)

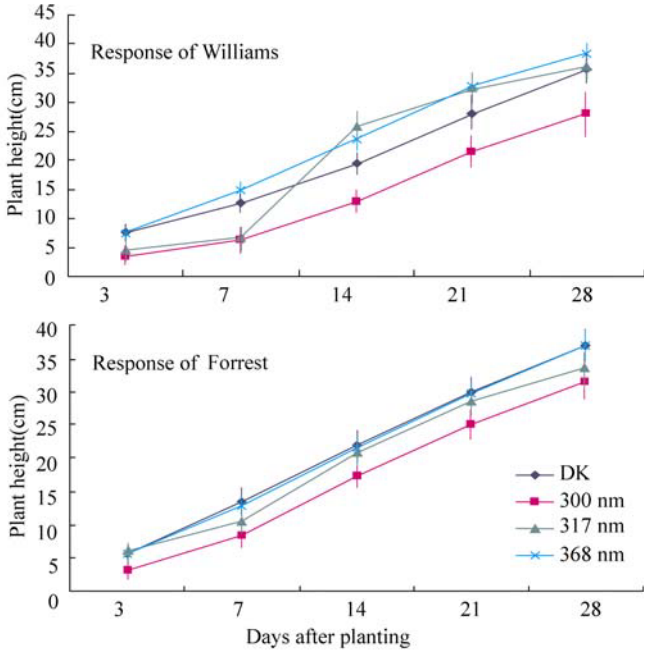

Figure 17.2 The response of soybean varieties Williams and Forrest to UV radiation treatment: a comparison of growth responses as assessed by height over 28 days post-planting. Sets of seedlings were treated with the UV wavelength shown (Untreated = mock pulse) and height measured every week from Day 3 after planting. Each data point is the result of 3 independently grown replicates of at least 20 seedlings. The SEMs are less than 10% for all points

When compared to untreated seedlings, there was only one clear difference in the manner of growth for the variety of Williams. Seedlings treated with 300 nm

experienced an immediate slowing of growth not observed for other treated and control seedlings of either variety. From 14 to 28 days post-irradiation, the rate of growth (i.e., slope of growth of sets of seedlings) was similar for all treatments. However, the main change in growth that occurred prior to 7 days post-irradiation persisted to 28 days after treatment for the 300 nm-treated seedlings (Fig. 17.2). The mean height of Williams "untreated" 35.95 ± 1.0 cm compared to the height of Williams "300 nm" at 29.9 ± 1.5 cm was significantly different (paired Student *t* test; mean height of 3 paired sets; $p = 0.04$). The 317 nm and 368 nm final height differences are less pronounced when compared to untreated seedlings ($34.5 + 0.9$ cm and $35.8 + 1.2$ cm, respectively), and are not statistically significant. Growth severely declines in response to 300 nm within the first week after exposure. The resumption of growth over time may be due to repair mechanisms and deployment of screening pigments (Warpeha et al., 2008; 2009).

The data of Table 17.1, and Figs. 17.1 and 17.2, indicate that the impact of UV radiation comes in the first week which could translate to losses of yield in the field for certain varieties. For example, while experiencing mortality in germinating seeds, the Forrest variety did not have as great a sensitivity in growth as those seedlings that survived the first week (Fig. 17.2). Williams experienced both high mortality in the germinating stage and delay in growth in the seedling stage. In soybean, there seems to be a great sensitivity to UV radiation, even with brief treatments early in the plant's life cycle, compared to Arabidopsis (Warpeha et al., 2008; 2009). There are also varietal-specific sensitivities as well as a variation to different wavelengths of light, as shown in our data. Recent reports show that the specific pigment responses in leaves to UV can vary, dependent upon the genetic variety of the seedlings (Sullivan et al., 2007), and occurs for a number of characteristics in soybean varieties (Biggs et al., 1981; Teramura and Murali, 1986; Reed et al., 1992), and *Pinus* species (Sullivan and Teramura, 1988). We are unsure of the mechanism of these intraspecific differences. More research is required at the ultrastructural level to look at the early development in vulnerable, fast-growing cells of young seedlings (i.e., meristems).

The first set of leaves inside the cotyledons is the site of rapid cell division and chloroplast development in the 7 days post-germination. As the cotyledons separate after coming up through the soil, the developing first pair of leaves is exposed to incident UV. Since there were seedlings that survived the first week of post-irradiation, but died by 28 days post-irradiation, it was of interest to determine if the brief UV radiation treatments had an effect on the young leaves, not immediately apparent in the germination or growth (height) characteristics, particularly for the more sensitive variety, Williams. Three-day-old dark-grown seedlings were given a brief (10^4 μmol m^{-2}) treatment of a specific UV radiation, then returned to darkness for 5 more days. The young leaves were then harvested to examine the effects on leaf expansion for Williams (Fig. 17.3; Forrest did not vary; data not shown).

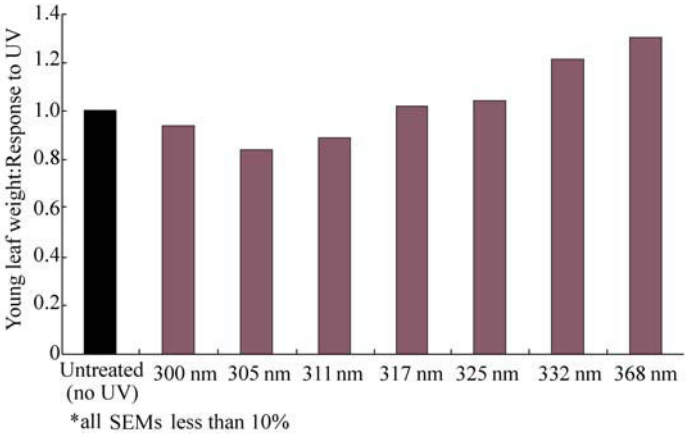

Figure 17.3 The response of soybean variety Williams to UV radiation treatment: a comparison of fresh weight accumulation. Seedlings were treated with the UV wavelength shown (Untreated = mock pulse) on Day 3 as described in Methods, returned to darkness, then harvested 5 days later to determine the effect of UV-B radiation on fresh weight accumulation. Each data point is the result of 3 independently grown replicates. The SEMs are less than 10% for all points

It is apparent from the data shown in Fig. 17.3 that UV-B wavelengths can prevent expansion of developing leaves in the first week post-irradiation. Conversely, UV-A wavelengths induce an increase in leaf expansion manifesting in increase in overall fresh weight compared to Untreated seedlings. The leaves are larger in appearance so it is not merely an increase in density and in soybean treated with UV-A wavelengths, but the plastid is more developed compared to Untreated seedlings (Warpeha et al., 2009). For wavelengths under 317 nm, the effect on live tissue is to prevent accumulation of structural materials and expansion. We know from experiments in Arabidopsis and soybean that cuticular function and expansion is adversely affected by UV-B wavelengths (Warpeha et al., 2008; 2009). Moreover, wavelengths below 317 nm cause aberrant changes to cell ultrastructure, including the structures of the developing plastid, the major site with more synthesis of phenylpropanoids (Warpeha et al., 2008; 2009).

17.2.2 Surviving Soybean: the Affect on Seed Production

The yield of soybean exposed to UV-B radiation can vary for different varieties but a mechanism for this effect has not been identified (Teramura and Murali, 1986). We examined the effects of early exposure of seedlings to UV-B on seed viability for both Williams and Forrest varieties.

On Day 3 after planting Williams and Forrest seed in darkness, different sets of germinating seeds were given a single dose of UV radiation (300 nm; 317 nm; 368 nm; total dose 10^4 μmol m^{-2}), or a mock irradiation (Untreated). The exposed

seedlings were then transferred to soil to grow outdoors in summer until seed set. Only Williams data for actual seed appearance is discussed herein as Forrest was unremarkable under these conditions (Fig. 17.4).

Figure 17.4 The response of soybean variety Williams to UV radiation treatment: a comparison of seed development. Seedlings were treated with the UV wavelength shown (Untreated = mock pulse) on Day 3, then grown until seed set. After natural ripening of seed pods, the pods were opened and the seeds were evaluated for appearance and level of development. The pod shown for Untreated is representative of pods and seeds of Untreated seedlings. The pods shown for 300 nm and 317 nm treatments are not the majority, occurring less than 10% of the time in the overall seed harvest. The seed that failed to develop to maturity (i.e., the aborted embryos shown for 300 nm and 317 nm treatments) were not used in the viability study

Mature pods were harvested and seeds were compared to the Control plants. Untreated seedlings produced uniform round seeds. Less than 1% of the seeds were deformed. Visible changes in appearance were observed for some seeds that were produced from seedlings treated with 300 nm or 317 nm (Fig. 17.4). The most common features observed in seed production by exposure to UV-B radiation were aborted embryos, or misshapen or arrested seed development. However, these effects were seen in only 10% or less of all seeds harvested from the experimental plants. Otherwise, seed morphology appeared normal and ripened at the same time as Untreated seeds.

Seeds harvested from plants producing seed, where some examples are shown in Fig. 17.4, were planted and assessed for viability and any abnormal growth characteristics in growth chamber studies under summer conditions. Seeds obtained from different varieties were planted similarly to those in the germination studies (see Sections 17.1 and 17.4), but were not treated on Day 3. The seeds were then transferred to 14:10 growth chambers and observed over a 10-day period (no additional treatments were given). From the data shown in Table 17.2, it is apparent that there is some negative effect on viability of the surviving mature seeds that were harvested from plants originally treated with 300 nm or 317 nm (on Day 3 of their growth cycle), even if they look normal. Only the viability of seed obtained from Williams seedlings treated with 300 nm was statistically different (paired Student *t* test; mean germination (79% vs. 100%) of paired sets; $p = 0.049$) from Untreated seed viability. If seedlings survive to yield seed, then the mature seed produced appears viable. There were no great losses in germination,

even though there was a reduction in viability for seedlings that originally experienced 300 nm or 317 nm treatments. The shoot apical meristem is most vulnerable in the first 7 days of growth (and we irradiate on Day 3); and indeed, plants are germinated containing all the meristems of the future tissues that will become the reproductive parts. We are currently investigating what layers of the meristems are most affected by UV and the scoreable differences of the changes induced.

Table 17.2 Viability of seed produced from plants treated with UV radiation on Day 3 (see Fig. 17.4). Seeds harvested from plants treated (Fig. 17.4) were planted in soil and assessed for germination under normal light (14 h light: 10 h dark), temperature (23˚C) and water conditions at 10 days after planting (normal germination is between Days 2 and 4)

Variety	300 nm	317 nm	368 nm	Untreated
Forrest	81%	88%	96%	100%
Williams	79%	84%	97%	100%

17.2.3 Assessment of Phenylpropanoids in Response to UV

The Williams variety of soybean was used for assessment of individual phenylpropanoids. On Day 7 after planting in darkness, separate growth trays were individually irradiated with 300 nm, 317 nm, 368 nm or Untreated. After irradiation, seedlings were returned to darkness until harvest of the primary leaf material 24 hours later. An analysis of materials produced in response to UV is shown in Table 17.3. All chemicals listed on the left were standardized with purified compounds in order to properly identify metabolites. Data indicate that 300 nm and 317 nm (both in UV-B region) seem to suppress the development of several groups of protective pigments (i.e., anthocyanins, synapic acid, flavanones) and unexpectedly 300 nm does not induce visible synthesis of quercetin. Both 300 nm and 317 nm treatments reduced the production of Phe itself; the amino acid that is the precursor to the phenylpropanoid pigments. This may be evidence that young germinating seeds and young seedlings cannot synthesize new pigments due to suppression of Phe production. For many higher plants, the most abundant screening compound for broad UV is the structure quercetin, identified as the main inducible pigment for UV-protection in many plant species (Sheahan and Rechnitz, 1993; reviewed in Rozema et al., 2002). It is likely to be very important in the very young seedling due to the reserves of quercetin compounds in the Arabidopsis seed (reviewed in Lepiniec et al., 2006). We may not observe changes in quercetin if there are sufficient seed reserves for our brief treatments in seedlings treated with 300 nm. Quercetin is not only an efficient absorber of UV-B, but also has strong antioxidant capabilities, likely to assist the seedling in times of stress (reviewed in Winkel-Shirley, 2002). In plants where it has been

examined, quercetin is the most efficient and prolific and abundant absorber of UV-B (Sheahan and Rechnitz, 1993; Rozema et al., 2002).

Table 17.3 Metabolome analysis of 8-day-old soybean etiolated seedling primary leaves treated with UV-B or UV-A radiation. Seedlings of Williams were grown for 7 days in complete darkness, treated with wavelengths shown (Untreated = mock pulse), then primary leaves harvested 24 h later to be ground in liquid nitrogen for metabolome analysis (see Methods). Malonyl dichloride is unchanged under different light/radiation regimes and is used herein as a negative control. + increase; **x** decrease; − no change compared to Untreated level. Untreated Plant Material = Value found in dark grown seedlings never exposed to UV, where the value is set to value 1.0

Metabolome compounds and substances	Dark	300 nm	317 nm	368 nm
Anthocyanins	1.0	x	−	+
p-coumaric Acid	1.0	−	+	+
3-Hydroxycinnamic Acid	1.0	+	+	+
Flavanone	1.0	x	−	−
Sinapic Acid	1.0	x	+	−
Quercetin	1.0	−	+	+
Malonyl Dichloride (control)	1.0	−	−	−
Phenylalanine	1.0	x	−	+

UV-B and UV-A wavelengths appear to induce or reduce the different phenylpropanoids possible in soybean (Table 17.3), which may indicate that UV-B and UV-A are using different signaling pathways to regulate pigment production. If there is significant damage to the developing plastids of the young plants, it is possible that appearance or disappearance of particular pigments occurs as an alarm response to deleterious effects of UV, like DNA alteration. Phe is directly responsible for making many pigments in dark-grown Arabidopsis, as evidenced by genetic and developmental studies (Warpeha et al., 2008). The same dependence on Phe may occur for soybean. However, currently under investigation, we do not know the exact quantity of pigments stored in soybean seed, nor do we have information on the exact Phe budget for the dormant seed as it converts to a germinating seed. Once these values are established, it will be easier to establish where and at what time soybean controls its pigment-synthesis and pigment-deployment responses.

17.3 Conclusions

Young seedlings are susceptible to UV radiation. If exposure is survived, there can be lasting effects that adversely affect seed germination, attenuate the growth seedlings, and even affect the “next generation” in terms of seed set and viability. Responses to UV-B can cause noticeable effects in different varieties of soybean.

The young developing leaves are particularly vulnerable to UV-B radiation. Pigment accumulation may be directly dependent upon Phe in response to various wavelengths.

17.4 Methods

17.4.1 Plant Materials and Accessions

Soybean (*Glycine max* L.) seed stocks of Williams and Forrest cultivated varieties were originally obtained from Bill Kenworthy at the University of Maryland. Seeds were propagated at the University of Illinois, Chicago (UIC) for long-term studies. Before growth protocols were utilized, seeds were surface sterilized for 30 min in 20% bleach and then rinsed with sterile water immediately prior to planting. Williams is primarily used for most experiments unless otherwise stated.

17.4.2 Plant Growth and Preparation of Tissue

Soybean of Williams and Forrest varieties were grown several ways, depending on the experiment. Studies where germinating seeds were treated with UV radiation (on Day 3), 30 seeds were planted (Day 0) on 0.8% agarose plates containing only 0.5 X Murashige and Skoog media as described in Lapik and Kaufman (2003). Soybean lie no deeper than 2 mm below the surface of agarose media.

Seedlings were grown in complete darkness for a various number of days, as described in the experiments (20 seeds planted, then utilized for 5 days after irradiation for fresh weight, ~100 seeds planted, grown for 7 days then irradiated for metabolome). Germinating seedlings were irradiated with a single pulse of 1,260 s or less (e.g., 1,260 s irradiation period for 300 nm; 1,080 s for 317 nm; 240 s for 368 nm) of low fluence UV (total fluence of 10^4 μmol m^{-2}; as measured by UV-A, UV-B monitor, (Warpeha and Kaufman, 1990; Warpeha et al., 1991; Warpeha et al., 2008)) or Untreated (no UV), on the third day after planting, or the seventh day after planting (the latter, metabolome studies only). Fluence levels used have been confirmed to be within reciprocity limits for BL/UV-A (Warpeha and Kaufman, 1990). Seedlings were placed back in the dark for times as indicated in experiments in the phytatrays.

Experiments for growth and viability were conducted on seedlings that were transplanted to soil on Day 3 and maintained in growth chambers (14:10) after which they were followed out for 28 days or 10 days, respectively (about 20 plants in each replicate). Plants assessed for yield were grown outdoors (20 − 30 plants) in soil from Day 3 until seed sets where pods were harvested and seed visually analyzed.

For fresh weight studies, the first set of developing leaves were harvested (Warpeha et al., 1991) from 20 seedlings. For metabolome studies, primary leaves were harvested from soybean grown in phytatrays and maintained in darkness aside from indicated irradiations (~20 plants per replicate).

17.4.3 Chemicals

All chemicals, including L-Phe and metabolome standards, unless otherwise noted, were obtained from Sigma (St. Louis, MO, USA).

17.4.4 UV Radiation Sources and Treatments

The USDA UV-B Monitoring and Research Program (UVMRP), Colorado State University, Fort Collins, CO, USA, has measured the actual UV exposure at the earth's surface for over a decade. This is an important tool for assessing the quantity and quality of radiation that plants are exposed to over time. It also enables a risk assessment of seedlings and older plants for injury development as well as assessing which plants are capable of developing sufficient defense mechanisms at different growth stages. The UV source (for wavelengths 300, 305, 311, 317, 325, 332 and 368 nm) was custom designed by William Durham of the UVMRP for specific UV-A and UV-B wavelengths (designated the Durham lamp) and assembled by the UVMRP, as originally described in Warpeha et al. (2008). Light is redirected by a mirror that reflects incident UV radiation, and allows the near infrared and infrared to pass out via a light-tight exhaust port so seedlings are not affected. Condensing lenses collect the reflected UV light and define the beam, which subsequently passes through one of seven narrow band filters of type Ultraviolet Multifilter Rotating Shadowband Radiometer (UVMFRSR). The narrow band-pass filters (Barr Associates, Westford, MA, USA) have a 2 nm FWHM at the following centered wavelengths: 300, 305, 311, 317, 325, 332 and 368 nm. The lengths of irradiation were selected to avoid reciprocity failure.

All treatments consisted of a total fluence (dose) of 10^4 μmol m^{-2} (Warpeha and Kaufman, 1990; Warpeha et al., 1991) as is normally used for photobiology studies. Our doses of UV do not exceed brief periods of direct sunlight at specific wavelengths estimated from measurements made at noon in June at the UVMRP Illinois site as discussed in Warpeha et al. (2008).

17.4.5 Metabolome Studies

Analysis of compounds was accomplished by high performance liquid chromatography (HPLC) and liquid chromatography—Mass Spectrometry (LC-MS)

and absorption spectra (anthocyanins; methods described in (Warpeha et al., 2006)). All HPLC and spectrophotometric methods and equipment are described in (Warpeha et al., 2006). Purified standards were obtained from Sigma and were dissolved according to manufacturer's recommendations. Standard profiles were obtained for picomolar to nanomolar quantities and the quantity of metabolite as listed in the Table 17.3 was determined in Untreated soybean primary leaves. That value was set to 1.00, whereby all subsequently analyzed samples of 300 nm, 317 nm, and 368 nm treatments where quantified and compared to the Untreated values. A simple up (+) or down (×) was used to indicate overall change as the quantities found in these very small tissues is difficult to numerically quantitate accurately on a per seedling basis. Each analysis consisted of at least 100 pairs of soybean leaves.

Acknowledgements

The authors wish to acknowledge the USDA UV-B Monitoring and Research Program, Colorado State University, Fort Collins, CO, and the scientists of the program, especially Jim Slusser, for support and assistance. The authors also wish to thank Bao-Shiang Lee and Lisanthi Jayathilaka for assistance with metabolome studies, Julia Adamiak, James Scios, Noranne Magee and John Pachego for greenhouse and field assistance, and Laurie Richards for tireless assistance with the manuscript.

References

Ajavon AN, Albritton DL, Megie G and Watson RT (2003) Scientific assessment of Ozone Depletion: 2002. Global Ozone and Monitoring Project—Report # 47. World Meteorological Organization, Geneva

Beerhues L, Robeneck H, and Wiermann R (1988) Chalcone synthesis from spinach (Spinacia aleracea L.) Ⅱ. Immunofluorescence and immunogold localization. Planta 173, 544－553

Bieza K and Lois R (2001) An Arabidopsis mutant tolerant to lethal ultraviolet-B levels shows constitutively elevated accumulation of flavonoids and other phenolics. Plant Physiology 126, 1105－1115

Biggs RH, Kossuth SV, and Teramura AH (1981) Response of 19 cultivars of soybeans to ultraviolet-B irradiance. Physiol. Plant. 53, 19－26

Bilger W, Hohnsen T and Schreiber U (2001) UV-excited chlorophyll fluorescence as a tool for the assessment of UV-protection by the epidermis of plants. Journal of Experimental Botany 52, 2007－2014

Bird SM, and Gray JE (2003) Signals from the cuticle affect epidermal cell differentiation. New Phytologist 157, 9－23

Blanding C, Simmons SJ, Casati P, Walbot V and Stapleton AE (2007) Coordinated regulation of maize genes during increasing exposure to ultraviolet radiation: identification of ultraviolet-responsive genes, functional processes and associated potential promoter motifs. Plant Biotechnology Journal 5, 677 – 695

Brown BA, Cloix C, Jiang GH, Kaiserli E, Herzyk P, Kliebenstein DJ, and Jenkins GI (2005) A UV-B-specific signaling component orchestrates plant UV protection. Proceedings of the National Academy of Science U.S.A. 102, 18225 – 18230

Brown BA and Jenkins GI (2008) UV-B signaling pathways with different fluence-rate response profiles are distinguished in mature Arabidopsis leaf tissue by requirement for UVR8, HY5, and HYH. Plant Physiology 146, 576 – 588

Burchard P, Bilger W and Weissenbock G (2000) Contribution of hydroxycinnamates and flavonoids to epidermal shielding of UV-A and UV-B radiation in developing rye primary leaves as assessed by ultraviolet-induced chlorophyll fluorescence measurements. Plant, Cell & Environment 23, 1373 – 1380

Caldwell MM, and Flint SD (1994) Stratospheric ozone reduction, solar UV-B radiation and terrestrial ecosystems. Climatic Change 28, 375 – 394

Caldwell M, Teramura AH, Tevini M, Bornman JF, Bjorn LO and Kulandevalu G (1995) Effects of increased solar ultraviolet radiation on terrestrial plants. AMBIO 24, 166 – 173

Caldwell MM, Ballare CL, Bornman JF, Flint SD, Bjorn LO, Teramura AH, Kulandaivelu G and Tevini M (2003) Terrestrial ecosystems, increased solar ultraviolet radiation and interactions with other climatic change factors. Photochemical and Photobiological Sciences 2, 29 – 38

Caldwell MM, Bornman JF, Ballare CL, Flint SD and Kulandaivelu G (2007) Terrestrial ecosystems, increased solar ultraviolet radiation, and interactions with other climate change factors. Photochemical and Photobiological Sciences 6, 252 – 266

Cartwright HN, Baucom C, Singh P, Smith KL and Stapleton AE (2001) Intraspecific comparisons reveal differences in the pattern of ultraviolet radiation responses in four maize (Zea mays L.) varieties. Journal of Photochemistry and Photobiology B: Biology 62, 88 – 96

Casati P and Walbot V (2005) Differential accumulation of maysin and rhamnosylisoorientin in leaves of high-altitude landraces of maize after UV-B exposure. Plant, Cell & Environment 28, 788 – 799

Chappell J, and Hahlbrock K (1984) Transcription of plant defense genes in response to UV light or fungal elicitor. Nature 311, 76 – 78

Chapple CCS, Shirley BW, Zook M, Hammerschmidt R and Somerville SC (1994) Secondary metabolism in Arabidopsis. In E M Meyerowitz and C R Somerville, eds, Arabidopsis, CSH laboratory Press, Plainview, New York, pp. 989 – 1030

Christie JM and Jenkins GI (1996) Distinct UV-B and UV-A/blue light signal transduction pathways induce chalcone synthase gene expression in Arabidopsis cells. Plant Cell 8, 1555 – 1567

Christie PJ, Alfenito MR and Walbot V (1994) Impact of low-temperature stress on general phenylpropanoid and anthocyanin pathways: Enhancement of transcript abundance and anthocyanin pigmentation in maize seedlings. Planta 194, 541 – 549

Cosio EG and McClure JW (1984) Kaempferol glycosides and enzymes of the flavonol biosynthesis in leaves of a soybean strain with low photosynthetic rates. Plant Physiology 74, 877 – 881

Davin LB and Lewis NG (1992) In HA Stafford and RK Ibrahim, eds Recent Advances in Phytochemistry, Plenum Press, New York 26, 325 – 375

Frohnmeyer H and Staiger D (2003) Ultraviolet-B radiation-mediated responses in plants. Balancing damage and protection. Plant Physiology 133, 1420 – 1428

Frohnmeyer H, Bowler C and Schafer E (1997) Evidence for some signal transduction elements involved in UV-light-dependent responses in parsley protoplasts. Journal of Experimental Botany 48, 739 – 750

Fuglevand G, Jackson JA and Jenkins GI (1996) UV-B, UV-A, and blue light signal transduction pathways interact synergistically to regulate chalcone synthase gene expression in Arabidopsis. Plant Cell 8, 2347 – 2357

Gilchrist DG and Kosuge T (1980) Aromatic amino acid biosynthesis and its regulation. In PK Stumpf, EE Conn, eds, The Biochemistry of Plants, Vol 5, B J Miflin, Academic Press, New York, pp 507 – 531

Gonzalez R, Paul ND, Percy K, Ambrose M, McLaughlin CK, Barnes JD, Areses M and Wellburn AR (1996) Responses to ultraviolet-B radiation (280 nm – 315 nm) of pea (Pisum sativum) lines differing in leaf surface wax. Physiologia Plantarum 98, 852 – 860

Grammatikopoulos G, Kyparissis A, Drilias P, Petropoulou Y and Manetas Y (1998) Effects of UV-B radiation on cuticle thickness and nutritional value of leaves in two mediterranean evergreen sclerophylls. Journal of Plant Physiology 153, 506 – 512

Gritz DC, Liu-Gritz L, Britz SJ, and Sullivan JH (2005) Ultraviolet B effects on stomatal density, water use efficiency and stable carbon isotope discrimination in four glasshouse-grown soybean (Glycine max) cultivars. Environ. Exp. Bot. 53, 343 – 355

Hahlbrock K and Scheel D (1989) Physiology and molecular biology of phenylpropanoid metabolism. Annual Review of Plant Physiology and Plant Molecular Biology 40, 347 – 369

Jansen MAK, Gaba V and Greenberg BM (1998) Higher plants and UV radiation: balancing damage repair and acclimation. Trends in Plant Sciences 3, 131 – 135

Jenkins GI and Brown BA (2007) UV-B perception and signal transduction. In Light and Plant Development, G.C. Whitelam and K.J. Halliday, eds (Oxford, UK: Blackwell Publishing), pp. 155 – 182

Kaiserli E and Jenkins GI (2007) UV-B promotes rapid nuclear translocation of the Arabidopsis UV-B-specific signaling component UVR8 and activates its function in the nucleus. Plant Cell 19, 2662 – 2673

Kim KS, Park SH, Kim DK and Jenks MA (2007) Influence of water deficit on leaf cuticular waxes of soybean (Glycine max [L.] Merr.) International Journal of Plant Science 168, 307 – 316

Kliebenstein DJ (2004) Secondary metabolites and plant/environment interactions: a view through Arabidopsis thaliana tinged glasses. Plant, Cell Environment 27, 675 – 684

Koti S, Reddy KR, Reddy VR, Kakani VG and Zhao DL (2005) Interactive effects of carbon dioxide, temperature, and ultraviolet-B radiation on soybean (Glycine max L.) flower and pollen morphology, pollen production, germination, and tube lengths. Journal of Experimental Botany 56, 725 – 736

Koti S, Reddy KR, Kakani VG, Zhao VG and Gao W (2007) Effects of carbon dioxide, temperature and ultraviolet-B radiation and their interactions on soybean (Glycine max L.) growth development. Environmental and Experimental Botany 60, 1 – 10

Landry LG, Chapple CCS and Last RL (1995) Arabidopsis mutants lacking phenolic sunscreens exhibit enhanced Ultraviolet-B injury and oxidative damage. Plant Physiology 109, 1159 – 1166

Lapik Y and Kaufman LS (2003) The Arabidopsis cupin domain protein AtPirin1 and AtGPA1, the Arabidopsis G subunit interact with each other and regulate seed germination and early seedling development. Plant Cell, 15, 1578 – 1590

Lepiniec L, Debeaujon I, Routaboul JM, Baudry A, Pourcel L, Nesi N and Caboche M (2006) Genetics and biochemistry of seed flavonoids. Annual Review of Plant Biology 57, 405 – 430

Lewis NG and Yamamoto E (1989) In RW Hemingway, JJ Karchesy, eds, Chemistry and significance of condensed tannins. Plenum Press, New York, pp 23 – 47

Leyva A, Jarillo JA, Salinas J and Martinez-Zapater JM (1995) Low temperature induces the accumulation of phenylalanine ammonia lyase and chalcone synthase mRNAs of Arabidopsis thaliana in a light dependent manner. Plant Physiology 108, 39 – 46

Li J, Ou-Lee I-M, Raba R, Amundson RG and Last RL (1993) Arabidopsis flavonoid mutants are hypersensitive to UV-B irradiation. Plant Cell 5, 171 – 179

Li Y, Zu YQ, Chen HY and Chen JJ (2003) Intraspecific differences in physiological response of 20 soybean cultivars to enhanced ultraviolet-B radiation under field conditions. Environmental and Experimental Botany 50, 87 – 97

Liu L and McClure JW (1995) Effects of UV-B on activities of enzymes of secondary phenolic metabolism in barley primary leaves. Physiologia Plantarum 93, 734 – 739

Liu L, Gitz DC and McClure JW (1995) Effects of UV-B on flavonoids, ferulic acid, growth and photosynthesis in barley primary leaves. Physiologia Plantarum 93, 725 – 733

Long LM, Patel HP, Cory WC and Stapleton AE (2003) The maize epicuticular wax layer provides UV protection. Functional Plant Biology 30, 75 – 81

Mahmoodzadeh H (2007) Effect of salinity stress on structural and ultrastructural features of apical meristems of two cultivars of canola (Brassica napus L.c.v.). Comparative biochemistry and Physiology A 146, S261 – S262

Margna U (1977) Control at the level of substrate supply — An alternative in the regulation of phenylpropanoid accumulation in plant cells. Phytochemistry 16, 419 – 426

Margna U, VainJarv T and Laanest L (1989) Different L-Phenylalanine pools available for the biosynthesis of phenolics in buckwheat seedling tissues. Phytochemistry 28, 469 – 475

Mazza CA, Boccalandro HE, Giordano CV, Battista D, Scopel AL and Ballare CL (2000) Functional significance and induction by solar radiation of ultraviolet-absorbing sunscreens in field-grown soybean crops. Plant Physiology 122, 117 – 125

Middleton EM, Kim MS, Krizek DT, and Bajwa RKS (2005) Symposium-in-Print: Ultraviolet Radiation and Terrestrial Ecosystems Evaluating UV-B Effects and EDU Protection in Soybean Leaves. Photochem. Photobiol. 81, 1075 – 1085

Nawrath C (2006) Unraveling the complex network of cuticular structure and function. Current Opinion Plant Biology 9, 281 – 287

Ohl S, Hahlbrock K and Schafer E (1989) A stable blue-light-derived signal modulates ultraviolet-light-induced activation of the chalcone-synthase gene in cultured parsley cells. Planta 177, 228 – 236

Oravecz A, Baumann A, Mate Z, Brzezinska A, Molinier J, Oakeley EJ, Adam E, Schafer E, Nagy F and Ulm R (2006) Constitutively Photomorphogenic1 is required for the UV-B response in Arabidopsis. Plant Cell 18, 1975 – 1990

Reed HE, Teramura AH, and Kenworthy WJ (1992) Ancestral U.S. soybean cultivars characterized for tolerance to ultraviolet-B radiation. Crop Science 32, 1214 – 1219

Reuber S, Bornman JF and Weissenböck G (1996) Phenylpropanoid compounds in primary leaf tissues of rye (Secale cereale): light response of their metabolism and the possible role in UV-B protection. Physiologia Plantarum 97, 160 – 168

Ries G, Heller W, Puchta H, Sandermann H, Seidlitz HK and Hohn B (2000) Elevated UV-B radiation reduces genome stability in plants. Nature 406, 98 – 1010

Robberecht R and Caldwell MM (1978) Leaf epidermal transmittance of ultraviolet radiation and its implications for plant sensitivity to ultraviolet radiation. Photochemistry and Photobiology 41, 95 – 99

Rozema J, vandeStaaij J, Bjorn LO and Caldwell M (1997) UV-B as an environmental factor in plant life: Stress and regulation. Trends in Ecology & Evolution 12, 22 – 28

Rozema J, Bjorn LO, Bornman JF, Gaberscik A, Hader D-P, Trost T, Germ M, Klisch M, Groniger A, Sinha RP, Lebert M, He Y-Y, Buffoni-Hall R, de Bakker NVJ, van de Stajj J and Meijkamp BB (2002) The role of UV-B radiation in aquatic and terrestrial ecosystems — an experimental and functional analysis of the evolution of UV-absorbing compounds. J. Photochem. Photobiol. B: Biology 66, 2 – 12

Rozema J, Boelen P and Blokker P (2005) Depletion of stratospheric ozone over the Antarctic and Arctic: Responses of plants of polar terrestrial ecosystems to enhanced UV-B. Environmental Pollution 137, 428 – 442

Sato T, Kang HS and Kumagai T (1994) Genetic study of resistance to inhibitory effects of UV-radiation in Rice (Oryza sativa). Physiologia Plantarum 91, 234 – 238

Sacks MM, Silk WK, and Burman P (1997) Effect of water stress on cortical cell division rates within the apical meristem of primary roots of maize. Plant Physiol. 114, 519 – 527

Sheahan JJ and Rechnitz GA (1993) Differential visualization of transparent testa mutants in Arabidopsis thaliana. Analytical Chemistry 65, 961 – 963

Sieber P, Schorderet M, Ryser U, Buchala A, Kolattukudy P, Metraux JP, and Nawrath C (2000) Transgenic Arabidopsis plants expressing a fungal cutinase show alterations in the structure and properties of the cuticle and postgenital organ fusions. Plant Cell 12, 721 – 737

Stapleton AE and Walbot V (1994) Flavonoids can protect maize DNA from induction of ultraviolet radiation damage. Plant Physiology 105, 881 – 889

Stapleton AE, Thornber CS and Walbot V (1997) UV-B component of sunlight causes measurable damage in field-grown maize (Zea mays L): Developmental and cellular heterogeneity of damage and repair. Plant, Cell & Environment 20, 279 – 290

Strid A, Chow WS and Anderson JM (1994) UV-B damage and protection at the molecular level in plants. Photosynthesis Research 39, 475 – 489

Sullivan JH (2005) Possible impacts of changes in UV-B radiation on North American trees and forests. Environmental Pollution 137, 380 – 389

Sullivan JH and Rozema J (1999) UV-B effects on terrestrial plant growth and photosynthesis. In, Stratospheric ozone depletion: the effects of enhanced UV-B radiation on terrestrial ecosystems (edited by J. Rozema), pp. 39 – 57. Backhays Publishers, Leiden, The Netherlands.

Sullivan JH and Teramura AH (1988) The effects of ultraviolet-B irradiation on seedling growth in the Pinaceae. American Journal of Botany 75, 225 – 230

Sullivan JH, Gitz DC, Peek MS, and McElrone AJ (2003) Response of three eastern tree species to supplemental UV-B radiation: leaf chemistry and gas exchange. Agricultural and Forest Meteorology. 120, 219 – 228

Sullivan JH, Gitz DC Ⅲ, Liu-Gitz L, Xu C, Gao W and Slusser J (2007) Coupling short-term changes in ambient UV-B levels with induction of UV-screening compounds. Photochemistry and Photobiology 83, 863 – 870

Tattini M, Gravano E, Pinelli P, Mulinacci N and Romani A (2000) Flavonoids accumulate in leaves and glandular trichomes of Phillyrea latifolia exposed to excess solar radiation. New Phytologist 148, 69 – 77

Teramura AH and Murali NS (1986) Intraspecific differences in growth and yield of soybean exposed to ultraviolet-B radiation under greenhouse and field conditions. Environ. and Experi. Botany. 26, 89 – 95

Teramura AH and Sullivan JH (1987) Soybean growth response to enhanced levels of ultraviolet-B radiation. American Journal of Botany 74, 975 – 979

Teramura AH, and Sullivan JH (1991) Potential effects of increased solar UV-B on global plant productivity. In: Riklis E (Ed.), Photobiology, Plenum Press, New York, pp 625 – 634

Teramura AH, Sullivan JH, and Lydon J (1990) Effects of solar UV-B radiation on Soybean yield and seed quality: a six-year field study. Physiologia Plantarum. 80, 5 – 11

Torabinejad J and Caldwell MM (2000) Inheritance of UV-B tolerance in seven ecotypes of Arabidopsis thaliana L. Heynh. and their F1 hybrids. Heredity 91, 228 – 233

Ulm R and Nagy F (2005) Signaling and gene regulation in response to ultraviolet light. Current Opinion in Plant Biology 8, 477 – 482

van Heerden PS, Neil Towers GH, and Lewis NG (1996) Nitrogen Metabolism in Lignifying Pinus taeda Cell Cultures. Journal of Biological Chemistry 271, 12350 – 12355

Wade HK, Bibikova TN, Valentine WJ and Jenkins GI (2001) Interactions within a network of phytochrome, cryptochrome, and UV-B phototransduction pathways regulate chalcone synthase gene expression in Arabidopsis leaf tissue. Plant Journal 25, 675 – 685

Warpeha KMF, and Kaufman LS (1990) Two distinct blue-light responses regulate the levels of transcripts of specific nuclear-coded genes in pea. Planta 182, 553 – 558

Warpeha KMF, Hamm HE, Rasenick MM, and Kaufman LS (1991) A blue-light activated GTP binding protein in the plasma membrane of etiolated pea. Proc. Natl. Acad. Sci. U.S.A. 88, 8925 – 8929

Warpeha KM, Lateef SS, Lapik Y, Anderson MB, Lee BS and Kaufman LS (2006) G-Protein-Coupled Receptor1, G-Protein G-Subunit1, and Prephenate Dehydratase1 Are Required for Blue Light-Induced Production of Phenylalanine in Etiolated Arabidopsis. Plant Physiology 140, 844 – 855

Warpeha KM, Gibbons J, Carol A, Slusser J, Tree R, Durham W, and Kaufman LS (2008) Presence of adequate phenylalanine mediated by G-protein is Critical for Protection from UV Radiation Damage in young etiolated Arabidopsis thaliana seedlings. Plant Cell and Env.

Warpeha KM, Sullivan JH, and Kaufman LS (2009) Phenylalanine provides critical protection from UV Radiation Damage in young soybean (*Glycine max*) seedlings. *Submitted*

Weinig C, Gravuer KA, Kane NC and Schmitt J (2004) Testing adaptive plasticity to UV: Costs and benefits of stem elongation and light-induced phenolics. Evolution 58, 2645 − 2656

West G, Inze D, and Beemster GTS (2004) Cell cycle modulation in the response of the primary root of Arabidopsis to salt stress. Plant Physiology 135, 1050 – 1058

Winkel-Shirley B (2002) Biosynthesis of flavonoids and effects of stress, Current Opinion in Plant Biology 5, 218 − 223

Yamada T, Matsuda F, Kasai K, Fukuoka S, Kitamura K, Tozawa Y, Miyagawa H and Wakasa K (2008) Mutation of a rice gene encoding a phenylalanine biosynthetic enzyme results in accumulation of phenylalanine and tryptophan. Plant Cell 20, 1316 − 1329

18 Characteristics of UV-B Radiation Tolerance in Broadleaf Trees in Southern USA

Yadong Qi[1], Gordon M. Heisler[2], Wei Gao[3], Thomas C. Vogelmann[4], and Shuju Bai[5]

[1] Urban Forestry Program, P.O. Box 11288, Southern University
Baton Rouge, LA 70813, USA
E-mail: yadong_qi@subr.edu
[2] USDA Forest Service Northeastern Research Station, c/o SUNY ESF,
5 Moon Library, Syracuse, NY 13210, USA
E-mail: gheisler@fs.fed.us
[3] USDA UV-B Radiation Monitoring Program, and Senior Research Scientist,
Natural Resource Ecology Laboratory, Colorado State University
Fort Collins, CO 80523-1499, USA
E-mail: wgao@uvb.nrel.colostate.edu
[4] Botany Department, University of Vermont, Burlington, VT 05405, USA
E-mail: Thomas.Vogelmann@uvm.edu
[5] Department of Computer Science, Southern University
Baton Rouge, LA 70813, USA
E-mail: bais@cmps.subr.edu

Abstract Research has indicated that the ozone layer in the earth's stratosphere has decreased significantly in the last two decades. Such a reduction has led to an increase in solar ultraviolet-B (UV-B) radiation (280 nm − 315 nm) striking the earth's surface. Nearly two-thirds of the 400 plant species and cultivars tested to date appear to be UV-B sensitive, one-third of which show certain tolerant characteristics. However, the majority of plants evaluated thus far have been annual agricultural species. Very few studies have been conducted on tree species which account for more than 80% of the global net primary production. Scientists from Southern University, the USDA Forest Service Northeastern Research Station, the USDA UV-B Monitoring and Research Program, and the University of Vermont, have recently completed a five-year program of collaborative research to assess UV-B (280 nm − 315 nm) radiation tolerance characteristics of more than 30 common broadleaf tree species in the southern US. The project has established a database of leaf optical properties, depth of UV-B penetration into leaves, concentration of UV-B absorbing compounds, and leaf anatomy. The study concluded that on a whole leaf basis, the tree leaves absorb 91% − 95%,

reflect 5%－9%, and transmit very little (＜1%) incident UV-B radiation. At the tissue level, the upper leaf epidermis appears to be the main site absorbing the most UV-B radiation. The study has identified 23 broadleaf tree species that possess strong epidermal UV-B screening functions and attenuate 92%－99% of the UV-B through their epidermal layers. These species include Arizona ash, chestnut oak, mocker nut hickory, pecan, American sycamore, bitternut hickory, green ash, sawtooth oak, American elm, blue Japanese oak, cherrybark oak, cottonwood, southern live oak, southern magnolia, shumard oak, sweetgum, American beech, white oak, Chinese tallow, water oak, yellow poplar, Bradford pear, and red maple. The epidermal attenuation is shown to be the dominant UV-B screening characteristic in most of the species studied. Thus, the effectiveness of the epidermal function of UV-B screening underlines the important aspect of the UV-B protection mechanism in the broadleaf trees. Within the species, there are cumulative increases in leaf thickness, leaf total concentration of UV-B absorbing compounds, and leaf chlorophyll content with an increase in UV-B radiation during the period of leaf growth and development (from April to August). The increased concentration in leaf UV-B absorbing compounds may help protect plants against the enhanced UV-B level during the growing season. Comparisons among the species, however, showed that large inter-specific variations exist in the leaf total UV-B absorbing compound concentration, leaf epidermal thickness, leaf total thickness, and depth of UV-B penetration, indicating the individualistic nature of the species. The knowledge of UV-B absorbing compounds and their strategic locations within leaf tissues may increase our current understanding of UV-B tolerance characteristics. Further research is necessary to identify and localize these compounds in leaf tissues. Such information may help us define the biochemical aspects of UV-B protection in broadleaf trees.

Keywords Leaf optical property, UV-B penetration, concentration of total UV-B absorbing compounds, UV-B tolerance, broadleaf tree species

18.1 Introduction

Decreased quantities of total-column ozone have been observed over large parts of the globe, permitting an increased penetration of solar ultraviolet-B (UV-B, 280 nm－315 nm) to the earth's surface (UNEP, 1998). The first reports of potential stratospheric ozone reduction were made more than 30 years ago (Johnston, 1971; Crutzen, 1972). The UV-B radiation on the earth's surface has increased by 6%－14% since the early 1980s (UNEP, 2002). More than 600 papers have been published with much attention directed on the effects of UV-B radiation on higher plants (Caldwell et al., 1998). Studies of the effects of increased solar UV-B at the ecosystem level (Caldwell et al., 1998) have only been undertaken in the past

10 years. Approximately 400 species of plants and cultivars have been screened for sensitivity to UV-B radiation, and of these, about two-thirds were found to be sensitive in some parameter (Sullivan and Rozema, 1999; Sullivan et al., 2003). The balance between damage and protection varies among species, even within varieties of crop species. Many species and varieties can accommodate increased UV-B. Tolerance of elevated UV-B by some species and crop varieties provides opportunities for genetic engineering and breeding to deal with potential crop yield reductions due to elevated UV-B in agricultural systems (UNEP, 1998).

Research indicates that increased UV-B exerts effects more often through altered patterns of gene activity than through damage. These UV-B effects on regulation manifest themselves in many ways, including changes in plant form and production of plant chemicals not directly involved in primary metabolism (UNEP, 1998). Much evidence suggests that plants have evolved two major strategies for resistance to UV-B radiation that involve repair and avoidance mechanisms. The former includes repair of DNA damages by excision repair or by repair of pyrimidine-dimers as photolyase, activated by UV-A and photosynthetically active radiation (PAR) (Taylor et al., 1997). The latter primarily includes epidermal screening of UV-B radiation to protect the mesophyll tissue of a leaf by the accumulation of UV-absorbing compounds in cell vacuoles and/or cell walls of the epidermis (Caldwell et al., 1983; Hutzler et al., 1998). Research has shown that flavonoids and related phenolics play an important role in plant defense against the UV-B radiation (Caldwell et al., 1983; Tevini et al., 1991; Day et al., 1992; Day, 1993; Li et al., 1993; Beggs and Wellmann, 1994; Day et al., 1994; Karabourniotis and Fasseas, 1996; Reuber et al., 1996; Bornman et al., 1997; Hutzler et al., 1998; Karabourniotis et al., 1998; Laakso et al., 2000; Sullivan et al., 2005).

Structural and biochemical changes induced by enhanced levels of UV-B radiation ultimately modify the penetration of UV radiation into plants. In order for UV radiation to be effective in plants, it must effectively penetrate into the tissues and be absorbed. The ability to predict the consequences of enhanced ambient UV-B levels on plants depends in part on our understanding of how much of this radiation reaches the chromophores within the mesophyll (Day, 1993). Ultraviolet penetration varies with plant species. Penetration of UV-B was found to be the greatest in herbaceous dicotyledons (broad-leafed plants) and was progressively less in woody dicotyledons, grasses and conifers (Day et al., 1992). The UV penetration also changes with leaf age; younger leaves attenuate UV-B radiation less than do the more mature leaves in some conifers (DeLucia et al., 1991; DeLucia et al., 1992).

Although some 400 plant species and cultivars have been studied, the vast majority tested have been herbaceous, annual agricultural species grown in laboratory or glasshouse conditions. Fewer than 5% of the studies have been conducted under field conditions. Relatively little information exists on the effects of UV-B radiation on forest tree species (Caldwell et al., 1998), which account for more than 80% of global net primary production (Whittaker, 1975; Barnes et

al., 1998). Tropical forests have received very little attention with respect to the ozone reduction problem (Searles et al., 1995; Caldwell et al., 1998) even though they represent nearly one half of global productivity and much of the total tree species diversity. Our knowledge is far from complete in regard to the effects of enhanced UV-B on trees and forest communities in various landscapes. The diverse range of UV-B radiation responses observed within annual plant species suggests that direct extrapolations from these species to long-lived woody plants many not be feasible. Therefore, it would be useful to know the differences in UV-B screening effectiveness in various tree species and to determine what general leaf properties are responsible for these differences. This paper is a result of a USDA-funded collaborative research project involving the scientists from Southern University, the USDA-FS Northeast Research Station, the USDA UV-B Monitoring and Research Program (UVMRP), and the University of Vermont. The research was the first in the southern US that focused on assessing UV-B radiation tolerance characteristics in diverse southern broadleaf tree species (Table 18.1, column 1). The specific objectives were to: (1) measure leaf reflectance, transmittance, and absorption of UV (280 nm − 400 nm) and visible (400 nm − 760 nm) radiation spectrums on a whole-leaf basis, (2) measure the light distribution and depth of UV-B light penetration (310 nm) into the leaves, (3) investigate leaf surface morphology and leaf anatomy, and (4) measure the total concentration of UV-B-absorbing compounds in the leaves throughout the growing season.

Table 18.1 Leaf reflectance (R_λ), transmittance (T_λ), and absorbance ($A_{\lambda)}$ to 300 nm UV-B radiation on a whole leaf basis, measured from the mature leaves of 35 southern tree species, grown in Baton Rouge, Louisiana, USA

Scientific name-common name	Whole leaf reflectance to 300nm (%) $R_{\lambda=300nm}$	Whole leaf transmittance to 300nm (%) $T_{\lambda=300nm}$	Whole leaf absorbance to 300nm (%) $A_{\lambda=300nm}$
Broadleaf evergreen trees			
Magnolia grandiflora - Southern magnolia	6.051	0.079	93.870
Magnolia virginiana - Sweet bay magnolia	6.004	0.003	93.993
Quercus glauca - Blue Japanese evergreen oak	6.756	0.005	93.239
Quercus virginiana - Southern live oak	8.475	0.000	91.525
Deciduous trees			
Acer rubrum - Red maple	6.017	0.003	93.979
Betula nigra - River birch	6.866	0.004	93.130
Carya cordiformis - Bitternut hickory	6.044	0.001	93.957
Carya illinoinensis - Pecan	8.576	0.010	91.415
Carya tomentosa - Mockernut hickory	6.223	0.002	93.775
Castanea dentata - American chestnut	7.852	0.000	92.148
Celis laevigata - Sugar hackberry	5.388	0.005	94.607

(Continued)

Scientific name-common name	Whole leaf reflectance to 300nm (%) $R_{\lambda=300nm}$	Whole leaf transmittance to 300nm (%) $T_{\lambda=300nm}$	Whole leaf absorbance to 300nm (%) $A_{\lambda=300nm}$
Cercis canadensis - Red bud	4.766	0.000	95.234
Cornus florida - Dogwood	8.610	0.048	91.342
Fagus grandifolia - American beech	6.970	0.003	93.027
Fraxinus pennsylvanica - Green ash	5.467	0.003	94.530
Fraxinus velutina - Arizona ash	6.570	0.003	93.427
Liquidamber styraciflua – Sweetgum	7.464	0.001	92.536
Liriodendron tulipifera - Yellow poplar	4.807	0.002	95.191
Morus rubra - Red mulberry	7.440	0.023	92.537
Platanus occidentails – Sycamore	6.824	0.012	93.164
Populus deltoides - Cottonwood	7.337	0.001	92.662
Pyrus calletyana "Bradford" - Bradford pear	6.088	0.002	93.910
Quercus acutissima - Sawtooth oak	6.634	0.167	93.199
Quercus alba - White oak	7.073	0.005	92.922
Quercus michauxii - Swamp chestnut oak	5.637	0.004	94.359
Quercus nigra - Water oak	7.186	0.001	92.813
Quercus palustris - Pin oak	5.843	0.005	94.152
Quercus phellos - Willow oak	5.503	0.008	94.490
Quercus shumardii- Shumard oak	8.144	0.005	91.851
Quercus stellata - Post oak	6.922	0.001	93.077
Quercus falcata - Southern red oak	5.974	0.004	94.022
Quercus falcata var. pagodifolia - Cherrybark oak	5.700	0.008	94.291
Sapium sebufrum - Chinese tallow	5.998	0.002	94.000
Ulmus americans - American elm	5.758	0.002	94.240
Ulmus parvifolia - Chinese elm	6.387	0.004	93.608
Mean	6.553	0.012	93.435
Max	8.610	0.167	95.234
Min	4.766	0.000	91.342
SD	1.005	0.031	1.008

The project has established a database of leaf optical properties (reflectance, transmittance, and absorbance to UV-B, UV-A, and visible light), leaf UV-B absorbing compound profiles, depth of UV-B penetration into leaves, and leaf anatomical characteristics. It is expected that through the comparative analyses of these properties across the species, we may have a better understanding of the biophysical and biochemical aspects of UV-B tolerance characteristics in diverse broadleaf trees in the South.

18.2 Methodology

18.2.1 Plant Materials

Leaves of the selected southern broadleaf tree species (Table 18.1, column 1) were collected from individual trees growing in Baton Rouge, Louisiana, USA, during two growing seasons from April to October in 2000 and in 2001. Leaf samples were collected each month from the sun portions of four unshaded individuals per species at the terminal 20 cm – 50 cm of a branch or stem, and were placed in humidified plastic bags in an insulated box for transporting to the laboratory. The experiment was a randomized complete block design with seven blocks arranged across time in a growing season. Each month was a block in which three trees per species were randomly selected for sampling. Species order was randomized. All species within a block were sampled in the shortest time possible during the first week of the month to minimize the environmental variation within the block. Samples were taken at approximately the same time each day between 8:00 a.m. – 10:00 a.m. Analyses were finished within the six hours of the sample collection. A total of 980 samples (35 species×4 samples/species/month×7 months) were collected in the field during the 2000 growing season to monitor the leaf optical properties, leaf UV-B absorbing compounds and chlorophyll concentration, and leaf thickness. The light penetration and spectral distribution within leaves and the anatomical research were conducted during the 2001 growing season.

18.2.2 Measuring Leaf Optical Properties

Leaf reflectance and transmittance were measured with an integrating sphere (Optronic IS-1000) following the procedures by Optronic Laboratories, Inc. (1997). The integrating sphere, powered by a constant power-output supply (OL 65 Programmable Current Source, Optronic, FL), was used in combination with an irradiance standard (Optronic OL Series 752-10) and a high accuracy UV/Visible spectroradiometer (OL 754) connected to a computer. Spectral scanning was performed from 250 nm – 800 nm at 5 nm intervals to produce a spectral distribution of the reflectance and transmittance on a whole-leaf basis for each species. Leaf adaxial/upper side was illuminated using a 200-W tungsten coiled-coil filament lamp with a 1.3 cm×7 cm quartz envelope. The spectral irradiance values were provided within the wavelength ranging from 250 nm to 800 nm and were based on the National Institute of Standard and Technology (NIST) 1973 scale of spectral irradiance (Saunders and Shumaker, 1977). Measurements of both spectral transmittance and reflectance were based on the procedure of direct substitution

(Optronic Laboratory, 1997). The spectral absorbance, A_λ, of a leaf sample, was computed from the knowledge of its spectral transmittance, T_λ, and spectral reflectance, R_λ, as follows:

$$A_\lambda = 1 - T_\lambda - R_\lambda$$

18.2.3 Measuring the Light Penetration and Distribution within Leaf Tissues

The depth of light penetration into leaves and spectral distribution within leaf tissues were measured using a fiber optic microprobe system (Fig. 18.1) (Qi et al., 2003a), which was modified based on Vogelmann and Bjorn (1984) and Vogelmann et al. (1991). The microprobes were fabricated in Dr. T. C. Vogelmann's lab, using 150 μm diameter (OD) multimode step-index fibers made of fused silica (Polymicro Technologies, Phoenix, AZ, USA). The fibers were heated and drawn to a tip diameter of around 10 μm. The tapered regions of the probes were then coated with evaporated chromium and truncated with a diamond knife. Thus, light entry was confined to the tip of the probes that had near-perfect Gaussian acceptance angles (50% acceptance half width) of 27° to 34°. To operate the microprobe, the tip was threaded through a needle eye and firmly glued onto it (Fig. 18.2(a)); the other end of the probe was connected to a spectroradiometer (Model 754, Optronic Laboratory, Florida, USA) (Fig. 18.2(b)). The needle carrying the probe tip was firmly mounted to a Stepper Mike (Model 18515, Oriel, Stratford, CT, USA) on an XYZ translator (Fig. 18.2(c)). The leaf sample was mounted between two aligned Plexiglas slides perforated with a 5 mm diameter opening in the center of both slides to allow the light to illuminate and the fiber to penetrate. The leaf sample was placed between the slides, with the abaxial side facing the fiber probe and the adaxial side facing the radiation beam from a 75-W Xenon-arc lamp (Hanovia 901C-1), which generated 4 $W/m^2/nm$ UV-B flux at 310 nm, or 0.23 W/m^2 erythemal UV-B at the leaf surface level. This amount of UV-B was comparable to the ambient level of the UV-B in Baton Rouge, LA, USA, measured by the USDA UVMRP. The erythemal UV-B radiation at the Baton Rouge Station peaked in June at 0.3 W/m^2 UV-B with the maximum daily sum of 8.2 kJ/m^2.

The measurements of light penetration were made at zero orientation at which the largest portion of light flux moves through the leaf. Photons captured by the microprobe were measured with the calibrated spectroradiometer. The light penetration was measured at four wavelengths including UV-B at 310 nm, UV-A at 360 nm, blue at 430 nm, and red at 680 nm. The spectroradiometer was preset for the wavelength selected before each measurement. The microprobe was auto-advanced at 4 μm/s through a vein-free region from the abaxial side toward the irradiated surface. Light transmitted to the probe was calculated as the relative amount of light, expressed as the ratio of light measured by the probe inside the

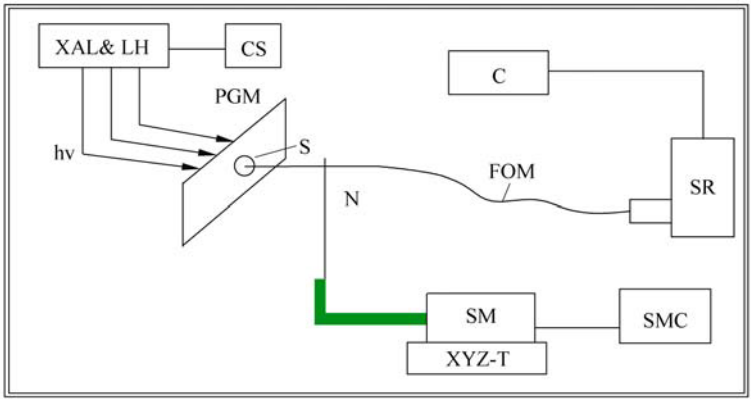

Figure 18.1 Diagram of the fiber optical microprobe system for measurement of light penetration, modified based on Vogelmann and Bjorn (1984). C = Computer, FOM = Fiber Optic Microprobe, S = Leaf Sample, N = Needle, SR = Spectroradiometer, SM = Stepper Motor, XYZ-T = XYZ Translator, SMC = Stepping Motor Controller, PGM = Plexiglas Mount, XAL&LH = Xenon-arc Lamp and Lamp House, CS = Current Source, hv = high voltage (Qi et al., 2003a)

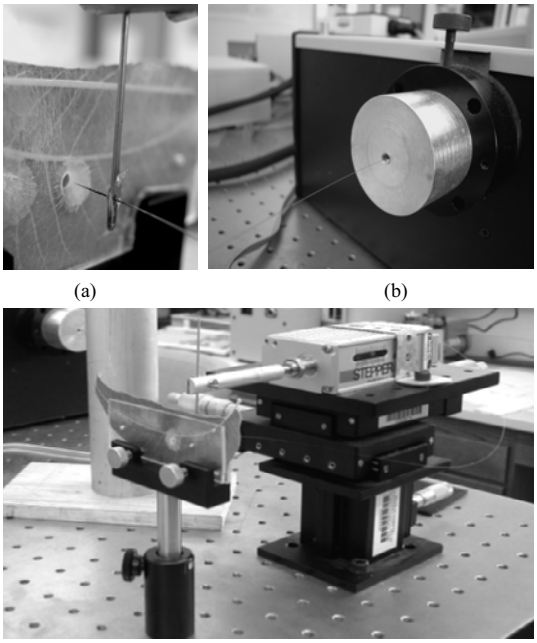

Figure 18.2 The fiber optic microprobe tip is threaded through the eye of a needle and firmly glued on to it (a), and the other end of the microprobe is connected to the OL754 Spectroradiometer (b). A leaf sample is mounted between two aligned Plexiglas slides perforated with a 5mm diameter opening in the center of each slide to allow the light to illuminate from the leaf adaxial surface and the microprobe to penetrate from the leaf abaxial surface (c)

tissue to light measured by the probe without the tissue (probe normal to incident light, the control). Fifteen mature leaves per species were measured for each of the four wavelengths selected.

18.2.4 Scanning Electron Microscopy and Light Microscopy of Leaves

Mature leaves were dissected, fixed in FAA (ethanol, glacial acetic acid, and formaldehyde), dehydrated in ethanol series, and dried in carbon dioxide using a Denton DCP-1 critical point drying apparatus. Leaves were mounted on stubs, coated with 25 nm gold palladium using a Hummer Ⅱ Sputter Coater, and examined using a Cambridge S-260 scanning electron microscope. Thicknesses of total leaf, upper and lower epidermis, mesophyll, and sponge tissues were measured with a light microscope equipped with a micrometer. The leaf thicknesses were monitored from April to October 2000 for all 35 species.

18.2.5 Measurements of UV-B Absorbing Compounds and Chlorophyll Concentrations

Extraction of leaf UV-B absorbing-compounds, mainly flavonoids and related phenolic compounds, was based on the method by Gorton and Vogelmann (1996). Two 10-mm-diameter leaf discs (the total leaf area was 1.57 cm^2) were placed in a 1.5 mL microfuge tube and ground to a fine powder in liquid nitrogen using a Teflon pestle. One mL of acidified methanol (methanol:H_2O:HCl 79:20:1 v/v) was added to the microfuge tube and homogenized well. The extracts were stored frozen ($-80^{\circ}C$) for up to one week, then clarified by centrifugation (Micro 12, National Labnet Company, Inc.). Forty μl of the supernatant were transferred to a quartz cuvette and diluted in 3 mL of extraction medium (resulting in a volume dilution factor of 76). Spectra of the extracts were obtained from 200 nm－820 nm with a computer-controlled, split-beam, dual-detector UV/Visible spectrophotometer (Genesis 2 Spectronic, Inc.) at 1 nm increments. The absorbance spectra of the extract were then standardized for the leaf area and volume to obtain the absorbance values on a leaf area basis (A/cm^2). In order to calculate the UV-B absorbing compound concentration for each sample, we decided to include the entire UV-B wavelength region by calculating the cumulative absorbance values from 280 nm－320 nm for each sample. This avoided the arbitrary selection of the absorbance at a single wavelength, e.g., at 300 nm, 310 nm, or 330 nm, which has been used in numerous studies. Our recent report also indicates that the values of UV-B absorbing compounds measured at 280 nm, 300 nm, and 310 nm were not always in agreement (R^2 ranged from 0.76－0.93) due to their wavelength specific nature (Qi et al., 2002). Therefore, the cumulative absorbance from

280 nm – 320 nm at 1 nm intervals was used, then standardized for leaf area and volume, and expressed as total absorbance ($A_{280\ nm-320\ nm}/cm^2$) to represent the total UV-B absorbing compound content or concentrations per unit of leaf area. Leaf total chlorophyll content was measured with a Minolta Chlorophyll Meter (Spad-502, Spectrum Technologies Inc, IL). The values were then converted to the true chlorophyll content based on the method developed by Yadava (1986).

18.2.6 Statistical Analysis

Data were analyzed using ANOVA ($p = 0.05$). Duncan's multiple range tests were used to compare means ($p = 0.05$). Regression analyses were used to assess the correlation and predictive power among the selected variables.

18.3 Results and Discussion

18.3.1 Leaf Optical Properties

Changes in leaf spectral reflectance, transmittance, and absorbance to UV/visible light of pecan leaves throughout a growing season are illustrated in Fig. 18.3. The changes in leaf optical properties were relatively small in UV-B (280 nm – 320 nm) and UV-A (320 nm – 400 nm) spectral regions compared to that of the visible spectral region (400 nm – 760 nm). Throughout the growing season, pecan leaves reflected 4% – 8%, transmitted 0% – 1%, and absorbed up to 96% of UV radiation (280 nm – 400 nm). In the visible light region, leaf absorbance to green light (at 555 nm) and to red light (at 680 nm) increased dramatically during leaf development from April to July. This trend seems to hold true for all other species studied. Since the leaf optical properties remained relatively steady within the UV region, this indicated we could make the species comparison at a single wavelength. Since our focus was primarily on UV-B, we chose 300 nm for the comparison of the leaf optical properties amongst the 35 species (Table 18.1). The species were ranked from the highest to the lowest based on their reflectance (Fig. 18.4). As shown in Table 18.1 and Fig. 18.4, leaf reflectance to the 300 nm UV-B was generally low across the species, ranging between 4.77% – 8.61% with a mean value of 6.55%, ± 1% of standard deviation. The leaf transmittance to the 300 nm was rather low for all the species, ranging between 0% – 0.17%. The leaf absorbance to the 300 nm UV-B was above 90% across the species, ranging between 91.34% – 95.23% with a mean value of 93.44%, ± 1% of standard deviation. These findings are generally in agreement with the results reported by Gausman et al. (1975), Robberecht et al. (1980), Cen and Bornman (1993), and Yang et al. (1995). It is generally agreed that leaves absorb over 90% of incident UV-B; leaf surface

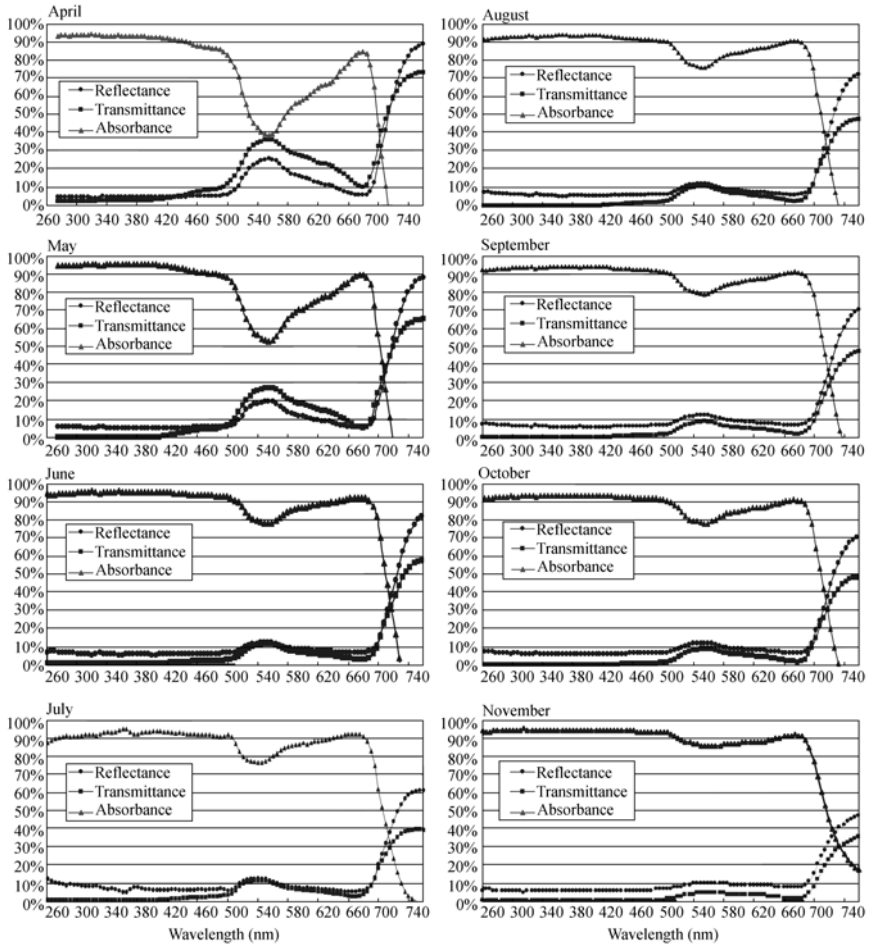

Figure 18.3 Leaf spectral reflectance, transmittance, and absorbance to UV/visible light during a growing season in leaves of pecan (Qi et al., 2003b)

reflection, as a first line of defense against UV-B, is less than 10% in most species, and there is negligible transmission of UV-B through leaves.

18.3.2 Depth of Light Penetration into Leaf Tissues

Light attenuation in pecan leaves at four wavelengths including UV-B, UV-A, blue light, and red light into leaf tissues is illustrated in Fig. 18.5. The depths of the light penetration into the leaf tissues are presented in Fig. 18.6. Pecan leaf epidermis strongly attenuated 310 nm UV-B, 98% of which was absorbed within the first 10 μm of the 15 μm-thick upper epidermal tissue (Figs. 18.5 and 18.6). High UV-B attenuation by the epidermal layer means low epidermal transmittance to UV-B.

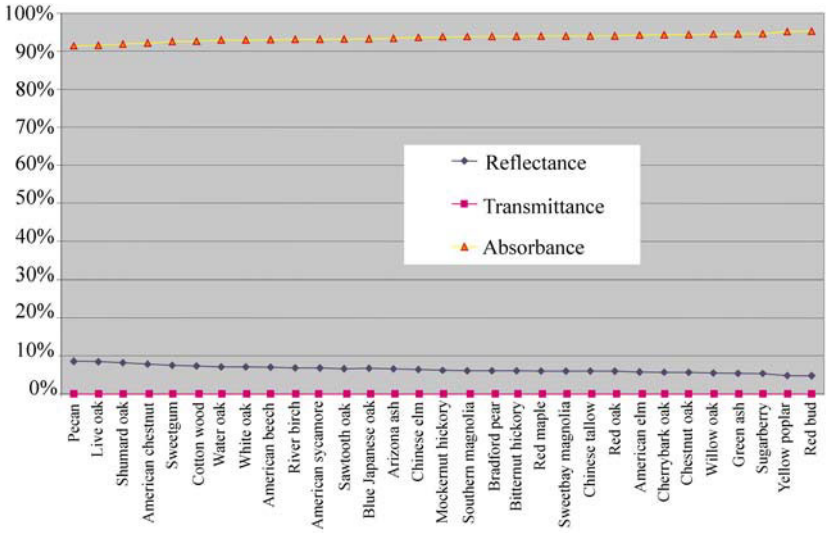

Figure 18.4 Leaf reflectance, transmittance, and absorbance to 300 nm UV-B radiation on a whole leaf basis in the selected broadleaf tree species. The measurements were made on the mature leaves collected in August in Baton Rouge, LA. The species were ranked based on the reflectance from the highest to the lowest

Since the epidermis of the pecan leaves allowed very little UV-B (< 2%) transmittance into the mesophyll tissues, the photosynthetic apparatus were essentially protected from the UV-B damage. Thus, such an effective epidermal function of the UV-B screening characterizes the UV-B tolerance mechanism in pecan. In addition to the UV-B attenuation, pecan leaf epidermis attenuated 96% of the UV-A (360 nm), 83% of the blue light (430 nm), and 58% of the red light (680 nm). However, the blue and the red light penetrated much deeper into the mesophyll tissues. The 430 nm light was mainly attenuated within the first 100 μm thickness of the leaf, including the upper epidermis and the palisade mesophyll tissue. The 680 nm penetrated even deeper into the sponge mesophyll and was mainly attenuated within the first 160 μm thickness of the leaf. Overall, mesophyll tissues alone attenuated 17% of the blue light and 42% of the red light that were available for photosynthesis (Figs. 18.5 and 18.6).

Comparisons among the species are presented in Fig. 18.7, which contains 31 species, excluding dogwood, red mulberry, pin oak, and post oak, for which the data were not available. The 31 species were ranked from the lowest to the highest based on their epidermal UV-B transmittance. The differences in the depth of the UV-B penetration, epidermal transmittance to UV-B, and upper epidermal thickness are clearly considerable amongst the species (Fig. 18.7). The first 23 species in Fig. 18.7, including Arizona ash, chestnut oak, mocker nut hickory, pecan, American sycamore, bitternut hickory, green ash, sawtooth oak, American elm, blue Japanese oak, cherrybark oak, cottonwood, southern live oak, southern magnolia, shumard oak,

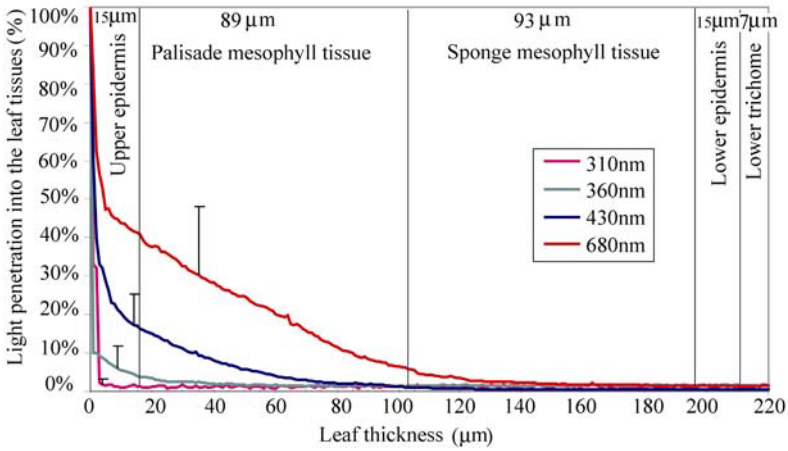

Figure 18.5 Light penetration into leaf tissues from the adaxial surfaces in pecan by four different wavelengths, the error bar represents +1SD. The measurements were made on 15 mature leaves sampled in August

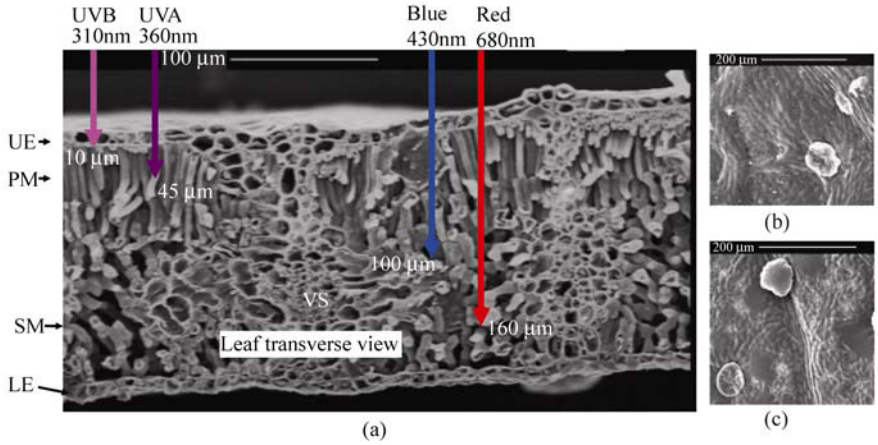

Figure 18.6 Visual illustration of the light penetration into leaf tissues in pecan. (a) Shows a pecan leaf cross-section. UE = upper epidermis, PM = palisade mesophyll, SM = sponge mesophyll, LE = lower epidermis, VS = vascular system. The downward arrows show the relative positions of depths of light penetration at different wavelengths; (b) shows the upper leaf surface and trichome; and (c) shows the lower leaf surface and trichome

sweetgum, American beech, white oak, Chinese tallow, water oak, yellow poplar, Bradford pear, and red maple, had relatively low epidermal transmittance, ranging from 1% – 8%. This means the leaf epidermises of these species were capable of attenuating 92% – 99% of the UV-B absorbed. Such a strong epidermal function of the UV-B screening underlies the fundamental UV-B protection mechanism in these species. This finding also concurs with the research by Caldwell et al.

(1983) and Day (1993), asserting that the epidermal attenuation appears to be the dominant UV-B screening mechanism in the majority of plants. On the other hand, the last five species in Fig. 18.7, including river birch, American chestnut, red bud, Chinese elm, and sugarberry, exhibited high epidermal transmittance (ranging from 27% − 49%). These species may be less UV-B tolerant. They may also experience up to 50% UV-B penetration into their mesophyll tissues, which could result in damage to their photosynthetic apparatus, unless there are additional UV-B absorbing compounds present in their mesophyll tissues. In addition, the three species in Fig. 18.7, including sweet bay magnolia, red oak, and willow oak, are intermediate regarding their epidermal transmittance (13% − 17%), which falls between the low values (under 8%) of the first 23 species and the high values (27% − 49%) shown by the last 5 species.

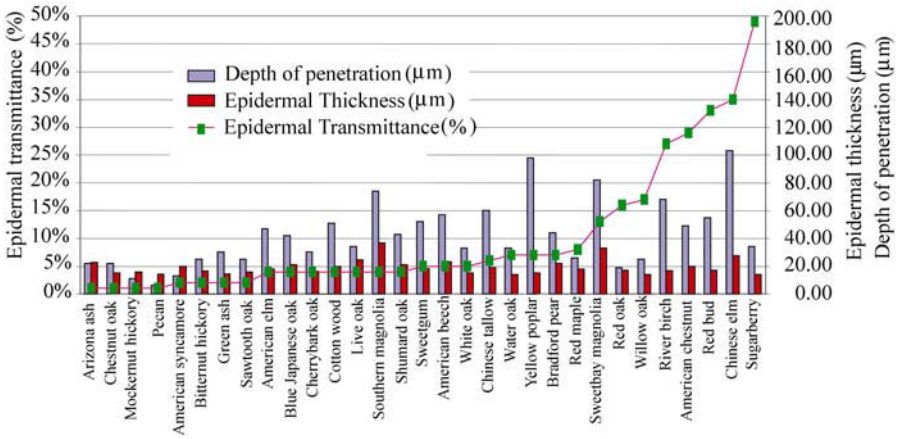

Figure 18.7 Comparisons of upper epidermal transmittance to 310 nm UV-B radiation, depth of 310 nm penetration into leaves, and epidermal thickness among the selected broadleaf tree species. Note: The species were ranked based on the epidermal transmittance from the lowest to the highest. In all cases, mature leaves were used and light was illuminated toward the upper leaf surfaces in the light penetration study

18.3.3 The Concentration of Leaf UV-B Absorbing Compounds

The inter-specific comparison of the total UV-B absorbing compound concentration per unit of leaf area ($A_{280\ nm-320\ nm}/cm^2$, assessed by integrating the absorbance values from 280 nm − 320 nm at 1 nm intervals) in the mature leaves is presented in Fig. 18.8. Large variations exist among the species. These UV-B absorbing compounds possess strong absorbance to the UV radiation (Qi et al., 2002; Qi et al., 2003b, c). It is possible that those species with the strong epidermal UV-B screening abilities, such as the first 23 species in Fig. 18.7, may have accumulated

more UV-B absorbing compounds in their epidermal layers than the rest of the species. Further research is necessary to localize the UV-B absorbing compounds in leaves. The accumulation of flavonoids in the epidermis has been shown to reduce epidermal transmittance of UV-B radiation (Robberecht and Caldwell, 1978; Tevini et al., 1991). Research by Karabourniotis and Fasseas (1996) and Karabourniotis et al. (1998) suggests that these flavonoids, and possibly other phenolics, are present throughout the leaf, but accumulate significantly in leaf trichomes and epidermal cells. Research has also demonstrated that the *Arabidopsis* mutants' lack of UV-B absorbing compounds (e.g., cinnnamic acid precursors and flavonoids) were hypersensitive to UV-B radiation (Li et al., 1993; Reuber et al., 1996). Those species with weak epidermal screening abilities, such as river birch, American chestnut, red bud, Chinese elm, and sugarberry (see Fig. 18.7), may be able to accumulate UV-B absorbing compounds throughout the leaf cross-sections in order to provide additional UV-B defense. Ultraviolet-absorbing compounds and specific leaf anatomical features are important in determining leaf screening efficiency (Bornman, 1999). The identifications and locations of flavonoids and related phenolics in leaf tissues have been advanced by many studies (Schnitzler et al., 1996; Hutzler et al., 1998; Laakso et al., 2000; Semerdjieva et al., 2003; Sullivan et al., 2005). Using fluorescence microscopy, Semerdjieva et al. (2003) discovered *Vaccinium myrtillus* contained the highest concentration of methanol-extractable UV-B absorbing compounds which were distributed throughout the leaf, and were particularly concentrated in chlorophyll-containing cells, while in *Vaccinium vitisidaea*, most phenolic compounds were cell wall-bound and concentrated in the walls of the epidermis. These two plants represent extreme forms of two divergent strategies for UV-B screening.

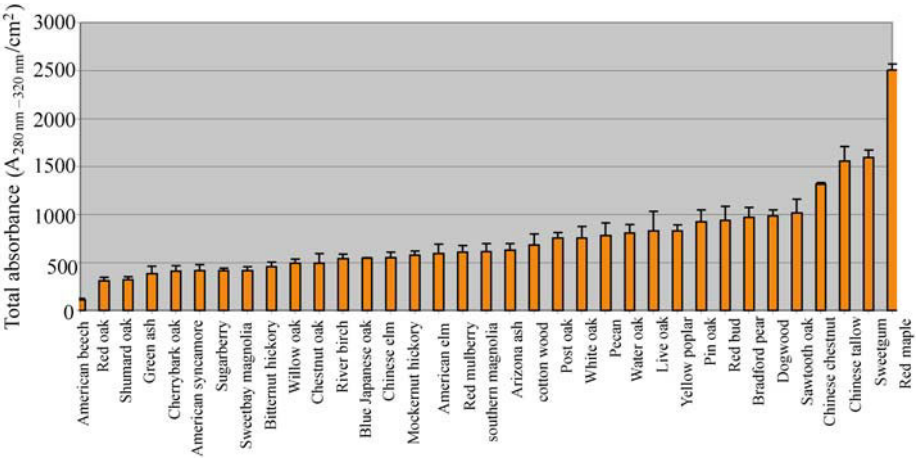

Figure 18.8 Comparisons of UV-B absorbing-compound concentrations in mature leaves among the selected broadleaf tree species grown in Baton Rouge, LA. The value for each species was the mean over four month measurements from July to Oct with four samples per month from sun-exposed leaves. The error bar indicates + 1SE

18.3.4 Correlations among the UV-B Related Variables within and among the Species

This study has shown that with increased UV-B radiation during the growing season (Fig. 18.9(a)), there are cumulative increases in leaf concentration of UV-B absorbing compounds (Fig. 18.9(b)), leaf total thickness (Fig. 18.9(c)), and leaf chlorophyll content (Fig. 18.9(d)), in all the 35 species combined. However, these parameters are all delayed responses from increasing solar UV levels. Although the leaves from each species were sampled in the first week of each month to represent that month, they perhaps better represent the previous month in relation to their responses to the UV-B radiation. Even so, there are still delays in the responses in UV-B absorbing compounds and other parameters as shown in Fig. 18.9. Perhaps a cumulative response might be in effect. The increased UV-B absorbing compound content over the growing season helps enhance the plants defense against the enhanced UV-B level. Correlation analyses of these variables (Table 18.2) indicated that during the growing season, there is a good correlation between total leaf thickness and total concentration of leaf UV-B absorbing compounds ($r = 0.9$). Also, considering that chlorophyll synthesis is very dynamic throughout the season, while UV-B absorbing compounds are probably only produced at very specific developmental stages it would make sense that chlorophyll concentrations would correlate much better with solar irradiance over the long haul than would UV-B absorbing compounds, which may be locked in at the time of synthesis and are not continuously being recycled. Thus, it is not surprising that the ambient UV-B radiation was correlated better to leaf chlorophyll content ($r = 0.94$) than to the concentration of UV-B absorbing compounds ($r = 0.45$). This may also be attributed to the fact that the UV-B radiation follows the trend of the total solar radiation, within which the PAR is well-correlated to chlorophyll development during the growing season. The chlorophyll content declined significantly in October (Fig. 18.9(d)) while the UV-B absorbing compound concentration remained at a steady state during the latter part of the growing season from August to October (Fig. 18.9(b)).

As we have demonstrated in Figs. 18.7 and 18.8, considerable inter-specific variations exist in the leaf total UV-B absorbing compound concentration, leaf epidermal thickness, and depth of UV-B penetration, as well as the epidermal transmittance among the species investigated. In order to reveal if there is any inter-specific correlation between these variables, we also performed the correlation analyses (Table 18.3). The results show there is a good inter-specific correlation between leaf total thickness and leaf epidermal thickness ($r = 0.84$), meaning that the species with thicker leaves may have thicker epidermis. Some positive inter-specific relationships seem to exist between the leaf total thickness and its chlorophyll content ($r = 0.66$), and between the epidermal thickness and the depth of UV-B penetration into leaves ($r = 0.53$). The correlation coefficients between the epidermal transmittance and depth of UV-B penetration ($r = 0.36$) and between

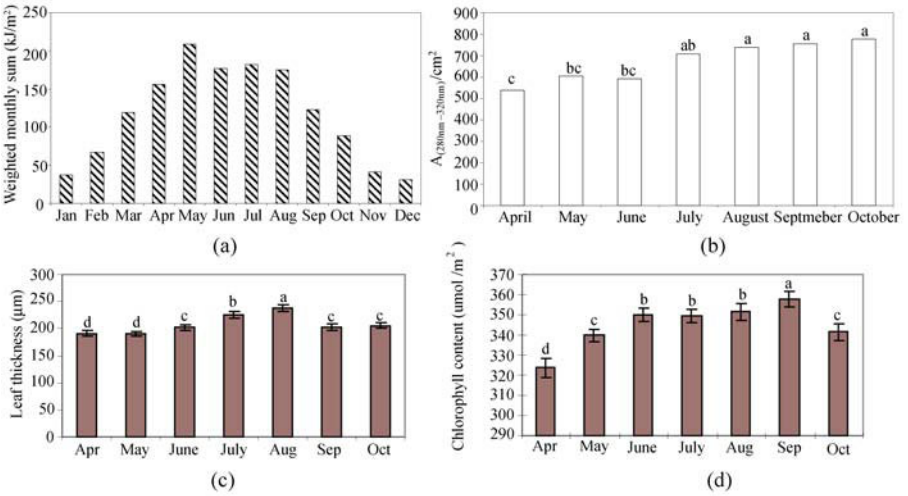

Figure 18.9 Monthly summation of ambient UV-B radiation in Baton Rouge, LA in year 2000 provided by the USDA-UV-B Monitoring Program Baton Rouge Station (a); and seasonal trends in leaf UV-B absorbing-compound concentration (b); leaf thickness (c); and leaf chlorophyll content (d); of the 35 species combined. Within each chart, means with unlike letters differ significantly according to Duncan's multiple range tests, $p \leqslant 0.05$. The error bars represent ± 1SE

Table 18.2 Correlation coefficients during leaf growth and development in all the species combined

Correlation coefficient	UV-B radiation (kJ/m^2/month)	Leaf thickness (μm)	Leaf chlorophyll (μmol/m^2)	Leaf UV-B absorbing compounds ($A_{280\ nm-320\ nm}/cm^2$)
UV-B radiation (kJ/m^2/month)	1			
Leaf thickness (μm)	0.48	1		
Leaf chlorophyll (μmol/m^2)	0.94	0.66	1	
Leaf UV-B absorbing-compounds $A_{280\ nm-320\ nm}/cm^2$	0.45	0.90	0.72	1

leaf total thickness and the depth of the penetration ($r = 0.36$) were too low to depict any inter-specific relationships. No inter-specific relationships were discovered between the leaf total UV-B absorbing compound concentration and any other variables, including leaf total thickness, epidermal thickness, epidermal transmittance, and depth of UV-B penetration (r values ranged from -0.02 to 0.06, as shown in Table 18.3). This may be attributed to the individualistic nature (randomness) of the species, or is perhaps due to the fact that the trees selected in this study,

Table 18.3 Correlation between the selected UV-B related properties in mature leaves across all the species studied

Correlation coefficient	Leaf total thickness (μm)	Leaf upper epidermal thickness (μm)	Leaf upper epidermal transmittance to 310 nm UVB (%)	Depth of 310 nm UVB penetration into leaves (μm)	Leaf concentration of total UV-B absorbing compounds ($A_{280\ nm\ -\ 320\ nm}/cm^2$)	Leaf chlorophyll content ($\mu mol/m^2$)
Leaf total thickness (μm)	1.00					
Leaf upper epidermal thickness (μm)	0.84	1.00				
Leaf upper epidermal transmittance to 310nm UVB (%)	−0.23	0.02	1.00			
Depth of 310 nm UVB penetration into leaves (μm)	0.36	0.53	0.36	1.00		
Leaf concentration of total UV-B absorbing compounds ($A_{280\ nm\ -\ 320\ nm}/cm^2$)	0.04	0.06	−0.02	0.02	1.00	
Chlorophyll content ($\mu mol/m^2$)	0.66	0.52	−0.17	0.10	−0.08	1.00

including 4 evergreen and 31 deciduous broadleaf species, generally belong to two life forms (evergreen angiosperms and deciduous dicotyledon trees) that may not be able to warrant for any significant correlations. A study involving species from 6 plant life forms (evergreen gymnosperms, evergreen angiosperms, deciduous dicotyledon trees, deciduous dicotyledon shrubs/vines, herbaceous dicotyledon, and grasses) did reveal better correlations between some of the UV-B related variables across the species (Day, 1993).

18.4 Conclusions

This study investigated the UV-B related biophysical, biochemical, and anatomical characteristics of more than 30 southern broadleaf tree species. It is concluded that leaves of the broadleaf trees generally reflect 4%−9%, transmit 0%−0.2%, and absorb 91%−95% of the incident UV-B radiation. The main site of UV-B attenuation takes place within the upper leaf epidermis. The project has identified 23 broadleaf tree species (Arizona ash, chestnut oak, mocker nut hickory, pecan, American sycamore, bitternut hickory, green ash, sawtooth oak, American elm, blue Japanese oak, cherrybark oak, cottonwood, southern live oak, southern magnolia, shumard oak, sweetgum, American beech, white oak, Chinese tallow, water oak, yellow poplar, Bradford pear, and red maple) possessing a strong epidermal UV-B screening functions (attenuating over 90% UV-B). The effectiveness of the epidermal function of the UV-B screening underlines the major UV-B protection mechanism in most of the trees studied. Three species (sweet bay magnolia, red oak, and willow oak) possessed intermediate epidermal screening function, and five other species (river birch, American chestnut, red bud, Chinese elm, and sugarberry) showed somewhat weak epidermal screening functions. Considerable inter-specific variations exist in leaf UV-B absorbing compound concentrations, depth of UV-B penetration, and leaf anatomical features. In addition to the epidermal screening function, the leaf UV-B absorbing compounds may play an important role in providing additional defense against UV-B radiation penetration into mesophyll tissues. Further studies are necessary to focus on localization and identification of UV-B absorbing compounds in leaf tissues, to promote a better understanding of the UV-B tolerance mechanisms in trees.

Acknowledgements

This research was supported by the USDA/CSREES/CBGP grant No. 98-38814-6386 to Y. Qi, and by Southern University Agricultural Research and Extension Center, Baton Rouge, LA, USA.

References

Barnes BV, Zak DR, Denton SR, and Spurr SH (1998) Forest Ecology, 2nd Ed. (p.774). Wiley, New York

Beggs CJ, and Wellmann E (1994) Photocontrol of flavonoid biosynthesis. In: Kendrick RE and Kronenberg GHM (Eds.), Photomorphogenesis in Plants, 2nd Ed. (pp. 733 – 751) Dordrecht, The Netherlands: Kluwer Academic Publishers

Bornman JF (1999) Localisation and functional significance of flavonoids and related compounds. In: J. Rozema (Ed.), Stratospheric Ozone Depletion: the Effects of Enhanced UV-B Radiation on Terrestrial Ecosystems (pp. 59 – 69). Leiden, The Netherlands: Backhuys Publishers

Bornman JF, Reuber S, Chen YP, and Weissenbock G (1997) Ultraviolet radiation as a stress factor and the role of protective pigments. In: Lumsden PJ (Ed.), Plants and UV-B: Responses to Environmental Change (pp. 157 – 168). Cambridge: Cambridge University Press

Caldwell MM, Robberecht R, and Flint SD (1983) Internal filters: prospects for UV-acclimation in higher plants, Physiologia Plantarum 58: 445 – 450

Caldwell MM, Björn LO, Bornman JF, Flint SD, Kulandaivelu G, Teramura AH, and Tevini M (1998) Effects of increased solar ultraviolet radiation on terrestrial ecosystems, Journal of Photochemistry and Photobiology B: Biology 46: 40 – 52

Cen YP, and Bornman JF (1993) The effect of exposure to enhanced UV-B radiation on the penetration of monochromatic and polychromatic UV-B radiation in leaves of Brassica napus, Physiologia Plantarum 87: 249 – 255

Crutzen PJ (1972) SSTs — a threat to the earth's ozone shield, Ambio 1: 41 – 51

Day TA (1993) Relative UV-B radiation screening effectiveness of foliage to absorbing-compound concentration and anatomical characteristics in a diverse group of plants. Oecologia 95: 542 – 550

Day TA, Vogelmann TC, and Delucia EH (1992) Are some plant life forms more effective at screening UV-B radiation? Oecologia 92: 513 – 519

Day TA, Howells BW, and Rice WJ (1994) Ultraviolet absorption and epidermal transmittance spectra in foliage, Physiologia Plantarum 92: 207 – 218

DeLucia EH, Day TA, and Vogelmann TC (1991) Ultraviolet-B radiation and the Rocky Mountain environment: measurement of incident light and penetration into foliage, Current Topics in Plant Biochemistry and Physiology 10: 32 – 48

DeLucia EH, Day TA, and Vogelmann TC (1992) Ultraviolet-B and visible light penetration into needles of two species of subalpine conifers during foliar development, Plant, Cell and Environment 15: 921 – 929

Gausman HW, Rodriquez RP, and Escobar DE (1975) UV-B reflectance, transmittance, and absorbance by plant leaf epidermises, Agron J 83: 391 – 396

Gorton HL, and Vogelmann TC (1996) Effects of epidermal cell shape and pigmentation on optical properties of Antirrhinum petals at visible and ultraviolet wavelengths, Plant Physiology 112: 879 – 888

Hutzler P, Fischbach R, Heller W, Jungblut TP, Reuber S, Schmitz R, Veit M, Weissenbock G, and Schnitzler JP (1998) Tissue localization of phenolic compounds in plants by confocal laser scanning microscopy, Journal of Experimental Botany 49: 953 – 965

Johnston HS (1971) Reduction of stratospheric ozone by nitrogen oxide catalysts from supersonic transport exhaust, Science 173: 517 – 522

Karabourniotis G, and Fasseas C (1996) The dense indumentum with its polyphenol content may replace the protective role of the epidermis in some young xeromorphic leaves, Can J Bot 74: 347 – 351

Karabourniotis G, Kofidis G, Fasseas C, Drossopoulos I, and Liakoura V (1998) Polyphenol deposition on the cell walls of some nonglandular leaf hairs during their development, Am J Bot 85: 1007 – 1012

Laakso K, Sullivan JH, and Huttunen S (2000) The effects of UV-B radiation on epidermal anatomy in loblolly pine (Pinus taeda L.) and Scots pine (Pinus sylvestris L.). Plant, Cell and Environment 23: 461 – 472

Li J, Ou-Lee TM, Raba R, Amundson RG, and Last RL (1993) Arabidopsis flavonoid mutants are hypersensitive to UV-B irradiation, Plant Cell 5: 171 – 179

Optronic Laboratories, Inc. (1997) Operational Manual for OL754 and its attachments. Florida USA: Optronic Laboratories, Inc.

Qi Y, Bai S, Vogelmann TC, Heisler GM, and Qin J (2002) Methodology for comprehensive evaluation of UV-B tolerance in trees, Proc SPIE 4482: 367 – 380

Qi Y, Bai S, Vogelmann TC, and Heisler GM (2003a) Penetration of UV-A, UV-B, blue and red light into leaf tissues of pecan measured by a fiber optic microprobe system, Proc SPIE 5156: 291 – 300

Qi Y, Bai S, and Heisler GM (2003b) Changes in ultraviolet-B and visible optical properties and absorbing pigment concentrations in pecan leaves during a growing season, Agriculture and Forest Meteorology 120: 229 – 240

Qi Y, Bai S, Gao W, and Heisler GM (2003c) Intra and inter-specific comparisons of UV-B absorbing compound concentrations in southern broadleaf trees in the USA, Proc SPIE 4896: 120 – 129

Reuber S, Bornman JF, and Weissenböck G (1996) A flavonoid mutant of barley (Hordeum vulgare L.) exhibits increased sensitivity to UV radiation in the primary leaf, Plant Cell and Environment 19: 593 – 601

Robberecht R and Caldwell WW (1978) Leaf epidermal transmittance of UV radiation and its implications for plant sensitivity to UV-radiation induced injury, Oecologia 32: 277 – 287

Robberecht R, Caldwell WW, and Billings WD (1980) Leaf UV optical properties along a latitude gradient in the arctic alpine life zone, Ecology 61: 612 – 619

Saunders RD, and Shumaker JB (1977) The 1973 NBS Scale of Spectral Irradiance, NBS Technology Note 594 – 613

Schnitzler JP, Jungblut TP, Heller W, Kofferlein M, Hutzler P, Heinzmann U, Schmezler E, Ernest D, Langebartels C, and Candermann H Jr (1996) Tissue localization of UV-B-screening pigments and of chalcone synthase mRNA in needles of Scots pine seedlings. New Phytologist 132: 247 – 258

Searles PS, Caldwell MM, and Winter K (1995) Responses of five tropical dicotyledon species to natural solar ultraviolet-B radiation, Amer J Botany 82: 445 – 453

Semerdjieva SI, Sheffield E, Phoenix GK, Gwynn-Jones D, Callaghan TV, and Johnson GN (2003) Contrasting strategies for UV B screening in sub-arctic dwarf shrubs. Plant, Cell and Environment 26: 957 – 964

Sullivan JH, and Rozema J (1999) UV-B effects on terrestrial plant growth and photosynthesis. In J. Rozema (Ed.), Stratospheric Ozone Depletion: The effect of Enhanced UV-B Radiation on Terrestrial Ecosystem (pp.39 – 57). Leiden, The Netherlands: Backhays Publishers

Sullivan JH, Gitz DC, Peek MS, and McElrone AJ (2003) Response of three eastern tree species to supplemental UV-B radiation: leaf chemistry and gas exchange, Agricultural and Forest Meteorology 120: 219 – 228

Sullivan JH, Xu C, Gao W, and Slusser JR (2005) Development of UV-B screening compounds in response to variation in ambient levels of UV-B radiation, Proc. SPIE 5886OL: 11

Taylor RM, Tobin AK, and Bray CM (1997) DNA damage and repair in plants. In: Lumsden PJ (Ed.), Plants and UV-B Responses to Environmental Change (pp. 53 – 76). Cambridge: Cambridge University Press

Tevini M, Braun J, and Fieser G (1991) The protective function of the epidermal layer of rye seedlings against ultraviolet-B radiation, Photochemistry and Photobiology 53: 329 – 333

UNEP (1998) Environmental Effects of Ozone Depletion, 1998 Assessment (p.103). United Nations Environment Programme

UNEP (2002) Scientific Assessment of Ozone Depletion: 2002. Global Ozone Research and Monitoring Project 47, United Nations Environment Programme/World Meteorological Organization, Nairobi, Kenya

Vogelmann TC, and Bjorn LO (1984) Measurement of light gradients and spectral regime in plant tissue with a fiber optic probe, Physiol Plant 60: 361 – 368

Vogelmann TC, Martin G, Chen G, and Buttry D (1991) Fiber optic microprobes and measurement of the light micro environment within plant tissues, Adv Botanical Res 18: 231 – 270

Whittaker RH (1975) Communities and Ecosystems (pp.76 – 87). New York: MacMillan Co

Yadava UL (1986) A rapid and nondestructive method to determine chlorophyll in intact leaves, HortScience 21: 449 – 450

Yang X, Heisler GM, Montgomery ME, Sullivan JH, Whereat EB, and Miller DR (1995) Radiative properties of hardwood leaves to ultraviolet irradiation, Int J Biometeorology 38: 60 – 66

Index